CRANFIELD UNIVERSITY
LIBRARY

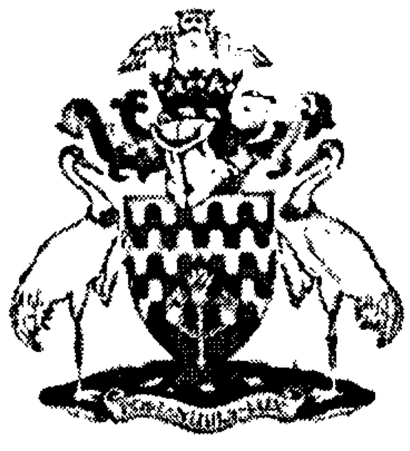

CRANFIELD UNIVERSITY

ELI EBER BATISTA GOMES

Operational Optimisation of Gas Turbines Distributed Generation Systems in Competitive Electricity Market

SCHOOL OF ENGINEERING

PhD Thesis

CRANFIELD UNIVERSITY

SCHOOL OF ENGINEERING

PhD Thesis

Academic Year 2003-2007

ELI EBER BATISTA GOMES

Operational Optimisation of Gas Turbines Distributed Generation Systems in Competitive Electricity Market

Supervisors:

Prof. Pericles Pilidis
Dr. Y. G. Li

April 2007

This thesis is submitted for the degree of Philosophy Doctor

©Cranfield University, 2007. All rights reserved. No part of this publication may be reproduced without the written permission of the copyright holder.

ACKNOWLEDGMENTS

My eternal gratitude to Jehovah God and his son Jesus Christ for the breath of life.

I would like to express my gratitude to Professor Pericles Pilidis for his guidance, support and encouragement since the beginning of this project. Also, my sincere thanks to Dr Y. Li for his support and advice.

I wish to acknowledge CAPES (the Brazilian federal agency under the Ministry of Education) for financial support to pursue a PhD degree at Cranfield University.

Special thanks to my colleagues in the Gas Turbine Engineering Group for their friendship and trust. My sincere appreciation goes to the staff of the Department of Power & Propulsion at Cranfield University for their hospitality and continuing encouragement.

I am extremely grateful to my parents Eber and Celia Gomes. Without their support, love and constant encouragement throughout so many years it would not have been possible for me to go this far with my studies. I also wish to express my gratitude to my dear wife Kenia Passos for her love, support and tolerance through the many difficult times of this project.

"The fear of the Lord is the beginning of wisdom; and the knowledge of the holy is understanding. For the Lord gives wisdom; out of his mouth comes knowledge and understanding." (Proverbs of Solomon, The Bible)

ABSTRACT

The development of power generation technologies and the deregulation of the power market has led to an increasing interest in distributed power generation, mainly the simultaneous exploitation of electricity and heat from the same energy source, known as combined heat and power (CHP) systems.

As a consequence of the high competitiveness of power markets and increasing environmental concerns, distributed power generators have to make reasonable choices at multiple levels of complexity. A key issue to successfully approaching these problems is the development of decision making support tools that rely on service life prediction, intelligent economic dispatch optimisation techniques and condition monitoring.

This research introduces the concept and development of a decision making support tool for a mini-pool nerve centre based on distributed gas turbine generation units operating in a competitive market. The nerve centre framework leads naturally to a multi-criteria optimisation problem which is solved in this research with a hybrid genetic algorithm adapted priority list and creep life assessment. The proposed hybrid approach can result in a significant saving to generators as it efficiently optimises mini-pool profits and service hours between failures in an acceptable computation time and accurately. Life cycle assessment combined with generation schedule optimisation can enhance the maintenance strategy activities and the competitiveness of gas turbine distributed generation plants, particularly for generators trading energy in a highly competitive market.

Gas turbine combined heat and power distributed generators are unlikely to succeed in competing individually with centralised generation technologies within the present market framework, but they can be more competitive in an information technology based mini-pool. Additionally, results show that the development of a low carbon emission power industry can result in an outstanding opportunity for combined heat and power mainly in power markets currently highly dependent on coal and oil powered stations.

CONTENTS

LIST OF FIGURES

LIST OF TABLES

LIST OF SYMBOLS AND ABBREVIATIONS

A	Area [m^2] or Availability
ACE	Avoided cost of electricity [£/period]
ACH	Avoided cost of heat [£/period]
ADC	Accounting depreciation charge [£/period]
ADE	Annual deficit of electricity [kWh/year]
AED	Annual electricity demand [kWh/year]
AEP	Annual electricity produced [kWh/year]
AFR	Air fuel ratio
AGC	Additional generation cost [£/kWh]
AHD	Annual heat demand [kW]
Ahr	Cross sectional area height ratio
a, b, c	Parameters of the polynomial fuel cost function FC(P)
ALP	Annual payments of principal and interest of the loan [£/period]
AMFC	Annual mass fuel consumption of the CHP system [kg/year]
A_n	Annulus area of the turbine blade
ANCF	Annual net cash flow [£/year]
AOP	Annual operation profit [£/year]
ASE	Annual surplus of electricity [kWh/year]
AT	Ambient temperature [K]
ATR	Annual tax rate
BCR	Benefit to cost ratio
BFTR	Fuel tariff rate for the boiler [£/kg]
BMC	Base maintenance cost [£/h]
C	Capital cost of the CHP system [£], Number of constraints or Absolute velocity
CCF	Mass content of carbon in the fuel [%]
CDP	Cost of power deficit [£/kWh]
cdtr	Carbon dioxide tax rate (carbon price) [£/ton]
CEP	Contract electricity price [£/kWh]
CF	Capacity factor

CHP	Combined heat and power
CHPED	Combined heat and power economic dispatch
CN	Non-dimensional constant speed
CO	Carbon monoxide
CO_2	Carbon dioxide
Cp	Specific heat coefficient at constant pressure [J/kgK]
CRF	Capital recovery factor
CS	Constant speed
CT	Cumulative up/down time [h]
DCA	Carbon dioxide allowance (% of annual emission)
DCF	Discounted cash flow
DCTax	Carbon dioxide tax cost
DED	Dynamic economic dispatch
DF	Demand factor
DG	Distribution Generation
DOD	Domestic object damage
DP	Deficit of power capacity [kW], design point or dynamic programming
DPB	Discounted payback period [years]
DP-PL	Hybrid dynamic programming priority list
DT	Downtime (outage) hours
DTC	Deficit of thermal capacity [kW]
DuP	Dual (partial-separable) programming
E	Young's modulus
e1, e2, e3	Elbow point of the piece-wise linear cost function
EA-PL	Evolutionary algorithm and priority list
EBP	Electricity buy price [£/kWh]
EC	Environmental constraints
ED	Electricity demand [kW]
EP	Electrical power output [kW]
ESP	Electricity sell price [£/kWh]
FAR	Fuel air ratio

FC	Fuel cost [£/period]
FCM	Fault coefficient matrix
FDI-GA	Fuzzy decision index and genetic algorithm
FOD	Foreign object damage
FOMC	Fixed operation and maintenance costs [£/period]
FT	Free turbine
Ftn	Fitness function
ftr	Fuel tariff rate [£/kg]
g	Acceleration of gravity [m/s^2]
GA	Genetic algorithm
GA-MU	Genetic algorithm and multiplier updating
GA-TS	Genetic algorithm tabu search
GC	Generation cost [£/kWh]
GG	Gas generator
GPA	Gas path analysis
GTEA	Gas turbine exhaust area [m^2]
GTED	Gas turbine exhaust density [kg/m^3]
GTEM	Gas turbine exhaust mach number
GTESP	Gas turbine exhaust static pressure [Pa]
GTEST	Gas turbine exhaust static temperature [K]
GTETP	Gas turbine exhaust total pressure [Pa]
GTETT	Gas turbine exhaust total temperature [K]
GTEV	Gas turbine exhaust velocity [m/s]
GTM	Gas turbine models
HC	Hydraulic constraints
HCL	Heat capacity limits [kW]
HDB	Heat demand balance [kW]
HD	Heat demand [kW]
HPR	Heat to power ratio
HR	Heat rate [kJ/kWh]
HRCR	Heat recovery steam generator cost rate
HSP	Heat selling price [£/kWh]

IC	Initial conditions
ICF	Initial cash flow [£/year]
ICM	Influence coefficient matrix
ICR	Installation, project and contingence cost rate
IMC	Incremental maintenance cost [£/kWh]
inc1, inc2, inc3	Incremental cost of the piece-wise linear cost function
IRR	Internal rate of return of investment
ISO	International organisation for standardisation
KB-GA	Knowledge-based genetic algorithm
L	Loan [£]
LFCF	Linear fuel cost function
LGPA	Linear gas path analysis
LHV	Low heat value of the fuel [kJ/kg]
LR	Lagrangian relaxation or Loan interest rate [%]
M	Momentum in axial or tangential direction
m	Stress exponent
m_b	Mass situated above of the cross sectional area
$\dot{m}$	Mass flow [kg/s]
MC	Maintenance cost [£/period]
MCO_2	Emission mass of carbon dioxide [kg/period]
MDT	Minimum down time [h]
MFC	Mass fuel consumption [kg/s]
MOF:min(PC,PHD)	Multi objective function minimise production cost and power and heat deviation
MPO	Maximum power output available
SHBM	Service hours between maintenance [h]
MTBF	Mean time between failure [h]
MUDT	Minimum up and down time [h]
MUT	Minimum up time [h]
N	Total number of operational units or rotational speed [rpm]
NC	Number of cycles
ND	Number of days per mounth

NDMF	Non-dimensional mass flow
NDRS	Non-dimensional rotational speed
NG	Natural gas
nl1, nl2, nl3	No load cost of the piece-wise linear cost function
NLGPA	Non linear gas path analysis
NO_x	Oxides of nitrogen
NPV	Net present value of the investment [£]
O&M	Operation and maintenance cost [£/period]
OD	Off-design
OF:max(UP)	Objective function maximises units' profit
OF:min(PC)	Objective function minimises production cost
OMC	Operation and maintenance cost [£/period]
P	Larson Miller parameter or Total pressure [Pa] or Power output [kW]
p	Static pressure [Pa]
PC	Production cost [£/period]
PD	Power demand [kW]
PDB	Power demand balance [kW]
PF_j	Penalty associated with constraint j
PHLD	Power-Heat linear diagram
P_{ISO}	Electric power at ISO conditions [kW]
PLFCF	Piecewise linear fuel cost function
Pmax	Upper generation limit [kW]
POL	Power output limits
Prf	Profit [£/period]
PR-GA	Parallel repair genetic algorithm
PSR	Power spinning reserve
Q	Heat capacity or activation energy for creep
QFCF	Quadratic fuel cost function
R	Specific gas constant (R=287 J/kgK)
RC	Regenerative Cycle
r_{cg}	Radius between the gravity centre and the centre of rotation

RC	Running cost [£/period]
RET	Recuperator entry temperature [K]
R	Revenue [£/period]
RL	Reduction of the unpaid part of loan at the end of period t [£/period]
RMS	Root mean square
rpm	Revolutions per minute
RRL	Ramp rates limits
RSCL	Reservoir storage capacity limits
RSE	Revenue from surplus excess electricity [£/period]
RV_T	Residual value of the investment at the end of the economic life [£]
SC	Simple cycle
SD	Shut down cost [£]
SED	Static economic dispatch
SGTC	Specific gas turbine cost [£/kW]
SOMC	Specific operation and maintenance costs [£/MWh]
SP	Surplus of power capacity [kW]
SPO	Shaft power output [kW]
SSC	Start-up and shut-down costs
STC	Surplus of thermal capacity [kW]
SU	Start-up cost [£]
T	Absolute total temperature [K], Economic life time of the investment [years], Total number of scheduling periods, Running time spend in each check point or Taxable income [£/period]
t	Static temperature [K]
T(K)	Metal temperature in Kelvin
Tamb	Ambient temperature [K]
TC	Thermal capacity [kW]
TCHPEff	Total CHP efficiency
TD	Thermal demand [kW] or Periods for depreciation [years]
TEff	Thermal efficiency

TEP	Turbine entry pressure [Pa]
TET	Turbine entry temperature [K]
T_f	Total engine running time [h]
TL	Time periods for loan repayment [years]
TMF	Total mass flow [kg/s]
TPL	Transmission Power Losses
TPrf	Total Profit of all N units over the time schedule [£]
t_r	Time to failure (stress rupture time) [h]
TR	Tax rate
T-S	Temperature - Entropy
UAS	Units' availability status (must run and must not run constraint)
UC	Unit commitment
UCDG(T&R)	Unit commitment distributed generation (thermal and renewable)
U_{cg}	blade tangential velocity at the gravity centre [m/s]
UCHTG	Unit commitment hydro-thermal generation
UCTG	Unit commitment thermal generation
UHC	Unburned hydrocarbons
u	Commitment state (0 if unit is offline;1 if unit is online)
v	Velocity [m/s]
Vlt_j	Violation of constraint j
VOMC	Variable operation and maintenance costs [£/MWh]
VS	Variable Speed
W	Air Mass Flow [kg/s]
Y	Distance from the neutral axis to the outer fibre

Greek Symbols

μ_{CO_2}	Emission of carbon dioxide per unit mass of fuel [kg CO_2/kg fuel]
Γ	Non-dimensional flow capacity
$\partial \in/\partial t$	Rate of dislocation creep
ω	Angular velocity
τ	Shear stress
σ_{UTS}	Ultimate tensile strength
$\sigma_{yso.2\%}$	0.2% proof strength
σ	Stress level
η	Efficiency
η_b	Boiler or combustor efficiency
η_e	Electrical efficiency
η_g	Electrical generator efficiency
η_C	Compressor isentropic efficiency
η_T	Turbine isentropic efficiency
η_{th}	Thermal efficiency
μ_j	Penalty multiplier associated with constraint j
α	Nozzle angle
γ_a	Air ratio of specific heat
γ_g	Gas ratio of specific heat
Δ	Change from original value
ΔV	Variation of velocity
Δt	Time interval
ρ	Density [kg/m^3]
ρ_b	Density of the blade alloy
ρ_f	Fuel density [kg/m^3]
φ	Flow coefficient

Subscripts

t	Index of time
C	Compressor
i	Index of units (i = 1 … N) or check points
m	Subscript indicates the months 1, 2, …, 12
t	Index of scheduling period (t = 0 … T)
T	Turbine
1,2,3, etc.	Station numbers
#	Selected parameter
a	Air
g	Exhaust gas
f	Fuel
I	Implanted degradation or Second moment of area
cg	Gravity centre
DP	Design point

Superscripts

–	Relative to design point (DP)

Chapter 1 – Introduction

1 - Introduction

This research addresses the fundamental issues regarding the concept and formulation of an innovative nerve centre for a mini-pool of distributed gas turbine generation units operating in a competitive power market. The concept proposed here is an alternative solution to manage the risks related to distributed generation systems in integrated (embedded) mini-grids, based on an association of generators. The multidisciplinary scope of this investigation includes the performance, diagnostics and life cycle assessment of a portfolio of gas turbines as well as financial optimisation and risk management in different time horizon lengths of distributed heat and power systems operating in a highly competitive market.

Distributed poly-generation (DPG), also called Distributed Energy or Onsite Generation, is a new trend in the generation of heat and electrical power. The DPG concept permits consumers who are generating electricity and/or heat for their own needs to send surplus electrical power back into the power grid, also known as net metering or shared excess, or heat via a heating distribution pipeline.

Distributed poly-generation is receiving greater attention throughout the world. This increased interest is attributed to the development of small scale power generation technologies and deregulation of the power industry which has led to increased competition and interest in the various technologies suitable for distributed power generation, mainly combined heat and power (CHP) systems. Due to its relatively high total energy efficiency, the application of CHP, i.e. the simultaneous exploitation of electricity and heat from the same energy source, is attracting increased attention. Today CHP is an essential element in the energy supply system in many countries and when environmental impact is considered important, CHP is a relevant option in many situations.

Typically the gas turbines used in distributed generation systems are in the medium-small size range because of the requirement of power demand and capacity matching. Despite current and significant benefits and design improvements, little work

has been performed on diagnostics and operational optimisation of power systems in small scale. This investigation aims to provide some comprehensive knowledge of technology behaviour and life cycle investigation. The prediction of possible faults in power systems can have a great impact on the maintenance programme efficiency as they can allow generators to optimise generation schedules and increase profits, mainly when trading electricity in a highly competitive market.

In some power markets, generators optimise the operation of the power plant by assessing the various elements of the cost of running a unit. In complex bidding structure markets, the problem of scheduling the generating units is normally formulated and solved by a centralised independent system operator (ISO), as a unit commitment problem (UC) in which the objective is to minimise the generators' (GENCOs) production costs (Figure 1.1).

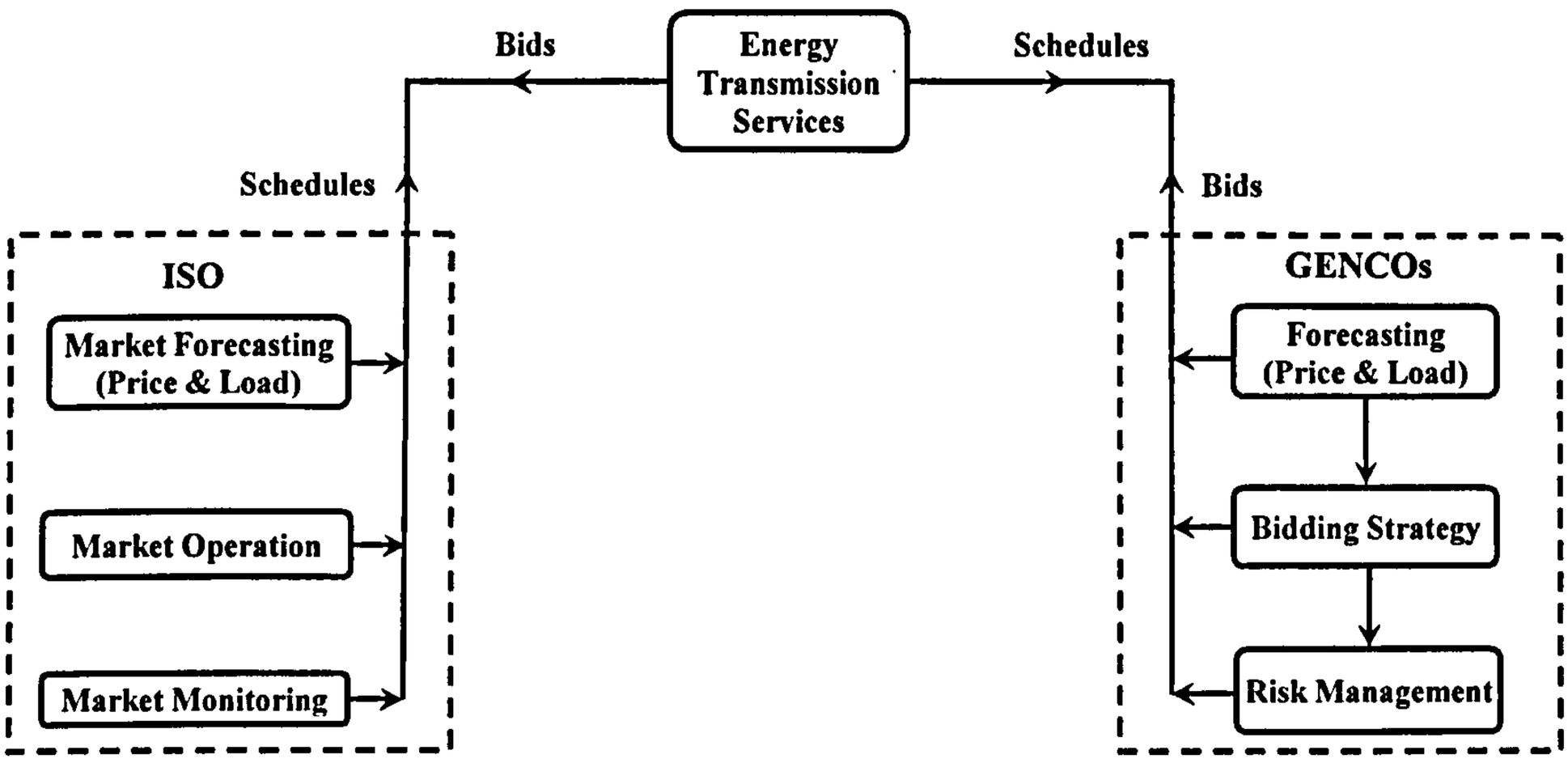

Figure 1.1 – Competitive-based electricity market structure

In a traditional vertically integrated power market, which has been replaced by a new wholesale competitive-based electricity market around the world, each power plant optimises its power scheduling independently of what other plants do. In an open competitive-based market, generators bid into the market in such a way as to maximise their total profit. Participants make offers on the amount of electricity they are willing to trade. These prices are ranked and taken in an increasing order until the balance of

supply and demand is achieved. Based on the offers and bids received, the system operator defines the market marginal price. Consumers pay this market marginal price whereas generators receive this price for every unit of energy trade. In fact the general structure of a competitive electricity market is such that electricity can be traded through a competitive market, bilateral contracts or a combination of both.

The penetration of distributed poly-generation and combined heat and power systems in the power market have been affected mainly by the low price paid for the excess of electricity sold to the grid, high fuel tariffs, and high fees for back-up supplies. The problem of the low revenue achieved by the excess of electricity sold to the network is mainly the consequence of a lack of interest by electric utilities in the surplus of electricity offered by independent power producers. The high fuel cost rate is highly dependent on the international oil price. Both these problems were not addressed in this investigation. However, the high cost of back-up supplies paid by generators is one of the benefits that the innovative nerve centre concept proposed in this study is able to mitigate throughout the optimisation of mini-grid integrated generators.

In order to improve the operation of such systems it is essential to have detailed and reliable optimisation models. The identification of optimisation techniques for power generation is an interesting issue, commonly known as unit or generation scheduling commitment, which was addressed in this research. Many generation scheduling optimisation studies have been reported in the technical literature, mainly for large power plant systems, but none of them has incorporated life cycle constraints or any maintenance management strategy for a mini-pool of distributed generation systems trading electricity in the competitive market.

Such a nerve centre schedules the most profitable operation of the generation units in order to be able to maintain the power plant in a very efficient way as well as quantify the risks involved. This enables an increase of operating profit and good availability by optimising dispatching of power units. Also the nerve centre is able to give financial support for long-term planning of such a mini-pool of units. Therefore short- and long-term contracts with different parties of the power market must be considered (Figure 1.2) which makes the problem more complex and effective risk management is a key issue.

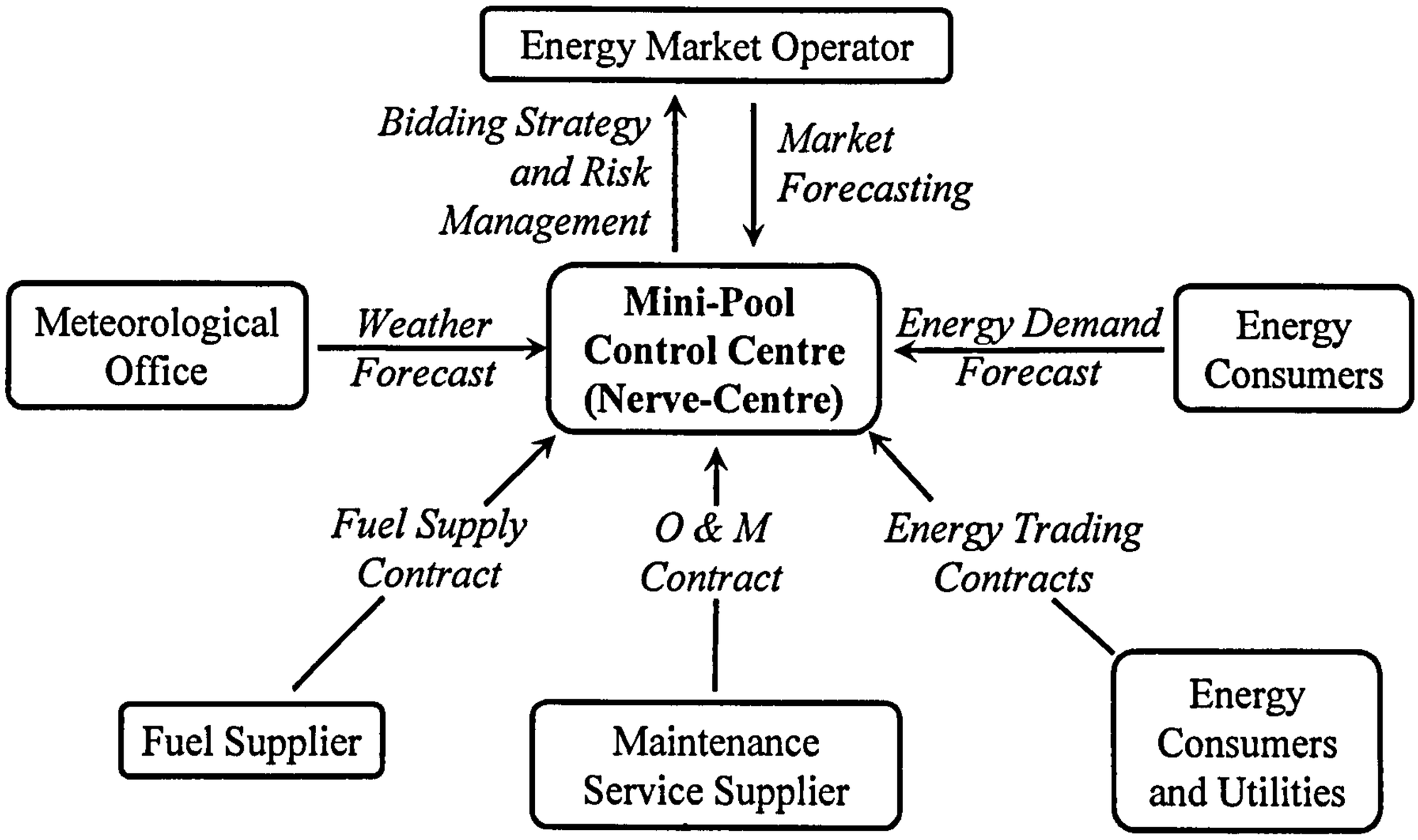

Figure 1.2 – Contractual structure of the nerve centre

The mini-pool control centre (nerve centre) exchanges and processes a large amount of technical, financial and contractual information in order to optimise and evaluate the risks involved (Figuren1.3). The information technology based nerve centre receives ambient condition forecasts from the meteorological office, market index prices, electricity network balance and legislative information from the energy market operator, power and heat demand forecasts from consumers, and others. It also must examine regularly the 'health' condition of the mini-pool power generation units and after further assessment give them appropriate control instructions for setting up generation scheduling and a maintenance strategy. The different modules can communicate with each other and update their status while the control centre processes and posts command instructions to the mini-pool. The author recognises that the development of a fast and robust nerve centre model is a difficult and time consuming project, of which this research can be considered as the first step.

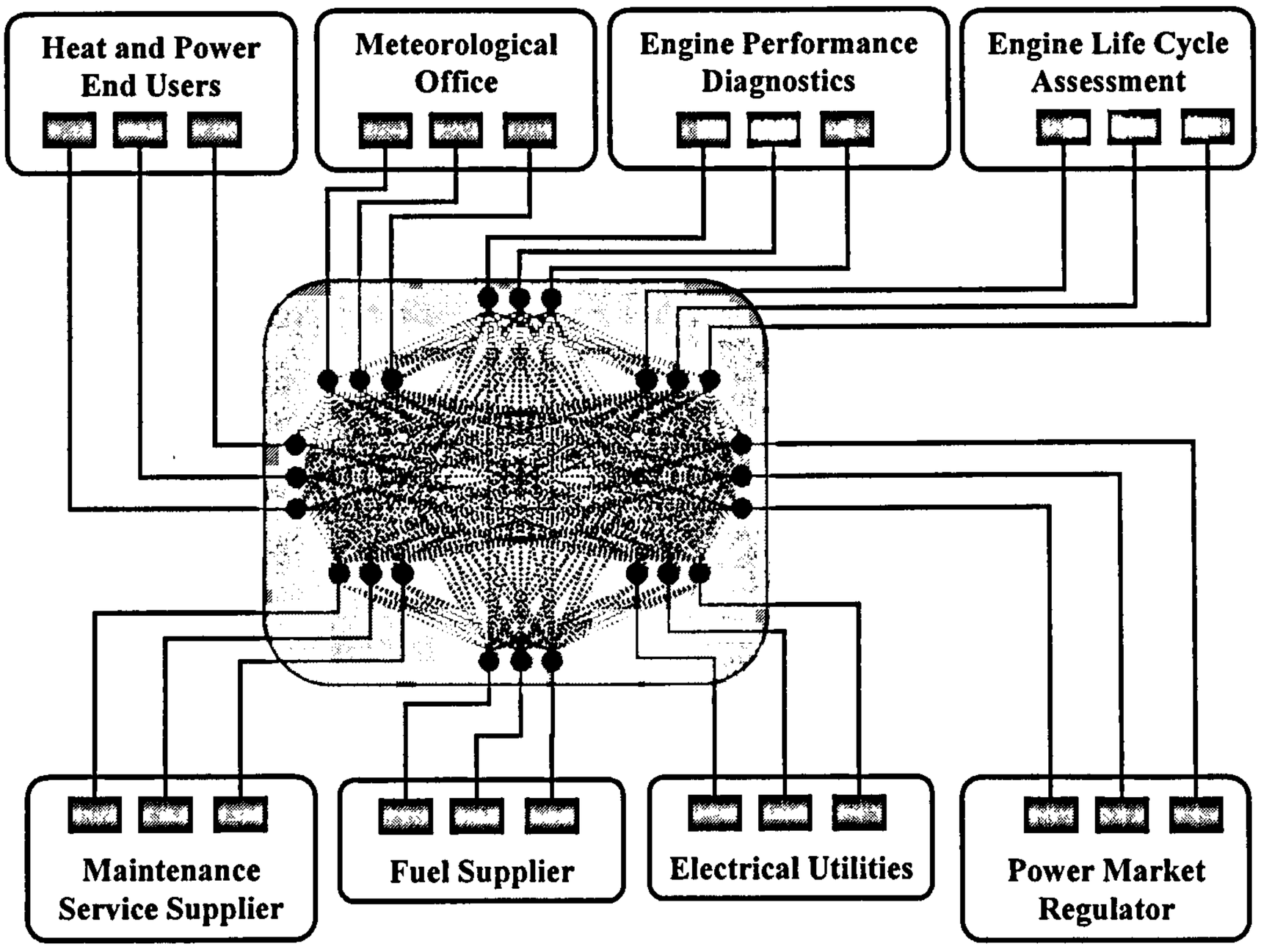

Figure 1.3 – Nerve centre information flow diagram

1.1 - Objectives of research

The main objective of this investigation is to develop the model of work of an innovative information technology based nerve centre for a mini-pool of distributed gas turbine generation plants able to manage the performance operation and risks associated with independent power production in a competitive electricity market. Such a nerve centre must be able to run the mini-pool of power units as profitably as possible while taking into consideration the performance conditions of engines, energy market price volatility, end-users' energy demands, and environmental conditions. This study is a multi-disciplinary operational optimisation problem in different time horizon lengths.

Human activities are becoming increasingly energy demanding and are affecting the environment. A better understanding of the relationship between human activity and energy consumption will aid informed policy and decision making for the mitigation of potential problems and adaptation to changes in market conditions. Detailed information on seasonal energy demand is very useful when evaluating human activities with the environment. An appropriate search in the open technical literature showed that there is a lack of such information in any one source and in sufficient detail. In any power system complex, before making any optimisation analysis,

expansion planning or investment, an evaluation of the energy demand of end-users must be carried out.

An extensive data acquisition has been carried out and presented in this study regarding energy consumption in the following applications over the seasons of the year: a ceramics factory, beverage industries, airport, a shopping centre, a hotel complex and a medium-size island. The data presented in this study are original and make a valuable contribution to the energy and environmental engineering field. Essentially the energy consumption data provided in this study are a reflection of the dynamic processes of human activities and they cover the secondary and tertiary (service) sectors of industry and also the residential segment.

A highly competitive energy market demands reductions in operation and maintenance costs as well as improvements in engine availability and reliability. In order to achieve such profitability and availability the right maintenance strategy needs to be implemented. In this investigation the maintenance strategy will be implemented through diagnosing engine faults, predicting an engine's useful lifetime and scheduling corrective actions.

Typically gas turbines for distributed power generation applications are designed in a simple or regenerative cycle in constant speed, and more recently in variable speed operation. The performance of a portfolio of gas turbines cycles and mechanical configurations were simulated covering the typical range size of distributed generation systems and combined heat and power plants. The 'health' conditions of the portfolio of engines described previously were assessed. The gas turbine health was monitored with an engine performance simulation system obtaining engine measurement information and then the diagnostic investigation was carried out with gas path analysis. Different single and multiple gas path faults were observed and the appropriate sets of sensors were identified to predict the engine's health.

In this investigation the turbine lifetime of gas turbines was estimated over their life cycle. The blade structure of the gas turbine engine is usually under more hostile operating conditions than any other mechanical device. The principal variables that take part in this context are time, temperature and stress loads; they and their combination are the precursors of the blade damage. Then the failure mechanism, stress

calculation and life assessment methods that usually are used in the blade mechanical design were investigated. The principal challenge of this analysis is how to generate a mathematical model able to relate the operation conditions against the blade failure.

Since the health conditions and life cycle of gas turbines can be assessed, a maintenance schedule strategy can be approached and the availability of such engines over their life cycle can be calculated. This is of significant importance when optimising the operation of power generators in markets of high volatility prices and competition.

The nerve centre aims to perform a financial optimisation of the generation units interconnected through a mini-grid and dispatching them at their optimal operating point during a specific period of time. The benefits of the nerve centre can be assessed by comparing the economic performance of such a mini-pool of units with similar individual units operating independently of each other: i.e. single against multi-unit optimisation. The operation of such a system in a consortium of units allows generators to manage the energy balance and profits more efficiently, thereby increasing the low revenue from a surplus of electricity and avoiding the high cost of back-up supplies usually paid by independent power producers set up in the conventional power market.

Traditionally the objective function of such optimisation studies aims to minimise the production costs of generators. However, in a competitive environment, independent generators bid in the market in order to maximise their profit. So, initially in this study each generator is modelled as an independent agent trying to maximise its profit. The disadvantage of such a model is the complexity in modelling units and system constraints and large dimension problems (i.e. systems with multi-units interconnected). A genetic algorithm based model was therefore developed to solve the multi-unit optimisation problem.

Genetic algorithms have been demonstrated to be an effective technique to solve the generation scheduling problems due to their capability in dealing with non-linear problems and ease in handling constraints. This investigation proposes a mechanism to solve the generation scheduling problem with a hybrid genetic algorithm-adapted priority list with heuristic rule crossover which allows the speeding up of the convergence process and obtains satisfactory solutions to the scheduling problem.

Short-, medium- and long-term analyses were carried out depending on the time horizon under consideration. Short-term analysis deals with hourly values from one to twenty-four hours ahead. In this investigation medium-term analysis covers horizons of one year in weekly periods. Long-term financial appraisal was carried out over the economic lifetime of the power systems. Because of the difficulty to accurately predict future events over a long-term horizon, the risk involved was assessed by a probabilistic analysis based on the Monte Carlo technique.

The life cycle assessment mentioned before and a carbon tax cost model were incorporated in the medium-term optimisation algorithm in order to manage the scheduling of units when considering the availability of such engines over their life cycle and the impact of implementing carbon tax in the energy market. Many CHP optimisation studies have been reported in the technical literature but none of them has incorporated such life cycle and environmental constraints in the competitive power market.

The effectiveness of the proposed methodology is illustrated in applications using the portfolio of energy demand consumers in a mini-pool with two, eight and forty gas turbine generation units.

1.2 - Model of Work

The implementation of the methodology proposed in this investigation was carried out through mathematical models and algorithms developed by the author in computational language as described below.

Turbomatch/Pythia: software developed in Cranfield University for the performance and diagnostic analysis of gas turbine cycles. It analyses the design and off-design point performance of gas turbines in different thermodynamic cycles and mechanical configurations. It is also able to evaluate the effects on performance due to compressor and turbine degradation and diagnostic assessment based on linear and non-linear gas path analysis. A computer code was developed by the author for each one of the portfolio of gas turbines evaluated in this investigation.

PowerProfit: software written in Fortran language for financial optmisation in different time horizon lengths of distributed generation systems, including combined

heat and power, operating in a competitive market. It allows users to perform single unit optimisation with dynamic programming methodology, or multi-unit optimisation with a hybrid genetic algorithm-adapted priority list.

GTLifeSpan: Fortran based program for gas turbine life cycle assessment. It is based on performance and structure mechanical resistance of the first row of turbine blades in gas turbines. The algorithm produces as output the availability of engines throughout creep life calculation and maintenance strategy specification.

PRisE (Project Risk Evaluation): program written in Fortran language for integration of risk analysis based on the Monte Carlo technique. For a given range of inputs variation the program produces a randomly Gaussian (normal) distribution for a large number of iterations.

DSPG (Decision Support for Power Generation): software written in Visual Basic language for investment decision support in distributed generation technologies, including combined heat and power with gas turbines trading electricity in both bilateral and competitive power markets. This software allows the user to calculate economic performance indices and to optimise scenarios by using the Monte Carlo risk analysis technique.

PowerScreen: software developed in graphical language LabVIEW™ 7.1 for remote monitoring, data acquisition and performance analysis of gas turbines. This program allows the user to follow component gas path measurements through a user-friendly interface screen and record the history of temperatures, pressures and fuel flow in file formats compatible with the majority of data processors.

GTPowerCycle: integration of the PowerProfit and GTLifeSpan software programs described before but also incorporating a carbon tax cost model and gas turbine maintenance reschedule with an exhaustive enumeration optimisation technique.

1.3 - Literature Review

Over recent years there has been an increasing interest in the condition monitoring assessment of gas-turbine engines and manufacturers are offering embedded health monitoring systems in order to follow the operational health of their engines carefully and take prompt maintenance actions when necessary. Degradation and

diagnostics of gas turbines are important issues, and they have been successfully studied and applied to large size simple cycle one and two shaft (with free turbine) gas turbines (Saravanamuttoo and Mac Isaac, 1983; Escher, 1995; Tarabrin et al., 1998; Ogaji and Singh, 2002). Smaller engines are believed to be more susceptible to degradation and little work has been performed on degradation and diagnostics performance of small sized regenerative stationary gas turbines.

The increasing economic targets in place worldwide have encouraged the research and development of combined management, financial, engineering and other techniques applied to physical assets in optimising economic life cycle costs (operating & maintenance), referred to as terotechnology. Condition management, the combination of condition based maintenance and terotechnology principles, is a powerful strategic tool for total quality management (TQM) and would involve a decision support tool that relies on condition monitoring assessment, service life prediction and economic dispatch of generation power systems.

The economic dispatch problem concerns the financial generation optimisation of power plants in service. It is regarding as the strategic choice to be made in order to determine which of the available power plants should be considered to supply energy, subject to a certain number of units and system constraints. The classical economic dispatch problem (Wood and Wollenberg, 1996) has been investigated in at least two different applications: economic dispatch of power systems only (power plants producing electricity power only) and economic dispatch of combined heat and power (CHP) or cogeneration plants (those producing electricity and heat simultaneously). The economic dispatch of power systems only is known in the technical literature as unit commitment or generation schedule problem, further abbreviated as UC or GS respectively. The economic dispatch of cogeneration systems is known as the combined heat and power economic dispatch (CHPED) problem.

CHPED is treated in the literature as a static economic dispatch problem. That simplifies the mathematical model, as the problem is not dependent on time-constraint parameters. UC is a dynamic economic dispatch problem solved during a period of time. The problem is divided into time intervals and some of the constraints are time

dependent which makes the problem more complex to solve than the static economic dispatch.

Most of the economic dispatch studies reported in the literature refer to large capacity centralised units (hydro and/or thermal or CHP plants). That means the problem is applicable to central power stations such as natural gas combined cycle, coal/fuel oil steam cycle, nuclear power plants and hydroelectric power stations, with total electric power capacity higher than 40MW and interconnected to the national transmission network. Only a few studies refer to the economic dispatch of distributed generation systems. Bakirtzis and Dokopoulos, 1988, and Contaxis and Kabouris, 1991 analysed the generation scheduling problem of distributed generation or autonomous energy system with a mix of power technologic portfolios: diesel generators, wind turbine and photovoltaic panels. The algorithm developed was applied to the isolated power system of a Greek island. Therefore the system is not interconnected with the national network and the model developed does not considerer trading surplus or deficit of electricity. Givanildo, 2005, investigated the impact of integrating wind power into a hydrothermal generation centralised network. The wind and hydro data bases are characterised by stochastic models and the mixed portfolio of wind-hydrothermal generation is approached with a system dynamics technique. The model developed is simulated with real data from the power market of the north-east of Brazil. Combined heat and power systems and competitive power market characteristic were not incorporated into the model.

The UC decision process decides whether units must be on or off in order to optimise the objective function following a list of constraints. Between these constraints the most common in thermal power system are: power output limits (POLs), power demand balance (PDB), minimum up/down time (MUDT) and power spinning reserve (PSR). In addition, some studies also take into account units' availability status (UAS) (must run/not run constraint), transmission power losses (TPLs), environmental constraints (ECs), units' initial conditions (ICs), ramp rate limits (RRLs) and hydraulic constraints (HCs). Traditionally the objective function is to minimise the production costs grouped into the following categories: fuel cost, maintenance cost, startup and shutdown costs. Fuel costs are modelled by a quadratic polynomial function, a piecewise constant function, or a piecewise linear function. Maintenance costs depend

on the base (fixed) and incremental (variable depending on the electricity produced) components. The startup cost is divided into cold and warm startup, and shutdown used to be constant over time.

The large changes the electrical power-supply industry has been passing through since the mid-1980s has led to privatisation, restructuring, and deregulation of the power sectors as a consequence of the increasing need for more efficiency in power production and delivery. This has also created many opportunities to research and develop projects focused on the modifications or replacement of traditional procedures to attend to the requirements of the modern power industry. In a restructured or deregulated power market, generators submit their bids to the market regulator which implements a power action to supply the forecasted demand. The traditional cost minimisation UC model used to optimise the economic dispatch of power plants can lead to suboptimal solutions and therefore its applicability in competitive power markets has been questioned (MacGregor and Puttgen, 1994; Sen and Kothari, 1998). As a result, a profit based UC problem has been formulated and solved by considering the volatility of competitive electricity market prices and allocating fixed and variable costs to the schedule period (Richter and Sheblé, 2000; Mendes, 1999).

In the CHPED problem there is a dependency between the heat production capacity and the electricity power generated. The multiple-demand and heat-power capacity dependency constraints of the CHP systems introduce an additional complication in the economic dispatch. In this type of analysis, production cost is modelled as a quadratic cost function depending on the power and heat output. A power and heat coupling-term constraint (power-heat linear diagram) is used to set minimum and maximum power and heat capacity. The objective function is to minimise production cost subjected to system constraints (power and heat balances) and units' constraints (power and heat capacity limits). No time dependent constraints are considered as part of the mathematical model. Despite all of the benefits of CHP systems, little work has been conducted in the combined heat and power economic dispatch (Table 1.1).

Different techniques have been developed to find the optimal solution of economic dispatch problems, such as exhaustive enumeration, priority list, dynamic

programming, Lagrangian relaxation, integer and linear programming, genetic algorithms, neural networks, expert and fuzzy systems, and others. In some studies a hybrid algorithm is developed which includes a mix of two or three different techniques.

Dynamic programming is used extensively to solve many optimisation problems throughout the world. Bakirtzis and Dokopoulos, 1988 developed a dynamic programming algorithm to solve the unit commitment problem and optimise the design of a distributed generation system with a mix of power technologic portfolios: diesel generators, wind turbine and photovoltaic panels. Contaxis and Kabouris, 1991 presented a hybrid dynamic programming priority list algorithm to solve the UC problem integrated with a probabilistic wind speed and demand load forecast model.

Many Lagrangian Relaxation (LR) based algorithms have been proposed to solve the UC problem in large size power systems. Some utilities have being using this technique regularly (Padhy, 2004). Wang et al., 1995, proposed an augmented Lagrangian relaxation for the short term generation scheduling problem of large size centralised power systems with transmission and environmental constraints. Guo et al., 1996 present a decomposed algorithm to solve the CHP static economic dispatch. The problem is modelled as a two-layer procedure: the heat and the power dispatch. The outer layer (power dispatch) is solved iteratively with the Lagrangian Relaxation technique. The inner layer solves the heat dispatch problem using the gradient searching method. The two sub-problems are connected by the heat-power feasibility constraints of CHP units.

Rooijers and Amerongen, 1994, proposed an iterative dual programming procedure to solve the CHP static economic dispatch. The algorithm uses a two level strategy solution. For a given power and heat output (lambda system) the lower level solves the economic dispatch problem, then the upper level updates the lambda's sensitivity coefficients. An iterative process is used to repeat the algorithm until the heat and power demand are fulfilled. Convergence of the optimal solution is guaranteed only if the objective cost function and/or feasible power-heat linear diagram are convex, otherwise a duality gap problem will occur similar to the Lagrange relaxation based technique.

In the last 30 years there has been an increasing interest in evolution and machine learning techniques, such as the genetic algorithms evolution based systems proposed by Holland, 1975 and reviewed and enhanced by Goldberg, 1989. In the power generation field, genetic algorithm (GA) has been employed successfully to solve the generation schedule problem (Sood et al., 2003). Kazarlis et al., 1996, deal with the UC problem using a GA with a varying quality function technique and problem specific operators. Maifeld and Sheblé, 1996, proposed a scheduling algorithm using a genetic algorithm with domain-specific mutation operators. Orero and Irving, 1998, presented a multiple step genetic algorithm to determine the optimal hourly generation schedule of a hydro thermal power system. Chang and Fu, 1998, introduced a multi-objective method by using a fuzzy decision index and the genetic algorithm, and Song and Xuan, 1998, incorporated an improved penalty function formulation in the GA to solve the static economic generation of CHP systems. Richter and Sheblé, 2000, applied the GA approach to a profit based UC problem for competitive markets. Sudhakaran and Slochanal, 2003, addressed the problem of CHP economic dispatch using a hybrid genetic algorithm tabu search procedure. The optimal solution search is divided into two steps: a simple GA to identify the optimal region solution and a tabu search technique to refine the solution with a fine tune local search. Su and Chiang, 2004, deal with the CHP economic dispatch problem through an integrated genetic algorithm with multiplier updating, allowing automatic adjustment of the random penalty function. Srinivasan and Chazelas, 2004 introduced a evolutionary algorithm procedure with genetic operators to solve the UC problem.

Table 1.1 summarises the most relevant studies on economic dispatch of power stations and CHP systems.

Table 1.1 – Economic dispatch problem for power plants

Reference	Economic Dispatch Model	Unit and System Constraints	Optim. Technique
Bakirtzis and Dokopoulos, 1988	UCDG(T&R) LFCF, SSC, DED, OF:min(PC)	POL, MUDT, PDB, UAS, PSR	DP
Contaxis and Kabouris, 1991	UCDG(T&R) PLFCF, SSC, DED, OF:min(PC)	POL, MUDT, PDB, UAS, PSR	DP-PL
Rooijers and Amerongen, 1994	CHPED, QFCF, SED, OF:min(PC)	POL, HCL, PHLD, PDB, HDB	DuP
Wang et al., 1995	UCTG, QFCF, SSC, DED, OF:min(PC)	POL, MUDT, PDB, PSR, TPL, EC	LR
Kazarlis et al., 1996	UCTG, PLFCF, SSC, DED, OF:min(PC)	POL, MUDT, PDB, IC	GA
Guo et al., 1996	CHPED, QFCF, SED, OF:min(PC)	POL, HCL, PHLD, PDB, HDB	LR
Orero and Irving, 1998	UCHTG, QFCF, DED, OF:min(PC)	POL, PDB, HC	GA
Song and Xuan, 1998	CHPED, QFCF, SED, OF:min(PC)	POL, HCL, PHLD, PDB, HDB	GA
Chang and Fu, 1998	CHPED, QFCF, SED, MOF:min(PC,PHD)	POL, HCL, PHLD, PDB, HDB, TPL	FDI-GA
Richter and Sheblé, 2000	UCTG, QFCF, SSC, DED, OF:max(UP)	POL, MUDT, RRL, PDB, PSR	GA
Aldridge et al., 2001	UCTG, PLFCF, SSC, DED, OF:min(PC)	POL, MUDT, RRL, PDB, PSR, TPL, IC	KB-GA
Arroyo and Conejo, 2002	UCTG, PLFCF, SSC, DED, OF:min(PC)	POL, MUDT, RRL, PDB, PSR	PR-GA
Sudhakaran and Slochanal, 2003	CHPED, QFCF, SED, OF:min(PC)	POL, HCL, PHLD, PDB, HDB	GA-TS
Gil et al., 2003	UCHTG, QFCF, DED, OF:min(PC)	POL, MUDT, PDB, HC, RSCL, PSR	GA
Su and Chiang, 2004	CHPED, QFCF, SED, OF:min(PC)	POL, HCL, PHLD, PDB, HDB	GA-MU
Srinivasan and Chazelas, 2004	UCTG, QFCF, SSC, DED, OF:min(PC)	POL, MUDT, PSR, PDB	EA-PL

1.4 - Contributions

The main author contributions are described below:

- This investigation presents real and detailed demand data collected from a portfolio of energy consumers' facilities. The energy demand patterns and the factors that influenced them were reported. The energy consumption information provided is useful for the elaboration of preliminary energy studies of heat and power demanding facilities. However, the information reported was not found in the technical literature in one source or in sufficient detail. Contributions were published in Gomes et al., 2004 and Gomes et al., 2007.

- A life cycle assessment for stationary gas turbines is presented and published in Gomes and Pilidis, 2007. The algorithm developed uses a time temperature parametric technique to evaluate long term creep life damage and incorporates a probabilistic Monte Carlo risk analysis. No research publication that combines these two techniques for gas turbine power generation systems was found to be available in the open literature.

- A new concept of a mini-pool of distributed generation units (named nerve centre) is introduced. The nerve centre economically optimises the generation schedule (GS) of gas turbine power plants interconnected through a mini-grid. Many GS studies have been reported in the technical literature, mainly for large scale centralised generation (Table 1.1). The few publications available regarding the GS of distributed generators (Bakirtzis and Dokopoulos, 1988; Contaxis and Kabouris, 1991) were not modelled as interconnected to the local network and do not consider trading electricity (surplus/deficit) in the competitive market as has been modelled in this work. The optimisation procedure developed is a Hybrid Genetic Algorithm Adapted Priority List (GA-APL) technique. The nerve centre concept is modelled in this investigation as a Multi-unit Optimisation (MUO) problem. It is not the main purpose of this investigation to present a genetic algorithm-based model against the state-of-the-art techniques to solve the

GS problem of power systems. However, one of the aims of this research is to demonstrate the advantages of such a nerve centre. In order to achieve this target the MUO economic performance is compared with two different approaches of DG: Conventional Case (CC) and Single Unit Optimisation (SUO). It is then applied to short-term GT DG generation schedule and medium-term GT CHP dynamic economic dispatch integrating the life cycle assessment mentioned before. The author did not find in the open literature any publication that approaches the generation scheduling of distributed generation systems as has been developed in this work. The contributions of this research were published in Gomes et al., 2007.

- A decision making support tool (DST) for Combined Heat and Power (CHP) schemes based on gas turbines was developed. The algorithm evaluates the economic performance of long-term investments in CHP systems. Many economic analyses of CHP systems reported in the literature are limited to a fixed interest rate discounted cash flow technique and sensitivity analysis (Gomes et al., 2003; Papamarcou, 2001). The DST developed in this research considers variable interest rates, highly volatile fuel tariffs and electricity rates over the economic life of the investment and performs an iterative risk evaluation based on a Monte Carlo risk analysis.

- The economic analyses carried out in this research (short- and medium-term generation scheduling and discounted cash flow technique) were based on gas turbine off-design performance. Compressor and turbine performance maps and the derating effects due to ambient conditions variation were taken into consideration. Although this makes the problem more complex to solve, it is nonetheless a particular contribution as most of the publications on financial appraisal of gas turbine power systems use design point performance.

- An experimental analysis was carried out with three different small gas turbines. Performance and emission levels were reported for engines fuelled with natural gas, diesel and kerosene. Contributions were published in Gomes et al., 2004.

- This research also studies the degradation performance effects and diagnostics of small gas turbines' constant and variable speed operation in simple and regenerative cycles (Gomes et al., 2006) on which subject there was found to be a lack of references in the public domain.

1.5 - Outline of the thesis

Chapter 1 is an introduction to this study. It describes the objectives and contributions of this research, and provides a review of the technical literature in this subject.

Chapter 2 presents an energy demand assessment for a portfolio of energy consumers in different industrial processes and tertiary services. Different gas turbines models were selected to supply the energy demand of each energy consumer facility assessed. The data collected and simulated in every period of time under consideration are displayed in Appendix A.

Chapter 3 presents a study on degradation performance effects and diagnostics of small gas turbines for power generation. Simple and regenerative cycles operating at constant and variable speed are analysed. The effects of the degradation in the compressor, turbine and recuperator on the performance of the engines are investigated. Diagnostics investigation is also carried out to obtain optimal instrumentation sets for degradation faults. Charts and tables with the results are available in Appendix B.

Chapter 4 provides an evaluation of the gas turbine lifetime during its operation over a life cycle and evaluates the risk involved in such assessment. A mathematical model is developed to calculate the principal variables that take part in life cycle assessment: time, temperature and stress loads. A Monte Carlo probabilistic risk analysis is carried out to properly evaluate the uncertainty involved.

Chapter 5 presents an experimental performance assessment and emission levels of two micro gas turbines fuelled by natural gas and diesel and a ground power unit (GPU) fuelled by kerosene.

Chapter 6 introduces a mini-pool of distributed generation units (named nerve centre) able to economically optimise the generation schedule of gas turbine power plants interconnected through a mini-grid in a short-term horizon. A hybrid genetic

algorithm adapted priority list technique is developed to solve the multi unit generation schedule optimisation problem. A case study with 8-units is presented. Appendix C displays charts and tables with results.

Chapter 7 displays an application of the optmisation algorithm described in chapter 6 to the GT CHP system, integrated with the life cycle assessment described in chapter 4 in a medium-term time interval. A maintenance reschedule algorithm is presented and the effects of carbon emission taxes on CHP systems are evaluated.

Chapter 8 describes an investment long-term decision making procedure for Combined Heat and Power (CHP) systems. The method is based on the variable discounted cash flow technique and Monte Carlo risk analysis. A case study for a portfolio of energy demand users is available.

Chapter 9 presents the final comments of this research and describes some suggestions for future research.

Finally all the references quoted in the text are listed in the Bibliography and References section.

Chapter 2 – Energy Demand Analysis

2 - Energy Demand Analysis

2.1 - Introduction

Combined heat and power (CHP) is recognised as an established efficient and environmentally friendly technology suitable for the local generation and provision of thermal and electrical energy requirements. The process of selecting a particular CHP generation unit requires understanding the main parameters of the consumer facility, such as electricity and heat load, process temperature, load factor (hours of operation per year) and others. When selecting a prime mover for a CHP plant a power or heat match must be selected. Ideally, the heat and power requirements would be at the same match point for a particular CHP plant, but this is almost never the case.

A decision must then be taken whether to have a deficit of heat or excess of electricity if the power-heat ratio of the CHP system is greater than the consumer, or have a deficit of electricity and excess of heat if the power-heat ratio if the consumer facility plant is greater than the CHP system (Figure 2.1). An energy demand assessment for a portfolio of energy consumers was therefore carried out.

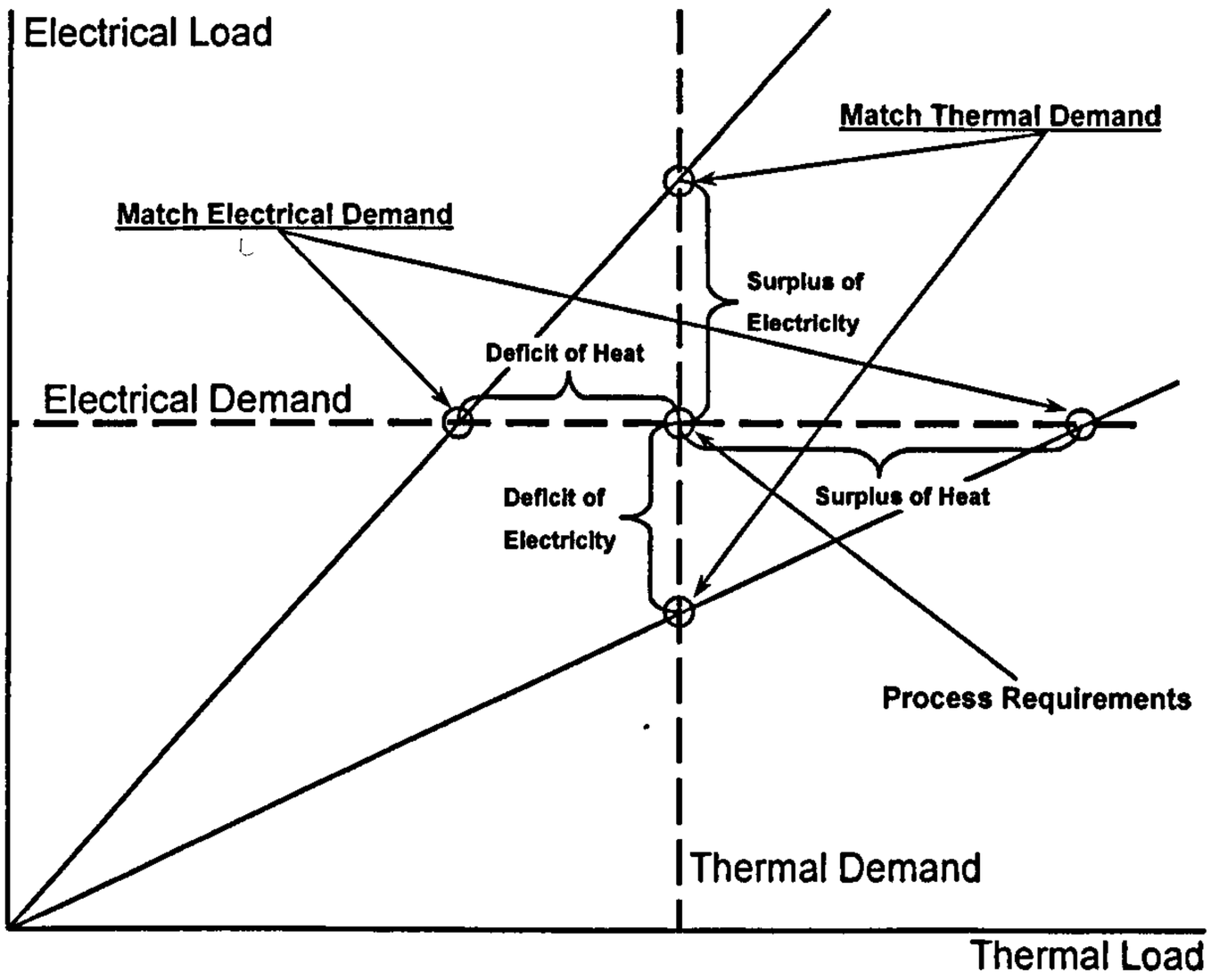

Figure 2.1 – Matching between CHP plant and consumer energy demand

The next section describes how the data acquisition was carried out. The analysis of the results of each of the facilities investigated is presented in section 2.3, and the heat and power demand profiles are presented in section 2.4. The database with all the information collected in the field and the off-design performance of the portfolio of gas turbine based CHP simulated is available in Appendix A.

2.2 - Energy demand survey

At the beginning of an energy demand assessment it is important to identify the types of energy used and where they have been used in the consumer's facilities. Once this has been understood the methodology must be chosen to quantify the amount of energy used.

Energy demand survey is a technical investigation of the control and flow of energy in a site over a given period, usually a year, with the aim of identifying cost-effective energy saving measures. The energy demand data acquisition can be conducted on a complex of buildings, entire process plants, individual manufacturing units, utility systems or even specific individual equipments. Usually it includes an examination of the energy conversion equipments, energy distribution systems, end users and possible management systems.

There is an increasing need for cost-effective energy conservation and increased energy productivity nowadays which can be implemented through energy-management procedures and equipments development. Energy consumption data provide valuable information to energy conservation studies as they can be used to improve energy productivity.

This analysis explicitly reveals the opportunities for reducing energy purchased, which also have the benefit of reducing detrimental environmental impact. Often during an energy survey, inefficient practices of energy utilisation are revealed. Demand side management practices can also be implemented by using the information obtained from energy demand acquisition, as they may reveal opportunities to improve load factors and thereby cut off the peak-demand element of energy charges.

Consumption data forecasts are needed for the expected lifespan of the potential CHP plant. If demands are forecast to change in the future, then data for each

year should be provided wherever possible. The greater the level of detail provided at this stage, the greater the potential accuracy of the subsequent financial evaluation. Economic viability is highly dependent on the demand for heat and power, as well as the price of electricity and fuel. Detailed energy demand profiles for both heat and electricity are fundamental to the appropriate design of CHP plants.

The main steps involved in raising energy demand profiles are summarised below:

- Become familiar with the site, the process involved and future plans;
- Understand how energy sources are currently managed;
- Gather knowledge about the main services facilities;
- Collect energy flow data consumed over the last year on a periodical base.

It is important to ensure that energy is used as efficiently as possible, eliminating energy wastage and improving the efficiency of energy consumption. The energy demand data need to be subdivided to a certain level. For heat use, the demand must be subdivided according to the different heat load temperatures. For the purposes of this study, it is sufficient to consider site consumption on both an annual and daily basis. The daily data were collected over a summer season and split into low, average and high production levels, and for industrial consumers. While this approach inevitably requires a certain amount of averaging, it should provide a sufficient degree of accuracy at this stage of the evaluation process.

Once a decision has been taken on the appropriate number of time periods, the electricity and heat demand data must be assessed and recorded in such a way that they can be readily used to calculate the potential energy cost savings. The site energy supply data required include:

- The number of hours of the year allocated to each time period. This should total 8760 hours, thereby representing demand over a full year.
- The average site electricity demand in kW for each time period.

- The average site heat demand in kW for each time period. The data should represent the heat supplied by the existing plant and equipment, and should include any distribution system losses.

Energy demand curves show the patterns of energy usage over specified time periods. In some instances, the local electricity supplier may be able to provide a load profile for a specific period of time. Where this is not an option, electrical current flows can be measured using non-intrusive clamp-on meters linked to a data logger. Careful interpretation is necessary to account for production and non-production periods and variations in production levels.

In order to evaluate heat loads it is necessary to carry out an investigation of heat users, including the type and grade of heat used in each case, and to combine this with hourly or half-hourly readings of boiler fuel or steam/heat meters over a period of time. Heat usage must be split into grades according to the temperature of use and separate profiles constructed for each grade.

2.3 - Analysis and discussion of results

In this study a database was created for a portfolio of different consumer facilities: a ceramics industrial park, two beverage industrial sites and a shopping centre located in the Brazilian northeast and southeast region (Gomes et al., 2004); an international airport, a hotel building complex, a island and a resort hotel located in Greece (Polizakis, 2007). These data were statistically processed and a parametric analysis is presented in the next sections. Detailed data are given in Appendix A.

2.4 - Ceramics Industrial Park

Electricity represents a significant manufacturing cost in ceramics processing and changes in the cost of energy have an immediate impact on profit. The main electrical energy users in ceramics processing are heaters, electrical motors and drives, and lighting systems.

Ceramics are defined as a class of inorganic, non-metallic solids that are subject to high temperature in manufacture and/or use. Generally high temperatures are part of ceramics processing and heat resistant or refractory materials are the main

product. The ceramics industry analysed in this approach is basically focused on the production of pottery and porcelain. The basic steps in the process for ceramic products manufacturing include raw material procurement, beneficiation, mixing, forming, drying, presinter thermal processing, glazing, firing, final processing and packaging. The rate of drying is controlled by temperature, relative humidity and airflow. These parameters largely determine the size of the dryer and technology used. A major factor in energy consumption is the volume of air used. Dryers do not function without adequate air and, if the airflow is too low, then temperature and humidity will not be distributed evenly. Dry powders often are granulated to improve flow, mixed directly with a binder solution and injected into a spray drying system. In spray drying, the ceramic powder in the form of slurry is atomised by means of a pressure nozzle or rotary atomiser and sprayed towards the top of the drying chamber. A descending stream of heated air flowing counter current to the spray dries the slurry as dense, homogeneous, spherical granules, which are collected at the base of the dryer (U.S. Environmental Protection Agency, 1996).

The potential application for energy savings in the ceramics industry is in the drying process. Spray dryers generally are gas-fired and have a potential heat demand which is ideal for combined heat and power applications (Figure 2.2 and Table 2.1).

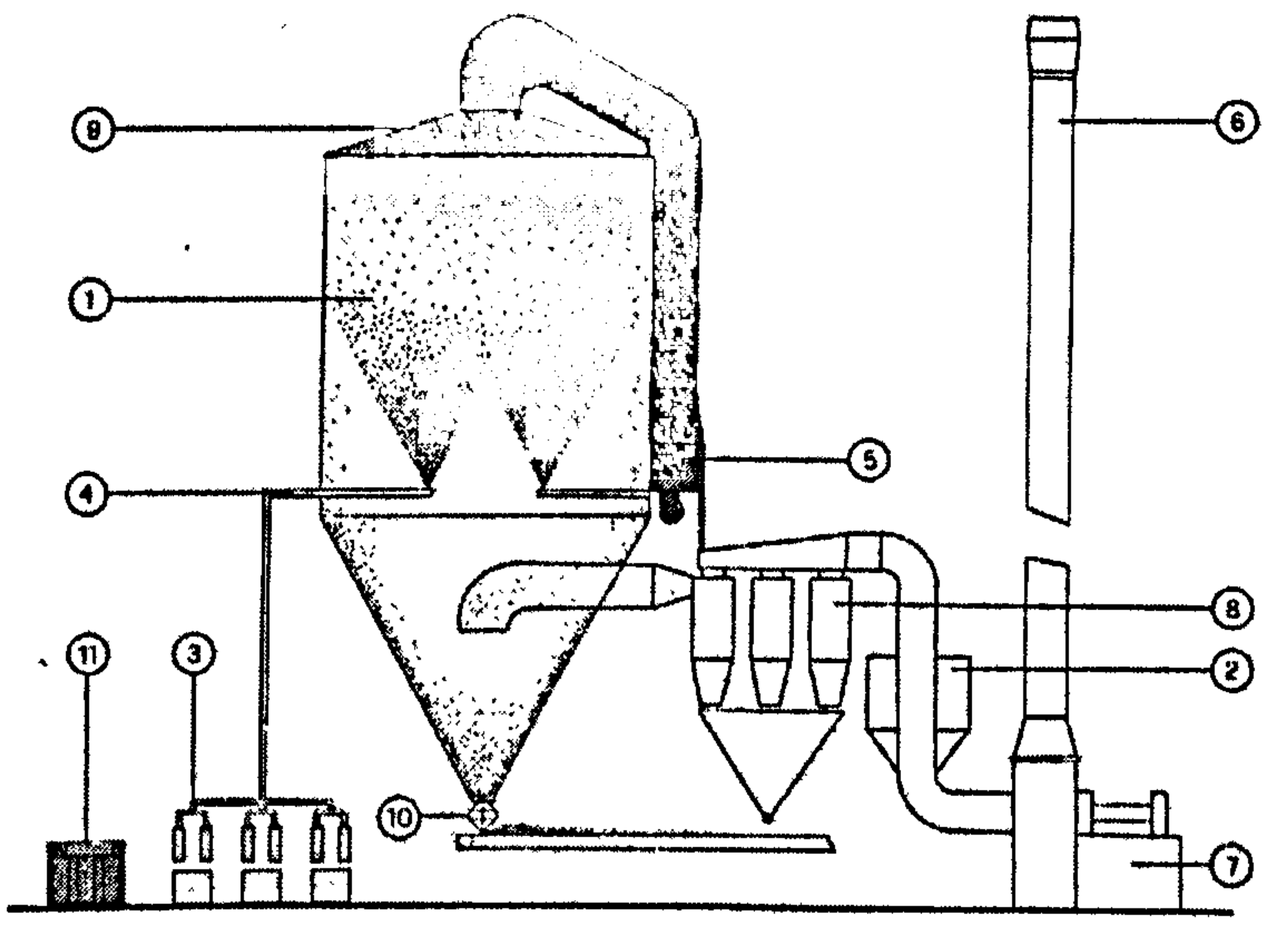

1	Dry tower
2	Scrubber
3	Pumps
4	Injectors
5	Combustor Chamber
6	Smoke stack
7	Centrifugal fan
8	Cyclone fiters
9	Diffuser
10	Discharge valve

Figure 2.2 - Spray dryer operation scheme

Table 2.1 - Technical characteristics of each spray dryer

Thermal power	MW	5.23
Maximum water evaporation rate	l H_2O/h	3,823
Specific thermal consumption	kJ / m^3 H_2O	4,925
Entry gas temperature	°C	400 - 600
Exhaust gas temperature	°C	80 - 100
Inlet relative humidity	%	32
Minimum outlet relative humidity	%	6
Dry tower pressure drop	Pa	196
Maximum gas flow	m^3/h	35,000
Maximum gas pressure	Pa	1,765
Nominal natural gas consumption	m^3/h	962,6
Natural Gas density	kg/m^3	0.7599
Natural Gas Low Heat Value	kJ/m^3	35,588

The ceramics industrial park investigated is located on the Northeast Brazilian coast and is divided into four sites. Table 2.2 shows the annual average consumption of power and heat during peak times (3 hours from 18:00h to 21:00h) and off-peak times (21 hours from 21:00h to 18:00h). The factory on site 1 is the oldest of the four and has a higher demand of power as a consequence of its higher production. Peak contracted power demand usually is lower than off-peak as a cost-saving measure. Manufacturers used to schedule lower production at peak times since peak electricity tariffs are more expensive. The factory on site 2 may have a potential saving on power if peak demand can be optimised. However further analysis is necessary. The spray dryer described above is located in site 1 and it supplies the other sites with pre-processed material.

Table 2.2 – Annual energy consumption of the ceramics industrial park

	Site#1		Site#2		Site#3		Site#4	
Electricity Demand	**Peak**	**Off-Peak**	**Peak**	**Off-Peak**	**Peak**	**Off-Peak**	**Peak**	**Off-Peak**
Contracted Power Demand [kW]	1,000	1,600	500	500	500	600	500	800
Electricity Consumed [MWh/year]	643	10,311	384	3,966	317	2,646	368	4,868
Thermal Demand								
Heat Demand	5,229 [kW]							
Annual Consumption	10,121 [MWh]							

The production data of the units on site 1, 3 and 4 are available in Appendix A. Figure 2.3 shows the variation of square metres produced over the year for units on sites 1 and 4. Production does not present a large variation over the year in the factory on site 1. Production from the factory on site 4 has fluctuated in the first two quarters of the year and then closed the year in a stable position. Lower production in June can be a consequence of low product sales, factory maintenance or a combination of both.

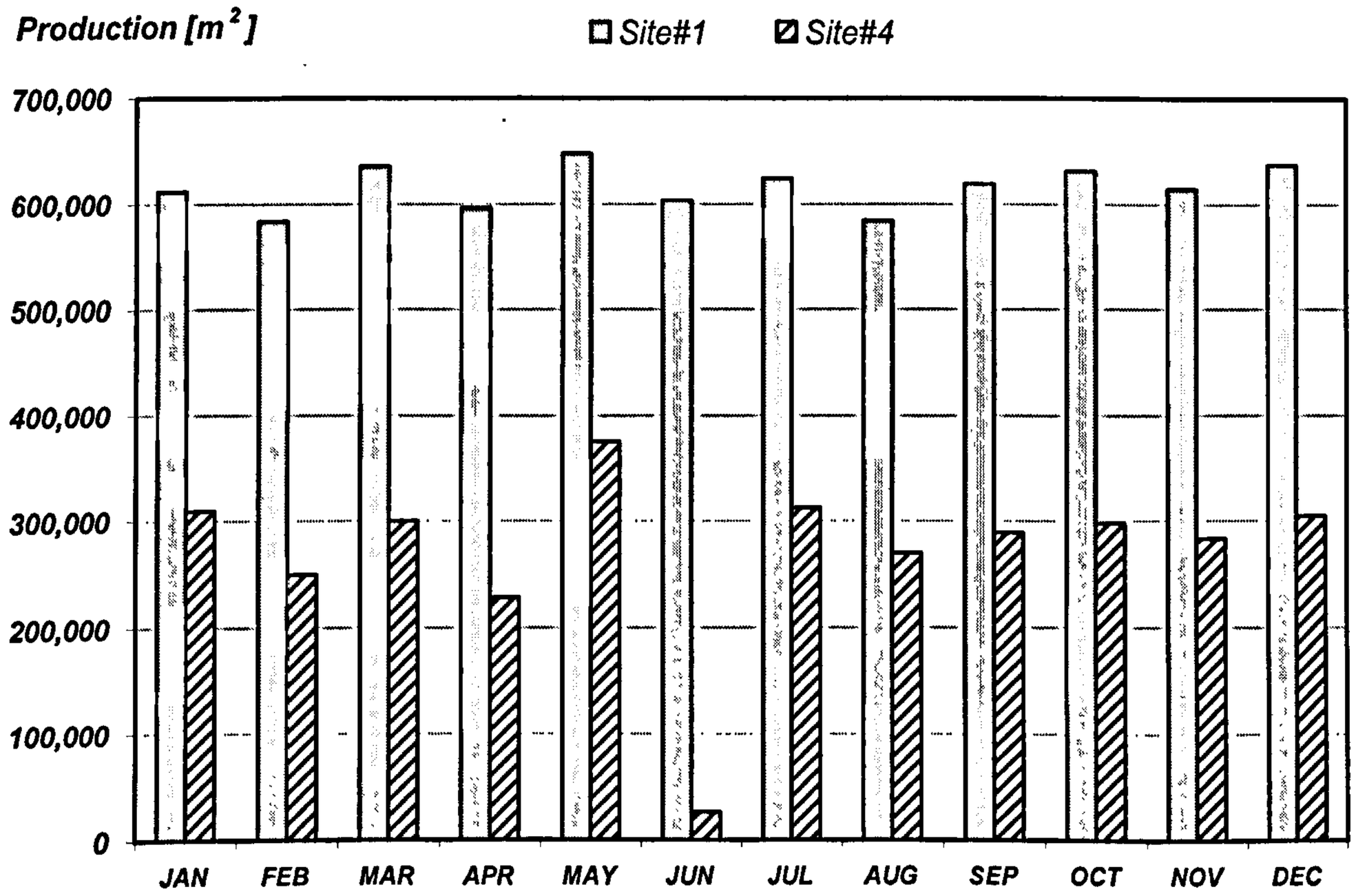

Figure 2.3 – Monthly production of the ceramics industrial park

Figure 2.4 shows the variation of electricity and heat consumption of the facilities investigated depending on their annual production. In this chart an average area of 0.25 m^2/unit produced is assumed. Electricity consumption is more related to the production capacity of the factory, mainly for production at a level higher than one million a month, as the factories used to operate at, or close to, full capacity most of the time. The heat demand is plotted against total ceramics industrial park production. Despite the production of the factory on site 2 not being available, this does not affect the total production significantly as it is the smallest facility of the four.

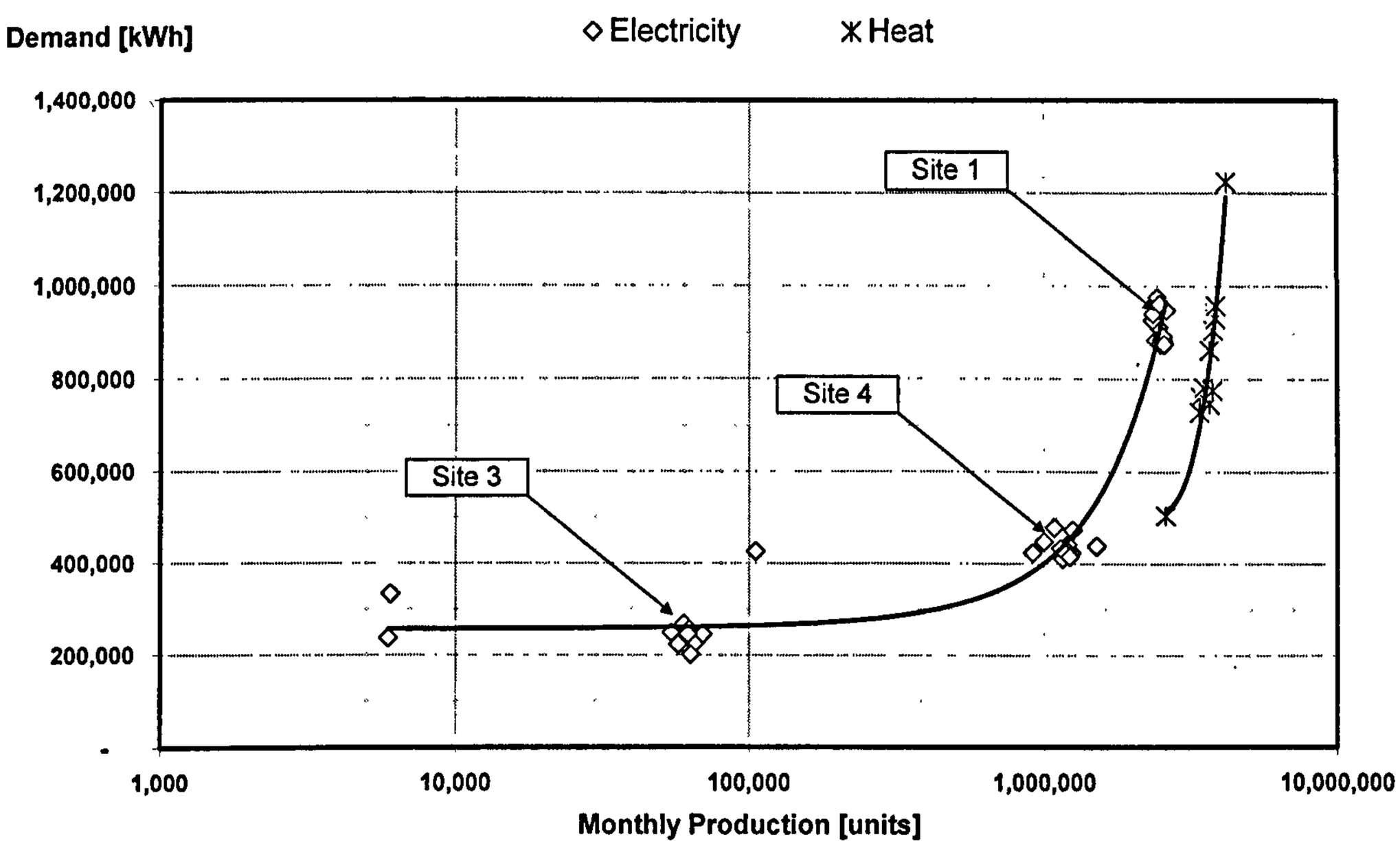

Figure 2.4 – Relation between energy consumption and factory production of the ceramics industries

The demand factor (DF) is an index that allows evaluating the relative variation of electricity used in the premises to be analysed. It is defined as the ratio between the average power demand over a specific time interval and the maximum demand recorded over that period. The average power demand is usually integrated over a specified time interval:

$$DF = \frac{\int_{\Delta t} PD(t)\,dt}{\Delta t \cdot \max(PD(t), \Delta t)}$$

Where PD is the power demand and Δt is the time interval. Figures 2.5 and 2.6 show the demand factor of the site investigated during off peak and peak hours, respectively. The factory on site 3 presents a lower demand factor over the year which means a higher variation on the power demand profile over the year.

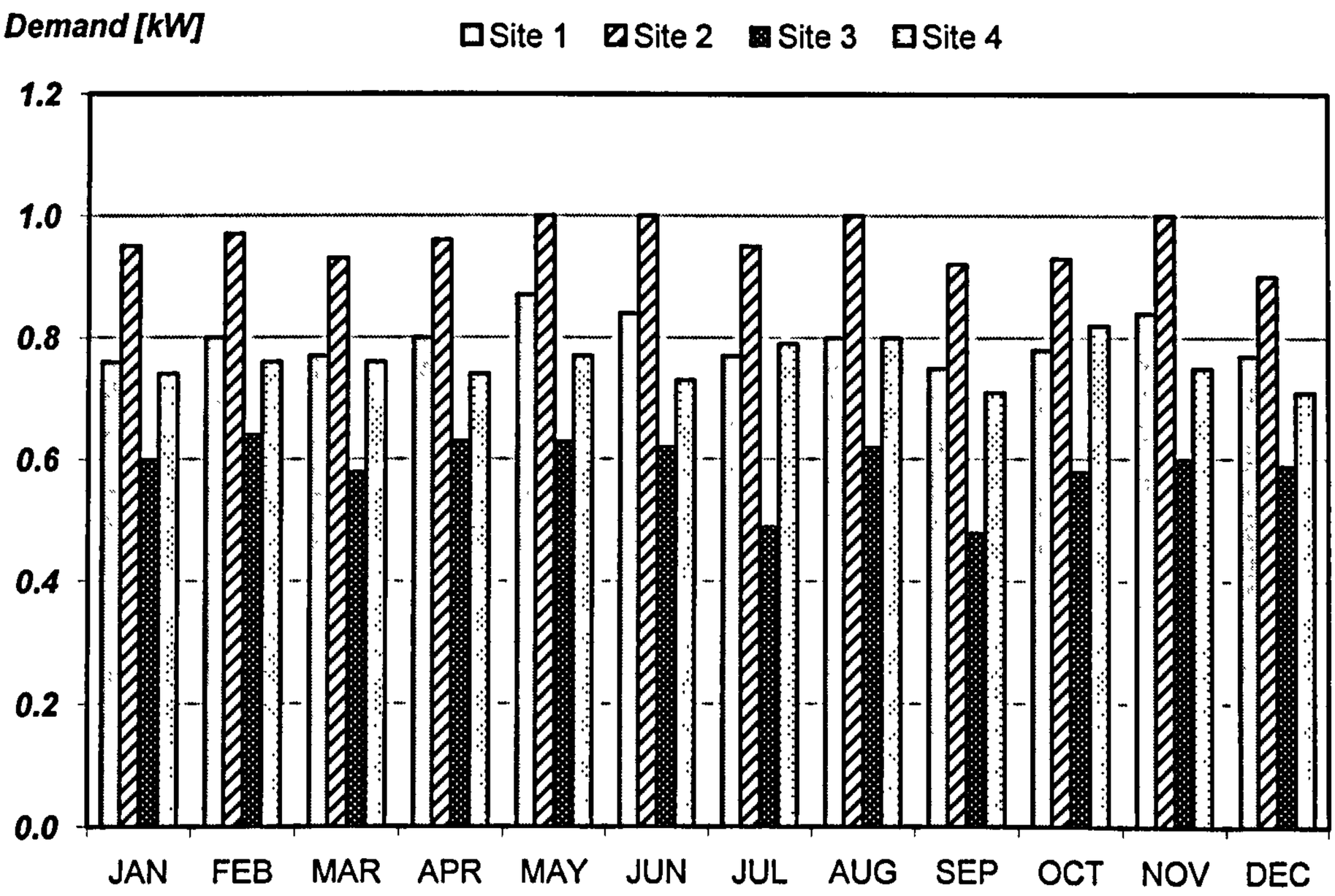

Figure 2.5 – Demand factor during off peak hours of the ceramics industries

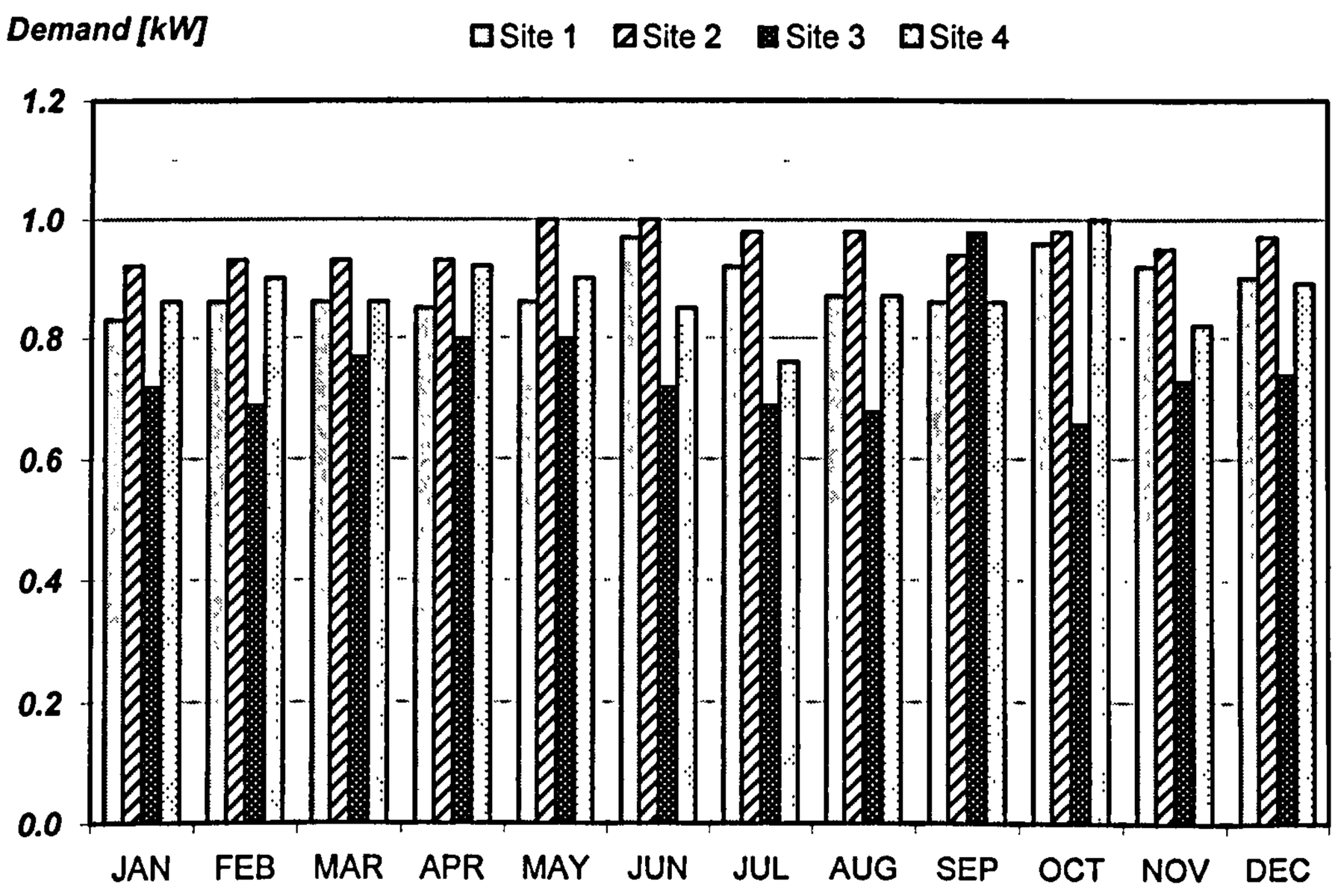

Figure 2.6 – Demand factor during peak hours of the ceramics industries

2.5 - Beverage Industrial Park

The beverage industrial park investigated in this research is also located in the north-eastern region of Brazil and is divided into two sites. They are classified in the food industry segment and are producers of beer and soft drinks as the main products, and carbon dioxide as a sub-product.

The processes of brewing are basically mashing, sparging, boiling, fermentation, and packaging. The first three processes before fermentation produce an extract of fermentable liquid (wort) from the mash (a mixture of water and grain). Then in the fermentation process a micro-organism called yeast turns the sugars in the wort to beer and carbon dioxide.

The main electricity loads are for the compressed air system, large-scale refrigeration plants, electrical motors and lighting. Both facilities operate over 24 hours per day 7 days per week. Basically the industrial area is divided into the following processes: compressed air supply plant, steam generator plant, refrigeration plant with compressor and cooler system, CO_2 compressor plant and peripheral systems. Table 2.3 present the annual energy consumption of both sites. In this case the local electricity supplier uses a tariff structure divided into Dry season (from May to November) and Wet season (from December to April). This tariff classification is used mainly because of the high share of hydropower stations in the Brazilian power market. The facility on site 2 has a higher production capacity than site 1 and consequently a higher power and heat demand. Because of the higher tariffs applied at peak times the off-peak contract demand is higher than the peak time at both sites as a consequence of an energy saving strategy being in place.

Table 2.3 – Annual energy consumption of the beverage industrial park

	Dry Season		Wet Season	
Site 1	**Peak**	**Off-Peak**	**Peak**	**Off-Peak**
Electricity Demand				
Contracted Power Demand [kW]	3,900	4,100	4,200	4,400
Electricity Consumed [MWh/year]	24,729			
Heat Demand				
Average Heat Demand	6,936 kW			
Beverage Production				
Annual Production	234 m^3			
CO_2 Production				
Annual Production	5,521 ton			
Site 2				
Electricity Demand				
Contracted Power Demand [kW]	7,370	8,100	7,370	8,100
Electricity Consumed [MWh/year]	42,351			
Heat Demand				
Average Heat Demand	11,754 kW			
Beverage Production				
Annual Production	619 m^3			
CO_2 Production				
Annual Production	10,878 ton			

Figures 2.7 and 2.8 show the relation between the production of beverage and carbon dioxide. The pattern of the charts indicates a lower production during winter, from June to August, and higher production during summer, from December to February, in the southern hemisphere.

Figure 2.9 shows the relation of the consumption of power and heat with relative monthly production of both facilities investigated. The charts show a linear relation between heat and power demand and relative monthly production. By comparing both charts it can be observed that in the beverage industry there is a higher demand of heat than power, and the specific heat demand rate (absolute kWh/relative production) is higher than specific power demand rate. That means for the variation of relative production there will be a higher variation on heat than electricity demand. Comparing both sites in the same chart distinct areas can be observed for each beverage and carbon dioxide curve depending on production capacity. Therefore, a manufacturer with a production capacity of between 31 and 74 cubic metres of beverage (equivalent

to 659 and 1,606 tons of CO_2) will have a heat and power demand between the two boundaries. The relation of power and heat demand with absolute monthly production of both facilities is shown in Figure 2.10.

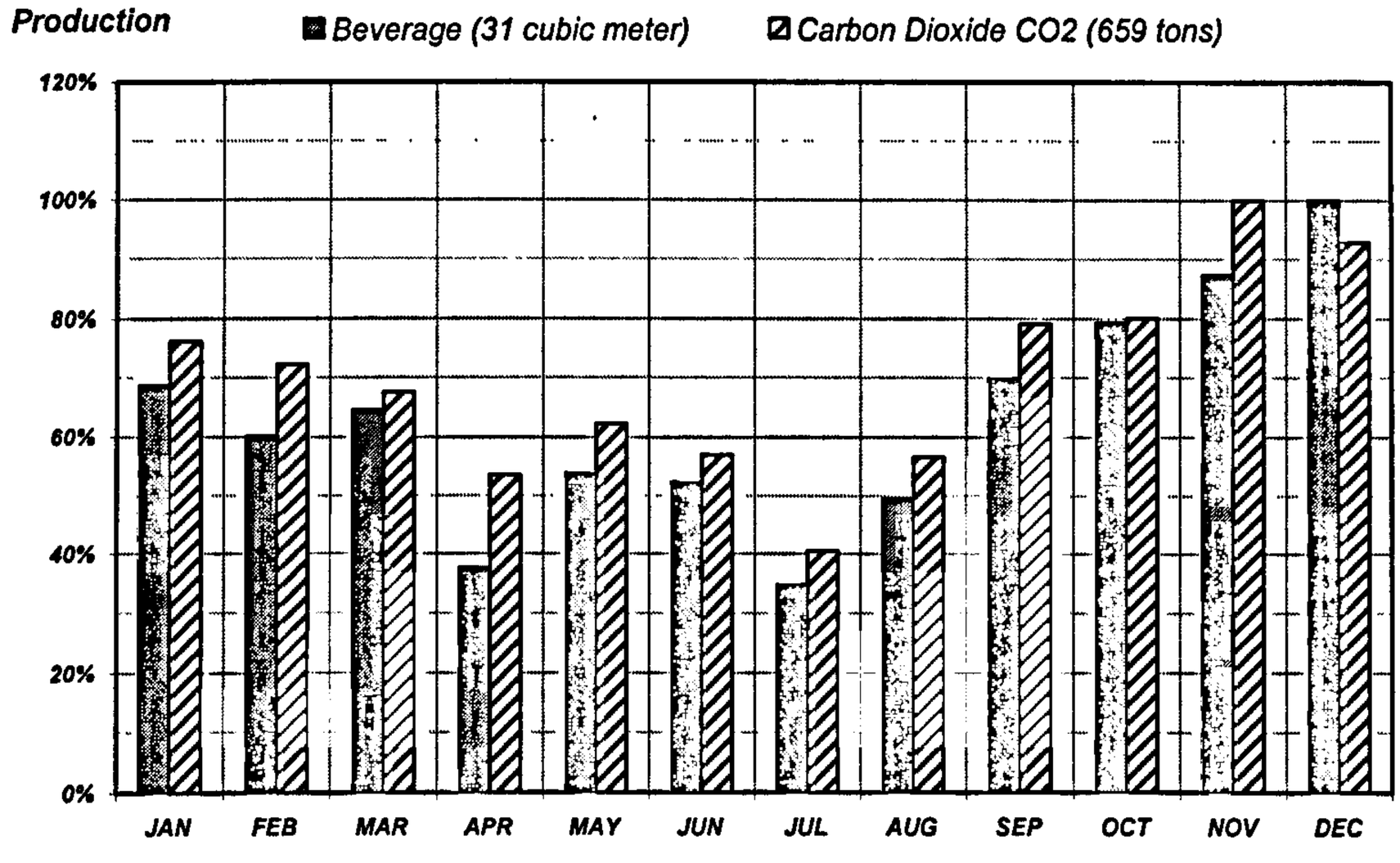

Figure 2.7 – Monthly production of the beverage industry site 1 (maximum capacity is given in parentheses)

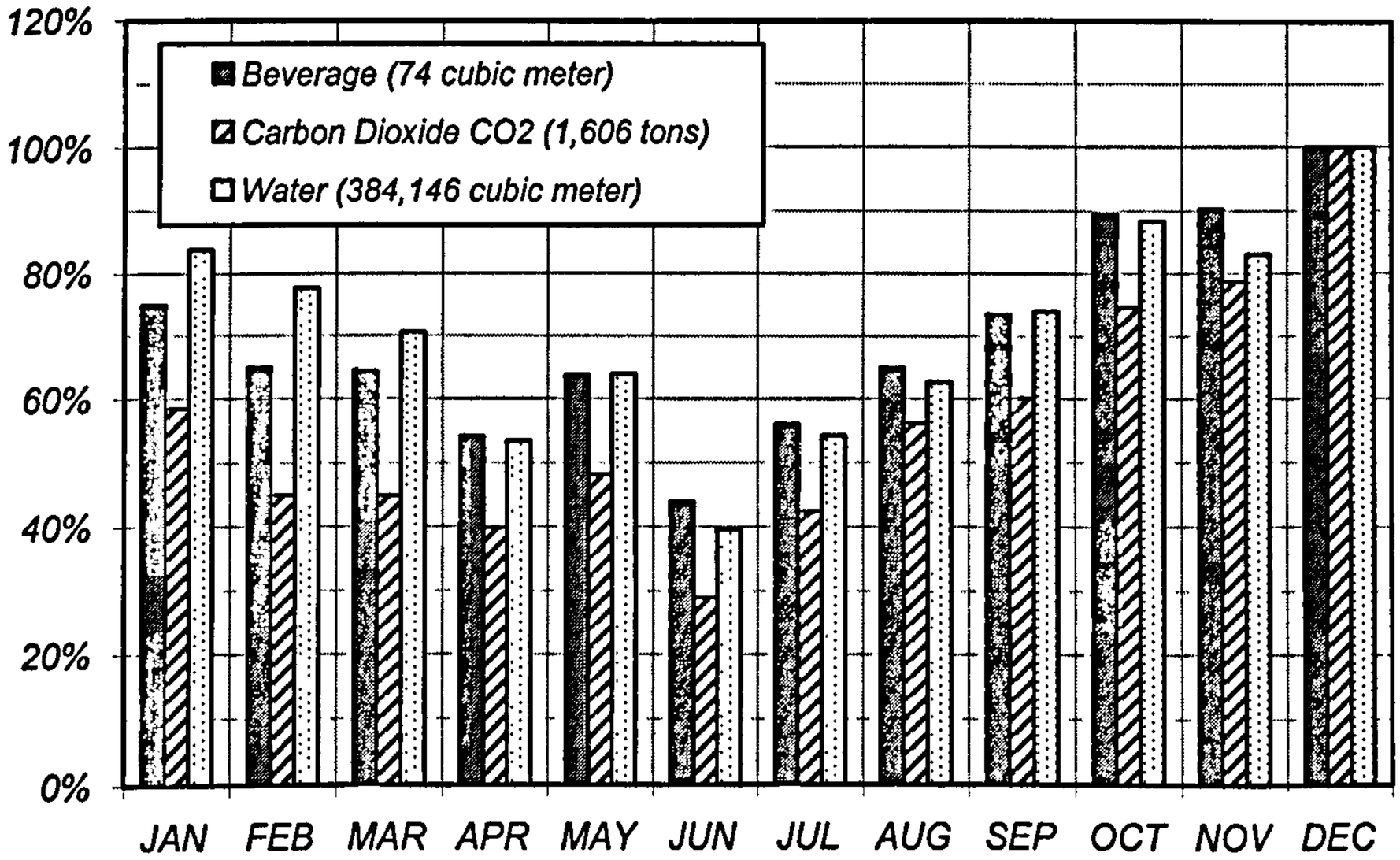

Figure 2.8 – Monthly production of the beverage industry site 2 (maximum capacity is given in parentheses)

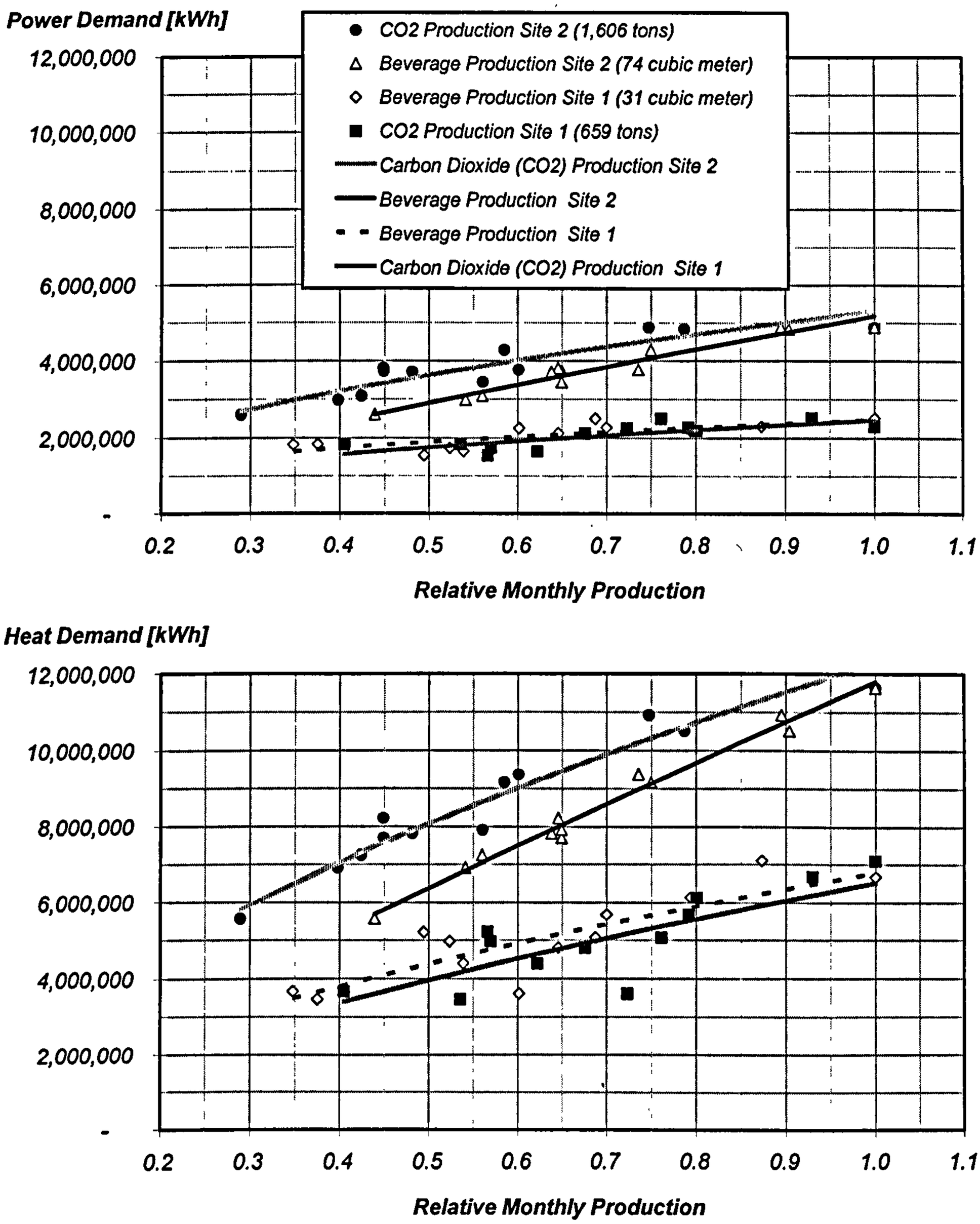

Figure 2.9 – Power and heat consumption and production relation of beverage industry park (sites 1 and 2) (figures in parentheses are the maximum capacity)

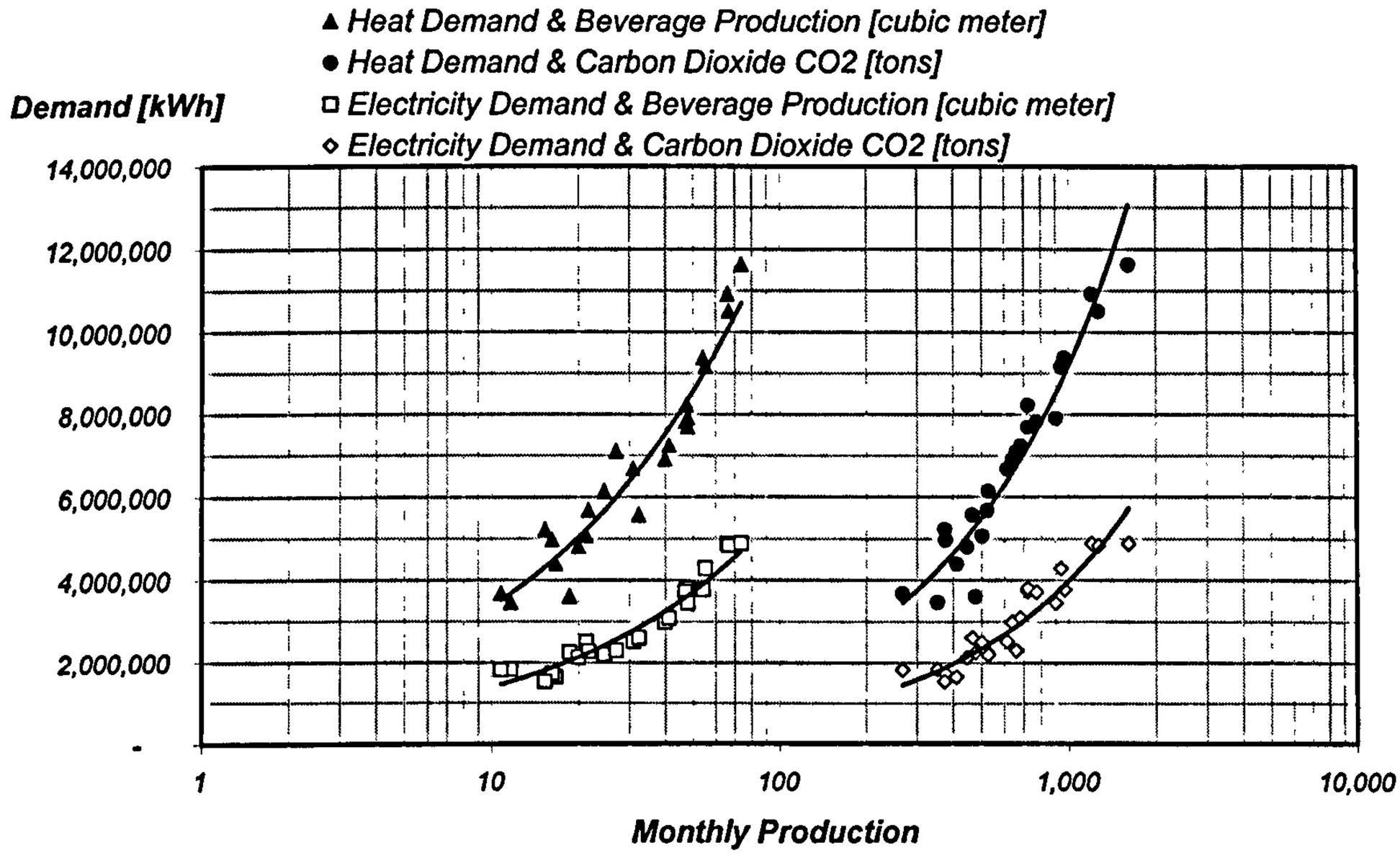

Figure 2.10 – Electricity and heat consumption depending on production of main and sub-product of the beverage industrial park (sites 1 and 2)

The daily manufacturing activity can be classified into three different categories: low, average and high production (Table 2.4). The effects of the economy of scale on the production activity can be observed in Figure 2.11. Higher production means using power more effectively in the production process and therefore a lower specific consumption can be obtained. The daily electricity demand is not constant but relatively small variations are observed in both sites, reflecting the different levels of production activity during summer season (Figure 2.12).

Table 2.4 – Specific electricity consumption of the beverage industrial park

	Site 1		Site 2	
	Daily Beverage Production	Specific Elect. Consumption	Daily Beverage Production	Specific Elect. Consumption
	m^3	kWh/m^3	m^3	kWh/m^3
Low Production	0.801	96,834	1.893	68,287
Average Production	1.026	80,079	2.691	56,471
High Production	1.258	68,614	3.427	48,386

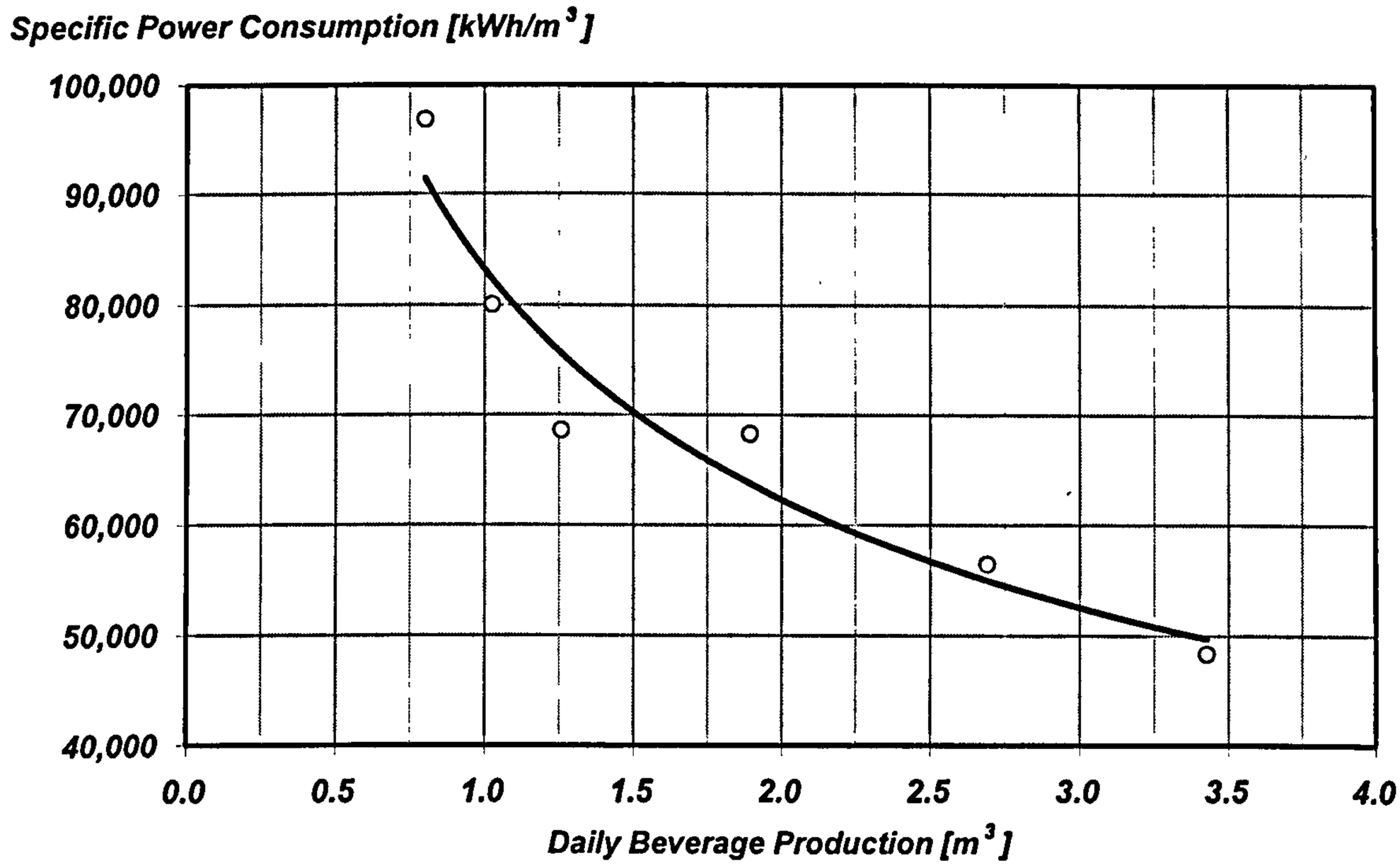

Figure 2.11 – Specific consumption of power behaviour with daily production of the beverage industrial park (sites 1 and 2)

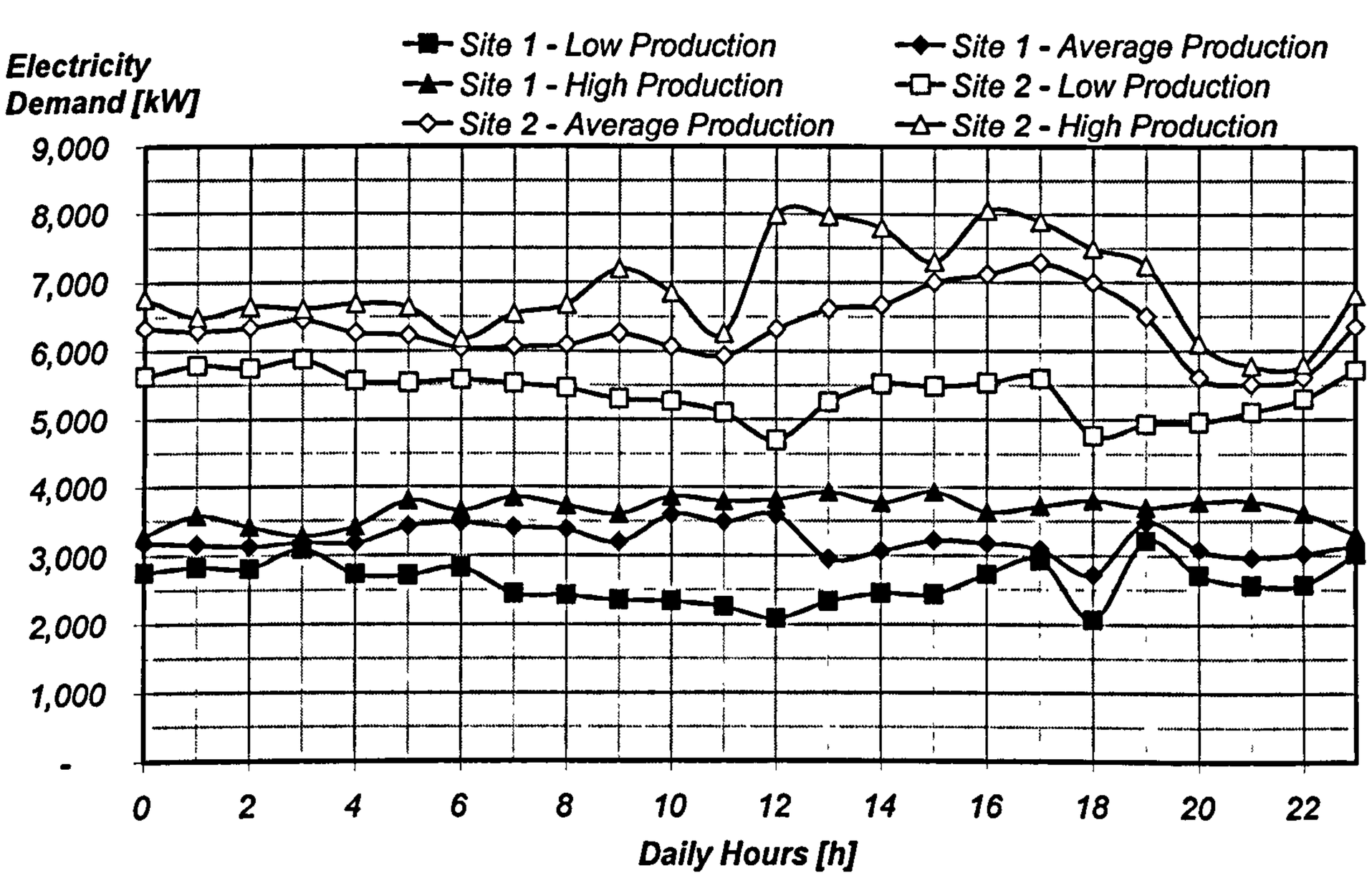

Figure 2.12 – Typical summer hourly electricity demand of the beverage industry park

2.6 - Shopping Centre

Facilities in the tertiary service are also great consumers of electricity. This section describes the electrical demand features of a shopping centre located in the south-eastern region of Brazil. It is a six storey building; three floors are for retail shopping including banks, eating places, cinema, supermarket and health centre. The other three levels are designed to accommodate 716 car parking spaces. On five floors there is no daylight penetration and the top floor is exposed to the weather. It opens to the public 7 days a week from 10:00am to 10:00pm. In this case the CHP plant must supply electricity to the end user and heat to a single-effect LiBr-water absorption chillers that produce cooling for the building's internal areas. Basically the electricity load includes lighting, and office and kitchen electrical devices.

Table 2.5 shows the energy consumption and main characteristics of the shopping centre investigated. Specific electricity consumption and specific power capacity installed are the ratio of annual electricity consumed and average electricity demand, respectively, to illuminated area.

Table 2.5 – Annual energy consumption of the shopping centre

Electricity Demand	
Contracted Electricity Demand [kW]	1,500
Average Electricity Demand [kW]	990
Electricity Consumed [MWh/year]	8,659
Thermal Demand	
Average Thermal Demand [kW]	1,533
Annual Thermal Demand [MWh/year]	6,329
Gross Internal Area [m^2]	
Temperature Controlled Area	35,696
Illuminated Area	53,085
Total Shopping Area	53,698
Average Specific Rates	
Specific Electricity Consumption [kWh/m^2]	163.12
Specific Power Capacity Installed [W/m^2]	18.65

2.7 - International Airport

The international airport investigated is located in the region of Thessaloniki, Greece. It serves 8,000,000 passengers per year. Electric consumption is mainly due to the air-conditioning, lighting of the internal space of the building, airfield lighting and the electromechanical installations. Particularly, it has been evident that the major part of the installed power is used for the central air-conditioning system while one third and one fifth of the installed power is used for the electromechanical installations and lighting respectively. The climate is basically mild summers and cold winters. Monthly ambient conditions, including solar radiation, wind speed and air humidity, are presented in Appendix A.

Table2.6 shows the energy consumption and main characteristics of the airport investigated. Specific electricity consumption and specific power capacity installed are the ratio of annual electricity consumed and average electricity demand, respectively, to total area. Specific heat consumption and specific heat capacity installed are the ratio of annual heat consumed and average heat demand, respectively, to temperature controlled area.

2.8 - Hotel Building Complex

The hotel complex investigated is located in the northern region of Greece and is divided into three sites. The particular characteristic of the hotel complex investigated is that its operation is seasonal; it opens in April and closes in October every year. Site 1 is divided into two buildings with a total of 500 rooms, swimming pool, restaurant, health centre, conference room, and tennis and basketball courts. Site 2 is also divided into two buildings with a total of 103 rooms, four swimming pools, 2 restaurants, health centre, conference room, roof garden, and tennis and basketball courts. Site 3 is a central building with a total of 215 rooms, swimming pool, restaurant, health centre, conference room, and tennis and basketball courts.

Table 2.6 – Annual energy consumption of the international airport

Electricity Demand	
Max Average Electricity Demand [kW]	4,964
Average Electricity Demand [kW]	4,036
Electricity Consumed [MWh/year]	35,403
Thermal Demand	
Max Average Heat Demand [kW]	6,750
Average Heat Demand [kW]	2,556
Annual Heat Demand [MWh/year]	22,265
Gross Internal Area [m^2]	
Public-passenger-check	55,500
VIPs area (CIPs Lounges)	3,000
Commercial and catering services	8,000
Offices	8,000
Luggage distribution area	11,250
Personal dressing rooms	3,750
Traffic areas	17,500
Electromechanical installation	8,000
Total area	115,000
Temperature Controlled Area	89,500
Average Specific Rates	
Specific Electricity Consumption [kWh/m^2]	307.85
Specific Heat Consumption [kWh/m^2]	248.77
Specific Power Capacity Installed [W/m^2]	35.09
Specific Heat Capacity Installed [W/m^2]	28.56

Table 2.7 presents the annual energy consumption and Figure 2.13 the occupancy of the hotel building complex. Figures 2.14 and 2.15 show the energy consumption depending on the overnight occupancy. Average specific rates were obtained as a ratio to total gross internal area. The hotel presents a higher electricity specific consumption but lower heat specific consumption when compared with the airport case. This is mainly related to the hotel's particular characteristics of seasonal operation, i.e. the hotel is not in operation during the winter when higher heat demands are expected. However there is strong need to maintain customer comfort during the rest of the year.

Table 2.7 – Annual energy consumption of the hotel building complex

Electricity Demand	
Max Average Electricity Demand [kW]	1,850
Average Electricity Demand [kW]	822
Electricity Consumed [MWh/year]	5,567
Thermal Demand	
Max Average Heat Demand [kW]	488
Average Heat Demand [kW]	204
Annual Heat Demand [MWh/year]	1,226
Gross Internal Area [m^2]	
Site#1	4,139
Site#2	4,355
Site#3	2,580
Total	**11,074**
Average Specific Rates	
Specific Electricity Consumption [kWh/m^2]	502.73
Specific Heat Consumption [kWh/m^2]	110.71
Specific Power Capacity Installed [W/m^2]	74.24
Specific Heat Capacity Installed [W/m^2]	18.46

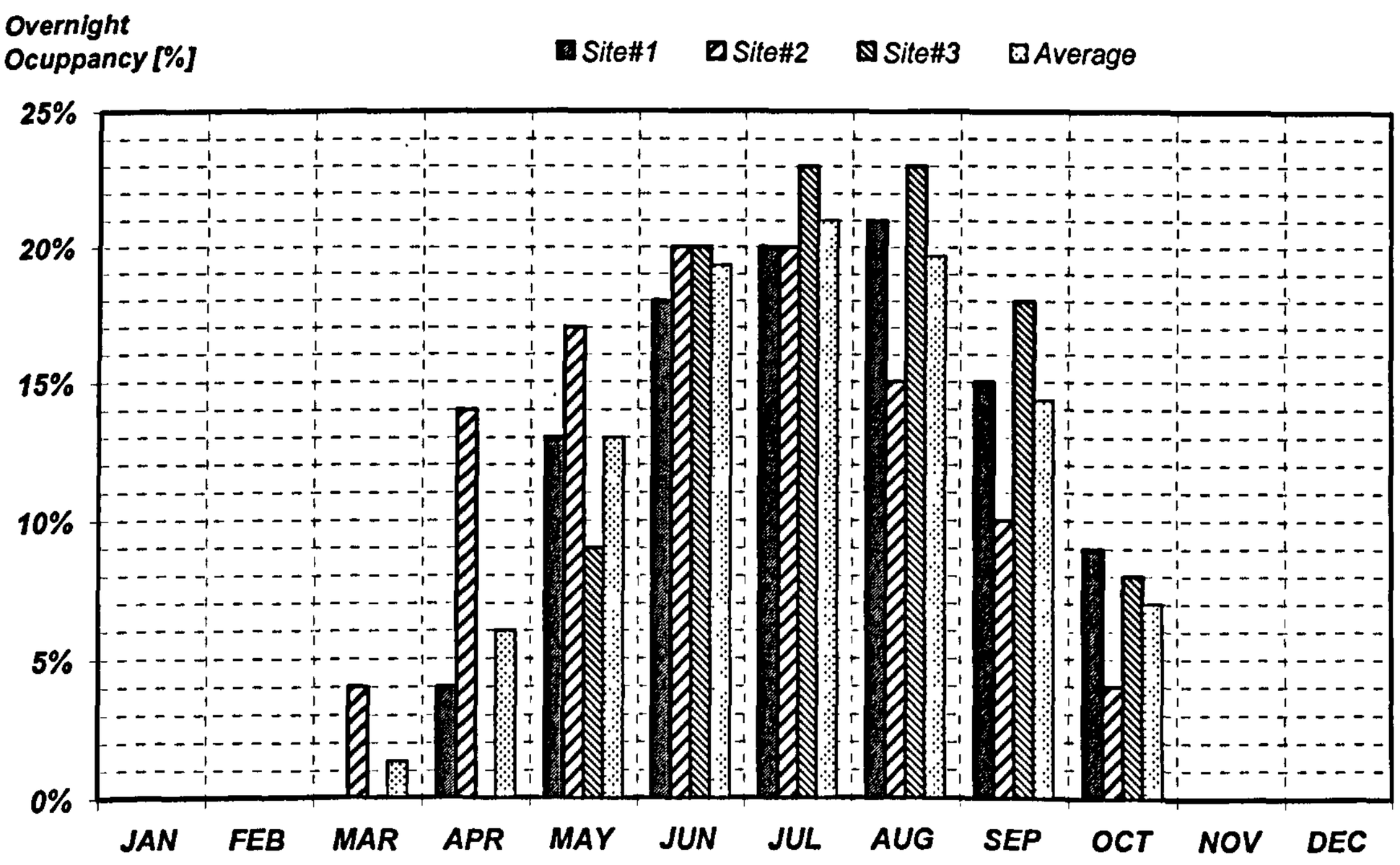

Figure 2.13 – Average monthly occupancy of the hotel building complex

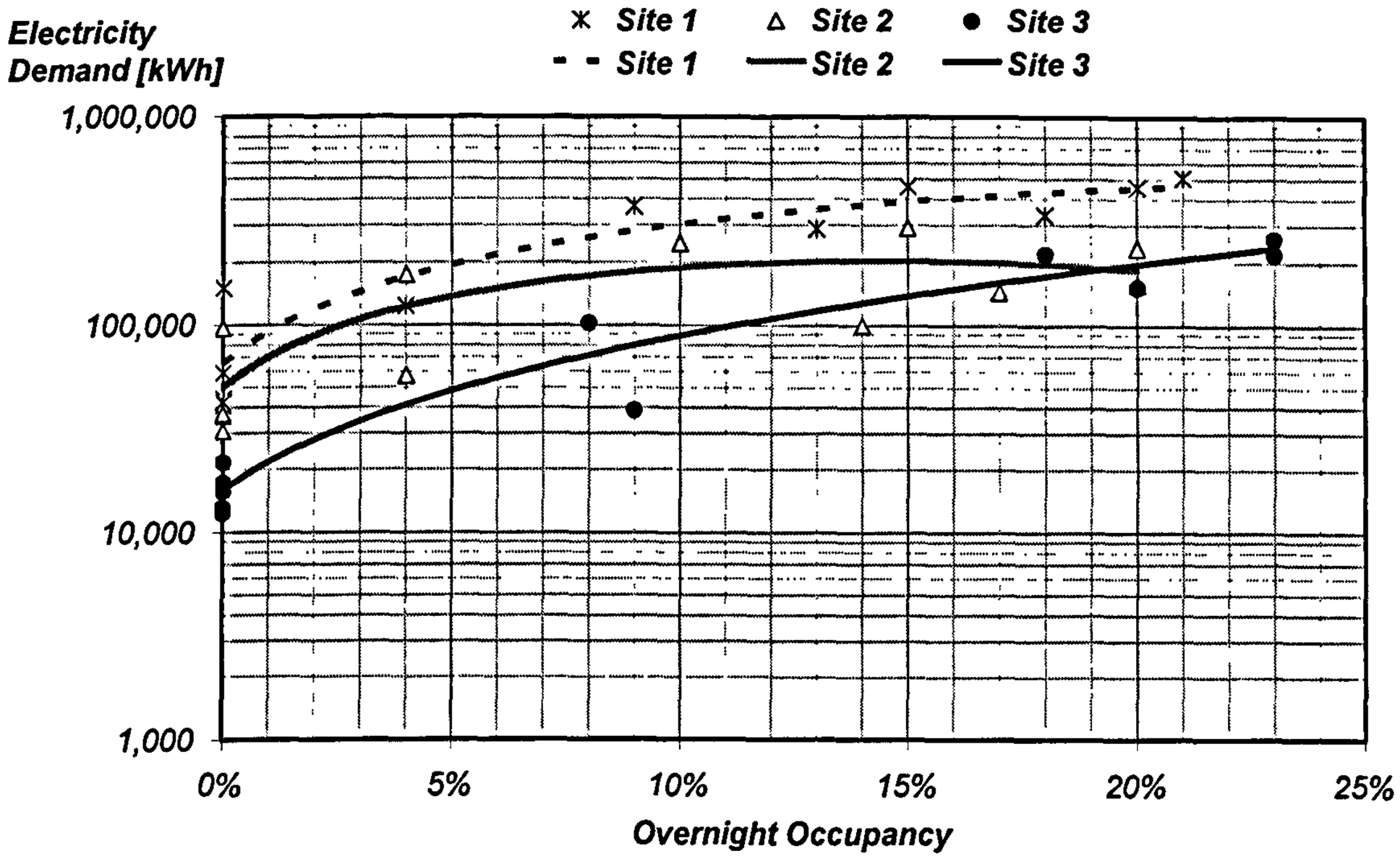

Figure 2.14 – Electricity consumption of hotel building complex depending on the overnight occupancy

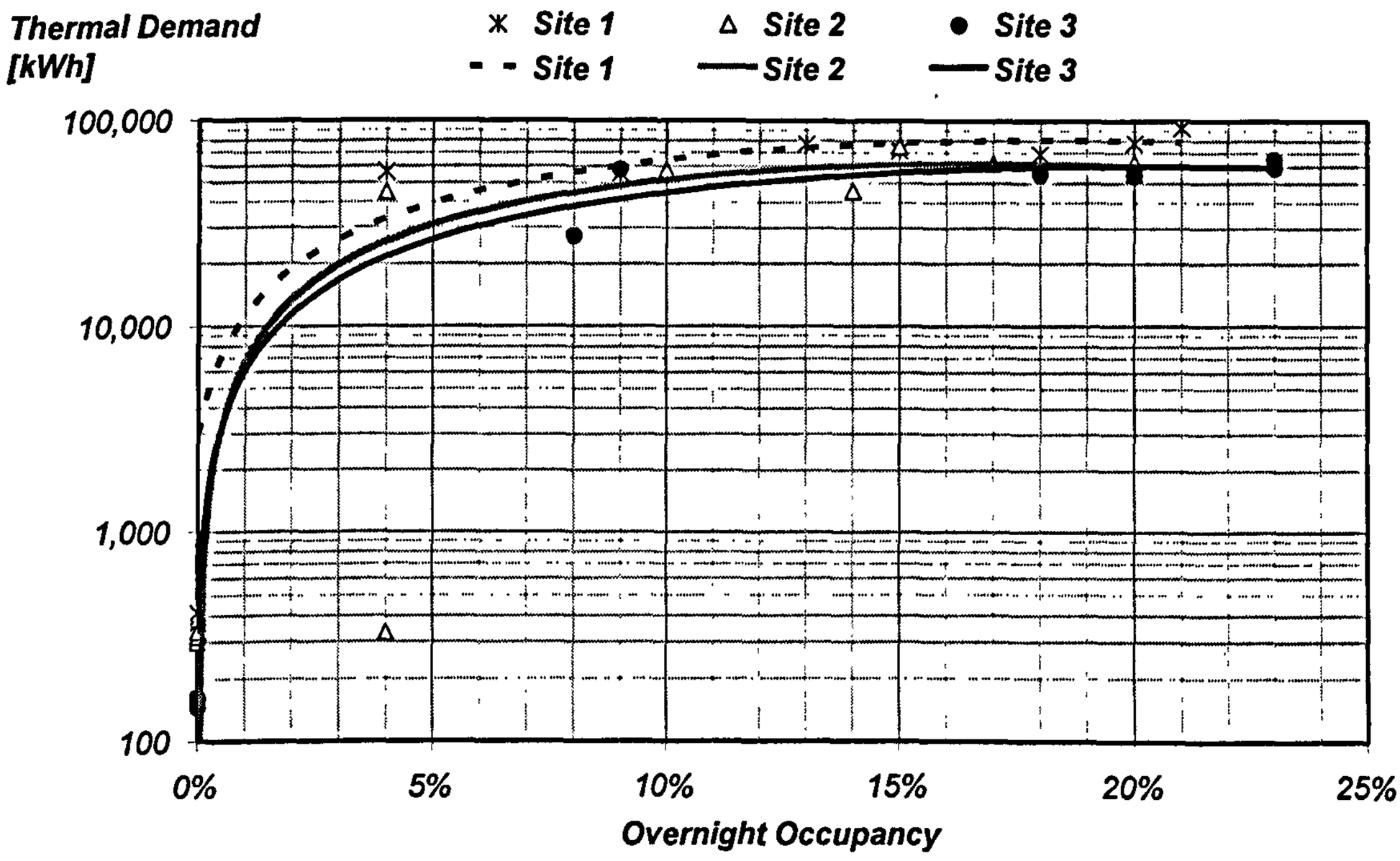

Figure 2.15 – Thermal consumption of hotel building complex depending on the overnight occupancy

2.9 - Mediterranean Island

The island investigated is located in the northern Aegean Sea and has a total area of 476 km^2. The total population, estimated in 1991, is 17,645 residents. The Mediterranean climate is basically that of a cold winter and mild summer. The consumption of electricity was supplied by the local utility company and represents the island's residential consumers (Table 2.8).

Table 2.8 – Annual energy consumption of the Mediterranean island

Electricity Demand	
Max Average Electricity Demand [kW]	8,198
Average Electricity Demand [kW]	6,188
Electricity Consumed [MWh/year]	54,258
Thermal Demand	
Max Average Thermal Demand [kW]	5,062
Average Thermal Demand [kW]	2,370
Annual Thermal Demand [MWh/year]	20,765

2.10 - Resort Hotel

The resort hotel examined is located on one of the Greek islands in the south-eastern Mediterranean. As with the hotel building complex, its operation is seasonal i.e. from March to October. It is divided into one main building and four independent smaller buildings with a total of 140 rooms, restaurant, entertainment halls, conference room and electromechanical house. Table 2.9 presents the annual energy consumption, and Figure 2.16 the occupancy of the resort hotel. Figure 2.17 shows the relationship between the demand and the overnight occupancy of the resort hotel studied.

Table 2.9 – Annual energy consumption of the resort hotel

Electricity Demand	
Max Average Electricity Demand [kW]	84.90
Average Electricity Demand [kW]	40.59
Electricity Consumed [MWh/year]	350.70
Thermal Demand	
Max Average Heat Demand [kW]	42.40
Average Heat Demand [kW]	18.80
Annual Heat Demand [MWh/year]	162.48

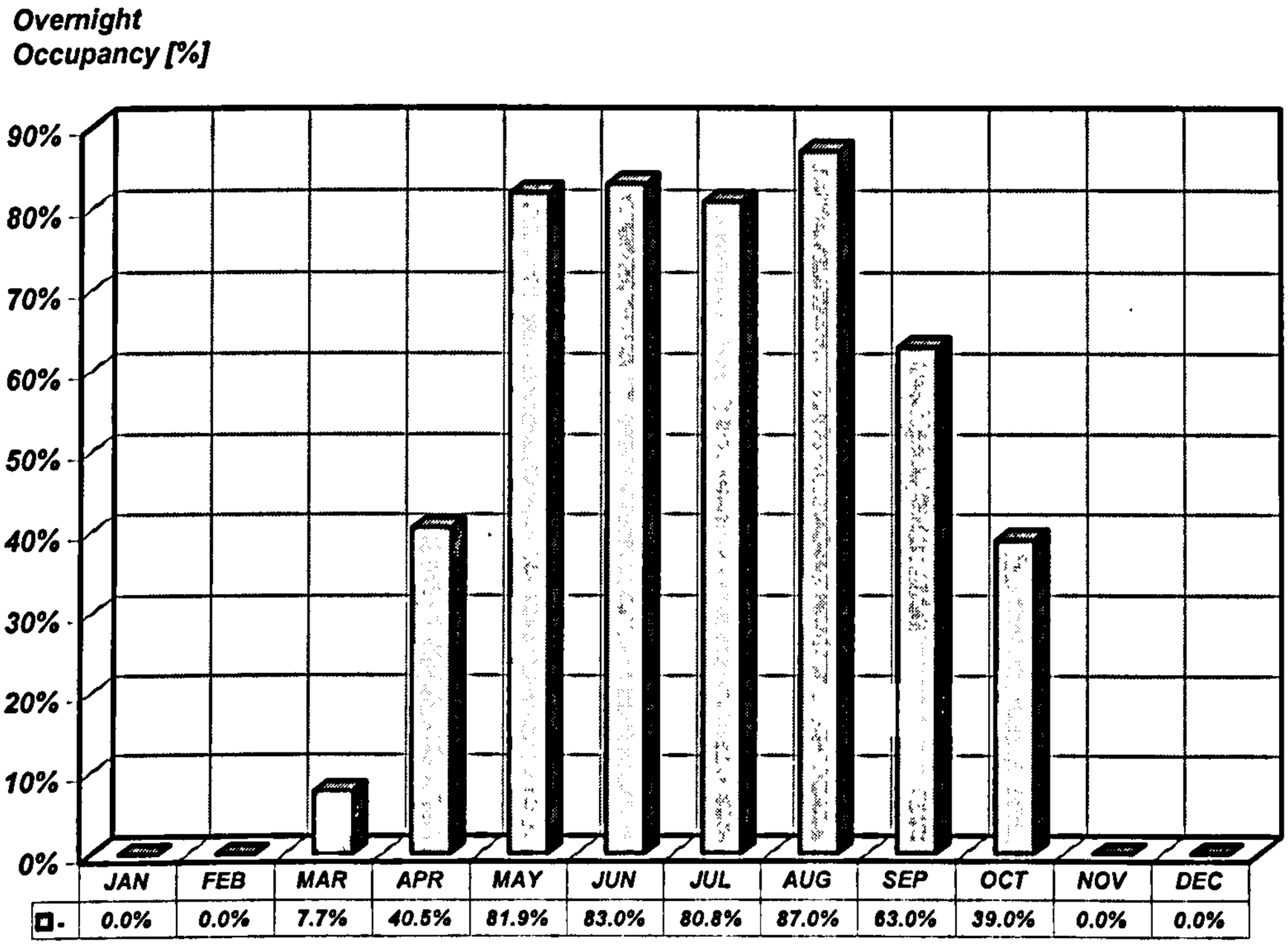

Figure 2.16 – Average monthly occupancy of the resort hotel

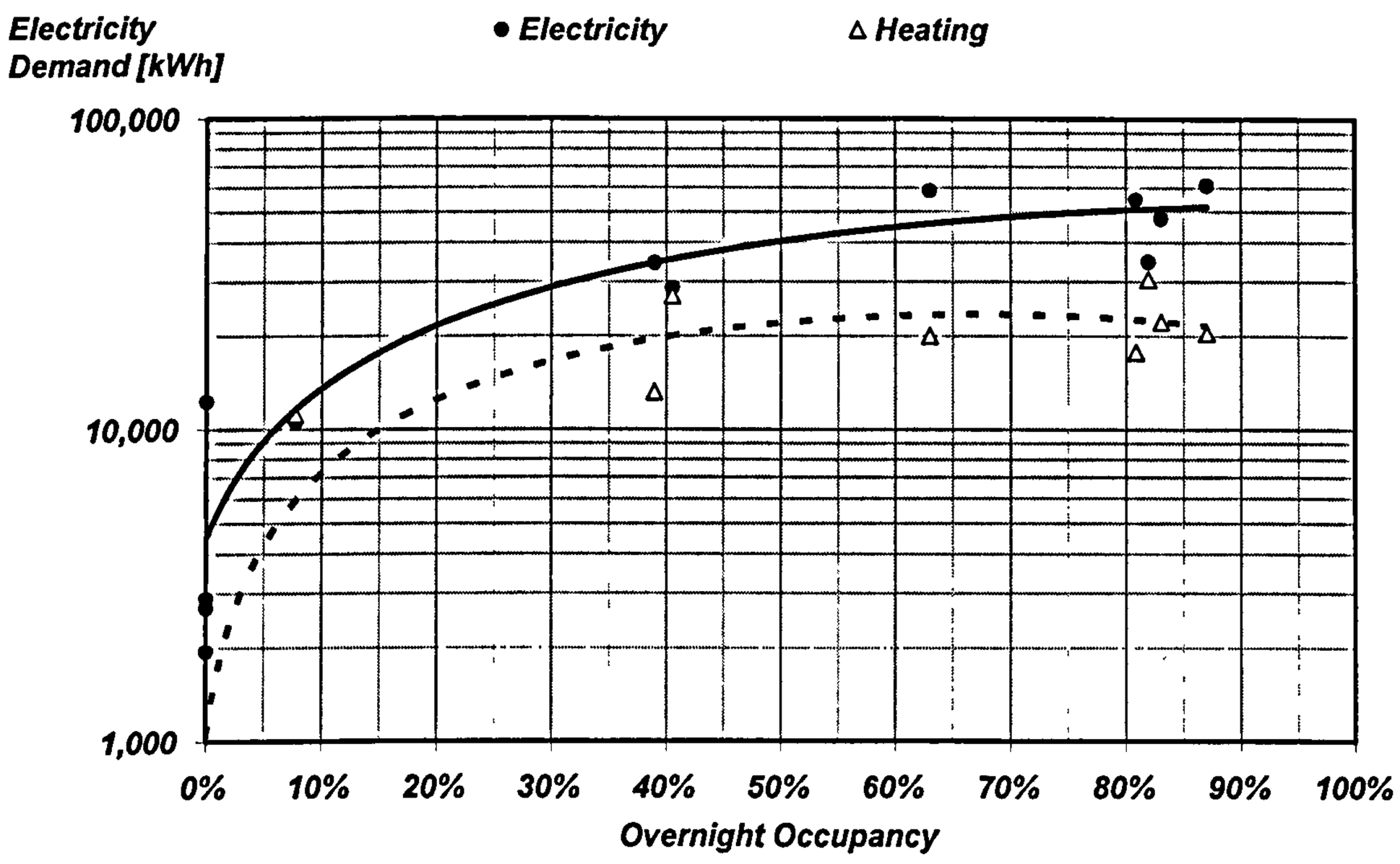

Figure 2.17 – Electricity and thermal consumption of resort hotel depending on the overnight occupancy

2.11 - Demand pattern analysis

The monthly heat and power demand profile of the facilities investigated over a year is presented in Figures 2.18 to 2.21. A summary of the main average parameters is given in Figures 2.22 to 2.25 where the bars represent the monthly variation over the year and the figures indicate the annual average.

The electricity and heat pattern of the beverage industrial park follows the monthly production profile: lower energy consumption during winter (from June to August) and higher during summer (from December to February). The typical average demand factor of the beverage industry is 0.645. Because of the high requirement of heat during the production process, the beverage industrial park presents the highest heat demand in the cases investigated and a relatively low power to heat ratio.

No large variations are observed in the power demand profile of the ceramics industrial park during the year and it follows the pattern of the production process. It displays the highest average demand factor between the consumer facilities investigated and the lowest power to heat ratio because of the high heat requirement of the spray dryer described in section 2.3.1.

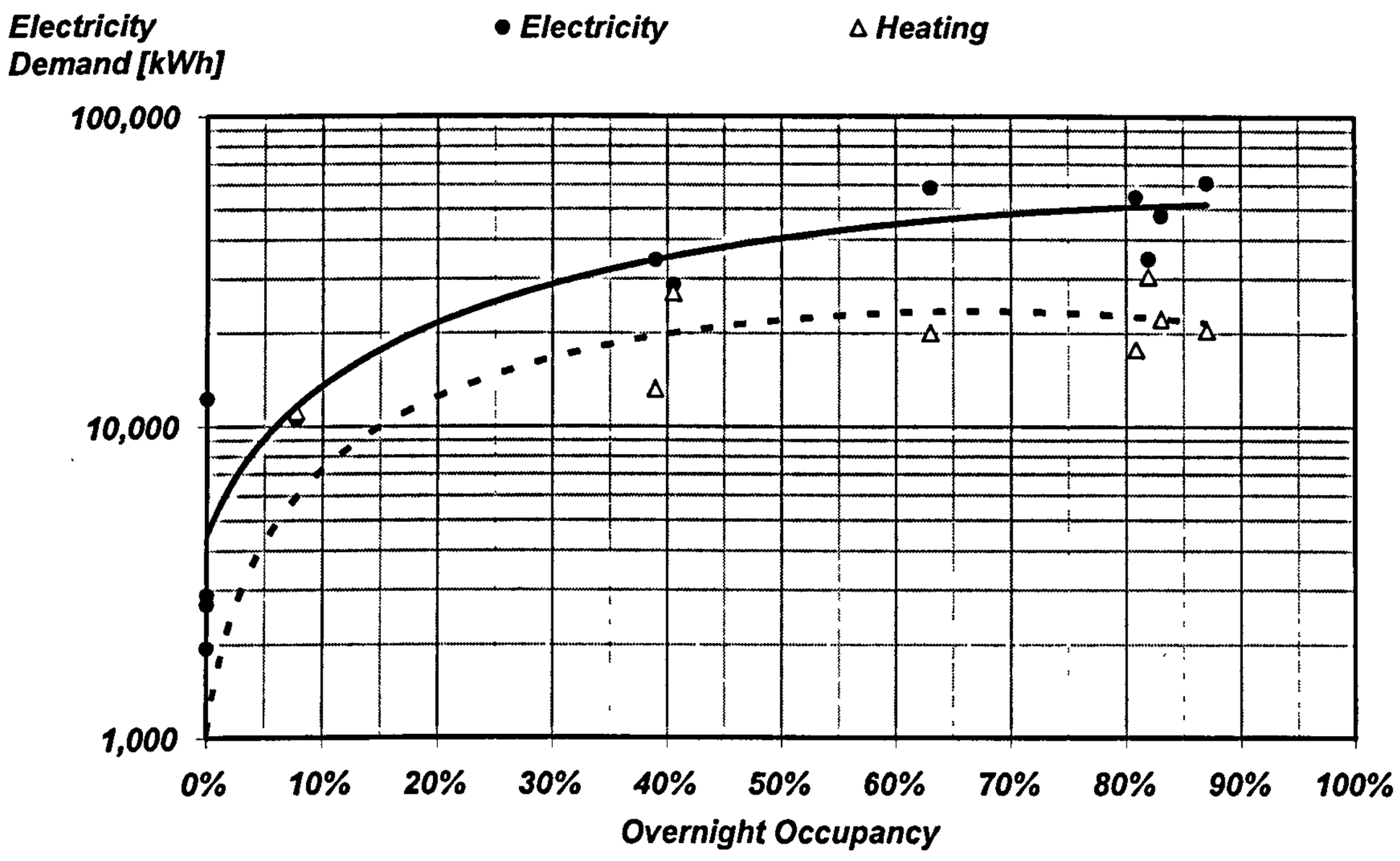

Figure 2.17 – Electricity and thermal consumption of resort hotel depending on the overnight occupancy

2.11 - Demand pattern analysis

The monthly heat and power demand profile of the facilities investigated over a year is presented in Figures 2.18 to 2.21. A summary of the main average parameters is given in Figures 2.22 to 2.25 where the bars represent the monthly variation over the year and the figures indicate the annual average.

The electricity and heat pattern of the beverage industrial park follows the monthly production profile: lower energy consumption during winter (from June to August) and higher during summer (from December to February). The typical average demand factor of the beverage industry is 0.645. Because of the high requirement of heat during the production process, the beverage industrial park presents the highest heat demand in the cases investigated and a relatively low power to heat ratio.

No large variations are observed in the power demand profile of the ceramics industrial park during the year and it follows the pattern of the production process. It displays the highest average demand factor between the consumer facilities investigated and the lowest power to heat ratio because of the high heat requirement of the spray dryer described in section 2.3.1.

The shopping centre demand is mainly related to hours of operation. No large variations are observed in the power demand with an average demand factor of 0.66. Higher demand figures are in the summer (from December to February) and lower in the winter (from June to August) because heat is used in an absorption chiller to supply cooling requirements.

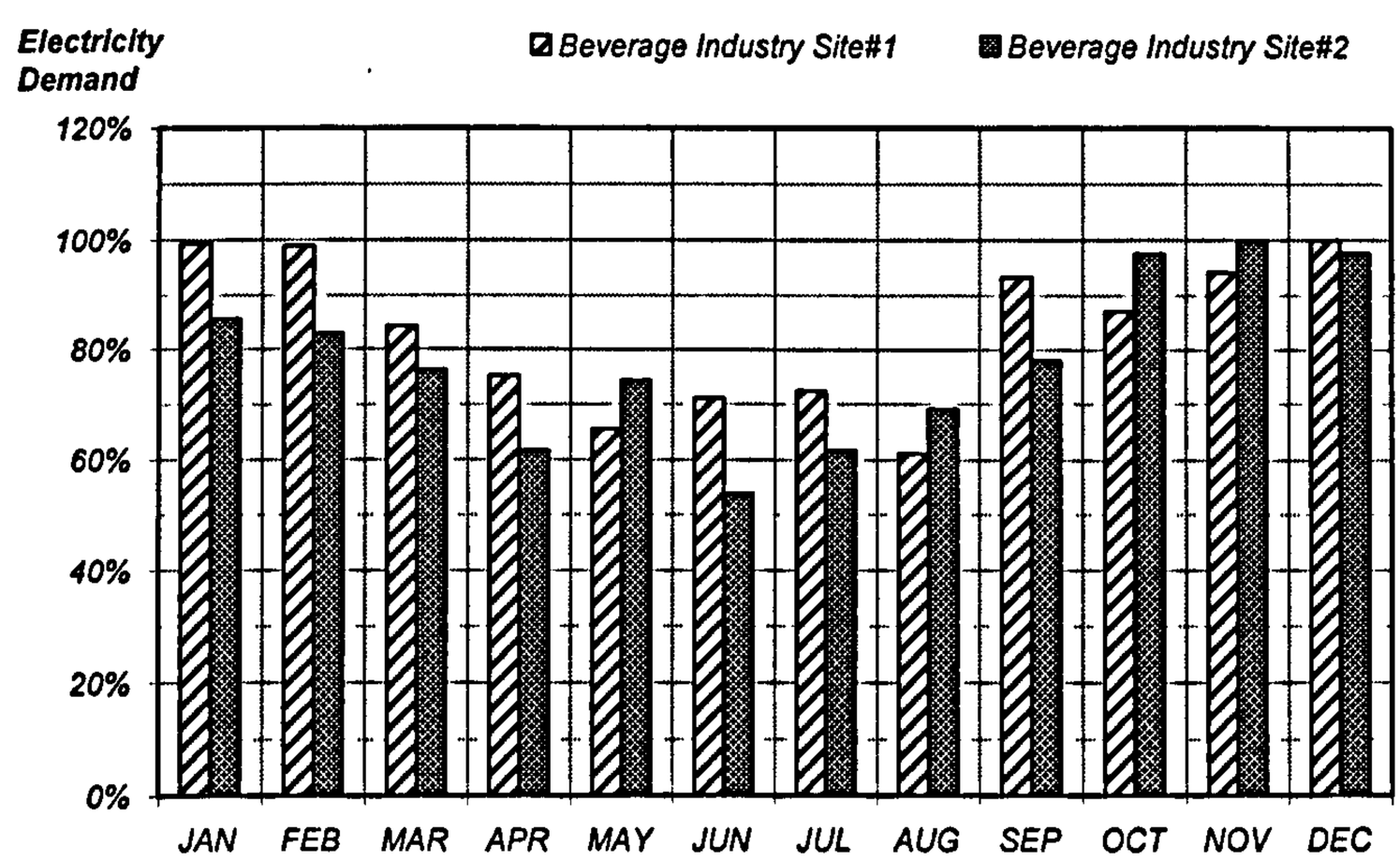

Figure 2.18 – Monthly electricity demand profile (industries and tertiary service)

The energy consumption of the airport and island studied are mainly related to the weather conditions (i.e. Mediterranean climate). Higher power demands and lower heat demands take place in the summer (from July to September in the northern

hemisphere), mostly attributed to a greater need for air conditioning and no need for space heating. Lower power demands and higher heat demands are required in the winter (from January to March in the northern hemisphere) as there is a greater need for space heating. The Mediterranean island presents the highest power demand investigated and it represents residential sector consumers. The airport presents the highest average and annual variation of power to heat ratio.

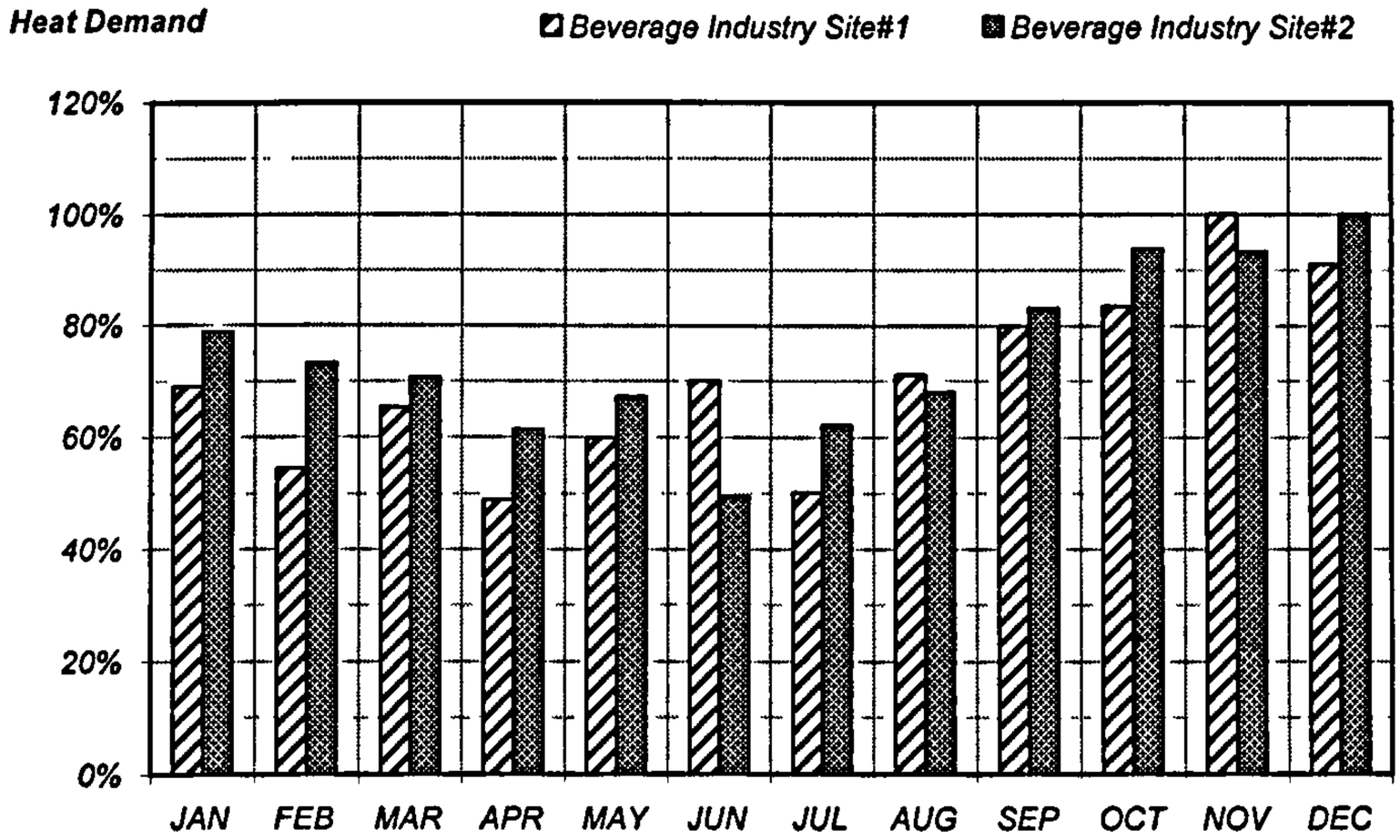

(a)

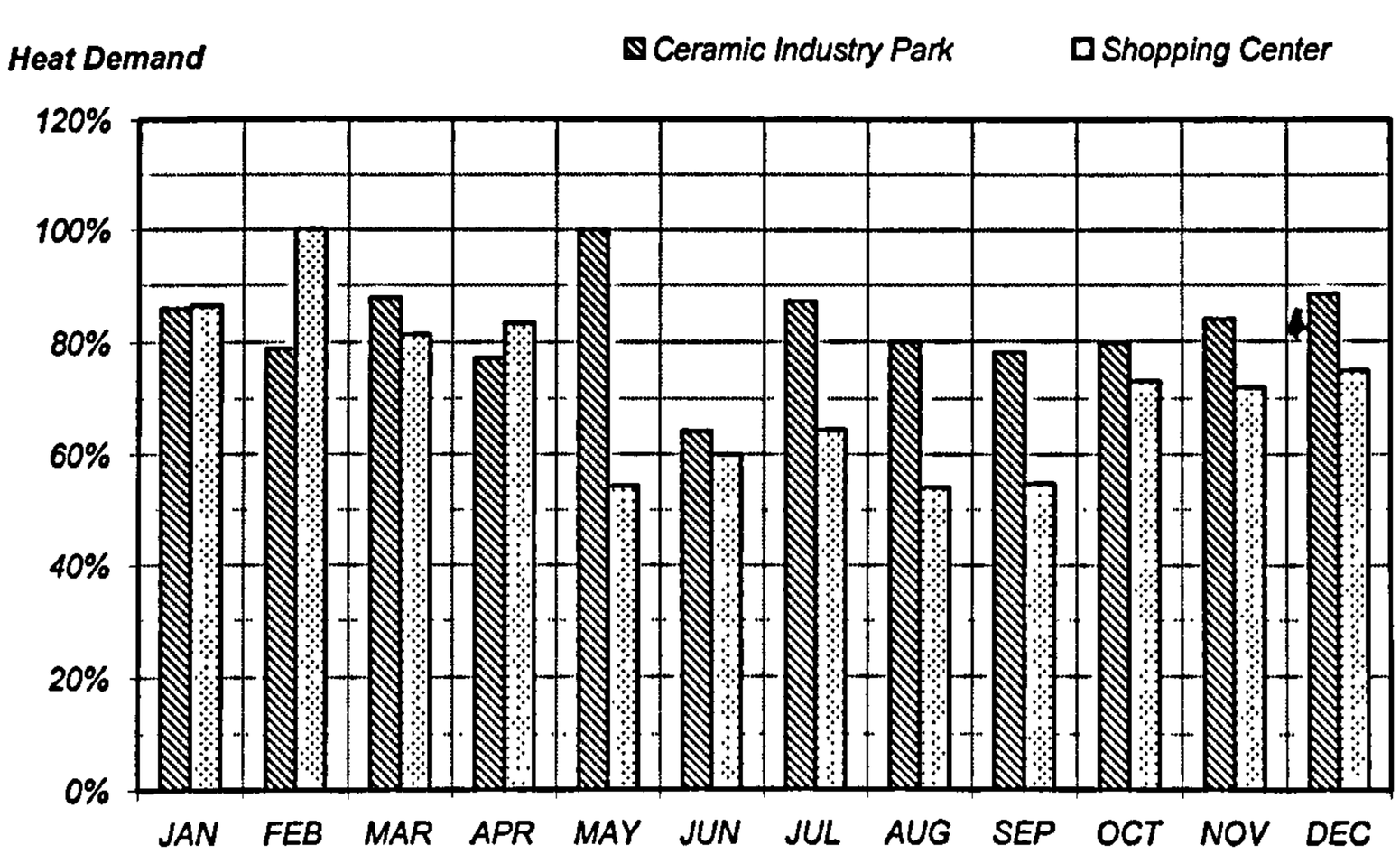

(b)

Figure 2.19 – Monthly thermal demand profile (industries and tertiary service)

The hotels' energy demand reflects their seasonal operation. Higher heat demand in May (hotel resort) and August (hotel complex) are explained by the need to keep customers comfortable all the time. Energy demand is highly dependent on occupancy which achieves its peak during the summer season. The hotels display the

lowest power and heat demand, and average demand factor between the facilities investigated.

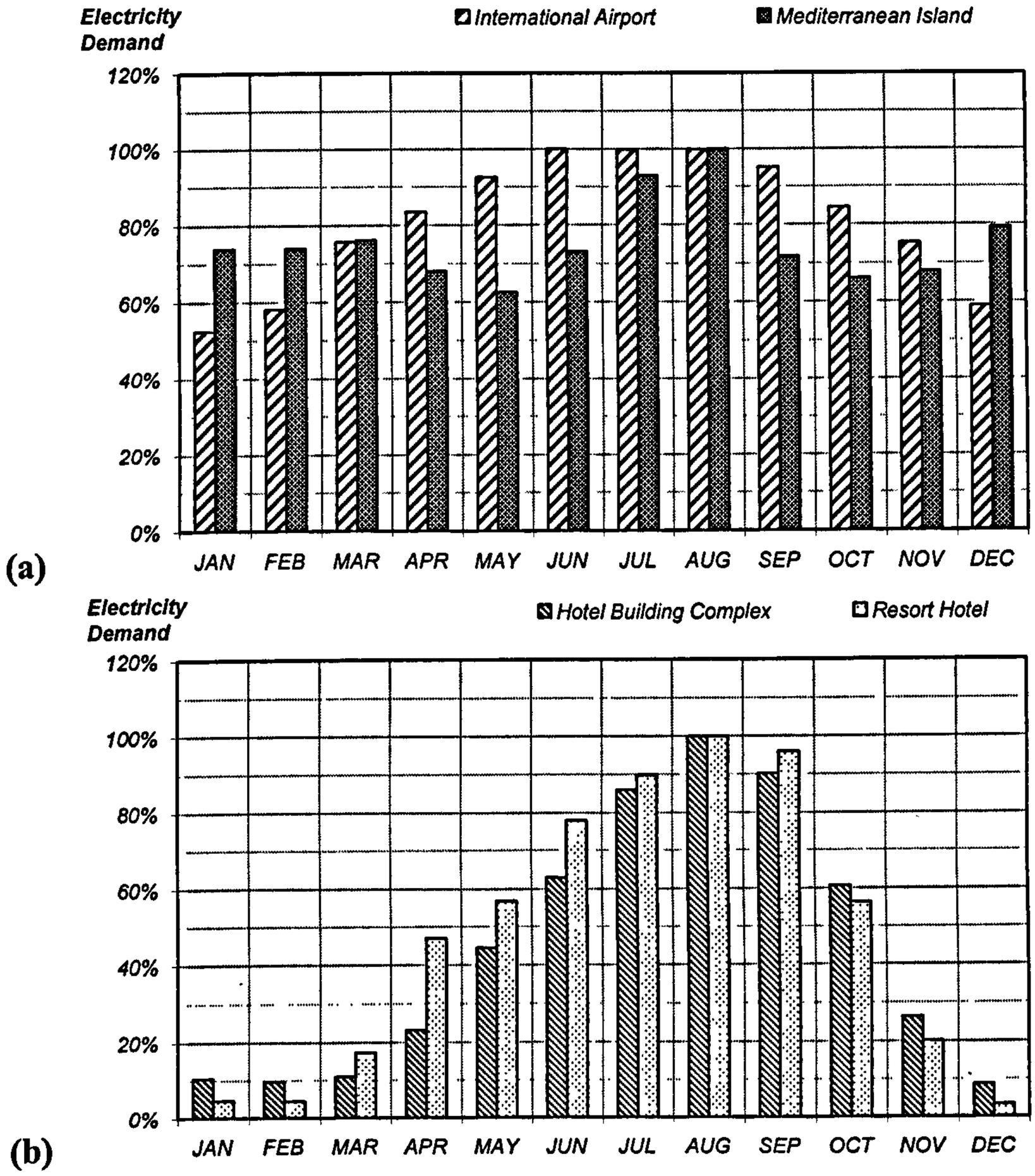

Figure 2.20 – Monthly electricity demand profile (airport, island and hotels)

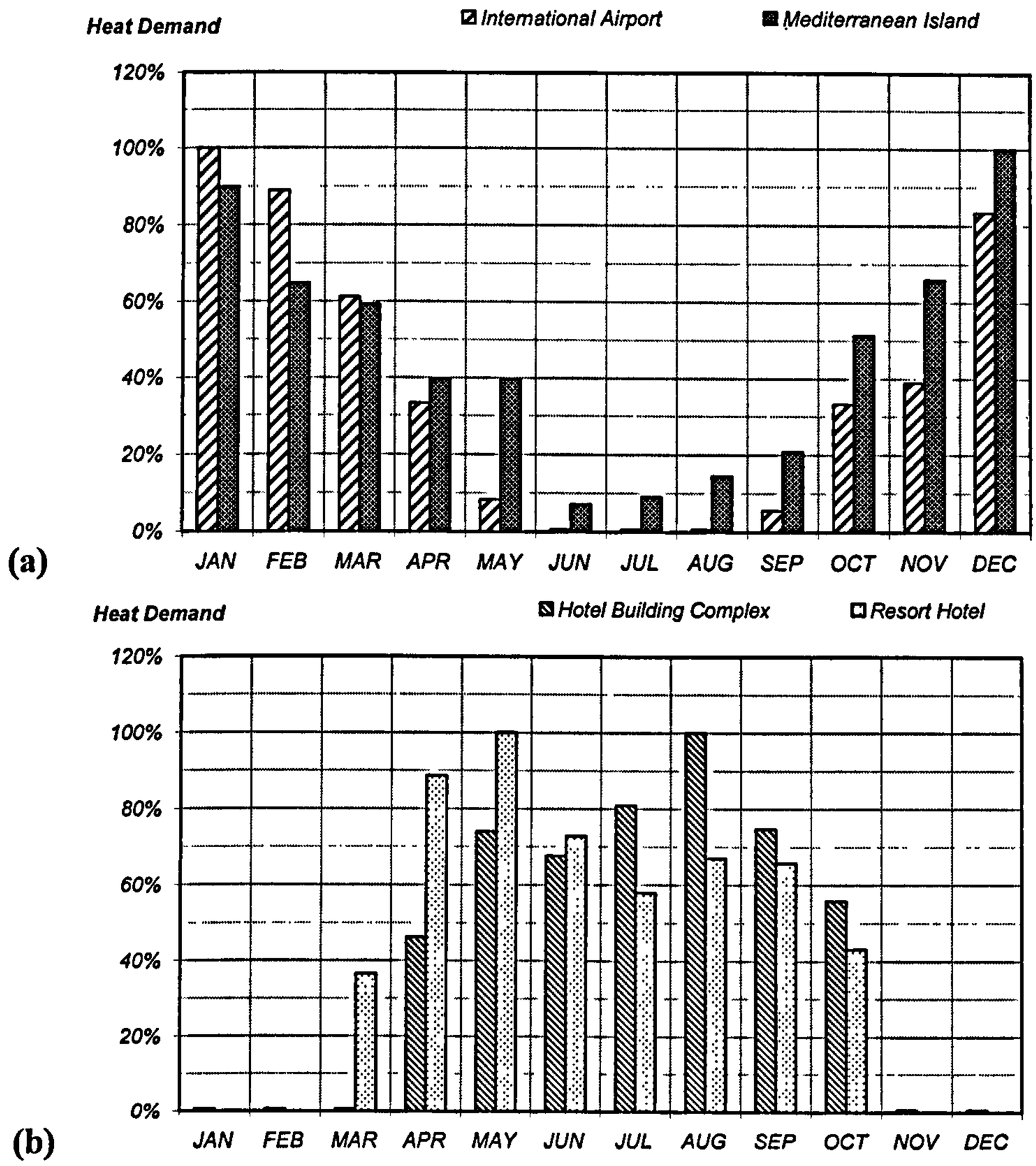

Figure 2.21 – Monthly thermal demand profile (airport, island and hotels)

The consumer sites studied under the Mediterranean climate present a higher variation of power to heat ratio over the year when compared with the sites in a tropical climate. This is because the energy demand is highly dependent on the weather conditions in most cases. In the tropical climate (mild winter and dry season, and hot summer and wet season) the ambient temperature variation is lower than that of the Mediterranean climate (mild summer and cold winter) over the year.

The energy end-users' facilities present an average power demand from 41 to 6,188 kW and heat demand from 19 to 11,754 kW. Based on the power demand the portfolio of consumers can be classified into two categories: medium sized consumers:

secondary industrial (manufacturing) sector, residential and large buildings; and small sized consumers: small buildings (service sector).

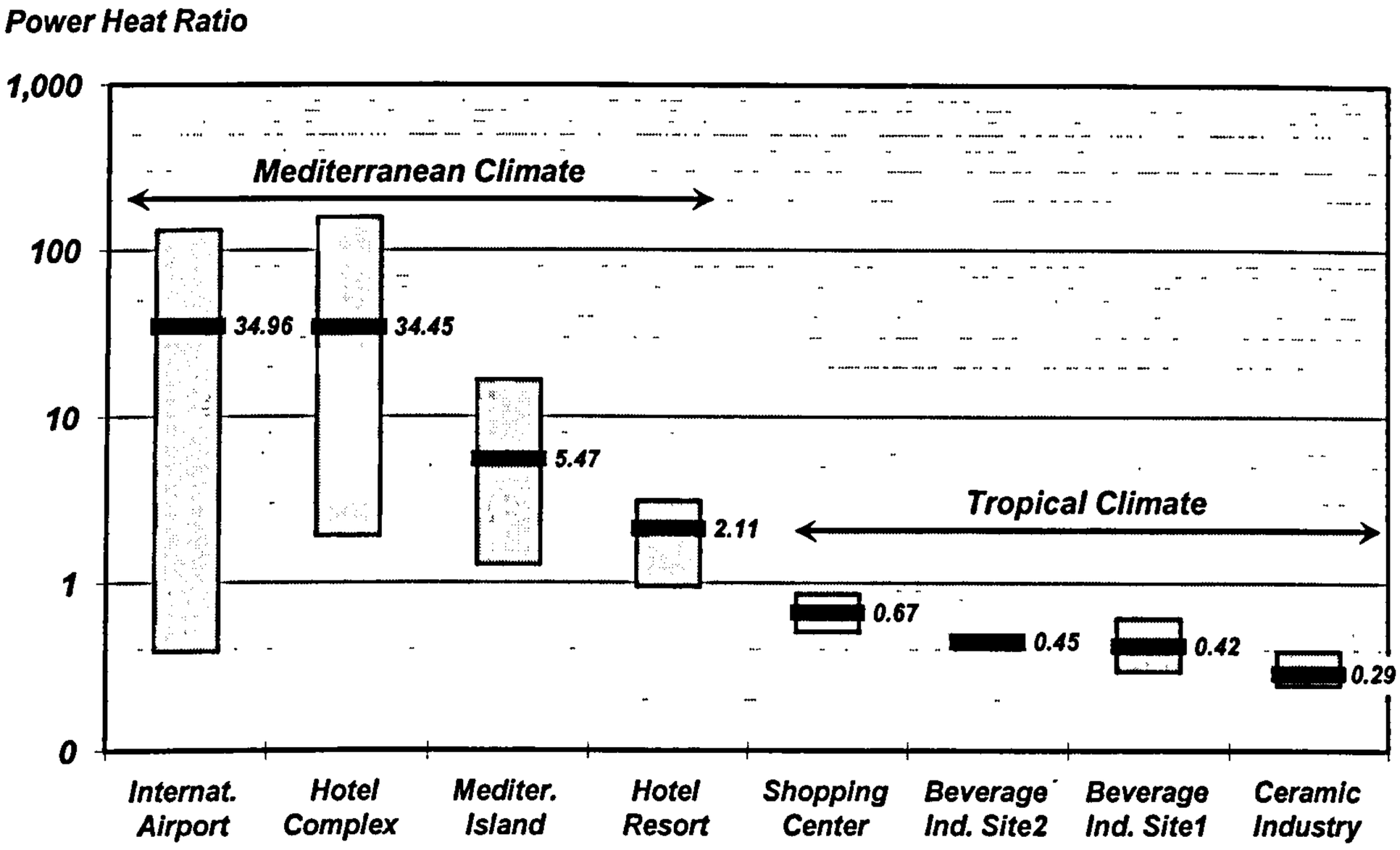

Figure 2.22 - Power heat ratio of the portfolio of consumers

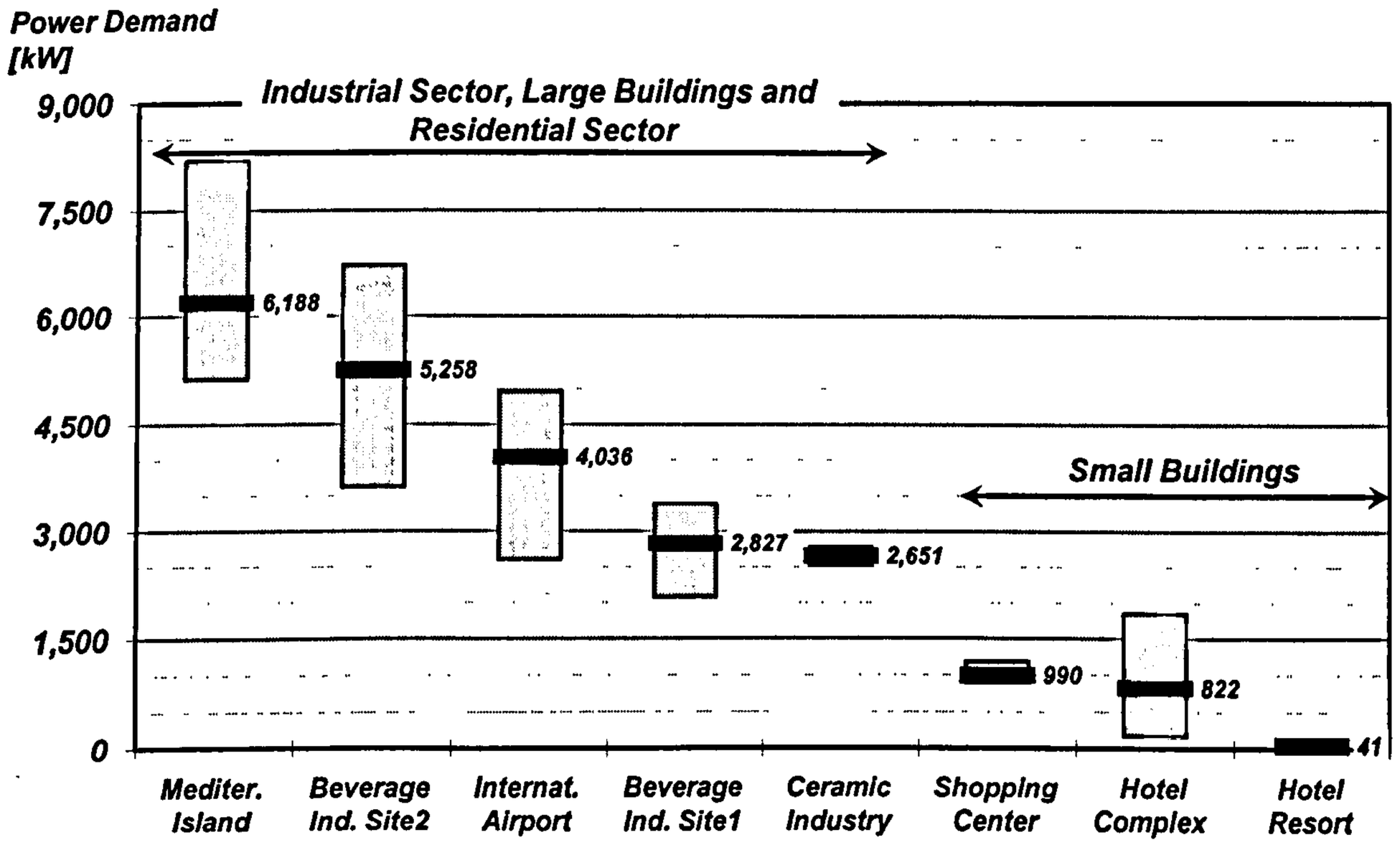

Figure 2.23 - Power demand of the portfolio of consumers

The average demand factor of all cases analysed varies from 0.37 to 0.73 and a clear classification can be made into two categories: low demand factor consumers: residential sector; and high demand factor consumers: secondary industrial (manufacturing) sector and buildings (service sector).

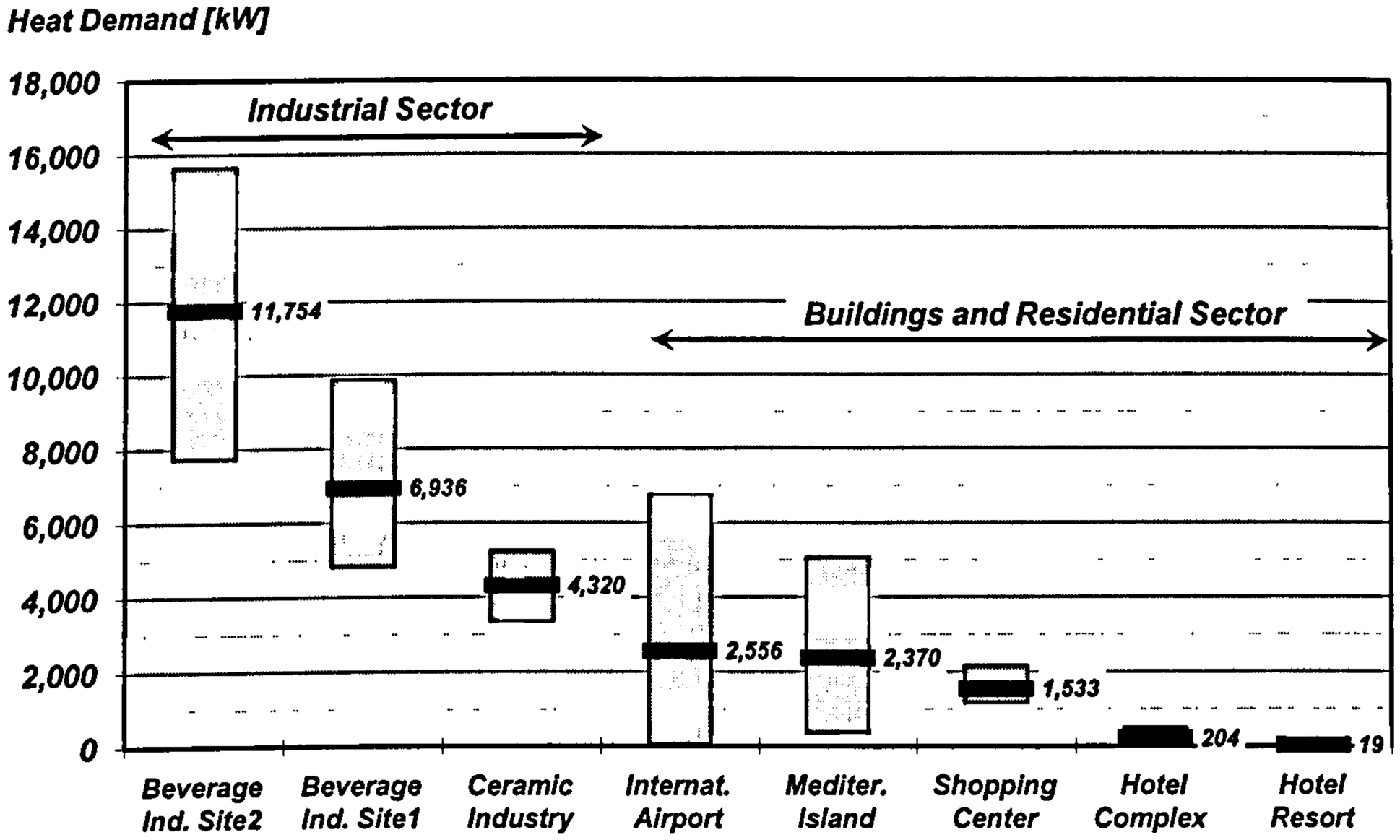

Figure 2.24 - Heat demand of the portfolio of consumers

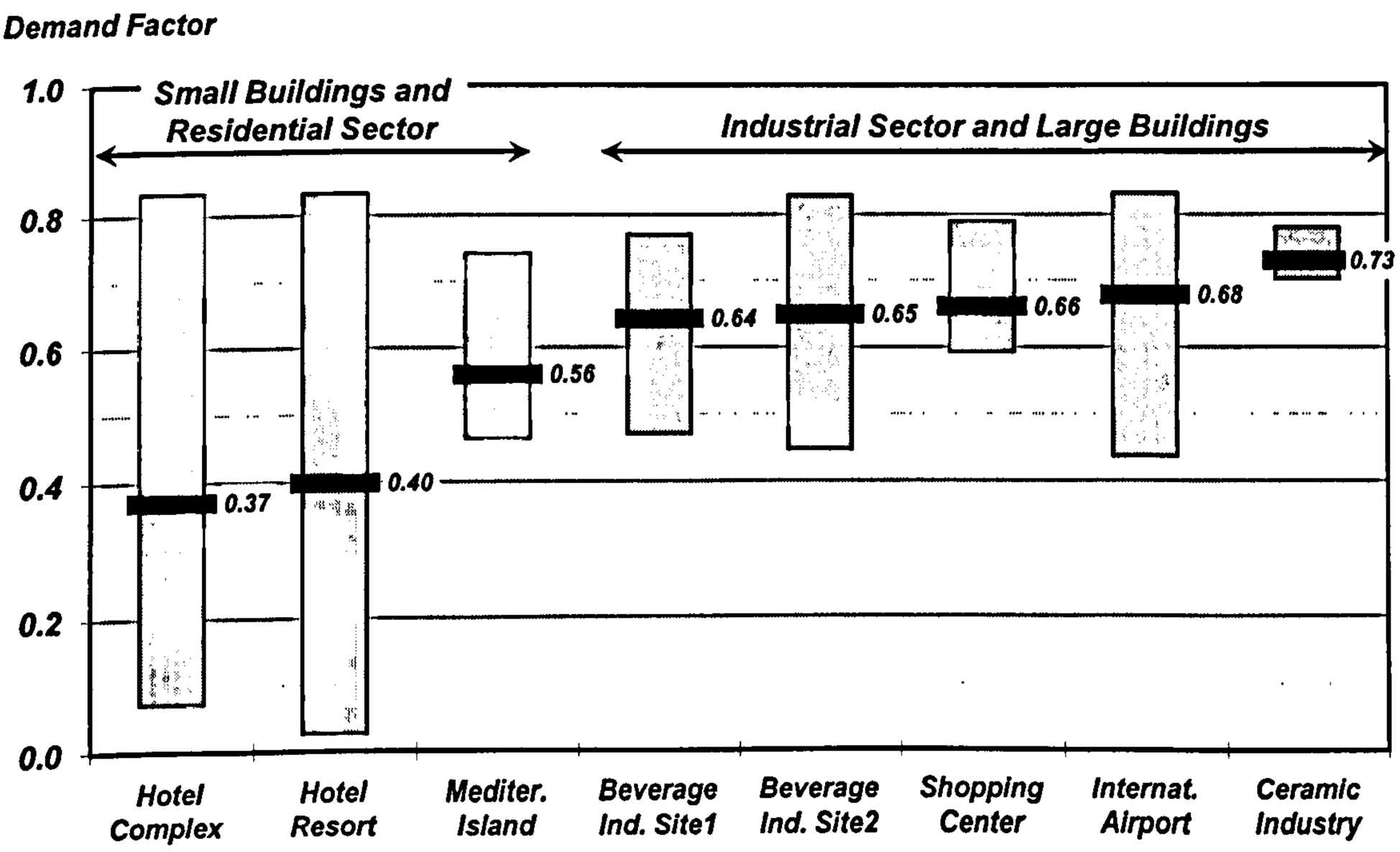

Figure 2.25 – Demand factor of the portfolio of consumers

2.12 - Selection of Gas Turbines

In this approach the power generation systems were selected with gas turbine based CHP plants using the detailed demand profiles collected for the supply of power and heat to the consumers' facilities. CHP units can operate in electricity priority mode, heat priority mode or mixed priority mode. In this study only CHP units operating in electricity priority mode were considered. That means the power demand has priority over the heat demand. Therefore the maximum power demand over the period analysed was used to select the size of the gas turbines but also taking into consideration a spinning reserve. Table 2.10 shows the size of the gas turbine selected for each unit. Turbomatch, the software developed in Cranfield University, was used to model and simulate the gas turbine design and off-design performance (Table 2.11).

The portfolio of gas turbines simulated in this study are hypothetical engines which means they do not simulate any particular engine performance but they represent the state-of-the-art gas turbines available for power generation in their respective capacity range and thermodynamic cycle. The mathematical models of these machines were validated by comparing their design point performance with the data from a range of commercial gas turbines in the respective power output capacity available (Gas Turbine World, 2005). The results of the off-design performance simulation are given in Appendix A.

Table 2.10 – Gas turbines selection matching for CHP units

	Unit	Maximum Power Demand [kW]	Gas Turbine Selected	Power Output ISO Conditions [kW]
International Airport	1	5,109	GT#2	5,300
Mediterranean Island	2	11,087	GT#1	11,690
Hotel Building Complex	3	2,446	GT#4	3,515
Ceramics Industry Park	4	3,500	GT#3	4,343
Beverage Industry - Site 1	5	4,400	GT#2	5,300
Beverage Industry - Site 2	6	8,100	GT#1	11,690
Shopping Centre	7	1,500	GT#5	1,850
Resort Hotel	8	107	GT#6	200

Table 2.11 – Gas turbines units design point performance

	GT#1	GT#2	GT#3	GT#4	GT#5	GT#6
Inlet Mass Flow [kg/s]	46.90	20.80	13.20	18.69	8.91	1.67
Compressor Pressure Ratio	15.5	13.5	18.0	12.5	9.5	5.0
Fuel Consumption [kg/s]	0.8344	0.3765	0.3356	0.2921	0.1549	0.0161
Turbine Entry Temperature [K]	1,288	1,276	1,290	1,184	1,200	1,203
Exhaust Total Temperature [K]	755	761	793	730	776	565
Shaft Power [kW]	11,690	5,300	4,343	3,515	1,850	200
Thermal Efficiency	0.325	0.326	0.300	0.279	0.277	0.288
Shaft Power Cycle	SC	SC	SC	SC	SC	RC

SC: Simple Cycle
RC: Regenerative Cycle

Chapter 3 – Gas Turbine Portfolio: Performance and Diagnostic

3 - Gas Turbine Portfolio: Performance and Diagnostic

3.1 - Introduction

Distributed power generation is receiving a great amount of attention throughout the world. This increased interest is attributed to the deregulation of electrical power industries which has led to increased competition and interest in the various technologies suitable for distributed power generation. Small gas turbines, also called micro gas turbines, are therefore emerging as an excellent option for such systems. Since the application of such technologies in the energy market, many studies have been carried out on design improvements of mechanical and electrical components, and economic assessment (Gomes et al., 2003; Gomes et al., 2004; Wang, et al., 2004). However, relatively less information is available on health monitoring and the diagnostics performance of such machines.

A high competitive energy market demands reductions in operation and maintenance costs as well as improvements in engine availability and reliability. In order to achieve such profitability and availability the right maintenance strategy needs to be implemented. In this investigation the maintenance strategy will be implemented through monitoring the gas turbine's health, diagnosing engine faults, predicting the turbine's lifetime and scheduling corrective actions.

The scope of the investigation in this section includes the performance, health monitoring and diagnostic assessment of a portfolio of gas turbines in the following configuration: simple cycle, regenerative cycle, one shaft with and without power turbine. Different techniques are available for gas turbine health monitoring and diagnostics: vibration monitoring, oil analysis, visual inspection, gas path analysis (GPA), and others. GPA is one of the most promising diagnostic techniques. The gas turbine health monitoring will be carried out with an engine performance simulation system obtaining engine measurement information through instrumentation and then the diagnostic investigation will be carried out with gas path analysis.

The question that can be raised from the maintenance strategy described before is that for a portfolio of gas turbines what is the optimum instrumentation set that thermodynamically correlates with the typical faults expected. Different single and multiple gas path faults can be observed in gas turbines, therefore knowledge of the appropriate set of sensors is indispensable to predict an engine's health.

This approach aims to identify the optimum set of instruments that can be used to diagnose single and multiple faults of engines. The relationship between measurements and component parameters is highly non-linear therefore appropriate estimation techniques have to be used. For a given set of sensors, some faults will be easier to identify than others so an instrumentation set should be properly chosen to detect the faults which are of interest. If a large number of performance parameters need to be evaluated, the cost of sensors may be a concern. In addition, the diagnostic system needs to be able to deal with noisy measurement.

In this study the software Turbomatch and Pythia, developed at Cranfield University, was used to simulate the gas turbine performance and carry out the diagnostic analysis respectively. It is a validated gas turbine gas path analysis software able to satisfy the requirements described above and provide the required engine health information for further analysis and decision making.

3.2 - Gas turbine for power generation

Gas turbines can be classified into three different power output ranges as follows: small, medium or large gas turbines.

Small turbines are those with a nominal power output lower them 1MW. Although their design is similar to the large gas turbines, some units have a centrifugal compressor or a combination of centrifugal and axial compressor and a radial turbine. Usually the engine components are: one stage centrifugal compressor with pressure ratio about 4:1, single combustor chamber with maximum temperature about 1200K and one stage radial turbine. Thermal efficiency is usually lower than large units due to the lower turbine inlet temperature and lower component efficiency. Because of the robustness and simple design they used to be able to run for several hours without outage. Some of them are designed in regenerative cycle (Figure 3.2) to improve

efficiency, as is discussed below. Most of them are available in a single shaft without free turbine (Figure 3.3) configuration but units with free turbine are also found in the market. Micro gas turbines are classified in this category, as their typical power output range is from 20 to 300kW. These machines have been conquering their space in the power market in the last few years. They have a large range of applications, mainly in the tertiary sector of industry (shopping centres, hotels, hospitals, airports), but also in landfill systems, airplanes (auxiliary power units), automobiles (turbochargers).

Medium gas turbines are those with nominal power output from 1 to 15MW. They can be divided into two categories from the design point of view: heavy duty (industrial stationary) or aero-derivative gas turbines. They can be found in both a single and two shaft configuration. Two shaft engines are more efficient in partial load as the gas generator can run at the optimal rotational speed mechanically independent of the free turbine generator shaft. The compressor is usually a subsonic 10-16 stages axial compressor with pressure ratio from 5 to 11:1. The gas generator turbine usually has 2 or 3 axial stages with cooling passages in the first stage. They have a large range of applications mainly in medium-large sized industries. The exhaust gases can be recovered in steam cycles (cogeneration or combine cycle power plants) producing higher total cycle efficiency.

Large gas turbines are those able to produce power higher than 15MW. They can also be classified in heavy duty aero-derivative gas turbines. The compressor and turbine are predominantly axial multi-stages and they have applications mainly in central power stations in both combined cycle and cogeneration system.

The basic work principle of open cycle gas turbines is given by the Joule-Brayton cycle, illustrated in Figure 3.1. The work fluid pressure is increased in the compressor and then in the combustor it increases its temperature through the combustion of the fuel injected. Then it is expanded in the turbine where its pressure decreases and disperses to the atmosphere. The turbine supplies power to the compressor and to the load mechanically connected, in this case a generator.

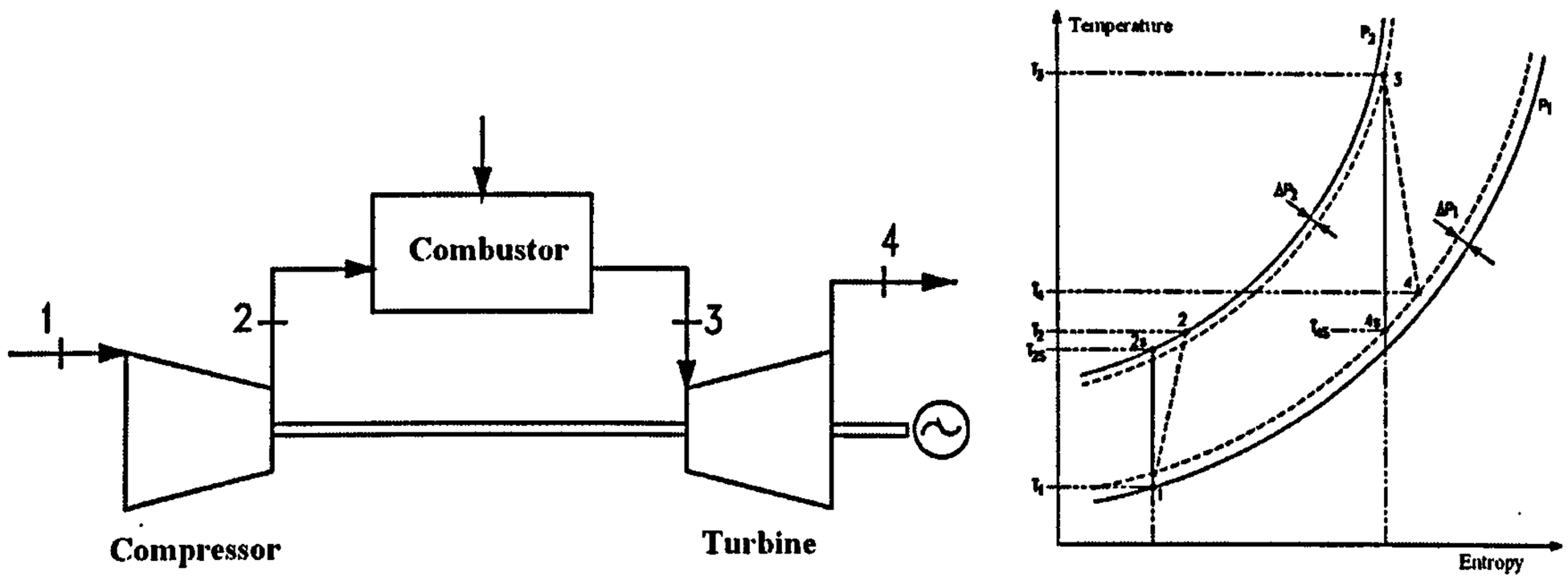

(a) (b)

Figure 3.1 - Gas turbine in simple cycle: (a) components scheme (b) T-S diagram

In the regenerative cycle (Figure 3.2), the air is pre-heated before being injected into the combustor by the turbine exhaust gases. This allows the engine to reduce the fuel consumption and then improve the thermal efficiency in both full and partial load operation.

A gas turbine can have different design configurations and components in order to improve the useful power output and thermal efficiency. Between the possible design configurations are: multiple compressor/turbine stages, intercooler between compressor stages, additional combustors chamber, heat exchangers (recuperators), and others. Also the number of shafts can change as discussed before. Figure 3.3 shows the configuration and characteristics of single and two shaft gas turbines, with and without free turbine.

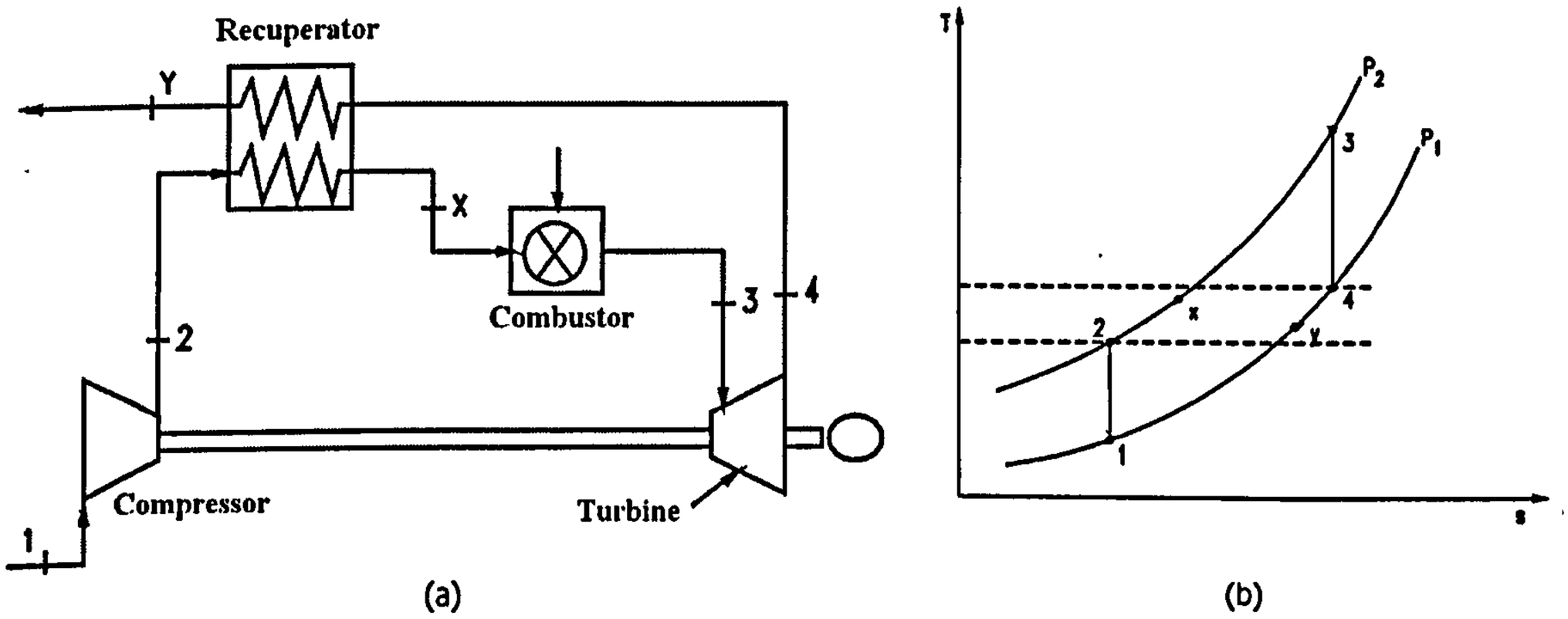

(a) (b)

Figure 3.2 – Regenerative gas turbine cycle: (a) components scheme (b) T-S diagram

	One Shaft	Two Shafts
Without Free Turbine	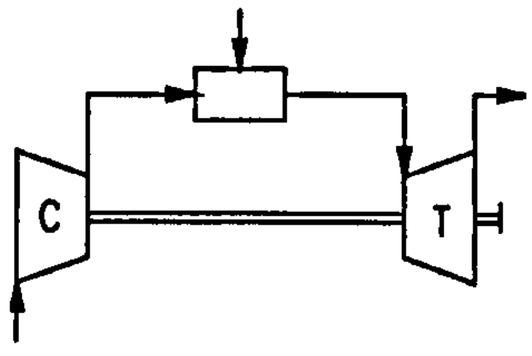 Constant speed and load operation. Typically for power generation applications.	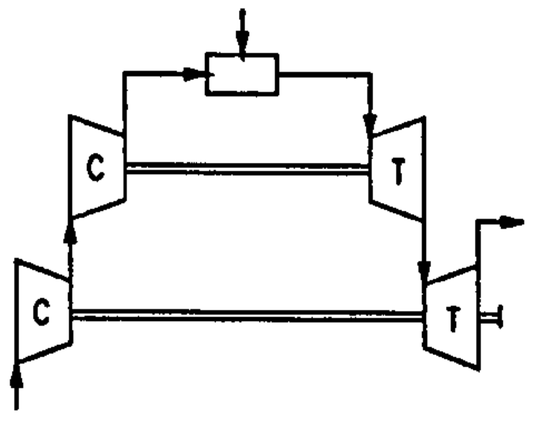 Higher pressure ratio and improved efficiency. Compressor (C) and turbine (T) divided in multi-stages.
With Free Turbine	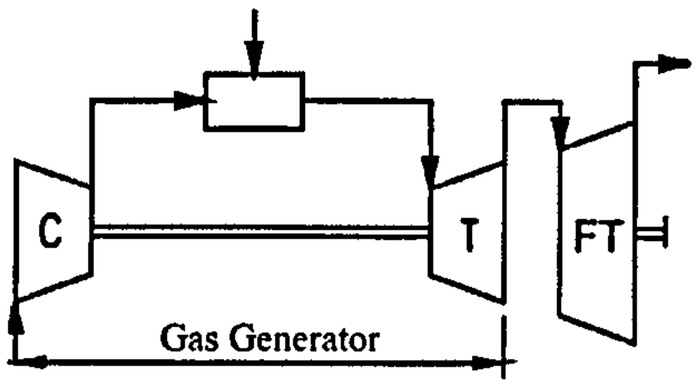 GG is mechanically independent of free turbine. Industrial (mechanical drive and power generation) and aeronautical applications.	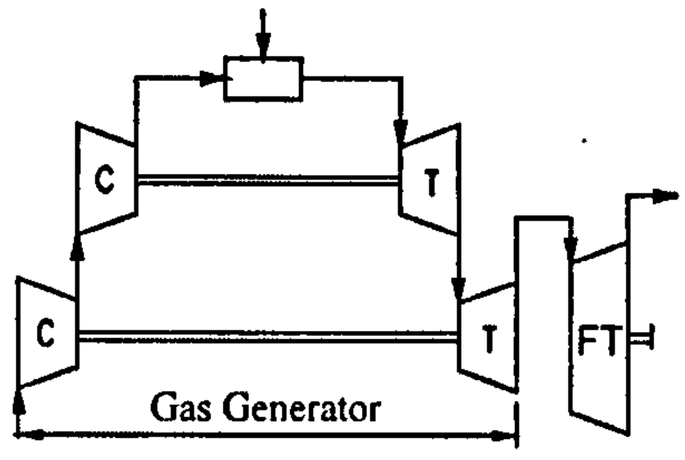 Typical of aeronautic engines in which the free turbine (FT) is replaced by a nozzle.

Figure 3.3 – Gas turbine shaft configuration (Nascimento et al., 2004)

Traditionally, gas turbines driving electrical generators run at a constant rotational speed. The equilibrium lines for these loads correspond to a particular line of constant non-dimensional speed as shown in Figure 3.4.

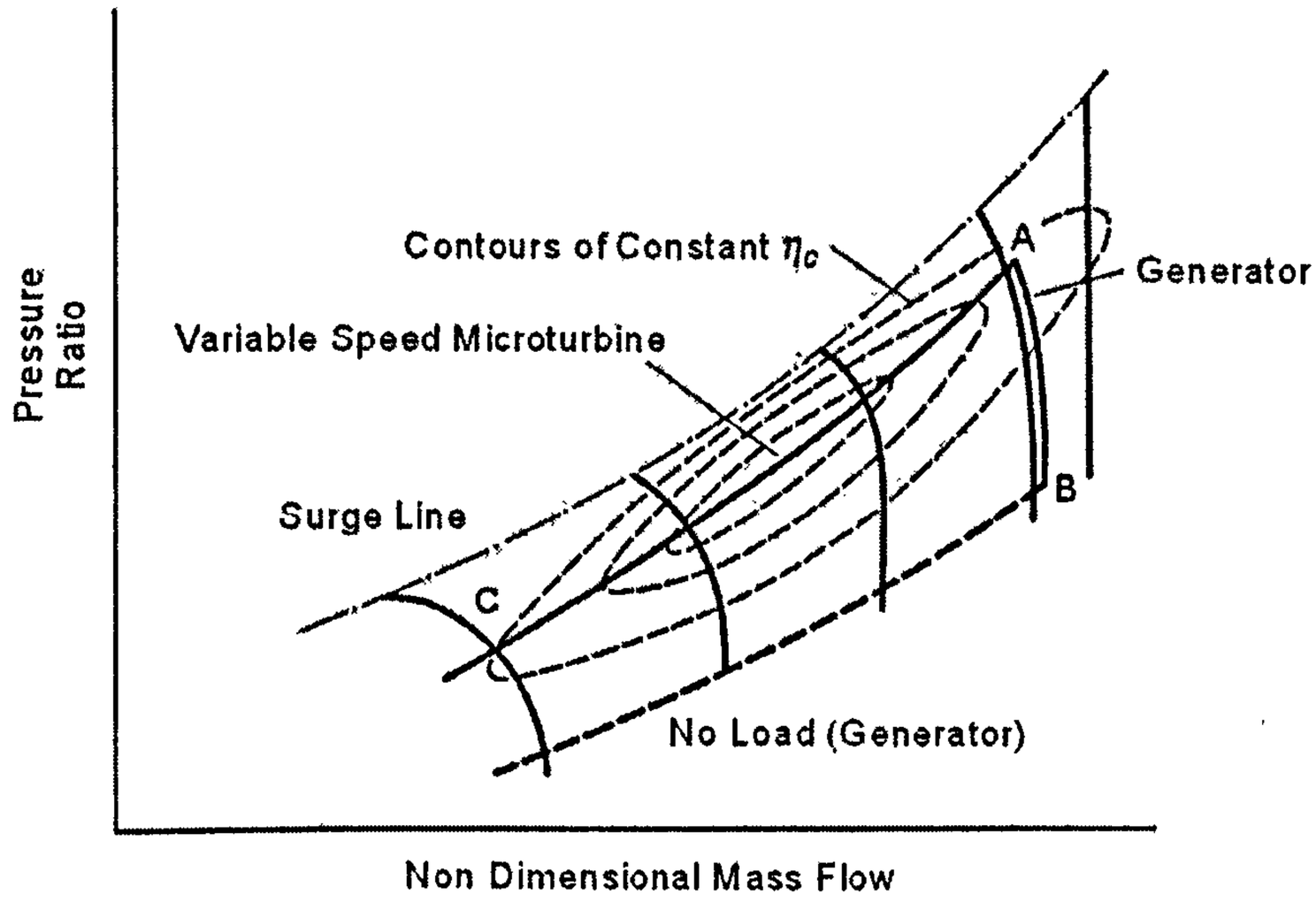

Figure 3.4 – Equilibrium running lines for constant speed and variable speed operation

Looking at the equilibrium running line for the generator (line A to B), each point on the line represents a different value of mass flow, fuel consumption, turbine entry temperature and power output. It can be seen that the equilibrium running line of the generator shows a sudden reduction in compressor efficiency as the load is reduced. In a gas turbine operating at constant speed, when the load changes the generating gas turbine still runs at the design rotational speed, which results in lower part load efficiency.

However, in a variable speed operation (line A to C), the equilibrium running line crosses different constant non-dimensional speed lines and higher compressor efficiency can therefore be maintained. The device that achieves this constant speed operation for the gas turbine is called a 'governor'. A governor is a speed-sensing device driven by the engine itself or by some mechanical equipment, such as a gearbox if the engine is connected with one. It actuates directly, or through an amplifier, in the fuel control of the engine. The ideal description of its operation is this: when the engine load increases, its speed momentarily drops; this is sensed by the governor, which causes the fuel admitted to the engine to be increased. This in turn increases the engine's torque and raises the speed against the new load until the equilibrium level is recovered. The electrical generator is the component which dictates whether the gas

turbine is operated at a variable or constant speed. The recent development of permanent magnet generators and electric power inverters make the variable speed operation a real design option for gas turbines in power generation applications. However, despite the current electrical engineering developments these electrical devices are only available in small capacity sizes (Rodgers et al., 2001).

The fundamental difference between constant speed and variable speed operation can be seen in Figure 3.5. It shows that gas turbines operating at constant speed do not produce any output power until they are running almost at full speed. On the other hand, variable speed engines begin to produce power at a lower rotational speed level.

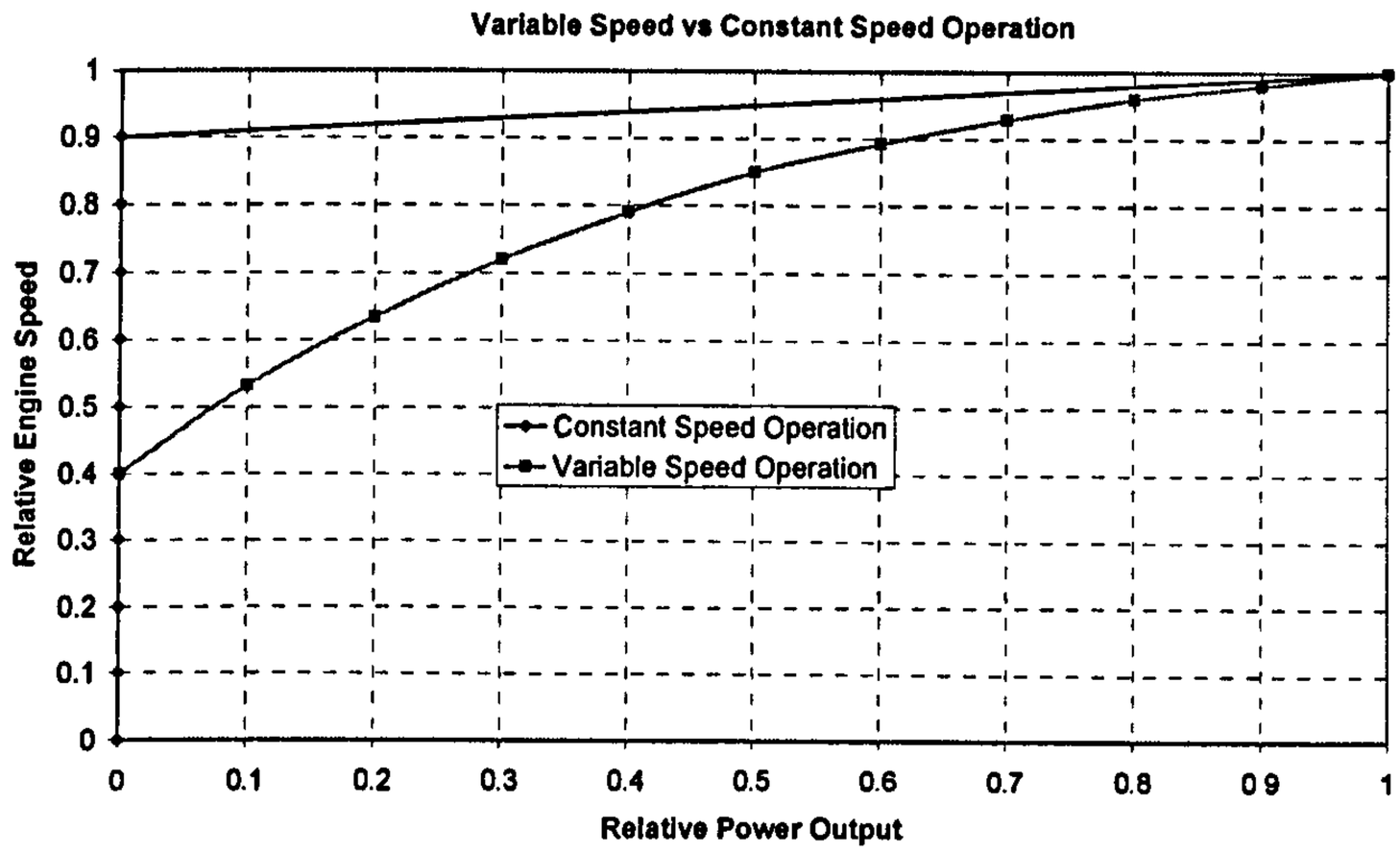

Figure 3.5 – Variable Speed versus Constant Speed Operation (Gomes et al., 2004)

The variable speed capability, together with the regenerative cycle advantages, gives a better performance at part load. In this investigation the degree of variation between the electrical generator power output and the gas generator rotational speed is given by a power law index of 4.8 risen experimentally. This index determines how the speed of the turbine varies with the load (Figure 3.6).

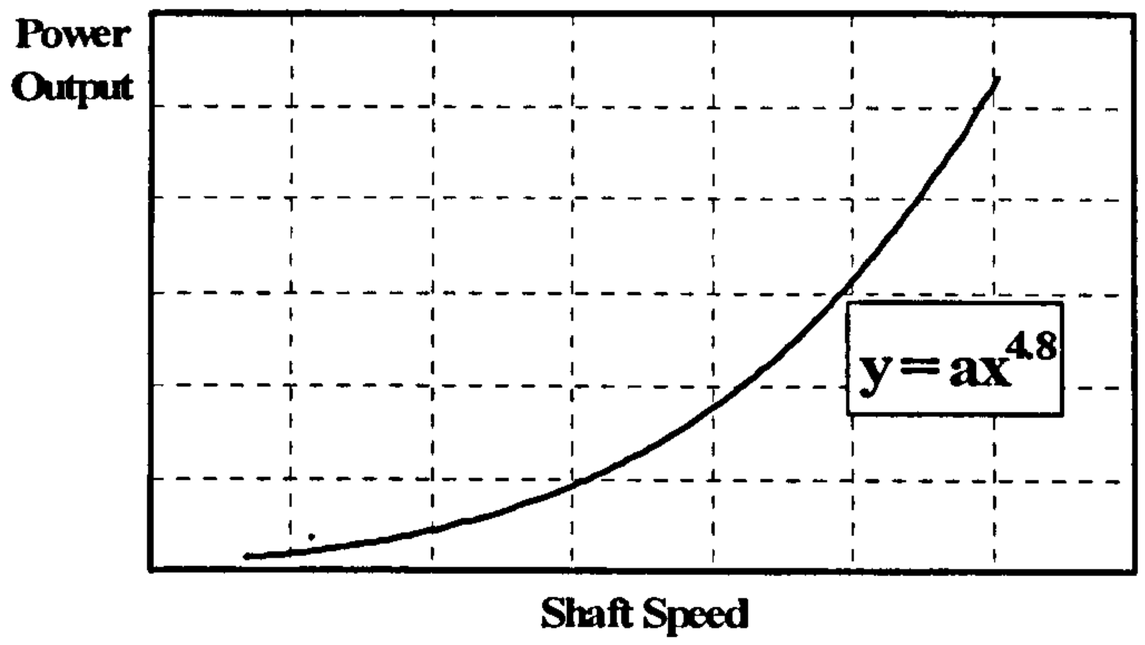

Figure 3.6 – Power law index of variable speed micro gas turbine

Figures 3.7 to 3.13 show the typical performance and financial data of current gas turbines available commercially. Heat to power ratio (HPR) is found between 1.3 and 2.9 (Figure 3.7). However, a higher HPR is possible despite some design constraints in the heat recovery system. Electrical efficiency of the regenerative cycle and combined heat and power systems is significantly higher as mentioned before (Figure 3.8). The engines analysed in this study do not include blade cooling systems, therefore the turbine inlet temperature is limited to around 1200K due to material restrictions (Figure 3.9). Mass flow is directly proportional to the power output as illustrated in Figure 3.10.

As a consequence of the higher efficiency improvements of the regenerative cycle, the gas turbine exhaust temperature is significantly lower than a simple cycle (Figure 3.11). Usually regenerative gas turbines are not appropriate to combine heat and power systems due to the relatively low exhaust temperature available for heat recovery and consequent low steam flow temperature for process. However, in micro-CHP (capacity between 20–300kW$_e$) applications, the temperature of the heat required for process application is not high; in fact, in many cases the heat is produced as hot saturated water with no need of steam production. The regenerative cycle can then be used with the advantage of higher electrical efficiency. Investment prices drop with power output and depend on the thermodynamic cycle, as in the regenerative cycle the recuperator can increase the engine cost by up to 30% in small units (Rodgers et al., 2001). Further information on gas turbine performance can be found in Pilidis, 2005.

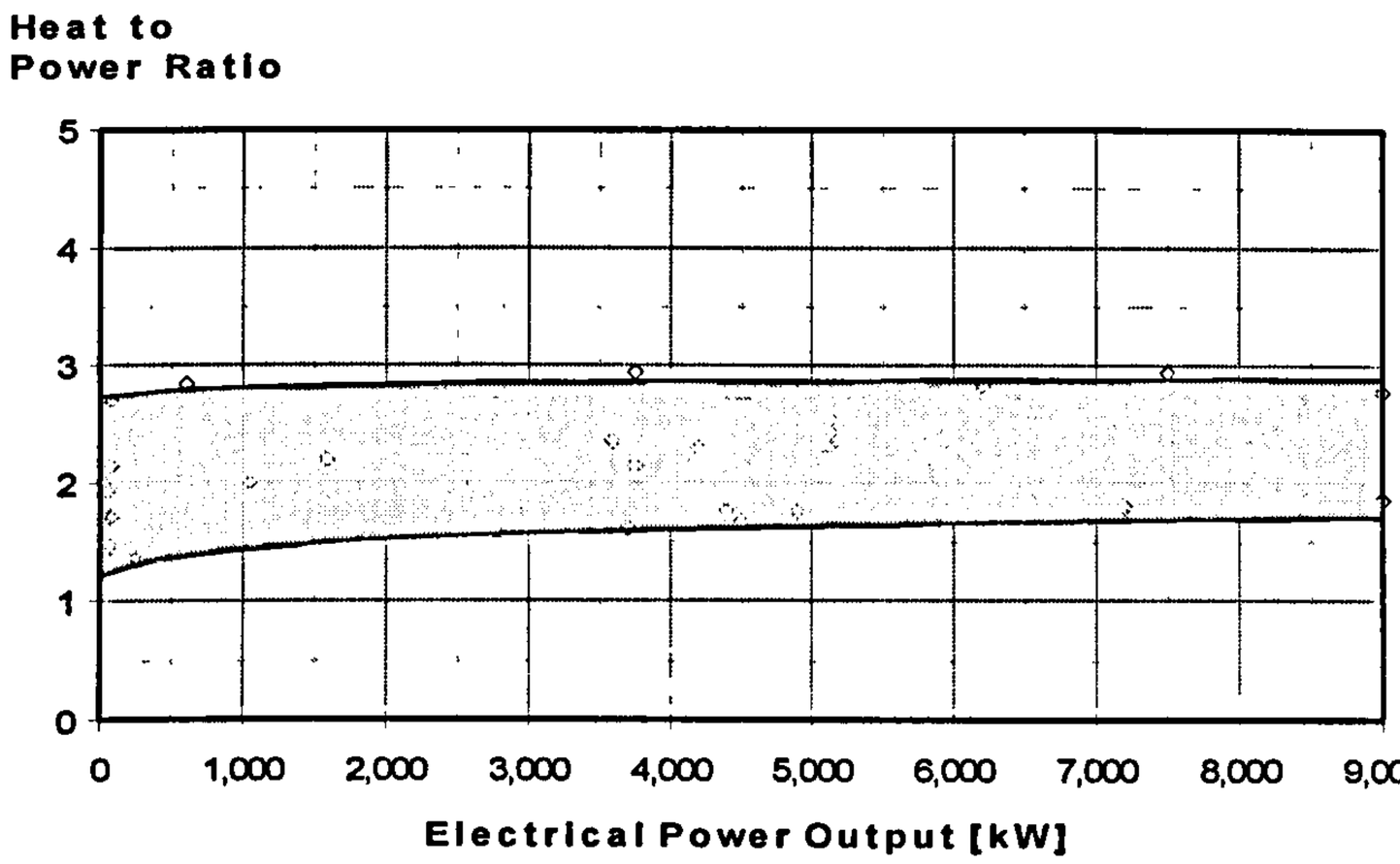

Figure 3.7 – Typical heat to power ratio of commercial gas turbines (Gas Turbine World, 2005)

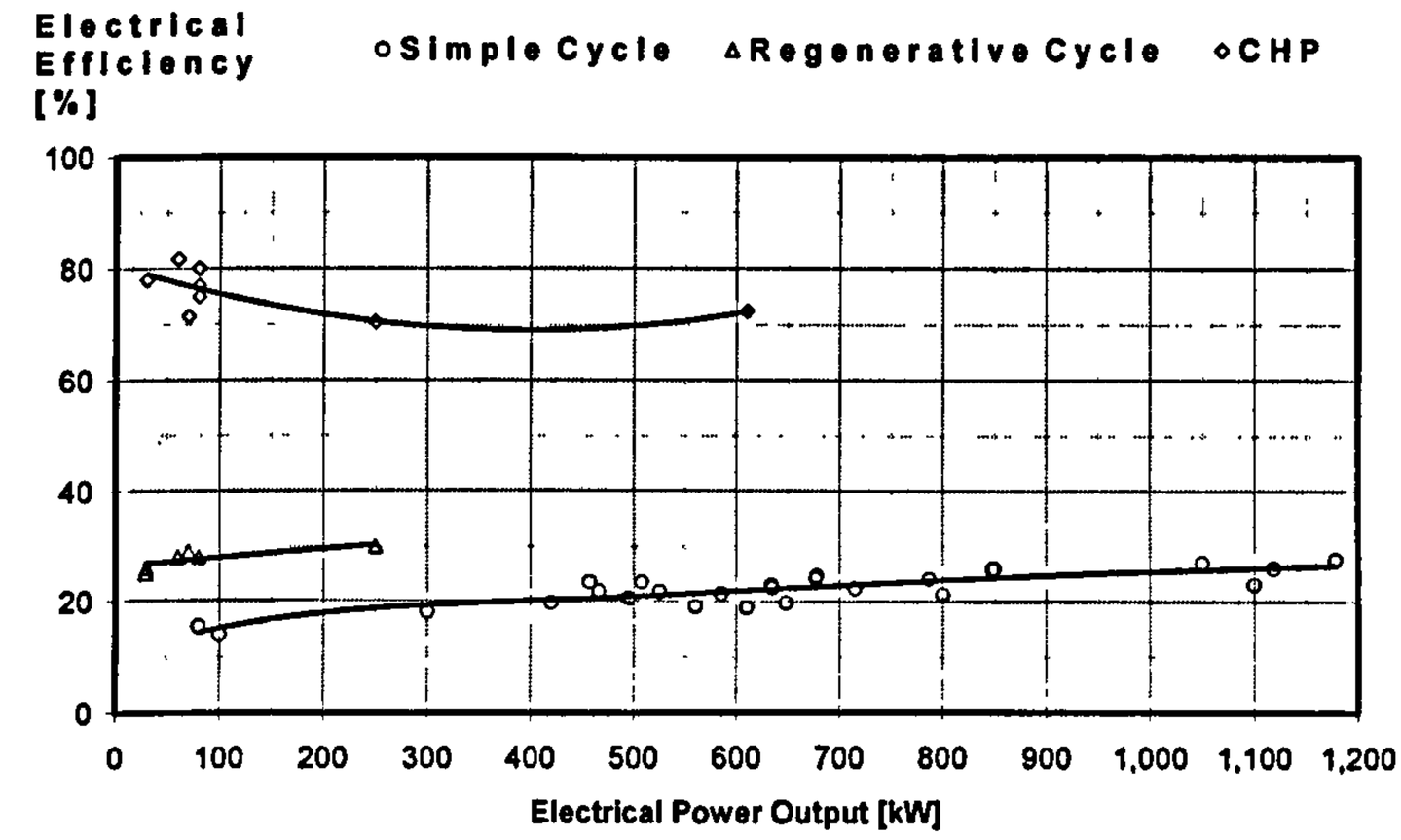

Figure 3.8 – Typical electrical efficiency of commercial gas turbines (Gas Turbine World, 2005)

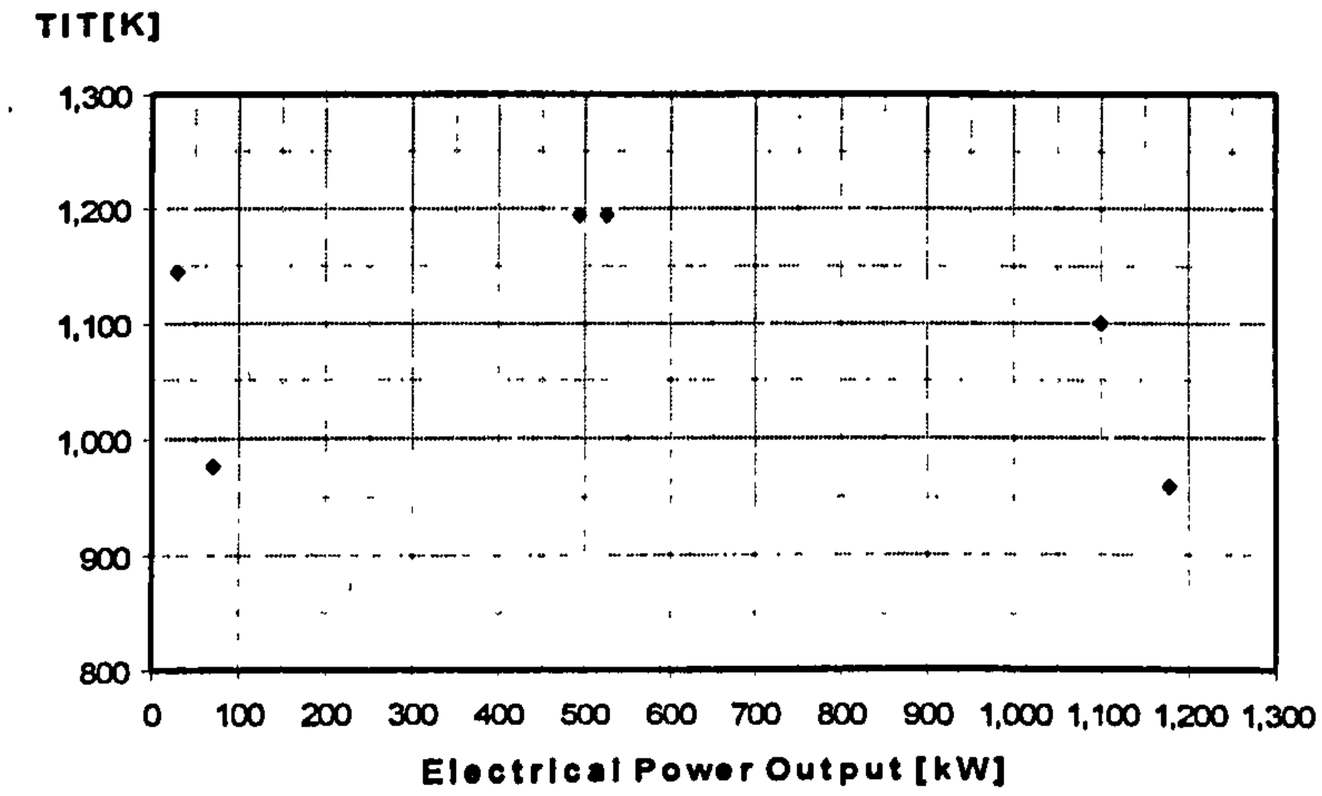

Figure 3.9 – Typical turbine inlet temperature of commercial gas turbines (Gas Turbine World, 2005)

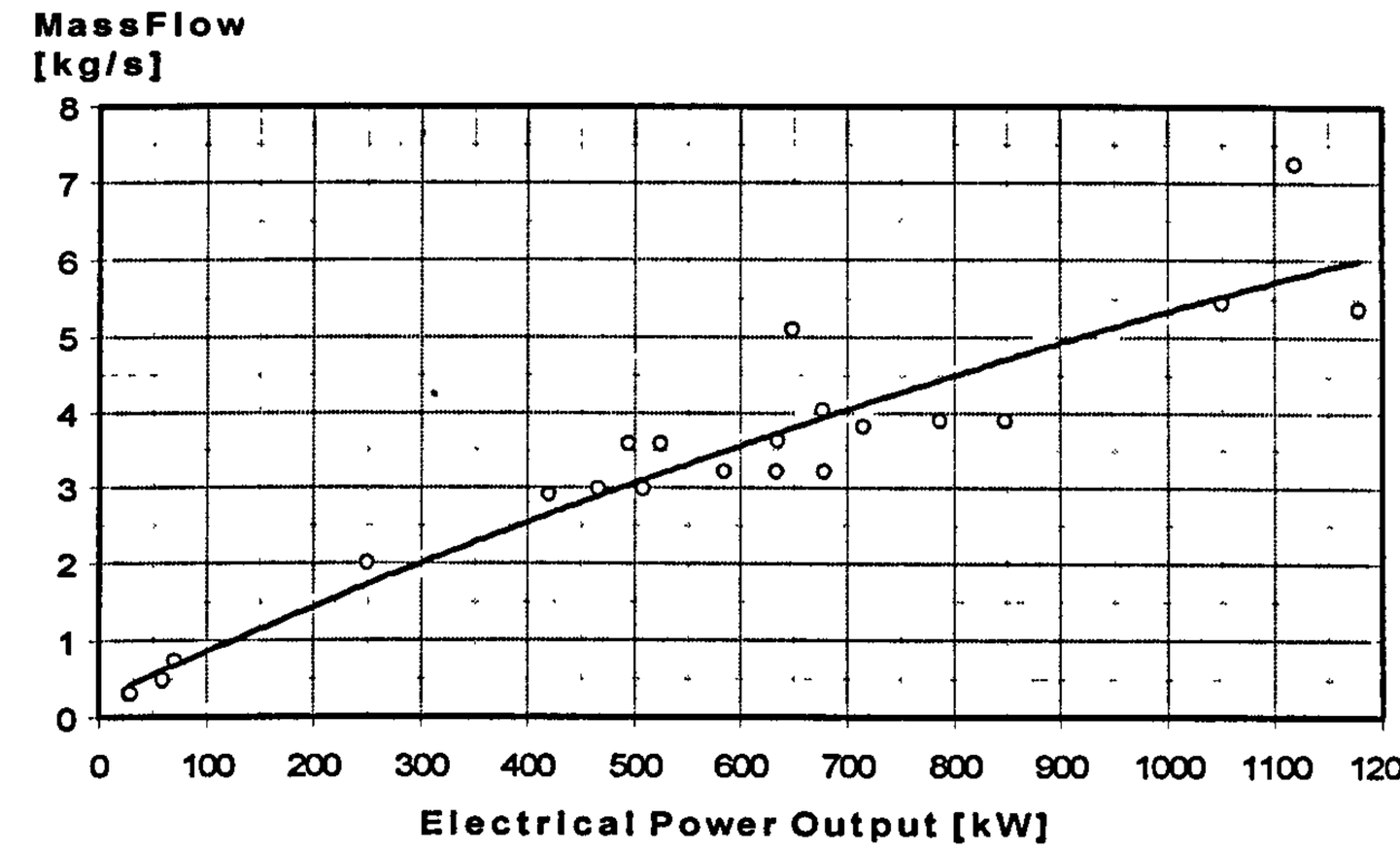

Figure 3.10 – Typical mass flow of commercial gas turbines (Gas Turbine World, 2005)

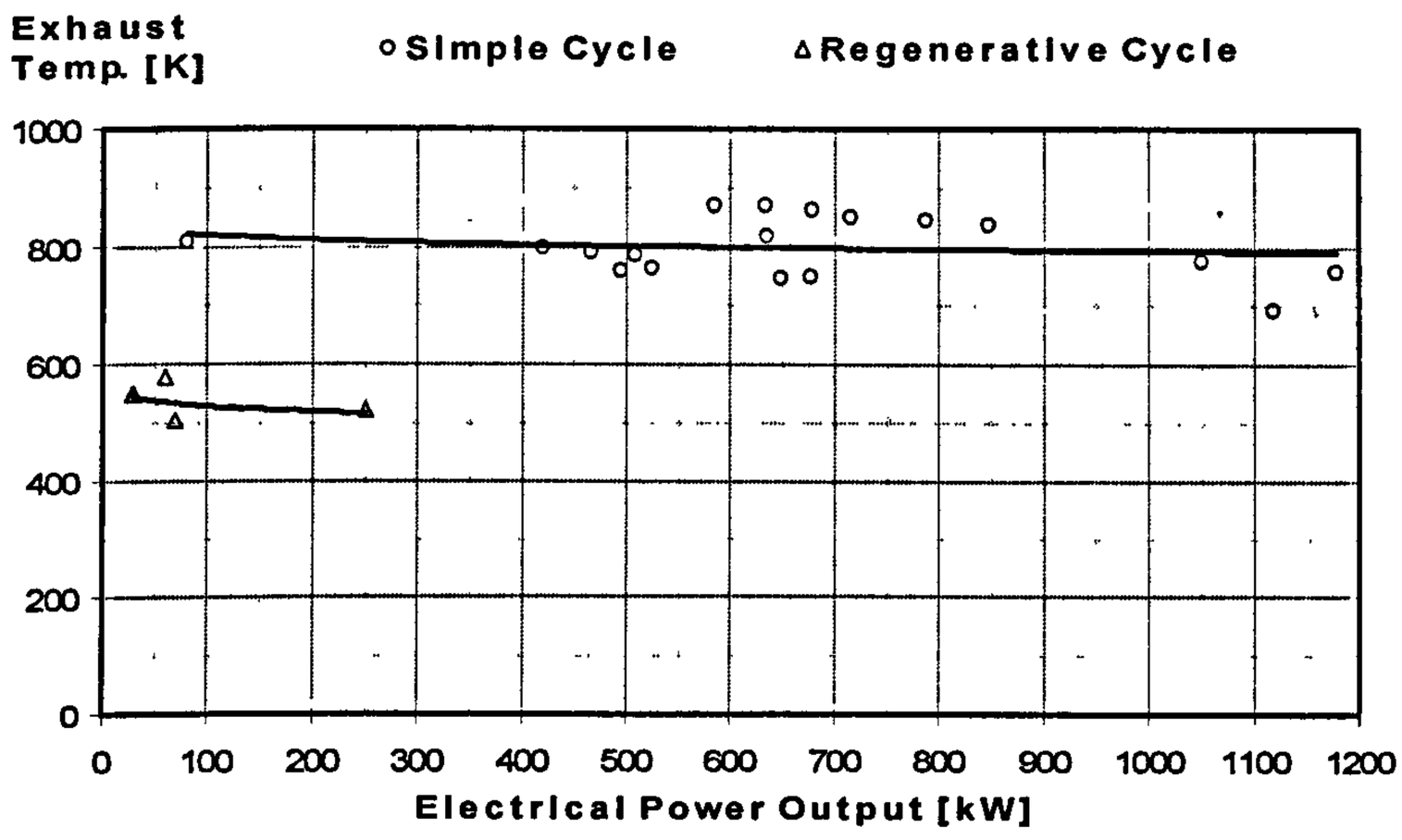

Figure 3.11 – Typical exhaust temperature of commercial gas turbines (Gas Turbine World, 2005)

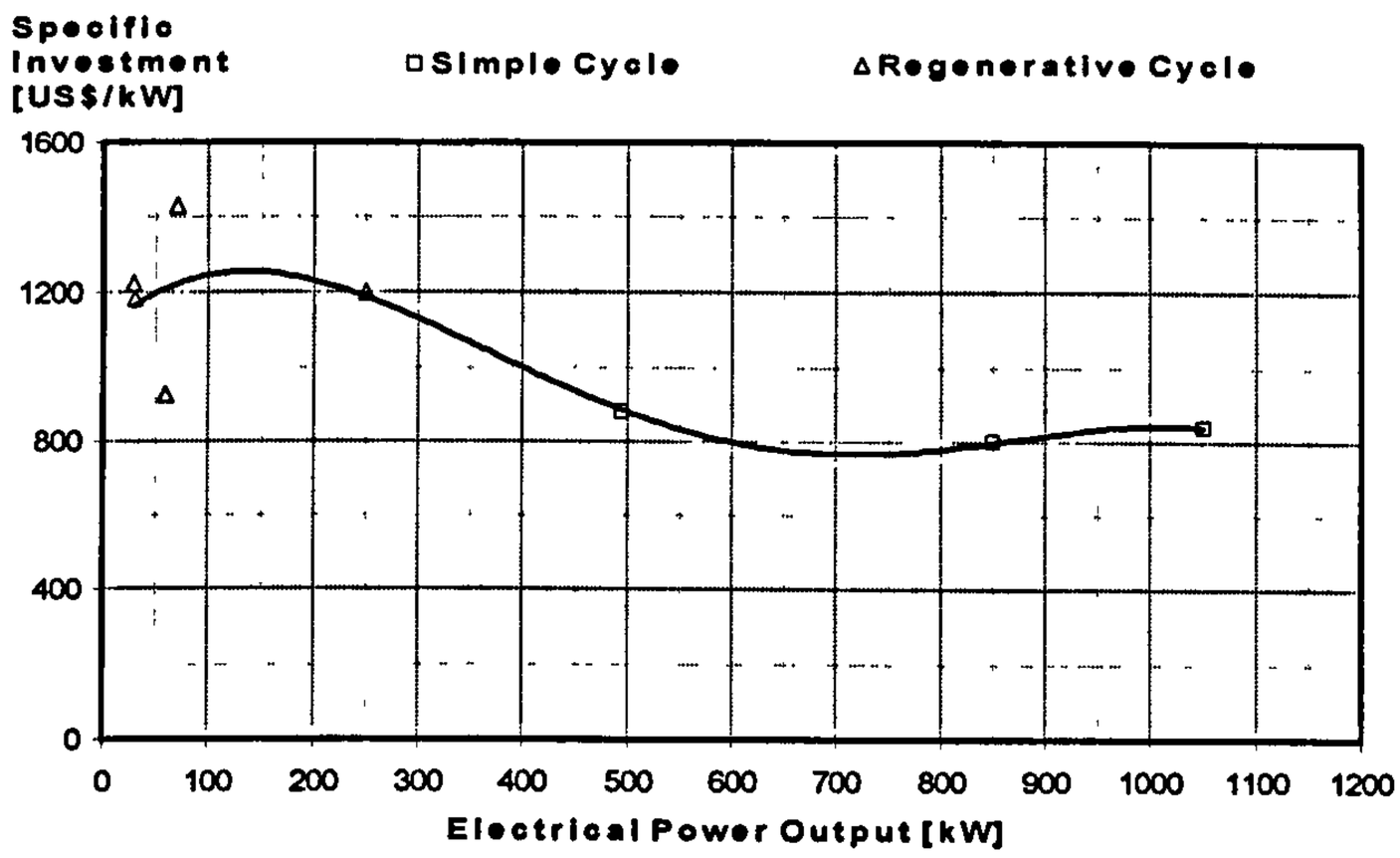

Figure 3.12 – Typical investment price of small commercial gas turbines (Gas Turbine World, 2005)

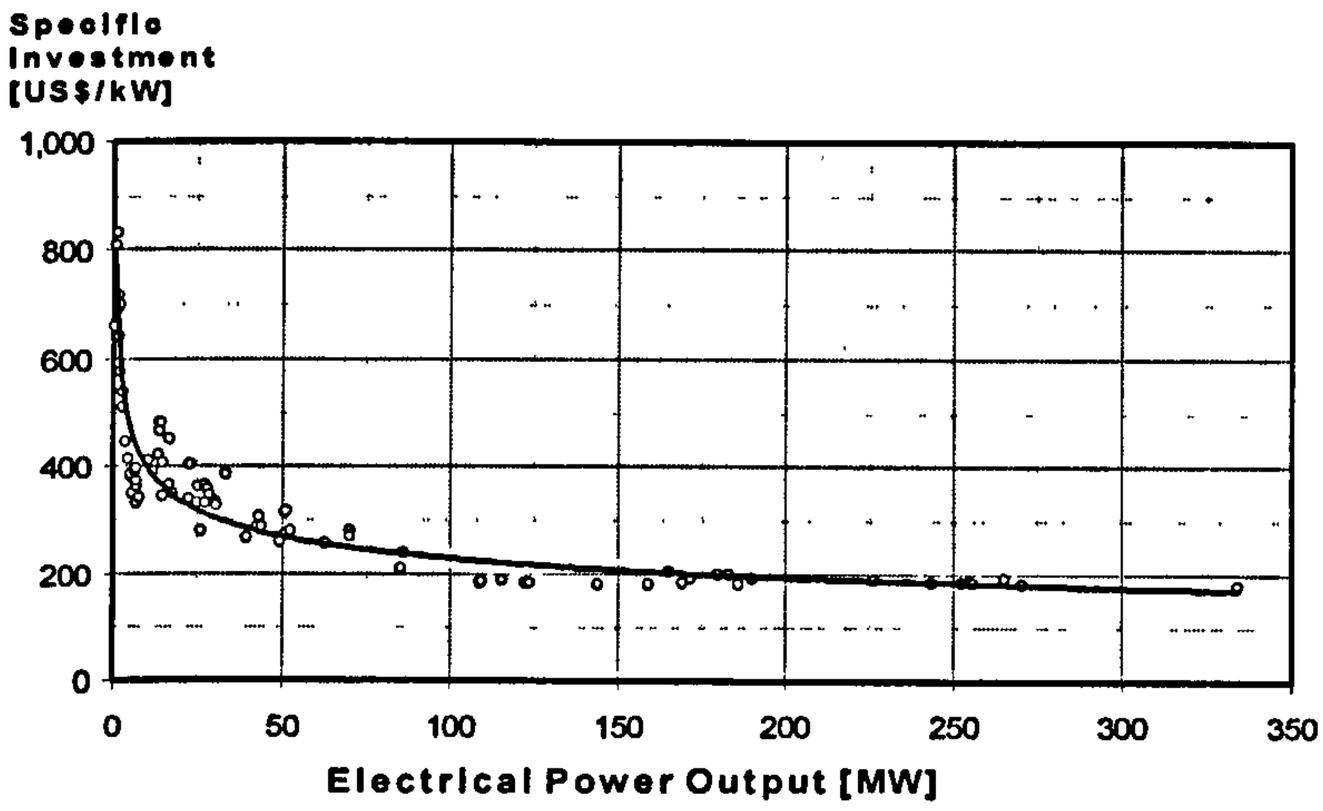

Figure 3.13 – Typical investment price of large commercial gas turbines (Gas Turbine World, 2005)

3.3 - Clean Engine Performance

This section presents a portfolio of gas turbines cycles that were investigated in this study. Typically, gas turbines for small-medium distributed generation systems are commercially available in a simple or regenerative thermodynamic cycle, constant or variable speed operation and with or without free turbine configuration.

The design point of any gas turbine is the particular point in the operating range when the engine is running at the particular speed, pressure ratio and mass flow for which the engine components were designed. The design point performance results of each engine provide the baseline to which the off design performance and degraded engine is compared.

Table 3.1 shows the design point performance of the portfolio of gas turbine models (GTMs) investigated in this study. For each engine model a code was written and simulated in the Turbomatch/Pythia software. The models do not represent any specific engine available commercially but they are hypothetical engines validated by the performance data presented previously. The pressure ratio, compressor and turbine isentropic efficiency were chosen based on the information presented by Boyce, 1982. The turbine entry temperature is the handle parameter and the electrical efficiency is the target parameter.

Table 3.1 – Design point performance of the gas turbine models

	GTM#1	GTM#2	GTM#3	GTM#4	GTM#5
Inlet Mass Flow [kg/s]	0.24	0.24	0.31	0.31	0.95
Compressure Pressure Ratio	4.0	4.0	4.0	4.0	4.0
Compressor Isentropic Efficiency	0.78	0.78	0.78	0.78	0.78
Fuel Consumption [kg/s]	0.0048	0.0048	0.0027	0.0027	0.0193
Turbine Entry Temperature [K]	1203	1203	1203	1203	1200
Turbine Isentropic Efficiency	0.80	0.80	0.80	0.80	0.80
Exhaust Total Temperature [K]	951	951	548	548	944
Electrical Power [kW]	29	29	29	29	120
Electrical Efficiency	0.141	0.141	0.252	0.252	0.145
Shaft Power Cycle	SC	SC	RC	RC	SC-FT
Regime of Operation	CS	VS	CS	VS	CS

SC: Simple Cycle
RC: Regenerative Cycle
FT: Free Turbine
CS: Constant Speed
VS: Variable Speed

3.4 - Deteriorated Engine Performance

Every gas turbine's performance deteriorates during operation due to degradation of the gas path components. This deterioration adversely affects the operation of the system. Understandings of the mechanisms that cause degradation, as well as the effects that the degradation of certain components can cause for the overall system are a matter of interest. Whilst various work has been performed on the degradation of large gas turbines (Zwebek and Pilidis, 2003; Kurz and Brun, 2001; Lakshmin et al., 1994), little work has been performed on the degradation of small gas

turbines. Tarabrin (1998), points that small gas turbines are more susceptible to degradation which is in contradiction with the conclusions of Aker and Saravanamuttoo (1988).

3.5 - Degradation Mechanisms

A brief introduction to the types and mechanisms of degradation are presented in this section. A comprehensive description of gas turbine degradation can be found in Li, 2002; Zwebek and Pilidis, 2003; Kurz and Brun, 2001; Lakshmin et al., 1994; Diakunchak, 1992. Several mechanisms can cause the degradation of engines. Different types of degradation include fouling, erosion, corrosion and foreign object damage.

Fouling – Fouling can be defined as the degradation of flow capacity and efficiency caused by the adherence of particular contaminants to the gas turbine airfoil and annulus surfaces. The result is a build up of material that causes increased surface roughness and to some degree changes the shape of the airfoil. Even with good filtration systems, particles will get through and be deposited on the blades. Typically, flow capacity is reduced by 3-8% and efficiency by 1% depending on the severity of the fouling. Fouling can normally be eliminated by cleaning. Fouling can occur in both the compressor and turbine. However, it is generally accepted that compressor fouling is the more common cause of performance deterioration. Turbine fouling is less likely and is largely dependent on the fuel used.

Erosion – Erosion can be defined as the abrasive removal of material from the flow path by particles impinging on the flow surfaces. Erosion of engine components causes blunting of aerofoil leading edges, thinning of trailing edges and increased surface roughness. The result of these is increased losses and thus performance deterioration. Occasionally, reduced trailing edge thickness may be beneficial to performance but unacceptable with regard to mechanical integrity considerations. Erosion is probably more of a problem for aero engine applications. This is because the filtration systems used for industrial engines will typically eliminate the bulk of the larger particles. Particles causing erosion are usually $20\mu m$ or more in diameter. In compressors, erosion increases pressure loss and decreases flow capacity and efficiency. In turbines, it increases the flow capacity and decreases the efficiency. Typically, flow

capacity for the turbine may be increased by 2% and the efficiency decreased by 1%. Unlike fouling, erosion cannot be recovered by washing but it can be restored through repair or replacement of the components.

Corrosion – Corrosion is the loss of material from flow path components caused by the chemical reaction between these components and contaminants that enter the gas turbine with the inlet air, fuel or in some cases injected water/steam. Corrosion usually results in surface roughness. Typically, compressor corrosion results in a reduction of the compressor flow capacity and isentropic efficiency. Turbine corrosion results in an increase in turbine effective area/flow capacity and a reduction in isentropic efficiency.

Foreign object damage (FOD) – Damage is often caused by foreign objects striking the flow path components. These objects may enter the engine with the inlet air or are the result of broken off pieces of the engine itself. The effect of foreign object damage (FOD) and domestic object damage (DOD) on performance degradation varies significantly with the severity of the damage. They result in flow path changes through the compressors and turbine and also alter the surface roughness. These can combine to reduce the flow capacity and efficiency. The risk of FOD is reduced for industrial gas turbines because of the use of air filtration at the inlet.

3.6 - Detection of degradation

The degradation of the gas path components results in changes in the gas turbine component's efficiency and flow capacity which produces observable variations in parameters such as temperature, pressure, rotational speeds, and fuel flow rate from their baseline clean engine performance. The degraded performance reflected from these measurements can be used to detect, isolate, and accommodate component faults. Such relationships were described by Urban, 1972.

Detection of any component degradation is a prerequisite before appropriate actions can be taken to restore a performance deficit. In an attempt to have high engine reliability and availability, gas turbine maintenance has been moving away from the preventative type to reliability centred maintenance based on engine health monitoring (condition monitoring) and fault diagnostics. An element of this investigation is to

simulate component degradations to determine the effect on the gas turbine performance. Once this is achieved optimal instrumentation sets sensitive to the implanted faults are required.

Condition monitoring provides a gas turbine operator with the information needed to carry out a condition-based maintenance programme, as opposed to the standard preventive maintenance programme. By scheduling major maintenance activities based on the actual condition of the machine, an operator may be able to stretch out the interval between overhauls. This translates directly into lower maintenance costs. This investigation is also merited based on the fact that there is a lack of information on small gas turbine degradation, health monitoring and diagnostics. Although gas turbines have relatively long maintenance intervals, improvements are possible if a substantial degradation and fault database were available.

3.7 - Degradation Modelling

In an attempt to cover a range of faults that may occur in a gas turbine it was first assumed that each component may degrade individually, and then the components were assumed to degrade together. The faults investigated are: compressor degradation, compressor isentropic efficiency degradation, turbine fouling, turbine erosion, turbine isentropic efficiency degradation, compressor and turbine fouling, compressor and turbine erosion, compressor and turbine isentropic efficiency degradation, and turbine exhaust (back) pressure (regenerative cycles).

3.7.1.1 - Fault Representation

In the previous studies on gas turbine degradation, the fault representation is modelled differently. In the absence of definitive values, the method used by Zwebek and Pilidis, 2003, and suggested by Diakunchak, 1992 and Saravanamuttoo et al., 1983, is employed along with a few modifications. These modifications include heat exchanger degradation through turbine back pressure increases. The faults implanted are defined as follows.

Fouling – Compressor or turbine fouling is represented by a reduction in the flow capacity at the inlet of the component plus a reduction in the component isentropic efficiency.

Erosion – Turbine erosion is represented by an increased flow capacity plus a reduction in the turbine isentropic efficiency.

Component Efficiency Degradation – The degradation of the efficiency of the individual components is modelled by reducing the isentropic efficiency of the component map and keeping the other parameters at the design point. It was assumed that component isentropic efficiency may decrease due to any reason, such as FOD or blade tip rubs.

Recuperator Degradation – Recuperator fouling can increase the pressure drop across this component. This can cause an increase in the turbine exit pressure also called turbine back pressure. Recuperator degradation is modelled in this approach as an increase in the turbine back pressure.

Faults in the compressor and turbine were simulated by altering the independent parameters from their DP values. This phenomenon is represented by changing the non-dimensional mass flow (Γ) and the component isentropic efficiency (η). These are known as the independent (non-measurable) parameters:

$$\Gamma = \frac{W\sqrt{T}}{PA} \tag{3.1}$$

The relationship between the non-dimensional flow capacity and isentropic efficiency for the relevant faults implanted is shown in Table 3.2. The representation of the component degradation is shown in Table 3.3. The effects of degradation on the gas turbine performance parameters (shaft power, thermal efficiency, exhaust mass flow and exhaust temperature) were evaluated. The results for each engine are available in Appendix B.

Table 3.2 – Implanted faults relation

Implanted Fault	Non-Dimensional Mass Flow Variation (ΔΓ)	Isentropic Efficiency Variation (Δη)	ΔΓ:Δη
Compressor Degradation	$\Gamma_C \downarrow$	$\eta_C \downarrow$	~1:0.5
Turbine Fouling & Corrosion	$\Gamma_T \downarrow$	$\eta_T \downarrow$	~1:0.5
Turbine Erosion	$\Gamma_T \uparrow$	$\eta_T \downarrow$	~1:0.5

Table 3.3 – Implanted fault representation

Implanted Fault	Represented by:	Range (%)
Compressor Fouling	Reduction in Γ	$0.0 \rightarrow (-5.0)$
	Reduction in η_C	$0.0 \rightarrow (-2.5)$
Compressor Erosion	Reduction in Γ	$0.0 \rightarrow (-5.0)$
	Reduction in η_C	$0.0 \rightarrow (-2.5)$
Turbine Fouling	Reduction in Γ	$0.0 \rightarrow (-5.0)$
	Reduction in η_T	$0.0 \rightarrow (-2.5)$
Turbine Erosion	Increase in Γ	$0.0 \rightarrow (+5.0)$
	Reduction in η_T	$0.0 \rightarrow (-2.5)$
Foreign object damage	Reduction in η_C and η_T	$0.0 \rightarrow (-5.0)$
Recuperator Degradation	Increase Turbine Back Pressure	$0.0 \rightarrow (+2.5)$

3.8 - Gas turbine health monitoring and diagnostics

The concept behind any gas path diagnostics method is that the diagnostic process calculates changes in the magnitudes of the component performance parameters (e.g. efficiency and flow capacity) for a given a set of measurements (e.g. temperatures, pressure, shaft speed and fuel flow) through the engine. A comparison of some characteristic values of an engine under examination with the corresponding values of an engine which is considered "healthy" is performed.

The parameters chosen and the means of measuring them distinguish each diagnostic method. The different techniques have not changed substantially since the 1970s and rely on the concept of gas path analysis that was first introduced by Urban, 1972. Different techniques that have evolved include linear GPA with ICM inversion,

non-linear GPA with ICM inversion, artificial neural networks and expert systems. Further information on these techniques can be found in Li, 2004.

The present study uses both linear and non-linear gas path analysis to select instrumentation that can detect component faults in simple and regenerative gas turbines, in constant and variable speed regimes of operation. The results for each engine investigated are available in Appendix B.

3.9 - Gas Path Analysis (GPA)

The software Pythia (Escher, 1995) performs a comparison of the deteriorated performance and the clean engine performance and changes in the monitored parameters will be detected through the application of gas path analysis (GPA). The aim of GPA is to detect, isolate and quantify some of the gas path faults that have observable effects on measurable or dependent parameters. This implies correctly that faults such as blade cracks or those caused by sudden failures such as fracture cannot be implicitly identified by gas path analyses. These sorts of failure mechanisms are addressed in chapter 4.

GPA uses two types of parameter in the engine analysis to discover the cause of a fault: independent parameters (i.e. efficiency and flow capacity) and dependent parameters (i.e. pressure, temperature, fuel flow).

Independent parameters are thermodynamically correlated with the dependent parameters. This means that changes in the dependent parameters are induced by changes in the independent parameters. The accurate identification of possible faulty components is reliant upon the choice of measurements taken.

Once the engine has degraded, the changes in the component parameters can be deduced from the changes in the dependent parameters using matrix notation. The deviation of the engine component parameters can be calculated with a fault matrix and is expressed as:

$$\Delta x = [FCM] \cdot \Delta y \tag{3.2}$$

Where [FCM] is the fault coefficient matrix, Δx represents the variations in the independent non-measurable parameters, and Δy represents the variations in the

dependent measurable parameters. Once this matrix has been calculated the deterioration of any independent parameter can be determined through knowledge of the changes in the measurable parameters used to build the [FCM].

3.9.1.1 - Linear (LGPA) versus Non-Linear Gas Path Analysis (NLGPA)

Linear gas path analysis (LGPA) assumes that changes in independent parameters are relatively small and the equation (3.2) can be expanded by a Taylor series. By doing so it is assumed that the independent parameters vary linearly with the dependent ones.

However, as the relationship between measurements and component parameters can be highly non-linear, a diagnostic method which can reflect this is required. NLGPA solves the non-linear relationship between the dependent and independent parameters with an iterative method such as the Newton-Rhapson method. This makes the method more accurate than LGPA, although the complex equations involved increase the calculation time slightly.

In this study, for the single component faults a comparison is made of the accuracy of the LGPA and NLGPA. A few studies have shown that the use of a non-linear GPA approach to instrumentation set selection provides a significant improvement when compared with linear GPA because it addresses the non-linear nature of the problem (House, 1992; Massart, 1997; Mustapha, 1995). Successive applications of linear GPA either diverge from, or converge to, an exact solution depending on the choice of instrumentation used.

3.9.1.2 - Gas turbine diagnostics

Before using the software to perform diagnostics, the user must decide upon the type and magnitude of the fault to be implanted. Also, the parameters which are to be measured must be chosen. The parameters measured are largely dependent on the instrumentation that would be installed on an actual engine.

Deteriorated modes and GPA were used in order to determine the degree of degradation for a given engine. Then a Fault Coefficient Matrix is generated by calculating component interrelationships numerically. The program generates

percentage changes in the chosen dependent parameters, the detected fault and the RMS error (which gives an indication of how accurate the diagnostic approach is).

For each measured parameter, the monitored changes are calculated according to the following formula:

$$\Delta\text{Monitored} = \frac{\text{Deteriorated Parameter} - \text{Baseline Parameter}}{\text{Baseline Parameter}} \cdot 100 \qquad \textbf{(3.3)}$$

The monitored deltas are used with the [FCM] to provide a prediction for the detected fault. Ideally, the detected fault and the implanted fault should be the same. However, in practice they differ. This difference is called the RMS (Root Mean Square) and is defined as:

$$\text{RMS} = \sqrt{\frac{\sum_{i=1}^{\text{No.Faults}} \left(\text{Implanted Fault}_i - \text{Detected Fault}_i\right)^2}{\text{No. Dependent Parameters}}} \qquad \textbf{(3.4)}$$

The FCM and RMS provide a means for a qualitative assessment of the various diagnostic approaches. There is no threshold for the RMS which declares a diagnostic approach is successful. However, the lower the RMS, the greater the confidence that can be had in the diagnostic approach.

3.9.1.3 - Diagnostics of faults

By implanting faults into the engine model, the performance of the engine is altered, simulating a deteriorated circumstance. In this investigation the components degraded are the compressor and turbine. The component's characteristics change when it degrades. Any type of deterioration, whether it is fouling or erosion will cause the running line of the engine to move to conform to the 'new' engine. In other words, for each level of deterioration, a new set of engine component characteristics will exist.

The compressor and turbine maps undergo a sort of shift as the components become degraded. It is this shift in the component maps that is used to simulate the various types of component degradation. This technique is complemented with the modification of the scaling factors that are calculated for the clean components during the design point simulation.

3.9.1.4 - Independent Parameters

For each gas turbine model, the faults analysed were compressor degradation, turbine fouling, turbine erosion, compressor degradation and turbine fouling, and compressor degradation and turbine erosion. Degradations of 3% were investigated. The fault representation and magnitudes were the same as those outlined in the degradation section.

3.9.1.5 - Selection of measured parameters

Depending on the varying effects of the different degradations on the measured parameters of the gas turbine, different selections of measurements will give different accuracies for the fault diagnostics. It is the purpose of the diagnostics investigation to determine which approaches are suitable for the different faults implanted.

The benefits of GPA can only be achieved with appropriate instrumentation that thermodynamically correlates with the desired faults. Furthermore, an optimal selection of instrumentation sets would allow for correct diagnosis of multiple faults. Knowledge of these optimum instrumentation sets to diagnose different faults would be indispensable to diagnostic engineers and developers.

Choosing which parameters to monitor is an important stage of the diagnostics approach. The parameters chosen for this study reflect the feasible instrumentation that would be present on a gas turbine. The parameters chosen for measurement were the compressor exit pressure and temperature, turbine exit pressure and temperature, fuel flow, gas generator speed and shaft power. The engines are modelled at sea level conditions and the ambient temperature and pressure are always constant.

3.9.1.6 - Engine Baseline

A baseline for each engine has to be established which serves as the reference condition to which the degraded performance can be compared. This baseline was taken as the clean engine performance data, i.e. when the engine is not subjected to any degradation. The baselines for each engine are established during the design point runs and are used for the diagnostics investigation.

3.9.1.7 - Handle Selection

Deteriorated performance is an off-design performance calculation. This involves a series of iterative loops in which the engine variables are adjusted to match with one particular variable, called the 'handle'. This handle specifies the engine power setting. In the actual engines, different options exist for the selection of this handle, e.g. compressor pressure ratio, exhaust temperature. For this investigation, handle selection is essentially a choice between turbine entry temperature (TET) and rotational speed. The idea behind this handle is that it cannot be a variable after being selected as the handle as it determines the engine power setting.

3.9.1.8 - Implementation of Faults

The approach used in this numerical calculation was to implant the component faults and then obtain the dependent parameters which were sensitive to the fault. Single and multiple faults in the compressor and turbine were implanted and different combinations of instrumentation sets were investigated. The different parameters measured and diagnostics approaches can be seen in Tables 3.4, 3.5 and 3.6. The symbol #'s mark the monitored parameters. The different faults are represented as explained in the previous section. The independent parameter is marked with the symbol "I".

Table 3.4 – Independent parameter selection for single and multiple faults diagnostic

	Single Fault			Multiple Fault	
Indep. Param.	Comp. Deg.	Turb. Fouling	Turb. Erosion	Comp. Deg. and Turb. Fouling	Comp. Deg. and Turb. Erosion
Γ_C	I			I	I
η_C	I			I	I
Γ_T		I	I	I	I
η_T		I	I	I	I

Table 3.5 – Single Component Fault Diagnostic Approaches

Measured Parameters	Approach Number																				
	1	2	3	4	5	6	7	8	9	10	11	12	13	14	15	16	17	18	19	20	21
Comp. Exit Pressure	#	#	#	#	#	#															
Comp. Exit Temp.	#						#	#	#	#	#										
Turbine Exit Pressure		#					#					#	#	#	#						
Turbine Exit Temp.			#					#				#				#	#	#			
Fuel Flow				#					#				#			#			#	#	
GG Speed					#					#				#			#		#		#
Shaft Power						#					#				#			#		#	#

Table 3.6 – Multiple Faults Diagnostic Approaches

Measured Parameters	Approach Number																															
	1	2	3	4	5	6	7	8	9	10	11	12	13	14	15	16	17	18	19	20	21	22	23	24	25	26	27	28	29	30	31	32
Comp. Exit Pressure	#	#	#	#	#	#		#	#	#	#		#	#	#		#	#	#	#	#	#		#	#					#		#
Comp. Exit Temp.	#	#	#	#	#		#	#	#	#			#			#	#	#	#	#	#			#			#		#	#	#	
Turbine Exit Pressure	#	#	#	#		#	#	#	#			#	#	#	#	#	#		#	#					#	#	#	#				#
Turbine Exit Temp.	#	#	#		#	#	#	#			#	#	#	#	#	#			#				#		#	#	#	#	#	#	#	#
Fuel Flow	#	#		#	#	#	#	#		#	#	#		#	#	#		#				#	#		#	#	#	#			#	
GG Speed	#	#	#	#	#	#	#		#	#	#	#		#	#	#	#	#			#	#	#	#				#	#	#		#
Shaft Power	#		#	#	#	#	#		#	#	#	#	#				#	#		#	#	#	#	#					#		#	

3.10 - Analysis of Results

3.11 - Compressor Degradation

The variable speed gas turbine displays greater sensitivity to compressor fouling than the constant speed in a regenerative cycle. However, compressor degradation has a similar effect on both the constant speed regenerative and the simple cycle.

For compressor degradation there is a decrease in flow capacity and efficiency. This flow capacity reduction causes a reduction in the pressure ratio due to the reduced gas mass flow through the turbine. This leads to a decrease in the gas turbine power output and to an increase in specific fuel consumption. The effect of compressor degradation in the simple cycle engine (GTM#1) performance is similar to those quoted by Diakunchak, 1992 and Hoeft, 1993.

For variable speed operation, the engine can operate on any non-dimensional rotational speed line. This entails that for a variation in TET, there is a corresponding range available for non-dimensional mass flow. For the constant speed engines, they are limited to operating over a non-dimensional speed line. Thus for a range of TET, there is a smaller range available for the non-dimensional mass flow variation, and for this reason the mass flow through the constant speed engines remains relatively constant.

There is a larger variation in the exhaust mass flow for the variable speed engines than the constant speed ones.

When the compressor fouls its characteristics change and the running line is forced to move to match the 'new' physical design of the engine. The fouling causes a reduction in the mass flow capacity and efficiency, and as a result of the efficiency change the temperature rise across the component increases. A new component map is created as a result of the compressor fouling with a reduction in pressure ratio and non-dimensional mass flow. For the variable speed regime of operation, there is a larger variation in pressure ratio, and thus mass flow which leads to a higher drop in shaft power.

3.12 - Turbine Fouling and Erosion

Turbine fouling has a significant impact on the performance of the gas turbine. Turbine fouling causes a reduction in the pressure ratio across the turbine, and then a reduction in the turbine mass flow and turbine isentropic efficiency. The variable speed engines are extremely sensitive to turbine fouling. Also the gas turbine displays greater sensitivity to turbine fouling when a recuperator is fitted.

Turbine erosion increases the turbine pressure ratio (for a fixed TET) and turbine fouling decreases. This explains why turbine fouling causes a greater reduction in performance than turbine erosion. The increased turbine pressure ratio helps to offset the power reduction. The effect of turbine erosion depends more on whether the cycle is regenerative or simple rather than if it operates at a variable or constant speed.

3.13 - Compressor Isentropic Efficiency Degradation

The output power and thermal efficiencies are reduced for reductions in component isentropic efficiencies. This degradation has no effect on the exhaust mass flow for the constant speed regenerative and simple cycle gas turbines.

There is no variation in the exhaust mass flows for the constant speed engines. However, reductions can be observed for the variable speed regenerative cycle. This can have a significant impact on a combined heat and power application, as the heat output capacity depends on the gas turbine exhaust mass flow and temperature.

Slight increases in exhaust temperature are observed for the variable speed micro gas turbine, i.e. 1.5% and 0.9% for the recuperated and simple cycle engines. However, negligible effects are seen on the constant speed micro gas turbines exhaust temperature.

For a single shaft gas turbine operating at constant speed, Tarabrin et al., 1998, found a 2.82% decrease in output power and a 1.41% decrease in thermal efficiency for a 1% decrease in compressor isentropic efficiency. This investigation found a 2.1% reduction in output power and a 1.9% decrease in thermal efficiency for a 1% decrease in compressor isentropic efficiency for a simple cycle constant speed engine.

3.14 - Turbine Isentropic Efficiency Degradation

Turbine isentropic efficiency degradation had a greater effect on the gas turbine performance than compressor isentropic efficiency degradation. As the turbine is producing power for both compressor and generator, any drop in the turbine efficiency will have a higher impact in the overall performance of the engine.

The effect of this degradation on the power and thermal efficiency is more dependent on whether the micro gas turbine is recuperated or not, rather than if it operates at variable or constant speed. Negligible effects are seen on the mass flow for the constant speed gas turbines, but a significant drop in mass flow is seen in the engines operating with variable speed. The turbine isentropic efficiency degradation has the same effect on the exhaust temperature as the combined compressor and turbine isentropic efficiency degradation for the constant speed simple cycle engine (GTM#1).

A drop of 1% in the turbine isentropic efficiency resulted in a reduction of 2.3% in the power output for the GTM#1. A similar performance was observed by Diakunchak, 1992, and Zwebek and Pilidis, 2003: i.e. 2.5% reduction for 1% turbine efficiency drop.

3.15 - Compressor and Turbine Isentropic Efficiency Degradation

For the isentropic efficiency degradations the mass flow capacities are at their DP values and thus the same pressure ratios. Therefore, the component isentropic

efficiencies degradation have negligible effects on the exhaust mass flow for the constant speed engines.

The exhaust temperatures are affected by the combined compressor and turbine isentropic efficiency degradation. An increase was also seen for the turbine isentropic efficiency degradation whilst negligible effects were seen for the compressor isentropic efficiency degradation for the constant speed engines. This can be attributed to the fact that less work is being extracted from the gas flow by the turbine and thus higher temperatures are observed. The constant speed engines' exhaust temperatures are unaffected by compressor isentropic efficiencies reduction. However, the exhaust temperatures for the variable speed engines are affected slightly by compressor isentropic efficiency degradation.

The compressor and turbine isentropic efficiency degradation has a greater effect on the power and thermal efficiency depending on whether the power cycle is a regenerative or simple cycle rather than if it operates at variable or constant speed. In fact, all the turbine degradations (erosion, fouling and efficiency) investigated exhibit this same characteristic. This is explained by the fact that the power and thermal efficiency displays greater sensitivity to turbine degradation than compressor degradation.

3.16 - Compressor Degradation and Turbine Erosion

Compressor degradation and turbine erosion causes a reduction in the component's isentropic efficiency. Flow capacity is reduced for the compressor but increased for the turbine. From the results, whilst the flow capacity has a substantial impact on the performance of all the engines investigated, it has less impact than the combined degradation of the compressor and turbine fouling. This is due to the fact that turbine erosion causes an increase in the compressor pressure ratio which helps to offset the power reduction caused by the mass flow reduction as a result of the compressor degradation.

3.17 - Compressor and Turbine Fouling

Compressor and turbine fouling causes a reduction in the component isentropic efficiencies and the flow capacities of each component. This causes a reduction in the pressure ratio across each component and, as a result of the components matching, a significant drop in the engine performance is observed.

Compressor and turbine fouling has a greater effect on the power and thermal efficiency depending on whether the power cycle is recuperated or not, rather than if it operates at variable or constant speed.

The combined degradation of compressor and turbine isentropic efficiencies, and turbine isentropic efficiency degradation on its own have a substantial impact on the power output and thermal efficiency of all the engines investigated.

The magnitude of the performance drop observed for the constant speed simple cycle engine (GTM#1) is not substantially different from those quoted in the literature. Unfortunately, due to lack of information on degradation performance of regenerative and variable speed gas turbines in the open literature, the results achieved with these models could not be compared. However, useful conclusions can be drawn from the various results that are presented.

3.18 - Recuperator Degradation

With reference to the heat exchanger degradation effect on engine performance (Appendix B), an increase in back pressure does not affect the exhaust temperature greatly for either the constant speed or variable speed engines. There is more reduction in shaft power for the variable speed engine than the constant speed engine. An increase in back pressure reduces substantially the output power as the pressure drop across the turbine is reduced.

As shaft power is related to mass flow, the greater reduction in mass flow for the variable speed engine causes the larger reduction in shaft power. The drop in mass flow for the constant speed engine is negligible as the compressor is limited to operating along a constant non-dimensional speed line and thus the range for the mass flow is limited. The efficiency follows the same trend as the power for increasing back pressure for both engines.

Gas turbine component degradation has different effects depending on the power cycle and whether the engine is operating at constant speed or variable speed. The engine displaying the greatest sensitivity to degradation is the variable speed regenerative cycle (GTM#4).

3.19 - Diagnostics Results Discussion

The results of the linear and non-linear GPA diagnostic investigations for each gas turbine model are presented in Appendix B. The four most accurate diagnostic approaches for each fault case and gas turbine model are shown in Tables 3.7 and 3.8. To find the instrumentation set of each approach number, refer to Tables 3.5 and 3.6.

Table 3.7 – Most Accurate Diagnostic Approaches for Single Component Faults

	Comp. Degradation				**Turbine Fouling**				**Turbine Erosion**			
	Approach Accuracy Decreasing ⇒				Approach Accuracy Decreasing ⇒				Approach Accuracy Decreasing ⇒			
GTM#1	9	1	4	11	9	17	14	5	20	3	10	19
GTM#2	1	9	8	11	19	3	11	5	8	11	5	18
GTM#3	4	1	9	17	1	10	19	4	18	9	11	4
GTM#4	9	17	1	4	1	4	17	13	9	19	1	3

Table 3.8 – Most Accurate Diagnostic Approaches for Multiple Component Faults

	Comp. Degradation and Turbine Fouling				**Comp. Degradation and Turbine Erosion**			
	Approach Accuracy Decreasing ⇒				Approach Accuracy Decreasing ⇒			
GTM#1	30	11	18	5	10	18	5	11
GTM#2	11	2	18	10	4	18	10	2
GTM#3	1	25	-	-	11	31	13	3
GTM#4	2	1	4	7	16	15	30	31

For the single fault diagnostic, several approaches have displayed low RMS errors. Such low values of error mean that the diagnostic approach not only detects the

fault but also detects the magnitude of the degradation. Multiple faults diagnostics show higher RMS error as they are more difficult to detect and quantify than single faults. Approaches involving all possible measured parameters do not give the most accurate diagnostic approach, which agrees with the conclusions of Ogaji and Singh, 2002.

Chapter 4 – Life Cycle Assessment

4 - Life Cycle Assessment

4.1 - Introduction

This investigation aims to develop an algorithm able to predict the lifetime of a turbine blade of a gas turbine in service. The scope of this approach includes the performance and mechanical assessment of "uncooled" gas turbines (those with no cooling passages in the blades). This section presents the failure mechanism, stress calculation and life assessment methods that are used in the blade's mechanical design. The blade structure of the gas turbine engine is usually under more hostile operating conditions than most other mechanical devices. The principal variables that take part in this context are time, temperature and stress loads; they and their combination are the precursors of blade damage.

The principal target of the mechanical engineers will be to generate a mathematical model, which will be able to relate the operating conditions to blade failure. Blade breakdown will happen when the blade loses its functionality or when the blade function presents an imminent risk in the safe operating of the turbine. The first assumption is related to the plastic, elastic, or corrosive loss of appropriate shape of the blade (deformation) and the second is more connected with fast crack propagation that could result in structural failure.

The numerical model that will represent blade behaviour needs input data which will came from the conversion of the operating conditions in input variables that will be part of the model. It is not an easy task to estimate the stress and temperature levels over the blade geometry in an engine operation using different regimes of operation. Also it is necessary to define the relations that will constitute the model which would relate these input parameters with the life assessment of the blade.

4.1.1 - Turbine blade failure mechanisms

Several criteria can be applied to gas turbine blade failure mechanism classification and it is very likely that more than one will be included in several categories.

4.1.1.1 - Short life failures

These failures occur after a short period of operation and there are several reasons that cause this kind of failure. The most common are: incorrect application of the design rules, a non fulfilment to determine accurately the likely loads to be imposed on the component, a dereliction in the manufacturing process and an oversight in the crack inspection process. Some examples of such failures are:

- Fast fracture by unstable crack propagation.
- Elastic instability leading to buckling.
- Plastic deformation leading to yielding.
- Excessive elastic deflection, causing component to jam or rub.
- Dynamic instability due to a resonance vibration.

4.1.1.2 - External factor induced failures

The external environment of the engine will be what motivates this kind of failure. Within this category, the most usual are: corrosion, erosion and foreign object damage (FOD). Generally, periodic inspections, other than maintenance actions (such as anti corrosion washing) and conditioning monitoring, are the tools available to avoid the external environment effects. The effects of the external environment on engine performance were investigated in greater detail in chapter 3.

4.1.1.3 - Turbine operating direct failures

High pressure turbine alloys experience a wide variety of thermal and mechanical loading cycles depending upon operating conditions. Creep and fatigue are the two failure mechanisms that are responsible for this degradation.

4.1.1.3.1 - Crack Formation

Cracking is a phenomenon that can occur suddenly or over an extended period. If sudden, it is called fracture, and if over a period of time it is known as fatigue. Fracture of engineering materials is classified as ductile or brittle.

4.1.1.3.1.1 - Ductile Fracture

Except in special circumstances such as high constraint or very high rates of strain application, ductile fracture occurs only in a limited class of engineering materials. Generally, overload fracture of metals is preceded by a period of plastic deformation in which the component strain must exceed, in many metals, 20-50% before fracture occurs. This is known as ductility and adds a safety margin relative to the possibility of failure of ductile materials.

4.1.1.3.1.2 - Brittle Fracture

Brittle materials fail without slip or void formation and hence do not experience plasticity or strain hardening. They fail suddenly, without permanent deformation prior to fracture. This is because when pre-existing cracks are loaded to the point that the stress surpasses the atomic bonding strength at the stress-intensity point ahead of the crack, the crack extends. When the crack extends, the stress intensity increases ensuring that the crack will extend still further. In this case the stress intensity is proportional to the square root of crack length. The process continues, even without further increase in stress until the fracture is complete. This makes brittle materials' strength very sensitive to the size of the largest pre-existing flaw in a stressed area.

4.1.1.3.1.3 - Fatigue

Fatigue happens when a component is subjected to fluctuating stresses, due to centrifugal, thermal or pressure loads because of the changing operational conditions that the engine experiences. These loads could lead to failure of the component, even though the maximum stress is lower than the static strength of the material. Fatigue can be considered as ensuing in the following three successive phases:

- Crack initiation at a stress concentration point, on the surface or within the body.
- Steady long crack growth in the direction normal to maximum tensile stress.
- Rapid crack growth and failure occur when the crack has so weakened the local material that the remaining cross-section of the component cannot withstand the imposed mechanical load.

In general, the amplitude and number of cycles of the applied load will decide the amount of time that a failure may occur. In this way, resistance to crack propagation is a desirable property, since it will give time to identify the generated crack, by different inspection techniques, and avoid failure by component replacement.

The fatigue failure can be classified by the amplitude and cycles of the applied loads into low cycle fatigue (LCF) or high cycle fatigue (HCF). In the same way, if the source of the stress levels is the temperature gradients, the fatigue process is classified as thermo mechanical fatigue (TMC) a condition that develops an LCF situation.

Low cycle fatigue (LCF): This is associated with a low numbers of cycles (around 10^3) in combination with high stress amplitude. The LCF usually carries plastic deformation, due to the high stress level. Thus, there is a substantial accumulation of energy in the form of plastic deformation. As a result, the proportion of life that the mechanical component spends in the crack initiation phase is short, but the time that it spends in the crack growth process is longer. Therefore it is easier to detect this kind of failure.

High cycle fatigue (HCF): This is associated with the application of a large number of low stress loads. The HCF is characterised by spending the greatest portion of time in the crack initiation and short crack growth phase which means it is difficult to be found in advance, i.e. before catastrophic failure. The HCF is associated with vibrations; the main causes are imbalance, misalignment, loose fitting installation and whirl, each of which can be originated by the design, manufacturing process, reparation of the engine or in-service causes. The strategy to avoid this kind of failure is to mitigate the vibratory sources.

Thermal fatigue or thermo mechanical fatigue (TMF): The temperature gradients to which turbine blade are exposed cause thermally induced stress which, when combined with high mechanical loading, results in localised high strain cycles and thereby produces thermal fatigue cracking in the blade, especially if repeated often enough. The cracks tend to be initiated on the component's surface, since the highest temperatures and stress levels occur there, and subsequently propagate through the bulk of blade. The components that are in direct contact with the high temperatures gases, such as turbine blades, nozzle guide vanes (which are completely immersed in the hot gas stream) and the turbine discs (which are partially immersed) are highly susceptible to thermal fatigue. Consequently, the thermal mechanical fatigue is dictated by the cyclic thermal, centrifugal and gas bending loads.

4.1.1.3.2 - Creep

Creep results in permanent deformation due to slip and void formation, but does take place over relatively long time spans. This is because creep is a thermally assisted diffusion process, where the slip and void formation are driven by the imposed stress field, but could not overcome atomic bounding forces without the aid of atomic-level vibratory motion associated with temperature rise in engineering materials.

A formal definition says that creep is the progressive plastic deformation of a material at constant temperature. In gas turbine cycles the situation is more complex because creep will result from a whole range of applied temperatures and loads. The creep mechanism is based on the migration of the material discontinuities or dislocations that exist in their crystal structure. These movements are stimulated by stress and temperature levels. At low temperatures there are two ongoing mechanisms which lead to a slow plastic flow of the material; grain boundary sliding and dislocation climb. At high temperatures, the mode of failure is known as inter crystalline failure. The creep process, from initial strain to fracture, can be idealised in four stages of phases (Figure 4.1):

- Instantaneous straining.
- Primary creep, the creep resistance increases as a function of its own deformation. It is the predominant stage at room temperature.

- Secondary creep, with a lower and constant creep rate, is the phase that will take the greatest proportion of the creep life. The secondary stage follows an Arrhenius equation, which has a power law dependence on the stress in the material:

$$\frac{\partial \in}{\partial t} = C \cdot \sigma^{m} \cdot e^{-Q/(R \cdot T)} \qquad (4.1)$$

Where $\partial \in / \partial t$ is the rate of dislocation creep, C is a constant parameter relating to the material, Q is the activation energy for creep, R is the universal gas constant, T is the absolute temperature, m is the stress exponent and is determined by the material composition (usually lies between 3 and 10).

- Tertiary creep is an unreal situation which occurs at high stress and temperatures. It occurs when there is an effective reduction in the cross-sectional area usually produced by necking.

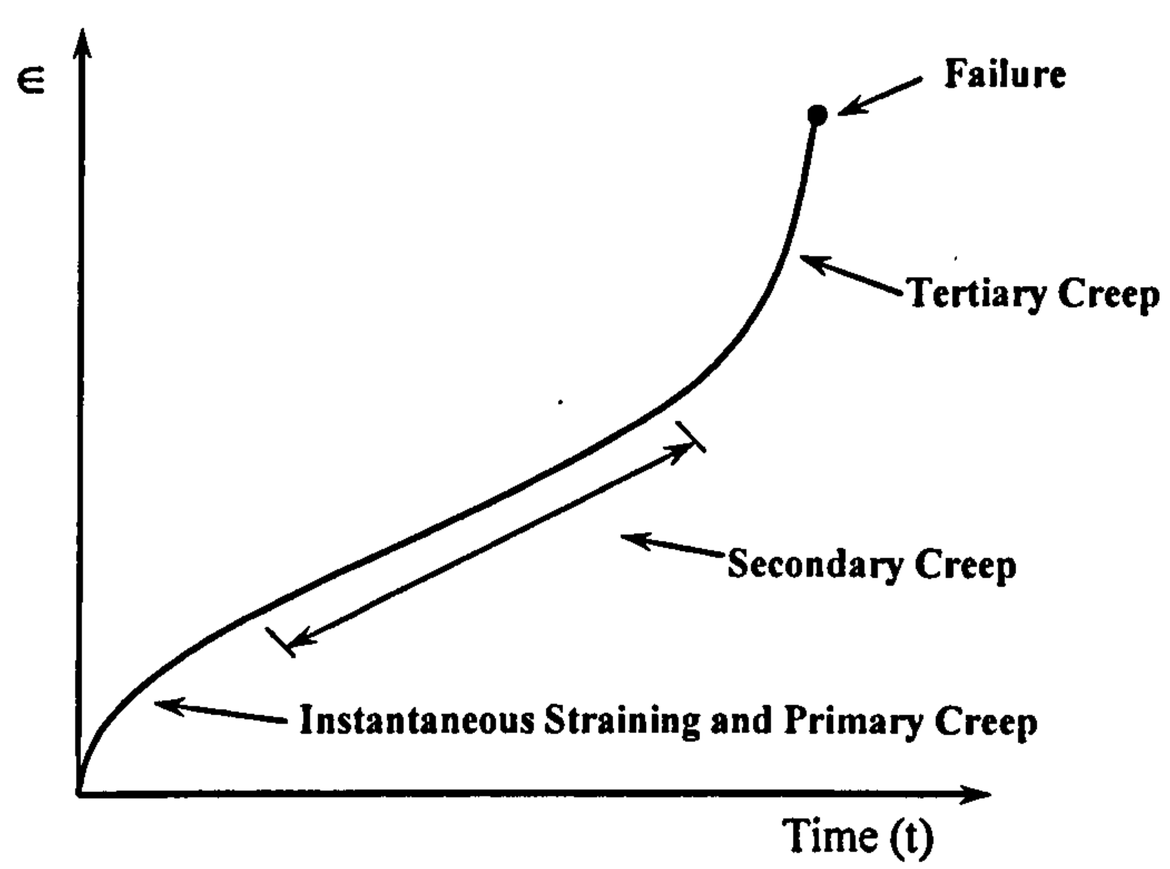

Figure 4.1 - Creep stages process

The life proportion that a component spends in the secondary creep will be a function of the applied stress and temperature. Generally the higher the temperature and stress level, the smaller the secondary creep proportion.

Equation (4.1) allows us to plot stress-rupture versus time graphs. However, the problem with such graphs is that they are very dependent on the material and heat treatment, and it is difficult to generalise from them to materials that such plots are not

available. Therefore, the approach used to calculate creep life is the Larson-Miller parameter, which will be discussed later in this chapter.

4.1.2 - Failure mechanism for life cycle assessment

The failure mechanisms described in the previous section will rule the life consumption of the turbine blades, under the load conditions that will be introduced over these components.

The short time failures will not be examined in this investigation, since they are addressed as design, manufacturing or inspection mistakes, as was commented on earlier.

The external environmentally induced failures will not be taken into account in the prediction of the lifetime of the engines due the random probability that they may happen. However, the effects of this important and complex mechanism on engine performance have been carefully analysed and described in chapter 3.

For the turbine experiencing direct failures, it is necessary to highlight that gas turbine components are subjected to a complicated combination of both steady and cyclical stress and thermal loads. These will inevitably bear the effects of creep and fatigue together which will eventually cause component failure. It is necessary, therefore, to understand the effects of this combination and to determine the safe life limit.

The stresses analysis of gas turbine engines is feasible but complex and requires data that are not available in the public domain. In this investigation, creep effects will be considered as the major life damage approach.

Ductile and brittle fractures will not be included in this investigation as they occur only in a limited class of engineering materials and also are addressed as manufacturing or inspection mistakes. Despite the extreme complexity of the physical mechanisms of fatigue, relatively simple engineering models have been developed and can provide guidance to the evaluation of the cumulative fatigue damage behaviour of materials.

The majority of fatigue damage in gas turbines occurs during the engine start-up. Then, as the fatigue damage increases with the number of cycles, the number of engine start-ups is the parameter used as a limit to a safe life. In this investigation the fatigue life cycle prediction results, achieved by McGraw et al., (1991) with the cast nickel-base superalloy MAR M-247, will be used as a reference.

4.2 - Blade metal temperature

Actual gas turbines are designed to run at high turbine inlet temperatures. Therefore, improved temperature capability materials, thermal barrier coatings and cooling systems are used to maintain acceptable life and operational requirements under such extreme conditions.

To design a turbine blade it is necessary to comprehend and implement a thermal model which represents the detailed hot gas flow physics that rule the gas turbine cycle. Blade metal temperature is one of the most important parameters concerning life cycle assessment and it depends on the combustor outlet temperature, blade geometry and on the blade cooling efficiency, if there is any cooling flow through the turbine blades.

In the present study, the maximum turbine entry temperature achieved by the portfolio of gas turbines studied is around 1200 K, which is below the actual levels of maximum temperature that can be achieved with "uncooled" turbines (i.e. those with no cooling passages in the blades). A detailed description of a reverse engineering process to calculate the metal temperature for gas turbines with blade cooling system is given by Holland and Thake, 1980. In this reference an inverse path was taken to predict and built a thermal model which related the amount of cooling air to the metal temperature.

Before going into details of blade metal temperature calculation, it is necessary to define the following gas turbine temperatures (Figure 4.2):

- Turbine entry temperature (TET): temperature at the leading edge of the first stator blade;
- Firing Temperature (FT): mass-flow mean total temperature at the first trailing edge of the first stator blade;

- Turbine Inlet Temperature (TIT): temperature defined by ISO 2314 – Gas Turbine Acceptance Tests. This is a reference temperature and is not generally a temperature that exists in a gas turbine cycle; it is calculated from a heat balance in the combustion system, using parameters obtained in the field tests;

- Turbine Rotor Inlet Temperature (TRIT): temperature mainly used in the design of turbine blades.

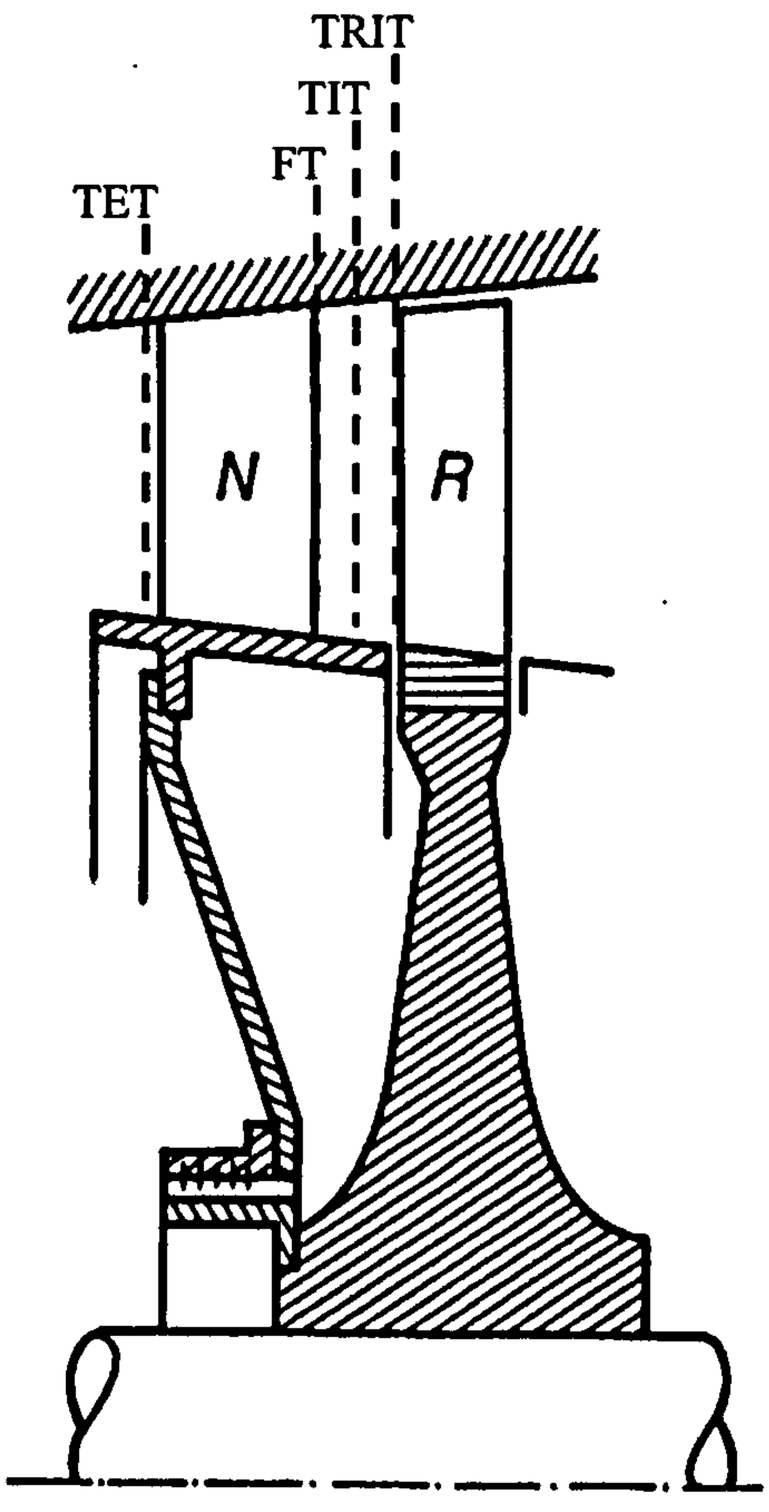

Figure 4.2- Temperature definitions at the turbine's first stage

The precise estimation of the blade metal temperature involves a complex iterative aerodynamic analysis and detailed heat transfer calculation throughout the blade. Dundas (1985) carried out a very detailed investigation and concluded that, at nominal rotational speed, blade average metal temperature is very close to the relative temperature of the gas. Therefore, in this study the turbine rotor inlet temperature

(TRIT) described in Figure 4.2 is considered equal to the static gas temperature, which is a conservative and acceptable assumption for the purpose of this investigation.

A typical gas temperature profile over the turbine blade can be seen in Figure 4.3. The midsection is in contact with the peak temperature while the root is in contact with a much cooler gas temperature. This profile is achieved by proper distribution of the combustor dilution air so that, while the average temperature is equal to the cycle temperature, the temperature at the radius is the average of the temperature around the circumference since that is the value of significance as far as the blade creep life is concerned. The calculation carried out in this approach will consider the temperature and velocities at the midsection blade or more exactly at the gravity centre radius (r_{cg}) between the blade gravity centre and the centre of rotation.

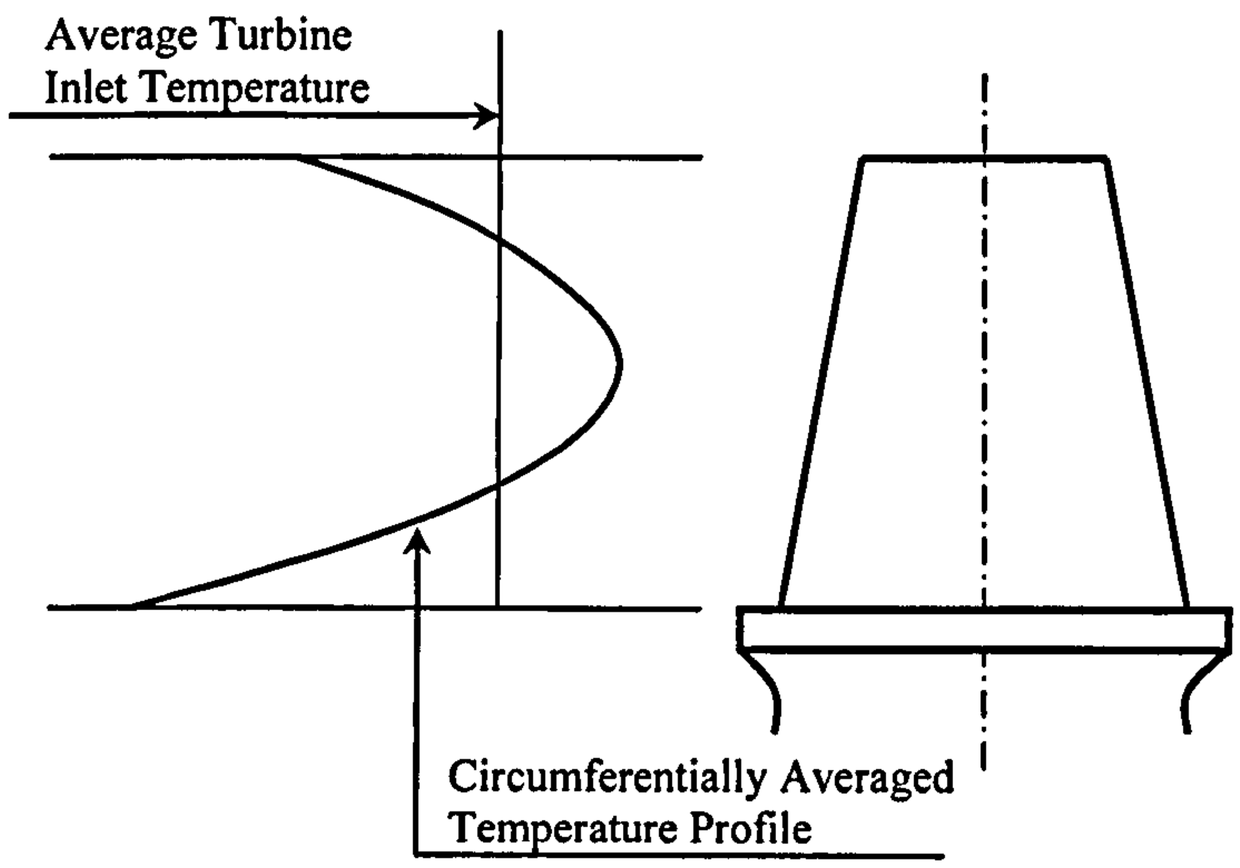

Figure 4.3 – Turbine inlet temperature profile (Dundas, 1985)

Figure 4.4 shows a typical axial turbine stage and respective velocity triangles. The gas enters the row of nozzle blades at station 1. Then it is expanded to station 2 and further expanded in the rotor blade passages to station 3.

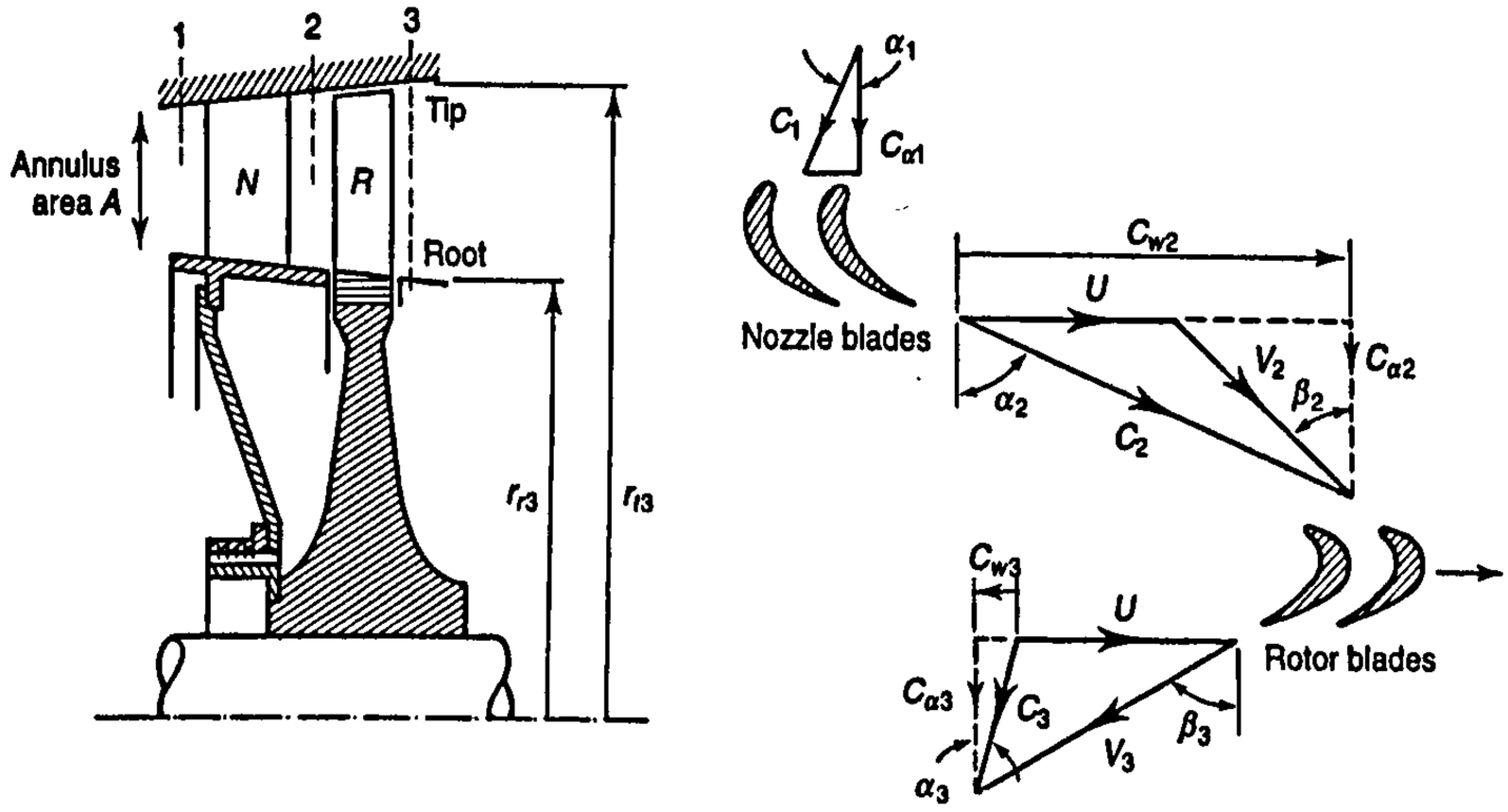

Figure 4.4 - Axial turbine stage (Saravanamuttoo et al., 2001)

In a gas turbine the hot combustor discharge gases enter the nozzle row at the relatively low Mach number and are accelerated in the nozzle row to the Mach number of 0.8 to 0.9 (velocities of as high as 610 m/s) and directed at the turbine blades to drive the turbine wheel by a combination of tangential impulse and reaction. The blade runs away from the nozzle exit stream with a tangential velocity (U_{cg}) so that the gas velocity that the blades see is given by the relative velocity (V_2). The relative velocity is substantially less than the absolute velocity, C_2, and decreases with increasing rotational speed. The static relative temperature (T_{2r}) is the maximum temperature that the blade sees even at the leading edge where stagnation conditions exist, and it is given by:

$$T_{2r} = T_{01} - \frac{C_2^2 - V_2^2}{2 \cdot c_p} \tag{4.2}$$

Where T_{01} is the total temperature at station 1, c_p is the gases specific heat at constant pressure, C_2 and V_2 are the absolute velocity and relative velocity at station 2 respectively (Figure 4.4) and can be written as:

$$C_2 = \frac{\varphi \cdot U_{cg}}{\cos \alpha_2} \tag{4.3}$$

$$V_2 = \sqrt{(\varphi \cdot U_{cg})^2 \cdot \left(1 + \left(tg\alpha_2 - \frac{1}{\varphi}\right)^2\right)} \tag{4.4}$$

Where α is the nozzle angle and φ is the flow coefficient given by:

$$\varphi = \frac{C_{a2}}{U_{cg}} \tag{4.5}$$

4.3 - Stress calculation

4.3.1 - General loads

The following are the main loads, and consequently main sources of stress, applied in gas turbine rotor blades:

- Centrifugal load: a force due to inertia. This load acts at any section of the aerofoil, and is produced by the material above that section.
- Gas load: the pressure and the momentum difference of gas when it passes across the aerofoil stage producing a reaction load on the blade.
- Thermal load: this load will be the consequence of thermal gradient on the blades which as a result produces dissimilar expansion.

These loads applied to the blade geometry will entail a general three axial state of stress, which should be calculated by a finite element analysis in order to achieve a high level of accuracy. Applying relatively simple rules of stress calculation to predict the general behaviour of loads in turbine blades is acceptable as these rules are widely used in the technical literature (Gomez, 2005; Arvantis, 1987; Marscher, 1985).

4.3.1.1 - Direct stress

The causes of direct stress (σ) are identified and classified below. The next sections also describe how this applied load results in forces and moments. In this section all the subscripts refer to the velocity triangles of Figure 4.4.

4.3.1.1.1 - Direct centrifugal stress (DCS)

This stress exists because of the blade weight and because it is under an inertial field. The centrifugal stress, for a given cross-sectional area (A), can by achieved by:

$$\sigma_{CF} = \frac{m_b \cdot r_{cg} \cdot \omega^2}{A} \tag{4.6}$$

Where m_b is the mass situated above the cross-sectional area, ω is the angular velocity [radians/s] and r_{cg} is the radius between the gravity centre and the centre of rotation. The angular velocity is given by the following equation:

$$\omega = 2\pi \cdot N \tag{4.7}$$

The blade speed at the gravity centre (U_{cg}) can be expressed in terms of the rotational speed (N) in [rev/s]:

$$U_{cg} = 2\pi \cdot N \cdot r_{cg} \tag{4.8}$$

Then:

$$\sigma_{CF} = \frac{m_b \cdot r_{cg} \cdot (2\pi \cdot N)^2}{A}$$

$$\sigma_{CF} = \frac{2\pi \cdot N \cdot m_b \cdot U_{cg}}{A} \tag{4.9}$$

In this study, the blade cross-sectional area is considered proportional to the blade height (h) ("uncooled" blades), as the relation below:

$$A = Ahr \cdot h \tag{4.10}$$

Where Ahr is the cross-sectional area-height ratio. The blade height can be given by the following expression:

$$h = \frac{A_n}{2\pi \cdot r_{cg}}$$

$$h = \frac{N \cdot A_n}{U_{cg}} \tag{4.11}$$

Where A_n is the annulus area of the turbine blade and can be calculated with the following expression:

$$A_n = \frac{\dot{m}}{\rho_2 \cdot C_{a2}}$$

Using the ideal gas equation of state and the definition of flow coefficient (φ):

$$\rho_2 = \frac{p_2}{R \cdot T_2}$$

$$\varphi = \frac{C_{a2}}{U_{cg}}$$

The following equation can be written:

$$A_n = \frac{R \cdot T_2 \cdot \dot{m}}{p_2 \cdot U_{cg} \cdot \varphi} \quad \textbf{(4.12)}$$

Where $\dot{m}$ is the gas mass flow [kg/s], T_2 is the static temperature [K], R is the specific gas constant (R=287 J/kgK), p_2 is the static pressure (Pa) and φ is the flow coefficient. The static temperature T_2 can be calculated by the following expression:

$$T_2 = T_{02} - \frac{C_2^{\,2}}{2 \cdot c_p}$$

Where T_{02} is the total temperature [K], c_p is the gases constant and α is the nozzle angle, C_2 is the velocity at station 2 [m/s]. Since $T_{02} = T_{01}$ and given the relations below:

$$C_2 = \frac{C_{a2}}{\cos\alpha_2}$$

$$\varphi = \frac{C_{a2}}{U_{cg}}$$

Then:

$$T_2 = T_{01} - \frac{\left(U_{cg} \cdot \varphi\right)^2}{2 \cdot c_p \cdot \cos^2 \alpha_2} \quad \textbf{(4.13)}$$

Where α_2 is the nozzle angle. The static pressure p_2 can be expressed by the following equation:

$$p_2 = p_{02} \cdot \left(\frac{T_2}{T_{02}} \right)^{\gamma_g / (\gamma_g - 1)}$$

Where p_{02} is the total pressure [Pa] and γ_g is the gases specific heat ratio. Since $p_{02} = p_{01}$ and from equation (4.8):

$$p_2 = p_{01} \cdot \left(1 - \frac{(U_{cg} \cdot \varphi)^2}{2 \cdot T_{01} \cdot c_p \cdot \cos^2 \alpha_2} \right)^{\gamma_g / (\gamma_g - 1)} \quad \textbf{(4.14)}$$

The calculation of the gases specific heat at constant pressure involves a very lengthy analysis of combustion products, mainly when dissociation is taken into account due the effects of the gases pressure. Accurate calculations concerning this issue have been made in Banes et al., 1967. Although in this approach the effects of pressure on the calculation of the gases specific heat will be not considered, it is an acceptable assumption for gas turbines designed to use turbine inlet temperatures lower then 1500K (Saravanamuttoo et al., 2001). Then, the gases specific heat at constant pressure (c_p) and the gases specific heat ratio (γ_g) for different temperatures of combustion and fuel/air ratio can be estimated based on Figure 4.5.

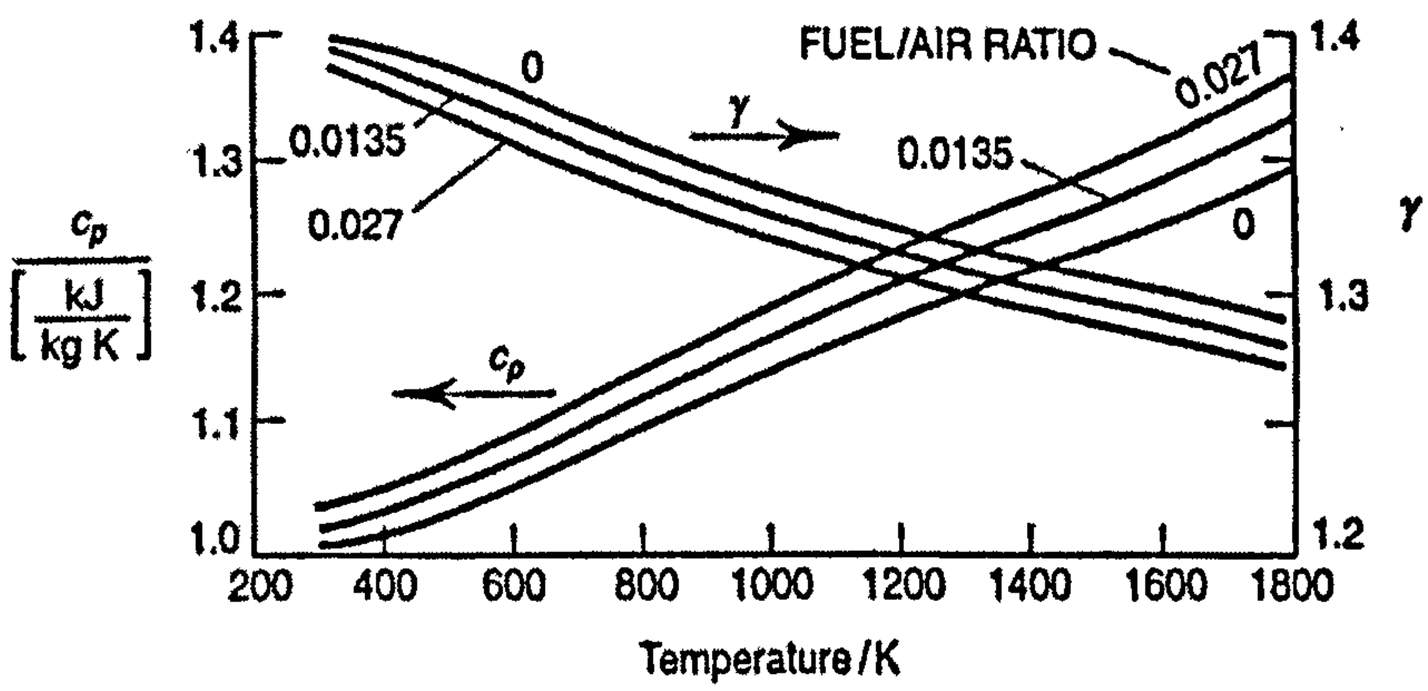

Figure 4.5 – Gases specific heat at constant pressure (c_p) and the gases specific heat ratio (γ_g) for typical combustion gases (Saravanamuttoo et al., 2001)

Finally the mass situated above of the cross-sectional area (m_b) is given by:

$$m_b = \frac{\rho_b \cdot A \cdot h}{2} \tag{4.15}$$

Where ρ_b is the density of the blade alloy.

4.3.1.1.2 - Gas bending stress

The difference of pressure due to work fluid passing through the blade produces a force acting on the blade. In addition, there is also a variation in velocity, which means that the momentum also will change and then another force will be induced (Figure 4.6). In the case of the velocity change, the force produced can be written as:

$$F_i = m_i \cdot \frac{\Delta V}{\Delta T} = \frac{m_i}{\Delta T}\Delta V = \dot{m}_i \cdot \Delta V \tag{4.16}$$

Where $\dot{m}_i$ is the mass flow that traverses each blade, ΔV and ΔT and are the variation of velocity and time respectively.

These forces will generate an axial bending moment and a tangential bending moment, but as the turbine blades used to be twisted, the ratio between the tangential and axial components will vary from root to tip. Knowledge of the rules of this variation in the axial and tangential velocity, together with the variation in the pressure for each cross-sectional area, allows an integration of them along the blade surface to find the total force that they generate and the action point that will produce the axial and tangential moments.

Then the bending moment is known, and the Bending Theory rule for cantilever beams can be applied with the intention of converting this into moments in stress (σ) values:

$$\frac{M}{I} = \frac{\sigma}{Y} \tag{4.17}$$

Where M is the momentum in axial or tangential direction, I is the second moment of area and Y is the distance from the neutral axis to the outer fibre.

4.3.1.1.3 - Centrifugal moment

When the centre of gravity of an aerofoil section does not lie on the radial from the axis of rotation through the centroid of the root section, a bending moment is produced due to the centrifugal applied load (Figure 4.6). A general expression to calculate this moment could be written as:

$$M_g = CF \cdot f(\alpha) \tag{4.18}$$

Where $f(\alpha)$ is a function which indicates the amount of leaning that the blade has for each cross-sectional area.

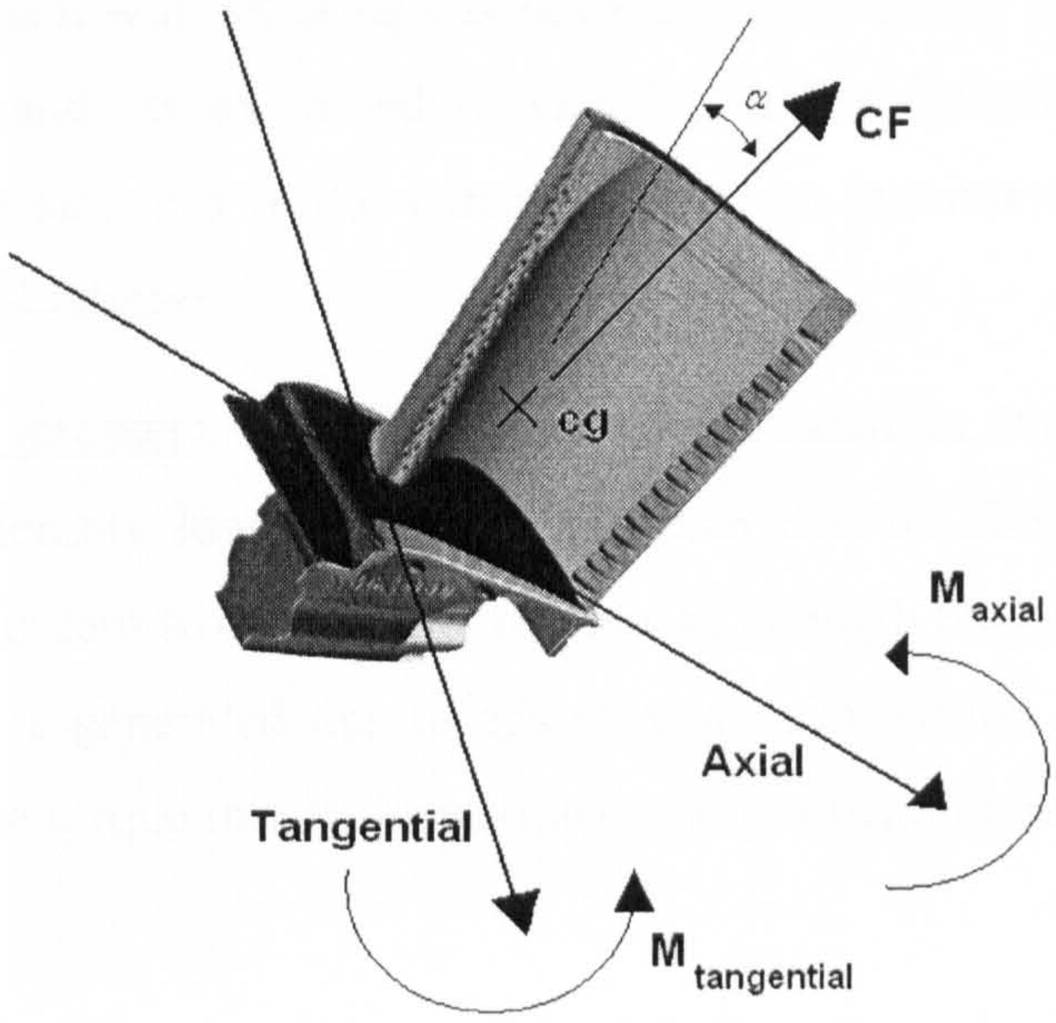

Figure 4.6 - Scheme of the forces and moments acting on the blade

4.3.2 - Assumptions and considerations

Some of the stress sources applied to turbine blades not described in the previous section such as the thermal load, vibrations, and others, and the reasons for that are explained in this section. The first reason is that some of them can be negligible in comparison with the loads described previously. Secondly, other loads carry a very complex methodology or need a very valuable input data (not available in the open literature) to be determined, which will convert into an excessive use of time for the contribution that they will make to the final results. On the other hand some of them can be considered out of context as the selected mechanisms of failure described previously do not take them into account, e.g. in the case for vibrations.

The following assumptions deserve particular clarification in order to properly define the analysis of this investigation's concern with the mechanical design scope:

- Thermal load: this stress comes from the thermal gradients in a blade, which can be spatial (they vary with the annular shape), or temporal (in relation to the cycle of operation of the engine). The second type is the most dangerous due to the relatively high difference of temperature that one blade can be exposed to, mainly in engines with blade cooling systems. The problem of the thermal load is dealt with by the thermal fatigue task that usually carries a very complex analysis (Marscher, 1992). Despite the complexity of such analysis it will not bring any relevant improvement to the final target of this study and, as explained previously, in this investigation the number of engine start-ups is the parameter used to monitor the damage caused by thermal fatigue.

- Shear stresses: The shear stresses produced in turbomachine blades are considerably lower in magnitude than that of direct stress. They can be insignificant from the point of view of strength but not from stiffness. Shear stress is generated due to gas pressure distribution along the blade length and the torque that the centrifugal and gas bending moments generate in the blade.

- Bending moments: As explained before, the principal causes of bending moments are the centrifugal force and the gas bending moments. The blade is usually leaned in the direction of rotation then it can balance all or part of the gas bending moment in the tangential direction. However, the blade can also be leaned axially with the objective to oppose the tangential and axial gas bending moments in a process known as "leaning or balancing". Obviously it is not possible to eliminate the effect of the gas bending moments for all operating conditions. However, in this investigation, stress produced by bending moments was not considered based on the reasonable assumption that bending moments produced by centrifugal forces have an equal magnitude to those that the gas produces.

Consequently, the load that is taken into account in this investigation is the centrifugal load, which produces a direct axial stress, as previously discussed.

4.4 - Creep life assessment

Single crystal Ni-base super alloys are commonly employed for use as high temperature creep and oxidation resistant blade alloys in the early stages of the modern gas turbine. Their excellent high temperature creep resistance is a result of the barriers to dislocation motion at high temperatures, achieved by a combination of solid solution strengthening and the absence of deleterious grain boundaries.

The complex geometry and anisotropy of blade components and the multi axial stress states they experience, have led to complex relationships between loads, temperature and deformation. It is necessary, therefore, to have a creep life consumption model that allows for the efficiency optimisation of turbine blades, and also prevents failure and avoids over design.

In this study the basic model selected for calculating the creep life consumption, caused by a given pattern of loading is the Larson-Miller time temperature parameter.

4.4.1 - The Larson-Miller parameter

The time temperature parametric method, to extrapolate long-term creep damage, is a technique which has shown great accuracy. The most popular of these methods is that of Larson and Miller. Although this method carries some assumptions it is considered accurate because it has been validated by experimental data and widely used in the engineering literature (Larson and Miller, 1952; Boyer, 1988; Jaske and Simonen, 1991; Bowman et al., 2004; Singh et al., 2005).

This method is based on the assumption that the time necessary to reach a particular strain can be traded for temperature; it means that an increase in operating temperature will reduce the time to reach a particular creep state. This assumption is absolutely true, but the problem that arises is how to relate those variables into a single expression which expresses the whole range of possible conditions. The definition of the Larson-Miller parameter is given by the following equation:

$$P = f(\sigma) = 1.8 \cdot T(K) \cdot 10^{-3} \cdot (\log t_r + C) \quad \textbf{(4.19)}$$

Where P is the Larson-Miller parameter that is a function of the stress level, T(K) is the metal temperature in Kelvin, t_r is the time to failure (stress rupture time) and C is a constant often taken as 20 in industrial applications.

The Larson-Miller parameter depends on the stress level and the blade material selected. This information used to be represented graphically for a specific material and such graphs are known as master curves. There are many kinds of advanced materials that can be used in turbine blades. However the master curves of such materials are not available in the open literature. Because of that, in this investigation all the calculations involving the Larson-Miller parameter will use the nickel base super alloy MAR-M 247 for which the master curve is presented in Figure 4.7.

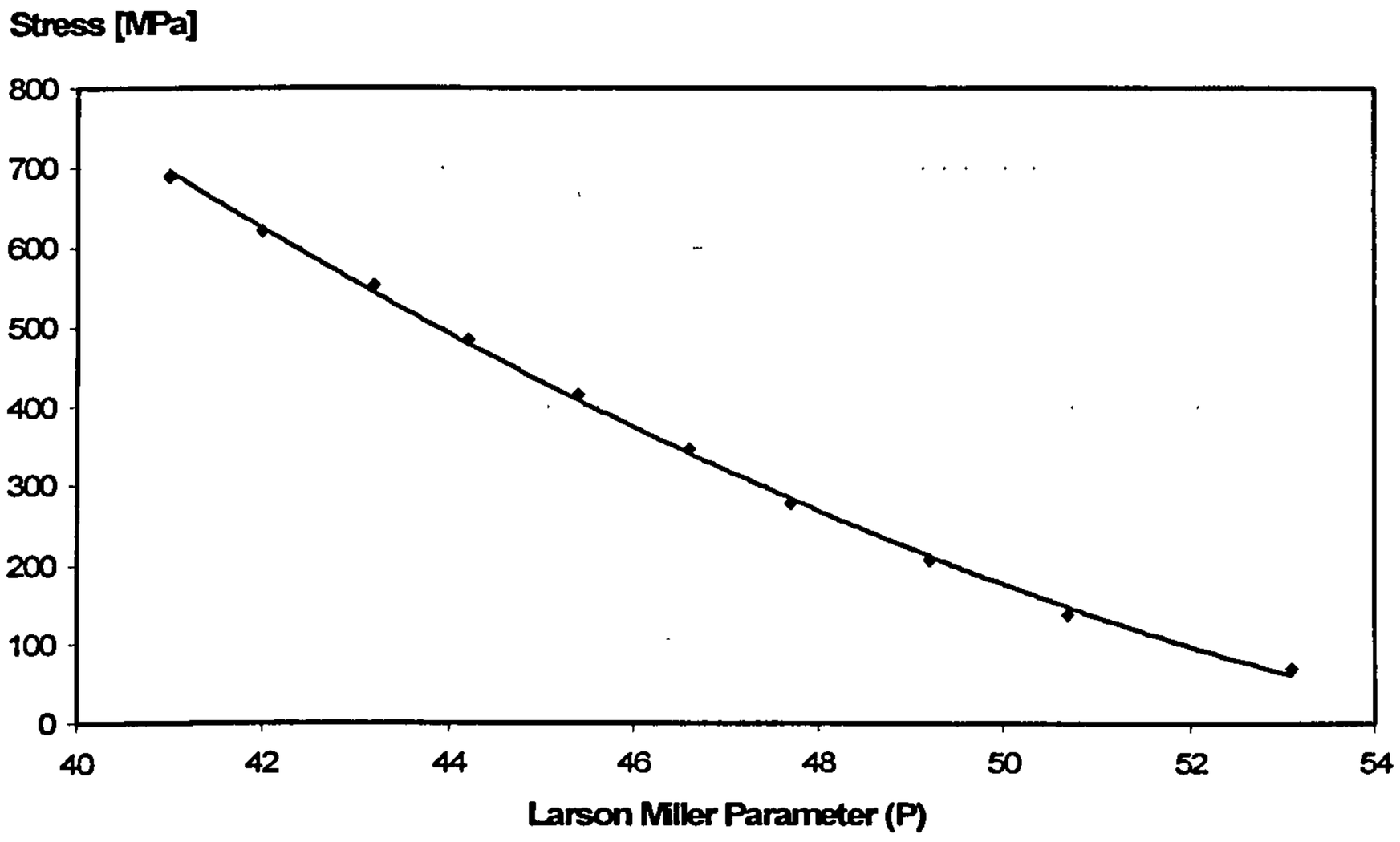

Figure 4.7 - MAR-M 247 master curve (Gomez, 2005)

Equation 4.19 can be understood as any combination of temperature and time which gives an equivalent value of the Larson-Miller parameter (P), which corresponds to an equivalent value of creep stress. The output of this simple expression will be the time to rupture that will be necessary at the temperature and stress conditions being studied. The advantage of this expression is that since the Larson-Miller parameter of a specific material can be found in the literature or obtained in the laboratory, the stress

rupture time can be estimated for a given stress and temperature (Figure 4.8). The Larson-Miller expression can be used with accuracy since the metal temperature is not extrapolated into high temperatures regions, as it is possible that metallurgical changes could take place, which essentially means that the properties of the material would change.

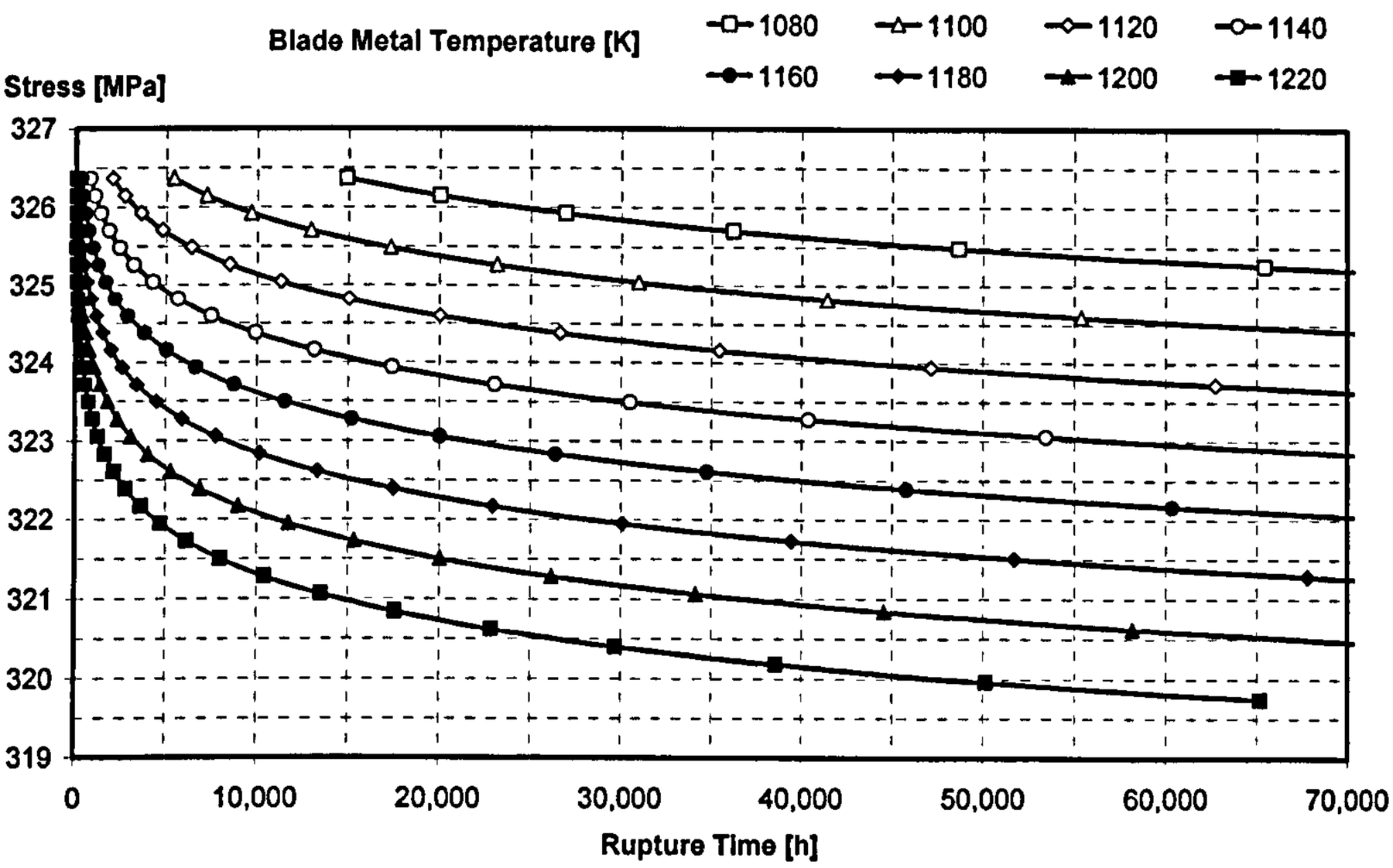

Figure 4.8 – Useful lifetime of the alloy MAR-M 247 given by Larson-Miller expression

The MAR-M 247 is nickel base, vacuum melted, cast super alloy with a high volume fraction (62%) and high refractory element (Ta+W+Mo). The alloy, developed in the very early 1970's by Danesi, Lund and others at Martin Metals Corporation, demonstrates high creep strength and good cast ability along with excellent oxidation resistance, resulting in increasing application in turbine engines (Roskosz, 2006). Under ambient room temperature conditions, the material has the following tensile properties (Table 4.1):

Table 4.1 - MAR-M 247 tensile properties

Young's Modulus (E)	221 GPa
0.2% Proof Strength ($\sigma_{yso.2\%}$)	801 MPa
Ultimate Tensile Strength (σ_{UTS})	1107 MPa

4.4.2 - Cumulative creep application

In this investigation the life cycle of the gas turbine will be assessed in several check points. In each check point the blade metal temperature and centrifugal stress will be estimated based on the operating conditions of the engine and the time to failure will be calculated using the Larson-Miller parameter expression. The blade metal temperature and centrifugal stress will be estimated using the mathematical model described in the previous section.

Turbine life cycling generally consists of repetitions of several combination of stress. Many theories have been proposed for how to combine the effects of these cycle groups. Two methods have been shown to have universal application to engineering materials: Miner's Rule and Fracture Mechanics.

The basic principle of fracture mechanics is that the progress of a pre-existing crack can be predicted cycle-by-cycle as a function of crack length and shape, stress, temperature and the corrosivity of the environment. It involves laboratory non-destructive tests and non-destructive testing inspections to produce a crack growth chart for the next cycle under similar temperature and environmental conditions to that expected for the component's service.

Miner (1945), popularised a rule that had first been proposed by A. Palmgren in 1924 and since then it has been used in many approaches involving life cycle engineering materials assessment (Tanaka and Akita, 1975; Shimokawa and Tanaka, 1980; Murakami, 1983; Leipholz, 1986; Sun, 1994; Boessioa et al., 2006). Miner's Rule can combine different factional life consumption failure theories such as fatigue and creep. Miner's law uses a linear damage sum assumption, which relates the damage that

the conditions of each period make to the component with the ratio between the time spent and the time to failure. The rule, also called Miner's rule or the Palmgren-Miner cumulative linear damage hypothesis, states an inverse sum law, such as:

$$\frac{T_f}{t_f} = \sum_{i=1}^{NC} \frac{T_i}{t_{ri}} \tag{4.20}$$

Where NC is the number of cycles, T_i is the running time spent in each check point, t_{ri} is the time to failure in the conditions of that check point predicted by the Larson-Miller expression, T_f is the total engine running time and t_f is the total running time to failure that this blade could spend until failure occurs.

4.5 - Monte Carlo Risk Analysis

The Monte Carlo technique is a numerical method of solving engineering problems by random sampling and it was first introduced by J. von Neumann and S. Ulam (Ulam et al., 1947; Metropolis and Ulam, 1949). The method usually involves complex problems in various areas of knowledge such as reliability engineering, nuclear engineering, astrophysics, agriculture, and many others. In the Monte Carlo method a random number is drawn and used in specific algorithm iterations. The process is repeated *N* times with each trial being independent of each other. From the randomness comes the convergence and a central value is derived.

4.5.1 - Random number generator

The random number generators available in the open literature are almost always linear congruent generators, which generate a sequence of integers between 0 and a large number by a recurrence equation. This equation will eventually repeat itself *M* times. Any initial "seed" choice of the random population is as good as any other and the sequence just takes off from that point.

Park and Miller have surveyed a large number of random number generators that have been used over the last 30 years or more. They proposed a "minimal standard" generator based on the choice for the recurrence equation constants first proposed by Lewis, Goodman and Miller in 1969. This generator has in subsequent years passed all new theoretical tests, and has accumulated a large amount of successful use.

In order to remove low-order serial correlations, Bays and Durham (1976), proposed an algorithm which shuffles the output of the minimal standard generator. This algorithm has been successfully tested with several statistics methods (Press et al., 1992).

4.5.2 - Random Gaussian distribution

Uncertainty in a mathematical model can be represented by a continuous or semi-continuous subjective probability distribution which expresses the relative chances that the variable being estimated will produce any particular value. Then it is convenient and appropriate to express a subjective probability distribution as a particular mathematical function, for example such as a Gaussian (normal) distribution.

For a given uniform variable x and its function y(x), the probability distribution of y (p(y)dy) is determined by:

$$p(y) = p(x)\left|\frac{dx}{dy}\right| \tag{4.21}$$

The solution of equation (4.21) for random variables with a Gaussian distribution is given by the Box-Muller method:

$$p(y)dy = \frac{1}{\sqrt{2\pi}} \cdot e^{-y^2/2}\, dy \tag{4.22}$$

Then the transformation between two uniform variables x_1, x_2, and two normal variables y_1, y_2 can be given by the following equations:

$$y_1 = \sqrt{-2 \cdot \ln(x_1)} \cdot \cos(2 \cdot \pi \cdot x_2) \tag{4.23}$$

$$y_2 = \sqrt{-2 \cdot \ln(x_1)} \cdot \sin(2 \cdot \pi \cdot x_2) \tag{4.24}$$

In this study, a Project Risk Evaluation Software (PRisE) has been written in Fortran language to produce the Gaussian distributed variables using the random number generator of Park and Miller with Bays-Durham shuffle and Box-Muller method to produce normal random variables.

4.6 - Turbine life assessment

The software Lifespan was written in Fortran language to carry out the life cycle assessment of a mini-pool of gas turbine units for power generation. In Figure 4.9 it is possible to see the scheme of the gas turbine life cycle assessment developed in this study. The units' off-design performance of engines were simulated using the software Turbomatch, described in chapter 1. The centrifugal stress and blade metal temperature were calculated based on the mathematical model developed in sections 4.2 and 4.3. The Monte Carlo risk analysis was carried out with the software PRisE described in the previous section.

Miner's law assumes that the component failure will happen when the sum of equation 4.20 is equal to one. However, in this analysis the maximum total consumed life allowed is 0.86, which can be considered as a conservative and low risk value. Then a Monte Carlo risk analysis is used to assess the uncertainty involved in the Miner's cumulative damage rule.

A case study for a gas turbine is described in Table 4.2. The unit is assumed to be working in different regimes of operation over the year, which include base load (case#1) and part-load operation (cases#2-5) as shown in Figure 4.10. The effects of ambient temperature were considered (Table 4.3) and the ambient pressure was taken as constant over the year.

Table 4.2 – Design Point Parameters

Total Mass Flow	46.90	kg/s
Rotational Speed	11,000	rpm
Turbine Entry Temperature	1,210.0	K
Blade Metal Temperature	1,209.8	K
Compressure Pressure Ratio	15.5	-
Flow Coefficient	0.9	-
Nozzle Angle	70	°
Power Output	10,300	kW
Thermal Efficiency	0.3317	-
Centrifugal Stress	84.21	Mpa
Larson Miller Parameter	52.3	-
Time to Failure	10,657	h

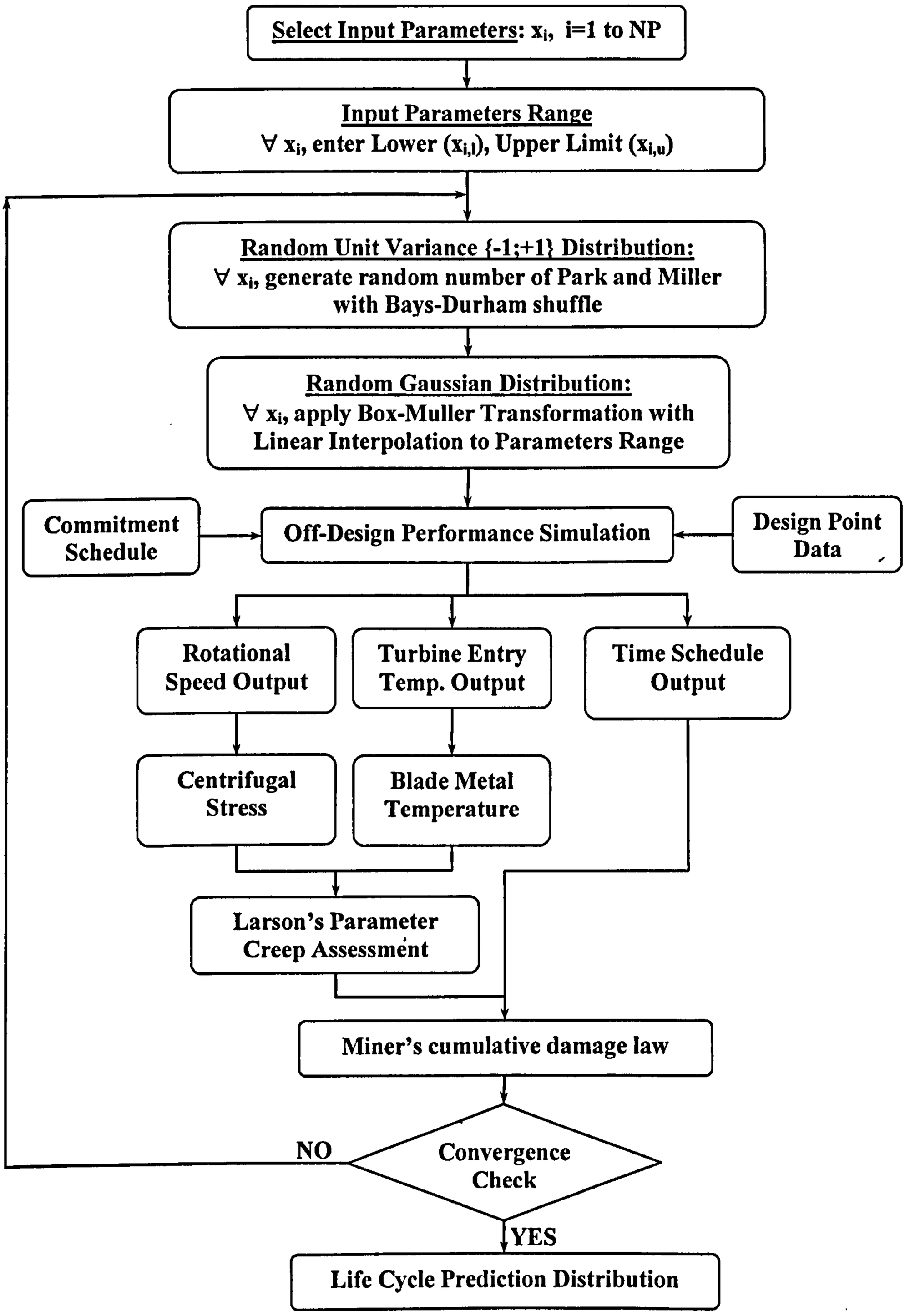

Figure 4.9 – General scheme of life cycle and probabilistic risk analysis assessment

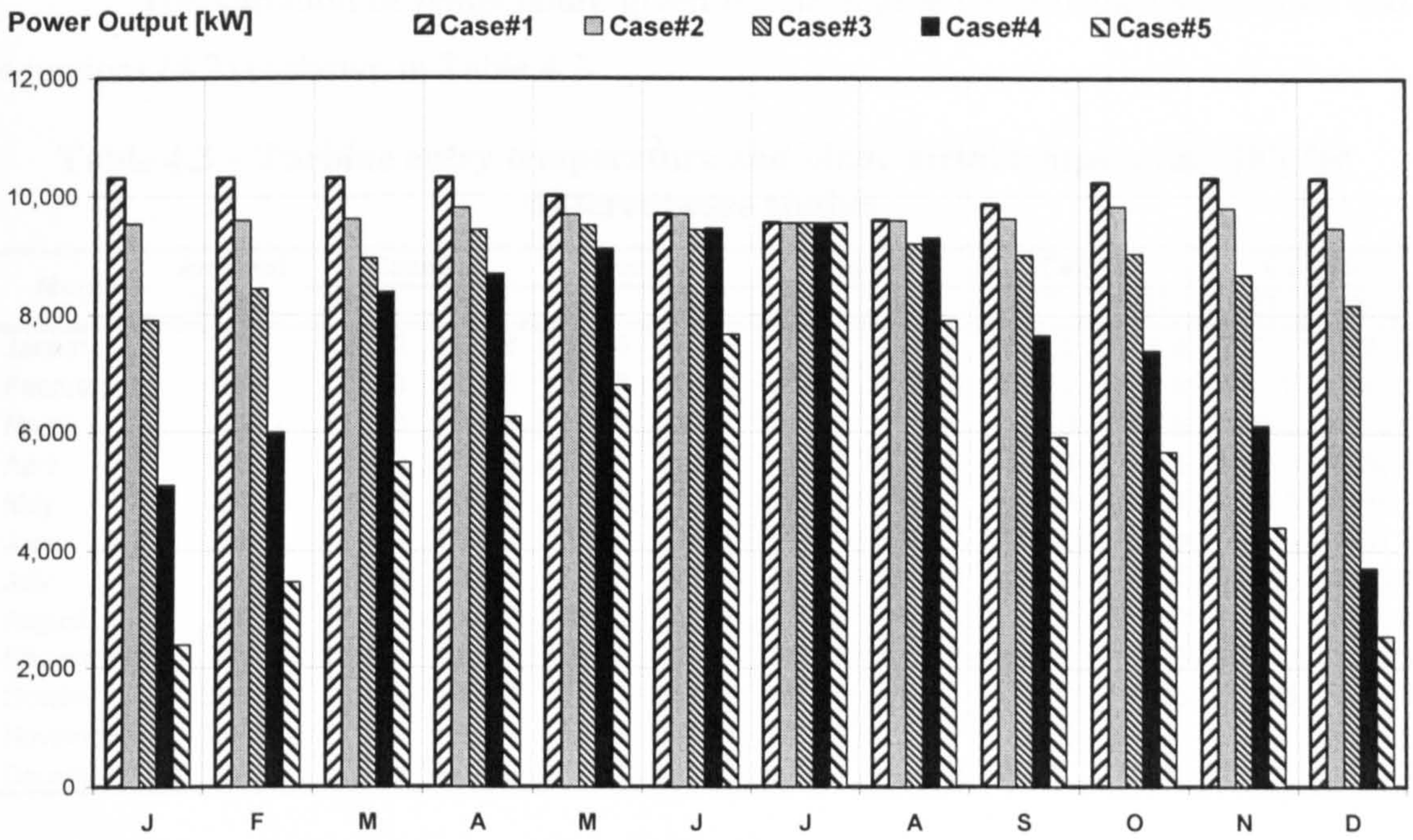

Figure 4.10 – Off-design performance over the year

In this approach a typical blade tip speed (U_{cg}) of 340 m/s is adopted as it is considered the maximum value that will lead to acceptable stresses. In current gas turbines the optimum value for flow coefficient (φ) is from 0.8 to 1.0 and the nozzle angle (α_2) from 60° to 80° (Saravanamuttoo et al., 2001). The density of the NI-Cr-co alloy used for gas turbines blades is about $\rho_b = 8000$ kg/m^3. The Area-height ratio (Ahr = 6.632 10^{-4} m^2) used in this investigation, between the blade cross-sectional area and height for an "uncooled" blade, is illustrated in Figure 4.11.

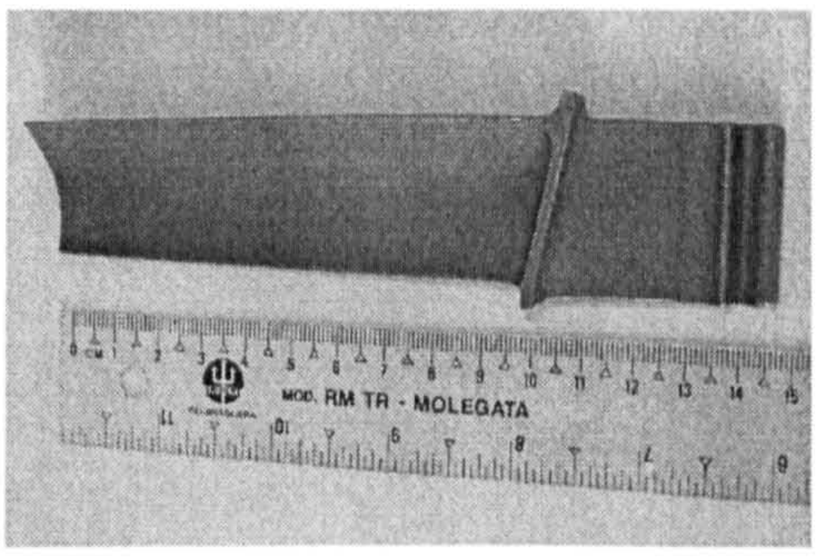

Figure 4.11 – Turbine blade: h = 0.105m, A = 6.964 10^{-5} m^2, Chord 0,031 m, Pitch 0,018 m

The variation of temperature given by the engine performance simulation and equations (4.2) is shown in Table 4.3.

Table 4.3 – Turbine entry temperature and blade metal temperature [K] for different case studies

Month	Ambient Temp.	Case#1		Case#2		Case#3		Case#4		Case#5	
		TET	BMT	TET	BMT	TET	BMT	TET	BMT	TET	BMT
January	278	1210.0	1209.8	1180.6	1180.4	1117.6	1117.4	1008.0	1007.8	900.0	899.8
February	280	1210.0	1209.8	1182.6	1182.4	1138.1	1137.9	1043.0	1042.8	943.0	942.8
March	283	1210.0	1209.8	1183.6	1183.4	1158.3	1158.1	1136.0	1135.8	1023.0	1022.8
April	287	1210.0	1209.8	1190.6	1190.4	1176.5	1176.3	1148.0	1147.8	1053.0	1052.8
May	293	1210.0	1209.8	1197.9	1197.7	1190.9	1190.7	1176.0	1175.8	1086.0	1085.8
June	298	1210.0	1209.8	1210.0	1209.8	1199.9	1199.7	1201.0	1200.8	1132.0	1131.8
July	300	1210.0	1209.8	1210.0	1209.8	1210.0	1209.8	1210.0	1209.8	1210.0	1209.8
August	299	1210.0	1209.8	1210.0	1209.8	1194.8	1194.6	1199.0	1198.8	1145.0	1144.8
September	295	1210.0	1209.8	1200.8	1200.6	1177.5	1177.3	1125.0	1124.8	1057.0	1056.8
October	289	1210.0	1209.8	1194.8	1194.6	1164.3	1164.1	1101.0	1100.8	1033.0	1032.8
November	284	1210.0	1209.8	1190.8	1190.6	1147.9	1147.7	1048.0	1047.8	980.0	979.8
December	280	1210.0	1209.8	1178.1	1177.9	1128.1	1127.9	953.0	952.8	907.0	906.8

The unit is scheduled for overhaul maintenance based on the life cycle prediction. During maintenance it is considered that all the hot parts are replaced by new components, including the turbine blades. The unit downtime (outage hours) was considered as 30 days and the period of analysis is 10 years with a monthly life assessment (120 check points). The mean time between failure (MTBF) and consumed life rate are illustrated in Figure 4.12. The line inclinations represents the consumed life rate (Figure 4.13). The low consumed life rate is a consequence of the partial load operation which results in lower turbine inlet temperature and lower turbine degradation. Consequently there is an increase in the time between failure.

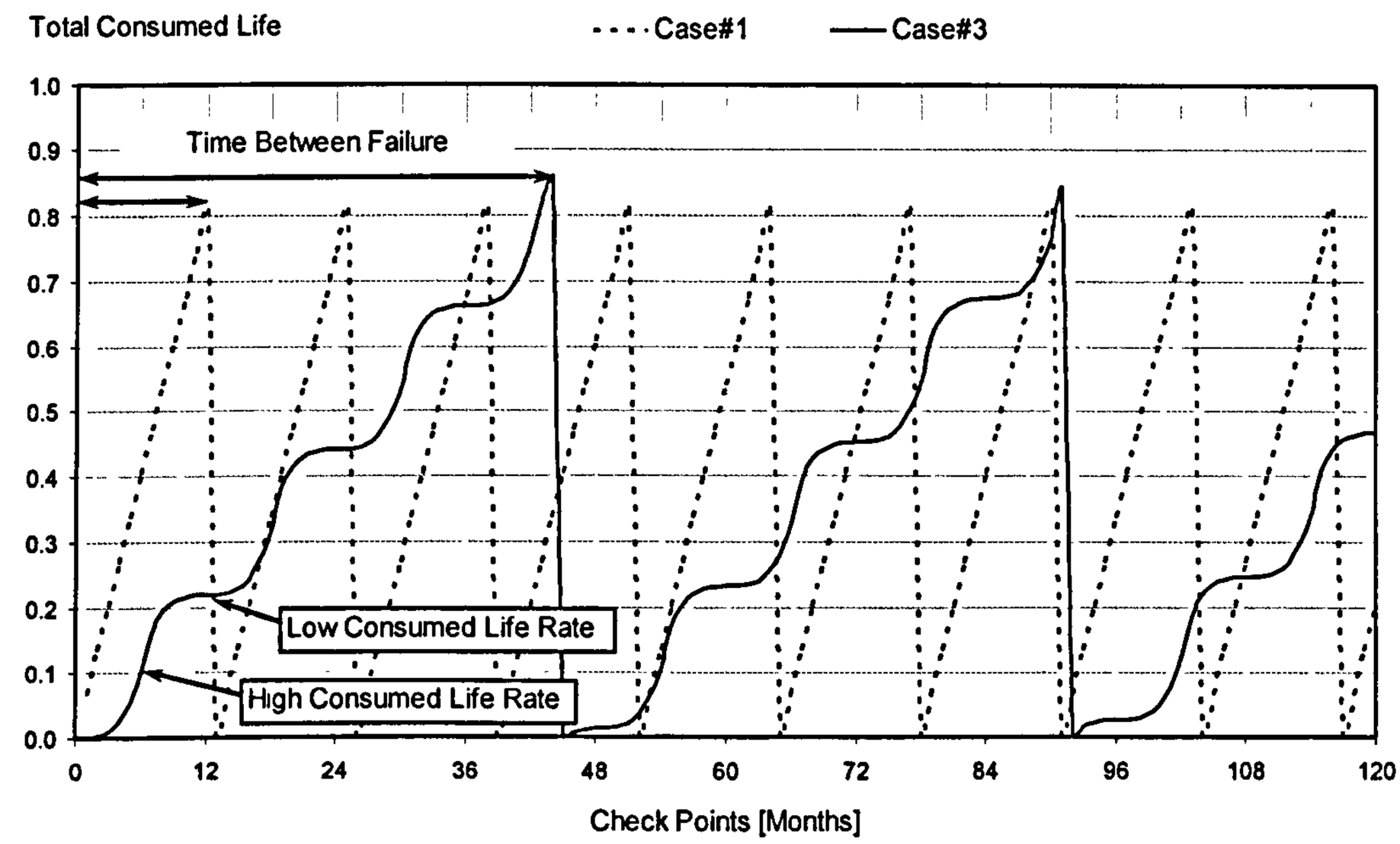

Figure 4.12 – Time of Operation between failure

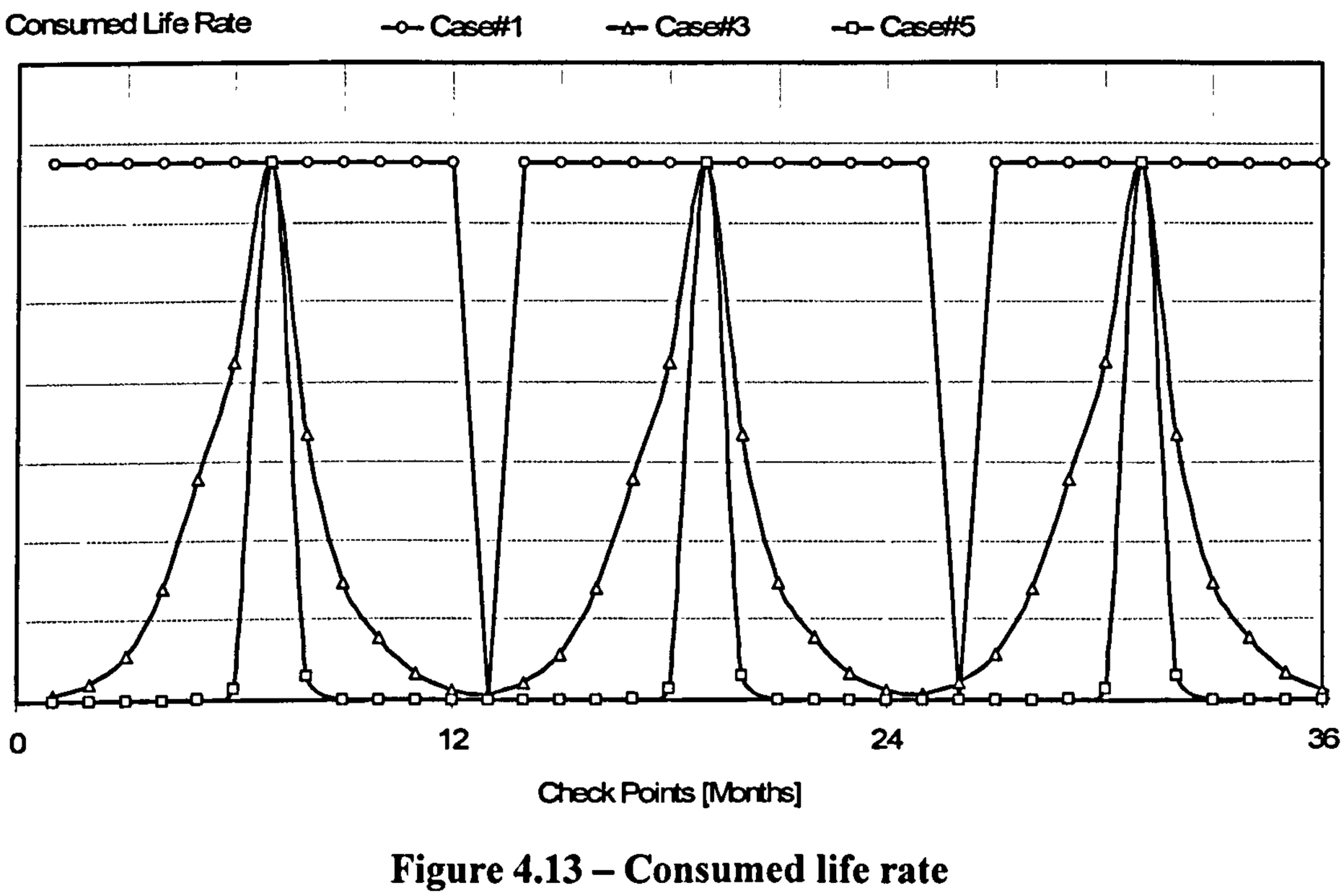

Figure 4.13 – Consumed life rate

The definition of availability (A) is given by the following equation. Where MTBF is mean time between failure and DT is downtime (outage hours):

$$A = \frac{MTBF}{MTBF + DT} \tag{4.25}$$

The definition of capacity factor (CF) is given by the following equation. Where EP_i is the electricity produced over each check point period, MPO_i is the maximum power output available over each check point period (Δt_i):

$$CF = \frac{\sum_{i=1}^{NCP} EP_i}{\sum_{i=1}^{NCP} MPO_i \cdot \Delta t_i} \tag{4.26}$$

Table 4.4 and Figure 4.14 show the capacity factor and availability behaviour for different case studies. The drop in capacity factor causes an increase in the useful lifetime and then higher availability is achieved.

Table 4.4 – Capacity Factor and Availability for different case studies

	Total Availability	Capacity Factor	Hours of Operation Between Failure [h]
Case#1	0.923	0.926	8,640
Case#2	0.957	0.918	15,840
Case#3	0.978	0.874	31,680
Case#4	0.986	0.734	49,480
Case#5	0.993	0.563	108,000

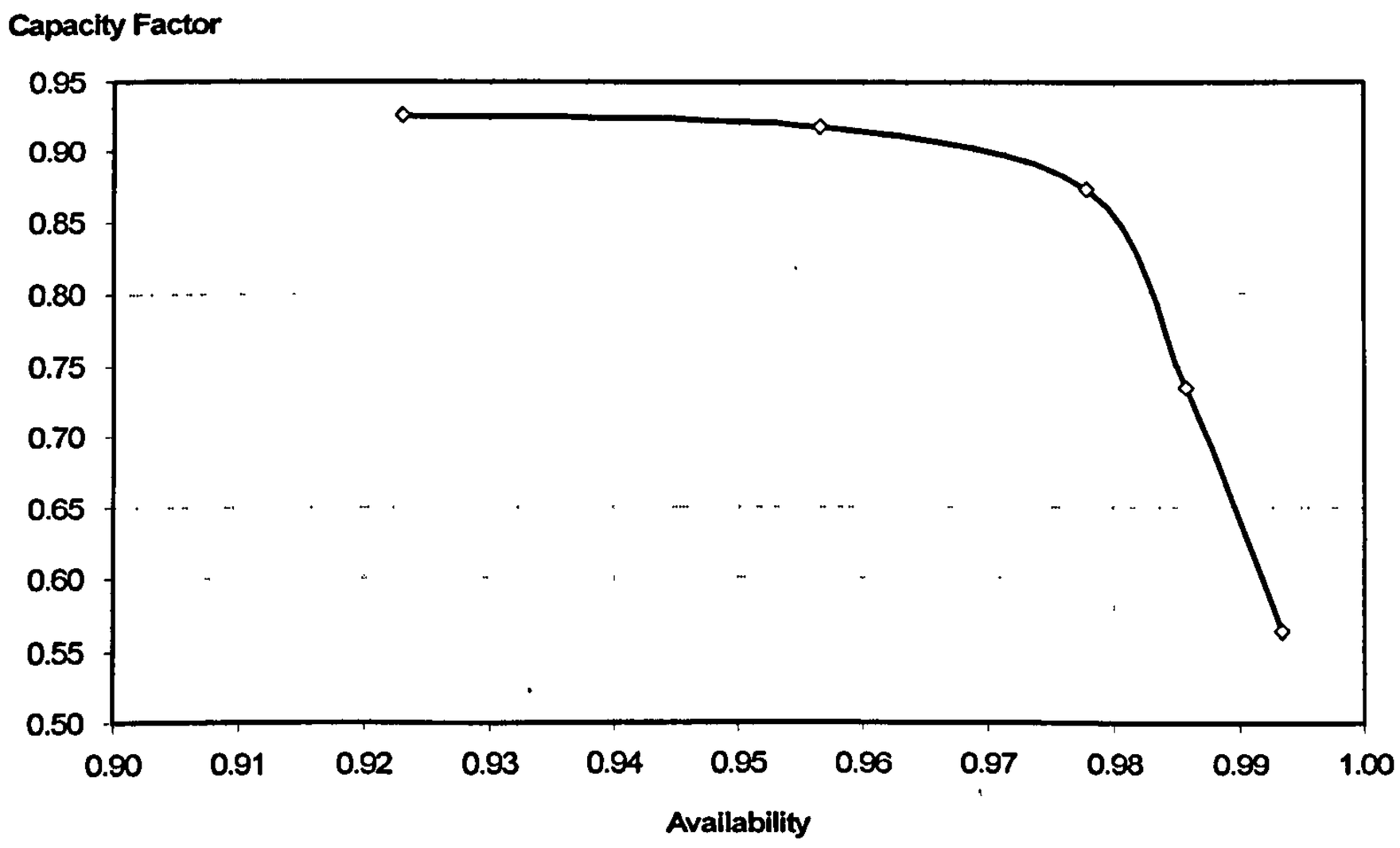

Figure 4.14 – Relation between capacity factor and availability

Again, Miner's law assumes that the component failure will happen when the sum of equation 4.20 is equal to one. However, due to the probabilistic nature of the failure mechanisms involved in life cycle assessment, this parameter shows a certain level of uncertainty and then a probabilistic risk analysis is required to properly evaluate it.

Figure 4.15 shows the input probability distribution of the maximum consumed life between 0.68 and 1.04. Figure 4.16 shows the risk involved in the life cycle assessment of case#1. Results show that there is 86% chance the mean time between failures be lower then 9,360 hours. A maximum of 10,800 hours is possible but with a probability of 2.6%.

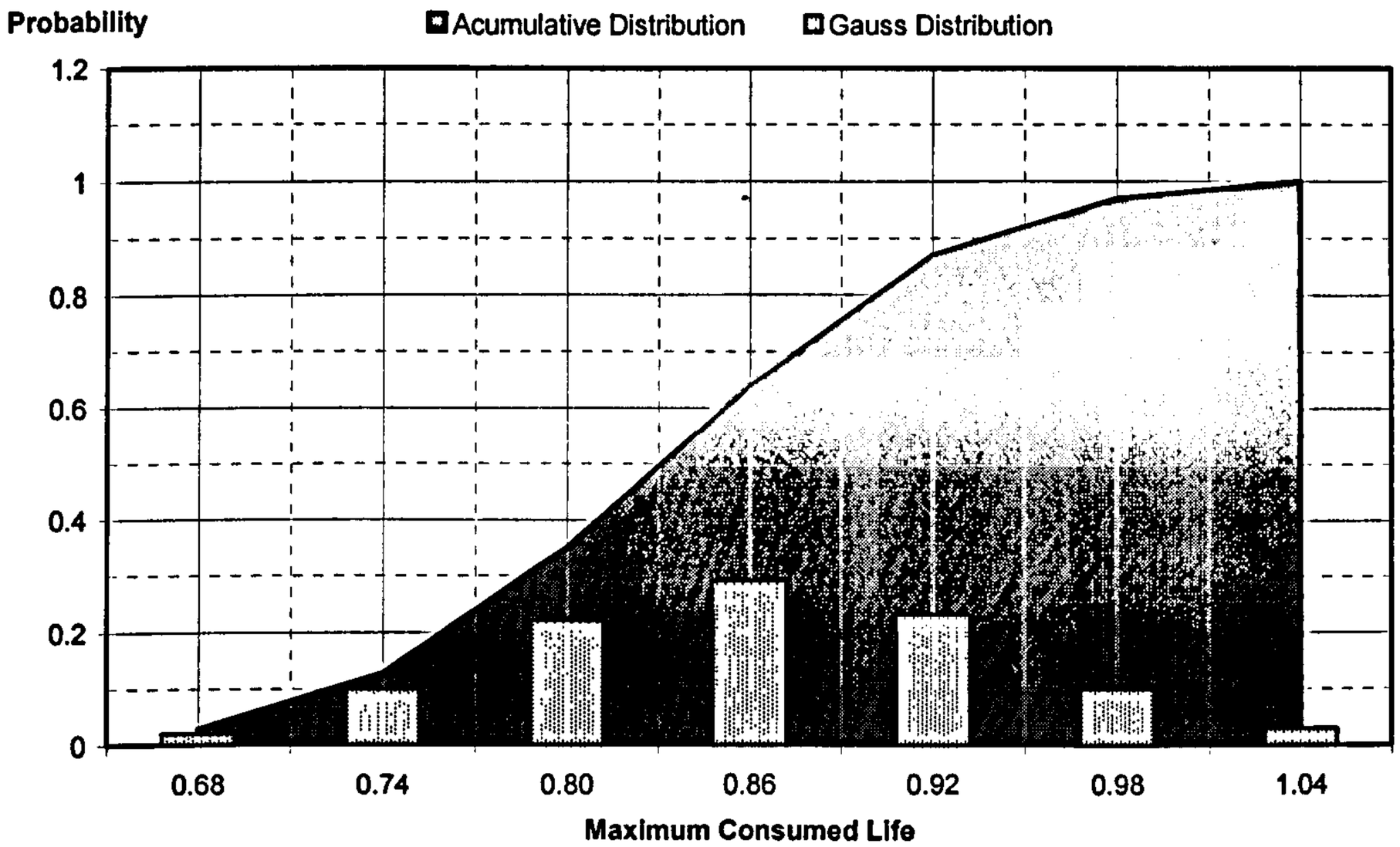

Figure 4.15 –Gaussian Distribution Input - Case#1

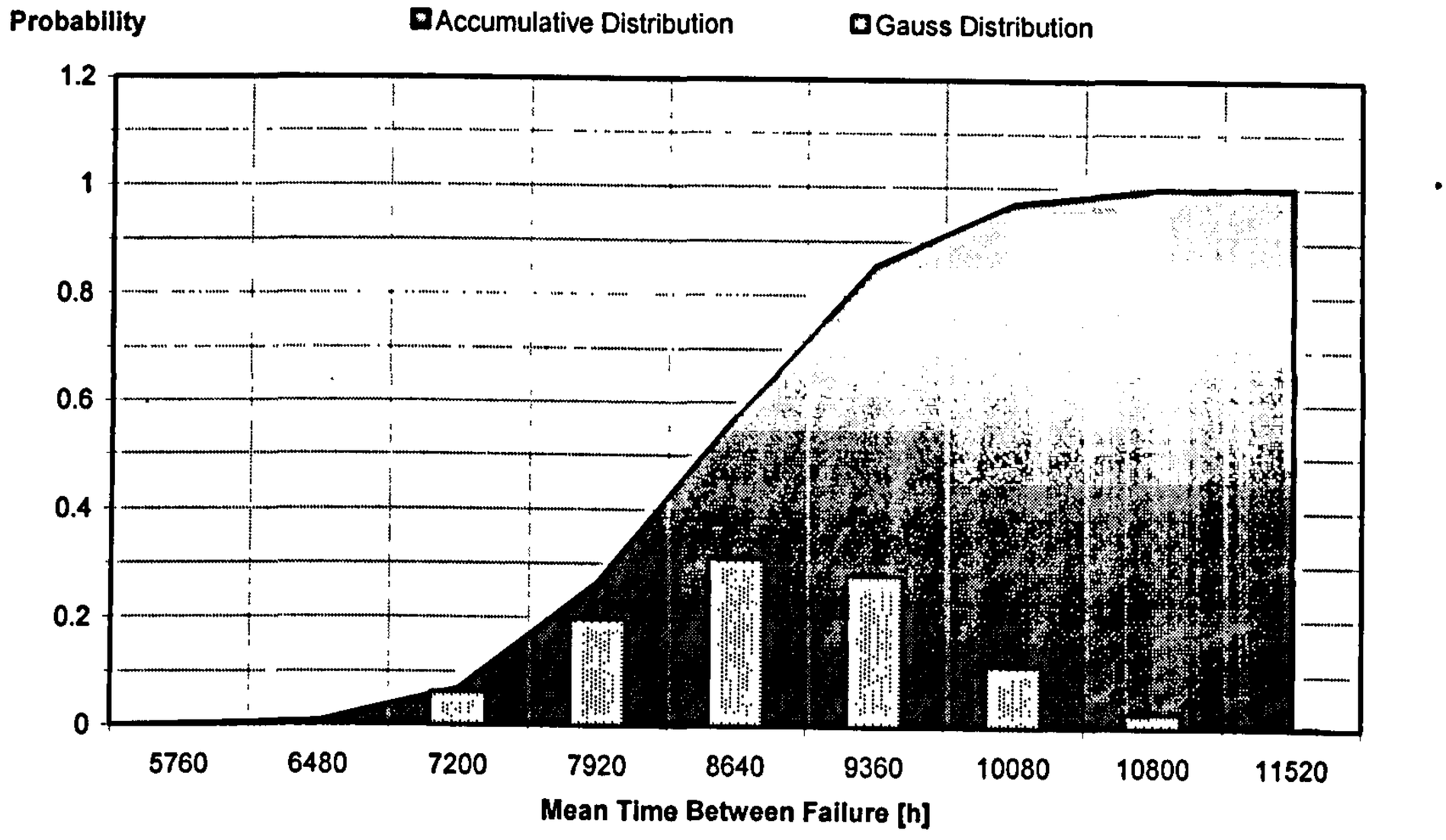

Figure 4.16 – Monte Carlo Risk Analysis Results – Case#1

The algorithm simulation was carried out in 2000 iterations which could be achieved in a few seconds of CPU Time (Pentium M Processor 1.73GHz). However, the analysis had shown convergence in 200 iterations (Figure 4.17).

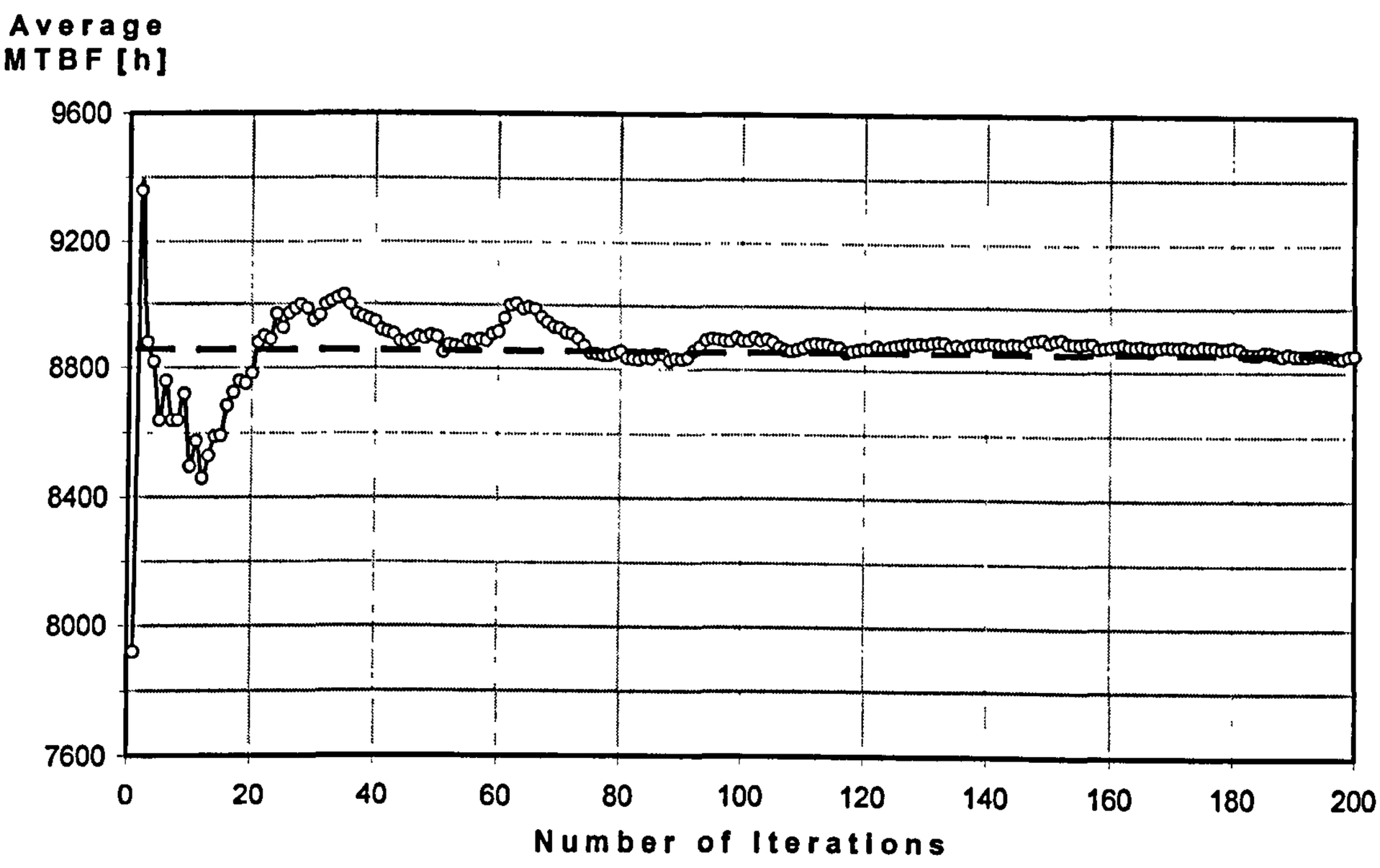

Figure 4.17 – Convergence of the Monte Carlo Risk Analysis – Case#1

Capacity factor represents an important parameter in life cycle assessment as it can change significantly the hours of operation between failures, as discussed before. Figure 4.18 shows the behaviour of the useful engine lifetime with capacity factor and availability.

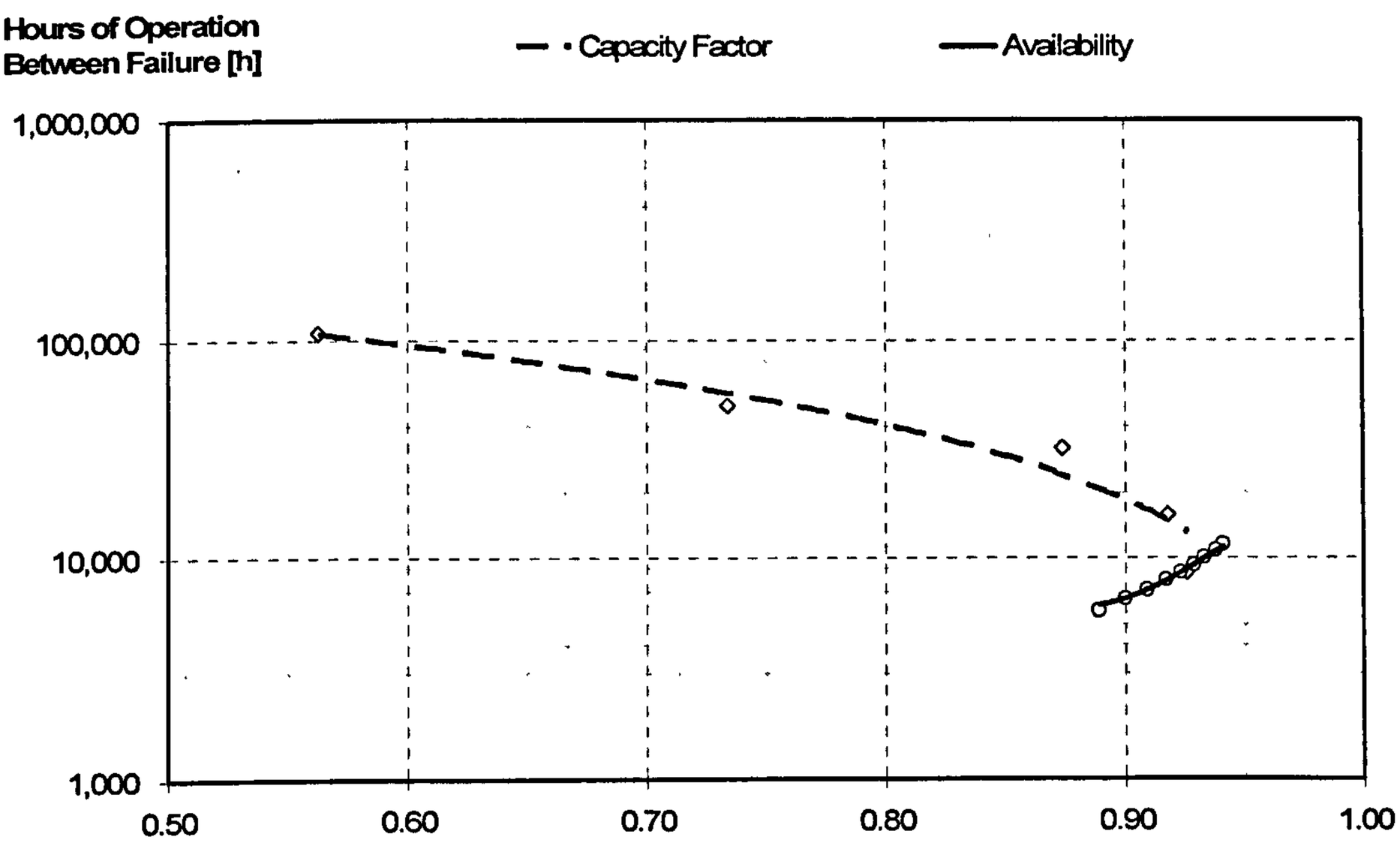

Figure 4.18 – Influence of Capacity Factor and Availability on the Life Cycle - Case#1

Chapter 5 – Performance and Emissions Evaluation of Micro Gas Turbines

5 - Performance and Emissions Evaluation of Micro Gas Turbines

5.1 - Introduction

This chapter presents a performance assessment and the emission levels of two micro gas turbines fuelled by natural gas and diesel, and a ground power unit (GPU) fuelled by kerosene. The data presented are based on experimental tests using these machines operating at partial and full load conditions.

Micro gas turbines are energy generators with typical capacity ranges from 15 to 300 kW. The principle of operation is the same as the open cycle gas turbine, but the machines have several distinctive features, such as: variable or constant speed capability, high rotational speed, compact size, simple operability, ease of installation, low maintenance, air or oil bearings. The high reliability and simple design of these engines make them an attractive prime mover in the generation and distribution of electricity in the small capacity range.

The state-of-the-art micro gas turbines have advanced considerably in recent years. Manufacturers have developed engines with different configurations. The configuration depends on the application, but usually the machine consists of a single turbo-compressor shaft, an annular combustor, a single stage radial flow compressor and turbine, with or without a recuperator. Acceptable thermal efficiencies are maintained by the partial recovery of the heat of the turbine exhaust which is transferred to the compressor outlet to preheat the air supply before it enters the combustor. This is usually done using an air-to-air heat exchanger called a recuperator or regenerator. Net cycle efficiencies are therefore increased to as much as 30% compared to the simple cycle average of 17% (Rodgers et al., 2001). The optimum rotational speed of these turbo machines at full power ratings is between 60,000 and 100,000 rpm. Some units are also able to operate in parallel with and/or isolated from the electric utility system and as multiple units for enhanced reliability.

Ground Power Units (GPUs) are relatively small, self-contained gas turbine generators found in military bases and airports, to service aircrafts between flights i.e. providing electricity and hydraulic pressure while the aircraft is on the ground. Typically they present the following features: constant speed, single-shaft design, single-stage centrifugal compressor, tangential can combustor, and a single-stage radial turbine. They also present high reliability and durability (Kidwell, 1989).

Emission control technologies and regulations for distributed generation systems are not yet precisely defined. However, control technologies exist that could reduce emissions from the fossil-fuelled components of a distributed generation system to levels similar to other traditional fossil-fuelled generation technologies. High temperature combustion produces a significant amount of NO_X, mainly Nitric Oxide (NO), which subsequently oxidises in the atmosphere to produce Nitrogen Dioxide. The combustion processes in micro gas turbines can result in the formation of significant amounts of NO_X (Nitrogen Oxides) and CO (Carbon Monoxide). Some manufacturers have developed advanced combustion technologies to minimise the formation of these pollutants as both have a negative effect on human beings.

5.2 - Performance and Emissions Tests

Data sampling was carried out during emissions and performance tests for approximately 30 minutes in order to allow the machine to achieve a permanent regime of operation in each power setting point. The exact installation location of the instrumentation had to be carefully selected in order have the lowest interference in the engine function and from the engine components. This was not an easy task mainly because the machines investigated are very compact and access to internal components is therefore very restricted.

Total and static exhaust pressures, and the engine gas path pressures and temperatures were measured in order to calculate the gas turbine mass flow and performance parameters. The mass flow is calculated with the procedure described below. The gas turbine exhaust mach number (GTEM) is given by the following equation, where GTETP is the gas turbine exhaust total pressure and GTESP is the gas turbine exhaust static pressure.

$$\text{GTEM} = \sqrt{\frac{2}{\gamma_g - 1} \cdot \left[\left(\frac{\text{GTETP}}{\text{GTESP}} \right)^{\frac{\gamma_g - 1}{\gamma_g}} - 1 \right]} \tag{5.1}$$

Then the gas turbine exhaust static temperature (GTEST) can be calculated with equation (5.2), where GTETT is the gas turbine exhaust total temperature

$$\text{GTEST} = \frac{\text{GTETT}}{1 + \frac{\gamma_g - 1}{2} \cdot (\text{GTEM})^2} \tag{5.2}$$

The exhaust gas mass flow ($\dot{m}_g$) is the product of the exhaust density (GTED), area (GTEA) and velocity (GTEV):

$$\dot{m}_g = \text{GTED} \cdot \text{GTEA} \cdot \text{GTEV} \tag{5.3}$$

$$\text{GTEV} = \text{GTEM} \cdot \sqrt{\gamma_g \cdot \text{GTEST} \cdot \text{R}} \tag{5.4}$$

Then air mass flow ($\dot{m}_a$) and air fuel ratio (AFR) are given by equations (5.5) and (5.6), respectively, where $\dot{m}_g$ is the exhaust gas mass flow.

$$\dot{m}_a = \dot{m}_g - \dot{m}_f \tag{5.5}$$

$$\text{AFR} = \frac{\dot{m}_a}{\dot{m}_f} \tag{5.6}$$

The engine performance is given by the equations below. The electrical efficiency (η_e) is:

$$\eta_e = \frac{\text{EPO}}{\dot{m}_f \cdot \text{LHV}} \tag{5.7}$$

Where EPO is the electric power output. The electrical efficiency and electric power output relative to the design point (ISO conditions) were calculated as follows:

$$\bar{\eta}_e = \frac{\eta_e}{\eta_{e,\text{DP}}} \tag{5.8}$$

$$\overline{EPO} = \frac{EPO}{EPO_{DP}} \tag{5.9}$$

Absolute and relative non-dimensional mass flow (NDMF) was calculated with equations (5.10) and (5.11) respectively:

$$NDMF = \frac{\dot{m}_a \cdot \sqrt{T_{01}}}{p_{01}} \tag{5.10}$$

$$\overline{NDMF} = \frac{NDMF}{NDMF_{DP}} \tag{5.11}$$

Absolute and relative non-dimensional rotational speed (NDRS) is given the equations below:

$$NDRS = \frac{RS}{\sqrt{T_{01}}} \tag{5.12}$$

$$\overline{NDRS} = \frac{NDRS}{NDRS_{DP}} \tag{5.13}$$

Finally the gas turbine exhaust total temperature (GTETT) and recuperator entry temperature (RET) relative to the design point conditions were calculated as follows:

$$\overline{GTETT} = \frac{GTETT}{GTETT_{DP}} \tag{5.14}$$

$$\overline{RET} = \frac{RET}{RET_{DP}} \tag{5.15}$$

During the emission data acquisition, the concentration of CO_2 (carbon dioxide), NO_X (NO and NO_2), CO, SO_2 (sulphur dioxide), N_2 (nitrogen), O_2 (oxygen) and exhaust temperature were measured in the exhaust stack at different power settings. The emissions measured were corrected for ambient concentrations of these pollutants and also to the standard 15% of oxygen (O_2).

5.3 - Analysis and Discussion of Results

The performance data were obtained from experimental tests with two Capstone C30 micro turbines fuelled by natural gas and liquid fuel. The operational behaviour of the micro turbines at part and full load were investigated. The performance of a Ground Power Unit (GPU) GTCP30-92 fuelled by kerosene was also assessed. The experimental tests were carried out at unload conditions and maximum rotation speed because of a GPU generator fault.

A software program named PowerScreen (Figure 5.1) was developed in graphical language LabVIEW™ 7.1 for remote monitoring, data acquisition and performance analysis. The software developed allows users to follow remotely the components gas path measurement through a user-friendly interface screen and to record historic temperatures, pressures, fuel flow, and electric power output in file formats compatible with the majority of data processors.

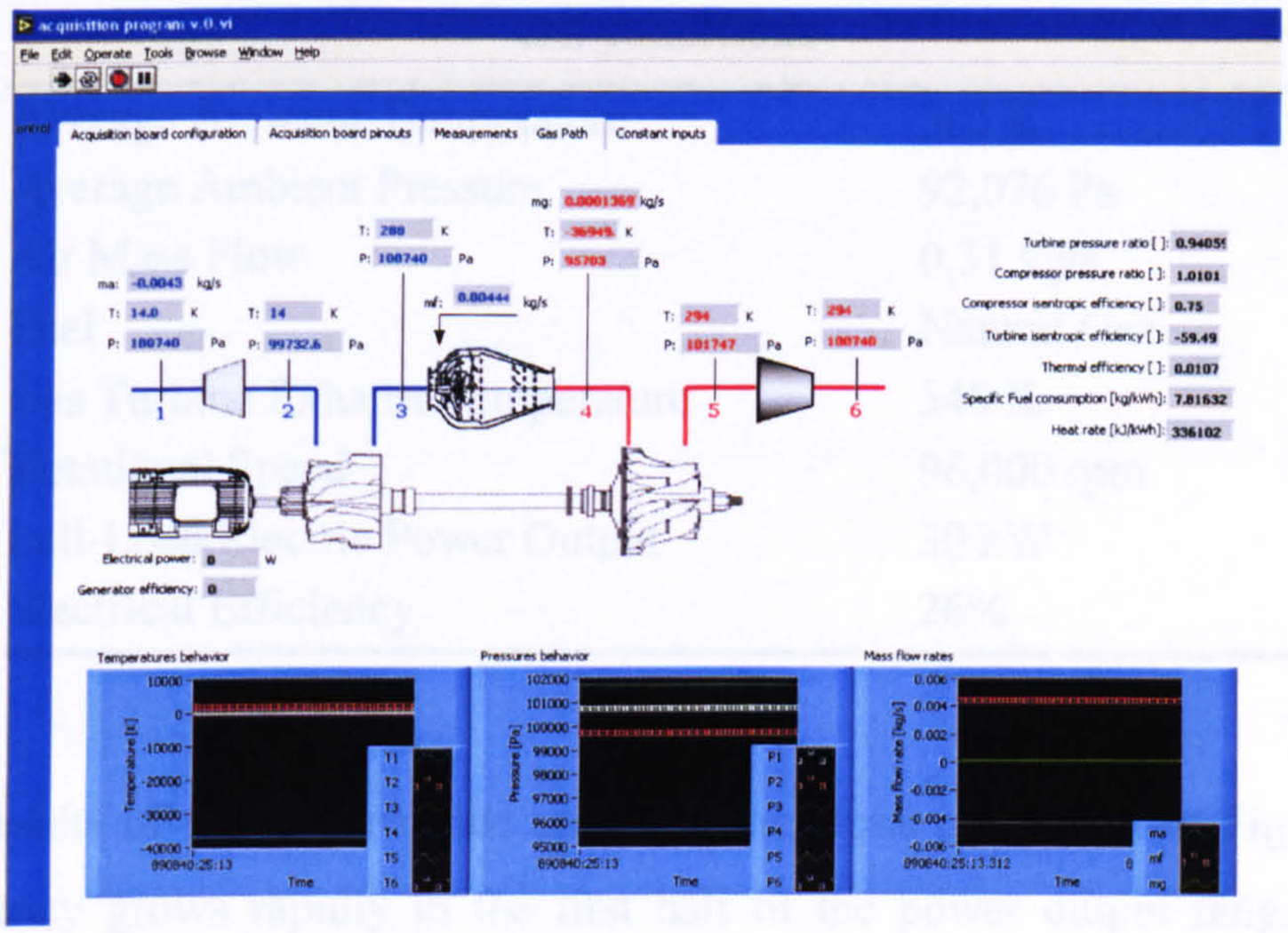

Figure 5.1 – Main screen of the data acquisition software (PowerScreen)

5.4 - Natural Gas Fuelled Microturbine

The micro gas turbine investigated operates in a regenerative gas turbine cycle (Figure 2.3) and consists basically of an air compressor, recuperator, combustor, turbine and a permanent magnet generator. An inverter-based electronic device is also installed allowing the generator to operate at high speeds and frequencies eliminating the need for a gearbox and associated moving parts. Generator, compressor impeller and turbine wheel are set up on a single shaft that rotates at 96,000 revolutions per minute (rpm) at full load.

Table 5.1 shows the design point data of this machine and the ambient test conditions. The natural gas micro turbine was tested while isolated from the electric utility system driving a resistive load. The system behaves as an independent voltage source and supplies the current demanded by the load.

Table 5.1 – Design point performance of natural gas micro turbine and ambient test conditions

Average Ambient Temperature	303 K
Average Ambient Pressure	92,076 Pa
Air Mass Flow	0.31 kg/s
Fuel	Natural Gas
Gas Turbine Exhaust Temperature	548 K
Rotational Speed	96,000 rpm
Full-Load Electric Power Output	30 kW
Electrical Efficiency	26%

Results of the performance and emissions tests are shown in Figures 5.2 and 5.3. Efficiency grows rapidly in the first half of the power output range due to the recuperator effectiveness. Over the second half there has been a slight increase in these parameters and they reach their highest at full load.

Low combustion temperatures reduce the NO_X formation but increase the emissions of CO. The natural gas micro turbine investigates uses a lean-premix combustion system to achieve low NO_X emissions levels at full load. Lean-premix combustion is achieved when higher air to fuel ratio (AFR) is achieved in the primary

combustion zone. Fuel injectors mix a large amount of air with fuel prior to combustion, resulting in a lower combustion temperature.

These machines also have a relatively large primary zone volume within their combustor chamber that allows the air and fuel mixture to remain in the combustion zone for a relatively long time period. This results in higher residence time and more complete combustion of CO.

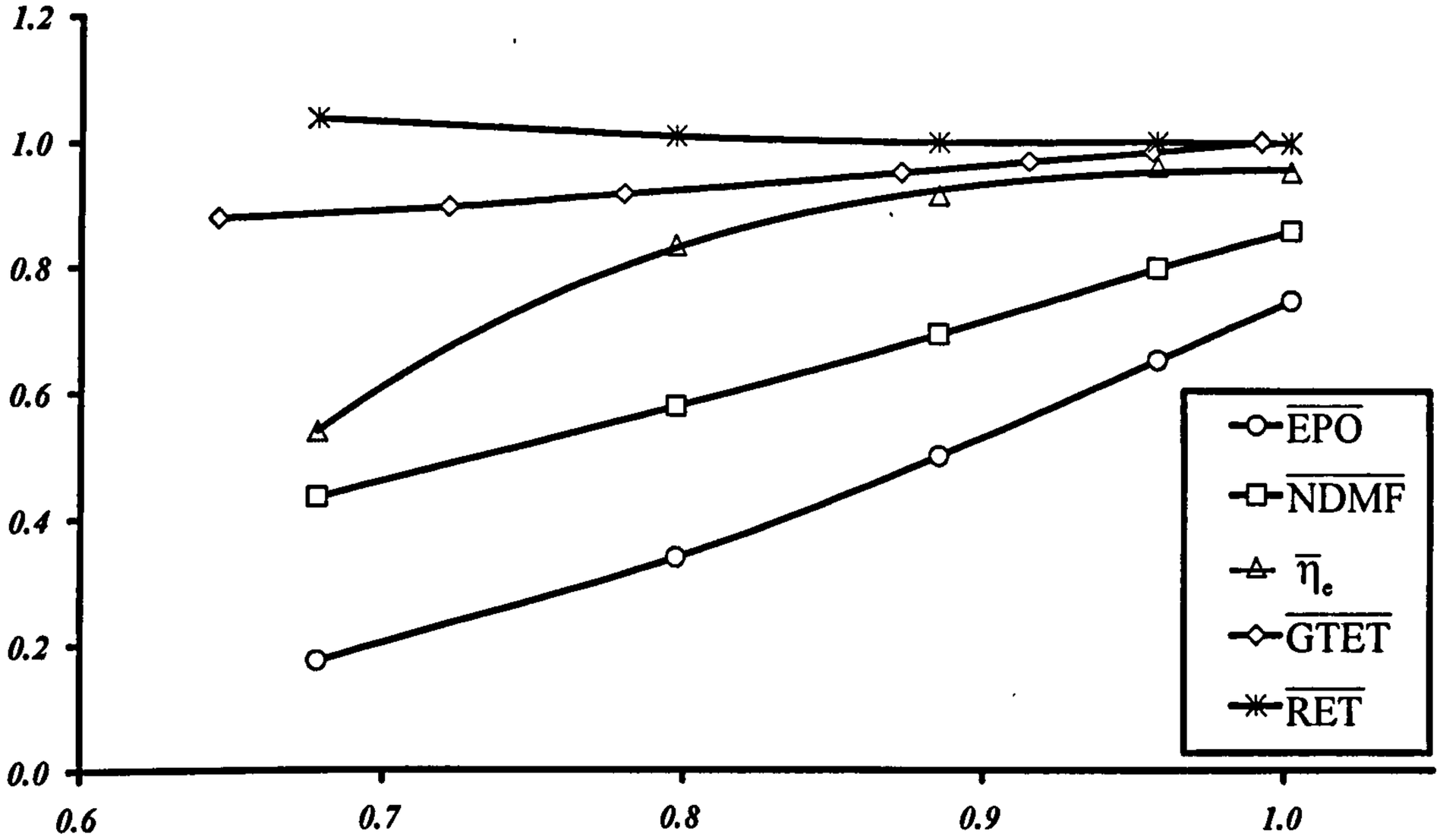

Figure 5.2 – Natural gas micro turbine performance at partial load

The combustion occurs in three stages (Figure 5.3). A hybrid fuel injector operates in different modes depending on the power output. A pilot burner is in operation at lower power levels resulting in a diffusion flame and higher NO_X emissions. The first stage is from start-up to about 5 kW when CO formation decreases and NO_X emissions increase rapidly. Then the fuel injector changes the mode of operation to a pre-mixed lean burning in two stages. The second stage is between 5 and 20 kW, where the CO formation reduces continuously and the NO_X emissions increase slowly to about 113 ppmv. In the final stage (power >20kW) the NO_X formation reduces to 5 ppmv.

Emissions of CO were all greatly affected by partial load operation. Emissions were low at full load but increased greatly as power output was reduced. Emissions of CO_2 (carbon dioxide) flattens at a level of 3.54% and they do not show any appreciable variation over the power output range.

The average concentration of oxygen (O_2) observed in the exhaust gases was 18.5% at 528 Kelvin. This condition makes the exhaust gases of these machines suitable for pre-heated air of downstream combustion or for direct heating in combined heat and power systems.

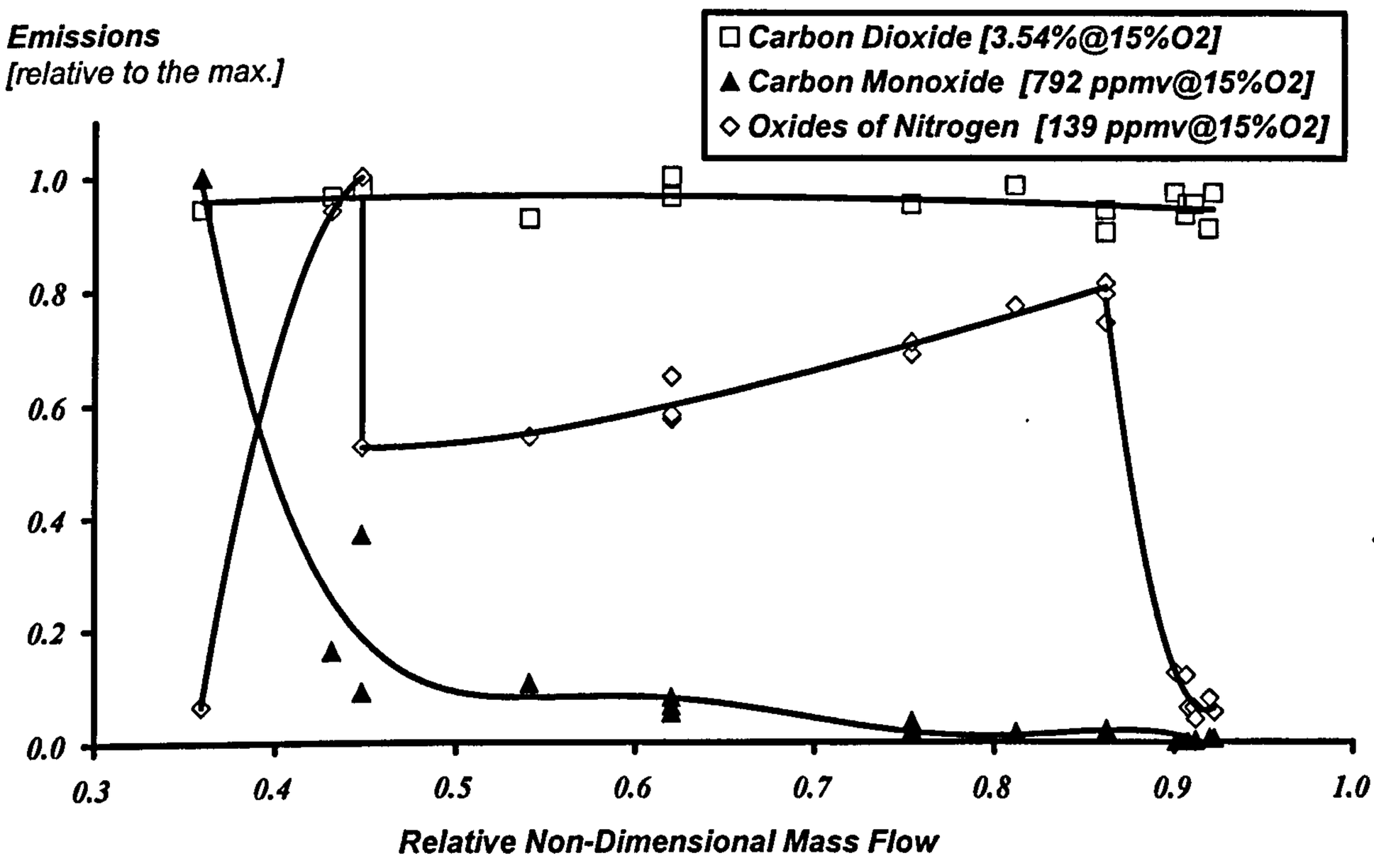

Figure 5.3 – Natural gas micro turbine emissions

5.5 - Liquid Fuelled Microturbine

The micro gas turbine fuelled with liquid fuel has a very similar configuration to the previous machine investigated with the exception that it is fitted with a liquid fuel injection system which operates with diffusion combustion. Table 5.2 shows the design point data of this machine and the ambient test conditions.

Table 5.2 – Design point performance of liquid fuelled micro turbine and ambient test conditions

Average Ambient Temperature	303 K
Average Ambient Pressure	92,076 Pa
Air Mass Flow	0.31 kg/s
Fuel	Diesel #2 (ASTM D975)
Gas Turbine Exhaust Temperature	548 K
Rotational Speed	96,000 rpm
Full-Load Electric Power Output	29 kW
Electrical Efficiency	25%

Figure 5.4 presents the performance behaviour of the liquid fuelled micro turbine. The performance variation of both natural gas and liquid fuelled micro turbines is very similar. This observation may be attributed to the similarity between the components of these machines since only the fuel injection system has an extensive design modification.

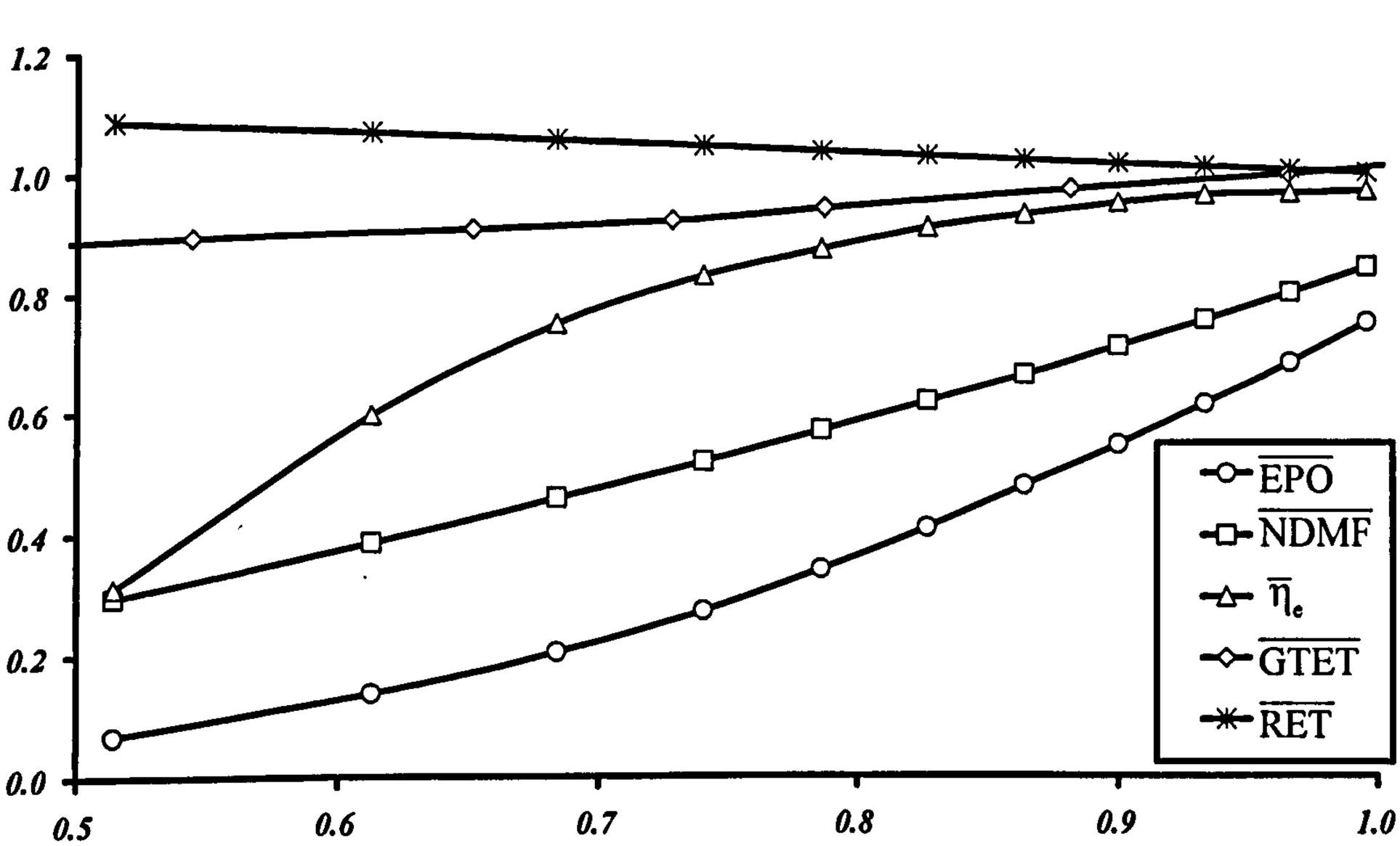

Figure 5.4 – Liquid fuelled micro turbine performance at partial load

Figure 5.5 shows the NO_X and CO emissions depending on the air fuel ratio. The single most important parameter that affects NO_X formation is the flame temperature. Lean mixtures (higher air fuel ratio) result in lower NO_X emissions but increases the formation of CO.

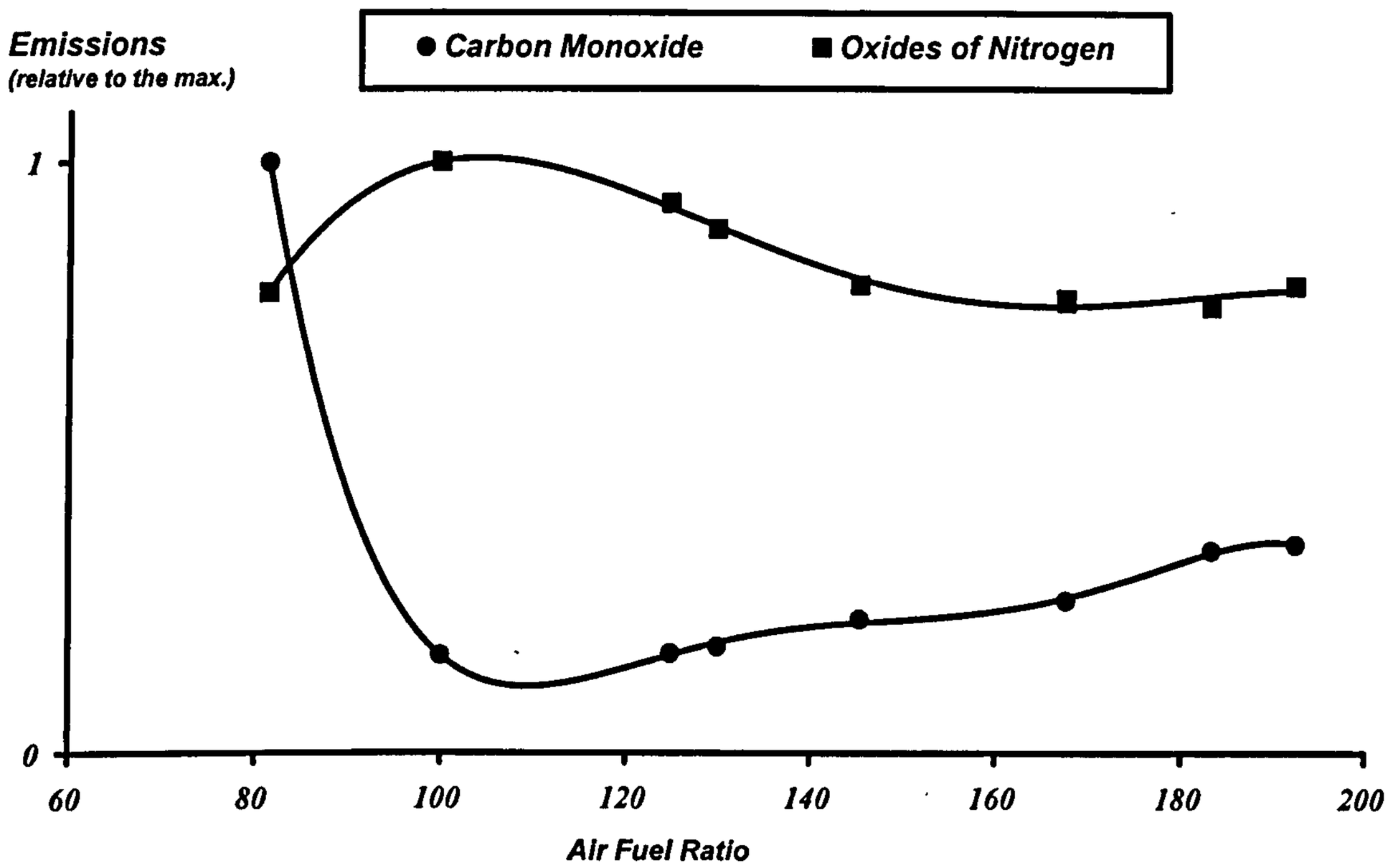

Figure 5.5 – Air fuel ratio effect on liquid fuel micro turbine emissions

Figure 5.6 shows CO, NO_X, CO_2 and SO_2 (sulphur dioxide) emissions for a liquid fuelled micro turbine. CO formation drops and NO_X emissions increase as the power output increases due to the increasing flame temperature. As well as in the natural gas micro turbine, CO_2 emissions do not present a significant variation over the non-dimensional mass flow range of the liquid fuelled micro turbine. However, a higher concentration is observed because of the higher content of carbon in the fuel. Sulphur dioxide emissions are an important concern for large scale centralised power generators fuelled with oil or coal. Sulphur dioxide concentrations lower than 44 ppmv were observed with micro turbines. However, CO_2 and SO_2 emissions depended highly on the properties of the liquid fuel used.

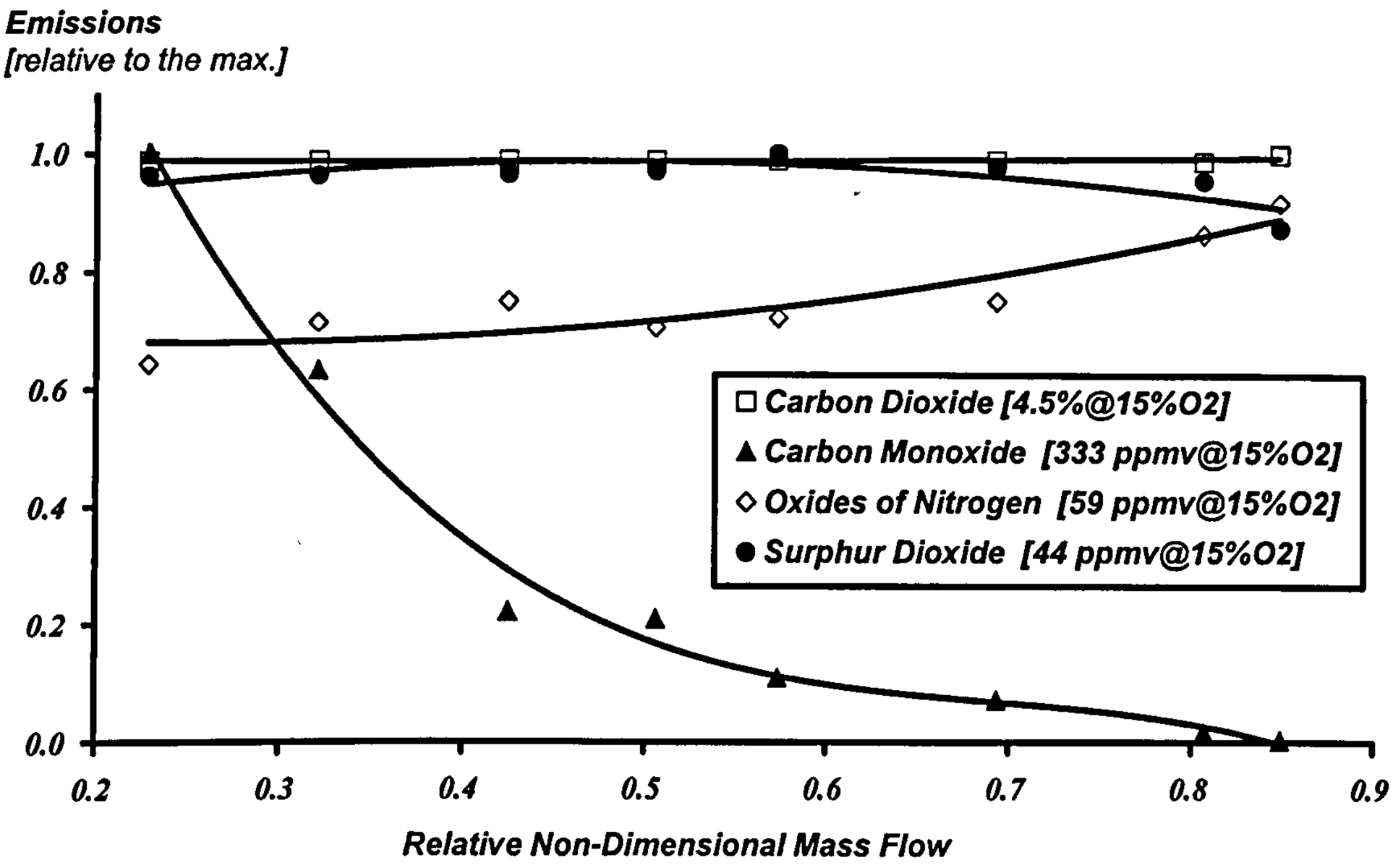

Figure 5.6 – Liquid fuel micro turbine emissions

Micro turbines and internal combustion reciprocating engines are both distributed generation technologies that compete in the same power market category. In the absence of a post combustion device such as a catalytic converter, reciprocating engines can have very high emission levels (Weston et al., 2001; Wartsila Corporation, 2001 and 2004). The emission levels of micro turbines are lower than those of internal combustion engines because combustion is a continuous process which allows more complete burning. Even for advanced engines with homogeneous charged compression ignition (HCCI), NO_X emissions can reach 100 ppmv at full load and have the disadvantages of high UHC and CO emissions (Martinez-Frias et al., 2002).

5.6 - Ground Power Unit (GPU)

The GPU investigated is a simple cycle gas turbine, gear drive assembly, single centrifugal compressor impeller and a single stage radial turbine wheel mounted in a one shaft constant speed operation with bearings lubricated by oil. A fuel meter was installed at the high pressure fuel line upstream to the combustor fuel atomiser assembly in order to measure the fuel volumetric flow.

The engine test was carried out with the gas turbine unload at maximum rotation and fuelled by kerosene. Unfortunately because of electrical generator core failure, it was not possible to test the engine at full load conditions. Table 5.3 presents the design point performance of ground power unit and gas path temperature and pressure.

Table 5.3 – Design point performance of ground power unit and ambient test conditions

Average Ambient Temperature	287 K
Average Ambient Pressure	100,740 Pa
Fuel	kerosene
Gas Turbine Exhaust Temperature	922 K
Rotational Speed	59,000 rpm
Full-Load Electric Power Output	20 kW
Electrical Efficiency	14%

Table 5.4 – Engine gas path total temperature and pressure (unload condition)

	Temperature [K]	Pressure [kPa]
1	287	100.74
2	287	99.73
3	391	220.70
4	653	209.67
5	539	102.28
6	538	101.27

Chapter 6 - Short-term Generation Schedule Optimisation

6 - Short-term Generation Schedule Optimisation

6.1 - Introduction

The determination of the most economical dispatch schedule of power generating units, which satisfies all the operating units, is considered as one of the major power system operation problems. In order to improve the operation of such systems it is essential to have detailed and reliable optimisation models. The identification of optimisation techniques for power generation is an interesting issue, commonly named as unit or generation scheduling commitment, which is addressed in this chapter. The commitment of a power generation unit means turn it on (start it up), bring it up to speed, synchronise it to the system, and connect it so that it can deliver power to consumers or network.

In this chapter the short-term generation schedule problem will be performed and restricted to distributed power generation with gas turbines. Scheduling generation units over a short-term horizon is a complex, large-scale, mixed-integer, non-linear optimisation problem. Short-term analysis deals with hourly load and price forecasts from one to twenty-four hours ahead and upwards. In this investigation the problem is divided into three sub-problems as follows: Conventional Case (CC) or baseline case, Single Unit Optimisation (SUO) and Multiple Units Optimisation (MUO).

In the conventional case units are committed individually. There is no exchange of power between units, but it may exchange power with the national network. In the single unit optimisation problem, units are scheduled in such way to produce optimal individual profit. As in the conventional case, there is no exchange of power between units, but there may be exchange of power with the national network. In the single unit optimisation problem, each unit represents an active agent in the market.

To solve the multiple units optimisation problem an intelligent information technology based nerve centre is proposed. Such nerve centre schedules the most profitable operation of the mini-pool of generation units respecting the units'

constraints. In the multiple units optimisation problem, units can exchange power between each other throughout a mini-grid independently of the national network and the mini-pool nerve centre represents just one active agent in the market. The high cost of back-up supplies used paid by generators in the traditional structure of operation is one of the benefits that the nerve centre concept proposed in this study is able to mitigate.

The classical objective of a unit commitment (UC) is to minimise the system operating costs, which is the sum of production, start-up and shut down costs of a power generation plant over the entire scheduled period. However, in competitive market, generators bid in the market in order to maximise their profit. In this study the problem consists of maximising the profit (objective function) of generators under a variety of unit's constraints. The unit's constraints can comprises demand and operation limit requirements in the classical unit commitment problem, such as spinning reserve, maximum capacity, minimum up time, minimum down time, crew constraints, and ramp rates. Each different electricity market may impose different rules on the scheduling algorithms, depending on the structure of their power system and market regulations.

In this investigation spinning reserve (surplus of electricity) has been considered as an option to increase revenue instead of a system constraint as it used to be modelled in the traditional unit commitment problem. Plant crew constraints were not included in the mathematical model as it was assumed that there are enough manpower resources to commit or not all the units necessary in a given time interval. Besides that, plant crew costs are included in the profit calculation model. Units derating have been considered. The off-design performance of power generation units was simulated depending on the ambient conditions variation over the scheduled period. Ramp up and down constraints were considered not to be relevant in this approach as the scope of work is restricted to small-medium size gas turbines.

6.2 - Conventional Case

The conventional case is mathematically modelled below, but in this case no optimisation technique is involved. It represents a baseline case where units are supposed to be on line during all the scheduled period (T) in a short-term horizon (24

hours). In a medium or long-term analysis, the conventional case model must consider the period in which the unit is not available for maintenance. In a short-term analysis, the assumption of keeping all the units in operation all the scheduled period independently of the power demand is possible and reasonable as generators have the option to sell the surplus of electricity, which may be an extra source of revenue depending on the market price paid for the electricity sold.

The following definition is used in this approach:

- $u_{i,t} = 1$, if unit i is online during time interval t;
- $u_{i,t} = 0$, if unit i is offline during time interval t;

Where $u_{i,t}$ is the commitment status of unit i at period t. Because this is a baseline case and no optimisation is involved, the units are assumed to be on line all the schedule period (T):

$$u_{i,t} = 1 \qquad \forall\ t=1, \ldots. T \text{ and } i=1. \ldots. N$$

The Total Profit (TPrf) is given by the following equation:

$$TPrf = \sum_{i=1}^{N}\sum_{t=1}^{T} Prf_{t,i} \tag{6.1}$$

The profit ($Prf_{t,i}$) of unit i at each time interval t is calculated by the balance between the revenue ($R_{t,i}$) from the production cost ($PC_{t,i}$), as given:

$$Prf_{i,t} = R_{i,t} - PC_{i,t} \tag{6.2}$$

The revenue is calculated by:

$$R_{i,t} = \left(u_{i,t} \cdot \left(ESP_t \cdot SP_{i,t} \cdot \Delta t\right) + \left(CEP_{i,t} \cdot ED_{i,t} \cdot \Delta t\right)\right) \tag{6.3}$$

Where ESP_t is the electricity sell price during time interval t, $SP_{i,t}$ is the surplus of power of unit i at period t, CEP_t is the contract electricity price during time interval t, $ED_{i,t}$ is the electricity demand of unit i at time interval t and Δt is the time interval at each period t.

The production costs can be written as a function of the Running Cost ($RC_{i,t}$) and Cost of Power Deficit ($CDP_{i,t}$):

$$PC_{i,t} = RC_{i,t} + CDP_{i,t} \tag{6.4}$$

The Running Cost is calculated as follows:

$$RC_{i,t} = u_{i,t} \cdot \left(FC_{i,t} + SU_{i,t}\right) + SD_{i,t} + MC_{i,t} \tag{6.5}$$

Where $FC_{i,t}$ is the fuel cost of unit i at period t, $SD_{i,t}$ is the shut down cost of unit i at period t, $SU_{i,t}$ is the start-up cost of unit i at period t, $MC_{i,t}$ is the maintenance cost of unit i at period t.

Because the units are suppose to be on line all the schedule period (T), start-up and shut down costs are defined as follows:

$SD_{i,t} = 0, \quad \forall \ t=1, \ldots, T$

$SU_{i,t} = 0, \quad$ if $(u_{i,t-1} = 1)$ and $(u_{i,t} = 1)$

$SU_{i,t} = SU_i, \quad$ if $(u_{i,t-1} = 0)$ and $(u_{i,t} = 1)$

Where SU_i is the start-up cost of unit i. A certain amount of energy must be expended to bring the unit online. This energy does not result in any power output and it is brought to this approach as a start-up cost. The start-up cost in any given time interval depends on the number of hours a unit has been off prior to start-up. This cost can be modelled by an exponential function of the form:

$$SU_i = C\,\&\,MC_i + FCS_i \cdot \left[1 - \exp\left(\frac{-CTO_{i,t}}{CT_i}\right)\right] \tag{6.6}$$

Where $C\&MC_i$ is the crew start-up costs and equipment maintenance cost of unit *i* during start-up, which is in part proportional to the accumulative number of start-ups. FCS_i is the fuel cost associated with the start-up of unit *i* from the cold condition, $CTO_{i,t}$ is the cumulative time the unit has been offline, CT_i is the cooling time of unit *i*.

In unit commitment problems the fuel cost function used to be represented by a polynomial cost function, such as:

$$FC_{i,t}(P_{i,t}) = a_i(P_{i,t}) + b_i(P_{i,t}) + c_i \tag{6.7}$$

Where $P_{i,t}$ is the electric power of unit i at time interval t and a_i, b_i, c_i are the parameters of the polynomial fuel cost function $FC_{i,t}$ $(P_{i,t})$. Fuel or production cost

model also appears in the literature as a piece-wise linear cost function such as the Willians line (Figure 6.1) represented below:

$$FC_{i,t}(P_{i,t}) = inc_{1,i}(P_{i,t}) + nl_{1,i} \qquad \text{If } P_{min,i} \le P_{i,t} \le e_{1,i}$$

$$FC_{i,t}(P_{i,t}) = inc_{2,i}(P_{i,t}) + nl_{2,i} \qquad \text{If } e_{1,i} \le P_{i,t} \le e_{2,i}$$

$$FC_{i,t}(P_{i,t}) = inc_{3,i}(P_{i,t}) + nl_{3,i} \qquad \text{If } e_{3,i} \le P_{i,t} \le P_{max,i}$$

Where $nl_{1,i}$, $nl_{2,i}$, $nl_{3,i}$ are no load cost of the piece-wise linear cost function of unit i; $inc_{1,i}$, $inc_{2,i}$, $inc_{3,i}$ are the incremental cost of the piece-wise linear cost function of unit i; $e_{1,i}$, $e_{2,i}$, $e_{3,i}$ are the elbow point of the piece-wise linear cost function of unit i; $P_{min,i}$ is the lower generation limit of unit i; $P_{max,i}$ is the upper generation limit of unit i.

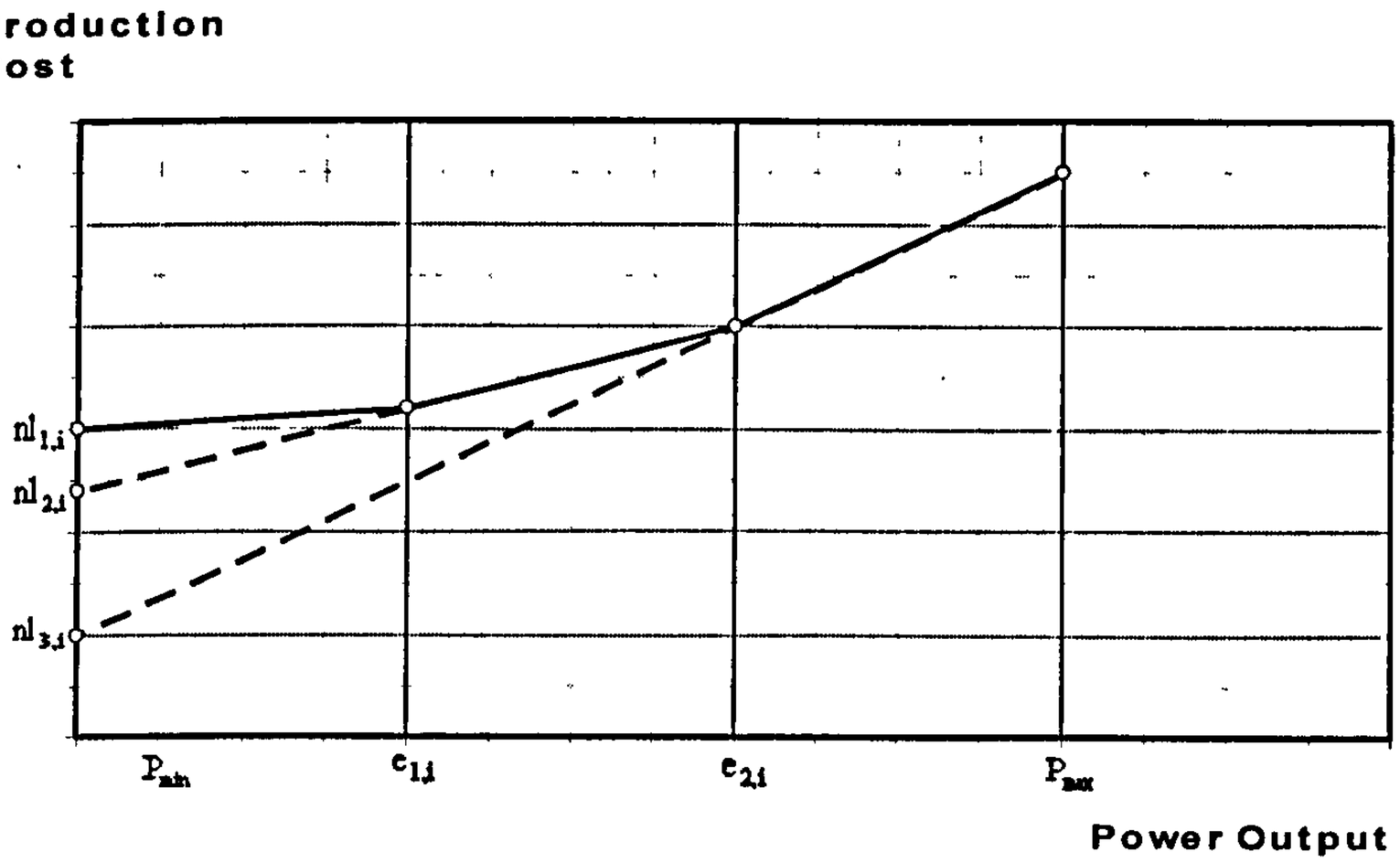

Figure 6.1 – Piece-wise linear cost functions (Willans line)

Studies that use the piece-wise linear cost function to dispatch power units are modelled as follows. It begins with all units at P_{min}, them raises the output of the unit with the lowest incremental cost segment. If the unit reaches the end elbow point of that segment or P_{max}, a search algorithm finds the unit with the lowest incremental cost segment and raises its output. This approach is repeated until the total power output is equal to the total demand (Wood and Wollenberg, 1996).

The piece-wise linear fuel cost function can aggregate a significant error to the calculation of the total operational cost, as it is a multiple segment linear approximation of the real production costs. In addition, the fuel cost of such thermal power plants depends on the off-design performance of the units, which depends on the ambient conditions and deterioration of engines, as describe in chapter 3. Both the polynomial cost function and piece-wise linear cost function do not take into account these effects and consequently are a common source of error in unit commitment problems involving thermal power units.

Fuel cost is directly proportional to the fuel consumption and price. In this investigation the fuel consumption is obtained from the off-design performance simulation of the gas turbine units considering the ambient conditions variation for every time interval. Clean and constant "health" condition of engines was assumed over the short-term scheduled period (24 hours). The software Turbomatch described previously was used to simulate the off-design gas turbine performance.

The following equation calculates the fuel cost:

$$FC_{i,t} = 3600 \cdot ftr_t \cdot MFC_{i,t} \cdot \Delta t \tag{6.8}$$

Where $ftr_{i,t}$ is the fuel tariff rate of unit i at period t, and $MFC_{i,t}$ is the mass fuel consumption of unit i at period t. The maintenance cost can be represented by the following equation:

$$MC_{i,t} = BMC_i \cdot \Delta t + u_{i,t} \cdot \left(IMC_i \cdot P_{i,t}\right) \cdot \Delta t \tag{6.9}$$

Where BMC_i is the base maintenance cost of unit i; and IMC_i is the incremental maintenance cost of unit i. The Cost of Power Deficit ($CDP_{i,t}$) is:

$$CDP_{i,t} = EBP_t \cdot DP_{i,t} \cdot \Delta t \tag{6.10}$$

Where EBP_t is the electricity buy price at period t and $DP_{i,t}$ is the deficit of power of unit i at period t. Finally,

$$Prf_{i,t} = R_{i,t} - PC_{i,t}$$

$$R_{i,t} = \left(u_{i,t} \cdot \left(ESP_t \cdot SP_{i,t} \cdot \Delta t\right) + \left(CEP_{i,t} \cdot ED_{i,t} \cdot \Delta t\right)\right)$$

$$PC_{i,t} = \left(u_{i,t} \cdot \left(FC_{i,t} + SU_{i,t}\right) + SD_{i,t} + MC_{i,t}\right) + EBP_{i,t} \cdot DP_{i,t} \cdot \Delta t \quad \textbf{(6.11)}$$

Then,

$$TPrf = \sum_{i=1}^{N} \sum_{t=1}^{T} Prf_{t,i}$$

6.2.1 - Units' and system constraints

The problem is limited to the following constraints: maximum capacity of generating units, electricity demand balance and initial conditions.

Generation limits: the generation units should only be scheduled to supply power within the limits set by their maximum capacity. In this investigation the maximum capacity of units was considered depending on the ambient conditions and off-design performance of units.

Electricity demand balance: this problem is divided into short periods of time of equal duration, in which the load demand forecasts is assumed constant. The unit commitment algorithm should provide the exact amount of power to balance the customer's demand ($ED_{i,t}$) in every time interval t. Hence, in this approach the following assumptions are considered regarding the electricity supply:

- Units are committed individually;
- If the total electrical capacity is installed it is not enough to supply the total electrical demand then the deficit of electricity is supplied by the national grid;
- If there is surplus of electricity, it can be sold to the national grid.

$$\left(u_{i,t} \cdot P_{i,t}\right) + DP_{i,t} \geq ED_{i,t} \quad \textbf{(6.12)}$$

Where $ED_{i,t}$ is the electricity demand of unit i at time interval t, $P_{i,t}$ is the electric power of unit i at time interval t, $DP_{i,t}$ is the deficit of power of unit i at period t.

Initial conditions: the initial condition of the units at the beginning of the scheduled period is considered known.

A subroutine has been written in Fortran language to simulate the conventional case model. Figure 6.3 illustrates how the algorithm works.

6.3 - Single Unit Commitment Optimisation

This section investigates the generation schedule optimisation of single (autonomous) power units. For a system of N units, and given a certain electricity price profile, it is necessary to determine the start-up/shut-down times and the power output levels of every individual unit at each time interval t over a specified time interval T, so that the generator's total profit is maximised subject to unit constraints (Figure 6.2).

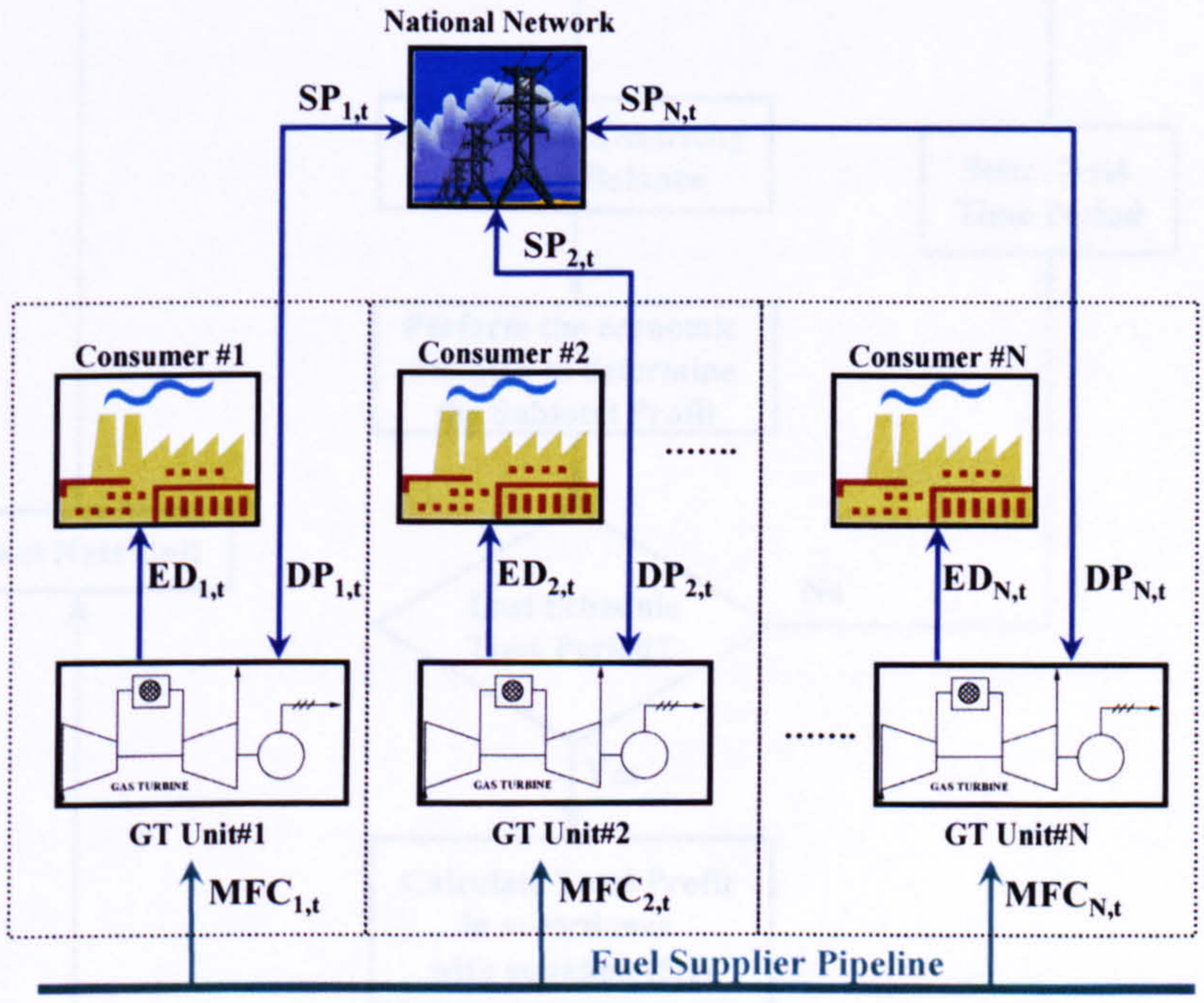

Figure 6.2 – Single unit operation structure diagram

Mathematically, the objective function or the total profit of the system can be written as in the previous section with equations (6.1) and (6.12):

$$\max_{u_{i,t}} (\mathrm{TPrf}) \Rightarrow \mathrm{TPrf} = \sum_{i=1}^{N} \sum_{t=1}^{T} \mathrm{Prf}_{t,i}$$

$$\mathrm{Prf}_{i,t} = \left(u_{i,t} \cdot \left(\mathrm{ESP}_t \cdot \mathrm{SP}_{i,t} \cdot \Delta t\right)\right) + \left(\mathrm{CEP}_{i,t} \cdot \mathrm{ED}_{i,t} \cdot \Delta t\right) - \left(u_{i,t} \cdot \left(\mathrm{FC}_{i,t} + \mathrm{SU}_{i,t}\right) + \mathrm{SD}_{i,t} + \mathrm{MC}_{i,t}\right) - \left(\mathrm{EBP}_t \cdot \mathrm{DP}_{i,t} \cdot \Delta t\right)$$

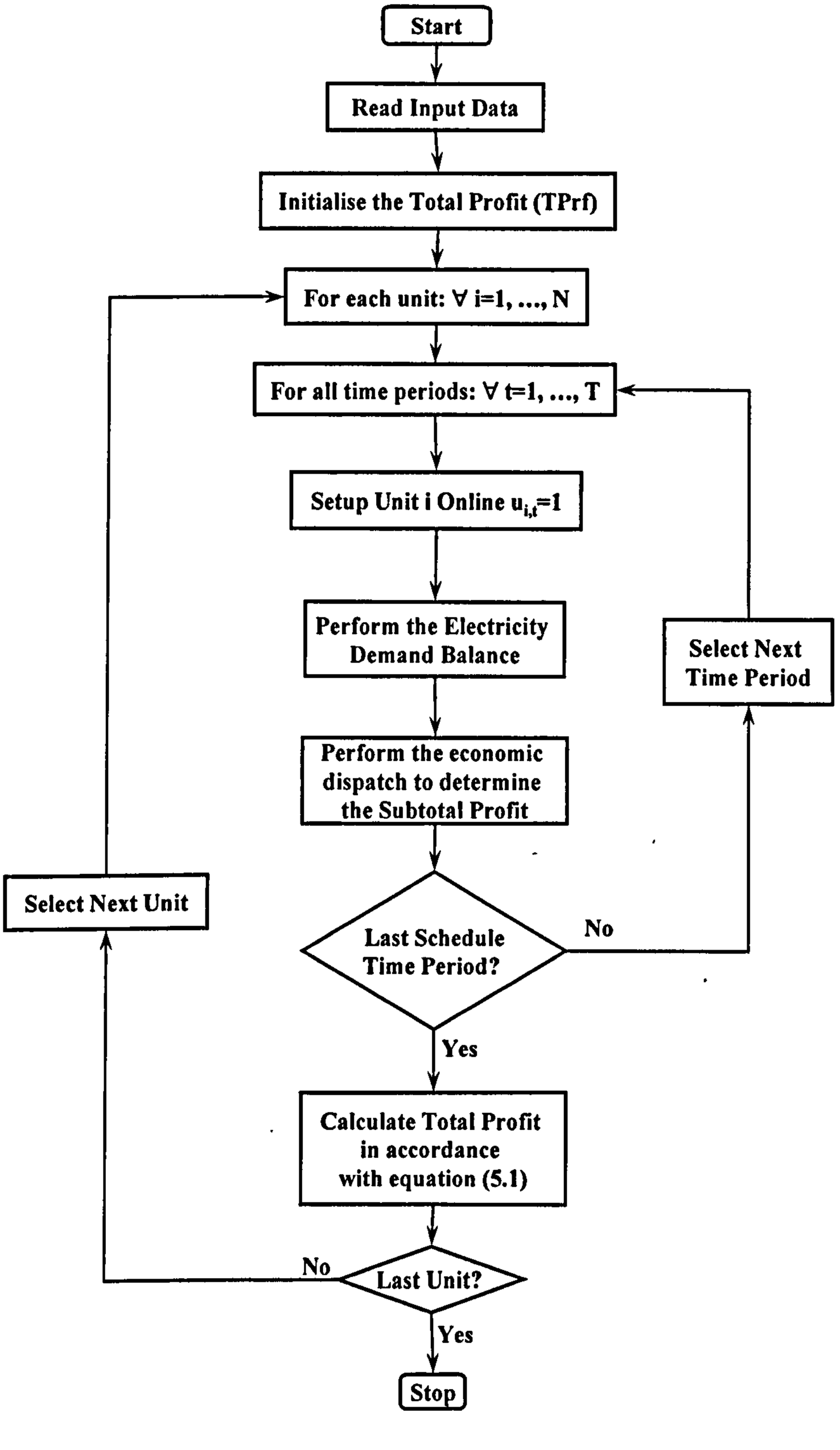

Figure 6.3 – Conventional case algorithm flowchart

Start-up and shut down costs are modelled as below:

$SU_{i,t} = 0$ and $SD_{i,t} = 0$, if $(u_{i,t-1} = 0)$ and $(u_{i,t} = 0)$ or $(u_{i,t-1} = 1)$ and $(u_{i,t} = 1)$

$SU_{i,t} = 0$ and $SD_{i,t} = SD_i$, if $(u_{i,t-1} = 1)$ and $(u_{i,t} = 0)$

$SU_{i,t} = SU_i$ and $SD_{i,t} = 0$, if $(u_{i,t-1} = 0)$ and $(u_{i,t} = 1)$

6.3.1 - Units' and system constraints and algorithm

As in the conventional case the units are limited to the maximum capacity of generating units, electricity demand balance, and initial conditions. However, minimum up and down time constraints were considered because in this case units can be switched on or off depending on the optimisation process.

Minimum Up (MUT) and Down (MDT) Time: once the generation unit is committed, it should remain online for a minimum period of time (MUT_i). Considering the cumulative time a unit has been running ($CT_{i,t}$) the minimum up time constraint can be modelled as follows:

$$\left(CT_{i,t} - MUT_i\right) \cdot \left(u_{i,t-1} - u_{i,t}\right) \geq 0 \qquad \textbf{(6.13)}$$

Once the generation unit is shut down, it should remains off for a minimum period of time (MDT_i) to allow the rotating parts of the engine to cool down. Considering the cumulative time a unit has been running ($CT_{i,t}$) the minimum up time constraint can be written as follows:

$$\left(-CT_{i,t} - MDT_i\right) \cdot \left(u_{i,t} - u_{i,t-1}\right) \geq 0 \qquad \textbf{(6.14)}$$

MUT and MDT are always positive numbers expressed in hours. CT can be a positive or negative number and it is also expressed in hours. If it is a negative number, this means that the engine has been offline; if positive, it means the engine has been online. The effects of MUT and MDT can be mathematically modelled in the following way:

$CT_{i,t} = CT_{i,t-1}$, if $(CT_{i,t-1}=-MDT_i)$ and $(u_{i,t}=0)$

$CT_{i,t} = CT_{i,t-1} - 1$, if $(-MDT_i < CT_{i,t-1} <= -1)$ and $(u_{i,t}=0)$

$CT_{i,t} = -1$, if $(CT_{i,t-1} = MUT_i)$ and $(u_{i,t}=0)$

$CT_{i,t} = CT_{i,t-1}$, if $(CT_{i,t-1}=MUT_i)$ and $(u_{i,t}=1)$ then

$CT_{i,t} = CT_{i,t-1} + 1$, if $(MUD_i > CT_{i,t-1} >= 1)$ and $(u_{i,t}=1)$

$CT_{i,t} = 1$, if $(CT_{i,t-1} = - MDT_i)$ and $(u_{i,t}=1)$

6.3.2 - Generation schedule commitment optimisation techniques

As described in Chapter 1 several techniques have been proposed to solve the problem of unit commitment problem. They can be categorized into three main groups: mathematical methods, like exhaustive enumeration, dynamic programming, integer and mixed programming, branch-and-bound methods, lagrangian relaxation and augmented lagrangian; heuristics methods, such as priority list, simulated anneling; and artificial intelligence methods like genetic algorithm, neural networks and expert systems.

Mathematical methods are the classical methods used to solve unit commitment optimisation. Exhaustive enumeration is a natural approach. The optimal solution can be obtained by a complete enumeration of all feasible combinations of generating unit's status, followed by the determination of the economic dispatch of each feasible solution. This technique requires the evaluation of $(2^N - 1)$ combinations for each scheduling interval and $(2^N - 1)^T$ combinations for the scheduling time horizon when scheduling N generating units over T scheduling intervals. The main disadvantage of this technique is that it leads to an enormous number of combinations.

Dynamic Programming (DP) technique is a systematic multi-stage searching procedure that achieves the optimal solution without assessing all the possible combinations. It is used extensively throughout the world and it has the advantage of being able to solve problems of a variety of applications and to be easily modified to model characteristics of specific utilities. The disadvantage of the dynamic programming is its suboptimal treatment in multiple unit's power systems which requires to limit the commitments considered at any hour and the difficulty in including constraints that affect a single-unit operation over time. The characteristic of Dynamic

Programming (DP) technique to solve unit commitment problems is more detailed explained in the next pages.

The Lagrangian relaxation technique decomposes the generation schedule problem into one dual and one primal sub-problem that are solved independently. It is a systematic method to schedule generating units, but the sensitivity of the units status to the adjustment in the Lagrangian multipliers may cause the process to converge to sub-optimal solutions or even fail to find a feasible solution within an acceptable number of iterations. The augmented Lagrangian method introduces quadratic penalty terms associated with the demand constraints to improve the convergence process.

Heuristics methods can reduce the dimension of unit commitment problems as much as possible without rejecting the optimal solution. However, this goal is not always achieved and hence the convergence to the optima solution cannot be guaranteed, due to the incomplete search of the solution space. Priority list is a heuristic technique that arranges the generating units in a priority ranking, which is then used to sequentially commit the units such that the system demand is satisfied. In the priority list method the units are committed in ascending order of the unit average full-load production cost so that the most economic base load units are committed first and the peak unit last in order to meet the load demand. Priority list based methods are very fast but highly heuristic and may result in a generation schedule with relatively low profit.

Artificial intelligence methods have been used to solve unit commitment problems. One of the main advantages of the artificial intelligence methods is that the complexity of the mathematical formulation can be avoided. However, the shortcoming of these methods is generally associated to the excessive computational resources that they require. With the advent of fast processors with larger memory artificial intelligence methods have become promising and are still evolving.

Generation schedule has recently been dealt by Genetic algorithms (GA), which are search techniques based on principles inspired on the evolutionary theory of genetic processes of biological organisms. When solving generation schedule problem for N generating units over T scheduling periods with GA one solution can be represented by a matrix containing the statuses of the units. The fitness value of the solution usually is set as the sum of the total operation cost of the solution and the

penalty function associated to the violations of system and unit constraints. The disadvantage is that it can be excessively time-consuming in large-scale power systems. A more detailed description of the Genetic Algorithm technique is provided in the next pages.

Artificial neural networks (ANN) have also been used to solve generation schedule problem. They are formed by a large number of neurons, interconnected to each. Each neuron has multi-inputs from other neurons with assigned weights to represent the strength of the input connections. The output of a neuron is determined by a signal, which is proportional to the sum of all the inputs. The operation of an ANN is based upon the presentation of a set of inputs and a subsequent forward propagation of this information through the network. A multi-layer ANN comprises an input layer, an output layer and a number of hidden layers. The ANN should be trained to produce the corresponding scheduling pattern for any input load profile. Once the network is trained the on-line operation would involve a sequence of simple arithmetic operations to generate the most economical schedule for the given demand load curve. If this solution is not feasible, it is used as an initial starting point for a near-optimum solution. The main characteristic of ANNs is that the previous knowledge of the solution and its behaviour in different circumstances can be used extensively for obtaining new solutions.

6.3.3 - Single Unit Optimisation with Dynamic Programming

Dynamic programming can solve optimisation problems which can be formulated as a sequence of decisions. There are many instances of applications in engineering, economic, industrial and military domains (Bellman and Dreyfus, 1962; Hastings, 1974). The Dynamic Programming technique employees a systematic multistage searching algorithm that tries to achieve the optimal solution without having to access all the possible combinations. It usually involves a table in which sub-problem solutions can be stored to avoid duplicate combinations.

A forward search algorithm can be applied which runs forward in time from the initial time to the final one, accumulating operating costs or profits in the process, and then backtracking from the last interval to the first to trace the optimal schedule. The main complexity with dynamic programming method is the dimension of the

problem. For an N-unit system, there will be 2^{N-1} possible unit combination at each stage. While the system and the unit constraint of typical power systems tend to significantly reduce this number storing all feasible combinations at every hour is still impossible even for moderate size systems. Thus heuristic techniques that search only a sub-set of all combinations are used. Heuristic do not guarantee optimal solutions and in a certain cases may require the relaxation of some the constraints to obtain a solution. However, since the single unit optimisation problem considers each unit individually, a single unit dynamic programming algorithm can be developed avoiding the dimensionality complexity.

Dynamic programming can be used to solve the profit maximisation problem because the problem satisfies the principle of optimality. An optimisation problem satisfies the principle of optimality if all parts of an optimal solution are themselves optimal solutions to sub-problems. The number of relevant sub-problems is limited by the schedule time and unit constraints. The solution to each larger sub-problem depends on a limited number of smaller sub-problems.

When solving generation schedule optimisation with dynamic programming the smallest sub-problems are solved first. This corresponds to defining the feasible state (whether 0 or 1), the associated nominal generation or dispatch, and the profit that it would result for each unit at each time interval. These solutions are then combined to solve larger sub-problems. In this case the individual profits are added together to give the total profit over the scheduling period, after which the path with the highest total profit is determined. This gives the optimal schedule for that unit for a given price profile.

The objective function is the one that gives the total profits for a unit *i* over the scheduling period, as shown in the following equation:

$$\max_{u_{i,t}} \left(\mathrm{TPrf}\right) \Rightarrow \mathrm{TPrf} = \sum_{i=1}^{N}\sum_{t=1}^{T} \mathrm{Prf}_{t,i}$$

$$\mathrm{Prf}_{i,t} = \left(u_{i,t} \cdot \left(\mathrm{ESP}_t \cdot \mathrm{SP}_{i,t} \cdot \Delta t\right)\right) + \left(\mathrm{CEP}_{i,t} \cdot \mathrm{ED}_{i,t} \cdot \Delta t\right) - \left(u_{i,t} \cdot \left(\mathrm{FC}_{i,t} + \mathrm{SU}_{i,t}\right) + \mathrm{SD}_{i,t} + \mathrm{MC}_{i,t}\right) - \left(\mathrm{EBP}_t \cdot \mathrm{DP}_{i,t} \cdot \Delta t\right)$$

The single unit optimisation proceeds as described above, but takes into account that decisions made at each stage must also respect the units' and system

constraints. All feasible solutions for each stage must be saved in order to backtrack the optimal schedule. Figure 6.5 shows the algorithm used in this investigation.

6.4 - Multi Unit Commitment Optimisation

This section investigates the generation schedule optimisation of a mini-pool of power units illustrated in Figure 6.4. The mini-pool nerve centre processes the information received in order to set up the optimal generation scheduling of units interconnected through a mini-grid.

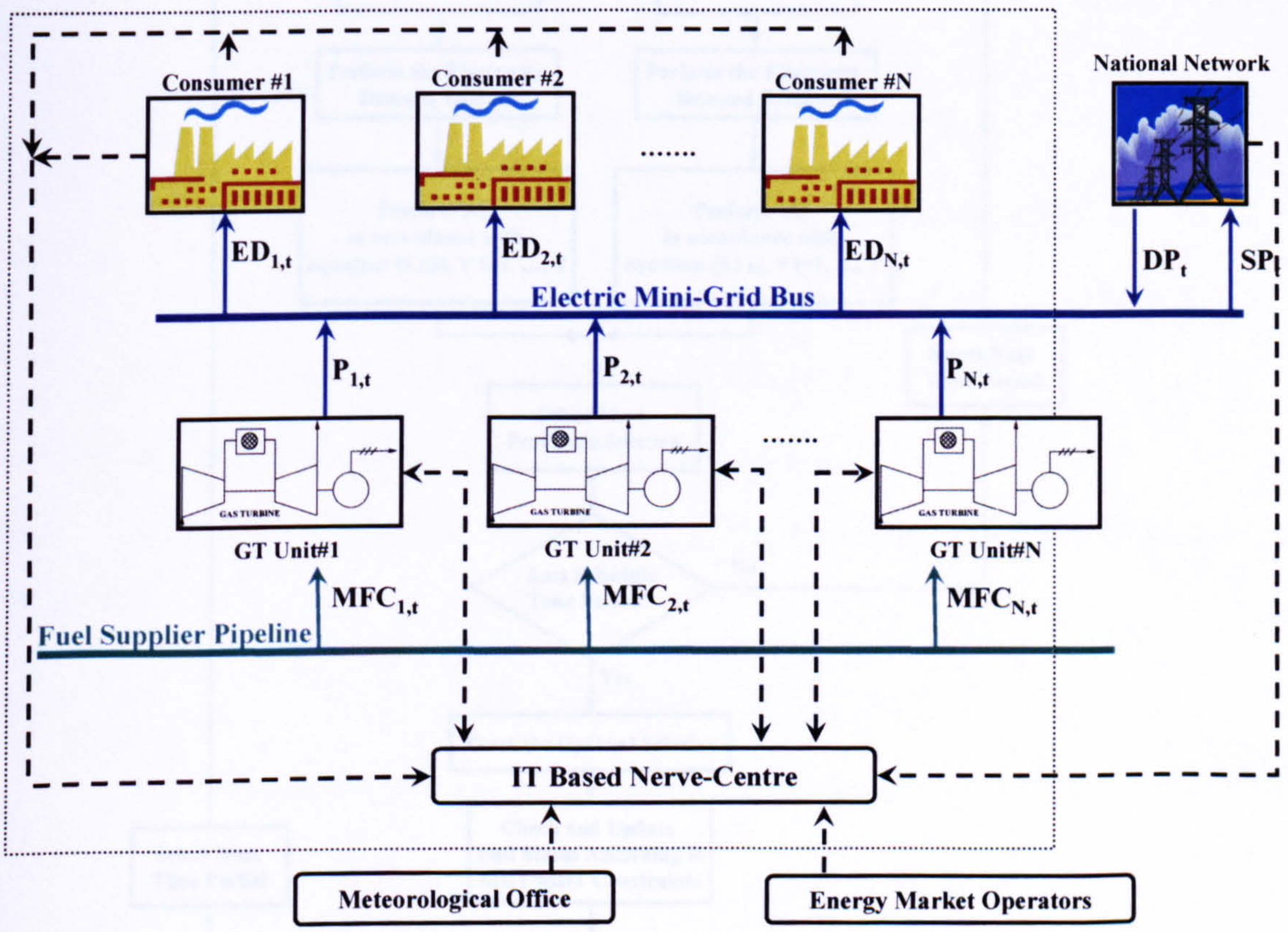

Figure 6.4 – Mini-pool structure diagram

The profit (Prf_t) at each time interval is calculated by subtracting the production cost (PC_t) during that interval from the revenue (R_t), as given:

$$Prf_t = R_t - PC_t \tag{6.15}$$

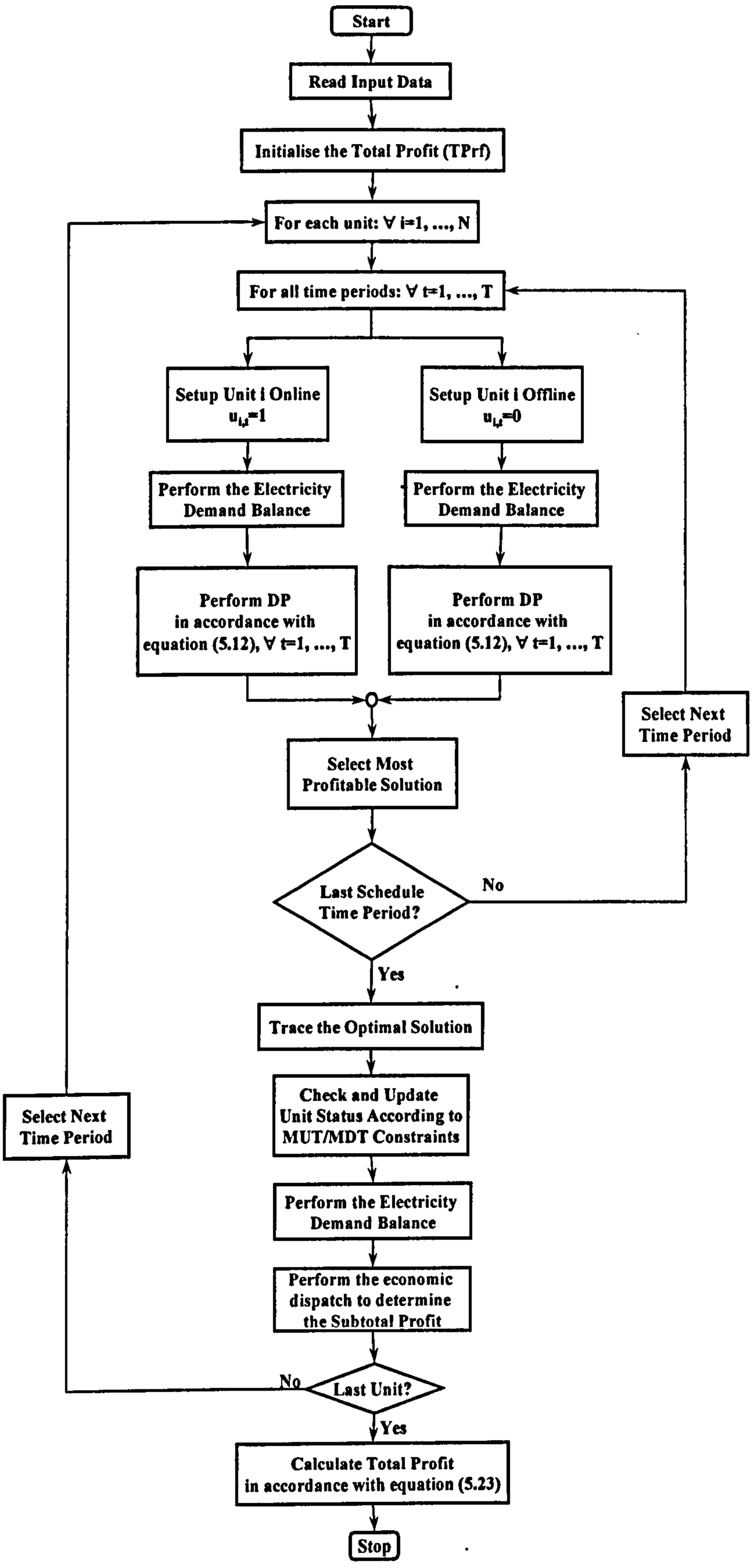

Figure 6.5 - Single Unit Optimisation Algorithm Flowchart

The revenue at each time interval is calculated by:

$$R_t = \left(ESP_t \cdot \sum_{i=1}^{N} \left(u_{i,t} \cdot SP_{i,t} \right) \cdot \Delta t \right) + \left(\sum_{i=1}^{N} \left(CEP_{i,t} \cdot ED_{i,t} \cdot \Delta t \right) \right)$$

$$R_t = \left(ESP_t \cdot SP_t \cdot \Delta t \right) + \left(\sum_{i=1}^{N} \left(CEP_{i,t} \cdot ED_{i,t} \cdot \Delta t \right) \right) \quad \textbf{(6.16)}$$

The production costs ($PC_{i,t}$) of the system can be written as follows:

$$PC_t = \sum_{i=1}^{N} RC_{i,t} + CDP_t \quad \textbf{(6.17)}$$

$$RC_{i,t} = u_{i,t} \cdot \left(FC_{i,t} + SU_{i,t} \right) + SD_{i,t} + MC_{i,t} \quad \textbf{(6.18)}$$

Stat-up and shutdown costs are calculated by the following algorithm:

$SU_{i,t} = 0$ and $SD_{i,t} = 0$, if $(u_{i,t-1} = 0)$ and $(u_{i,t} = 0)$ or $(u_{i,t-1} = 1)$ and $(u_{i,t} = 1)$

$SU_{i,t} = 0$ and $SD_{i,t} = SD_i$, if $(u_{i,t-1} = 1)$ and $(u_{i,t} = 0)$

$SU_{i,t} = SU_i$ and $SD_{i,t} = 0$, if $(u_{i,t-1} = 0)$ and $(u_{i,t} = 1)$

Where SU_i is given by equation (6.6). The following equation calculates the fuel cost:

$$FC_{i,t} = 3600 \cdot ftr_{i,t} \cdot MFC_{i,t} \cdot \Delta t \quad \textbf{(6.19)}$$

The maintenance cost can be represented by the following equation:

$$MC_{i,t} = BMC_i \cdot \Delta t + u_{i,t} \cdot \left(IMC_i \cdot P_{i,t} \right) \cdot \Delta t \quad \textbf{(6.20)}$$

The cost of deficit of power is:

$$CDP_t = EBP_t \cdot \sum_{i=1}^{N} DP_{i,t} \cdot \Delta t$$

$$CDP_t = EBP_t \cdot DP_t \cdot \Delta t \quad \textbf{(6.21)}$$

Total Profit ($TPrf_i$) is given by the following equation:

$$TPrf_i = \sum_{t=1}^{T} Prf_t \quad \textbf{(6.22)}$$

The unit is limited to the following constraints: maximum capacity, minimum up and down time, electricity demand balance, and initial conditions.

6.4.1 - Multi Unit Commitment Optimisation with Genetic Algorithms

Genetic algorithms (GAs) are general-purpose search techniques based on principles inspired from the genetic and evolutionary mechanisms observed in natural systems and populations of living beings. Their basic principle is the maintenance of a population of solutions to a problem (genotypes) in the form of coded information individuals that evolve in time. The evolution is based on the laws of natural selection (survival of the fittest) and genetic information recombination within the population. The evolving population samples the search space and accumulates knowledge about good and bad quality areas and recombine this knowledge to form solutions with optimal performance to the specific problem.

At first a population of solutions is generated randomly. Each member of the population is then decoded to a real problem solution and a "fitness" value is assigned to it by a quality function that gives a measure of the solution quality.

When the evaluation is completed, individuals from the population are selected in pairs to replicate and form "offspring" individuals or new problem solutions. The selection is performed probabilistically so that an individual's selection probability is proportional to the individual's fitness. This assures that high-quality solutions will be selected many times and become "parents" of many new solutions while low-quality solutions will contribute less to the new population with the probability not to be chosen for reproduction at all.

When two parents are selected they are combined to produce an "offspring" solution using specific operators. The reproduction process is driven by operators such as selection, crossover and mutation. Crossover simply combines the parents to form a new chromosome that inherits solution characteristics from both parents. Although crossover being the primary search operator, it cannot produce information that does not already exist within the population. Mutation covers this need by injecting new information in the produced offspring. The injection is done randomly by altering parts

of the new chromosome. Mutation is the operator that gives a specific probability to every solution to be considered and evaluated.

When a sufficient number of solutions have been produced, they are considered as a new generation and they totally replace the "parents" to proceed with the evolution. Many generations are necessary to converge to the optimum or near-optimum solution according to the problem complexity level.

The genetic algorithm multi-units generation schedule optimisation problem was modelled as follows. A chromosome is composed of the solution of all units N over the schedule period of time T. Then each chromosome is a $(N \cdot T)$ bit chromosome formed with 1 and 0, which indicates the ON and OFF unit status respectively. The search space can then be extensively large. For a 40 unit system and 24 hour scheduling period the, solution is formed of 40 x 24 = 960 bits, resulting in a search space of $2^{960} = 9.75 \times 10^{288}$.

The fitness (Ftn) of each solution is calculated with the equations below.

$$Ftn = TPrf + \sum_{j=1}^{C} PF_j \tag{6.23}$$

$$PF_j = \mu_j \cdot Vlt_j \tag{6.24}$$

The total profit is computed as described in the previous section. A penalty term function (PF_j) proportional to the amount of the constraint violation (Vlt_j) is added to the fitness function if the solution is not according to any units' or system constraints. The chosen penalty multipliers (μ_j) must be sufficiently large to discourage the selection of solutions with violated constraints.

After the evaluation of the initial randomly generated population the genetic algorithm begins the creation of the new generation of solutions. Basically the total profit, penalties and fitness function are assessed. Then the fittest chromosome is sorted out. The program runs until the number of generations achieves its maximum defined by the user. The whole population is replaced in each generation (Figure 6.6).

Two "genotypes" are selected using the Roulette Wheel parent section algorithm using a probability proportional to the genotype's relative fitness. Each time a

parent chromosome is needed, a random number is drawn and a chromosome found from the "roulette wheel". The disadvantage of this technique is that a single generation schedule can dominate the selection process and lead to premature convergence.

```
Suppose the fitness of N individuals in a population are:
f1,f2,f3,..., fN.
In roulette wheel selection, the probability of an individual
being selected is Probi=fi/(f1+f2+...+fN).
Then a parent is selected by going through the following steps:
Generate a random value r between 0 and 1.
Set sum=0;
For i=1 to N do
      begin
      sum=sum+Probi;
      if (sum>=r)
            return i   (parent selected);
end
```

Then a new "offspring genotype" (new generation schedule) is produced by means of the two basic genetic operators: crossover and mutation. Crossover is an operator applied with certain probability. It combines the parent's genotypes exchanging parts of them to form to new genotypes that inherit solution characteristics from both parents.

Initially, traditional crossover operators were used in this investigation but failed to get convergence. Therefore, a heuristic rule crossover was proposed and used. This operator generates one child (chd) from the two parents (prt1) and (prt2), where the fitness of prt1 is greater than or equal to the fitness of prt2, and according to the following rule:

IF $(prt1_t = 0)$ and $(prt2_t = 0)$, THEN $(chd_t = 0)$

IF $(prt1_t = 0)$ and $(prt2_t = 1)$, THEN $(chd_t = 0)$

IF $(prt1_t = 1)$ and $(prt2_t = 0)$, THEN $(chd_t = 1)$

IF $(prt1_t = 1)$ and $(prt2_t = 1)$, THEN $(chd_t = 1)$

To introduce innovation and diversity in the population, a uniform mutation operator is used in order to prevent premature convergence. In this operation bits of the chromosomes (the mutation points) were randomly chosen and have a specific

probability to be inversed. Figure 6.6 shows the sequence of operators used in the genetic algorithm optimisation.

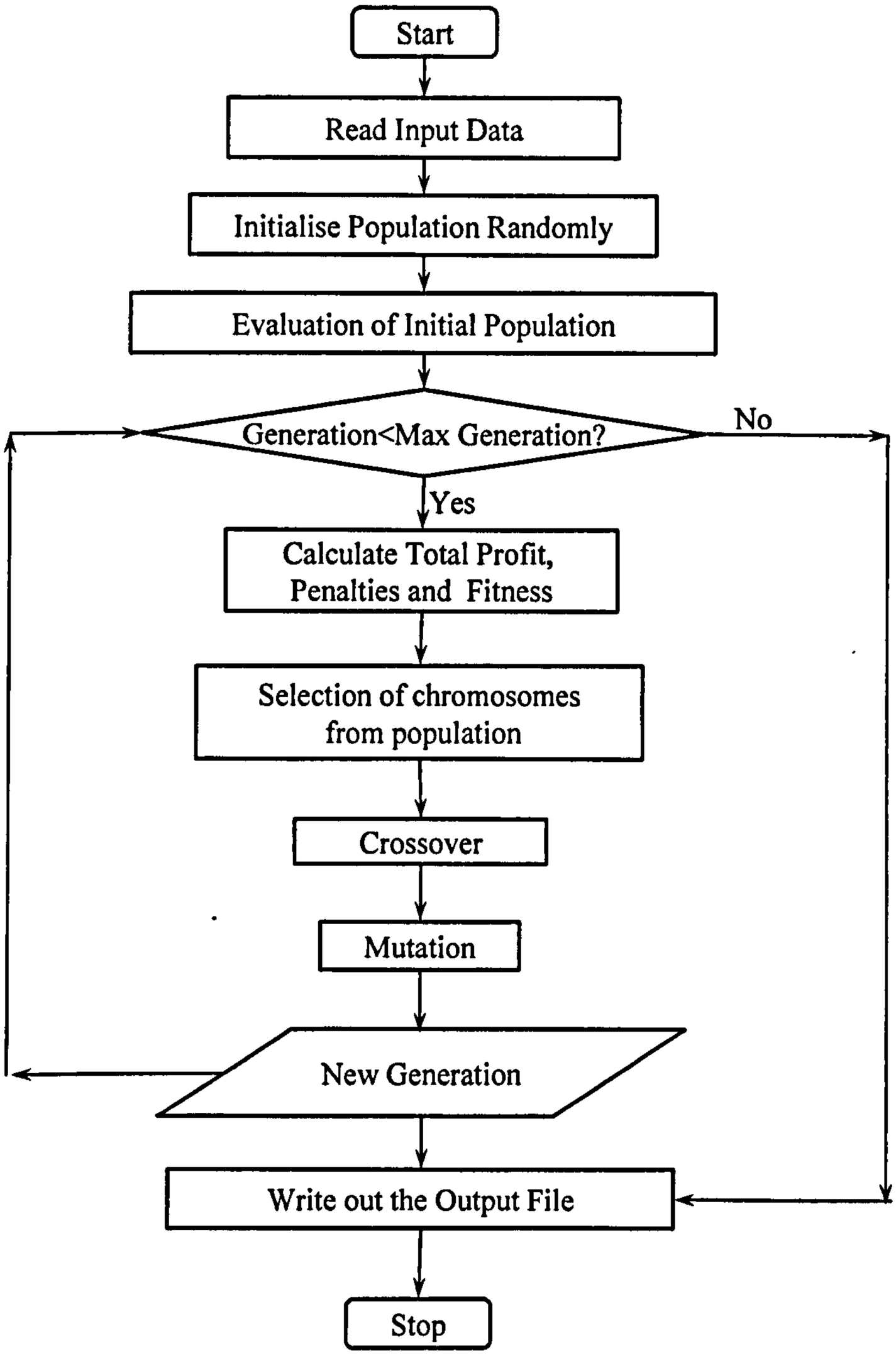

Figure 6.6 – Flowchart of generation schedule optimisation with genetic algorithms

6.4.1.1 - Initialisation of population

In traditional genetic algorithm optimisation the initial population is usually obtained from randomly generated solutions. However, these randomly generated solutions are generally far from the optimal solution in the solution space. Thus the convergence is slow and it may results in a local minimum convergence. In this study, part of the initial population was still generated randomly to maintain the population

diversity, but the remaining population was generated using an Adapted Priority List method.

In a Priority List (PL) technique, in each time interval of the schedule period, units are connected in a preset order until load demand requirements are observed. This order is usually setup based on the generation cost of units. The less costly units are committed first and the more costly units are committed only if the load demand is higher than the total power dispatched.

The traditional priority list technique is not an effective solution for the initialisation of the genetic algorithm developed in this study, because it does not consider the spinning reserve (excess of power capacity) as an option for electricity trading, but just as a system constraint. Then, an Adapted Priority List (APL) is proposed based on the rules described below.

The generation cost ($GC_{i,ISO}$) of each unit i under ISO conditions is given by:

$$FCR_{i,ISO} = 3600 \cdot ftr_{i,ISO} \cdot MFC_{i,ISO} \tag{6.25}$$

$$GC_{i,ISO} = \frac{FCR_{i,ISO}}{P_{i,ISO}} \tag{6.26}$$

Where $FCR_{i,ISO}$ is the fuel cost rate of each unit i under ISO conditions. After sorting out the units to ascending generation cost, dispatch the units starting from the least costly unit (lower $GC_{i,ISO}$) according to the following rule:

DO (i = 1)

IF ($GC_{i,ISO}$ <= $EBP_{i,t}$) THEN ($u_{i,t} = 1$)

IF $GC_{i,ISO} > EBP_{i,t}$, THEN ($u_{i,t} = 0$)

UNTIL (Power Balance: $(u_{i,t} \cdot P_{i,t}) \geq ED_{i,t}$ **)** **(6.27)**

Then, starting from the latest unit dispatched in the previous algorithm (unit k), schedule the power capacity of the remaining units according the following rule:

DO (i = k)

IF $GC_{i,ISO}$ <= $ESP_{i,t}$, THEN ($u_{i,t} = 1$)

IF $GC_{i,ISO} > ESP_{i,t}$, THEN ($u_{i,t} = 0$)

UNTIL (Last unit: i = N)

6.5 - Software Testing and Verification

A Software program PowerProfit has been written for generation schedule optimisation in different time horizon lengths of distributed generation systems operating in competitive market. After translate the algorithm to Fortran language each function was compiled using a Compaq Visual Fortran Compiler and debugged for syntax error test.

A dynamic testing was carried out to check the program for possible run-time, logical and design errors. The program was executed in parts and tested using a set of data such that every logical path in it was run through at least once. Different types of data (simple, typical and extreme) were used with the intention of finding any possible design errors.

In the simple data dynamic test the problem is optimise one or two units with arbitrary hourly prices over a 6-hour trading period. The results are compared with dynamic programming optimisation carried out step by step in a Microsoft® Office Excel spread sheet.

The typical data dynamic test was set in 8 units over a 24-hour trading period. The electricity demand and generation units performance were taken from chapter 2 and Appendix A. Electricity and fuel prices were taken arbitrarily within the typical range of these variables in the UK power market.

The extreme data dynamic was set in 40 units over a 24-hour trading period. The system is divided in 5 groups of 8 units. This test simulates how the software reacts to the high volatility of the energy market. Then the following input data were used throughout the entire schedule period and during peaks intervals: very low and very high demand electricity, very low and very high electricity and fuel prices, high minimum up and down times constraints.

6.6 - Analysis and Discussion of Results

Two cases were carried out: a typical system (8 units) and an extreme system (40 units), both over a 24-hour trading period. In this investigation the maintenance costs of gas turbines units used was 3.62£/MWh of electricity produced and the (natural gas) fuel tariff rate is 0.0585 £/kg. The gas turbines units were assumed off initially (schedule time 0). The start-up cost and minimum up and down time units were taken from Wang *et al*, 1995.

The contracted electricity price used in this study is shown in Table 6.1. It usually is a result of medium or long-term agreement between generator and consumer. That means it does not change over a short-term period.

Table 6.1 – Contracted electricity price of units

UNIT	CEP £/kWh
1	0.0185
2	0.0173
3	0.0224
4	0.0169
5	0.0180
6	0.0175
7	0.0194
8	0.0285

The electricity demanded forecasts by each unit is given by Figure 6.7 and the power produced by each unit is given by Figure 6.8. It is based on the data presented in Appendix A.

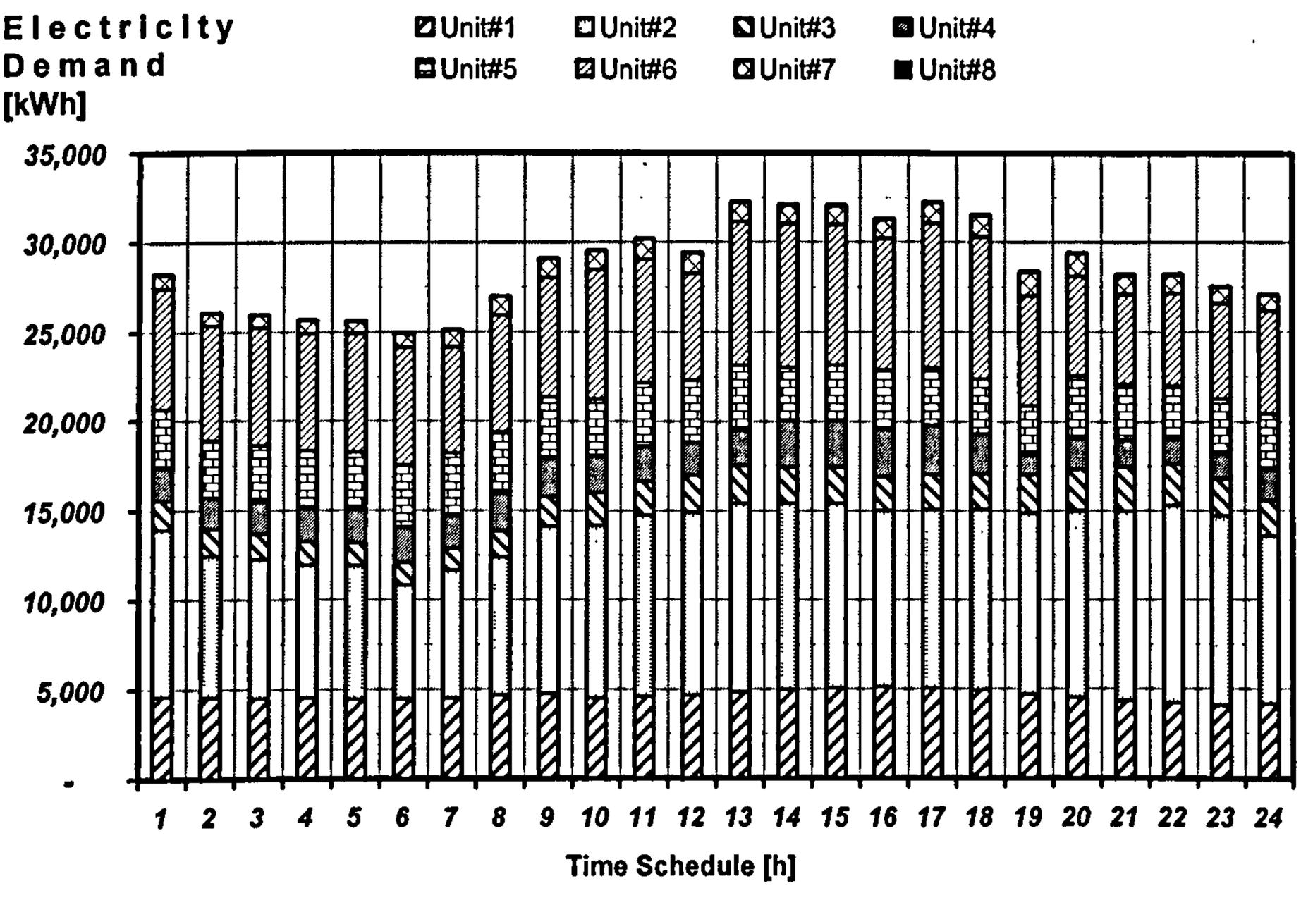

Figure 6.7 - 8-units mini-pool electricity demand forecasts

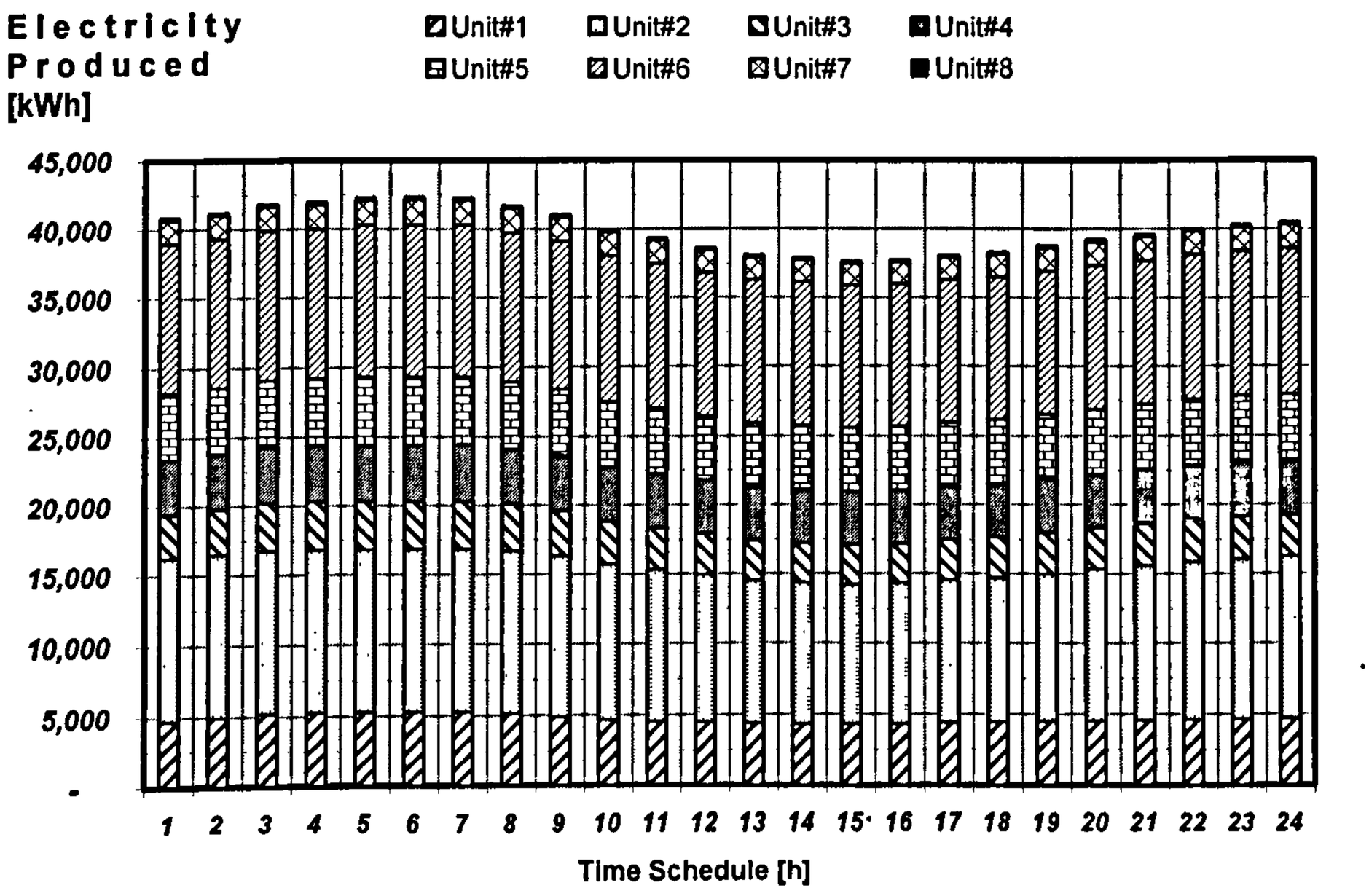

Figure 6.8 – 8-units mini-pool off-design power output

The electricity price forecasts of each unit are presented in Figure 6.9. It reflects the volatility of the power market.

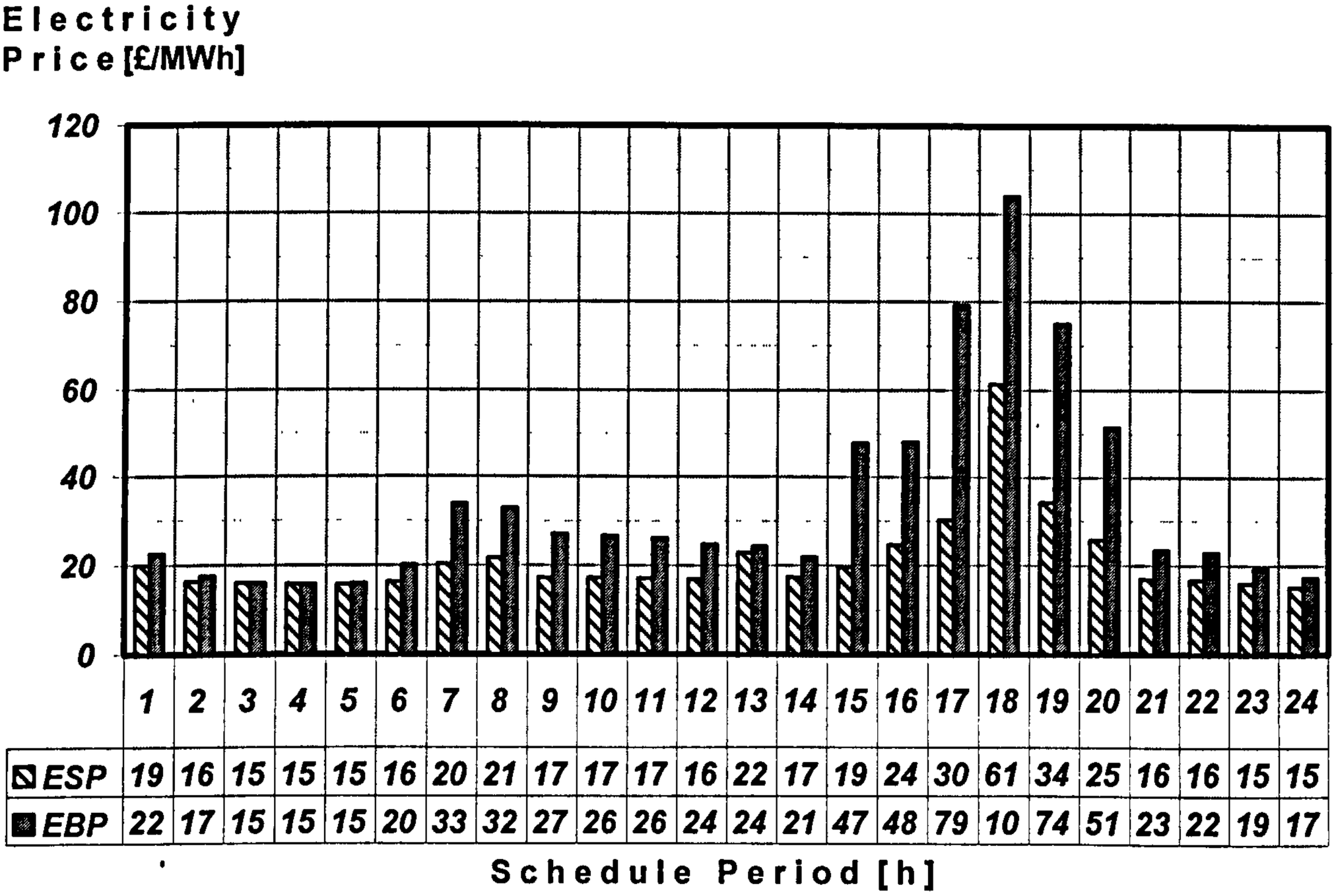

Figure 6.9 – Electricity Price Forecasts

The optimal solution of the single unit commitment with dynamic programming algorithm for the 8-unit system is shown in Table 6.2 (1 means unit is on-line, 0 means unit is off-line). In this case there is no exchange of power between units. The software program identifies the best time in the schedule period to switch the unit on and also the time during which to generate electricity is not feasible (unit is switched off).

Table 6.2 – Optimal 8-units mini-pool schedule obtained by single unit commitment algorithm

t [h]	1	2	3	4	5	6	7	8	9	10	11	12	13	14	15	16	17	18	19	20	21	22	23	24
Unit#1	1	1	0	0	0	1	1	1	1	1	1	1	1	1	1	1	1	1	1	1	1	1	1	1
Unit#2	1	1	0	0	0	1	1	1	1	1	1	1	1	1	1	1	1	1	1	1	1	1	1	1
Unit#3	1	0	0	0	0	0	1	1	1	1	1	1	1	1	1	1	1	1	1	1	1	1	0	0
Unit#4	1	0	0	0	0	0	1	1	1	1	1	1	1	1	1	1	1	1	1	1	1	1	0	0
Unit#5	1	1	0	0	0	1	1	1	1	1	1	1	1	1	1	1	1	1	1	1	1	1	1	0
Unit#6	1	1	0	0	0	1	1	1	1	1	1	1	1	1	1	1	1	1	1	1	1	1	1	0
Unit#7	1	0	0	0	0	0	1	1	1	1	1	1	1	1	1	1	1	1	1	1	1	1	0	0
Unit#8	1	0	0	0	0	0	1	1	1	1	1	1	1	1	1	1	1	1	1	1	1	1	0	0

Figure 6.10 shows the total profit of each unit obtained with the dynamic programming algorithm. The peak of profit occurs at the same time as the peak of electricity market price because of the higher revenue from selling the surplus of electricity.

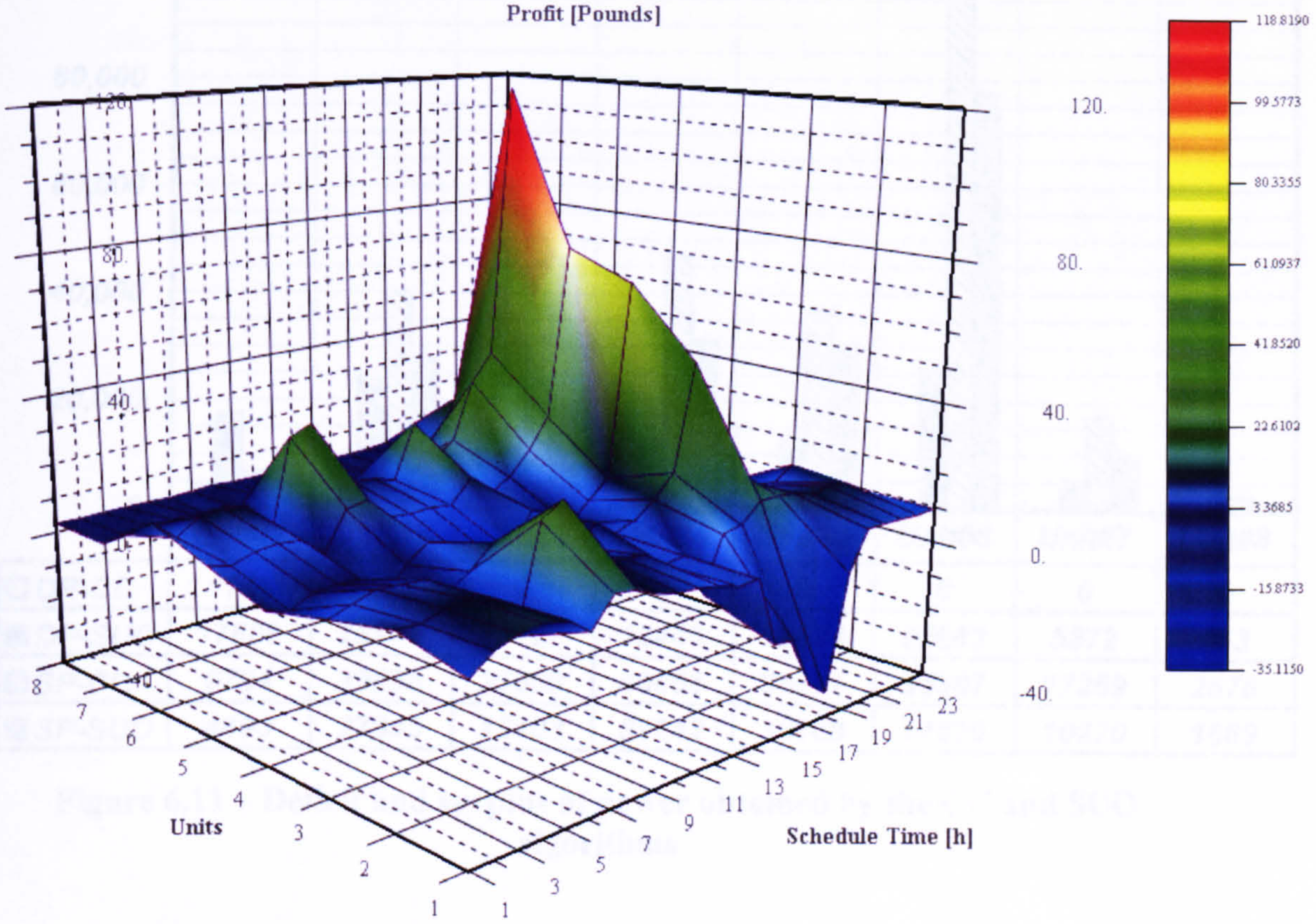

Figure 6.10 – Profit schedule obtained by single unit commitment algorithm

Figure 6.11 shows the comparison between the conventional case and single unit commitment. The single unit optimisation problem shows an increase in the deficit of power and decrease of surplus when comparing with the conventional case due to the shut-down of units over period of time during which is not feasible to produce power. Consequently the revenue from a surplus of electricity decreases as shown in Figure 6.12. The production cost supposes to increase due to the higher deficit of power. However, it drops as seen in Figure 6.12 and it can be explained by the fact that the contribution of the deficit of power is lower than the running costs: 87.1% against 12.9% (Figure 6.13). The running cost represents the majority of the production costs

mainly because of the fuel costs, which can be responsible for up to 80% of running costs (Figure 6.14).

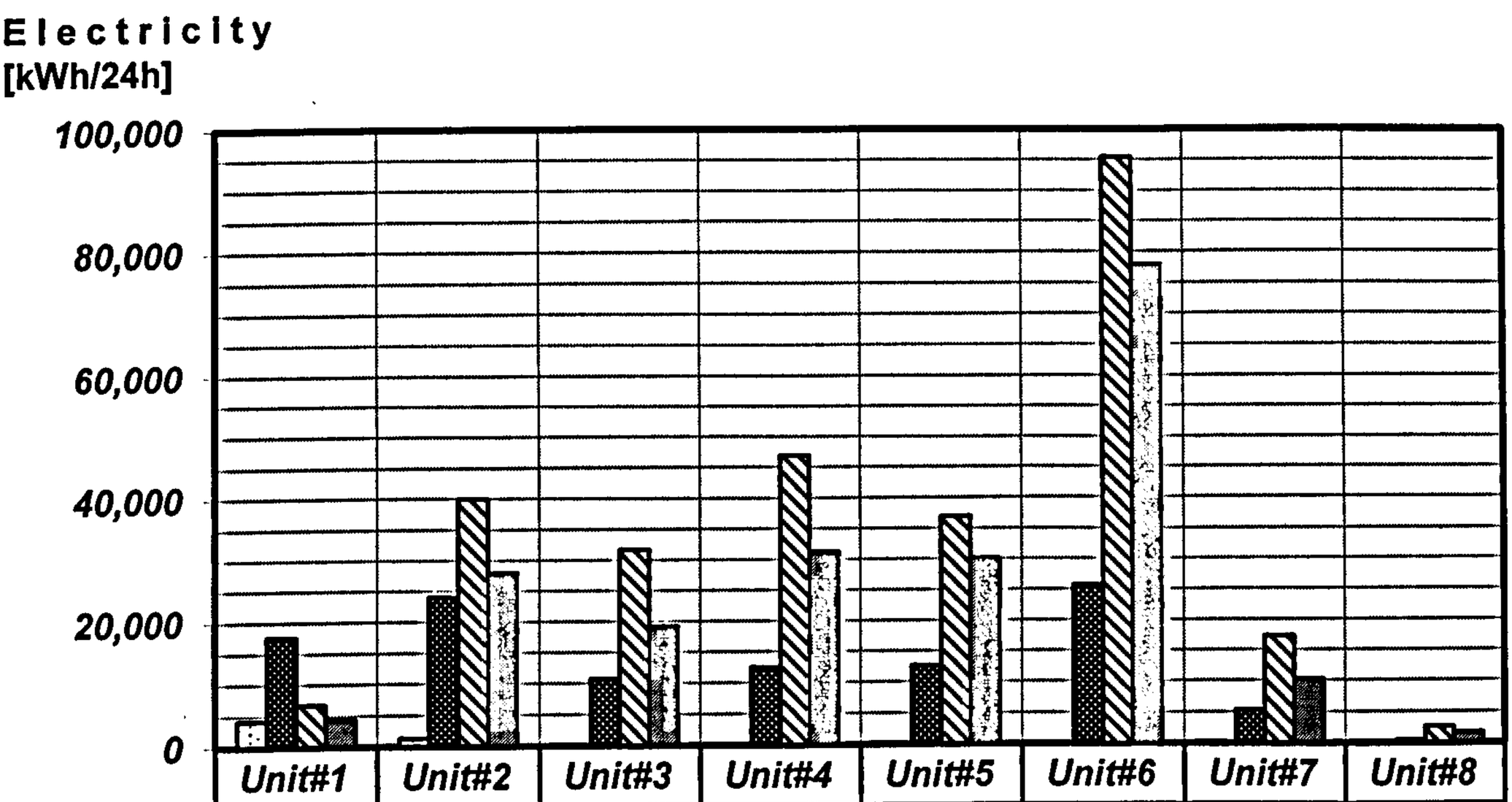

	Unit#1	Unit#2	Unit#3	Unit#4	Unit#5	Unit#6	Unit#7	Unit#8
DP-CC	4146	1270	0	0	0	0	0	0
DP-SUO	17606	23998	10727	12446	12634	25683	5372	453
SP-CC	6724	39936	31658	46856	36971	95387	17259	2575
SP-SUO	4490	27945	19103	31242	30168	77879	10220	1669

Figure 6.11 – Deficit and surplus of power obtained by the CC and SUO algorithms

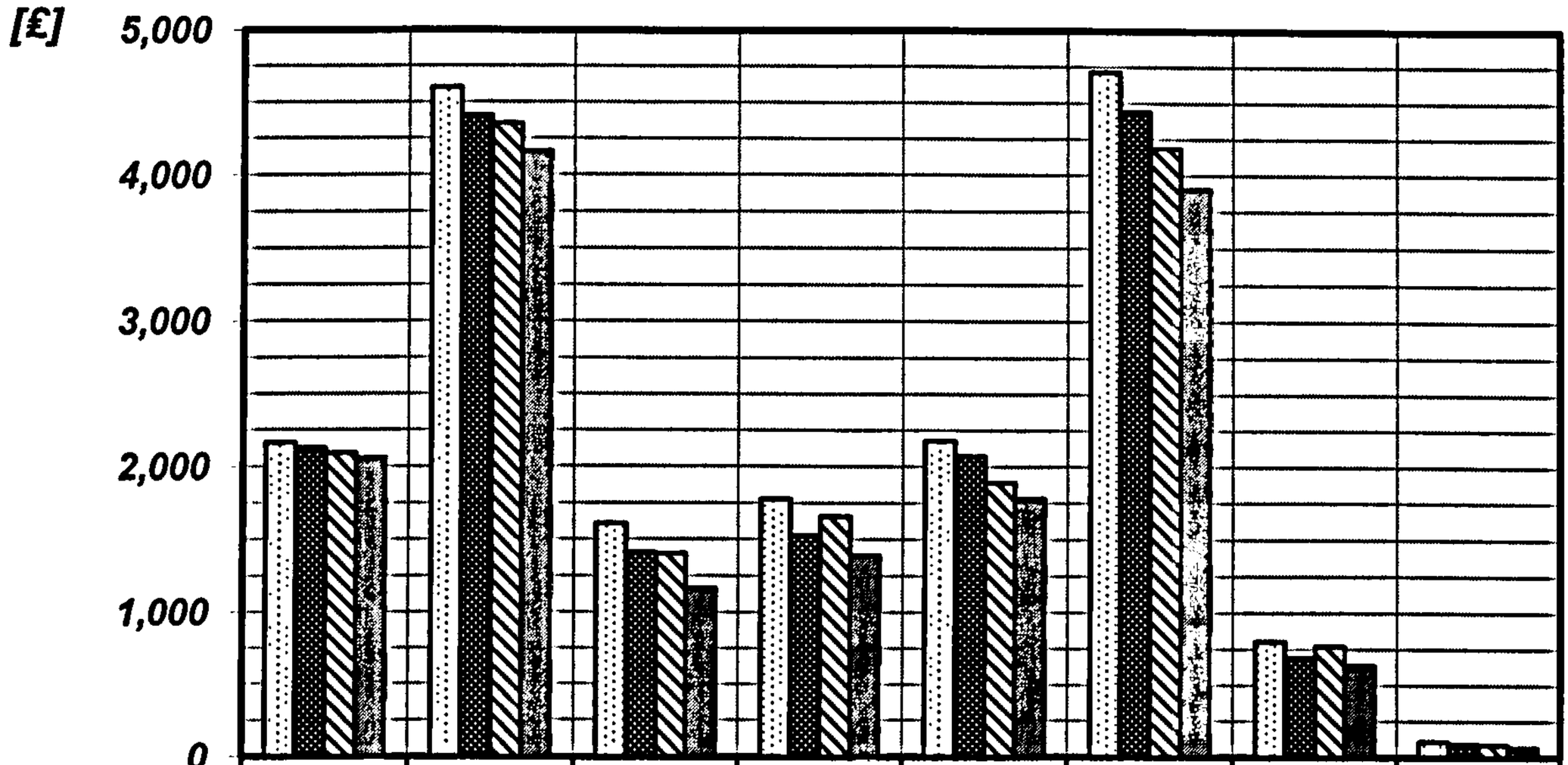

	Unit#1	Unit#2	Unit#3	Unit#4	Unit#5	Unit#6	Unit#7	Unit#8
Rev-CC	2159	4597	1610	1776	2178	4711	803	106
Rev-SUO	2123	4408	1411	1529	2072	4439	691	92
PC-CC	2090	4351	1402	1657	1888	4188	769	82
PC-SUO	2055	4159	1164	1388	1778	3905	636	66

Figure 6.12 – Revenue (Rev) and production cost (PC) obtained by the CC and SUO algorithm

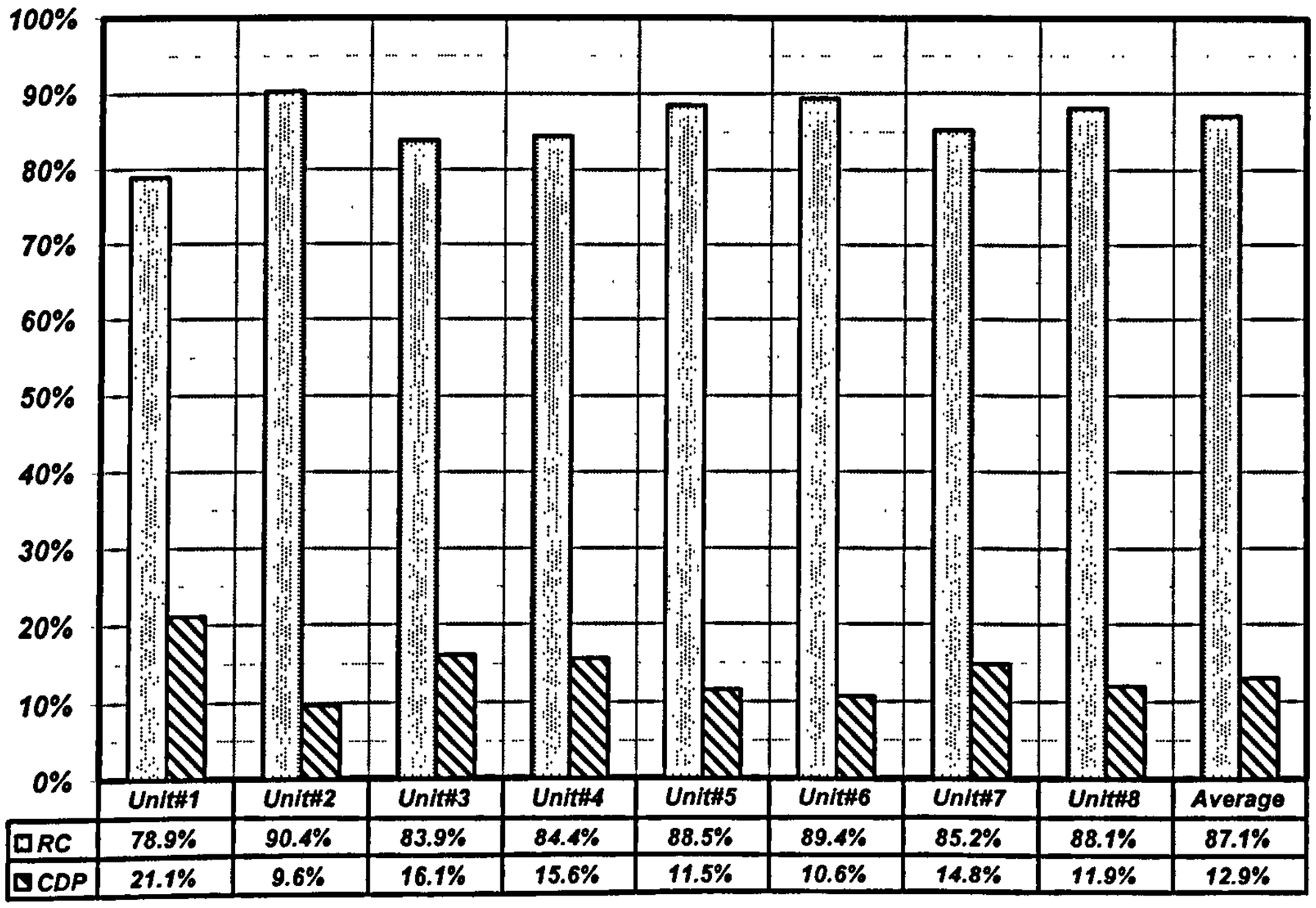

	Unit#1	Unit#2	Unit#3	Unit#4	Unit#5	Unit#6	Unit#7	Unit#8	Average
RC	78.9%	90.4%	83.9%	84.4%	88.5%	89.4%	85.2%	88.1%	87.1%
CDP	21.1%	9.6%	16.1%	15.6%	11.5%	10.6%	14.8%	11.9%	12.9%

Figure 6.13 – Production cost breakdown of an 8-units mini-pool

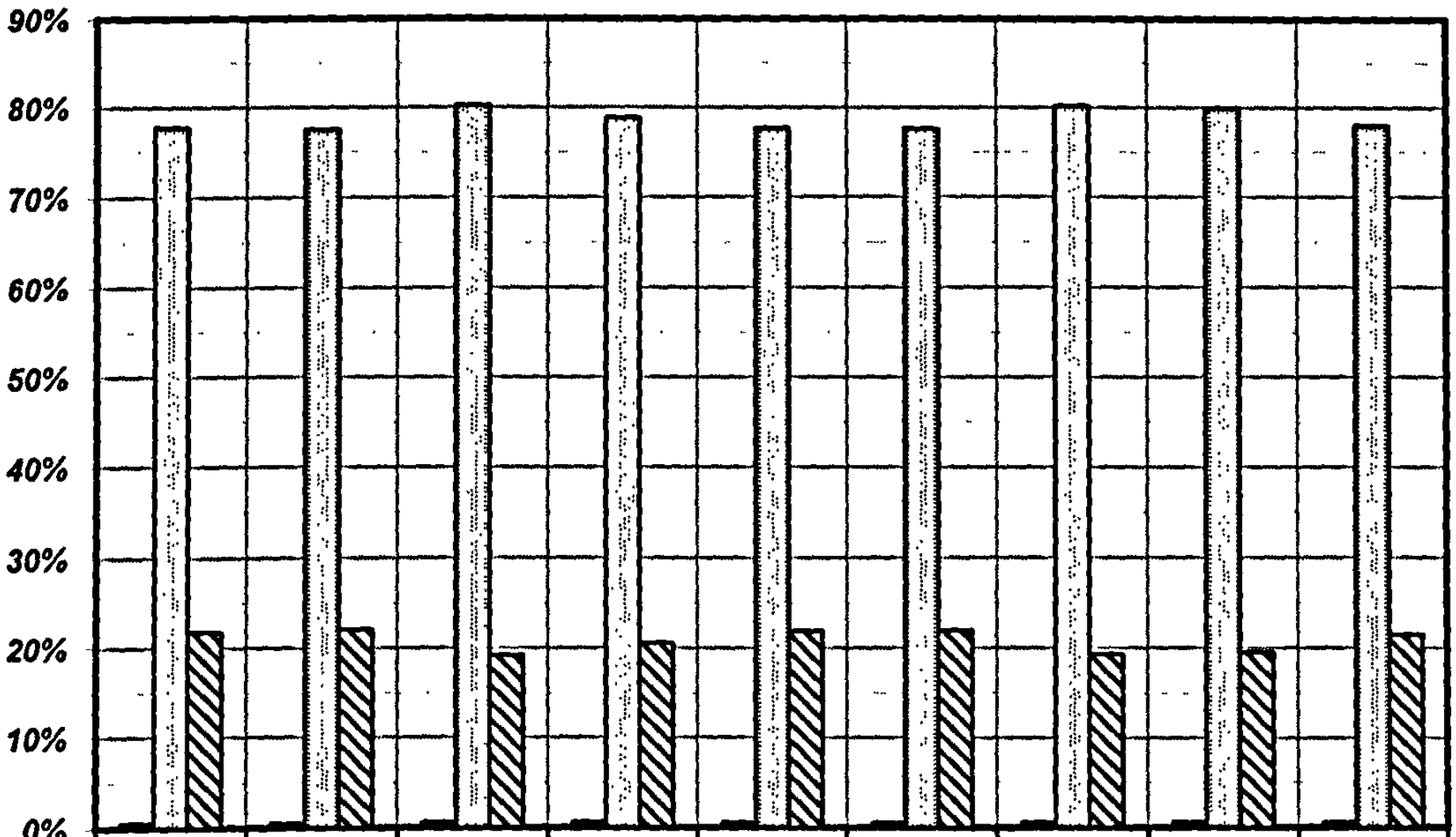

	Unit#1	Unit#2	Unit#3	Unit#4	Unit#5	Unit#6	Unit#7	Unit#8	Average
SU	0.54%	0.50%	0.60%	0.62%	0.56%	0.54%	0.57%	0.58%	0.54%
FC	77.7%	77.5%	80.2%	78.8%	77.6%	77.6%	80.2%	79.9%	78.0%
MC	21.8%	22.0%	19.2%	20.6%	21.8%	21.9%	19.3%	19.5%	21.5%

Figure 6.14 – Running cost breakdown of an 8-units mini-pool

The single unit commitment optimisation with dynamic programming can introduce a considerable benefit to generators' profit, saving 6.79% in an 8-units mini-pool. Table 6.3 shows that the savings can aggregate up to £37,435 on an annual basis, where DP is the deficit of power and SP is the surplus of power.

Table 6.3 – Savings with SUO of the an 8-units mini-pool

	CC	SUO	Saving	Annual Saving [£]
DP [kWh]	5,416	108,919	-	-
SP [kWh]	277,366	202,716	-	-
Rev [£]	17,939	16,765	-6.55%	-428,551
PC [£]	16,428	15,152	-7.77%	-465,988
Prf [£]	1,510	1,613	6.79%	37,435
Profitability	8%	10%	14.27%	

Table 6.4 shows the optimal solution of an 8-units mini-pool obtained by the hybrid genetic algorithm and adapted priority list (GA-APL). The underlined bold character figures represent the units whose status has changed from the single unit

commitment schedule (Table 6.4) to the multi-units commitment by the hybrid GA-APL.

Table 6.4 – Optimal 8-units mini-pool schedule obtained by multi-units commitment algorithm

t [h]	1	2	3	4	5	6	7	8	9	10	11	12	13	14	15	16	17	18	19	20	21	22	23	24
Unit#1	1	1	0	0	0	1	1	1	1	1	1	1	1	1	1	1	1	1	1	1	1	1	1	1
Unit#2	1	1	0	0	0	1	1	1	1	1	1	1	1	1	1	1	1	1	1	1	1	1	1	1
Unit#3	1	0	0	0	0	0	1	1	0	0	0	0	1	0	1	1	1	1	1	1	0	0	0	0
Unit#4	1	0	0	0	0	0	1	1	0	0	0	0	1	1	1	1	1	1	1	1	0	0	0	0
Unit#5	1	0	0	0	0	0	1	1	1	1	1	1	1	1	1	1	1	1	1	1	1	1	1	0
Unit#6	1	1	0	0	0	1	1	1	1	1	1	1	1	1	1	1	1	1	1	1	1	1	1	1
Unit#7	1	0	0	0	0	0	1	1	0	0	0	0	1	0	1	1	1	1	1	1	0	0	0	0
Unit#8	1	0	0	0	0	0	1	1	0	0	0	0	1	0	0	1	1	1	1	1	0	0	0	0

The priority list of units committed first is presented in Table 6.5. The decision comparative parameter is the generation cost (GC). Units with a lower GC are committed first until covering the total demand in each period of scheduled time. Then the GC is compared with the electricity sell price to decide whether to dispatch the reserve capacity or not. That is the Adapted Priority List which produces a 'seed' solution to the multi-unit commitment program with genetic algorithm.

Table 6.5 – Sequence of units dispatched of 8-unit system achieved with APL

	GCI [£/kWh]	PL Position
Unit#1	0.01291	4th
Unit#2	0.01256	1st
Unit#3	0.01500	8th
Unit#4	0.01378	5th
Unit#5	0.01279	3rd
Unit#6	0.01275	2nd
Unit#7	0.01488	7th
Unit#8	0.01418	6th

The method of initialising the genetic algorithm with a 'seed' solution aims to speed up the convergence process. Despite the 'seed' solution being far from the optimal solution, it is a better approach when compared with a randomly generated

solution. Figure 6.15 illustrates the benefits achieved with the hybrid genetic algorithm and adapted priority list (GA-APL).

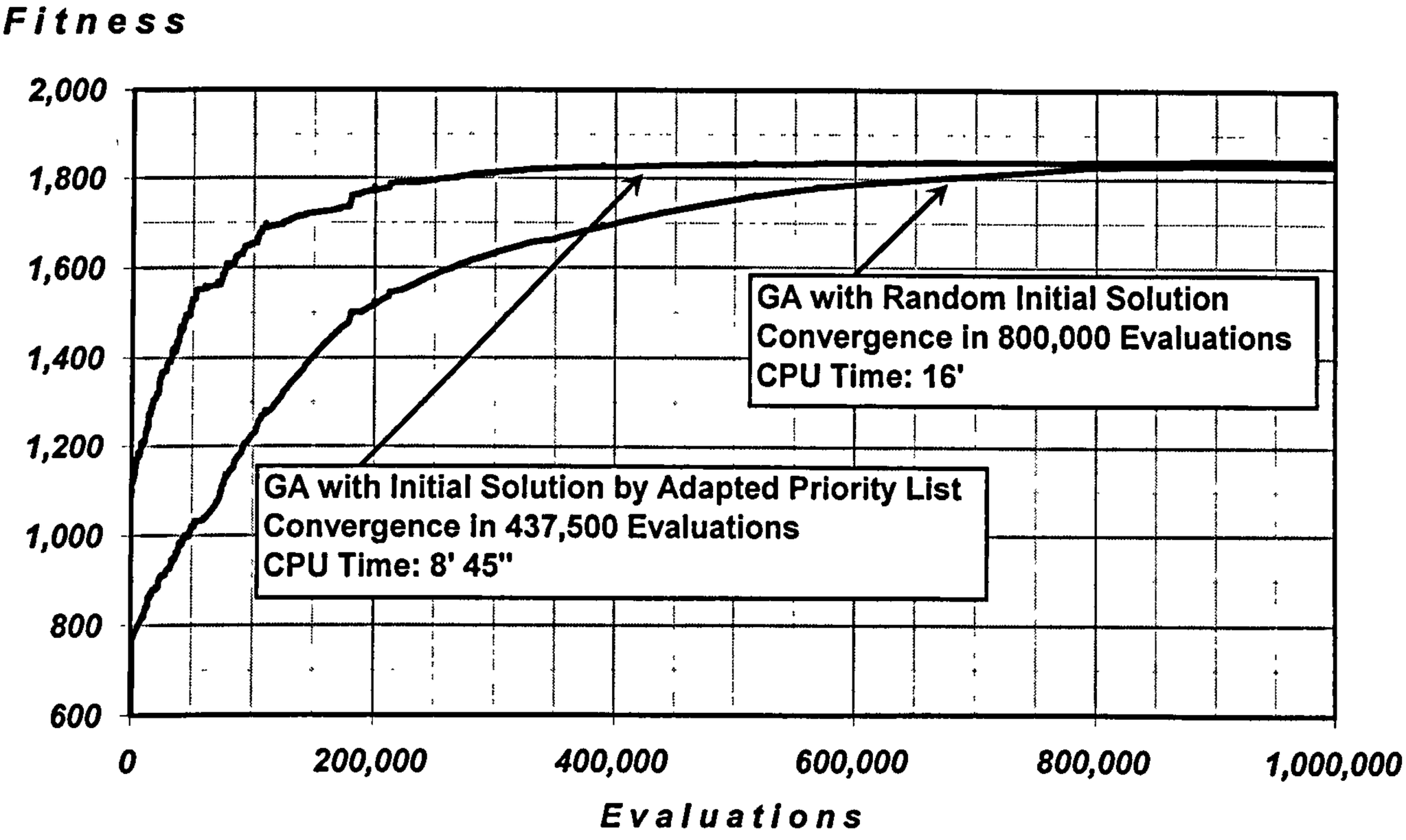

Figure 6.15 – Convergence (average of 10 runs) obtained by Hybrid GA-APL against GA (8-units mini-pool)

The savings achieved in the multiple units optimisation with hybrid genetic algorithm adapted priority list can be up to 14% when compared with single unit optimisation with dynamic programming and up to 21% compared with conventional case in an 8-units mini-pool. On an annual basis this can represent an accumulative saving of £120,948 (Tables 6.6 and 6.7).

Table 6.6 – Savings of the an 8-units mini-pool with MUO against SUC

	SUO	MUO	Saving	Annual Saving [£]
DP [kWh]	108,919	77,614	-	-
SP [kWh]	202,716	114,155	-	-
Rev [£]	16,765	15,235	-9.12%	-558,288
PC [£]	15,152	13,393	-11.60%	-641,796
Prf [£]	1,613	1,842	14.19%	83,513
Profitability	10%	12%	25.65%	

Table 6.7 – Savings of the an 8-units mini-pool with MUO against CC

	CC	MUO	Saving	Annual Saving [£]
DP [kWh]	5,416	77,614	-	-
SP [kWh]	277,366	114,155	-	-
Rev [£]	17,939	15,235	-15.07%	-986,839
PC [£]	16,428	13,393	-18.47%	-1,107,783
Prf [£]	1,510	1,842	21.94%	120,948
Profitability	8%	12%	43.58%	

The revenue of the system comes from both bilateral contracted electricity (TEC) and electricity trade in the competitive power market (TESM). Figure 6.16 shows that most of the profit still comes from bilateral contracts. However during peak time of market electricity prices a significant part of the revenue may be produced by trading electricity in the competitive market. Running costs (RC) make a bigger contribution to the production costs, but the cost of deficit of electricity (CDP) can also have a significant impact on the operation of the mini-pool during periods of time when it is not feasible to produce electricity (units are shut down) (Figure 6.17).

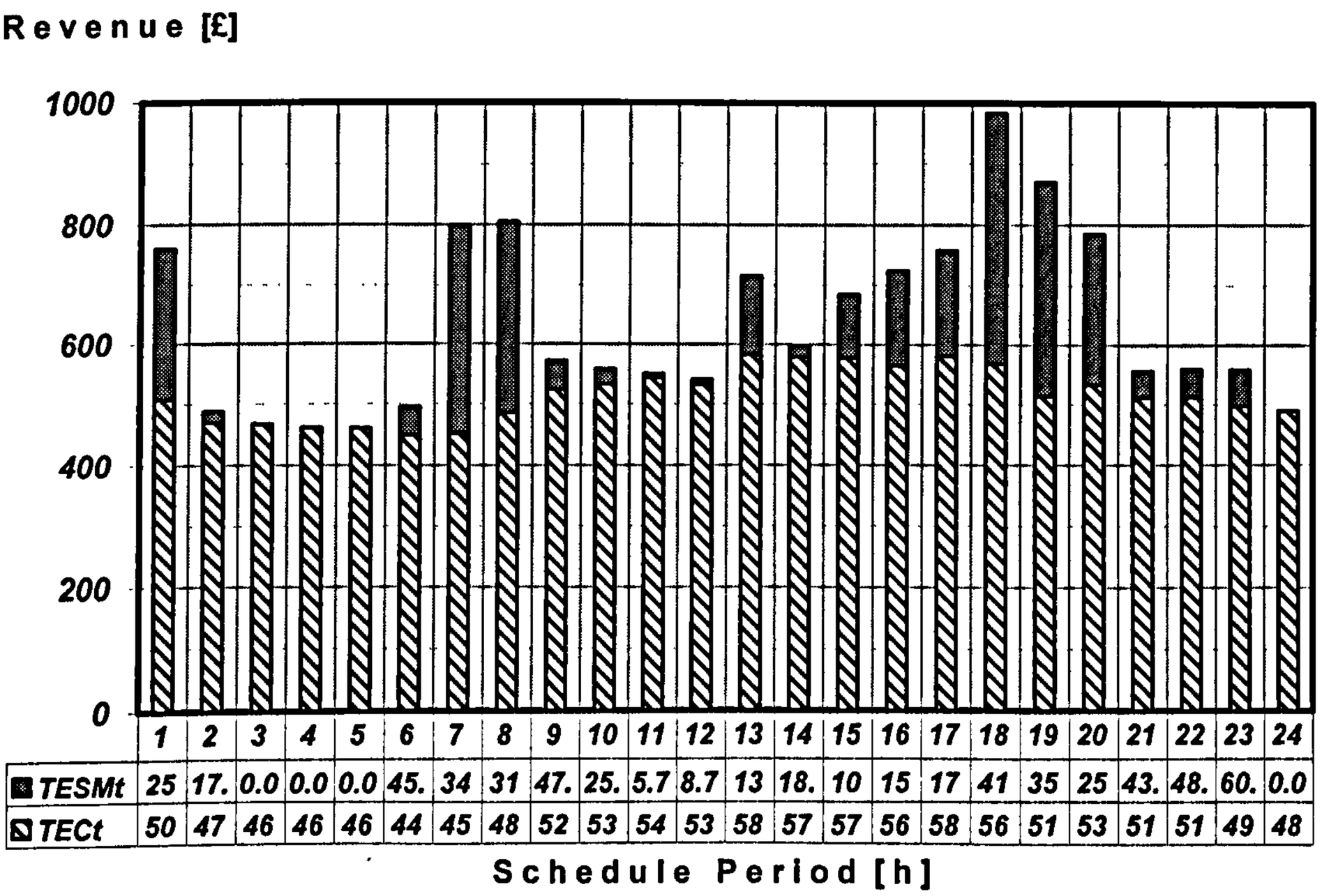

Figure 6.16 – Revenue breakdown of an 8-units mini-pool obtained by MUO algorithm

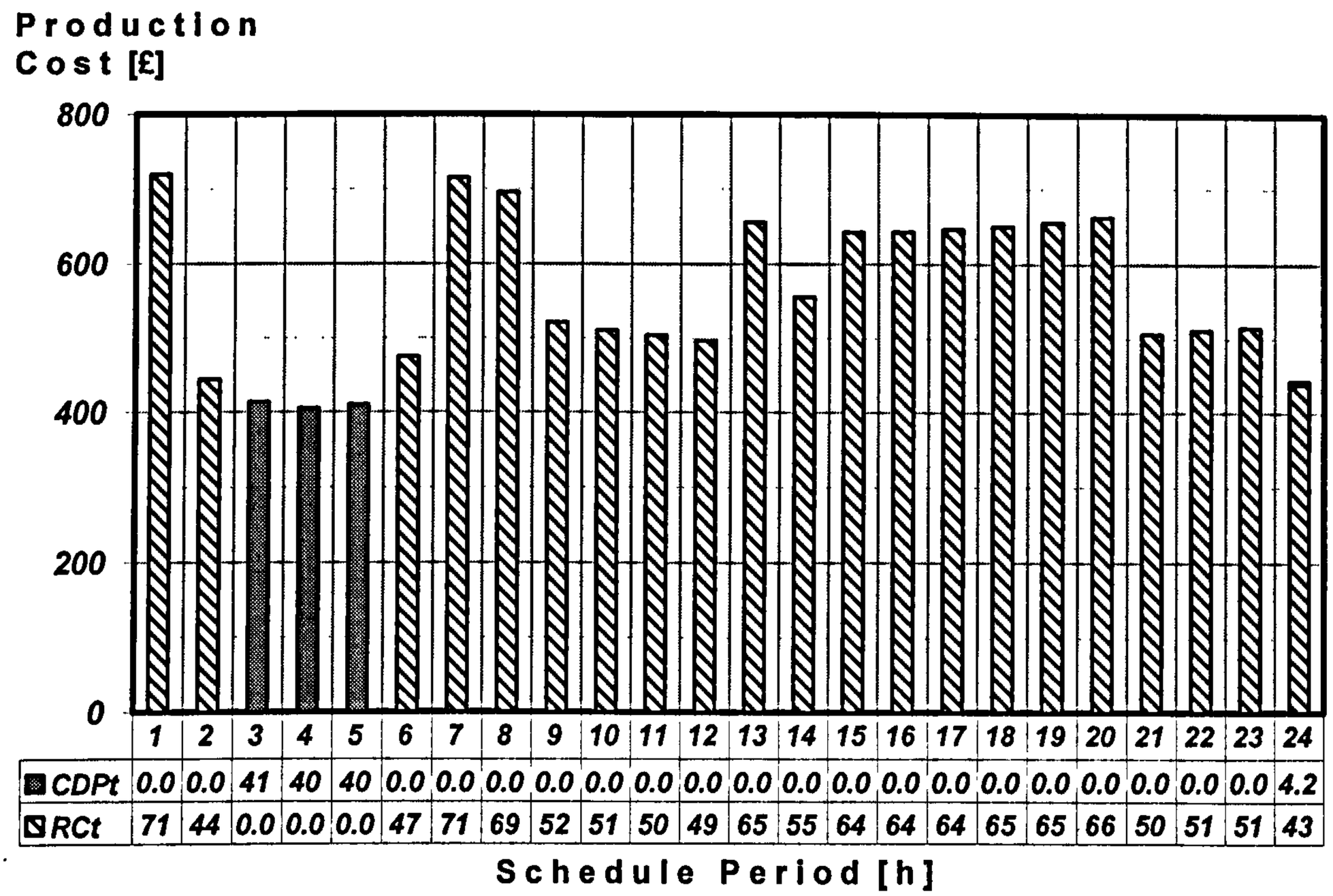

	1	2	3	4	5	6	7	8	9	10	11	12	13	14	15	16	17	18	19	20	21	22	23	24
CDPt	0.0	0.0	41	40	40	0.0	0.0	0.0	0.0	0.0	0.0	0.0	0.0	0.0	0.0	0.0	0.0	0.0	0.0	0.0	0.0	0.0	0.0	4.2
RCt	71	44	0.0	0.0	0.0	47	71	69	52	51	50	49	65	55	64	64	64	65	65	66	50	51	51	43

Figure 6.17 – Production cost of an 8-units mini-pool obtained by MUO algorithm

Despite the relatively high production costs observed in this case study, it is possible to make profit over all the schedule period as shown in Figure 6.18. The peak of profit coincides with the peak of electricity market prices, confirming the initial idea of making profit by running the units of the mini-pool during the best times of the market.

The genetic algorithm convergence procedure can provide global optimal or close-to-optimal solution. The results of 40 runs of the software PowerProfit show that there is a 70% chance of achieving convergence with the Hybrid GA-APL for an 8-units mini-pool problem and an error lower than 0.41% (Figure 6.19). Figure 6.20 shows the distribution of the evaluation of convergence after 40 runs.

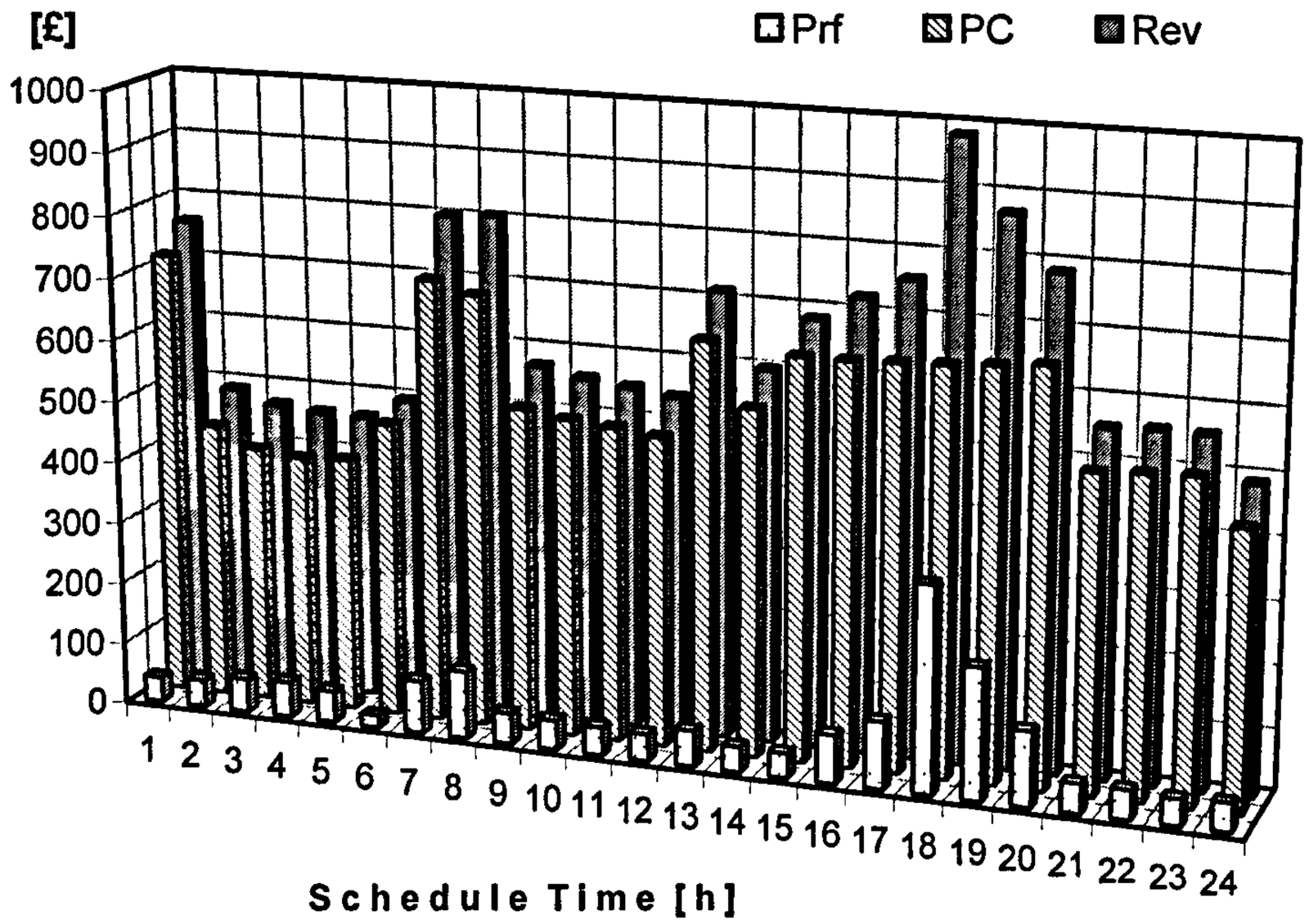

	1	2	3	4	5	6	7	8	9	10	11	12	13	14	15	16	17	18	19	20	21	22	23	24
Prf	40.4	43.9	54.3	57.0	51.0	20.2	85.2	109.	50.3	47.7	46.3	44.5	59.2	42.1	41.0	80.1	110.	333.	213.	123.	48.9	48.6	43.6	46.6
PC	719.	443.	412.	404.	409.	474.	714.	695.	520.	510.	503.	496.	655.	555.	642.	643.	646.	650.	655.	662.	506.	511.	514.	442.
Rev	759.	487.	467.	461.	460.	494.	799.	804.	571.	557.	550.	541.	714.	597.	683.	723.	757.	983.	869.	785.	555.	559.	558.	489.

Figure 6.18 - Profit schedule obtained by multi-unit commitment algorithm

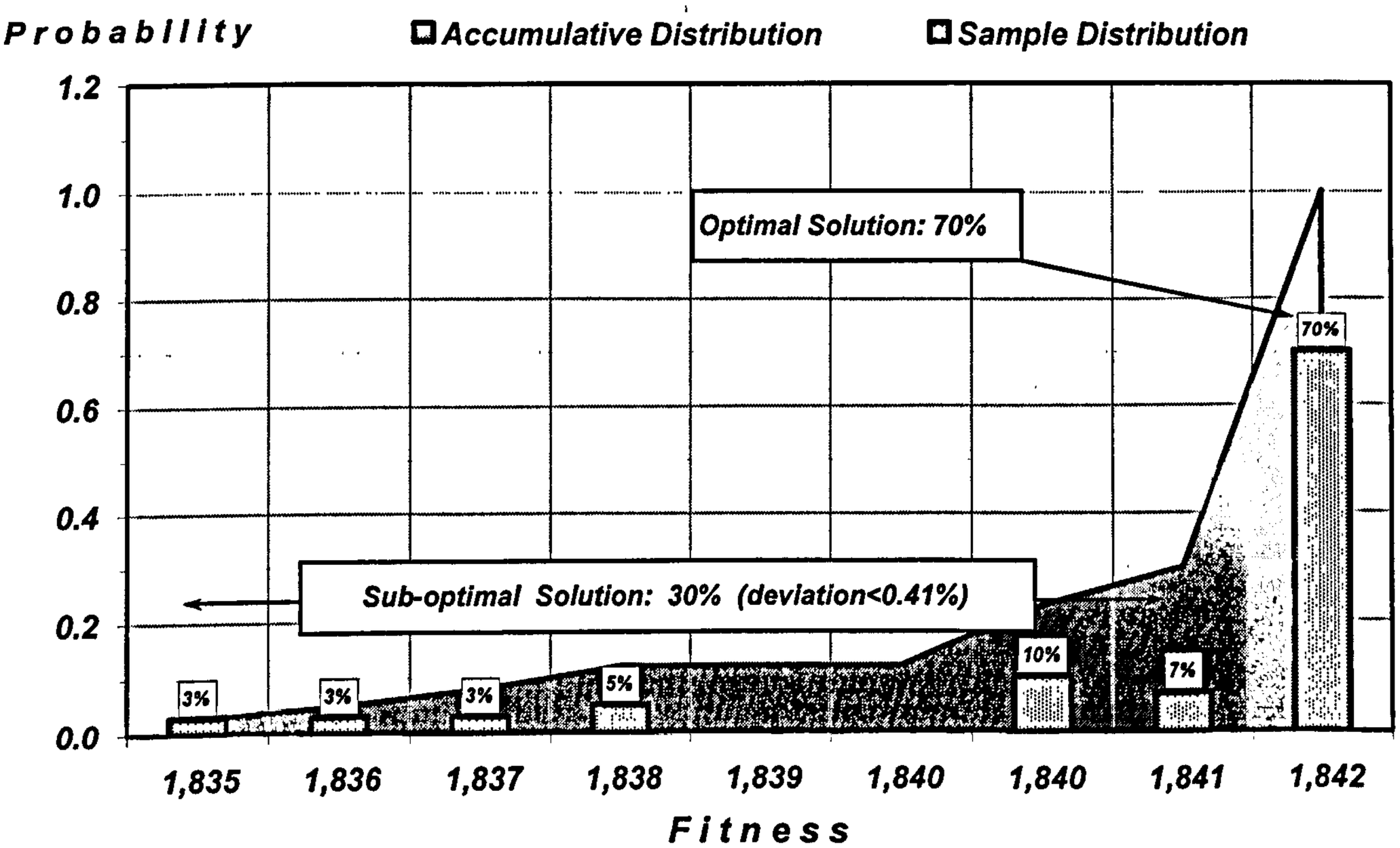

Figure 6.19 – Probability distribution of total profit obtained by Hybrid GA-APL in 40 runs (8-units mini-pool)

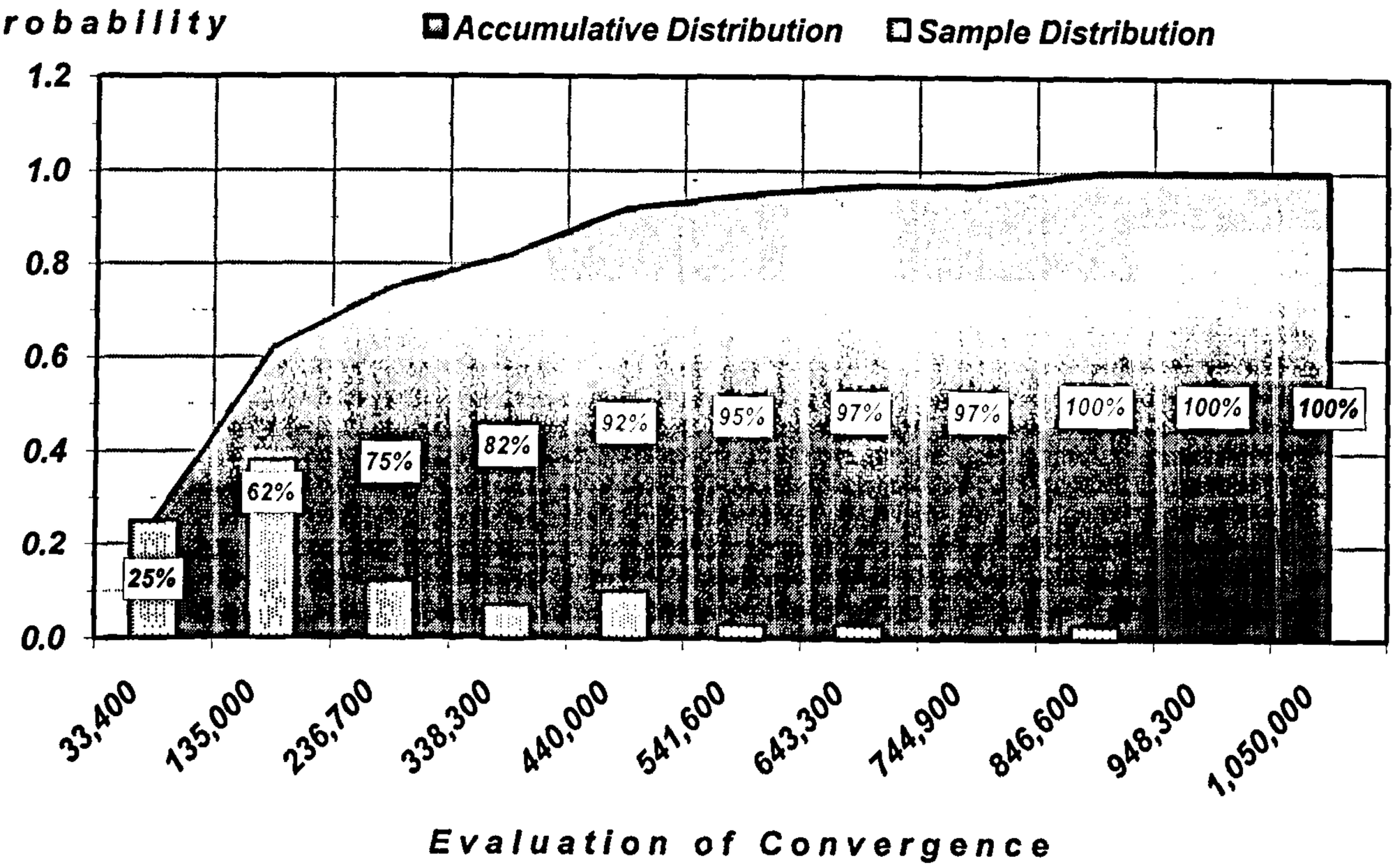

Figure 6.20 - Probability distribution of iteration of convergence obtained by Hybrid GA-APL in 40 runs (8-units mini-pool)

Processing time is another concern of genetic algorithm based optimisation software. Figure 6.21 shows the CPU time spend in a Pentium M Processor 1.73GHz on each run of the PowerProfit program for different problems sizes, however with the same population size (100 evaluations) and a maximum of a ten thousand (10,000) generations. Dimension of the problem (D) is defined by the product between the number of units (N) and time schedule (T).

$$D = N \cdot T \tag{6.28}$$

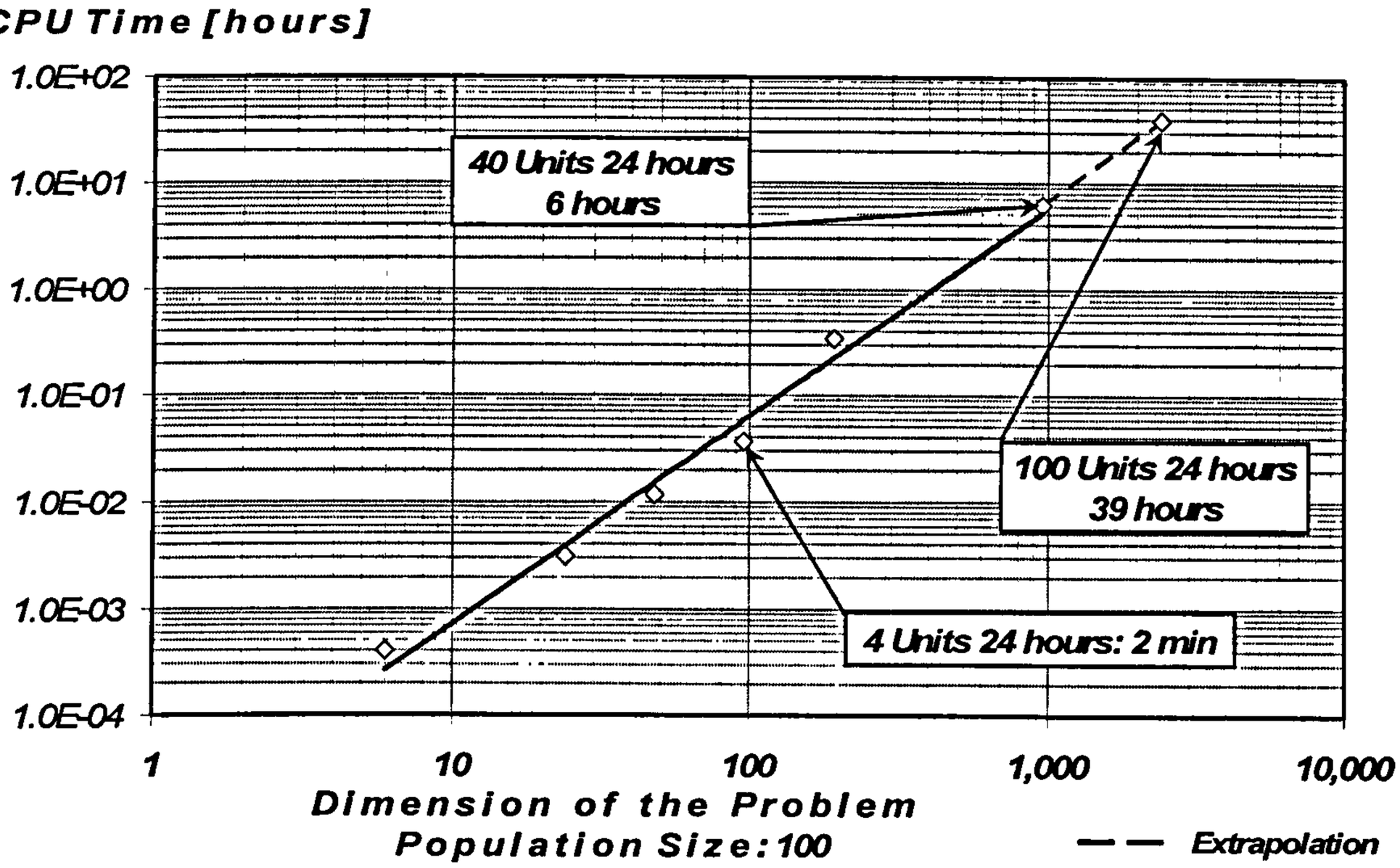

Figure 6.21 – CPU time spent in each run to against the dimension of the problem

The results of an 8-unit mini-pool optimisation with minimum up and down time constraints is presented in Appendix C. In the same appendix it can also be found the results for a generation schedule optimisation of a 40-units mini-pool.

Chapter 7 - Medium-term Generation Schedule Optimisation

7 - Medium-term Generation Schedule Optimisation

7.1 - Introduction

This section presents the generation and maintenance schedule problem for a mini-pool CHP system in a competitive market during a period of one year divided into 52 time intervals of one week's duration (168 hours).

7.2 - Mathematical Model

The model of the structure of the mini-pool CHP units proposed in this study is illustrated in Figure 7.1.

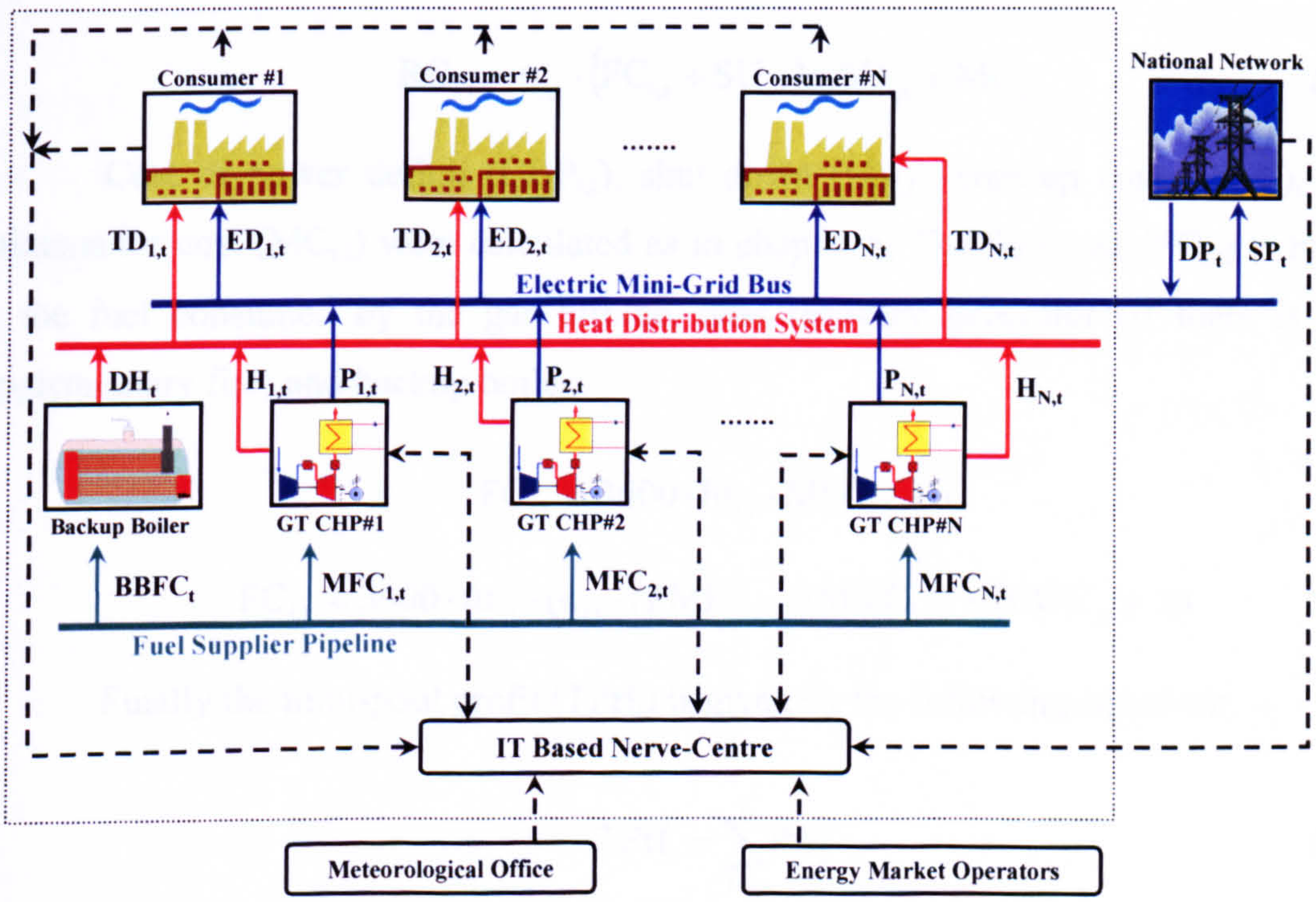

Figure 7.1 – Mini-pool structure diagram

As in the short-term analysis the profit (Prf_t) at each time interval is calculated by subtracting the production cost (PC_t) during that interval from the revenue (R_t), as given:

$$Prf_t = R_t - PC_t \tag{7.1}$$

The revenue includes the income from selling electricity and heat as follows:

$$R_t = \left(ESP_t \cdot \sum_{i=1}^{N}\left(u_{i,t} \cdot SP_{i,t}\right)\cdot \Delta t\right) + \left(\sum_{i=1}^{N}\left(CEP_{i,t} \cdot ED_{i,t} \cdot \Delta t\right)\right) + \left(\sum_{i=1}^{N}\left(TD_{i,t} \cdot HSP_{i,t}\right)\cdot \Delta t\right) \tag{7.2}$$

Where $TD_{i,t}$ is the thermal demand of unit i at period t and $HSP_{i,t}$ is the heat selling price of unit i at period t. The production costs ($PC_{i,t}$) of the system can be written as follows:

$$PC_{i,t} = RC_{i,t} + CDP_{i,t} \tag{7.3}$$

The Running Cost ($RC_{i,t}$) is calculated as follows:

$$RC_{i,t} = u_{i,t} \cdot \left(FC_{i,t} + SU_{i,t}\right) + SD_{i,t} + MC_{i,t} \tag{7.4}$$

Cost of power deficit ($CDP_{i,t}$), shut down ($SD_{i,t}$), start-up costs ($SU_{i,t}$), and maintenance cost ($MC_{i,t}$) were calculated as in chapter 6. The fuel cost ($FC_{i,t}$) is based on the fuel consumed by the gas turbine, heat recovery generator (if there is any supplementary fire) and backup boiler:

$$FC_{i,t} = 3600 \cdot ftr_{i,t} \cdot MFC_{i,t} \cdot \Delta t$$

$$FC_{i,t} = 3600 \cdot ftr_{i,t} \cdot (u_{i,t} \cdot (PMFC_{i,t} + SFFC_{i,t}) + BBFC_{i,t}) \cdot \Delta t \tag{7.5}$$

Finally the mini-pool profit ($TPrf_i$) is given by the following equation:

$$TPrf_i = \sum_{t=1}^{T} Prf_t \tag{7.6}$$

The medium-term generation schedule problem is limited to the following constraints as described in chapter 6: maximum capacity, electricity demand balance, and initial conditions. Also the units' availability constraint is taken into account based on the gas turbine life cycle assessment presented in chapter 4.

7.3 - Carbon emissions cost

The main pollutants found in the gas turbine exhaust gases are: carbon dioxide (CO_2), carbon monoxide (CO), nitrogen oxides (NO_x), sulphur oxides (SO_x, usually sulphur dioxide SO_2), unburned hydrocarbons (C_xH_y, HC or UHC) and solid particles ("particulates").

Carbon dioxide emissions depend primarily on the type, quality (heat value) and quantity (mass flow) of the fuel used. This approach assumes complete combustion in the gas turbine combustor which is very close to reality when combustion takes place with an excess of air and the combustor is not degraded. Then the CO_2 emission is calculated by the following equation:

$$MCO_{2i,t} = \mu_{CO_2} \cdot MFC_{i,t} \tag{7.7}$$

$$\mu_{CO_2} = \frac{44}{12} \cdot CCF \tag{7.8}$$

Where $MCO_{2i,t}$ is the emission mass of carbon dioxide, μ_{CO_2} is the emission of carbon dioxide per unit mass of fuel (Table 7.1), the constant CCF is the mass content of carbon in the fuel.

Table 7.1 – Carbon content of typical fuel used in power generation (Educogen, 2002)

Fuel	Carbon Content (CCF) [%]	μ_{CO_2} [kg CO_2/kg fuel]	Lower Heat Value [kJ/kg]
Natural gas	75	2.75	49000
Diesel oil	83	3.05	42500
Fuel oil 0.7% S	86.5	3.17	41500
Fuel oil 2% S	85	3.12	41000
Peat[1]	58	2.13	7800
Lignite[1]	64	2.35	24000
Coal[1]	80	2.93	30000

[1] Fuel with no moisture and ash

Carbon taxation is modelled in the generation schedule as follows. Where DCTax is the carbon dioxide tax cost, cdtr is the carbon dioxide tax rate (carbon price) and DCA is the carbon dioxide allowance (% of annual emission). In this investigation

the dioxide carbon allowance is always considered as 100% of annual emission (DCA = 1.0).

$$RC_{i,t} = FC_{i,t} + SU_{i,t} + SD_{i,t} + MC_{i,t} + CDTax_{i,t} \quad \textbf{(7.9)}$$

$$CDTax_{i,t} = 3600 \cdot \Delta t \cdot cdtr \cdot \left(2.75 \cdot MFC_{i,t}\right) \cdot DCA \quad \textbf{(7.10)}$$

7.4 - Gas Turbine Reschedule Maintenance

The methodology detail described in chapter 4 is used to predict the gas turbine life cycle during its operation. The model calculates the principal variables that take part in the life cycle assessment, (i.e. time, temperature and stress loads), and produces the expected time to failure. Then the effects of the combination of different levels of these parameters on the turbine life cycling are assessed over the period of time studied. The outcome is the gas turbine service hours between maintenance for a defined maintenance period.

Therefore the algorithm searches for the optimal solution which maximises both mini-pool profit and average service hours between maintenance as described by the following equation:

$$\textbf{Objective Function} = \max_{u_{i,t}}(\text{Mini - Pool Profit}, \text{Average SHBM}_i) \quad \textbf{(7.11)}$$

The search algorithm is based on an enumeration and search approach. It generates and inspects all possible combinations in the stated space that are guaranteed to contain the desired solution (objective function) respecting the given constraints. Exhaustive enumeration is an effective technique as the convergence to the optimal solution is always guaranteed.

A software program (GTPowerCycle) has been written in Fortran language to simulate the medium-term generation and maintenance schedule optimisation model which is illustrated in Figure 7.2.

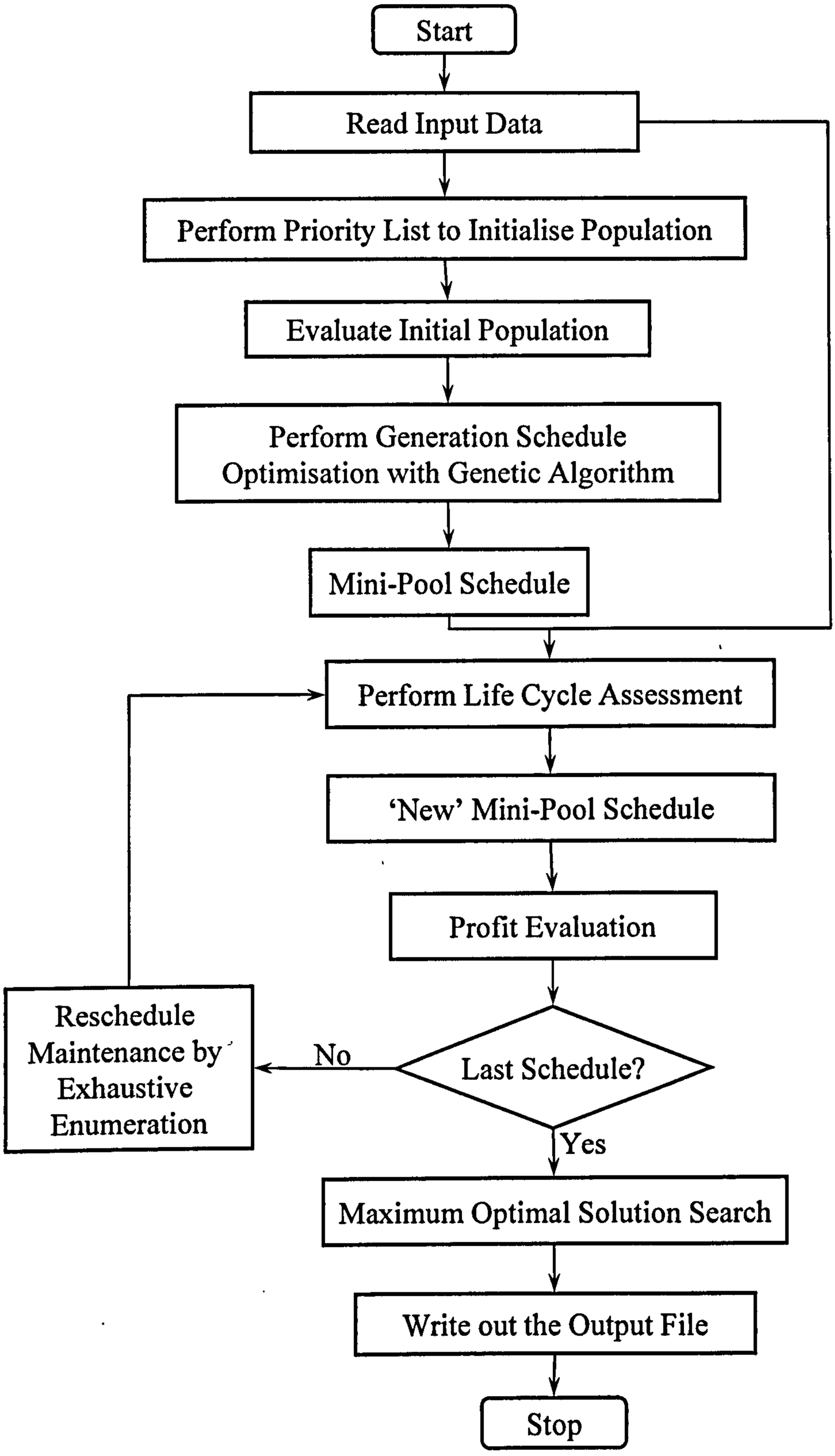

Figure 7.2 – Flowchart of medium-term mini-pool generation and maintenance schedule optimisation

7.5 - Case Study and Analysis of Results

In this case study, a mini-pool of two gas turbine CHP plants (units 4 and 6, chapter 2) was evaluated. A symbolic heat sell price (HSP) of 0.0025 £/kWh$_t$ was used and the contract electricity price (CEP) was considered as 33.5 £/MWh$_e$. A 4-week period of gas turbine maintenance is assumed. Figure 7.3 shows the variation of the market electricity prices over the 52-week schedule period.

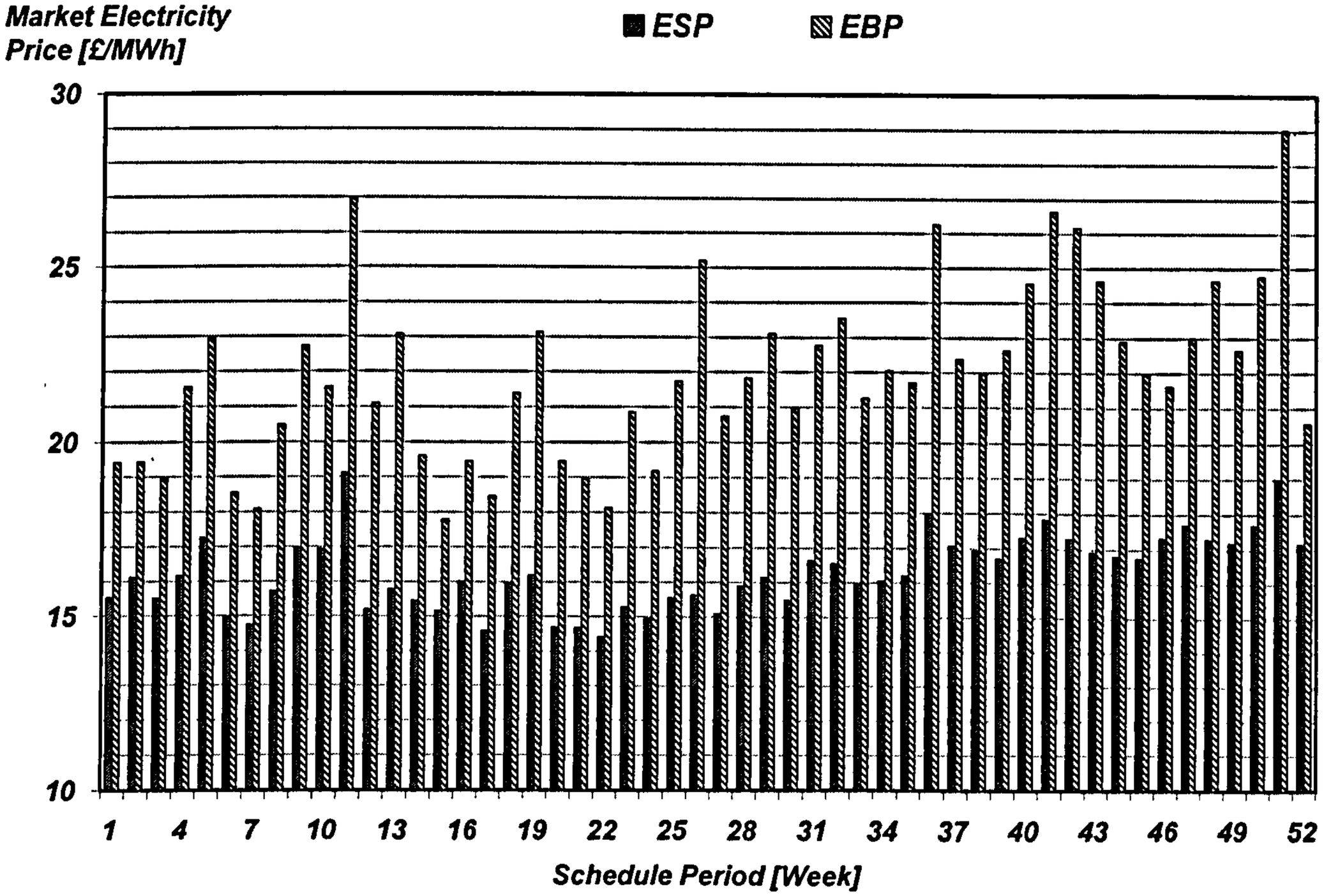

Figure 7.3 – Market electricity prices over schedule period

In the medium-term generation schedule problem fuel prices present a significant variation over the year, as illustrated Figure 7.4, mainly because of the close dependency of the international oil price. The average natural gas price used is about 21p/therm (Figure 7.5) with a maximum peak of 52p/therm (Figure 7.4).

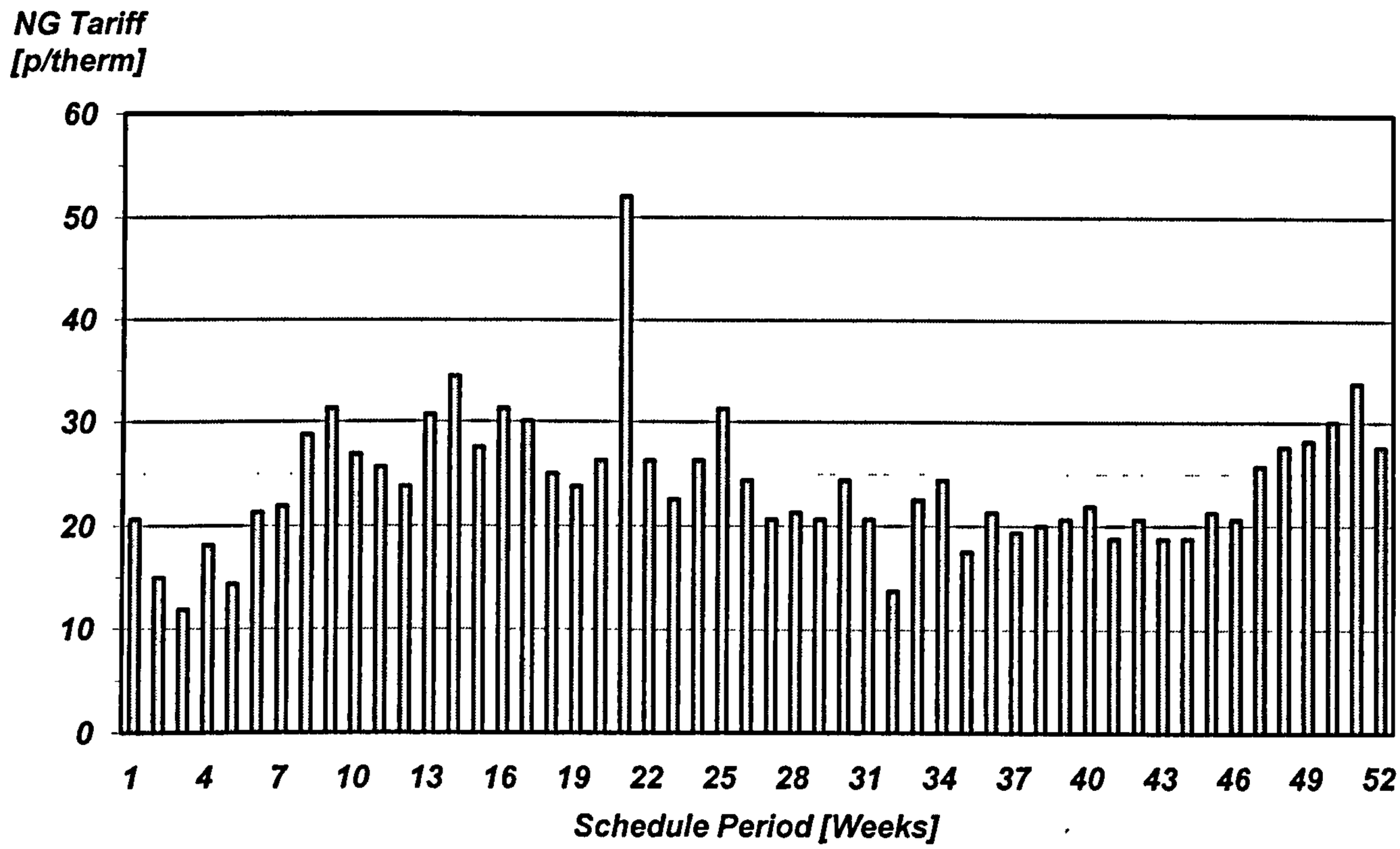

Figure 7.4 – Natural gas tariff over schedule period (Sikorski, 2006)

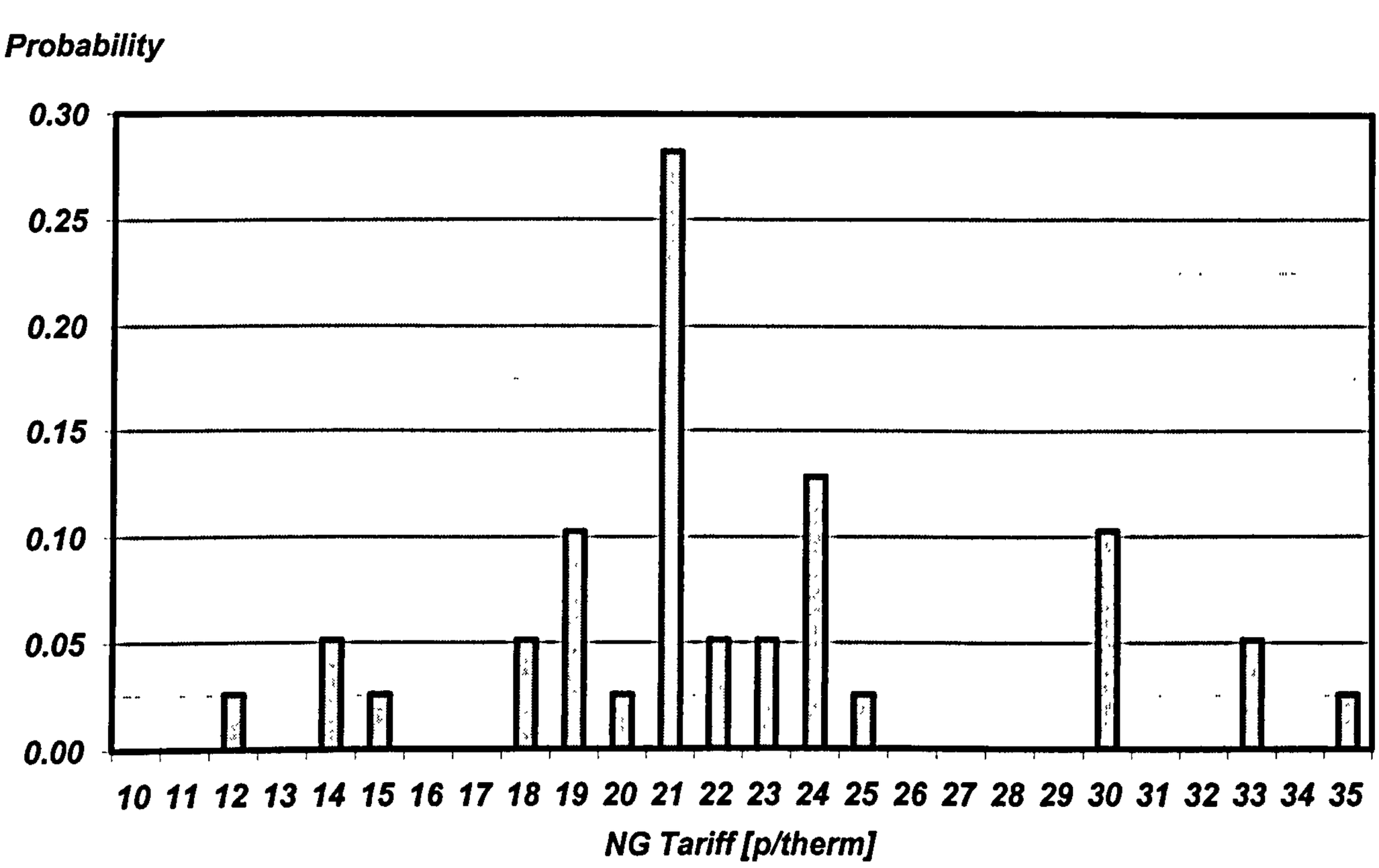

Figure 7.5 – Natural gas price probability distribution

Table 7.2 shows the life cycle of the gas turbines investigated in this case study. Figure 7.6 illustrates the convergence of the generation schedule optimisation algorithm. The software program converges to the mini-pool profit of £216,891 in approximately 80 seconds and a total of 72,000 evaluations. The majority of a sample of 100 runs (68%) converges to the optimal solution and the maximum error expected is lower than 1% (Figure 7.7).

Table 7.2 – Design point creep life assessment

	Unit 4	Unit 6	
Total Mass Flow	18	48	kg/s
Rotational Speed	14,943	11,000	rpm
Turbine Entry Temperature	1,290	1,288	K
Blade Metal Temperature	1,236	1,232	K
Compressure Pressure Ratio	15.5	16.5	-
Nozzle Angle	54	54	°
Power Output	4,343	10,300	kW
Thermal Efficiency	0.300	0.325	-
Centrifugal Stress	41	48	MPa
Larson Miller Parameter	53	53	-
Time to Failure	10,374	10,349	h

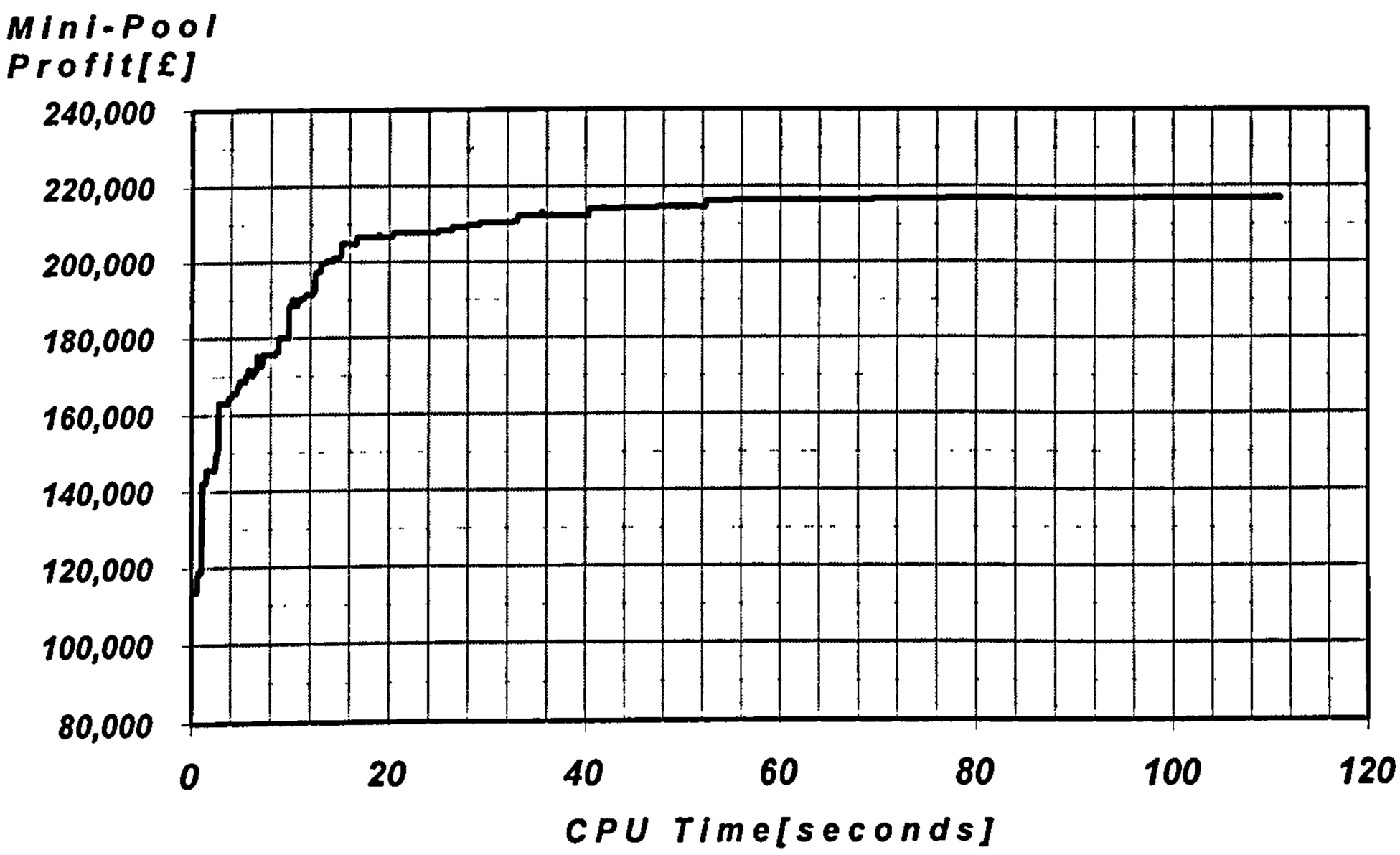

Figure 7.6 – Mini-pool profit convergence with hybrid genetic algorithm priority list (average of 100 runs)

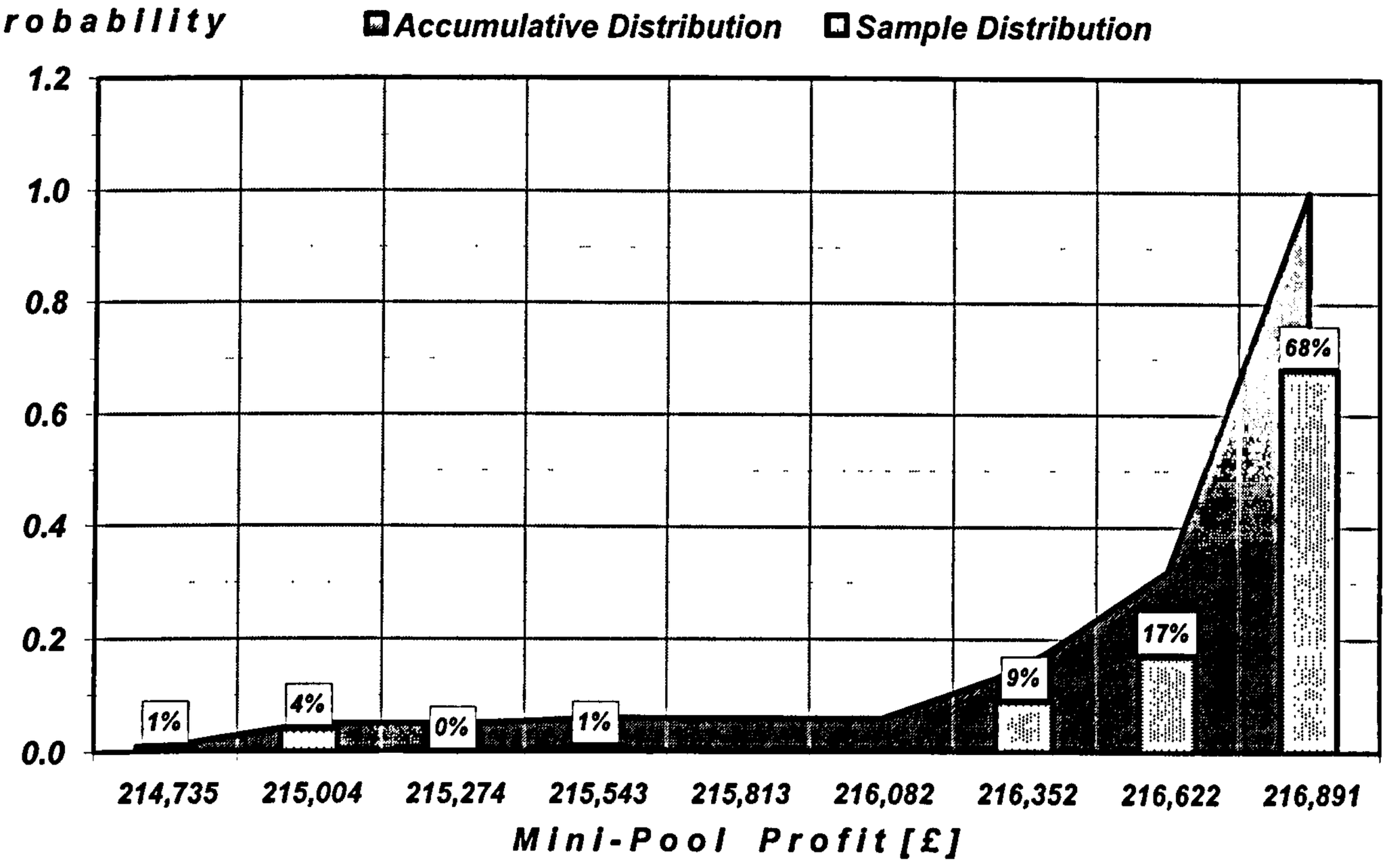

Figure 7.7 – Mini-pool profit probability distribution (sample of 100 runs)

The off-design gas turbine life cycle assessment described in chapter 4 and the exhaustive enumeration search illustrated in Figure 7.8 were used to incorporate the maintenance schedule into the mini-pool generation schedule. All possible combinations in a given lifetime window were investigated and the mini-pool schedule that produces the maximum profit and service hours between maintenance is the global optimal solution.

In this case study a total of 2,704 combinations were analysed in approximately 160 seconds of CPU time. Many mini-pool schedules are able to produce the maximum profit of £216,891 (Figure 7.9). However the best global solution is the one able to maximise both profit and service hours between maintenance. Figure 7.10 shows the maximum global solution found. The units' status between the dotted lines represents the maintenance period. The life cycle time window investigated is between 7,896 and 11,508h and the average maximum service hours between maintenance found was 9,660h.

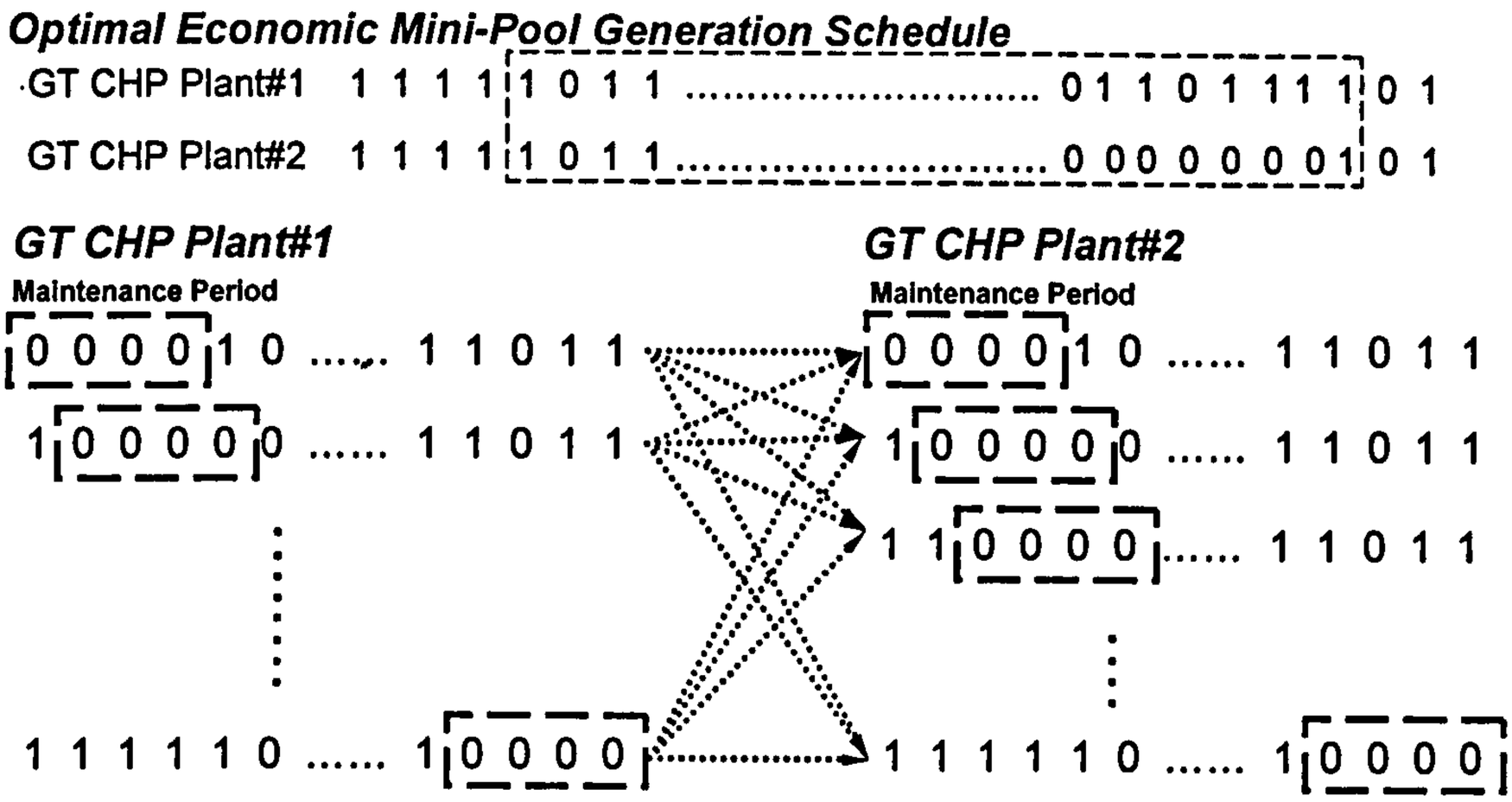

Figure 7.8 – Reschedule maintenance by exhaustive enumeration

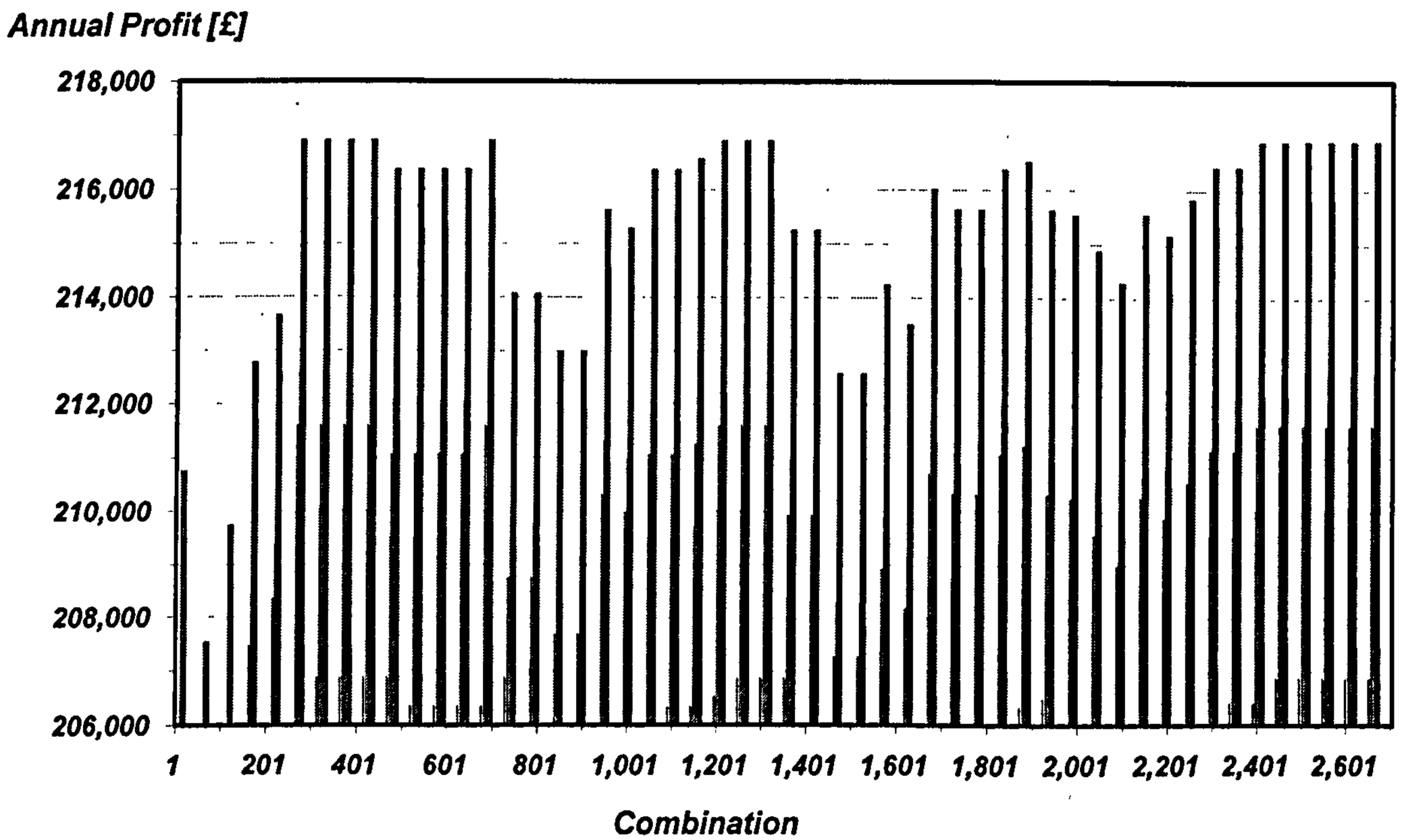

Figure 7.9 – Evolution of all rescheduled combinations

Week	1	2	3	4	5	6	7	8	9	10	11	12	13	14	15	16	17	18	19	20	21	22	23	24	25	26	27	28	29	30	31	32	33	34	35	36	37	38	39	40	41	42	43	44	45	46	47	48	49	50	51	52
GT CHP Unit 4	0	1	1	1	1	0	0	0	0	0	0	0	1	0	0	0	0	1	0	1	0	1	1	0	0	0	0	0	0	1	0	1	0	0	1	1	1	0	0	0	1	1	1	1	0	1	0	0	0	0	0	0
GT CHP Unit 6	1	1	1	1	1	1	1	0	1	1	1	1	0	0	0	0	0	0	1	1	0	0	0	0	0	1	1	1	1	0	1	1	1	1	1	1	1	1	1	1	1	1	1	1	1	1	1	1	1	1	1	1

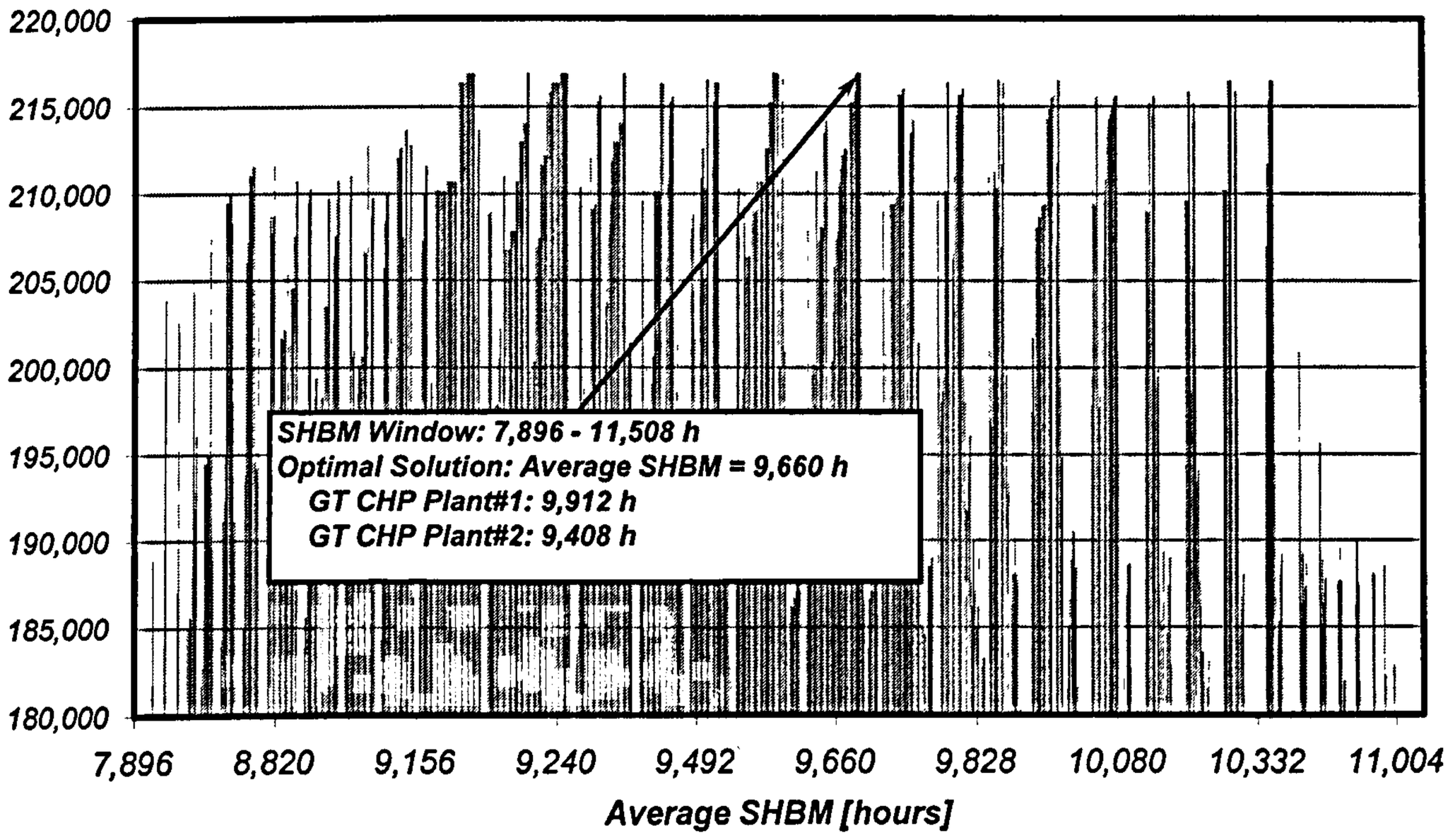

Figure 7.10 – Maximum global solution searching

The EU Emissions Trading Scheme (EU ETS) has recently been implemented in Europe and carbon price is expected to have a significant impact on the cost of generating electricity (PB Power, 2006). The effects of the carbon tax on the generation cost of the mini-pool CHP system were evaluated in this research using the generation and maintenance scheduling algorithm described before. The profit of the mini-pool CHP (units 4 and 6) was analysed in four different market scenarios:

- Scenario#1: predominantly Natural Gas Combined Cycle power plants;
- Scenario#2: predominantly Fuel Oil Steam Cycle power plants;
- Scenario#3: predominantly Coal Steam Cycle power plants;
- Scenario#4: a mix of different technologies: 25% Natural Gas Combined Cycle, 25% Fuel Oil Steam Cycle, 25% Coal Steam Cycle and 25% Nuclear, Hydroelectric and Wind power stations.

Basically the effect of carbon price on power generation is directly related to the content of carbon in the fuel, power technology efficiency and the price of carbon. The additional generation cost (AGC) due to the carbon tax was calculated based on the following equation:

$$AGC = \frac{3.6 \cdot dctr \cdot \mu_{CO2} \cdot DCA}{\eta_e \cdot LHV} \quad (7.12)$$

Where η_e is the electrical efficiency of the power generation technology. The impact of carbon dioxide tax rate up to 40 £/ton was investigated. Figure 7.11 presents the additional generation cost due to carbon taxes for different power generation technologies.

The additional generation costs were incorporated into the electricity prices used in the CHP generation schedule model described before in order to evaluate the effects of such a levy on the CHP financial performance. The baseline electricity market prices correspond to those available in a mix technology portfolio (scenario#4). For simplicity reasons the same baseline electricity market prices were considered for each scenario. This is an acceptable assumption for the purpose of this preliminary carbon emission tax assessment. Figure 7.12 displays the results of the simulation of the medium-term generation schedule algorithm in different power markets. Mini-pool CHP profit increases in a power market predominantly composed of coal and oil fuelled power stations but it drops in a marketplace mainly fuelled with natural gas combined cycle power plants.

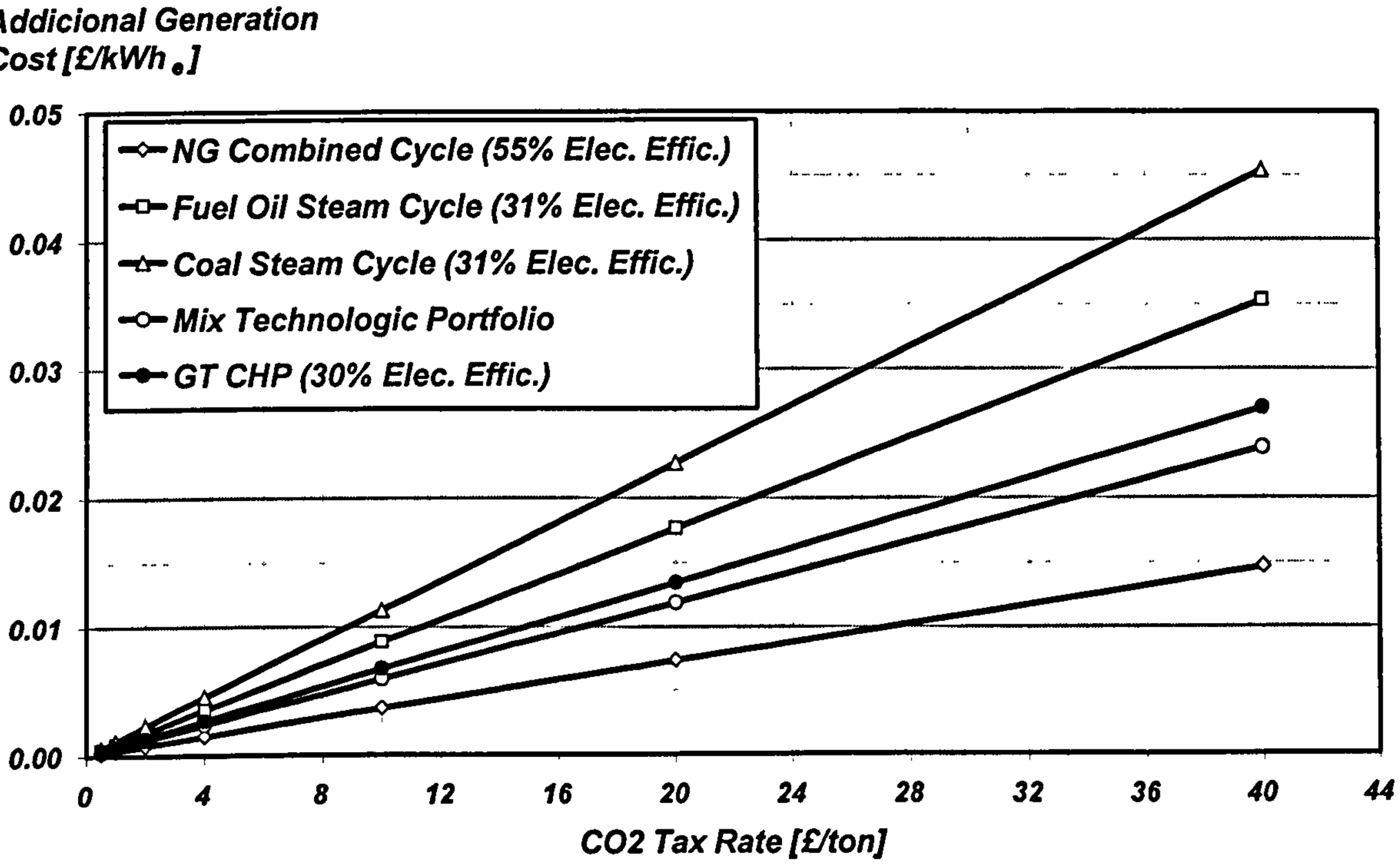

Figure 7.11 – Additional generation cost for different power generation technologies

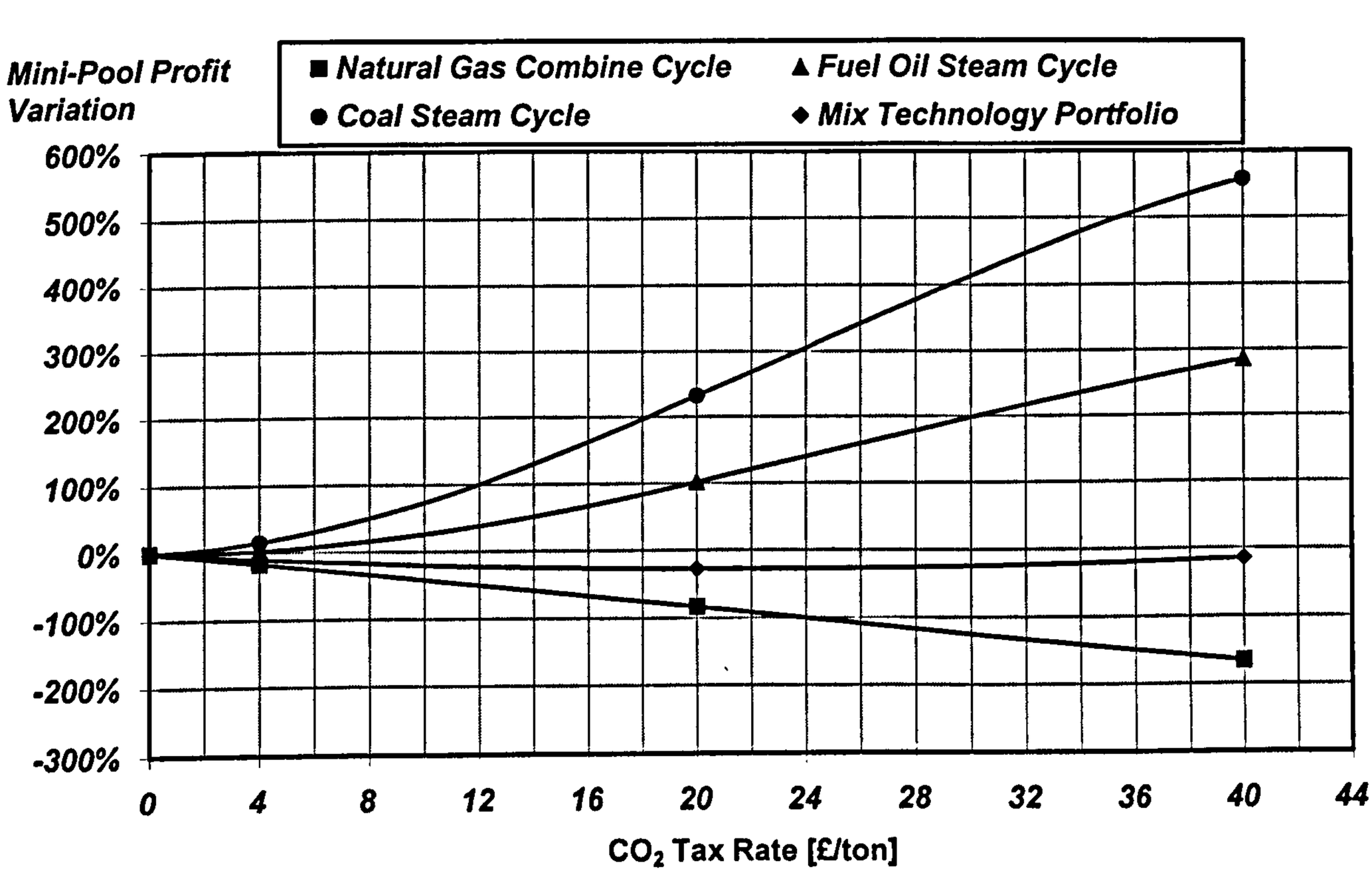

Figure 7.12 – Mini-pool CHP profit impact due to carbon emissions tax

Chapter 8 – Long-term Decision Making Support Tool

8 - Long-term Decision Making Support Tool

8.1 - Introduction

This chapter describes an investment decision for making a support tool for Combined Heat and Power (CHP) systems. The main focus of this investigation is the financial evaluation of the Combined Heat and Power proposal. Over the last few years there has been an increasing interest in decision making support tools that combines management, financial, engineering and other disciplines applied to physical assets in optimising the economic life cycle costs of power plants. This approach aims to give industries, manufacturers of heat and power equipments, policymakers and other professionals the ability to understand and evaluate the energy solution of combined heat and power (CHP) plants.

CHP systems can be configured depending on the site requirements, by different prime moving technologies. In this investigation the CHP system analysed is based on an open cycle gas turbine with direct heating or with a heat recovery steam generator (Figure 8.1). The monthly heat and power demand profile and off-design performance of the CHP units described in chapter 2 and detailed presented in Appendix A were used to carry out the case studies.

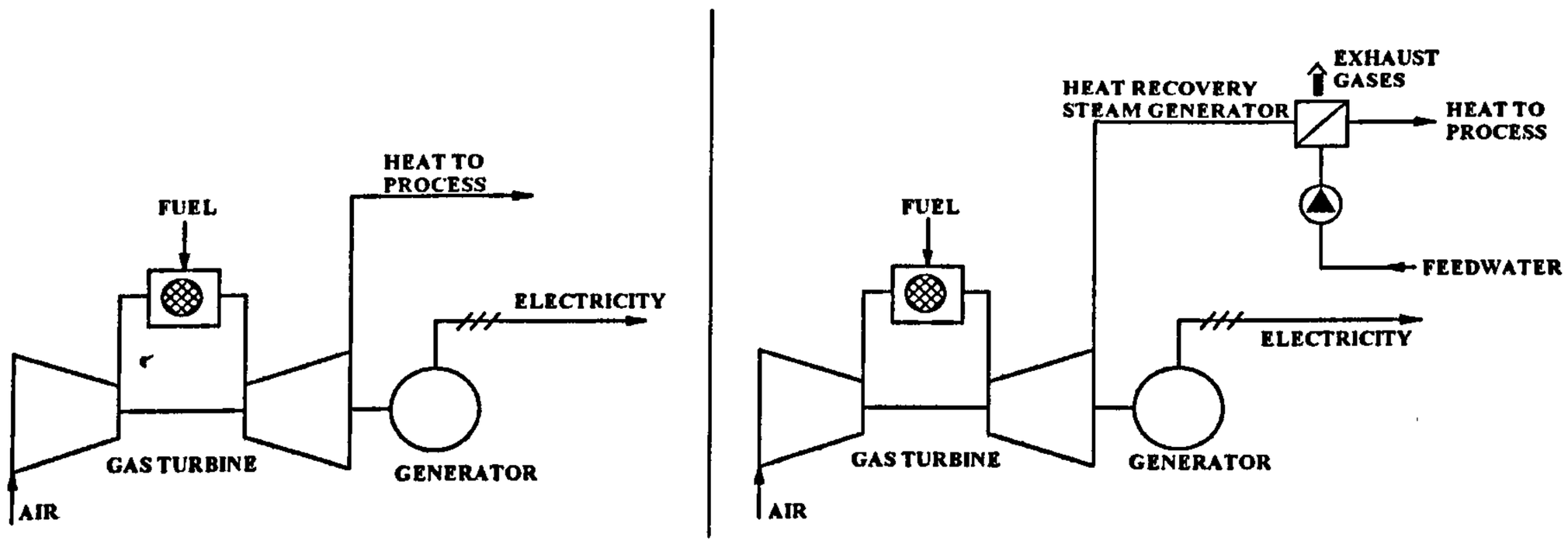

Figure 8.1 - CHP schemes with gas turbines

8.2 - Financial appraisal and risk analysis

8.2.1 - Financial appraisal

The financial analysis is based on the discounted cash flow technique with variable economic input rates. The mathematical model aims to calculate the parameters' Net Present Value (NPV), Internal Rate of Return (IRR), Discounted Payback Period (DPB) and Generation Cost (GC_t) of the project proposal.

Initially the annual CHP plant power balance is calculated as follows. The annual electricity demanded (AED), annual electricity produced (AEP) and annual mass fuel consumption (AMFC) were calculated by the sums below over the 12 months of the year.

$$AED_t = \sum_{m=1}^{12} ED_{t,m} \cdot ND_m \cdot 24 \tag{8.1}$$

$$AEP_t = \sum_{m=1}^{12} \left(P_{t,m} \cdot ND_m \cdot 24\right) \cdot A_t \tag{8.2}$$

$$AMFC_t = \sum_{m=1}^{12} \left(MFC_{t,m} \cdot ND_m \cdot 3600 \cdot 24\right) \cdot A_t \tag{8.3}$$

Where $ED_{t,m}$ is electricity demand at year t and month m, ND_m is the number of days at month m, $P_{t,m}$ is electric power at time interval t and month m, $MFC_{t,m}$ mass fuel consumption of the CHP system at year t and month m and A_t is the availability of the CHP system at year t. The constants 24 and 3600 refer to the daily number of hours and hourly number of seconds, respectively.

The gas turbine availability is given by the gas turbine life cycle algorithm described in chapter 4. The annual mass flow consumption includes fuel flow from both the gas turbine and back-up boiler used to supply the heat demand when the CHP unit is not available or if there is any deficit of heat. As mentioned in chapter 2 the CHP plants in consideration in this investigation are under the electricity priority mode of operation. The power and heat demand matching were carried out as illustrated in Figure 8.2. Deficit and excess of power and heat can be calculated with the equations below.

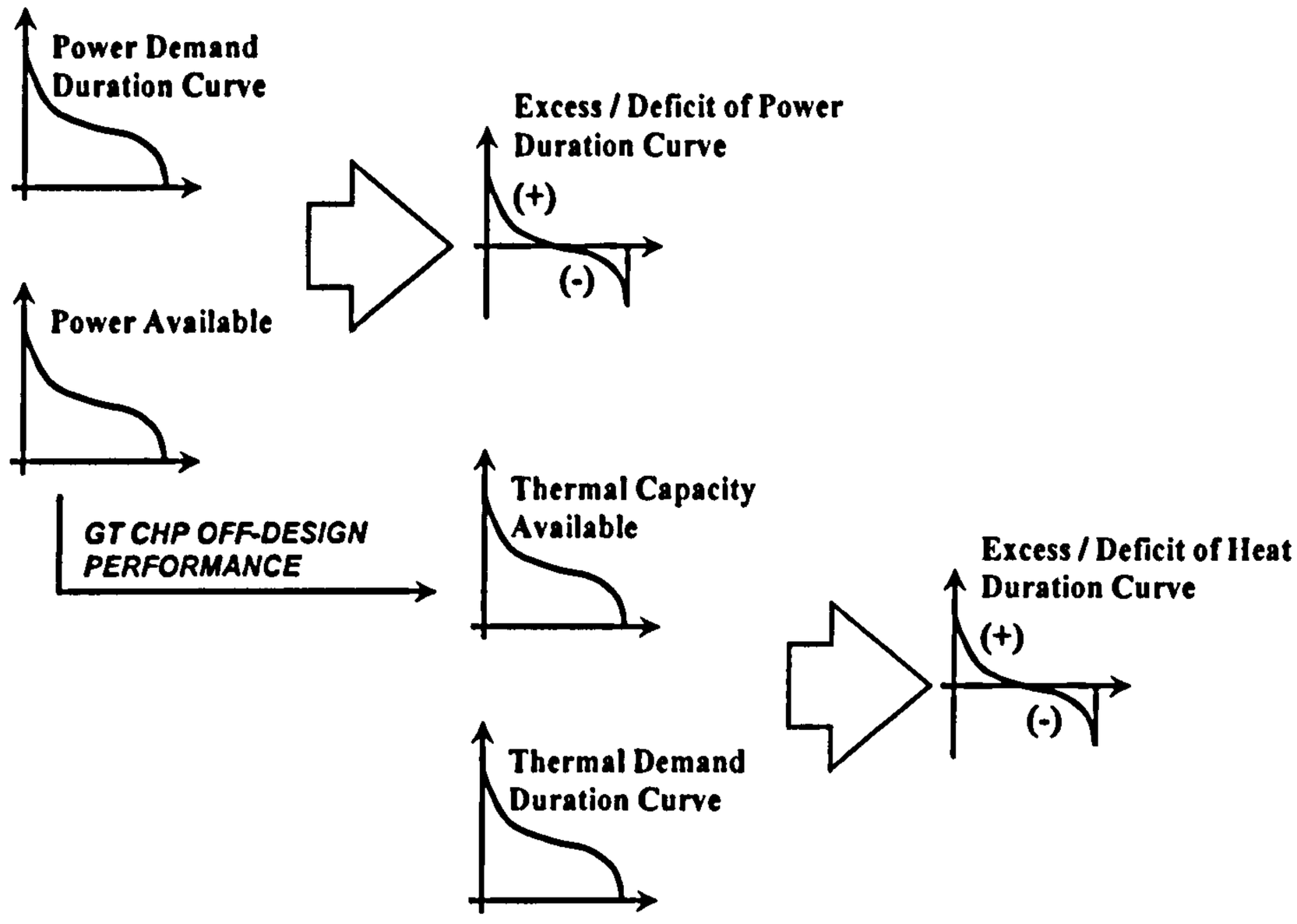

Figure 8.2 – GT CHP power priority model convolution

If there is deficit of power, then the annual deficit of electricity (ADE_t) is given by equation (8.4) and if there is surplus of power, then the annual surplus of electricity (ASE_t) is given by equation (8.5).

$$ADE_t = AED_t - AEP_t \tag{8.4}$$

$$ASE_t = AEP_t - AED_t \tag{8.5}$$

The initial cash flow (ICF) if the investment is given by the following equation.

$$ICF = L - C \tag{8.6}$$

If total capital costs (C) are not paid in full with private funds then a loan (L) component is part of the initial cash flow. The total capital cost (C) is defined by:

$$C = \frac{P_{ISO} \cdot SGTC}{1 - HRCR - ICR} \tag{8.7}$$

Where HRCR is the heat recovery steam generator (HRSG) cost rate, ICR is the installation, project and contingency cost rate, SGTC is the specific gas turbine cost and P_{ISO} is the electric power of the gas turbine at ISO conditions. In this investigation the HRSG capital cost is considered to be 12% of total capital cost, and installation, project and contingence cost 26% (Jennekens, 1989; Belding, 1982).

The annual operation profit (AOP_t) of the CHP system is the balance of incomes, savings (avoided cost) and the production costs of an investment throughout its cycle life. It is calculated by the following equation:

$$AOP_t = ACE_t + RSE_t + ACH_t - FC_t - OMC_t - CDP_t \tag{8.8}$$

Where the avoided cost of electricity (ACE_t) is given by the product of annual electricity demanded (AED_t) and contract electricity price (CEP_t):

$$ACE_t = AED_t \cdot CEP_t \tag{8.9}$$

The revenue from selling surplus electricity (RSE_t) to the grid is calculated with equation (8.10) and the cost of deficit of power (CDP_t) with equation (8.11).

$$RSE_t = ASE_t \cdot ESP_t \tag{8.10}$$

$$CDP_t = ADE_t \cdot EBP_t \tag{8.11}$$

Where ESP_t and EBP_t are electricity sell price and electricity buy price, respectively. The avoided cost of heat (ACH_t) is the cost of fuel used to feed a boiler that would supply the total thermal demand if not produced by a CHP system (conventional heat production) and is given by equation (8.12). Where $BFTR_t$ is the fuel tariff rate of the conventional system, LHV is the low heat value of the fuel used (natural gas LHV = 46,000 [kJ/kg]), and η_B is the thermal efficiency of the boiler (80% in this investigation). The annual heat demanded (AHD_t) is provided by equation (8.13) where HD_t is the useful thermal demand over the year.

$$ACH_t = BFTR_t \cdot \frac{AHD_t}{LHV \cdot \eta_B} \tag{8.12}$$

$$AHD_t = \sum_{m=1}^{12} \left(HD_{t,m} \cdot ND_m \cdot 24 \right) \tag{8.13}$$

The fuel cost (FC_t) and operation and maintenance cost (OMC_t) of the CHP system were calculated with equations (8.14) and (8.15), respectively. Where FTR_t is the fuel tariff rate and $SOMC_t$ is the specific operation and maintenance cost (per unit of electricity produced). Typically the average specific operation and maintenance cost of gas turbines is 3.8 £/MWh.

$$FC_t = FTR_t \cdot AMFC_t \tag{8.14}$$

$$OMC_t = SOMC \cdot AEP_t \cdot 1000 \tag{8.15}$$

The net cash flow ($ANCF_t$) is the balance between the operational profit and loan and tax annual payments (ALP_t and ATR_t respectively). In the last year of the economic life of the investment (T = 11 years in this investigation) a residual value (RV_t) may be considered.

$$ANCF_t = AOP_t - ALP_t - ATR_t, \quad t = 1, 2, \ldots, T-1 \tag{8.16}$$

$$ANCF_t = AOP_t - ALP_t - ATR_t + RV_T, \quad t = T \tag{8.17}$$

Assuming a fixed-rate loan over the economic life of the investment, the annual loan repayment is calculated with equations (8.18) and (8.19), where TL is the time period for loan repayment, LR is the loan interest rate and CRF(TL, LR) is the capital recovery factor given by equation (8.20).

$$ALP_t = L \cdot CRF(TL, LR), t=1, 2, \ldots, TL \tag{8.18}$$

$$ALP_t = 0, t > TL \tag{8.19}$$

$$CRF(TL, LR) = \frac{LR \cdot (1+LR)^{TL}}{(1+LR)^{TL} - 1} \tag{8.20}$$

The annual tax payment is defined by the following equation:

$$ATP_t = TR_t \cdot T_t \tag{8.21}$$

The taxable income (T_t) is determined by equation (8.22) where ADC_t is the accounting depreciation charge and LIC_t is the loan interest charged.

$$T_t = AOP_t - ADC_t - LIC_t \tag{8.22}$$

Assuming a straight-line depreciation, the accounting depreciation charge (ADC_t) can be determined with equations (8.23) and (8.24) where TD is the time period for depreciation.

$$ADC_t = \frac{C}{TD}, t = 1, 2, \ldots, TD \quad (8.23)$$

$$ADC_t = 0, t > TD \quad (8.24)$$

Net present value (NPV) is the balance of debts and revenues of an investment's cash flow in present value terms for a given interest (discount) rate and economic life time (T). The net present value of the CHP investment cash flow considering a variable annual interest rate (IR_t) is given by equation (8.25).

$$NPV = ICF + \sum_{t=1}^{T} \frac{ANCF_t}{\prod_{i=1}^{t}(1 + IR_t)} \quad (8.25)$$

Mathematically the IRR is defined as an interest rate that results in a net present value of an investment cash flow equal to zero (equation (8.26)).

$$ICF + \sum_{t=1}^{T} \frac{ANCF_t}{(1 + IRR)^t} = 0 \quad (8.26)$$

Discounted payback period (DPB) is defined as the period of time required for a net cash flow to recover the sum of the original investment for a given interest (discount) rate. Mathematically the discounted payback period is equal to the minimum period of time interval that satisfies the equation (8.27):

$$ICF + \sum_{t=1}^{DPB} \frac{ANCF_t}{\prod_{i=1}^{t}(1 + IR_t)} \geq 0 \quad (8.27)$$

The generation cost (GC_t) is also used to evaluate the economic performance of the CHP system and is defined as the ratio of all production costs to the total electricity produced (equation 8.28).

$$GC_t = \frac{FC_t + OMC_t + ALP_t + ATP_t}{AEP_t} \quad (8.28)$$

The economic model is limited to the CHP power generation capacity and electricity demand balance constraints. The gas turbine units must supply power within the limits set by their maximum capacity. In this investigation the maximum capacity of the units was considered depending on the ambient conditions (off-design performance). If the total electrical capacity ($P_{it,m}$) is not enough to supply the total demand ($ED_{it,m}$) then the deficit of power ($DP_{t,m}$) is supplied by the local network. Therefore:

$$P_{t,m} + DP_{t,m} \geq ED_{t,m} \quad (8.29)$$

8.2.2 - Risk Analysis

A level of uncertainty is attached to the financial appraisal described in the previous section as it involves dealing with future projections. Therefore a risk analysis must be carried out in order to identify the possible range of financial outcomes of the project proposal.

The Monte-Carlo risk analysis described in chapter 4 is used to evaluate the financial risk involved in this investigation. A list of input parameters was selected and random values were generated following a Gaussian probability distribution on a range of variation. Then the discounted cash flow algorithm was used to produce the economic parameters' probability distribution. A large number of individual evaluations were carried out with different stochastic input values selected from their specific probability distribution in random combinations. If a sufficient number of evaluations have been carried out, the shape of the output histogram will be insensitive to both changes in the number of evaluations and in the sequence of random input values used. That is an indication of the algorithm convergence.

8.3 - Case Studies and Discussion

A software program (DSPG) was developed in Visual Basic language to perform the algorithm described. Program testing was carried out by first correcting all syntax errors, and then checking for run-time and design errors, using dynamic testing. Each function has been compiled using a Visual Basic Compiler and debugged. During the dynamic testing the program was executed in parts and tested using a set of carefully

test data such that every logical path in it was run through at least once. Different types of data were also used with the intent of finding any possible design errors.

Initially the financial analysis was carried out for every CHP unit described in chapter 2 and the mini-pool of all units in three different scenarios: low (not favourable), base and high (favourable). Table 8.1 shows the variations of main inputs of each individual scenario at the end of the economic life of the investment. Figures 8.3 to 8.5 show the annual variation of the main inputs in each scenario.

Table 8.1 – Total variation of the inputs parameters in different scenarios over the economic life of the project

	Low	Base	High
Electricity Prices (ESP, EBP, CEP)	+15%	+51%	+137%
Fuel Tariffs (FTR, BFTR)	+29%	-40%	-63%
Interest Rate (IR)	+69%	+6%	-16%
Heat and Power Demand (AED, AHD)	+5%	+16%	+28%

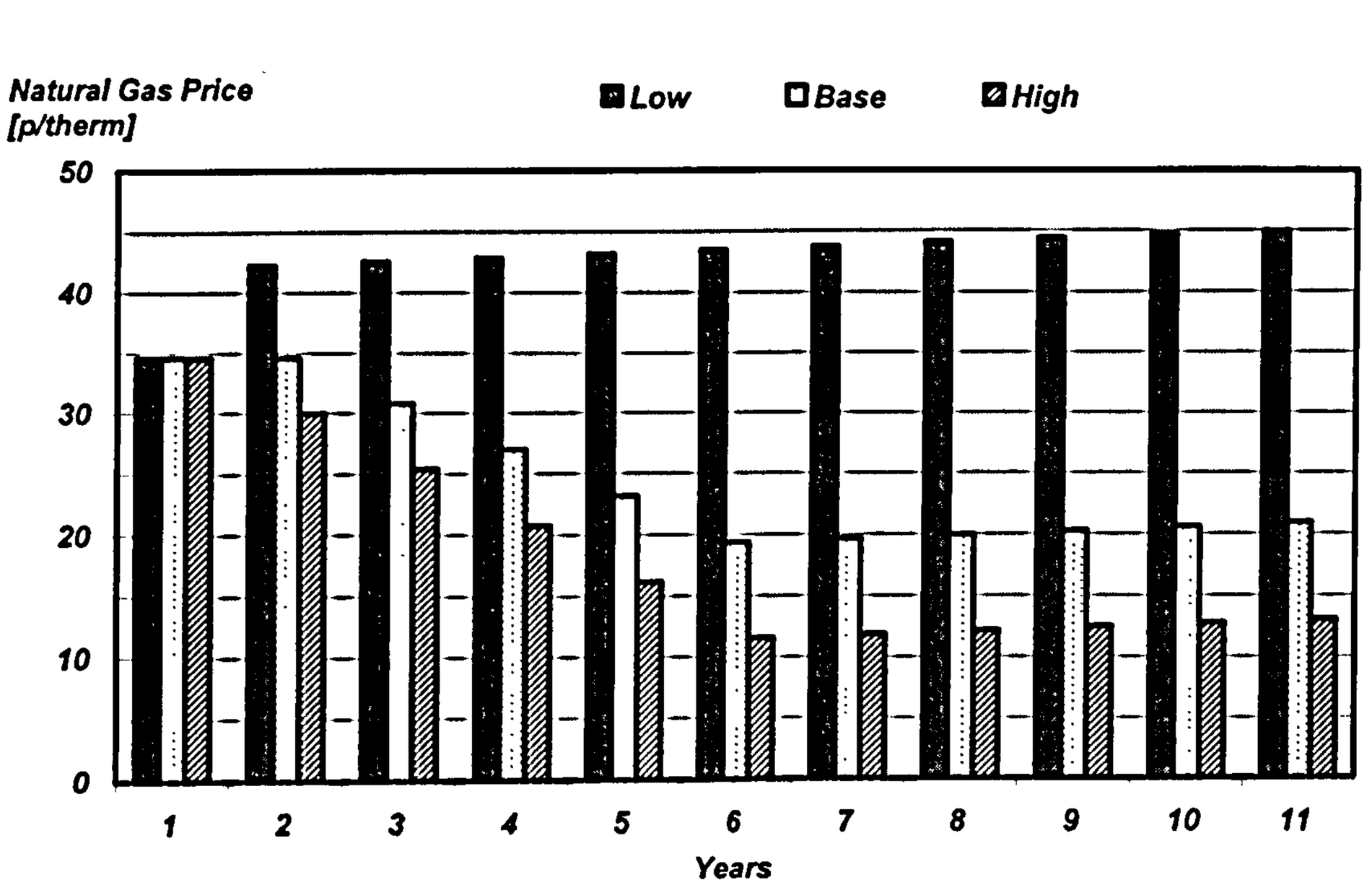

Figure 8.3 – Fuel tariff projection over the economic life of the investment (DTI, 2006)

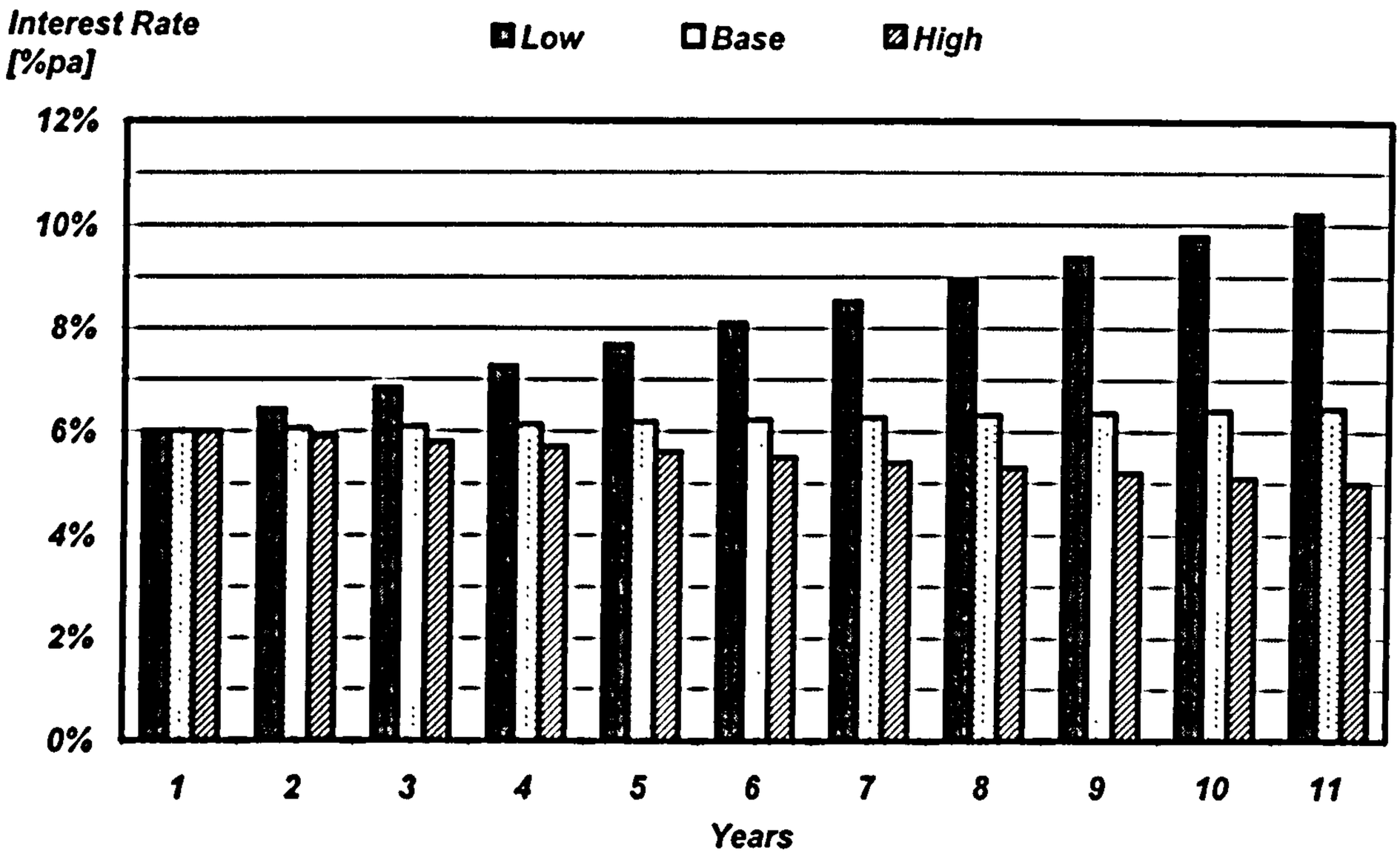

Figure 8.4 – Interest rate projection over the economic life of the investment

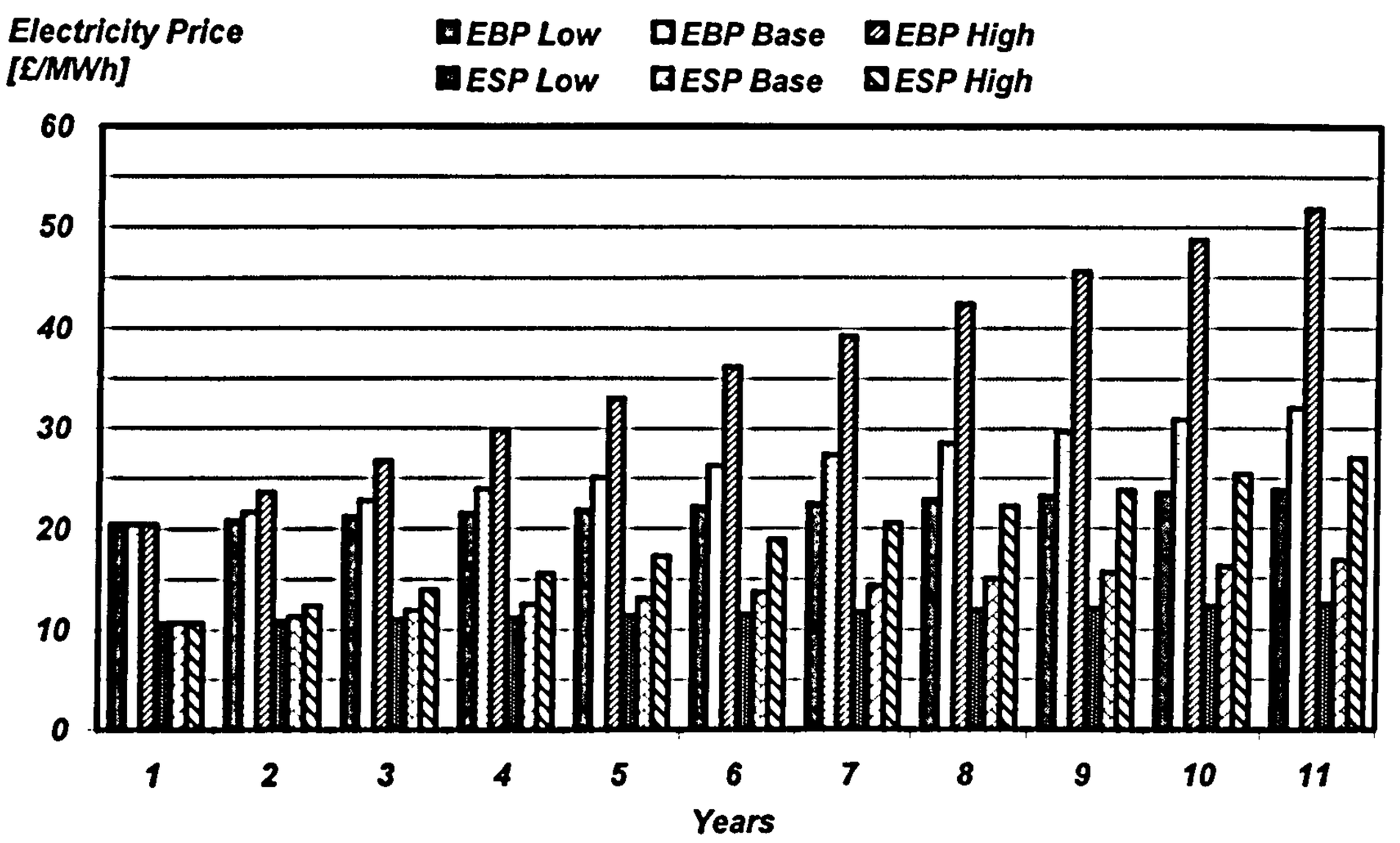

Figure 8.5 – Electricity price projection over the economic life of the investment (DTI, 2006)

Figures 8.6 to 8.8 display the main results of the financial appraisal of the CHP portfolio in the base scenario. Both the hotels and the shopping centre project investigated showed negative net present value and higher discounted payback period. A discounted payback period higher than the economic life of the investment means that the project will not be able to recover the investment required over its lifetime. The lower economic performance of the hotels is attributed mainly to the lower power demand factor and lower thermal efficiency of the CHP prime movers. The avoided cost of electricity of the CHP project is not able to offset the production costs (mainly fuel cost) resulting in negative savings.

The international airport and the ceramics industrial park present the most economically attractive options with a net present value of £6.7 and £4.0 million (base scenario) and discounted payback period of 7.1 and 7.8 years (base scenario), respectively. This is mainly because of the higher demand factor of both end-users. Higher revenues and avoided costs produce higher savings that can offset the capital and production costs with a higher positive net present value at the end of the economic life of the investment.

An interesting result can be observed with both beverage industries. The beverage industry on site 1 presents a positive net present value while the net present value of the beverage industry on site 2 is negative. This is mainly because of the higher investment, higher variation of demand factor and excess of power available on site 2. The revenue from selling the surplus of power is not enough to offset the production costs (mainly fuel costs). A CHP plant with lower power and heat capacity would be an alternative more economically attractive for the beverage industry on site 2.

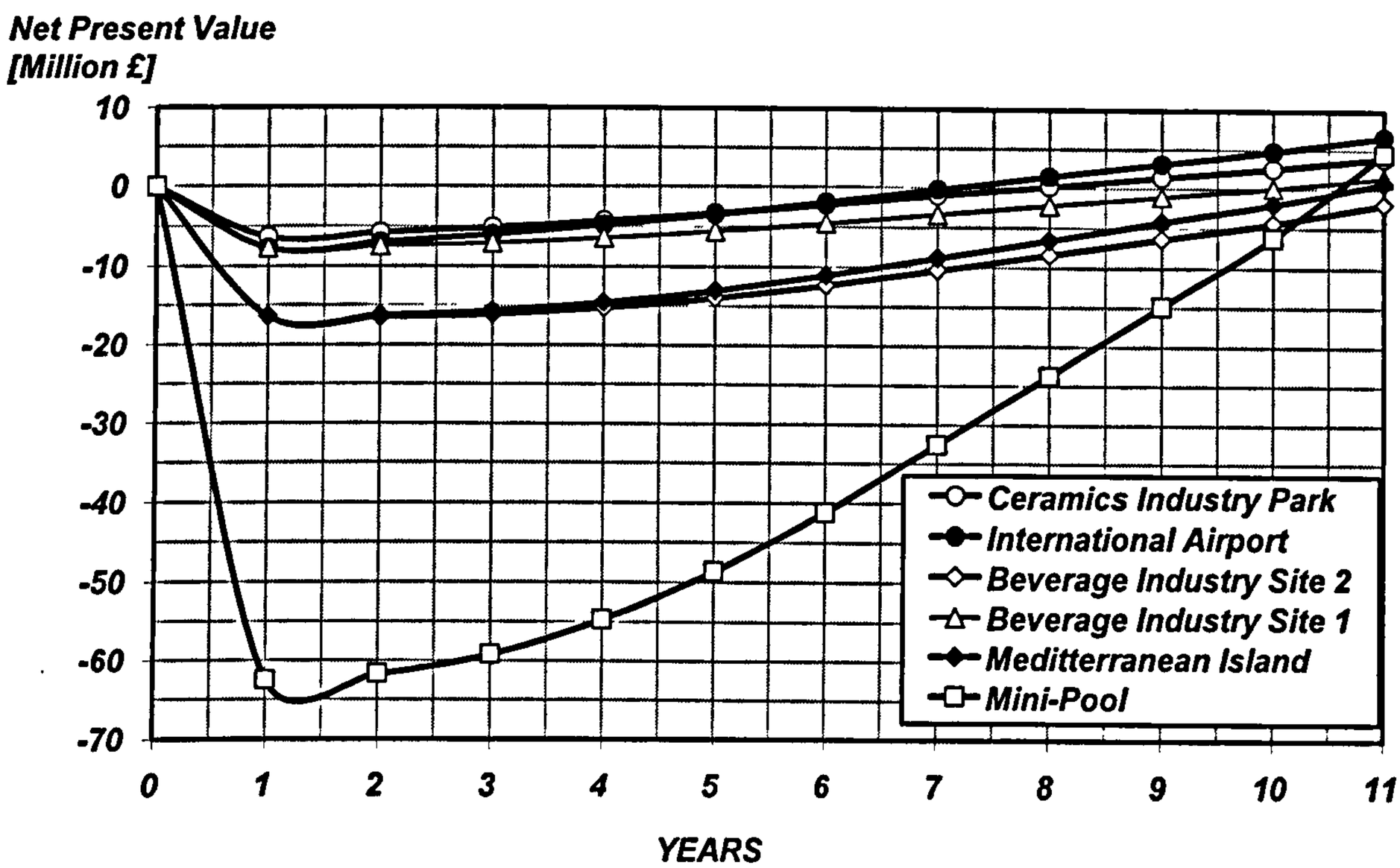

Figure 8.6 – Discounted cash flow of the portfolio of CHP projects: base scenario

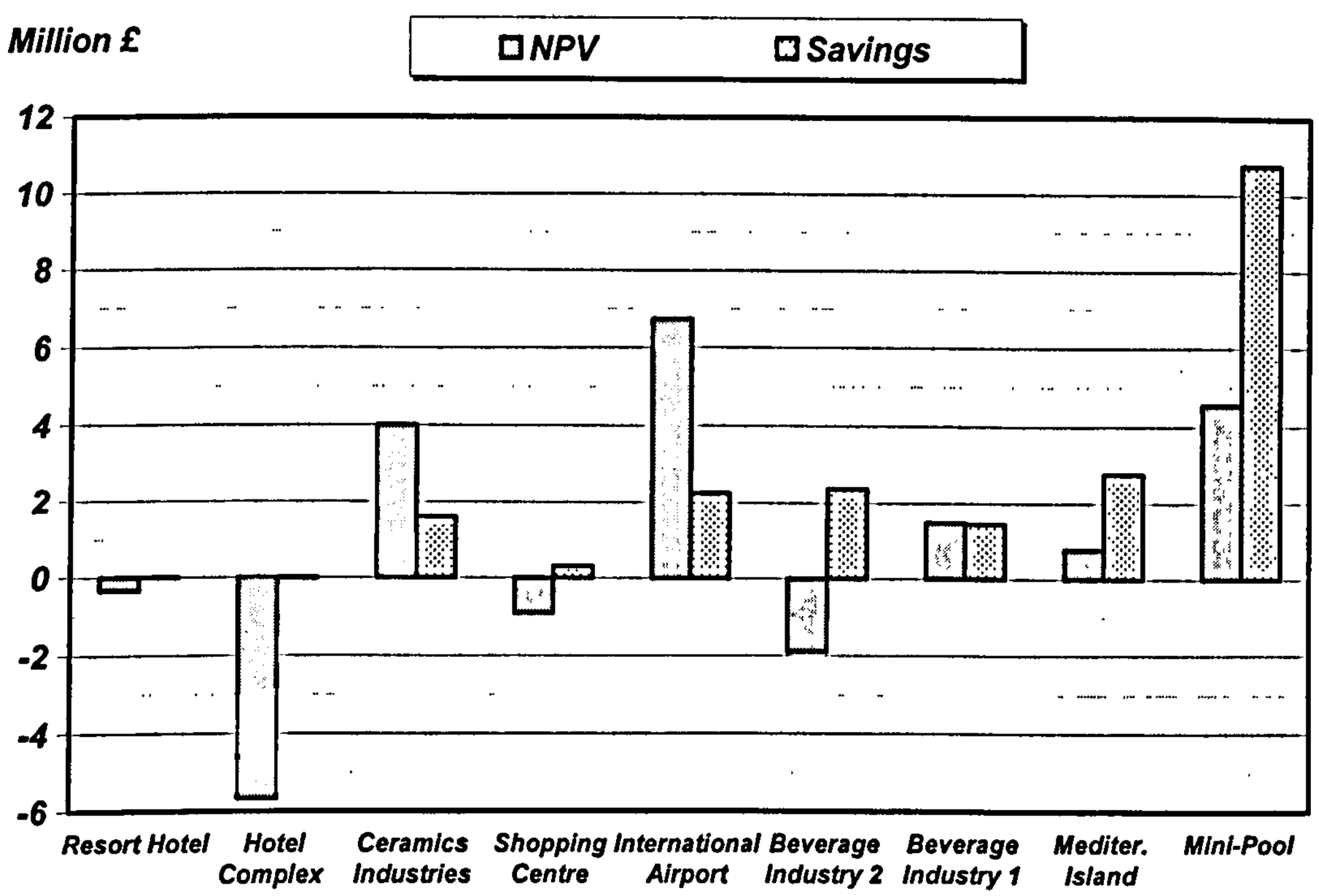

Figure 8.7 – Net present value and annual saving (average net cash flow) of the portfolio of CHP projects: base scenario

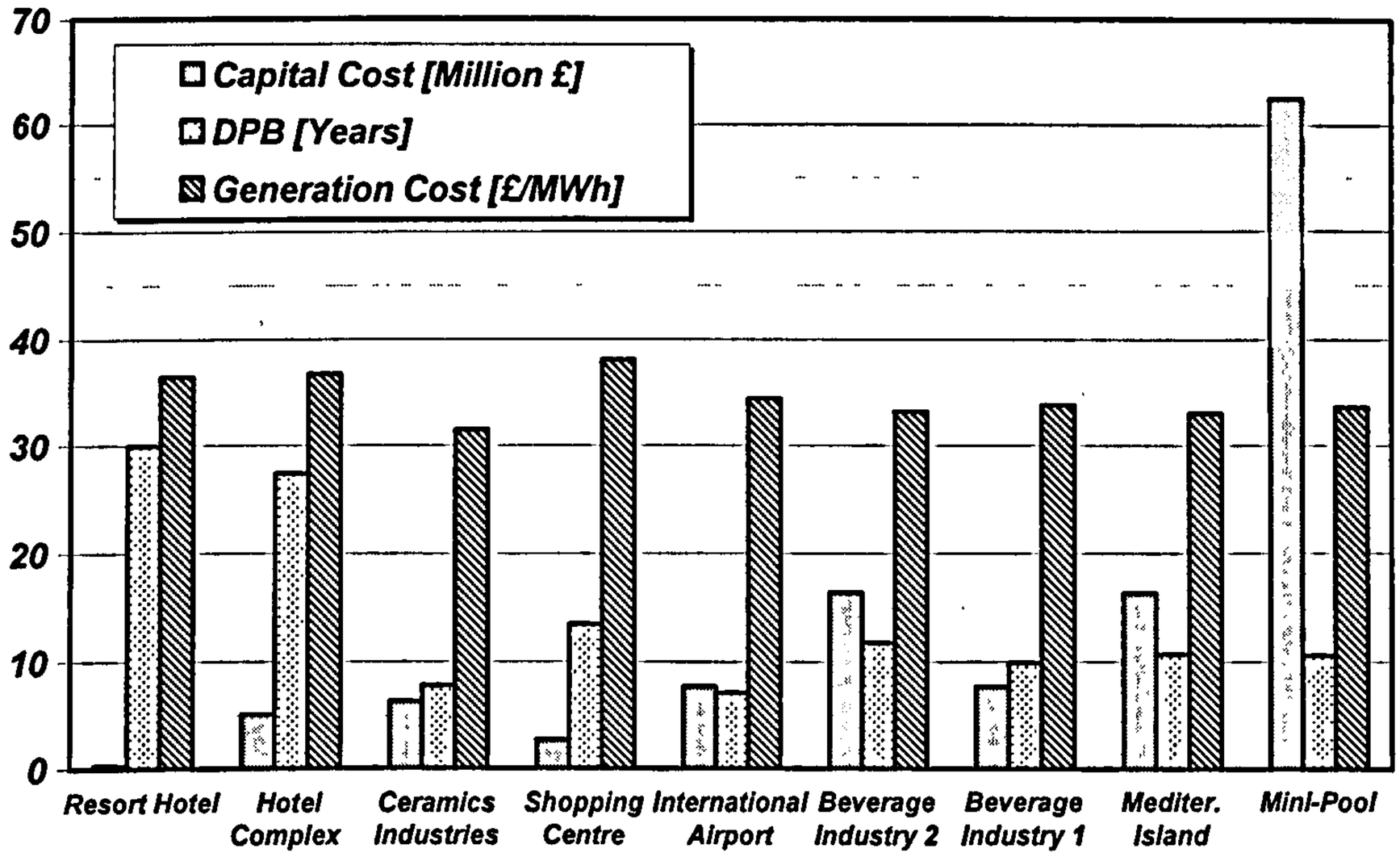

Figure 8.8 – Financial evaluation of the portfolio of CHP projects: base scenario

The results of the CHP portfolio financial appraisal in the high scenario are summarised in Figure 8.9. Figure 8.10 shows the sensitivity of the net present value to the interest rate. The point the net present value is equal to zero is defined as the internal rate of return of the investment. Because of the higher cash flow involved in the mini-pool project a higher volatility is observed with interest rate variation.

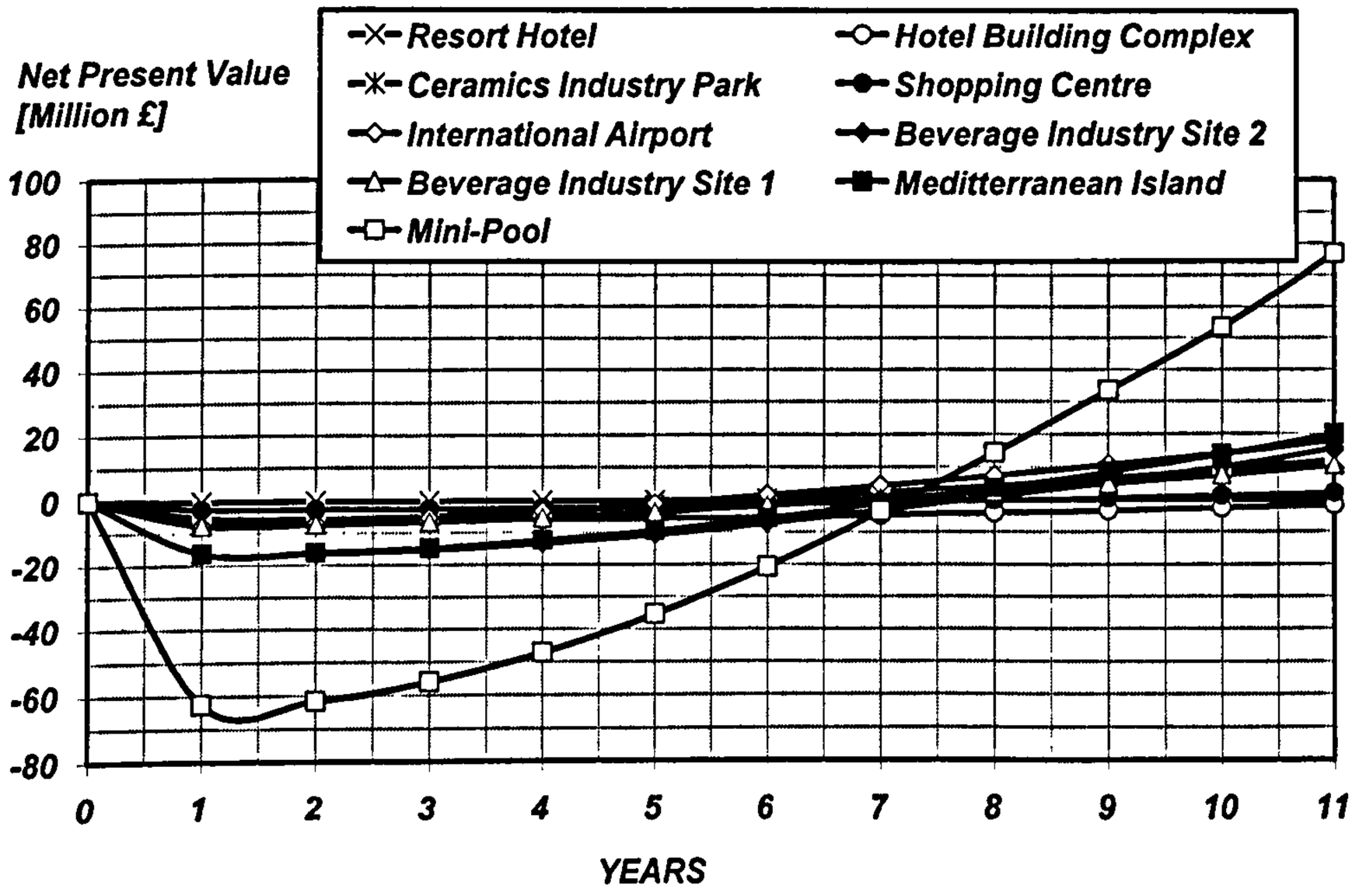

Figure 8.9 - Discounted cash flow evaluation of the portfolio of CHP projects: high scenario

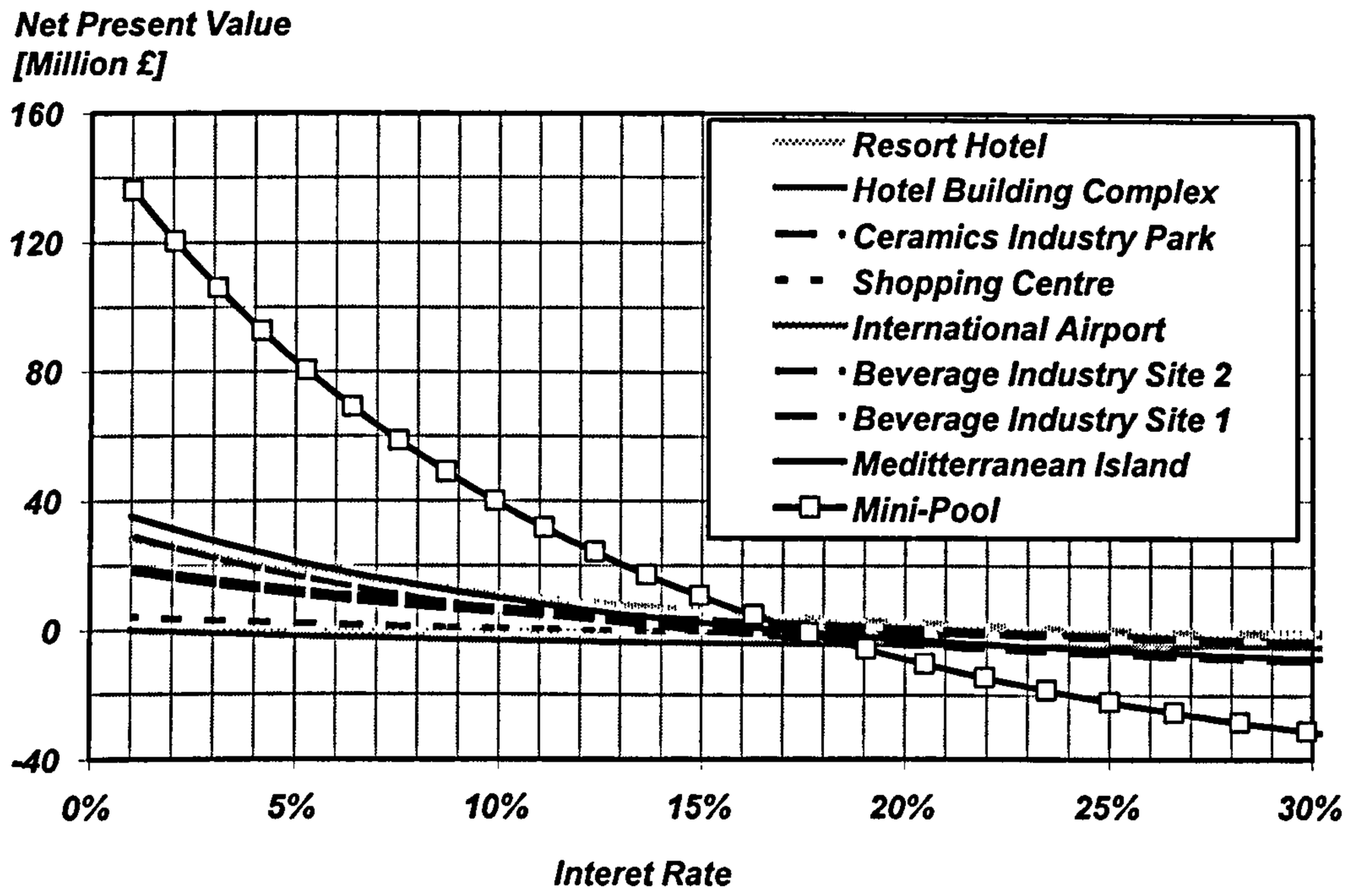

Figure 8.10 – Effects of the interest rate on the net present value of the portfolio of CHP projects: high scenario

A summary of the results in the low, base and high scenarios is presented in Figures 8.11 to 8.16. The mini-pool project is composed of the CHP portfolio of all facilities investigated. Therefore higher capital costs and annual savings are observed and the cash flow becomes more sensitive to the market fluctuations. It is a very good opportunity for the resort and complex hotels, and the shopping centre as the CHP project showed that it was not economically attractive when evaluated individually. The mini-pool scheme would not bring the same economic benefit to the airport and ceramics industries but it can still be useful supplying heat and power backup during the CHP outage hours avoiding the backup penalties applied by the bilateral market. The mini-pool average generation cost is 33.63 £/MWh which is lower than the average UK electricity price (Figure 8.13). The effect of the market scenarios on the mini-pool net present value is displayed in Figure 8.15.

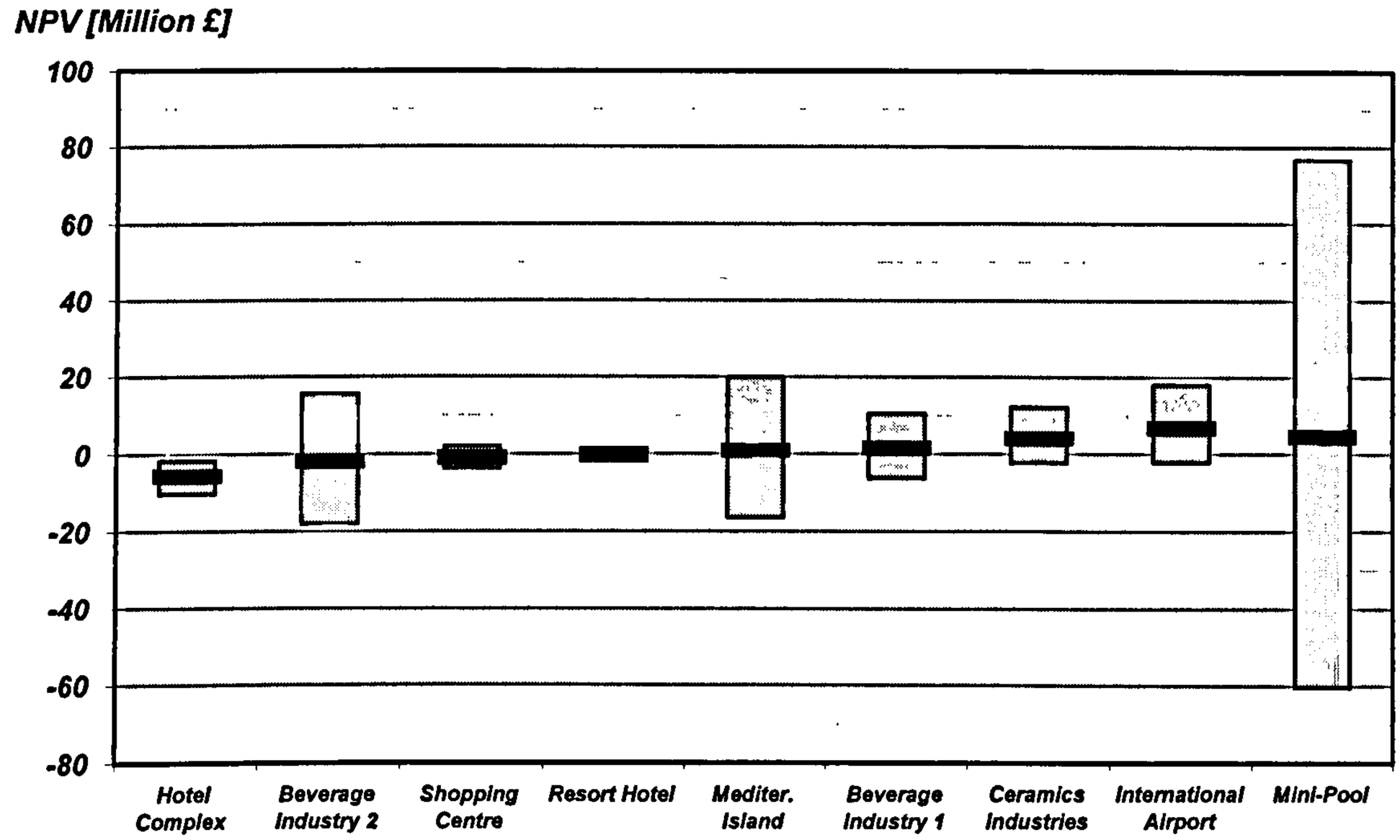

Figure 8.11 - Net present value of the portfolio of CHP projects: low, base and high scenarios

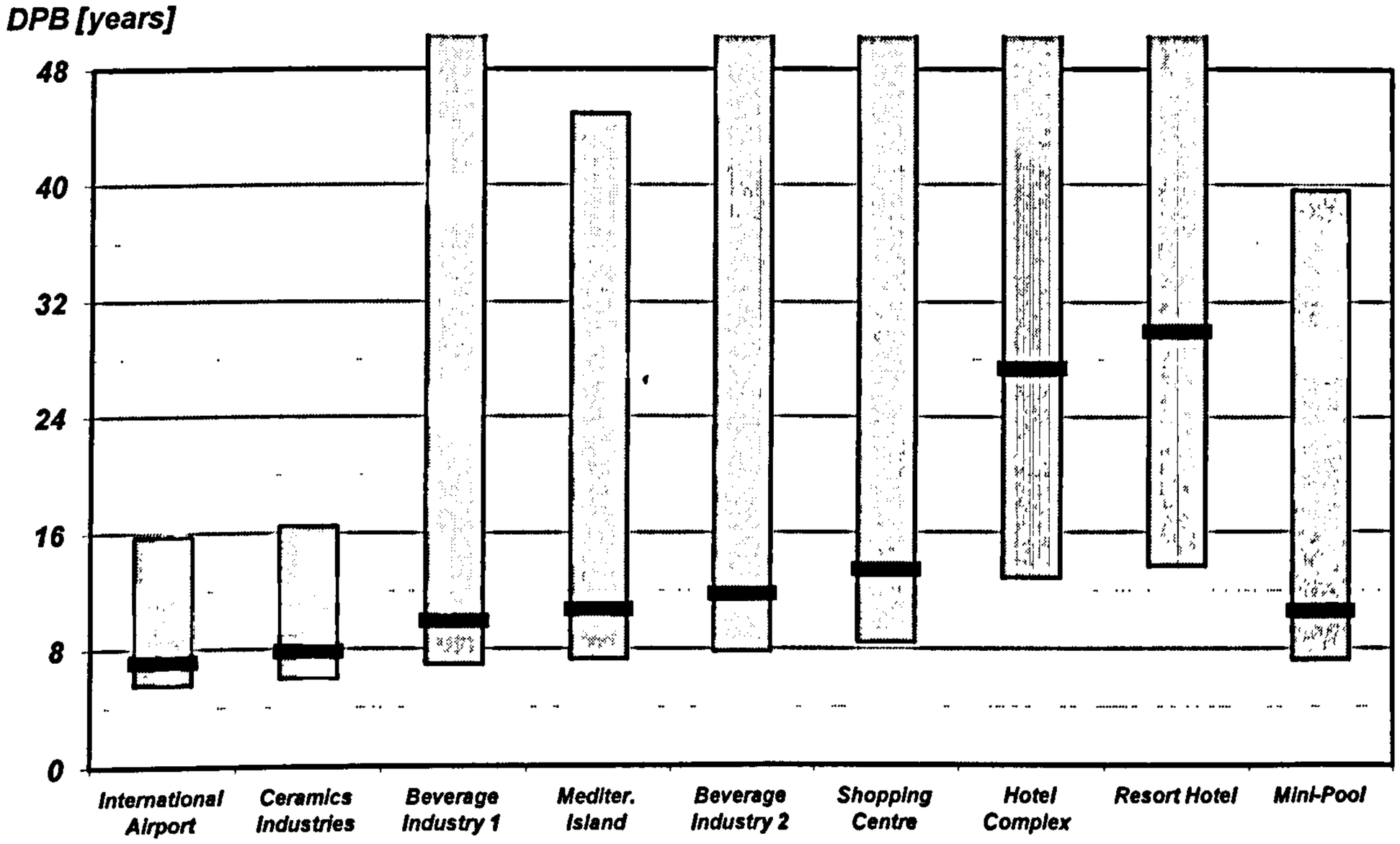

Figure 8.12 – Discounted payback period of the portfolio of CHP projects: low, base and high scenarios

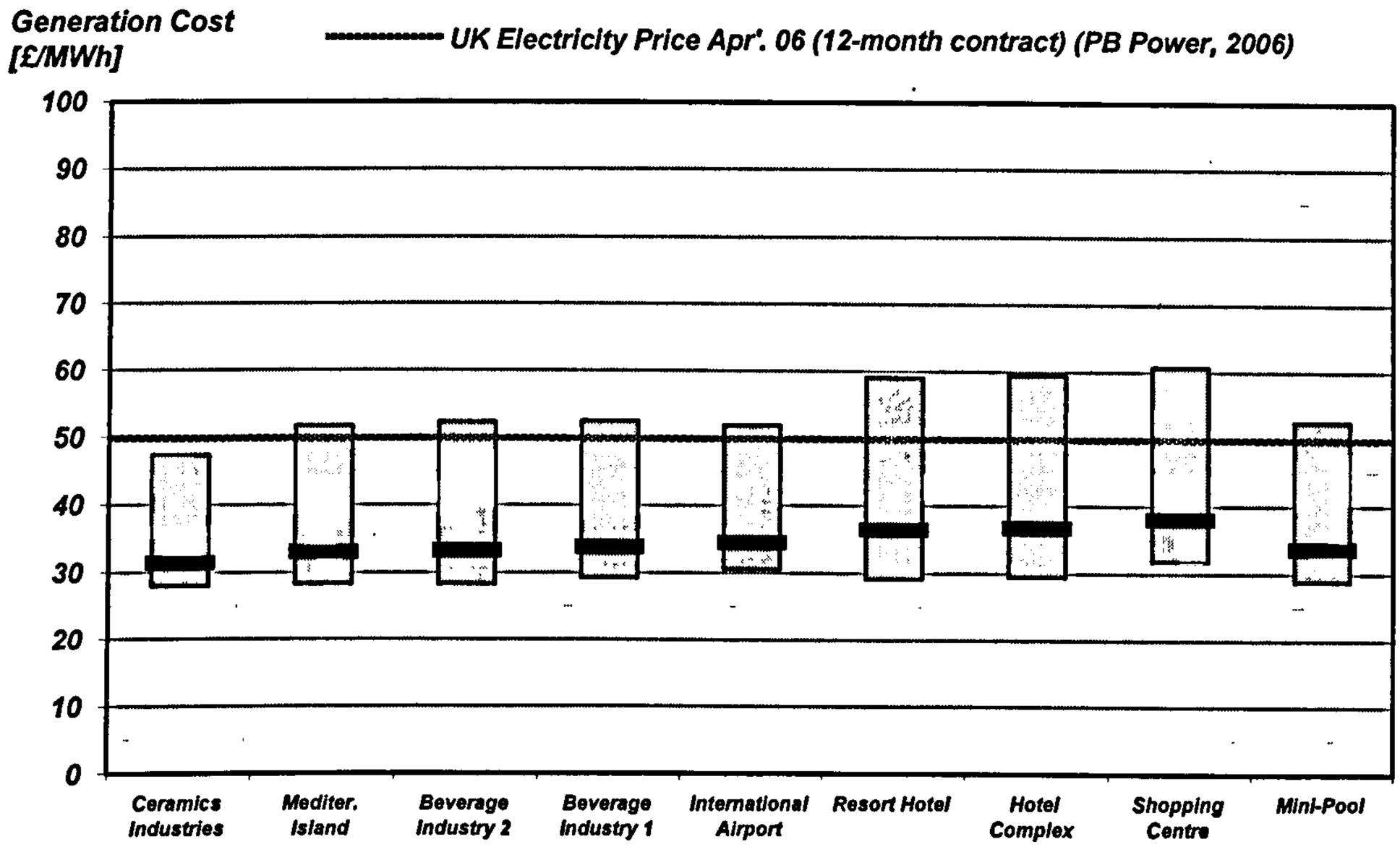

Figure 8.13 – Generation cost of the portfolio of CHP projects: low, base and high scenarios against UK electricity price

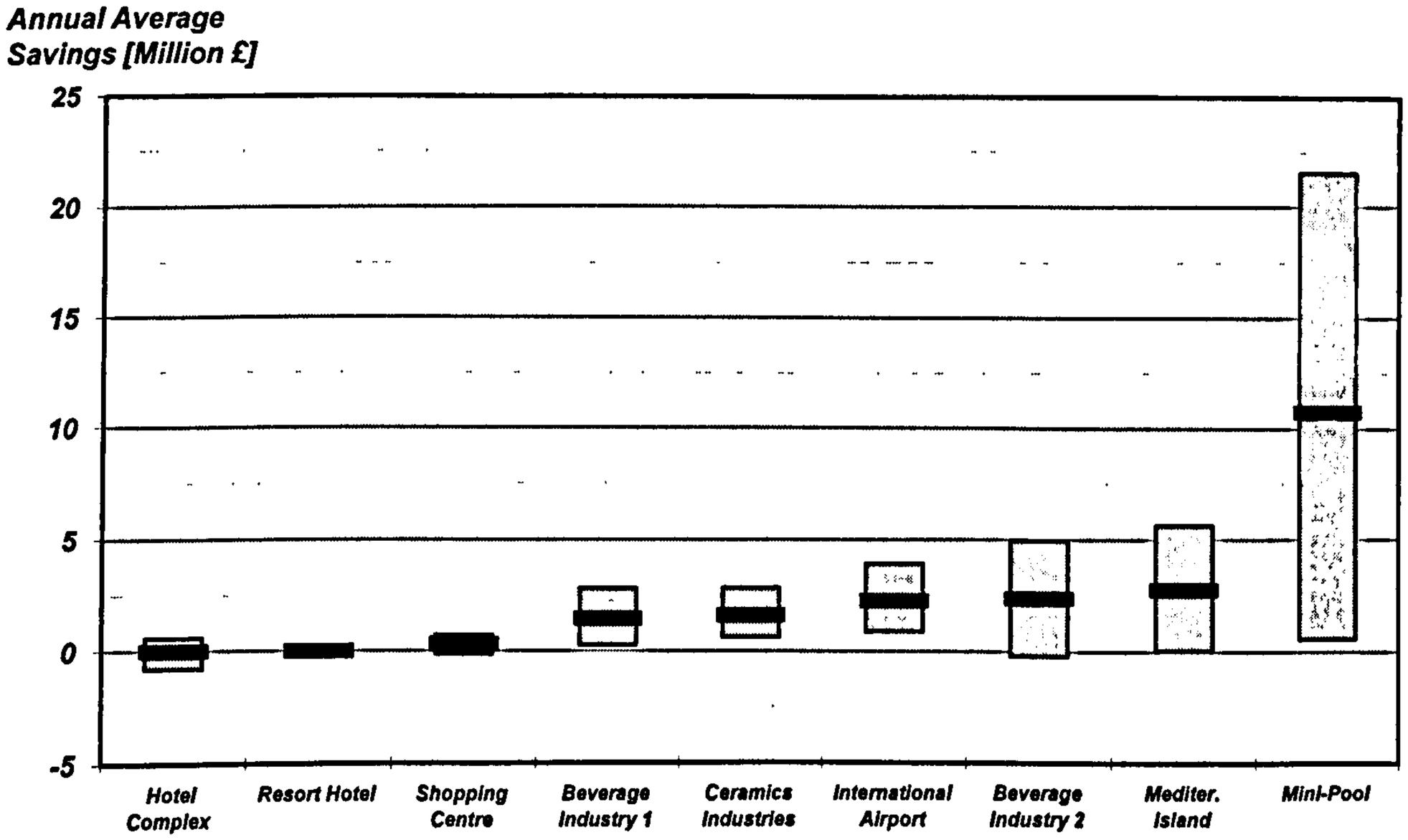

Figure 8.14 - Annual saving (average net cash flow) of the portfolio of CHP projects: low, base and high scenarios

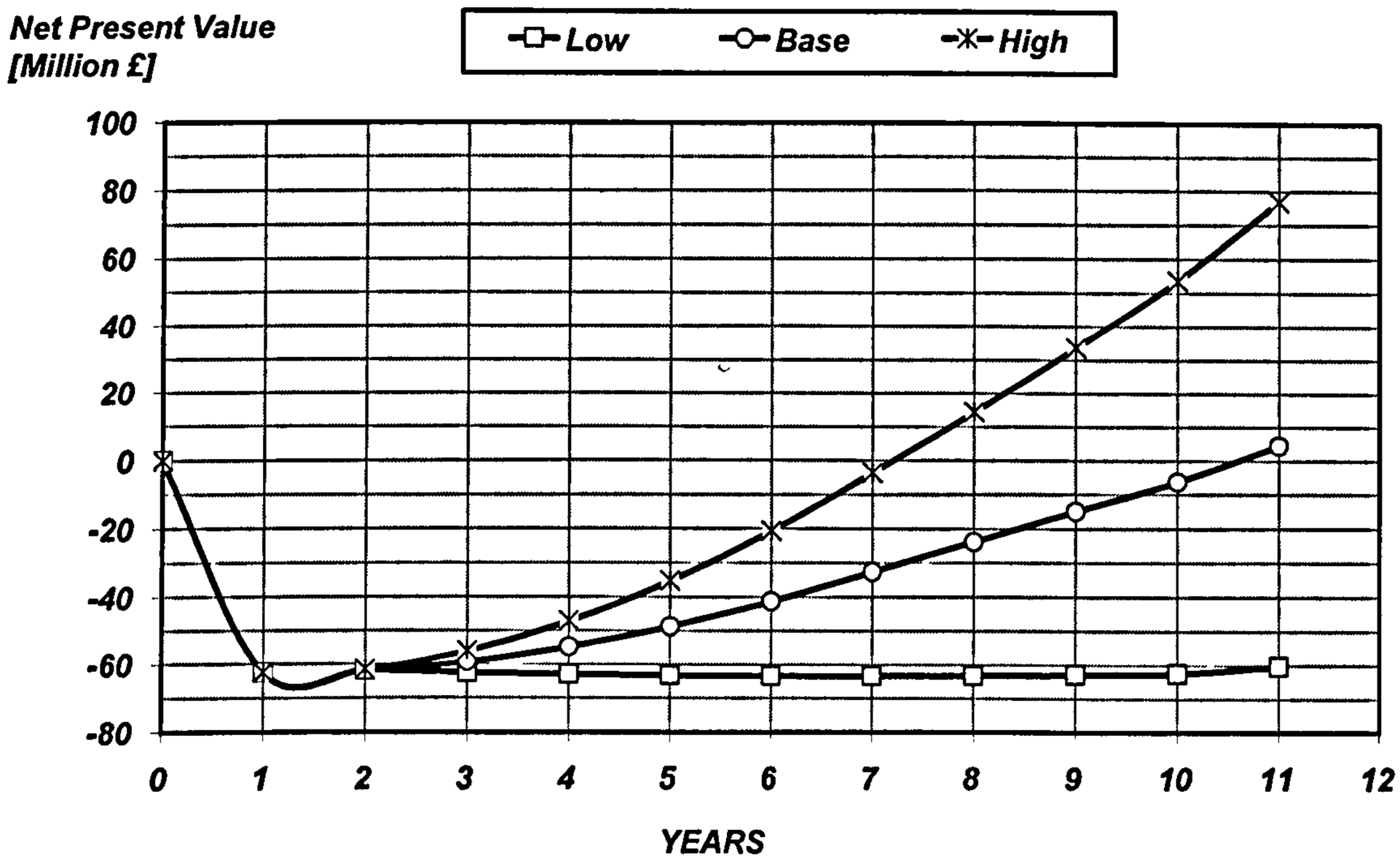

Figure 8.15 - Mini-pool discounted cash flow: low, base and high scenarios

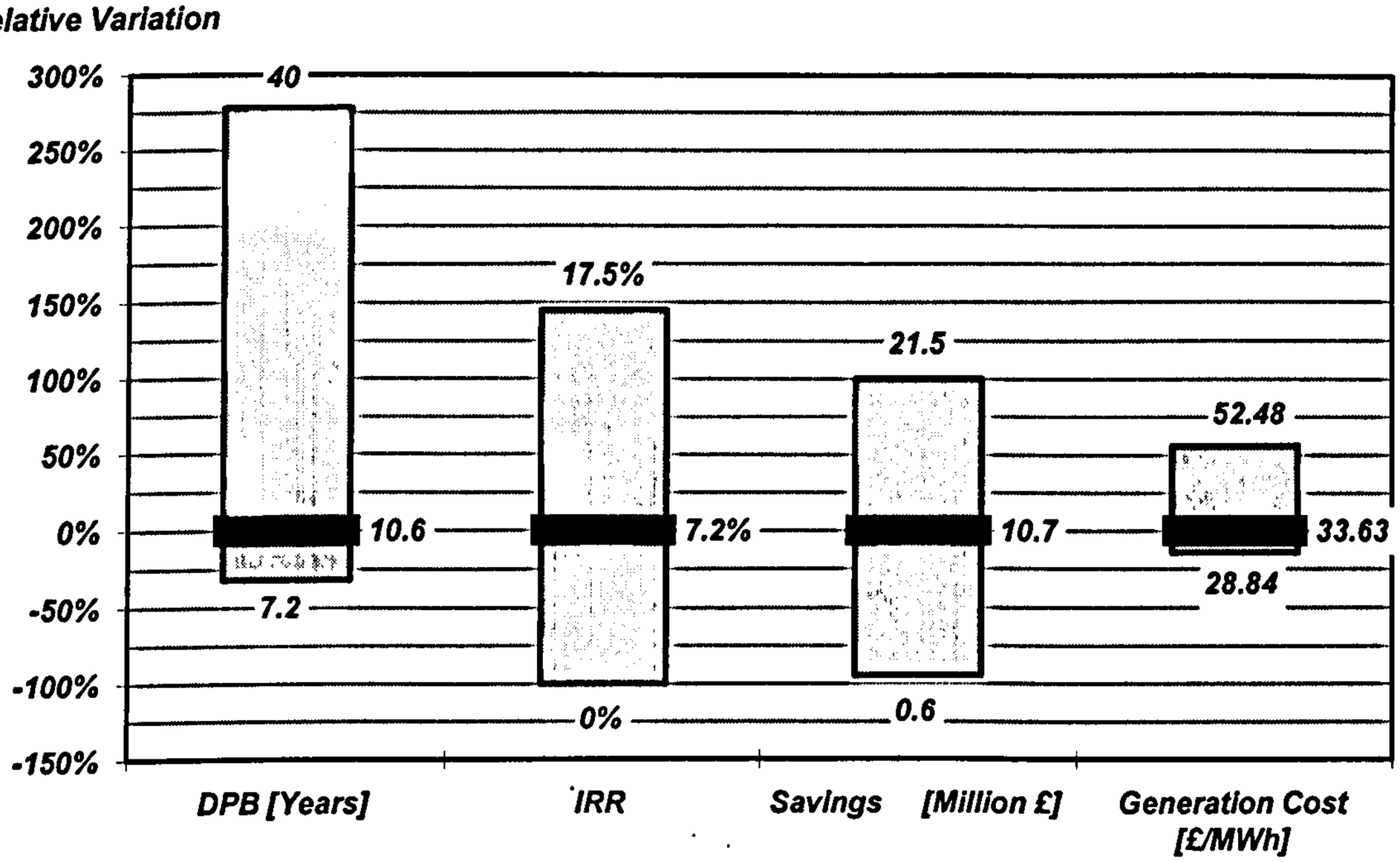

Figure 8.16 – Mini-pool financial appraisal summary: low, base and high scenarios

Table 8.2 introduces the input of the risk analysis of the mini-pool project and Figure 8.17 presents the convergence process. A total of 2,000 evaluations were carried

out but the algorithm found convergence in approximately 800 evaluations. Figures 8.18 and 8.19 display the output distribution of economic parameters observed. There is an accumulative probability of 37% of net present value of the mini-pool CHP project being higher than 3.9 years and 63% probability of discounted payback period being lower than 10 years for the input distribution given in Table 8.2. A minimum discounted payback period of 6.6 years is possible but with a probability of 0.4%.

Table 8.2 – Range of variation of the mini-pool risk analysis inputs (Gaussian distribution)

Interest Rates (IR)	+/- 20%
Fuel Tariffs (FTR)	+/- 60%
Electricity Prices (EBP, ESP and CEP)	+/- 120%
GT Capital Costs (SGTC)	+/- 44%
Installation Costs (ICR)	+/- 56%
Maintenance Costs (SOMC)	+/- 32%

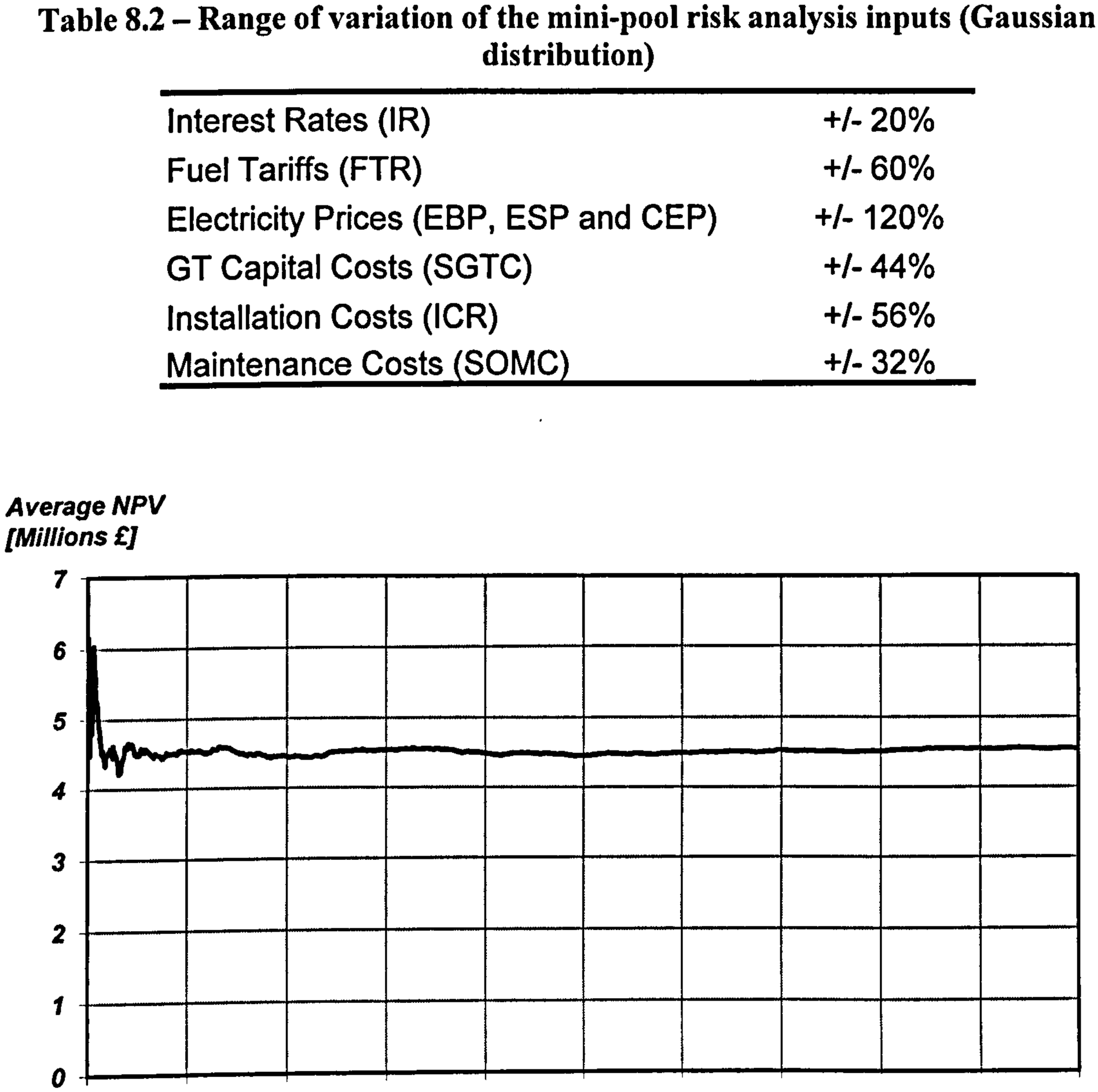

Figure 8.17 - Convergence of the mini-pool risk analysis

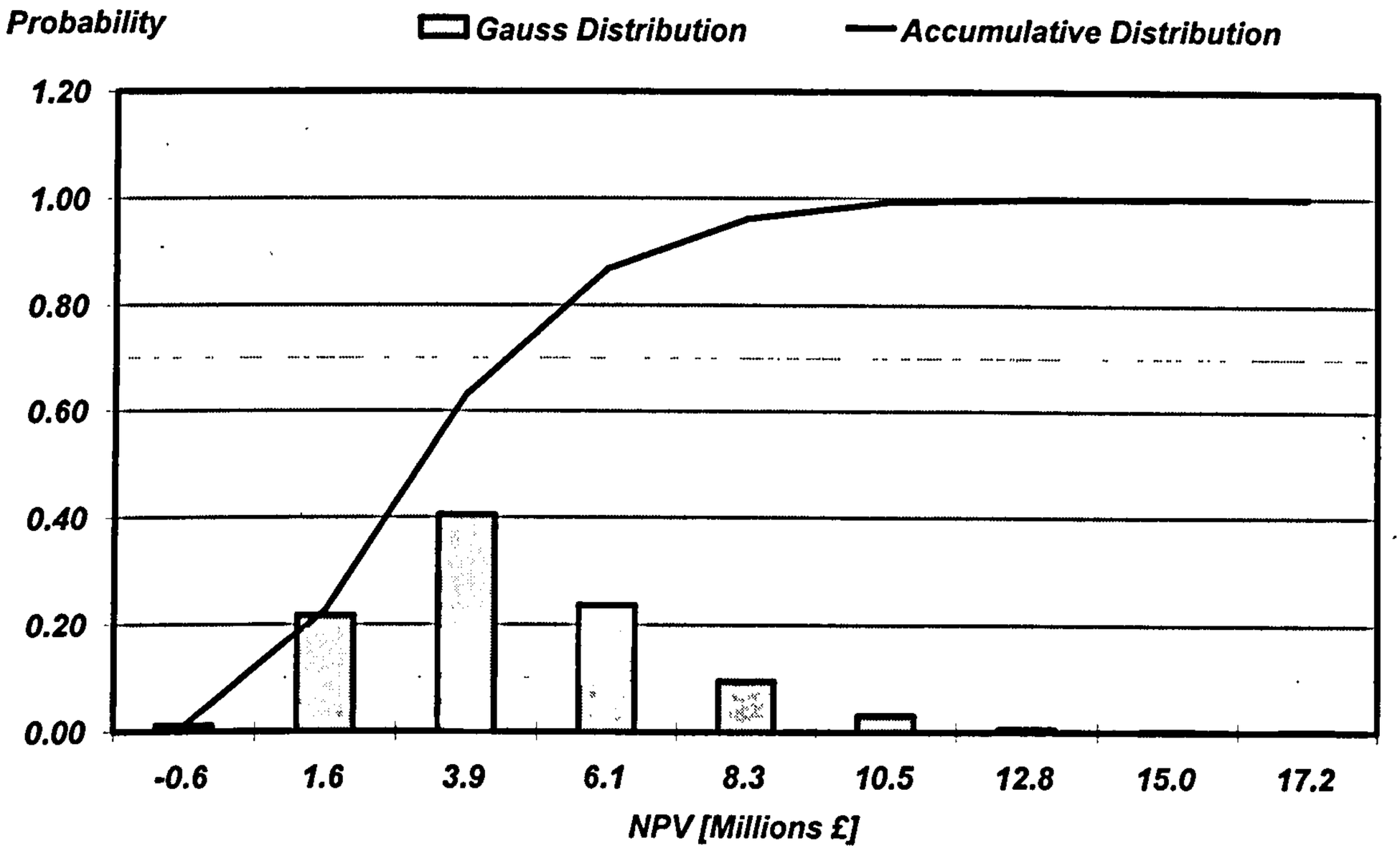

Figure 8.18 – Risk analysis output histogram: mini-pool net present value

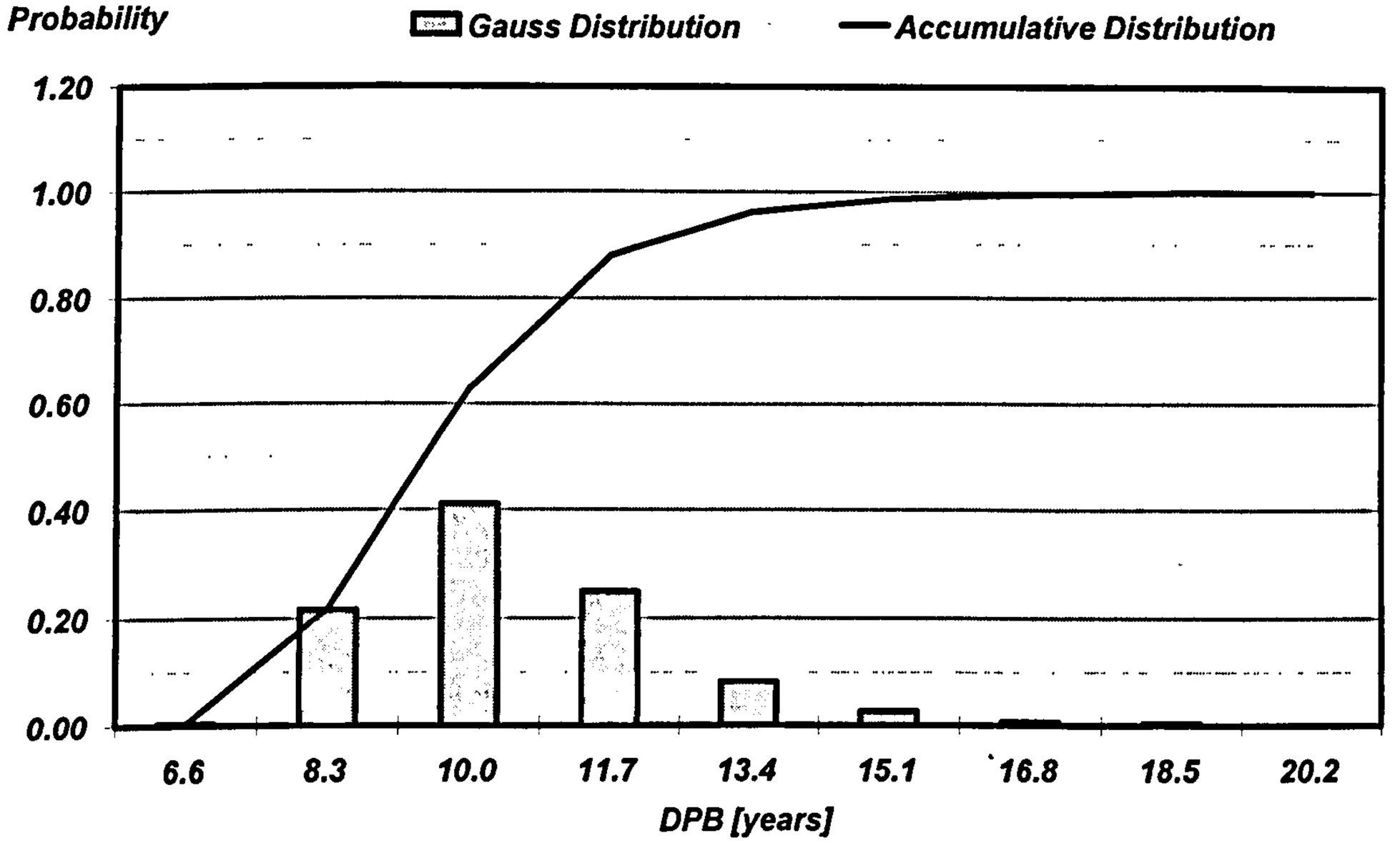

Figure 8.19 - Risk analysis output histogram: mini-pool discounted payback period

Chapter 9 - Conclusions and Recommendations

9 - Conclusions

This research introduces an innovative nerve centre concept through the optimisation of mini-grid integrated generators (mini-pool). Such a mini-pool operates in a competitive market producing heat and power to end users. A multidisciplinary investigation was carried out involving diagnostics, life cycle assessment, financial and risk optimisation in different time horizon lengths.

The technological scope of the mini-pool investigated is composed of a portfolio of energy consumers, and gas turbine distributed combined heat and power (CHP) generation. The higher participation of private companies in the power market and the recent technological advances in small scale power generation technologies has increased the interest for distributed generation systems, mainly combined heat and power (CHP) systems. Despite the thermodynamically efficient and environmental benefits of CHP, its share in the power market of many countries is still modest. One of the barriers for the widespread use of such systems is the need and cost of power supplies when the CHP units are not available. This is one of the issues with which the mini-pool nerve centre concept proposed in this research is concerned.

A multi objective optimisation algorithm was developed and real demand data patterns collected in a portfolio of heat and power demand users were used as input data. Heat and power consumer facilities in secondary industries, tertiary (service), and residential sectors located in the Mediterranean and tropical climate areas were examined and seasonal data was collected, statically processed and then a parametric analysis was carried out.

The strategic energy consumption information provided is useful for the elaboration of preliminary energy studies of many installations and for the quantitative evaluation of human interactions with the environment. In addition, this analysis allows end users to identify possible energy and cost saving opportunities when comparing specific energy consumption charts with references.

Secondary industries and the airport investigated have a reasonably steady pattern of demand with only minor variations resulting mainly from production and site

activities or plant availability. Other consumers (mainly residential and the tertiary service) have well-defined and predictable demand profiles related to regular working activities. Ambient conditions play a very important role in demanding energy resources. Sites located in the Mediterranean region and requiring large amounts of energy for space heating presented a significant change between winter and summer heat demands.

The findings of this research can have a significant contribution on the future energy production and consumption development challenges faced for many institutions as a consequence of the increasing population, demands for higher standards of living and lower pollution levels.

This research also evaluated the gas turbine life time and the risk involved during its operation over a life cycle. Creep life assessment of turbine blades in gas turbines used to be quoted in design point conditions. However the turbine life cycling consists of repetitions of a combination of different regimes of operation and ambient conditions.

The trend of creep consumption life can be determined and appropriate maintenance action can be planned before damage occurs. Therefore engine downtime can be minimised and high levels of availability achieved. The risk analysis algorithm produces the expected window time in which the turbine blade is expected to fail and its respective probability. Algorithm convergence is possible to be achieved in realistic and practical computational time.

Condition monitoring and life cycle techniques can optimise the availability of power engines resulting in higher competitiveness. This assessment can be of considerable value for gas turbine power generators as it allows users to approach the most suitable maintenance or operation strategy thereby increasing the gas turbine component life. This is of significant importance when optimising the operation of power generators particularly in markets of high competition.

The performance and emission concentration of small liquid fuel and natural gas turbines was experimentally analysed. The units experimentally tested have clean combustion technology to achieve low emissions for all classes of pollutants investigated. NO_X emissions are lower than average fossil fuel power plants reported by

Weston et al., 2002. These units are clean enough to be sited within a community among residential and commercial establishments and are clearly designed to operate at full load. The data presented in this study are original and make a valuable contribution to energy and the environmental engineering field.

A Hybrid Genetic Algorithm Adapted Priority List has been developed to solve the Multi Unit Optimisation problem. The initial population has been seeded with an Adapted Priority List solution. The introduction of this reasonably good solution in the initial population, even if not a feasible solution, makes the search start closer to the optimum, leading to a faster convergence and better results.

Comparison of Multi and Single Unit Schedule Optimisations with traditionally distributed generation systems indicates that the proposed nerve centre concept can result in significant savings to generators and also shows that the proposed algorithms efficiently find optimal results in a reasonable computation time for small and medium sized systems.

Units and system constraints could be easily modelled in the Hybrid Genetic Algorithm Adapted Priority List mainly because of its flexible characteristics. Results show that despite the stochastic nature of the proposed algorithm the risk of convergence to suboptimal solutions is relatively low.

The algorithm developed was not only able to optimise the profit of the proposed mini-pool in the short-term horizon but also to maximise the service hours between failures in medium-term planning. Life cycle assessment combined with generation schedule optimisation can enhance the maintenance strategy activities and the competitiveness of gas turbine distributed generation plants, particularly for generators trading energy in a highly competitive market.

Environmental issues are expected to play a key role in decision making processes in the future power generation industry. In this study, an environmental constraint (carbon emission tax) was also incorporated in the mini-pool generation schedule algorithm. Results show that CHP will become more competitive as carbon taxes are implemented mainly in power markets driven by coal/oil centralised power stations

In this investigation the distributed generators are responsible for supplying the energy demand of the end user and maximising their profits. It is supposed here that a long term contract is established between the end user and the energy supplier – typically an energy service company (ESCO). It is also supposed that the ESCO can manage the energy supply as they like, including the option of buying electricity from the network instead of producing it and then reselling it to the user, if there is any advantage in that. Power plant owners and end users would be unlikely to accept such an approach during the initial stages of a feasibility study of a power plant. However, many power plants in countries in which the power market is fully deregulated (high competition) are at present facing the hard decision of whether to produce power or shut down their engines and resell the fuel contracted due to the high fuel prices and competitiveness they are facing.

The author understand that there is a perception barrier to implement the nerve centre concept proposed as generators have the idea that shutting down their engines will necessarily decrease their profit. This maybe absolutely true for centralised power plants generators trading electricity in the bilateral market. However, as it is demonstrated in this research, a mini-pool of distributed generators interconnected through a mini-grid operating in a competitive power market can maximise their profit by scheduling their engines according to the volatile prices of the market. In some circumstances this will inevitably involve shutting down engines for some periods of time.

All CHP units investigated were considered to be electrically interconnected to the national network which is reasonable and practical in all cases analysed. Regarding the issue with the interconnection between the island and the mini-grid, two scenarios must be considered depending on whether the mini-pool is physically located on the continent or on the island. If the mini-pool is located on the island it can be connected to the local network as can any other independent power generator. If the mini-pool is located on the continent, the island can be connected to the mini-pool through two different ways:

- using the connection of the national continent network if the local legislation allows and the local transmission lines/utility owner agrees. In

this case a transmission charge will be applied which will increase production costs; or

- building up a private electrical connection with the mini-pool mini grid if local legislation allows. In this case there will be an extra capital cost which may be financed over the first years of operation but will also increase production costs until the investment is totally paid off.

The island demand was added to this investigation in order to give diversity to the analysis of a wide portfolio of energy demand patterns. The island demand has a typical residential consumer profile on a larger scale. It can be considered equivalent to any other large group of residential consumers such as residential buildings or even an entire city.

Electricity and gas prices and local consumer demand forecasts are very important input parameters in the proposed mini-pool nerve centre methodology as they are associated with decision making in a competitive market. This subject has been investigated over recent years and an acceptable level of performance has been reached since the restructuring of the energy industry. Adaptive time series and artificial intelligence techniques have been developed to forecast load and price in short-term competitive markets achieving errors lower than 2% (Bunn and Farmer, 1985) and 8.8% (Zhang et al., 2003) respectively.

When approaching market forecasts it is important to treat end users separately in residential, commercial, and industrial sectors as this has contributed to more accurate forecasts mainly for medium term planning (Bunn and Farmer, 1985). With regard to this issue, this research has made a particular contribution with all the energy demands and weather conditions data collected and reported for facilities in all three sectors.

A major challenge is common in both engineering and economic disciplines which is to make reasonable strategic choices among several possible solutions to an important and practical problem. An investment in a Combined Heat and Power (CHP) system is ruled by complex dynamics frameworks and affected by various uncertainties.

A decision making support tool for Gas Turbine CHP systems is proposed in this research based on financial and probabilistic risk analysis. The CHP units were first analysed individually and then interconnected in a mini-pool arrangement.

The ultimate goal in this decision-making support tool is to optimise economic performance. Therefore, it is very important to properly understand and quantify the trade-offs and their relevant consequences over the economic life of the investment. The interaction between the different model components is a non-linear process. These components are supposed to be deterministic but the outcome of some of them depends on unpredictable factors that are treated in stochastic terms. For this reason the decision-making support process was first modelled in simulation scenarios and later with an uncertainty probabilistic analysis. Scenario simulation investigation is an important tool for assessing the range of economic performance variation in different market trends while uncertainty analysis and the parameters probability distribution function (PDF) were used in dealing with uncertain conditions in order to reduce risks involved.

Natural gas CHP can contribute not only to the economic benefits of the end user but also to a whole nation. CHP units can be a limiting factor to the installation of new conventional electrical units and considerable carbon emissions can be saved mainly in power markets predominantly using coal and oil powered generation technology.

Some of facilities studied showed economically feasible combined heat and power production in the baseline scenario. However, other factors, such as the availability of technical and maintenance support, environmental issues, and the reliability of the fuel supply, must be considered before any decision is made.

Initially it was thought that distributed CHP would be a suitable choice of power and heat supply to hotels because of the requirement to maintain customer comfort. The results show that a CHP proposal is not as economically attractive for service sector facilities (hotels and shopping centre) as it is for industrial companies and airports. This is mainly because CHP systems require a matched heat load to provide maximum benefit. However, in a mini-pool arrangement, enterprises in the tertiary sector can have an outstanding opportunity to produce their own independent power and heat demand in a more profitable way. The industries and airport investigated will not

have the same economic benefit in a mini-pool arrangement, but they still can have a significant contribution if reliability of independent power and heat supply is a priority issue for their business.

CHP generators are unlikely to succeed in competing individually with centralised generation technologies within the present market framework, but they can be more competitive in an integrated co-operation of multi generators (mini-pool). However, the cash flow of the mini-pool presents more volatility than the cash flow of the individual units because of the higher amount of money involved in each time period. Therefore the economic feasibility of the investment is more volatile to market fluctuations.

The features described before make the proposed mini-pool nerve centre concept a possible alternative for actual and future power system management tools resulting in the restructuring of the power industry.

Despite the potential market for micro power technologies, manufacturers of micro gas turbines have encountered many barriers to overcome performance and reliability. Therefore, an investigation of the performance and degradation effects of micro gas turbines in different thermodynamic cycles and design regimes of operation was carried out.

Variable speed regenerative micro gas turbines have a potential application in small scale distributed generation systems because of the substantially greater thermal efficiency and better part-load performance compared with constant speed simple cycle engines. This conclusion was observed in both computational simulation and experimental analysis with natural gas and liquid fuelled engines. On the other hand, the regenerative variable speed cycle is more sensitive to component degradations and consequently will present higher maintenance costs. Determination of the appropriate set of instrumentation is more dependent on whether the cycle is regenerative or not rather than if it operates at a variable or constant speed.

In some cases investigated, gas path analysis (GPA) was not able to give an accurate prediction of the engine fault. This is attributed to the fact that physical faults are not always related to independent parameter change. The GPA diagnostic technique is highly dependent on the accuracy and reliability of instrumentation measurements.

Deteriorated instrumentation will present higher error measurements and can result in misleading fault detections. Consequently unnecessary maintenance actions may take place.

The development of a robust gas turbine condition monitoring system is a very complex issue because of the many different faults that are possible. However, a combination of different techniques such as borescope inspection, vibration monitoring, oil inspection can complement the GPA diagnostic. Instrumentation acquisition, installation and maintenance costs, and users' perception and experience must also be carefully analysed before any investment in condition monitoring systems is made.

9.1 - Recommendations and Future Work

Materials that are subjected to progressive cyclic and fluctuating strains will eventually present permanent structural damage (fatigue). Fatigue life assessment can have a positive impact reducing gas turbines life cycle costs (Devereux, 1992) as frequent cycling will increase thermal stresses, which results in increased maintenance costs and reduced life time. It is not the purpose of this research to investigate the effects of fatigue on gas turbine off-design operation. However, because of the possible start-up and shut-down repetitions that the proposed generation schedule algorithm may result in, the implementing of a fatigue life assessment can contribute to a more robust gas turbine blade life cycle assessment and generation schedule optimisation.

Turbine blade cooling is used to maintain the blade life in an acceptable range as blades are designed to run under extreme head load conditions in order to increase the cycle efficiency. However, blade cooling also has its disadvantages as it increases thermodynamic and aerodynamic losses, and manufacturing costs significantly. This research is restricted to stationary medium- and small-sized gas turbines used for distributed power generation. Typically the turbine blades of these machines have no complex internal cooling channels which are often present in large-sized industrial and aero gas turbines. It would be an interesting topic to extend the scope of work of the proposed mini-pool nerve centre to large-sized industrial gas turbines, mainly those in combined heat and power cycles. Following this line of thought, it would be very useful to incorporate turbines blade with internal cooling in the life cycle assessment proposed.

Essentially it would require an evaluation on the effects of cooling flow rates in the blade metal temperature.

Forecasts of power and heat demand for different sectors of industry, and prices in the competitive power market is another very interesting area that would aggregate significant value to the methodology proposed in this research. Demand and price forecasts in the competitive market require an investigation into the demand and supply chains as there is a very close connection between these two parameters. In competitive energy markets, demand and price forecasts need to be detailed and well defined for bidding purposes. This requires the elaboration of computationally intensive methods involving variable segmentation, combinations and neurotechnology as well as the integration of weather forecasts. The size of the market share is also an important parameter to be investigated as it aggregates a significant uncertainty and adds a new dimension to the price forecasting process.

As a complement to the demand and prices forecast described before, it would be a very useful contribution to extend the demand data acquisition to other facilities in the secondary and tertiary sectors of industry, such as petrochemicals, food, cement and glass, primary metals, textile and paper, hospitals, leisure centres, and others.

Bibliography and References

Aker, G.F. and Saravanamuttoo, H.I.H., Predicting the Gas Turbine Performance Degradation due to Compressor Fouling Using Computer Simulation Techniques. ASME Report No. 88-GT-206, 1988.

Aldridge, C. J., McKee, S., McDonald, J. R., Galloway, S. J., Dahal, K. P., Bradley, M. E. and Macqueen, J. F. Knowledge-based genetic algorithm for unit Commitment. IEE Proceedings on Generation, Transmission and Distribution, 148 (2), March 2001, 146-152.

Arroyo, J. M. and Conejo, A. J. A Parallel Repair Genetic Algorithm to Solve the Unit Commitment Problem. IEEE Transactions on Power Systems, 17 (4), November 2002. 1216-1224.

Arvantis, S.T., Symko, Y.B., Tadros, R.N. Multi axial life prediction system for turbine components. Journal of Engineering for Gas Turbines and Power, 109, 1987. 107-114.

Bakirtzis, A. G. and Dokopoulos, P. S. Short therm generation scheduling in a small autonomous system with unconvencional energy sources. IEEE Transactions on Power Systems, 3 (3), August 1988, 1230-1236.

Banes, B., McIntyre, R. W. and Sims, J. A. Properties of air and combustion products with kerosine and hydrogen fuels : equilibrium composition and thermodynamic properties for air and systems. Bristol Siddeley Engines on behalf of the Propulsion and Energetics Panel of the Advisory Group for Aerospace Research and Development, 1967.

Bays, C. and Durham, S. D. Improving a poor random number generator, 2(1), 1976, 59-64. Cited in: Press, W. H; Teukolsky, S. A.; Willian, T. V., and Brian, P. F. Numerical Recipes in Fortran - The art of Scientific Computing. Second ed. Cambridge University Press, 1992.

Belding, J. A. In: Cogeneration, in Industrial Energy Conservation – Manual 15, edited by E. P. Gyftopoulos, The MIT Press, Cambridge, Ma., 1982.

Bellman, R. E. and Dreyfus, S. E. Applied Dynamic Programming, Princeton: Princeton University Press, 1962.

Boessioa, M. L.; Morsch, I. B., and Awruch. A. M. Fatigue lifetime estimation of commercial vehicles. Journal of Sound and Vibration, 291 (1-2), 2006, 169-191.

Bowman, R., Ritzert, F., and Freedman, M. Evaluation of candidate materials for a high-temperature stirling convertor heater head. NASA/TM2003-212734. Space Technology and Applications International Forum (STAIF2004), 2004.

Boyce, M. P. Gas turbine engineering handbook. Gulf Publishing Company, 1982.

Boyer, H. E. Atlas of Creep and Stress-Rupture Curves. USA: ASME International, 1988.

Bunn, D. W. and Farmer, E. D. Comparative models for electrical load forecasting. Chichester, U.K.: Wiley, 1985.

Chang, C. S. and Fu, W. Stochastic multi-objective generation dispatch of combined heat and power systems, IEE Proceedings on Generation, Transmission and Distribution, 145 (5), 1998, 583–591.

Contaxis, G.C. and Kabouris, J. Short Term Scheduling in a Wind/Diesel Autonomous Energy System. IEEE Transactions on Power Systems, 6 (3), August 1991, 1161-1167.

Devereux, B. Improving life usage of the F404 engine through thrust rating, MSc. Thesis, UK: Cranfield University, 1992.

Diakunchak, I. S. Performance Deterioration in Industrial Gas Turbines, ASME Journal of Engineering for Gas Turbines and Power, 114 (2), 1992, 161-168.

DTI, The UK Fuel Poverty Strategy and Annual Monitoring, Annual Progress Report, Fourth edition, June 2006. http://www.dti.gov.uk/energy/fuel-poverty/strategy/index.html (accessed 28th March 2007).

DTI, UK Energy and CO2 Emissions Projections UEP26 - Updated Projections to 2020, February 2006, http://www.dti.gov.uk/files/file31861.pdf (accessed 28th March 2007).

Dundas, R. E. Mechanical design of the gas turbine. In: Sawyer's gas turbine engineering handbook, edited by J. W. Sawyer. Third edition, Volume I, USA: Turbomachinery International Publications, 1985.

Educogen, The European Education Tool on Energy-Efficiency through the Use of Cogeneration, EC SAVE Programme Final Report XVII/4.1031/P/99-159, 2002.

Escher, P. C. Pythia: an object-oriented gas-path analysis computer program for general applications. PhD Thesis, UK: Cranfield University; 1995.

Gas Turbine World, Gas Turbine World Handbook 2005, USA: Pequot Publishing Inc., 2005.

Gil, E., Bustos, J., and Rudnick, H. Short-term hydrothermal generation scheduling model using a genetic algorithm, IEEE Transactions on Power Systems, 18(4), November 2003, 1256–1264.

Givanildo, J. de A. Renewable energy – overcoming intermittency. PhD Thesis, London: University of London, 2005.

Goldberg, D. Genetic Algorithms in Search, Optimization & Machine Learning. Reading, MA: Addison-Wesley Publishing Company, Inc., 1989.

Gomes, E. E. B. and Pilidis, P; Polizakis, A. Sort-term generation schedule optimisation for gas turbine power systems. In: Proceedings of ASME Turbo Expo Conference, Montreal, Canada, May 14-17 2007. Montreal, Canada: ASME, 2007.

Gomes, E. E. B.; Pilidis, P; Polizakis, A; Short-term Generation Schedule Optimisation with Genetic Algorithm for Distributed Generation Systems; Energy The International Journal, submitted on 17 October 2006 and accepted for publication on 30 March 2007.

Gomes, E. E. B.; Cobas, V. M., and Teixeira, F. N. In: Thermal Power Generation Cases in Brazil, edited by Lora, E. E. S. and Nascimento, M. A. R. do. Thermal Power Generation: Planning, Design and Operation, Vol. II, First ed., Rio de Janeiro, Brazil: Interciencia; 2004 (in Portuguese language).

Gomes, E. E. B.; McCaffrey, D; Garces, M J M; Polizakis, A L, and Pilidis, P. Comparative Analysis of Microturbines Performance Deterioration and Diagnostics. In: Proceedings of ASME Turbo Expo Conference, Barcelona, Spain, May 8-11 2006, part A, 269-276. Barcelona, Spain: ASME, 2006.

Gomes, E. E. B.; Nascimento, M. A. R. do, and Lora, E. E. S. Case studies of distributed generation projects with microturbines in Brazil. In: Proceedings of 2003 International Joint Power Generation Conference, Atlanta, GA, June 16-19 2003, 1031-1037. Atlanta, GA: ASME, 2003.

Gomes, E. E. B.; Nascimento, M. A. R. do; Lora, E. E. S.; Pilidis, P; Haslam, A; Performance evaluation and case studies of microturbines fuelled with natural gas and diesel, Journal of Power and Energy, The Proceedings of the Institution of Mechanical Engineering, 218(A), 2004.

Gomes, E. E. B.; Pilidis, P. Gas Turbine Life Cycle Assessment and Preliminary Risk Analysis, In: Proceedings of ASME Turbo Expo Conference, Montreal, Canada, May 14-17 2007. Montreal, Canada: ASME, 2007.

Gomez, D. G. Variable Cooling Supply. MSc Thesis, UK: Cranfield University; 2005.

Guo, T., Henwood, M.I., Ooijen, M. van. An algorithm for combined heat and power economic dispatch, IEEE Transactions on Power Systems, 11(4), 1996, 1778–1784.

Hastings, N.A.J. Dynamic Programming with Management Applications, Operational Research Quarterly, 25(3), 1974. 502-503.

Hoeft, R.F. Heavy Duty Gas Turbine Operating and Maintenance Considerations, GER-3620B. GE I&PS, 1993.

Holland, J. H. Adaptation in Natural and Artificial Systems. Ann Arbor: University of Michigan Press, 1975.

Holland, M. J. and Thake, T. F. Rotor Blade Cooling in High Pressure Turbines. Journal of Aircraft 17 (6), 1980. 412-418.

House, P., Gas Path Analysis Techniques Applied to Turboshaft Engines, MSc Thesis, UK: Cranfield University, 1992.

Jaske, C. E. and Simonen, F. A. Creep-rupture properties for use in the life assessment of fired heater tubes. In: Proceedings First International Conference on Heat-Resistant Materials, Fontana, Wisconsin, September 23-26 1991, 485-493. Fontana, Wisconsin: ASME: 1991.

Jennekens, M. Learning from Experiences with Small Scale Cogeneration. Center for the Analysis and Dissemination of Demonstrated Energy Technologies Analyses Series No. 1. Sittard, The Netherlands: CADDET, 1989.

Kazarlis, S. A., Bakirtzis, A. G., Petridis, V. A genetic algorithm solution to the unit commitment problem, IEEE Transactions on Power Systems, 11(1), 1996. 83–92.

Kidwell, J. R. Garrett multipurpose small power unit (MPSPU). Journal of Aerospace, 98(1), 1989. 1490-1497.

Kurz, R., and Brun, K., Degradation in Gas Turbine Systems, ASME Journal of Engineering for Gas Turbines and Power, 123 (1), 2001. 70-77.

Lakshmin, A. N., Boyce, M. P. and Meher-Homji, C. B. Modelling and Analysis of Gas Turbine Performance Deterioration, ASME Journal of Engineering for Gas Turbines and Power, 116(1), 1994.

Larson, F. R. and Miller, J. A time-temperature relationship for rupture and creep stress. Transations of ASME, 74, 1952. 765–775.

Leipholz, H. H. E. On The Modified S-N Curve For Metal Fatigue Prediction and its Experimental Verification, Engineering Fracture Mechanics Journal, 23(3), 1986. 495-505.

Li, Y.G. Performance analysis based gas turbine diagnostics: a review, Journal of Power and Energy, The Proceedings of the Institution of Mechanical Engineering, 216(A), 2002. 363–377.

Li, Y.G., Gas Turbine Diagnostics, Thermal Power Lecture Notes, Cranfield University, 2004

MacGregor, P. R. and Puttgen, H. B., The integration of nonutility generation and spot prices within utility generation scheduling. IEEE Transactions on Power Systems, 9(3), 1994. 1302 – 1308.

Maifeld, T. and Sheblé, G., Genetic-based unit commitment. IEEE Transactions on Power Systems, 11(3), 1996, 1359-1370.

Marscher, W. D. Structural Analysis: Fatigue Life Assessment. In: Radial Turbines, edited by N. C. Baines and C. H. Sieverding. Lecture Series 1992-05. Belgium: Karman Institute for Fluid Dynamics; 1992.

Marscher, W. D. Structural design and analysis of modern turbomachinery systems. In: Sawyer's gas turbine engineering handbook, edited by J. W. Sawyer. Third edition, Volume I, USA: Turbomachinery International Publications, 1985.

Martinez-Frias, J., Aceves, S. M., Flowers, D. Smith, J. R., Dibble, R. Thermal Charge Conditioning for Optimal HCCI Engine Operation, Journal of Energy Resources Technology, 124, 2002. 67-75.

Massart, E. Performance and Deterioration Analysis of a Small Gas Turbine for Road Vehicles. MSc Thesis. UK: Cranfield University; 1997.

McGraw, M. A.; Halford, G. R., and Kalluri, S. Cumulative fatigue damage behaviour of MAR M-247. NASA/CP10064. USA: NASA-Lewis Research Center; 1991.

Mendes, D. P. Generation scheduling, pricing mechanisms and bidding strategies in competitive electricity markets. PhD Thesis, Manchester: University of Manchester; 1999.

Metropolis, N. and Ulam, S. The Monte Carlo method. Journal of the American Statistical Association, 44, 1949. 335-341.

Miner, M. A. Cumulative damage in fatigue, Journal of Applied Mechanics, 1945, A159–A163.

Murakami, Y.; Harada, S.; Endo, T.; Tani-Ishis, H., and Fukushima, Y. Correlations among growth law of small cracks, low-cycle fatigue law and applicability of Miner's rule. Engineering Fracture Mechanics Journal, 18(5), 1983. 909-924.

Mustapha, N.A.K., The Application of Gas Path Analysis to Combined Cycle Gas Turbines, MSc Thesis, UK: Cranfield University, 1995.

Nascimento, M. A. R. do; Gomes, E. E. B., and Venturini, O. J. Gas Turbines. In: Thermal Power Generation Cases in Brazil, edited by Lora, E. E. S. and Nascimento, M. A. R. do. Thermal Power Generation: Planning, Design and Operation, Vol. I, First ed., Rio de Janeiro, Brazil: Interciencia; 2004 (in Portuguese language).

Ogaji, S.O.T., Singh, R., and Probert, S.D. Multiple sensor fault diagnoses for a 2 shaft stationery gas turbine, Journal of Engineering for Applied Energy, 71, 2002. 321-339.

Orero, S. O. and Irving, M. R. A genetic algorithm modelling framework and solution technique for sort-term optimal hydrothermal scheduling, IEEE Transactions on Power Systems, 13, 1998, 501–518.

Padhy, N. P. Unit Commitment - A bibliographical survey, IEEE Transactions on Power Systems, 19 (2), 2004. 1196-1205.

Papamarcou, M. and Kalogirou, S. Financial appraisal of a combined heat and power system for a hotel in Cyprus, Energy Conversion and Management Journal, 42(6), 2001. 689-708.

PB Power, Powering the nation, London: Parsons Brinckerhoff Ltd, 2006.

Pilidis, P. Gas Turbine Theory and Performance, Thermal Power Lecture Notes, Cranfield University, 2005

Polizakis, A. L., Techno-economic Evaluation of Trigeneration Plant: Gas Turbine Performance, Absorption Cooling and District Heating, PhD Thesis, UK: Cranfield University, 2007

Press, W. H; Teukolsky, S. A.; Willian, T. V., and Brian, P. F. Numerical Recipes in Fortran - The art of Scientific Computing. Second ed. UK: Cambridge University Press, 1992.

Richter, C. W. and Sheblé, G. B. A Profit-Based Unit Commitment GA for the Competitive Environment, IEEE Transactions on Power Systems, 15(2), 2000. 715-721.

Rodgers, C.; Watts, J.; Thoren, D.; Nichols, K. & Brent, R. Microturbines, In: Distributed Generation – The Power Paradigm for the New Millennium, edited by Anne-Marie Borbely & Jan F. Kreider, CRC Press LLC., USA, 2001.

Rooijers, F.J. and Amerongen, R. A. M. van Static Economic Dispatch for Co-generation Systems, IEEE Transaction on Power Systems, 9 (3), 1994. 1392-1398.

Roskosz, S., Staszewski, M. and Cwajna, J. A complex procedure for describing porosity in precision cast elements of aircraft engines made of MAR-M 247 and MAR-M 509 superalloys. Materials Characterization, 56(4-5), 2006. 405-413.

Saravanamuttoo, H. I. H.; Rogers, C. F. G., and Cohen, H. Gas Turbine Theory. 5th edition ed. London: Pearson Education Limited; 2001.

Saravanamuttoo, H.I.H. and Mac Isaac, B.D., Thermodynamic models for pipeline gas turbine diagnostics, ASME Journal of Engineering for Gas Turbines and Power, 105 (A), 1983. 875-894.

Sen, S. and Kothari, D. P. Evaluation of benefit of inter-area energy exchange of the indian power systems based on multi-area unit commitment approach. Electric Machines and Power Systems, 26, 1998. 801–813.

Shimokawa, T. and Tanaka, S. A statistical consideration of Miner's rule. International Journal of Fatigue, 4, 1980, 165-170.

Sikorski, T. UK Gas Market: Supply and Demand Outlook. In: New Build and Retrofit Challenges in the UK Conference, London, 9-10 November 2006. London, UK: Wilmington Conferences, 2006.

Singh, M. P.; Thakur, B. K., and Sullivan, W. E. Assessing useful life of turbomachinery components. In: Proceedings of the thirty-fourth turbomachinery symposium. Houston, Texas, September 12-15 2005, 177-192. Houston, Texas: Texas A&M University, 2005.

Song, Y. H. and Xuan, Q. Y. Combined heat and power economic dispatch using genetic algorithm based penalty function method, Electric Machines and Power Systems, 26 (4), 1998. 363-372

Sood, Y. R.; Padhy, N. P., and Gupta, H. O. Discussion on optimal power flow by enhanced genetic algorithms, IEEE Transactions on Power Systems, 18, 2003, 1219-1220.

Srinivasan, D. and Chazelas J. A priority list-based evolutionary algorithm to solve large scale unit commitment problem. In: 2004 International Conference on Power System Technology - POWERCON 2004. Singapore, 21-24 November 2004, 1746-1751. Reprint: IEEE; 2004.

Su, C. –T. and Chiang, C –L. An incorporated algorithm for combined heat and power economic dispatch. Electric Power Systems Research, 69, 2004. 187–195.

Sudhakaran, M. and Slochanal, S. M. R. Integrating Genetic Algorithms and Tabu Economic Dispatch Search For Combined Heat And Power, In: Proceedings of IEEE Annual International Conference TENCON 2003, 1, 2003. 67-71.

Sun, Y. S. Revised Miner's Rule and its Application in Calculating Equivalent Loads for Components. 43, 1994. 319-324.

Tanaka, S. and Akita, S. On the Miner's damage hypothesis in notched specimens with emphasis on scatter of fatigue life. Engineering Fracture Mechanics Journal, 7, 1975. 473-480.

Tarabrin, A.P., Schurovsky, V. A., Bodrov, A.I., and Stalder, J.P., Influence of Axial Compressor Fouling on Gas Turbine Unit Performance Based on Different Schemes and With Different Initial Parameters, ASME International Gas Turbine and Aeroengine Congress, Stockholm, Sweden, June 1998. ASME Paper No.98-GT-416. Stockholm, Sweden: ASME, 1998.

U. S. Environmental Protection Agency, Ceramic products manufacturing - emission factor documentation for AP-42, EPA-68-D2-0159/III-01. USA: EPA, 1996.

Ulam, S.; Richtmyer, R. D., and von Neumann, J. Statistical methods in neutron diffusion. Report LAMS551. USA: Los Alamos Scientific Laboratory; 1947.

Urban, L. A. Gas Path Analysis Applied to Turbine Engine Condition Monitoring, AIAA Paper No. 72-1082, 1972.

Wang, S. J.; Shahidehpour, S. M.; Kirschen, D. S.; Mokhtari, S., and Irisarri, G. D. Short-term generation scheduling with transmission and enviromental constraints using an augmented lagrangian relaxation. IEEE Transactions on Power Systems, 10(3), 1995, 1294-1301.

Wang, W., Ruixian, C., and Zhang, N. General Characteristics of Single Shaft Microturbine Set at Variable Speed Operation and its Optimisation, Journal of Engineering for Applied Thermal Engineering, 24, 2004, 851-1863.

Wartsila Corporation, Environmental Report 2000 – Power for Land and Sea. http://www.wartsila.com (accessed 18th July 2004).

Wartsila Corporation, Wartsila 20 – Technology Review, White Paper, Finland. http://www.wartsila.com (accessed 18th July 2004).

Weston, F., Seidman, N., L., James, C. Model Regulations for the Output of Specified Air Emissions from Smaller-Scale Electric Generation Resources, The Regulatory Assistance Project, 2002. http://www.raponline.org (accessed 28th March 2007).

Wood, A. J. and Wollenberg, B. F. Power generation, operation, and control. Second ed. New York: John Wiley & Sons, Inc., 1996.

Zhang, L. L., Luh, P. B., Kasiviswanathan, K. Energy Clearing Price Prediction and Confidence Interval Estimation With Cascaded Neural Networks, IEEE Transactions on Power Systems, 18(1), 2003. 99-105.

Zwebek, A., and Pilidis, P. Degradation Effects on Combined Cycle Power Plant Performance – Part 1: Gas Turbine Cycle Component Degradation Effects, ASME Journal of Engineering for Gas Turbines and Power, 125(1), 2003. 651-657.

Chapter 10 – Appendix A Combined Heat and Power Portfolio: Demand and Off-Design Performance

10 - Appendix A Combined Heat and Power Portfolio: Demand and Off-Design Performance

10.1 - Ceramics Industrial Park

Table 10.1 – Monthly ambient temperature in Northeastern Brazil

	Ambient Temperature		
	Average	Maximum	Minimum
	[°C]	[°C]	[°C]
JAN	26	32	23
FEB	25	30	22
MAR	28	30	21
APR	26	29	23
MAY	27	29	22
JUN	26	28	22
JUL	24	27	20
AUG	26	28	22
SEP	28	28	19
OCT	28	29	23
NOV	27	29	23
DEC	24	30	23

Table 10.2 – Monthly thermal load of the ceramics industrial park

	Average Fuel Consumption	Hours of Operation	Average Heat Demand	
	kg/s	h/month	kW	kWh
JAN	0.1200	201	4497	904,921
FEB	0.1101	185	4125	761,372
MAR	0.1225	205	4589	942,598
APR	0.1077	181	4035	728,623
MAY	0.1396	234	5229	1,223,539
JUN	0.0896	150	3357	504,269
JUL	0.1217	204	4559	930,277
AUG	0.1115	187	4179	781,556
SEP	0.1090	183	4084	746,587
OCT	0.1112	186	4165	776,149
NOV	0.1172	197	4391	862,857
DEC	0.1235	207	4627	958,097

Table 10.3 – Monthly production of the ceramics industrial park

	Site#1 [m^2]	Site#3 [units]	Site#4 [m^2]
JAN	611,582	61,745	309,026
FEB	583,382	57,293	249,338
MAR	635,316	65,031	299,712
APR	596,674	65,738	228,374
MAY	647,813	69,563	375,169
JUN	603,556	59,864	26,334
JUL	624,356	63,241	312,622
AUG	584,067	62,446	270,009
SEP	618,929	6,019	288,701
OCT	631,361	5,915	297,566
NOV	614,397	54,355	283,032
DEC	637,447	61,857	304,396

Table 10.4 – Monthly electricity consumption of the ceramics industrial park

	JAN	FEB	MAR	APR	MAY	JUN	JUL	AUG	SEP	OCT	NOV	DEC	Total
Site#1													
Peak Electricity Demand [kWh]	56,645	55,200	55,200	52,800	55,200	53,618	49,502	50,868	49,533	51,512	56,562	56,328	642,969
Off-Peak Electricity Demand [kWh]	854,448	871,200	825,600	830,400	892,800	921,936	834,912	889,200	826,464	840,192	904,368	819,120	10,310,640
Total Electricity Demand [kWh]	911,093	926,400	880,800	883,200	948,000	975,554	884,414	940,068	875,997	891,704	960,930	875,448	10,953,609
Site#2													
Peak Electricity Demand [kWh]	30,960	30,960	31,680	30,960	33,120	33,931	32,164	32,486	31,125	32,474	32,427	31,680	383,966
Off-Peak Electricity Demand [kWh]	326,880	339,120	326,160	325,440	350,640	351,215	321,631	340,464	313,406	316,962	342,531	311,760	3,966,208
Total Electricity Demand [kWh]	357,840	370,080	357,840	356,400	383,760	385,145	353,795	372,949	344,531	349,436	374,957	343,440	4,350,174
Site#3													
Peak Electricity Demand [kWh]	16,800	15,600	16,800	15,600	16800	35,849	17,463	48,354	80,400	21,156	15,428	16,800	317,050
Off-Peak Electricity Demand [kWh]	224,400	207,600	220,800	211,200	228000	231,751	184,137	207,246	252,000	216,444	232,972	229,200	2,645,750
Total Electricity Demand [kWh]	241,200	223,200	237,600	226,800	244,800	267,600	201,600	255,600	332,400	237,600	248,400	246,000	2,962,800
Site#4													
Peak Electricity Demand [kWh]	28,290	29,520	29,520	29,520	28,800	30,750	35,670	33,210	29,520	34,440	28,290	30,750	368,280
Off-Peak Electricity Demand [kWh]	394,830	418,200	412,050	393,600	409,200	394,830	436,650	444,030	381,300	394,830	404,670	383,760	4,867,950
Total Electricity Demand [kWh]	423,120	447,720	441,570	423,120	438,000	425,580	472,320	477,240	410,820	429,270	432,960	414,510	5,236,230
Ceramic Industrial Park													
Peak Electricity Demand [kWh]	132,695	131,280	133,200	128,880	133,920	154,148	134,799	164,918	190,578	139,582	132,707	135,558	1,712,265
Off-Peak Electricity Demand [kWh]	1,800,558	1,836,120	1,784,610	1,760,640	1,880,640	1,899,732	1,777,330	1,880,940	1,773,170	1,768,428	1,884,541	1,743,840	21,790,548
Total Electricity Demand [kWh]	1,933,253	1,967,400	1,917,810	1,889,520	2,014,560	2,053,879	1,912,129	2,045,858	1,963,747	1,908,010	2,017,248	1,879,398	23,502,812

Table 10.5 – Monthly demand factor of the ceramics industrial park

	JAN	FEB	MAR	APR	MAY	JUN	JUL	AUG	SEP	OCT	NOV	DEC	Annual Average
Site#1													
Peak Demand Factor	0.83	0.86	0.86	0.85	0.86	0.97	0.92	0.87	0.86	0.96	0.92	0.90	0.89
Off-Peak Demand Factor	0.76	0 80	0.77	0 80	0.87	0.84	0.77	0.80	0.75	0.78	0.84	0.77	0.80
Site#2													
Peak Demand Factor	0.92	0.93	0.93	0.93	1.01	1.03	0.98	0.98	0.94	0.98	0.95	0.97	0.96
Off-Peak Demand Factor	0.95	0 97	0.93	0.96	1.03	1.04	0 95	1.01	0.92	0.93	1.01	0.90	0.97
Site#3													
Peak Demand Factor	0.72	0.69	0.77	0.80	0.80	0.72	0.69	0.68	0.98	0.66	0.73	0.74	0.75
Off-Peak Demand Factor	0.60	0.64	0.58	0 63	0 63	0.62	0.49	0.62	0.48	0.58	0 60	0 59	0 59
Site#4													
Peak Demand Factor	0.86	0.90	0.86	0.92	0.90	0.85	0.76	0.87	0.86	1.00	0.82	0.89	0.87
Off-Peak Demand Factor	0.74	0.76	0.76	0.74	0.77	0.73	0.79	0.80	0.71	0.82	0.75	0.71	0.76

Table 10.6 – Monthly electricity demand of the ceramics industrial park

	JAN	FEB	MAR	APR	MAY	JUN	JUL	AUG	SEP	OCT	NOV	DEC	Annual Average	Annual Minimum	Annual Maximum
Site#1															
Maximum Peak Power Demand [kW]	1,056	984	984	960	984	847	824	897	885	828	941	966	930	824	1,056
Maximum Off-Peak Power Demand [kW]	1,695	1,632	1,608	1,560	1,536	1,659	1,640	1,682	1,667	1,617	1,624	1,609	1,627	1,536	1,695
Maximum Power Demand [kW]	1,695	1,632	1,608	1,560	1,536	1,659	1,640	1,682	1,667	1,617	1,624	1,609	1,627	1,536	1,695
Average Peak Power Demand [kW]	876	846	846	816	846	821	758	780	761	794	866	869	823	758	876
Average Off-Peak Power Demand [kW]	1,288	1,306	1,238	1,248	1,336	1,393	1,263	1,346	1,250	1,261	1,364	1,239	1,294	1,238	1,393
Average Power Demand [kW]	1,237	1,248	1,189	1,194	1,275	1,322	1,199	1,275	1,189	1,203	1,302	1,193	1,235	1,189	1,322
Site#2															
Maximum Peak Power Demand [kW]	518	511	526	511	504	507	507	510	510	508	526	504	512	504	526
Maximum Off-Peak Power Demand [kW]	518	526	526	511	511	508	507	507	511	514	511	518	514	507	526
Maximum Power Demand [kW]	518	526	526	511	511	508	507	510	511	514	526	518	515	507	526
Average Peak Power Demand [kW]	477	475	489	475	509	522	497	500	479	498	499	489	492	475	522
Average Off-Peak Power Demand [kW]	492	510	489	491	527	528	482	512	470	478	516	467	497	467	528
Average Power Demand [kW]	491	506	489	489	524	527	483	510	471	481	514	469	496	469	527
Site#3															
Maximum Peak Power Demand [kW]	360	348	336	300	324	421	396	431	468	492	324	348	379	300	492
Maximum Off-Peak Power Demand [kW]	564	576	576	504	540	588	564	564	588	564	588	558	565	504	588
Maximum Power Demand [kW]	564	576	576	504	540	588	564	564	588	564	588	558	565	504	588
Average Peak Power Demand [kW]	259	240	259	240	259	303	273	293	459	325	237	258	284	237	459
Average Off-Peak Power Demand [kW]	338	369	334	318	340	365	276	350	282	327	353	329	332	276	369
Average Power Demand [kW]	329	353	325	308	330	357	276	343	304	327	338	320	326	276	357
Site#4															
Maximum Peak Power Demand [kW]	504	504	529	492	492	554	726	590	529	529	529	529	542	492	726
Maximum Off-Peak Power Demand [kW]	800	824	812	800	804	811	836	836	812	726	812	812	807	726	836
Maximum Power Demand [kW]	800	824	812	800	804	811	836	836	812	726	812	812	807	726	836
Average Peak Power Demand [kW]	434	454	455	453	443	470	552	514	455	529	434	471	472	434	552
Average Off-Peak Power Demand [kW]	592	626	617	592	619	592	661	669	576	595	609	576	610	576	669
Average Power Demand [kW]	572	605	597	574	597	577	647	650	561	587	587	563	593	561	650
Ceramic Industrial Park															
Maximum Peak Power Demand [kW]	2,439	2,348	2,375	2,263	2,304	2,328	2,452	2,428	2,392	2,357	2,319	2,347	2,363	2,263	2,452
Maximum Off-Peak Power Demand [kW]	3,577	3,558	3,521	3,375	3,391	3,565	3,547	3,589	3,578	3,420	3,535	3,497	3,513	3,375	3,589
Maximum Power Demand [kW]	3,577	3,558	3,521	3,375	3,391	3,565	3,547	3,589	3,578	3,420	3,535	3,497	3,513	3,375	3,589
Average Peak Power Demand [kW]	2,097	2,113	2,042	2,082	2,074	2,117	1,864	2,112	2,057	2,357	1,902	2,089	2,075	1,864	2,357
Average Off-Peak Power Demand [kW]	2,711	2,810	2,678	2,648	2,822	2,878	2,681	2,876	2,579	2,661	2,842	2,611	2,733	2,579	2,878
Average Power Demand [kW]	2,634	2,723	2,599	2,577	2,729	2,783	2,579	2,781	2,514	2,623	2,725	2,546	2,651	2,514	2,783

Table 10.7 – Average monthly energy demand of the ceramics industrial park

	Heating		Electricity	
MONTHS	**[kW]**	**[kWh]**	**[kW]**	**[kWh]**
JAN	4,497	904,921	2,634	1,933,253
FEB	4,125	761,372	2,723	1,967,400
MAR	4,589	942,598	2,599	1,917,810
APR	4,035	728,623	2,577	1,889,520
MAY	5,229	1,223,539	2,729	2,014,560
JUN	3,357	504,269	2,783	2,053,879
JUL	4,559	930,277	2,579	1,912,129
AUG	4,179	781,556	2,781	2,045,858
SEP	4,084	746,587	2,514	1,963,747
OCT	4,165	776,149	2,623	1,908,010
NOV	4,391	862,857	2,725	2,017,248
DEC	4,627	958,097	2,546	1,879,398
Maximum	5,229	1,223,539	2,783	2,053,879
Average	4,404	879,827	2,658	1,968,731

Table 10.8 – Typical summer hourly electricity demand of the ceramics industrial park

	Electricity [kW]		
	Average Production	High Production	Low Production
0	1,915	2,485	1,433
1	1,765	2,538	1,453
2	1,792	2,609	1,472
3	1,851	2,814	1,500
4	1,855	2,886	1,528
5	1,960	2,987	1,512
6	1,836	3,176	1,680
7	2,113	3,353	1,907
8	2,190	3,365	1,979
9	2,040	3,425	1,959
10	1,980	3,575	2,052
11	1,871	3,509	2,186
12	2,053	3,514	2,160
13	2,692	3,516	2,142
14	2,712	3,421	2,112
15	2,767	3,212	2,047
16	2,821	2,879	1,912
17	2,276	2,784	1,599
18	1,880	2,819	1,559
19	1,792	2,869	1,482
20	1,577	2,796	1,471
21	1,432	2,788	1,456
22	1,488	2,887	1,407
23	1,735	2,924	1,324
Average	2,016	3,047	1,722
Max	2,821	3,575	2,186

10.2 - Beverage Industries

Table 10.9 – Average monthly electricity demand and production of the beverage industry site 1

	Electricity		Demand Factor	Production
MONTHS	**[kW]**	**[kWh]**	**[-]**	**[m^3]**
JAN	3,362	2,501,668	0.764	21.25
FEB	3,347	2,249,268	0.761	18.61
MAR	2,853	2,122,497	0.648	19.96
APR	2,544	1,831,772	0.578	11.60
MAY	2,219	1,651,055	0.504	16.66
JUN	2,406	1,732,110	0.547	16.18
JUL	2,450	1,822,850	0.557	10.76
AUG	2,070	1,539,745	0.470	15.29
SEP	3,156	2,272,194	0.717	21.64
OCT	2,947	2,192,888	0.670	24.54
NOV	3,188	2,295,467	0.725	27.00
DEC	3,384	2,517,709	0.769	30.92
Total	-	24,729,223	-	234
Maximum	3,384	2,517,709	0.769	30.92
Average	2,827	2,060,769	0.643	19.53

Table 10.10 – Average monthly thermal demand and CO_2 production of the beverage industry site 1

	Heating		CO_2
MONTHS	**[kW]**	**[kWh]**	**[tons]**
JAN	6,817	5,071,820	501.46
FEB	5,378	3,613,892	476.30
MAR	6,462	4,807,948	445.16
APR	4,821	3,471,253	352.76
MAY	5,909	4,396,420	409.88
JUN	6,909	4,974,573	375.32
JUL	4,945	3,678,873	266.74
AUG	7,012	5,216,969	373.03
SEP	7,888	5,679,147	521.52
OCT	8,244	6,133,288	527.55
NOV	9,864	7,102,387	658.85
DEC	8,981	6,682,057	612.27
Total	-	60,828,628	5,521
Maximum	9,864	7,102,387	659
Average	6,936	5,069,052	460

Table 10.11 – Average monthly electricity demand and production of the beverage industry site 2

	Electricity		Demand Factor	Production
MONTHS	**[kW]**	**[kWh]**	**[-]**	**[m^3]**
JAN	5,752	4,279,228	0.710	55.22
FEB	5,570	3,743,355	0.688	47.84
MAR	5,126	3,813,578	0.633	47.55
APR	4,150	2,988,039	0.512	39.86
MAY	4,991	3,713,483	0.616	46.99
JUN	3,621	2,606,914	0.447	32.35
JUL	4,154	3,090,943	0.513	41.24
AUG	4,642	3,453,445	0.573	47.82
SEP	5,246	3,777,038	0.648	54.18
OCT	6,556	4,877,576	0.809	65.91
NOV	6,716	4,835,724	0.829	66.55
DEC	6,566	4,885,368	0.811	73.66
Total	-	46,064,691	-	619
Maximum	6,716	4,885,368	0.829	73.66
Average	5,258	3,838,724	0.649	51.60

Table 10.12 – Average monthly thermal demand, CO_2 production and water consumption of the beverage industry site 2

	Heating		CO2	Water
MONTHS	**[kW]**	**[kWh]**	**[tons]**	**[m3]**
JAN	12,326	9,170,825	940	321,742
FEB	11,462	7,702,208	722	298,499
MAR	11,060	8,229,006	721	271,116
APR	9,603	6,914,488	639	205,018
MAY	10,521	7,827,971	773	245,551
JUN	7,735	5,568,976	465	152,198
JUL	9,740	7,246,450	681	207,867
AUG	10,641	7,916,662	901	240,524
SEP	13,025	9,377,741	965	284,342
OCT	14,687	10,926,789	1,200	339,716
NOV	14,609	10,518,779	1,264	319,067
DEC	15,643	11,638,048	1,606	384,146
Total	-	103,037,942	10,878	3,269,786
Maximum	15,643	11,638,048	1,606	384,146
Average	11,754	8,586,495	906	272,482

Table 10.13 –Typical summer hourly electricity demand of the beverage industry park

Hour	Electricity Demand [kW]					
	Site 1			Site 2		
	Low Production	Average Production	High Production	Low Production	Average Production	High Production
0	2,760	3,185	3,281	5,626	6,333	6,762
1	2,832	3,152	3,575	5,789	6,289	6,489
2	2,813	3,123	3,418	5,746	6,345	6,653
3	3,093	3,189	3,282	5,877	6,460	6,612
4	2,733	3,178	3,424	5,566	6,268	6,694
5	2,721	3,427	3,807	5,539	6,228	6,639
6	2,830	3,477	3,661	5,585	6,045	6,183
7	2,456	3,409	3,855	5,530	6,065	6,543
8	2,427	3,383	3,737	5,464	6,096	6,680
9	2,356	3,196	3,613	5,304	6,259	7,199
10	2,339	3,600	3,862	5,266	6,069	6,844
11	2,265	3,497	3,792	5,100	5,933	6,256
12	2,088	3,592	3,820	4,701	6,316	7,991
13	2,335	2,950	3,934	5,257	6,605	7,978
14	2,453	3,065	3,774	5,523	6,662	7,800
15	2,437	3,220	3,936	5,487	7,001	7,295
16	2,727	3,182	3,640	5,540	7,114	8,060
17	2,931	3,092	3,724	5,599	7,280	7,896
18	2,072	2,716	3,808	4,765	6,990	7,492
19	3,216	3,481	3,701	4,932	6,492	7,241
20	2,714	3,087	3,784	4,959	5,617	6,110
21	2,568	2,969	3,794	5,109	5,514	5,782
22	2,578	3,028	3,620	5,300	5,617	5,803
23	3,022	3,144	3,309	5,724	6,351	6,804
Max	3,216	3,600	3,936	5,877	7,280	8,060
Total	62,765	77,342	88,151	129,287	151,950	165,802
Average	2,615	3,223	3,673	5,387	6,331	6,908

10.3 - Shopping Centre

Table 10.14 – Monthly ambient temperature in Southeastern Brazil

	Ambient Temperature		
	Average	Maximum	Minimum
MONTHS	[°C]	[°C]	[°C]
JAN	26.0	29.0	16.0
FEB	27.0	30.0	16.0
MAR	26.0	29.0	16.0
APR	24.0	28.0	15.0
MAY	23.0	27.0	14.0
JUN	22.0	25.0	12.0
JUL	21.0	26.0	11.0
AUG	22.0	26.0	12.0
SEP	22.0	25.0	12.0
OCT	23.0	26.0	13.0
NOV	24.0	27.0	15.0
DEC	25.0	29.0	15.0

Table 10.15 – Average monthly energy demand of the shopping centre

	Electricity		Demand Factor	Heating	
MONTHS	[kW]	[kWh]	[-]	[kW]	[kWh]
JAN	1,016	755,632	0.677	1,854	632,055
FEB	1,184	795,351	0.789	2,143	638,641
MAR	889	661,649	0.593	1,744	594,638
APR	1,013	729,632	0.676	1,785	587,112
MAY	1,003	746,561	0.669	1,164	348,022
JUN	1,068	769,261	0.712	1,284	545,732
JUL	889	661,518	0.593	1,380	425,105
AUG	966	718,596	0.644	1,156	408,193
SEP	936	673,873	0.624	1,173	451,430
OCT	929	691,132	0.619	1,563	533,099
NOV	1,000	719,687	0.666	1,540	545,025
DEC	990	736,350	0.660	1,605	619,631
Total	-	8,659,242	-	-	6,328,682
Maximum	1,184	795,351	0.789	2,143	638,641
Average	990	721,604	0.660	1,533	527,390

10.4 - International Airport

Table 10.16 – Monthly climatic conditions in Thessaloniki region

Month	Barometric Pressure	Average Air Temperature	Maximum Air Temperature	Minimum Air Temperature	Sunlight	Relative Humidity	Average Cloudiness
	mmHg	[°C]	[°C]	[°C]	h	%	%
1	1019.1	5.2	20.8	-14.0	91.6	76.1	4.7
2	1017.9	6.7	23.2	-12.8	94.8	73.0	4.8
3	1016.6	9.7	25.8	-7.2	150.2	72.4	4.9
4	1013.3	14.2	31.2	-1.2	203.5	67.8	4.4
5	1013.9	19.6	36.0	3.0	267.2	63.8	4.1
6	1013.1	24.4	39.8	6.8	288.6	55.9	3.2
7	1012.8	26.6	42.0	9.6	320.4	53.2	2.2
8	1013.4	26.0	40.4	8.2	263.8	55.3	2.1
9	1016.4	21.8	36.2	2.6	221.0	62.0	2.7
10	1018.9	16.2	31.6	-1.4	161.8	70.2	3.9
11	1018.6	11.0	26.6	-6.2	121.0	76.8	4.7
12	1018.1	6.9	22.6	-9.2	102.9	78.0	4.8

Table 10.17 – Operation hours of the heating system for a typical day

Months	1	2	3	4	5	6	7	8	9	10	11	12
Operation hours per day	18	16	11	6	1,5	0,1	0,1	0,1	1	6	7	15

Table 10.18 – Average monthly energy demand and production of the international airport

	Electricity		Demand Factor	Heating	
MONTHS	[kW]	[kWh]	[-]	[kW]	[kWh]
JAN	2,602	1,935,888	0.437	6,750	5,022,000
FEB	2,889	1,941,408	0.485	6,000	4,032,000
MAR	3,759	2,796,696	0.631	4,125	3,069,000
APR	4,140	2,980,560	0.695	2,250	1,620,000
MAY	4,596	3,419,424	0.772	563	418,872
JUN	4,964	3,574,320	0.833	38	27,360
JUL	4,953	3,684,784	0.831	38	28,272
AUG	4,954	3,685,528	0.832	38	28,272
SEP	4,721	3,398,880	0.792	375	270,000
OCT	4,197	3,122,568	0.705	2,250	1,674,000
NOV	3,735	2,689,440	0.627	2,625	1,890,000
DEC	2,922	2,173,720	0.490	5,625	4,185,000
Total	-	35,403,216	-	-	22,264,776
Maximum	4,964	3,685,528	0.833	6,750	5,022,000
Average	4,036	2,950,268	0.677	2,556	1,855,398

10.5 - Hotel Building Complex

Table 10.19 – Average monthly occupancy of the hotel building complex

MONTHS	Overnight Ocuppancy [%]			
	Site#1	Site#2	Site#3	Average
JAN	0.0%	0.0%	0.0%	0.0%
FEB	0.0%	0.0%	0.0%	0.0%
MAR	0.0%	4.0%	0.0%	1.3%
APR	4.0%	14.0%	0.0%	6.0%
MAY	13.0%	17.0%	9.0%	13.0%
JUN	18.0%	20.0%	20.0%	19.3%
JUL	20.0%	20.0%	23.0%	21.0%
AUG	21.0%	15.0%	23.0%	19.7%
SEP	15.0%	10.0%	18.0%	14.3%
OCT	9.0%	4.0%	8.0%	7.0%
NOV	0.0%	0.0%	0.0%	0.0%
DEC	0.0%	0.0%	0.0%	0.0%
Maximum	21.0%	20.0%	23.0%	21.0%
Average	8.3%	8.7%	8.4%	8.5%

Table 10.20 – Average monthly electricity demand of the hotel building complex

MONTHS	Electricity [kW]				Demand Factor [-]	[kWh]			
	Site#1	Site#2	Site#3	Total		Site#1	Site#2	Site#3	Total
JAN	102.5	63.6	27.4	193.5	0.087	58,663	36,373	15,707	110,743
FEB	85.2	59.2	33.2	177.7	0.080	44,055	30,613	17,173	91,842
MAR	71.2	99.7	30.3	201.2	0.091	40,726	57,040	17,360	115,126
APR	223.4	180.6	23.8	427.8	0.193	123,754	100,000	13,200	236,954
MAY	503.5	252.8	67.9	824.2	0.371	288,180	144,667	38,853	471,700
JUN	602.6	284.6	275.9	1,163.1	0.524	333,763	157,600	152,800	644,163
JUL	797.9	408.8	382.8	1,589.5	0.716	456,642	233,947	219,067	909,656
AUG	888.2	509.9	452.1	1,850.2	0.833	508,319	291,813	258,747	1,058,879
SEP	829.2	444.9	394.3	1,668.4	0.751	459,255	246,400	218,400	924,055
OCT	640.8	303.3	178.8	1,122.9	0.506	366,725	173,600	102,300	642,625
NOV	273.0	174.8	39.0	486.8	0.219	151,194	96,800	21,600	269,594
DEC	73.8	65.0	21.7	160.5	0 072	42,261	37,200	12,400	91,861
Total	-	-	-	-	-	2,873,538	1,606,053	1,087,607	5,567,198
Maximum	888	510	452	1,850	0.833	508,319	291,813	258,747	1,058,879
Average	424	237	161	822	0.370	239,462	133,838	90,634	463,933

Table 10.21 – Average monthly thermal demand of the hotel building complex

MONTHS	Heating							
	[kW]				[kWh]			
	Site#1	Site#2	Site#3	Total	Site#1	Site#2	Site#3	Total
JAN	1.7	0.6	0.9	3.16	413	334	162	909
FEB	1.7	0.6	0.9	3.14	370	299	146	815
MAR	1.7	0.6	0.9	3.14	409	331	162	902
APR	156.6	68.3	0.9	225.81	56,380	45,540	157	102,077
MAY	206.2	89.9	65.1	361.19	76,693	61,948	58,041	196,683
JUN	190.9	83.5	55.6	330.02	68,727	55,669	54,491	178,888
JUL	209.4	114.5	70.7	394.56	77,896	63,096	59,058	200,050
AUG	249.0	136.1	102.9	488.01	92,614	75,018	64,946	232,578
SEP	198.0	108.0	58.6	364.50	71,277	57,574	55,013	183,864
OCT	149.0	81.3	42.7	273.00	55,433	44,817	27,215	127,465
NOV	1.6	0.6	0.9	3.11	392	317	156	865
DEC	1.7	0.6	0.9	3.16	413	334	162	909
Total	-	-	-	-	501,019	405,276	319,710	1,226,005
Maximum	249	136	103	488	92,614.256	75,018	64,946	232,578
Average	114	57	33	204	41,751.584	33,773	26,643	102,167

10.6 - Mediterranean Island

Table 10.22 – Monthly climatic conditions in Northern Aegean Sea region

Month	Barometric Pressure	Average Air Temperature	Maximum Air Temperature	Minimum Air Temperature	Sunlight	Relative Humidity	Average Cloudiness
	mmHg	[°C]	[°C]	[°C]	h	%	%
1	1019.4	7.4	18.8	-5.2	82.0	76.8	4.8
2	1018.3	7.7	19.0	-5.8	110.7	74.8	4.7
3	1016.8	9.7	22.0	-6.0	162.1	75.1	4.1
4	1013.6	13.6	25.8	0.0	221.7	73.8	3.5
5	1014.0	18.4	31.0	3.0	294.4	68.7	2.9
6	1012.8	23.4	34.4	3.4	326.7	60.4	1.8
7	1012.6	25.6	39.4	12.0	344.7	57.2	0.9
8	1013.1	24.9	35.8	12.0	338.4	61.7	0.9
9	1016.1	21.4	32.8	8.2	264.9	66.3	1.5
10	1018.5	16.7	31.8	1.6	197.8	73.2	3.0
11	1018.8	12.2	24.0	-2.0	127.6	77.8	4.4
12	1018.4	9.2	19.2	-3.6	94.6	78.6	4.8

Table 10.23 – Monthly energy demand of the Mediterranean island

	Electricity		Demand Factor	Heating	
MONTHS	[kW]	[kWh]	[-]	[kW]	[kWh]
JAN	6,063	4,510,565	0.548	4,547	3,382,924
FEB	6,070	4,078,727	0.548	3,278	2,202,513
MAR	6,244	4,645,296	0.564	2,997	2,229,742
APR	5,578	4,016,070	0.504	2,008	1,445,785
MAY	5,130	3,816,432	0.464	2,001	1,488,408
JUN	5,998	4,318,411	0.542	360	259,105
JUL	7,623	5,671,677	0.689	457	340,301
AUG	8,198	6,098,961	0.741	738	548,906
SEP	5,885	4,236,875	0.532	1,059	762,638
OCT	5,414	4,027,754	0.489	2,599	1,933,322
NOV	5,568	4,008,751	0.503	3,341	2,405,251
DEC	6,490	4,828,548	0.586	5,062	3,766,267
Maximum	8,198	6,098,961	0.741	5,062	3,766,267
Average	6,188	4,521,506	0.559	2,370	1,730,430

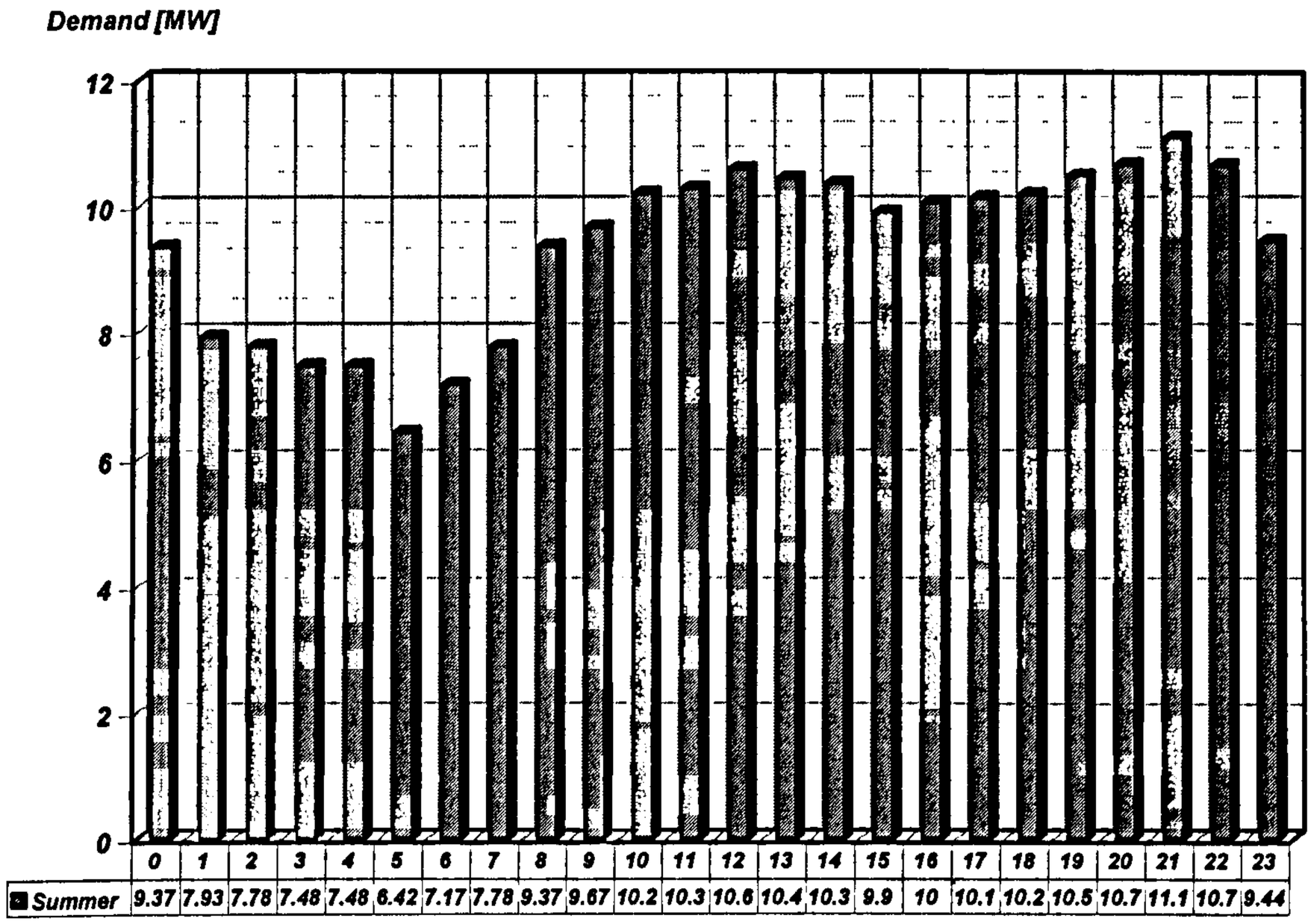

	0	1	2	3	4	5	6	7	8	9	10	11	12	13	14	15	16	17	18	19	20	21	22	23
Summer	9.37	7.93	7.78	7.48	7.48	6.42	7.17	7.78	9.37	9.67	10.2	10.3	10.6	10.4	10.3	9.9	10	10.1	10.2	10.5	10.7	11.1	10.7	9.44

Figure 10.1 – Typical summer hourly electricity demand of the Mediterranean island

10.7 - Resort Hotel

Table 10.24 – Monthly climatic conditions in southeastern Mediterranean region

	Barometric Pressure	Average Air Temperature	Maximum Air Temperature	Minimum Air Temperature	Sunlight	Relative Humidity	Average Cloudiness
Month	mmHg	[°C]	[°C]	[°C]	h	%	%
1	1015.7	12.9	24.9	0.8	110.3	69	5.6
2	1014.8	13.1	25.4	2	132.2	67	5.3
3	1013.4	14.4	28.5	3	157	65	4.6
4	1012	19	33.2	5.4	218	64	3.8
5	1011.7	20.7	37	9.8	300	64	2.7
6	1009.8	24.9	37.5	13.6	335	61	1.6
7	1006.9	26.8	41.4	15	373.1	60	0.9
8	1007.5	26.9	39.3	16.4	350.2	61	1
9	1011.4	24.3	38	13.6	263.7	64	2.4
10	1014.7	20.8	35	8.8	166.1	67	4.1
11	1016.4	17.9	30.5	6.8	165.8	68	4.3
12	1015.8	14.8	28	2.4	112.9	67	5.3

Table 10.25 – Average monthly energy demand of the resort hotel

	Electricity		Demand Factor	Heating	
MONTHS	[kW]	[kWh]	[-]	[kW]	[kWh]
JAN	4	2,893	0.039	0.0	0
FEB	4	2,700	0.037	0.0	0
MAR	15	10,575	0.144	15.5	11,139
APR	40	28,689	0.392	37.6	27,083
MAY	48	34,714	0.473	42.4	30,516
JUN	66	47,700	0.650	30.9	22,278
JUL	76	54,871	0.748	24.6	17,729
AUG	85	61,100	0.833	28.4	20,475
SEP	82	58,673	0.800	27.9	20,063
OCT	48	34,525	0.470	18.3	13,198
NOV	17	12,302	0.168	0.0	0
DEC	3	1,953	0.027	0.0	0
Total	-	350,695	-	-	162,481
Maximum	85	61,100	0.833	42	30,516
Average	41	29,225	0.398	19	13,540

10.8 - CHP Off-design Performance

Table 10.26 – CHP Unit#1 International Airport: Monthly Performance

	AT [°C]	SPO [kW]	FMF [kg/s]	TMF [kg/s]	TEff [%]	TET [°C]	TEP [Pa]	ET [°C]	TC [kW]	TD [kW]	STC [kW]	DTC [kW]	EPO [kW]	PD [kW]	SP [kW]	DP [kW]	TCHPEff [%]
JAN	5.2	5,300	0.3113	21.176	32.7	1,276	12,590	761	6,546	6,750	0	204	5,247	2,602	2,645	0	72.8
FEB	6.7	5,300	0.3113	21.176	32.7	1,276	12,590	761	6,546	6,000	546	0	5,247	2,889	2,358	0	72.8
MAR	9.7	5,300	0.3113	21.176	32.7	1,276	12,590	761	6,546	4,125	2,421	0	5,247	3,759	1,488	0	72.8
APR	14.2	5,300	0.3113	21.176	32.7	1,276	12,590	761	6,546	2,250	4,296	0	5,247	4,140	1,107	0	72.8
MAY	19.6	5,116	0.3035	20.788	32.4	1,276	12,382	764	6,478	563	5,915	0	5,065	4,596	469	0	73.1
JUN	24.4	4,930	0.2956	20.396	32.1	1,276	12,171	768	6,425	38	6,387	0	4,881	4,964	0	83	73.6
JUL	26.6	4,831	0.2921	20.221	31.8	1,276	12,076	770	6,404	38	6,366	0	4,782	4,953	0	171	73.7
AUG	26.0	4,872	0.2930	20.268	32.0	1,276	12,102	769	6,401	38	6,363	0	4,823	4,954	0	131	73.7
SEP	21.8	5,022	0.2998	20.606	32.2	1,276	12,285	766	6,456	375	6,081	0	4,972	4,721	251	0	73.3
OCT	16.2	5,242	0.3093	21.074	32.6	1,276	12,536	762	6,532	2,250	4,282	0	5,190	4,197	993	0	72.9
NOV	11.0	5,306	0.3113	21.176	32.8	1,276	12,591	761	6,546	2,625	3,921	0	5,253	3,735	1,518	0	72.9
DEC	6 9	5,306	0 3113	21 176	32 8	1,276	12,591	761	6,546	5,625	921	0	5,253	2,922	2,331	0	72 9

Table 10.27 – CHP Unit#2 Mediterranean Island: Monthly Performance

	AT [°C]	SPO [kW]	FMF [kg/s]	TMF [kg/s]	TEff [%]	TET [°C]	TEP [Pa]	ET [°C]	TC [kW]	TD [kW]	STC [kW]	DTC [kW]	EPO [kW]	PD [kW]	SP [kW]	DP [kW]	TCHPEff [%]
JAN	7.4	11,690	0.6899	47.734	32.6	1,288	14,456	755	14,515	4,530	9,985	0	11,573	6,040	5,533	0	72.7
FEB	7.7	11,690	0.6899	47.734	32.6	1,288	14,456	755	14,515	2,851	11,664	0	11,573	5,280	6,293	0	72.7
MAR	9.7	11,690	0.6899	47.734	32.6	1,288	14,456	755	14,515	2,573	11,942	0	11,573	5,360	6,213	0	72.7
APR	13.6	11,690	0.6899	47.734	32.6	1,288	14,456	755	14,515	1,994	12,521	0	11,573	5,540	6,033	0	72.7
MAY	18.4	11,379	0.6771	47.086	32.3	1,288	14,268	757	14,397	2,071	12,326	0	11,265	5,310	5,955	0	72.9
JUN	23.4	11,021	0.6588	46.160	32.2	1,288	14,003	759	14,191	345	13,846	0	10,911	5,750	5,161	0	73.3
JUL	25.6	10,813	0.6509	45.763	31.9	1,288	13,888	761	14,146	446	13,700	0	10,705	7,430	3,275	0	73.4
AUG	24.9	10,910	0.6534	45 889	32.1	1,288	13,924	760	14,147	721	13,426	0	10,801	8,010	2,791	0	73.4
SEP	21.4	11,166	0.6660	46.527	32.2	1,288	14,108	758	14,265	1,037	13,228	0	11,054	5,760	5,294	0	73.1
OCT	16.7	11,545	0.6835	47.408	32.5	1,288	14,361	756	14,456	2,462	11,994	0	11,430	5,130	6,300	0	72.8
NOV	12.2	11,724	0.6900	47.735	32.7	1,288	14,455	754	14,475	3,060	11,415	0	11,607	5,100	6,507	0	72.7
DEC	9 2	11,724	0 6900	47 735	32 7	1,288	14,455	754	14,475	4,688	9,787	0	11,607	6,010	5,597	0	72 7

Table 10.28 – CHP Unit#3 Hotel Building Complex: Monthly Performance

	AT [°C]	SPO [kW]	FMF [kg/s]	TMF [kg/s]	TEff [%]	TET [°C]	TEP [Pa]	ET [°C]	TC [kW]	TD [kW]	STC [kW]	DTC [kW]	EPO [kW]	PD [kW]	SP [kW]	DP [kW]	TCHPEff [%]
JAN	5.2	3,515	0.2416	18.982	27.9	1,184	11,658	729.94	6,648	2	6,646	0	3,480	159	3,321	0	80.6
FEB	6.7	3,515	0.2416	18.982	27.9	1,184	11,658	729.94	6,648	2	6,646	0	3,480	185	3,295	0	80.6
MAR	9.7	3,515	0.2416	18.982	27.9	1,184	11,658	729.94	6,648	57	6,591	0	3,480	234	3,246	0	80.6
APR	14.2	3,515	0.2416	18.982	27.9	1,184	11,658	729.94	6,648	150	6,498	0	3,480	404	3,076	0	80.6
MAY	19.6	3,407	0.2354	18.635	27.8	1,184	11,460	731.76	6,562	418	6,145	0	3,373	903	2,470	0	81.2
JUN	24.4	3,283	0.2290	18.284	27.5	1,184	11,261	734.28	6,486	391	6,095	0	3,250	1,182	2,068	0	81.8
JUL	26.6	3,203	0.2262	18.127	27.2	1,184	11,174	736.62	6,475	427	6,047	0	3,171	1,323	1,848	0	82.0
AUG	26.0	3,243	0.2270	18.169	27.4	1,184	11,197	735	6,461	508	5,952	0	3,211	1,761	1,450	0	81.9
SEP	21.8	3,334	0.2324	18.472	27.5	1,184	11,369	733.65	6,541	398	6,143	0	3,301	1,330	1,971	0	81.4
OCT	16.2	3,478	0.2400	18.890	27.8	1,184	11,604	730.88	6,635	297	6,337	0	3,443	1,136	2,307	0	80.8
NOV	11.0	3,536	0.2416	18.982	28.1	1,184	11,655	729 01	6,630	213	6,417	0	3,501	774	2,727	0	80.6
DEC	6 9	3,536	0 2416	18 982	28 1	1,184	11,655	729 01	6,630	2	6,628	0	3,501	258	3,243	0	80.6

Table 10.29 – CHP Unit#4 Ceramics Industry: Monthly Performance

	AT	SPO	FMF	TMF	TEff	TET	TEP	ET	TC	TD	STC	DTC	EPO	PD	SP	DP	TCHPEff
	[°C]	[kW]	[kg/s]	[kg/s]	[%]	[°C]	[Pa]	[°C]	[kW]	[kW]	[kW]	[kW]	[kW]	[kW]	[kW]	[kW]	[%]
JAN	26.0	4,028	0.2614	17.541	29.6	1,290	11,823	798	7,385	4,497	2,888	0	3,988	2,740	1,248	0	83.7
FEB	25.0	4,053	0 2628	17.610	29.7	1,290	11,865	798	7,414	4,125	3,289	0	4,013	2,951	1,062	0	83.6
MAR	28.0	3,965	0.2586	17.405	29.5	1,290	11,740	800	7,364	4,589	2,775	0	3,925	2,930	995	0	83.9
APR	26.0	4,032	0.2614	17.541	29.7	1,290	11,823	798	7,385	4,035	3,350	0	3,991	2,795	1,196	0	83.7
MAY	27.0	3,982	0.2600	17.472	29.4	1,290	11,782	800	7,392	5,229	2,163	0	3,942	2,799	1,143	0	83.8
JUN	26.0	4,028	0.2614	17.541	29.6	1,290	11,823	798	7,385	3,357	4,028	0	3,988	2,927	1,061	0	83.7
JUL	24.0	4,090	0.2643	17.679	29 8	1,290	11,909	797	7,424	4,559	2,865	0	4,049	2,724	1,325	0	83.5
AUG	26.0	4,005	0.2614	17.541	29.5	1,290	11,824	799	7,403	4,179	3,224	0	3,965	2,840	1,125	0	83.6
SEP	28.0	3,952	0.2586	17.405	29.4	1,290	11,740	800	7,364	4,084	3,280	0	3,913	2,715	1,198	0	83.8
OCT	28.0	3,952	0.2586	17.405	29.4	1,290	11,740	800	7,364	4,165	3,199	0	3,913	2,807	1,106	0	83.8
NOV	27.0	3,999	0.2600	17.472	29 6	1,290	11,781	799	7,374	4,391	2,983	0	3,959	2,895	1,064	0	83 8
DEC	24 0	4,074	0 2643	17 679	29 6	1,290	11,909	798	7,443	4,627	2,816	0	4,034	2,768	1,266	0	83.5

Table 10.30 – CHP Unit#5 Beverage Industry Site 1: Monthly Performance

	AT	SPO	FMF	TMF	TEff	TET	TEP	ET	TC	TD	STC	DTC	EPO	PD	SP	DP	TCHPEff
	[°C]	[kW]	[kg/s]	[kg/s]	[%]	[°C]	[Pa]	[°C]	[kW]	[kW]	[kW]	[kW]	[kW]	[kW]	[kW]	[kW]	[%]
JAN	26.0	4,872	0.2930	20.268	32.0	1,276	12,102	769	6,401	6,817	0	416	4,823	3,362	1,461	0	73.7
FEB	25.0	4,909	0.2946	20.348	32.0	1,276	12,145	768	6,410	5,378	1,032	0	4,860	3,347	1,513	0	73.6
MAR	28.0	4,774	0.2898	20.110	31.7	1,276	12,016	771	6,385	6,462	0	77	4,727	3,853	874	0	73.7
APR	26.0	4,882	0.2930	20 268	32.0	1,276	12,102	768	6,384	4,821	1,563	0	4,833	2,544	2,289	0	73.6
MAY	27.0	4,821	0.2914	20.189	31.8	1,276	12,059	770	6,393	5,909	484	0	4,772	2,219	2,553	0	73.7
JUN	26.0	4,874	0.2930	20.268	32.0	1,276	12,102	768	6,384	6,909	0	525	4,825	2,406	2,419	0	73.6
JUL	24.0	4,953	0.2962	20.428	32.2	1,276	12,189	767	6,418	4,945	1,473	0	4,904	2,450	2,454	0	73.5
AUG	26.0	4,853	0.2930	20.268	31.9	1,276	12,102	769	6,401	7,012	0	611	4,805	2,070	2,735	0	73.5
SEP	28.0	4,782	0.2898	20.110	31.7	1,276	12,016	771	6,385	7,888	0	1503	4,734	3,156	1,578	0	73 8
OCT	28.0	4,782	0.2898	20.110	31.7	1,276	12,016	771	6,385	8,244	0	1859	4,734	2,947	1,787	0	73.8
NOV	27.0	4,837	0.2914	20.189	31.9	1,276	12,060	769	6,376	9,864	0	3488	4,788	3,188	1,600	0	73.7
DEC	24 0	4,960	0 2962	20 428	32 2	1,276	12,189	767	6,418	8,981	0	2563	4,910	3,384	1,526	0	73 5

Table 10.31 – CHP Unit#6 Beverage Industry Site 2: Monthly Performance

	AT	SPO	FMF	TMF	TEff	TET	TEP	ET	TC	TD	STC	DTC	EPO	PD	SP	DP	TCHPEff
	[°C]	[kW]	[kg/s]	[kg/s]	[%]	[°C]	[Pa]	[°C]	[kW]	[kW]	[kW]	[kW]	[kW]	[kW]	[kW]	[kW]	[%]
JAN	26.0	10,824	0.6494	45.692	32.1	1,288	13,869	761	14,124	12,326	1,798	0	10,716	5,757	4,959	0	73.6
FEB	25.0	10,899	0.6530	45.871	32.1	1,288	13,919	760	14,141	11,462	2,679	0	10,790	5,570	5,220	0	73.4
MAR	28.0	10,618	0.6424	45.337	31.8	1,288	13,765	763	14,091	11,060	3,031	0	10,512	5,126	5,386	0	73.6
APR	26.0	10,844	0.6495	45 692	32.1	1,288	13,869	760	14,086	9,603	4,483	0	10,736	4,150	6,586	0	73.5
MAY	27.0	10,715	0.6459	45.514	31.9	1,288	13,816	762	14,108	10,521	3,587	0	10,608	4,991	5,617	0	73.6
JUN	26.0	10,826	0.6495	45.692	32.1	1,288	13,868	761	14,124	7,735	6,389	0	10,718	3,621	7,097	0	73.6
JUL	24.0	10,991	0.6566	46.051	32.2	1,288	13,972	759	14,158	9,740	4,418	0	10,881	4,154	6,727	0	73.3
AUG	26.0	10,782	0.6495	45.692	31.9	1,288	13,868	762	14,163	10,641	3,522	0	10,674	4,642	6,032	0	73.5
SEP	28.0	10,636	0.6424	45.337	31.8	1,288	13,765	763	14,091	13,025	1,066	0	10,530	5,246	5,284	0	73.7
OCT	28.0	10,636	0.6424	45.337	31.8	1,288	13,765	763	14,091	14,687	0	596	10,530	6,556	3,974	0	73.7
NOV	27.0	10,749	0.6459	45.514	32.0	1,288	13,817	762	14,108	14,609	0	501	10,642	6,716	3,926	0	73.7
DEC	24 0	11,004	0 6566	46 051	32.2	1,288	13,972	759	14,158	15,643	0	1485	10,894	6,566	4,328	0	73 4

Table 10.32 – CHP Unit#7 Shopping Centre: Monthly Performance

	AT [°C]	SPO [kW]	FMF [kg/s]	TMF [kg/s]	TEff [%]	TET [°C]	TEP [Pa]	ET [°C]	TC [kW]	TD [kW]	STC [kW]	DTC [kW]	EPO [kW]	PD [kW]	SP [kW]	DP [kW]	TCHPEff [%]
JAN	26.0	1,708	0.1208	8.710	27.2	1,200	8,547	782	3,522	1,632	1,890	0	1,691	811	880	0	83.0
FEB	27.0	1,682	0.1202	8.678	26.9	1,200	8,521	784	3,527	1,806	1,721	0	1,665	951	714	0	83.1
MAR	26.0	1,706	0.1208	8.709	27.2	1,200	8,548	782	3,522	1,280	2,242	0	1,689	785	904	0	82.9
APR	24.0	1,733	0.1221	8.772	27.3	1,200	8,602	781	3,538	1,703	1,835	0	1,716	872	844	0	82.7
MAY	23.0	1,733	0.1228	8 806	27.1	1,200	8,624	782	3,561	1,029	2,532	0	1,716	777	939	0	82.6
JUN	22.0	1,760	0.1234	8.835	27.4	1,200	8,658	780	3,554	1,279	2,275	0	1,743	849	894	0	82.5
JUL	21.0	1,760	0.1241	8.870	27.3	1,200	8,680	781	3,578	1,193	2,385	0	1,743	717	1,026	0	82.4
AUG	22.0	1,760	0.1234	8.835	27.4	1,200	8,658	780	3,554	1,077	2,477	0	1,743	775	968	0	82.5
SEP	22.0	1,760	0.1234	8.835	27.4	1,200	8,658	780	3,554	1,250	2,304	0	1,743	836	907	0	82.5
OCT	23.0	1,736	0.1227	8.803	27.2	1,200	8,631	781	3,550	1,303	2,247	0	1,718	841	877	0	82.6
NOV	24.0	1,725	0.1221	8.771	27.2	1,200	8,603	782	3,547	1,490	2,057	0	1,708	909	799	0	82.8
DEC	25 0	1,711	0.1215	8 740	27.1	1,200	8,576	782	3,534	1,559	1,975	0	1,694	857	837	0	82 8

Table 10.33 – CHP Unit#8 Resort Hotel: Monthly Performance

	AT [°C]	SPO [kW]	FMF [kg/s]	TMF [kg/s]	TEff [%]	TET [°C]	TEP [Pa]	ET [°C]	TC [kW]	TD [kW]	STC [kW]	DTC [kW]	EPO [kW]	PD [kW]	SP [kW]	DP [kW]	TCHPEff [%]
JAN	12.9	200	0.0133	1.686	28.8	1,203	4,613	565	301	0	301	0	198	4	194	0	72.1
FEB	13.1	200	0.0133	1.686	28.8	1,203	4,613	565	301	0	301	0	198	4	194	0	72.1
MAR	14.4	200	0.0133	1.686	28.8	1,203	4,613	565	301	16	286	0	198	15	183	0	72.1
APR	19.0	195	0.0133	1.686	28.2	1,203	4,613	571	312	38	274	0	193	40	153	0	73.1
MAY	20.7	193	0.0133	1.686	27.9	1,203	4,613	573	315	42	273	0	191	48	143	0	73.4
JUN	24.9	188	0.0132	1.686	27.2	1,203	4,613	579	326	31	295	0	186	66	120	0	74.3
JUL	26.8	186	0.0132	1.686	26.9	1,203	4,613	582	331	25	307	0	184	76	108	0	74.9
AUG	26.9	186	0.0132	1.686	26.9	1,203	4,613	582	331	28	303	0	184	85	99	0	74 8
SEP	24.3	189	0.0133	1.686	27.3	1,203	4,613	578	324	28	296	0	187	82	105	0	74.0
OCT	20.8	193	0.0133	1.686	27.9	1,203	4,613	574	317	18	299	0	191	48	143	0	73.5
NOV	17.9	197	0.0133	1.686	28.3	1,203	4,613	570	310	0	310	0	195	17	178	0	72.8
DEC	14 8	200	0 0133	1 686	28 8	1,203	4,613	565	301	0	301	0	198	3	195	0	72 1

Chapter 11 – Appendix B Gas Turbine Portfolio: Degraded Performance and Diagnostic Analysis

11 - Appendix B Gas Turbine Portfolio: Degraded Performance and Diagnostic Analysis

11.1 - Degraded Performance

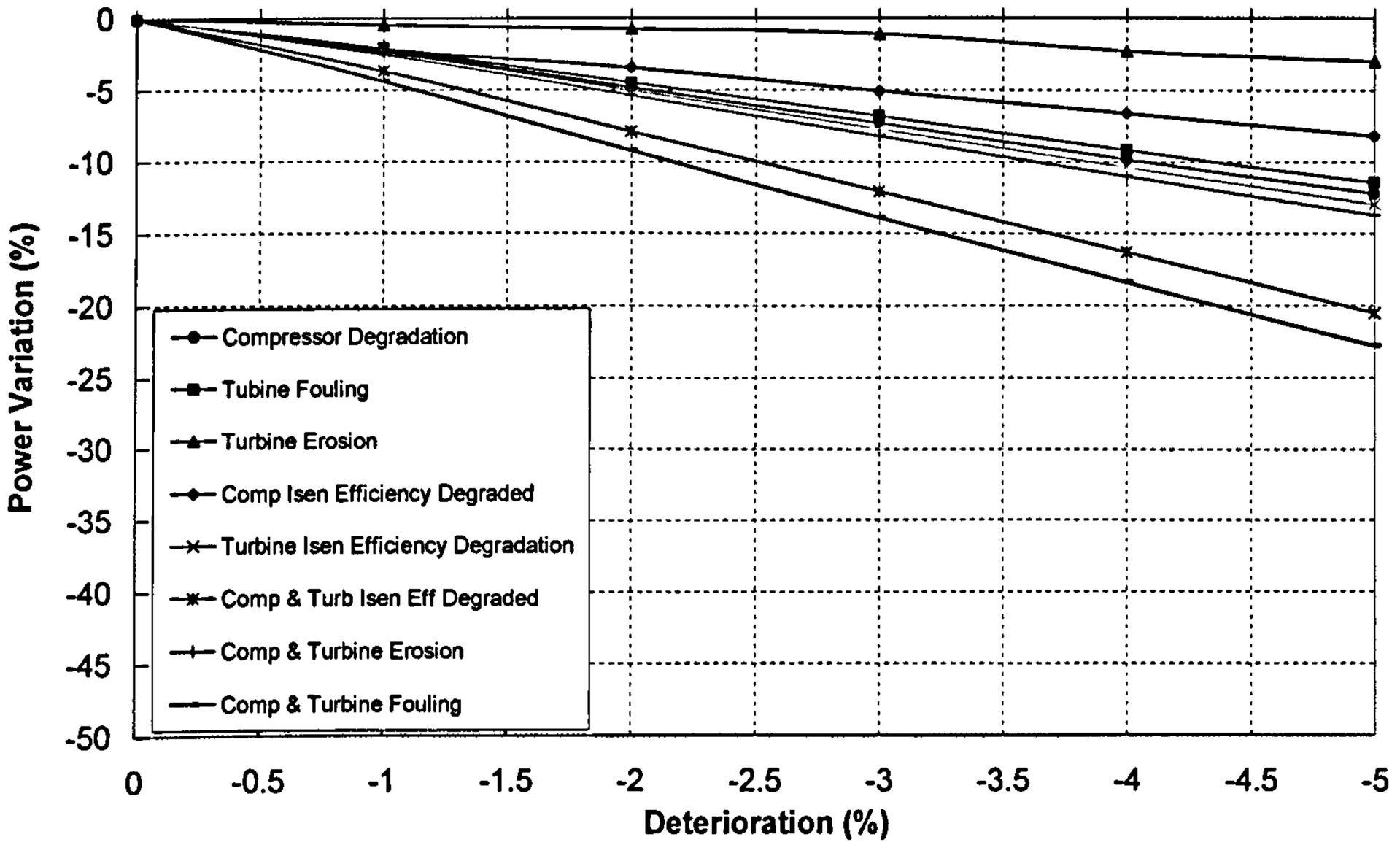

Figure 11.1 - Degradation Effect on GTM#1 power

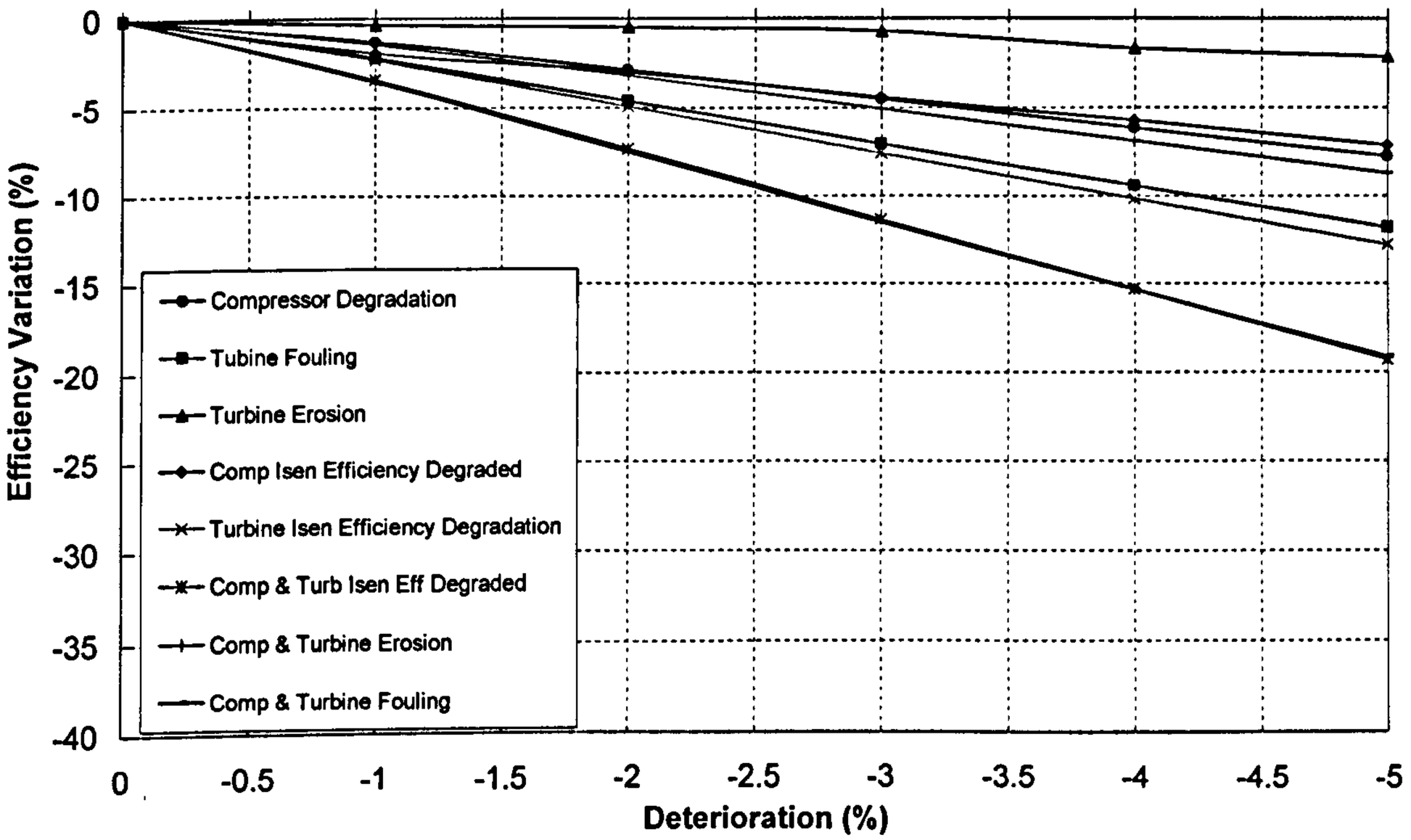

Figure 11.2 - Degradation Effect on GTM#1 efficiency

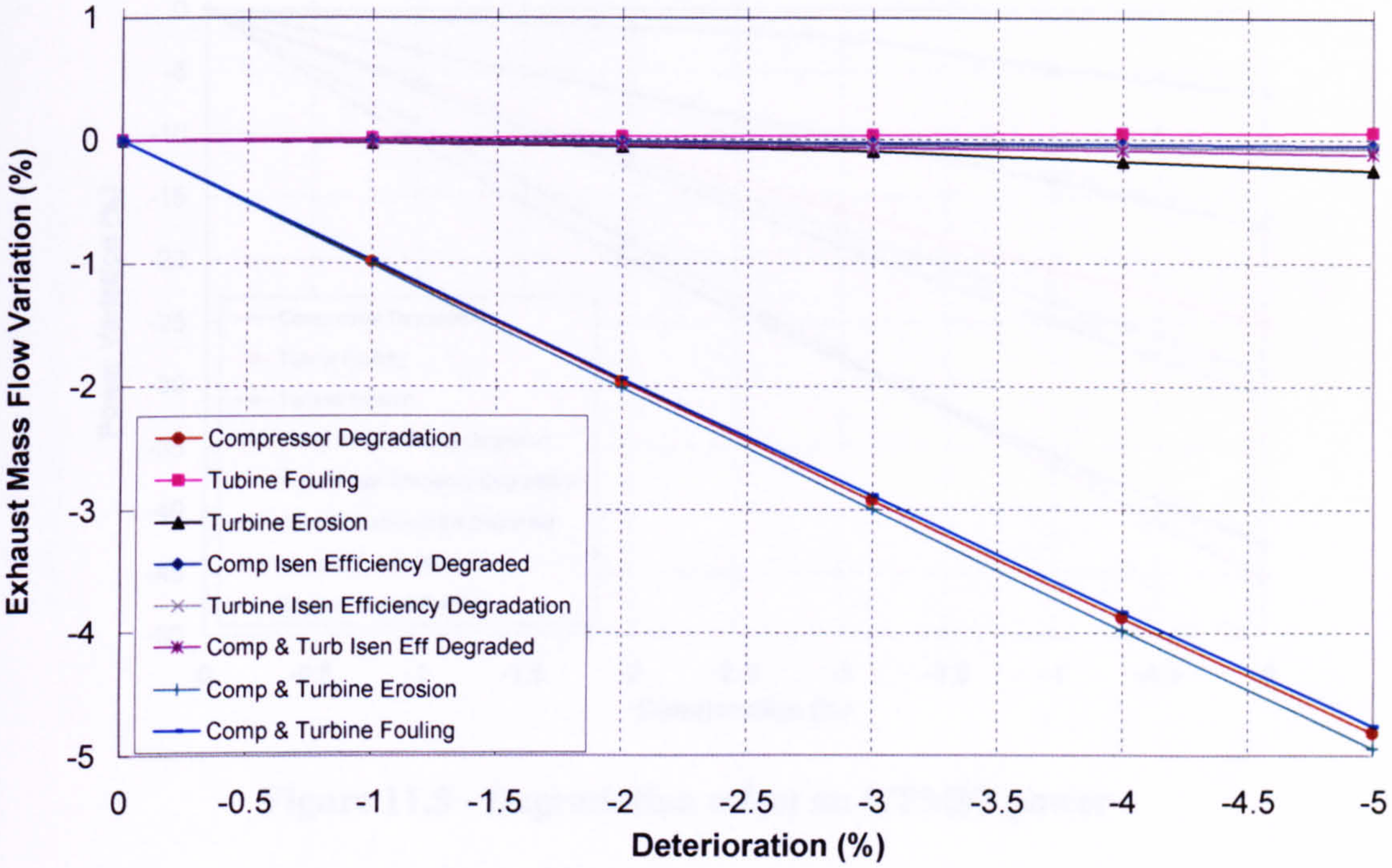

Figure 11.3 - Degradation effect on GTM#1 exhaust mass flow

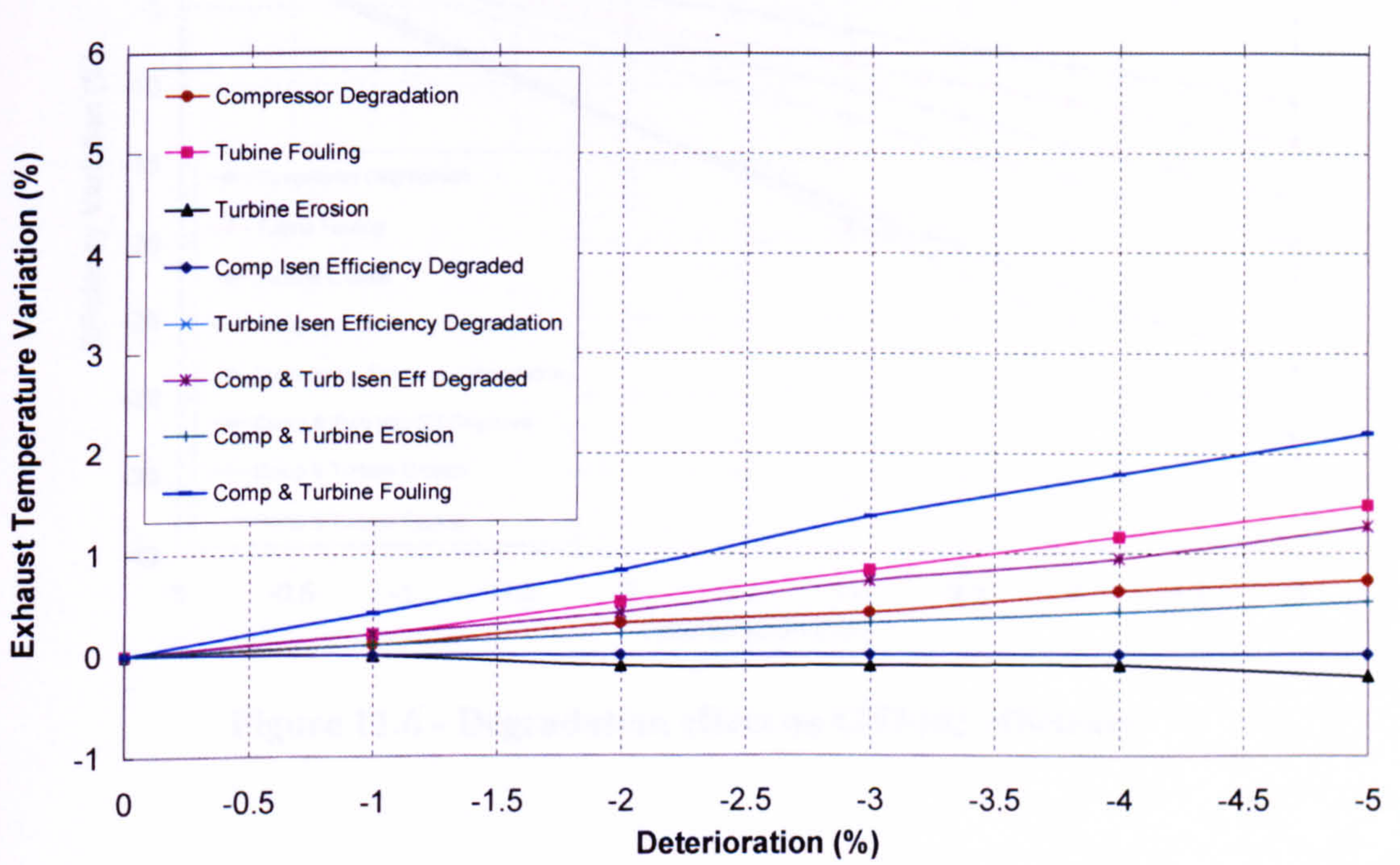

Figure 11.4 - Degradation effect on GTM#1 exhaust temperature

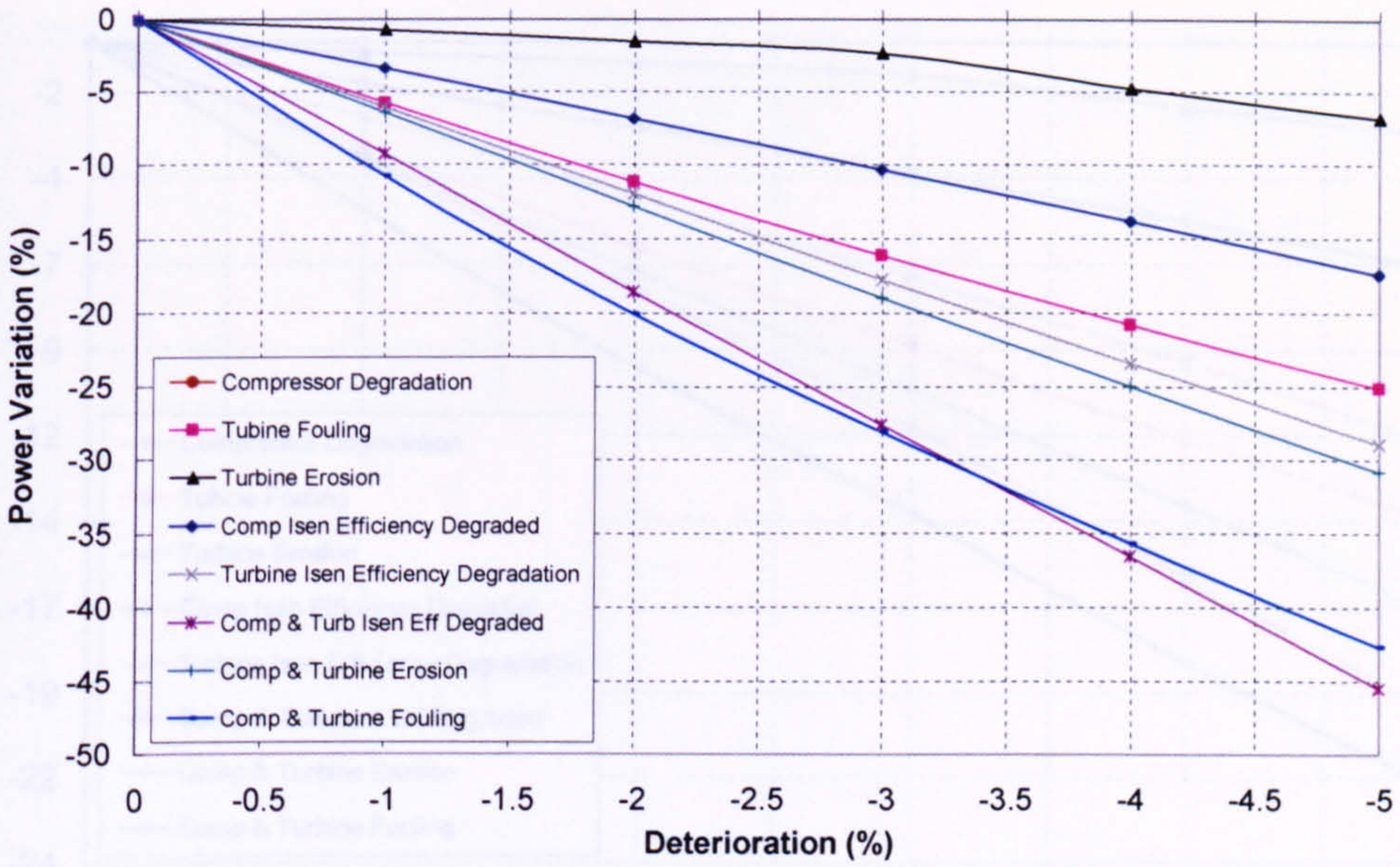

Figure 11.5 - Degradation effect on GTM#2 power

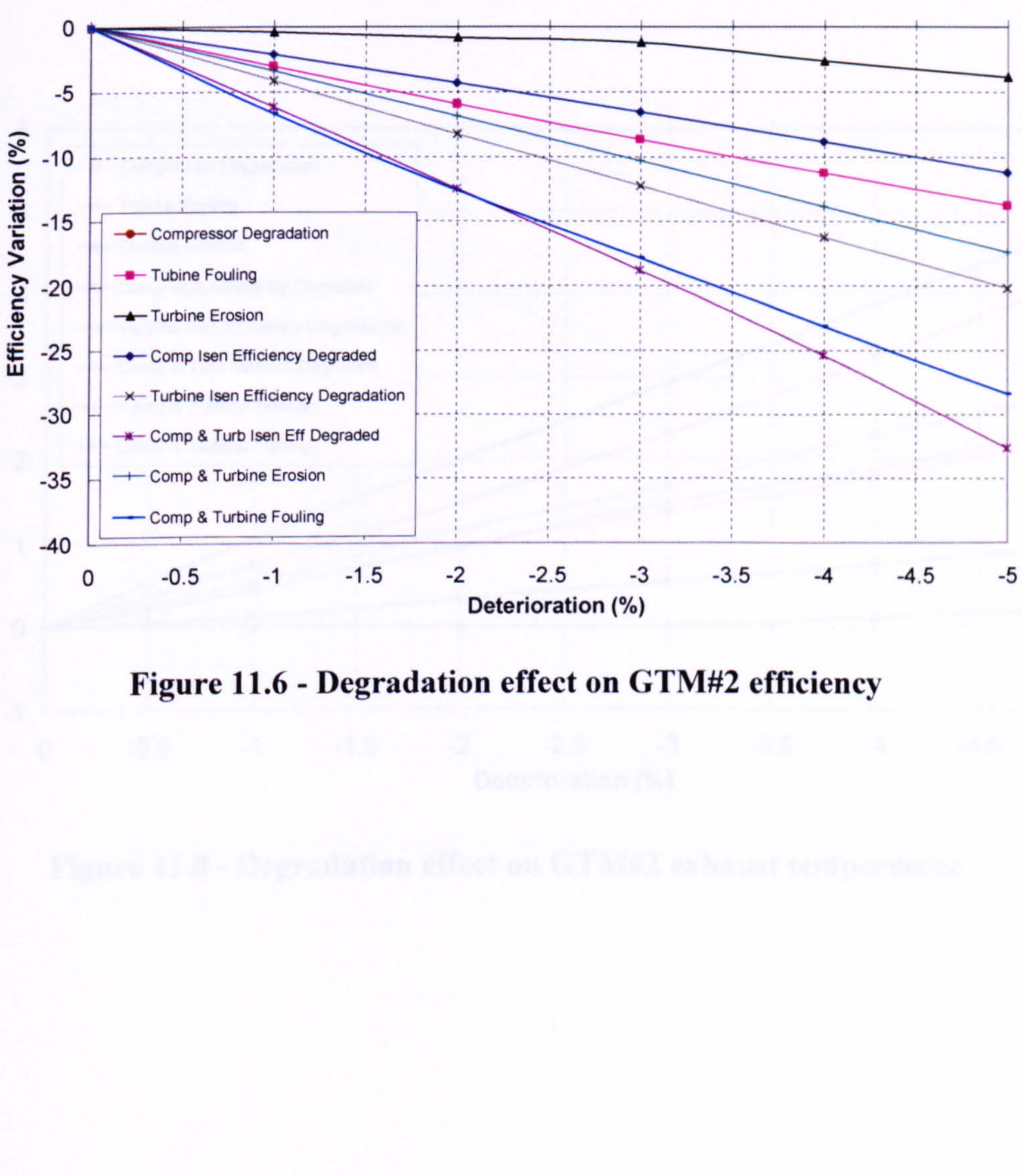

Figure 11.6 - Degradation effect on GTM#2 efficiency

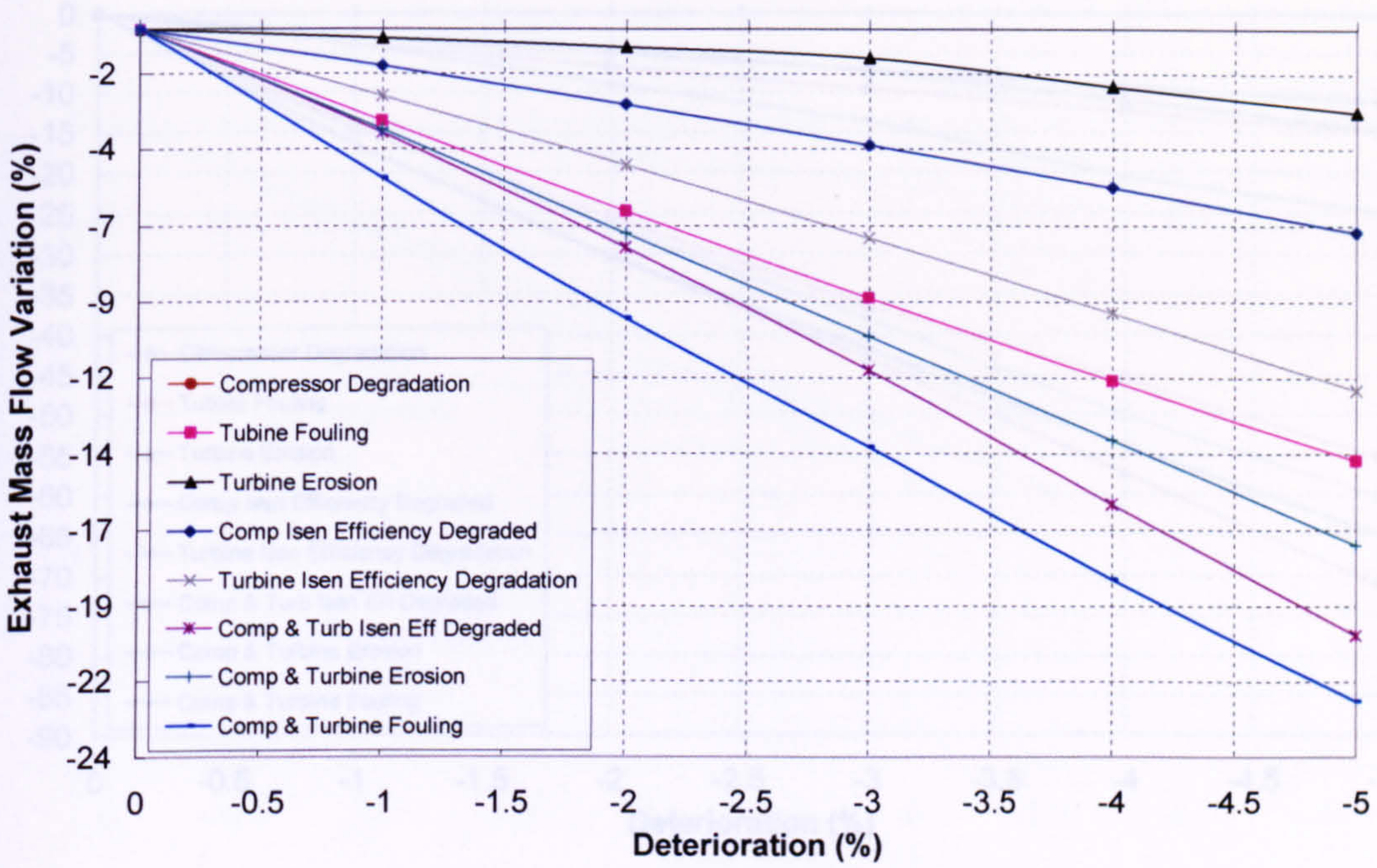

Figure 11.7 - Degradation effect on GTM#2 exhaust mass flow

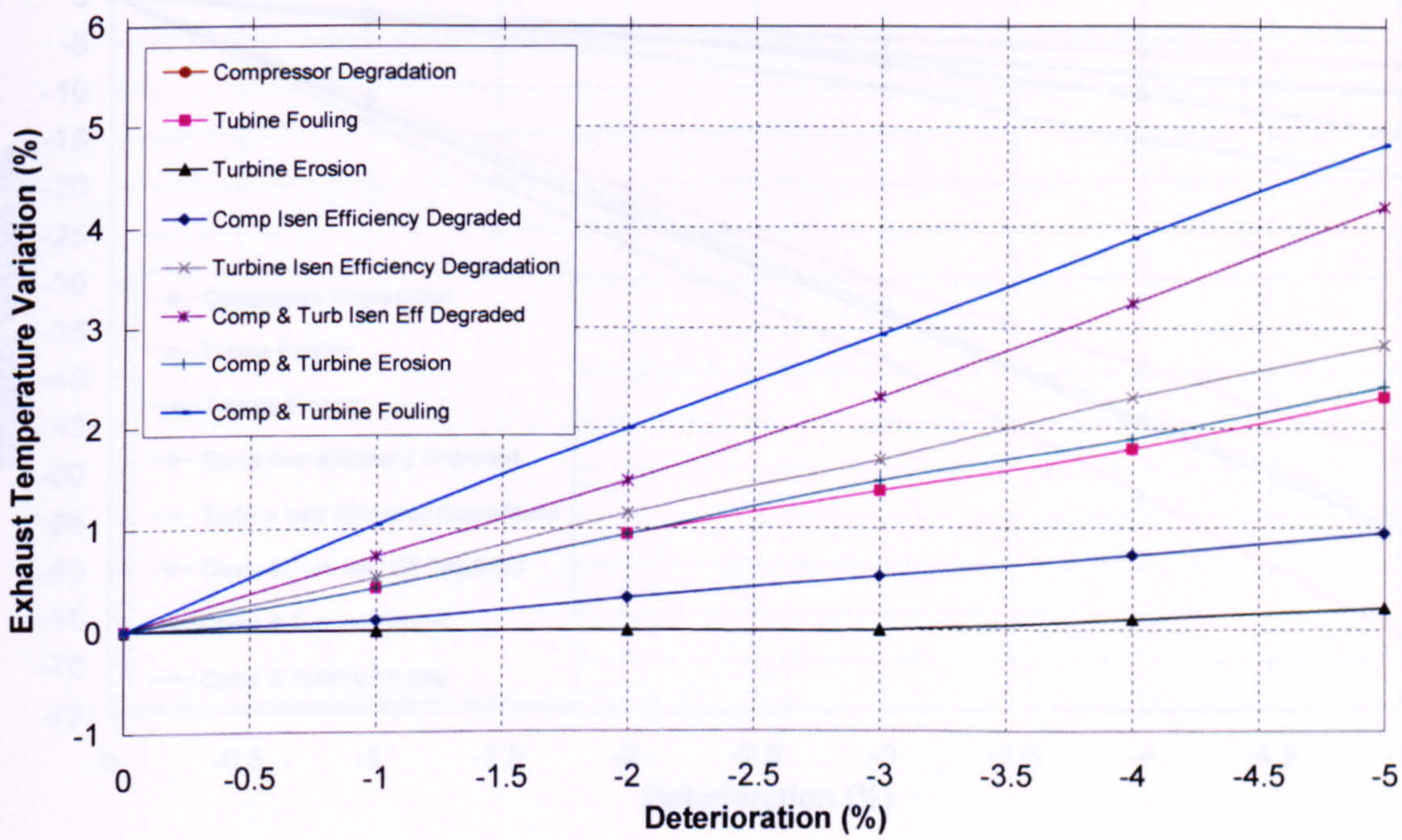

Figure 11.8 - Degradation effect on GTM#2 exhaust temperature

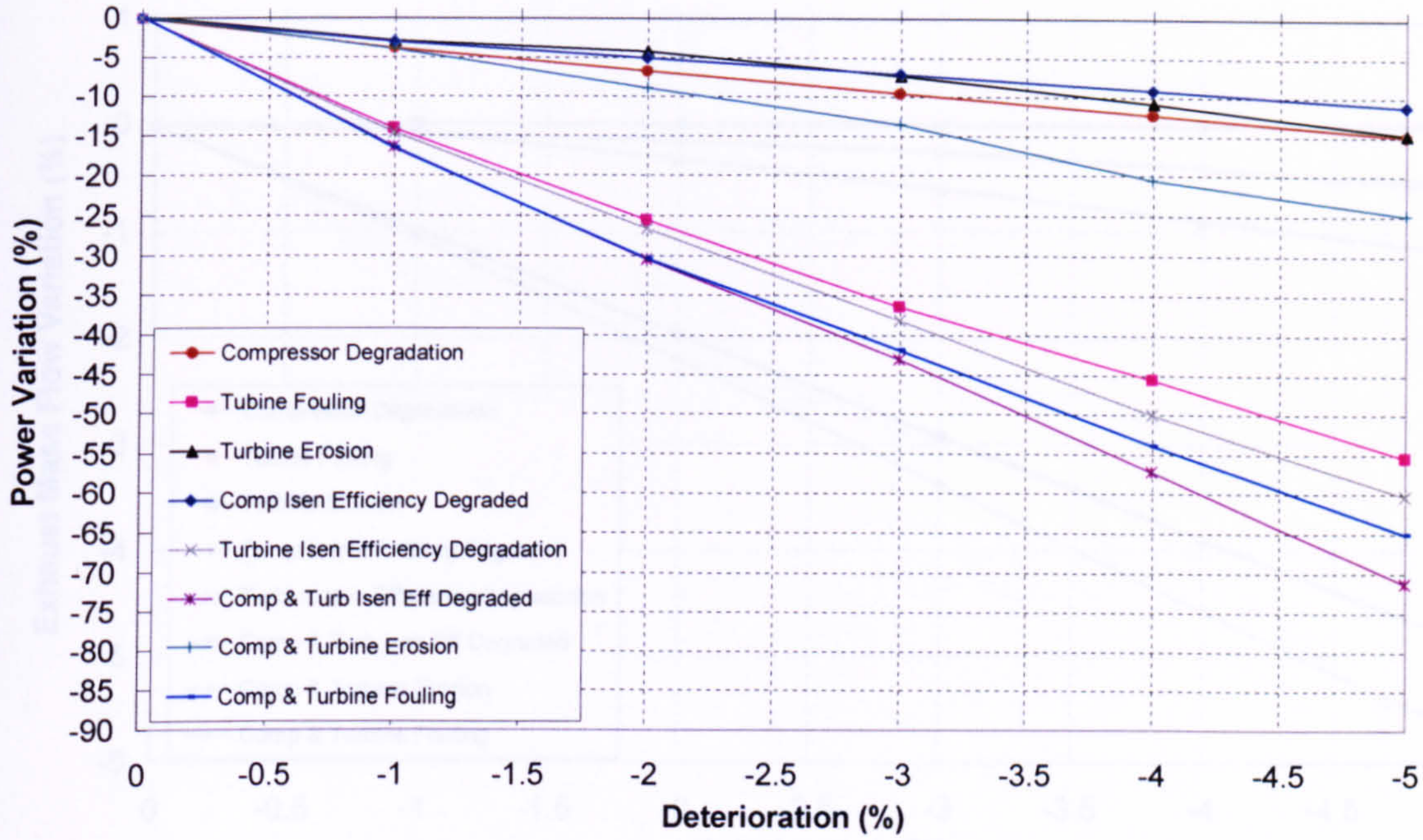

Figure 11.9 - Degradation effect on GTM#3 power

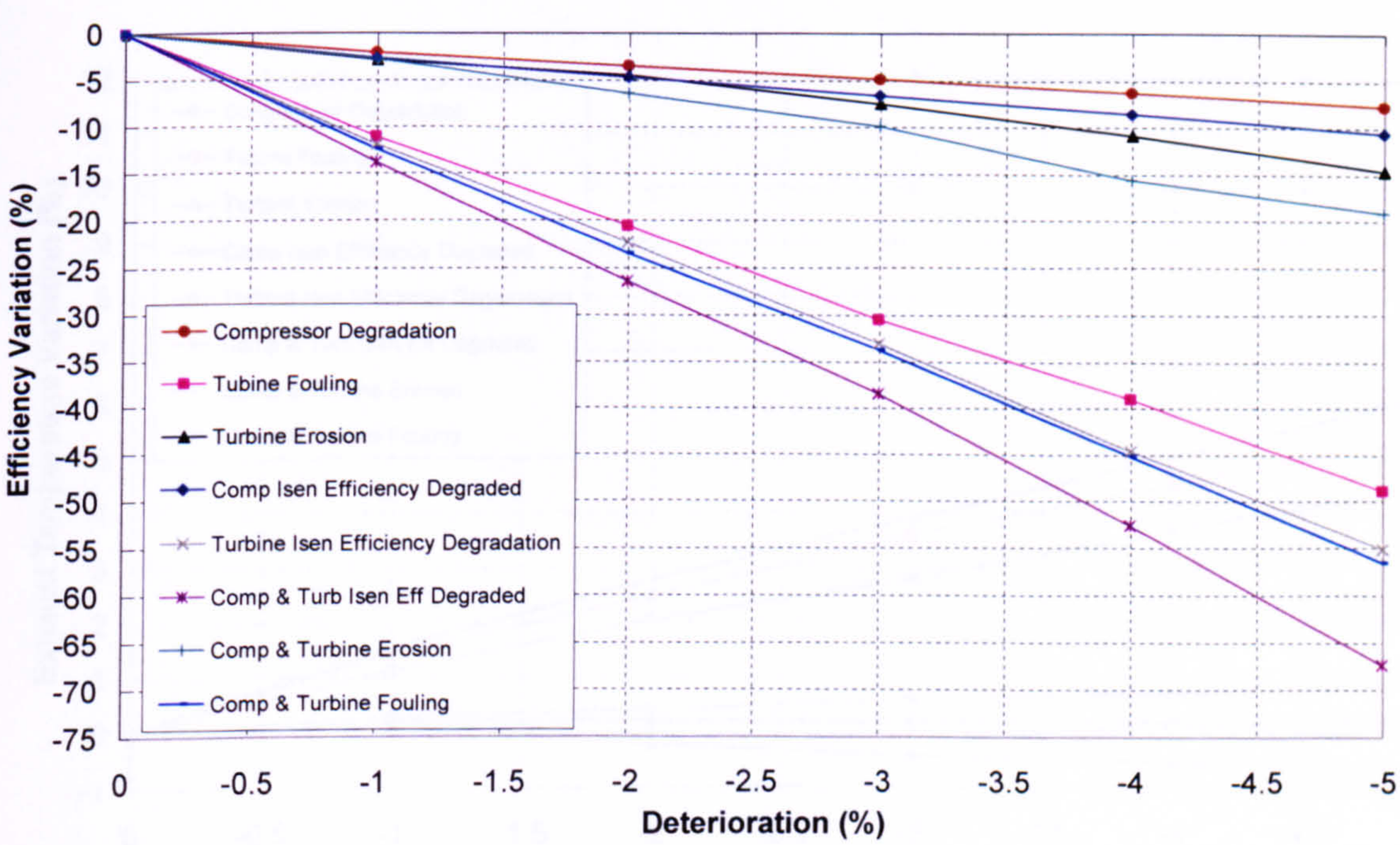

Figure 11.10 - Degradation effect on GTM#3 efficiency

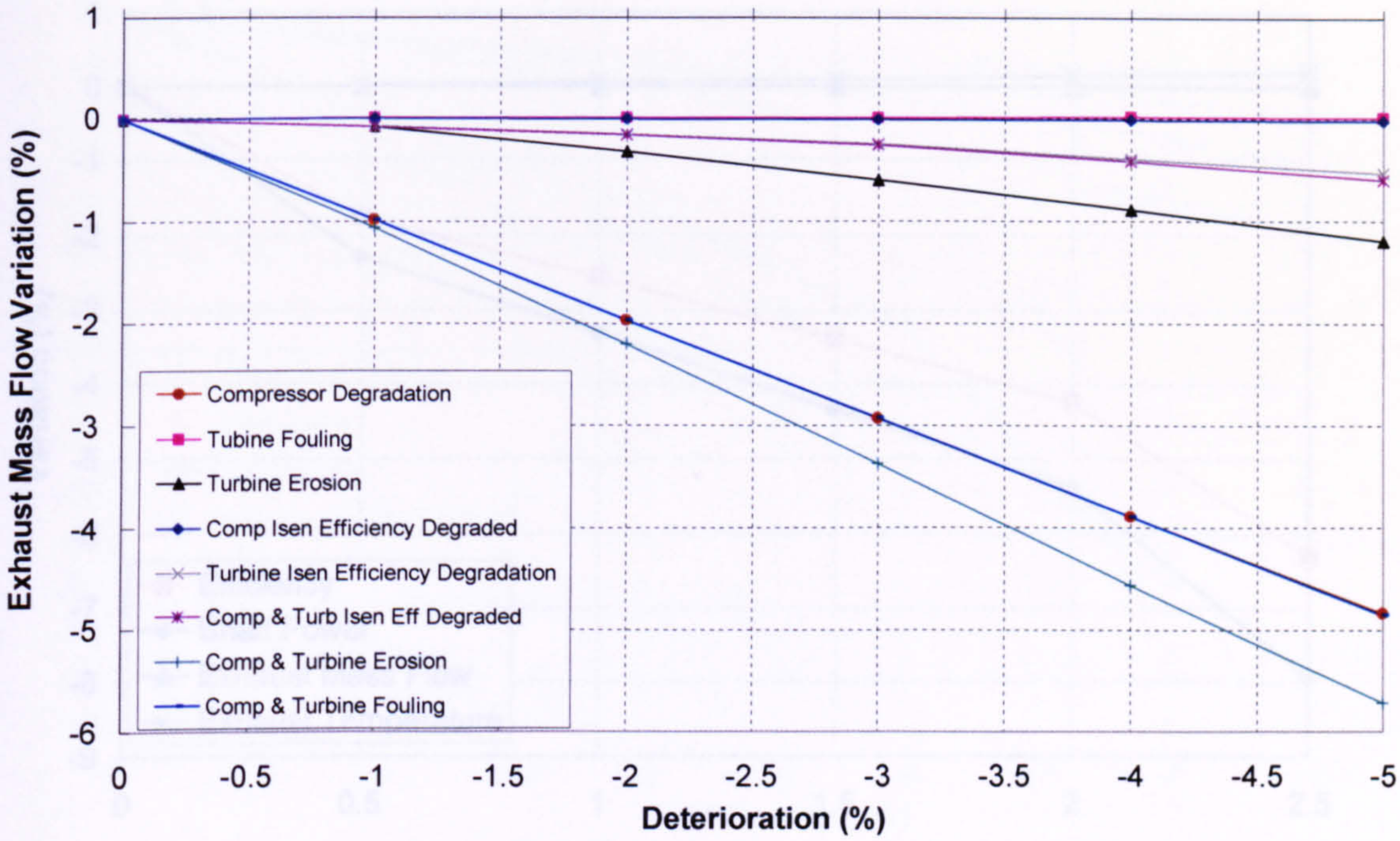

Figure 11.11 - Degradation effect on GTM#3 exhaust mass flow

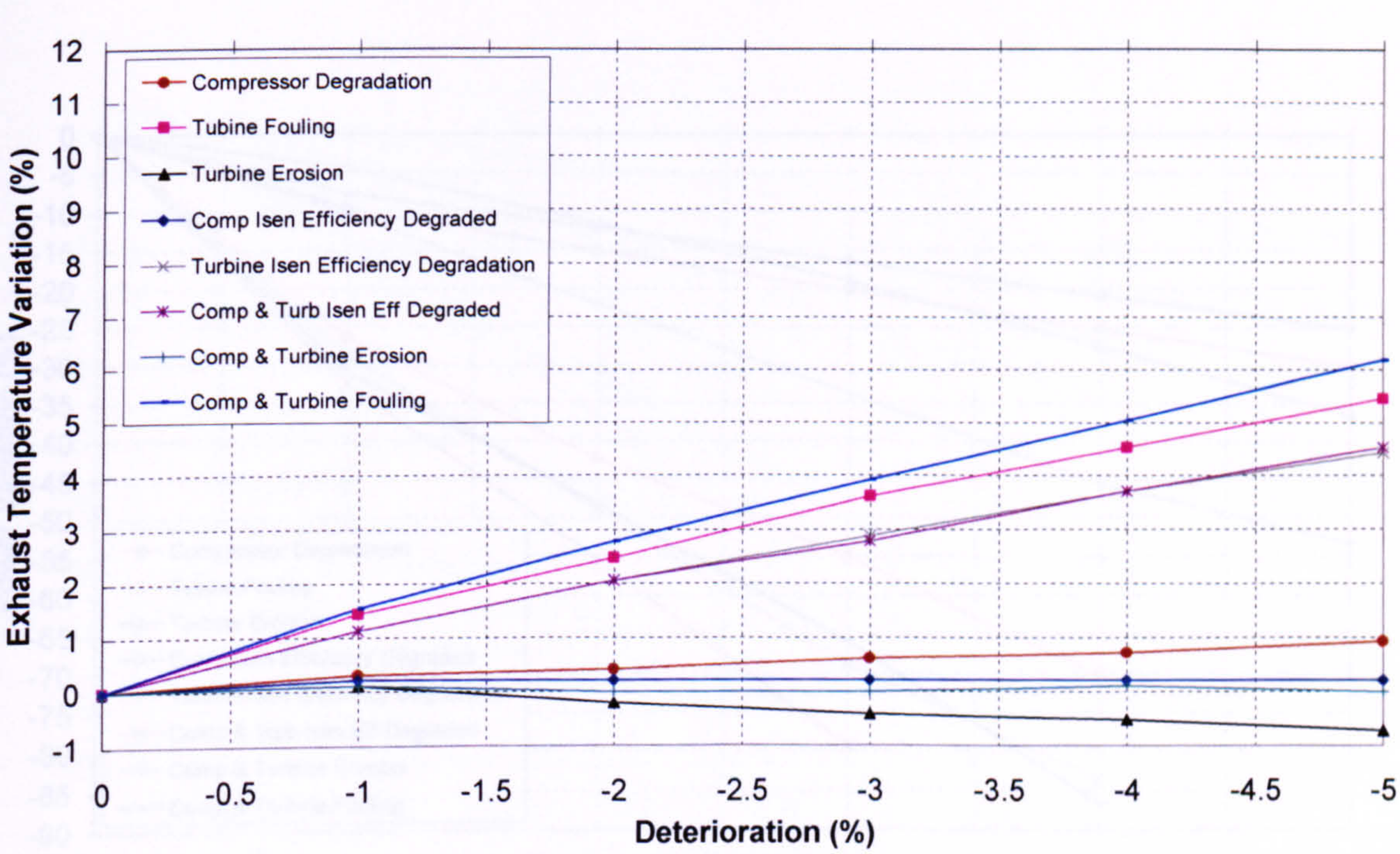

Figure 11.12 - Degradation effect on GTM#3 exhaust temperature

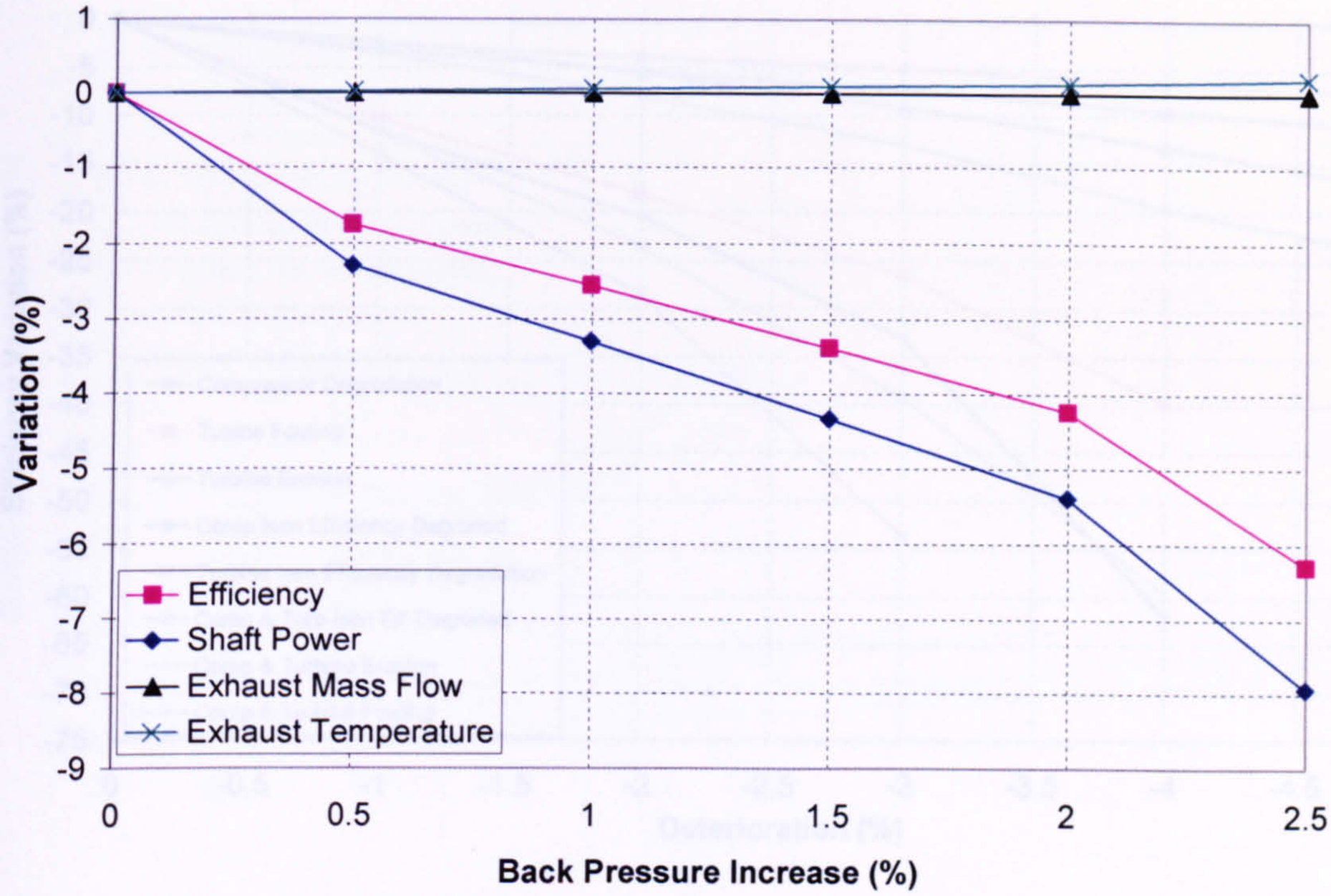

Figure 11.13 – Back Pressure effect on GTM#3 performance due recuperator degradation

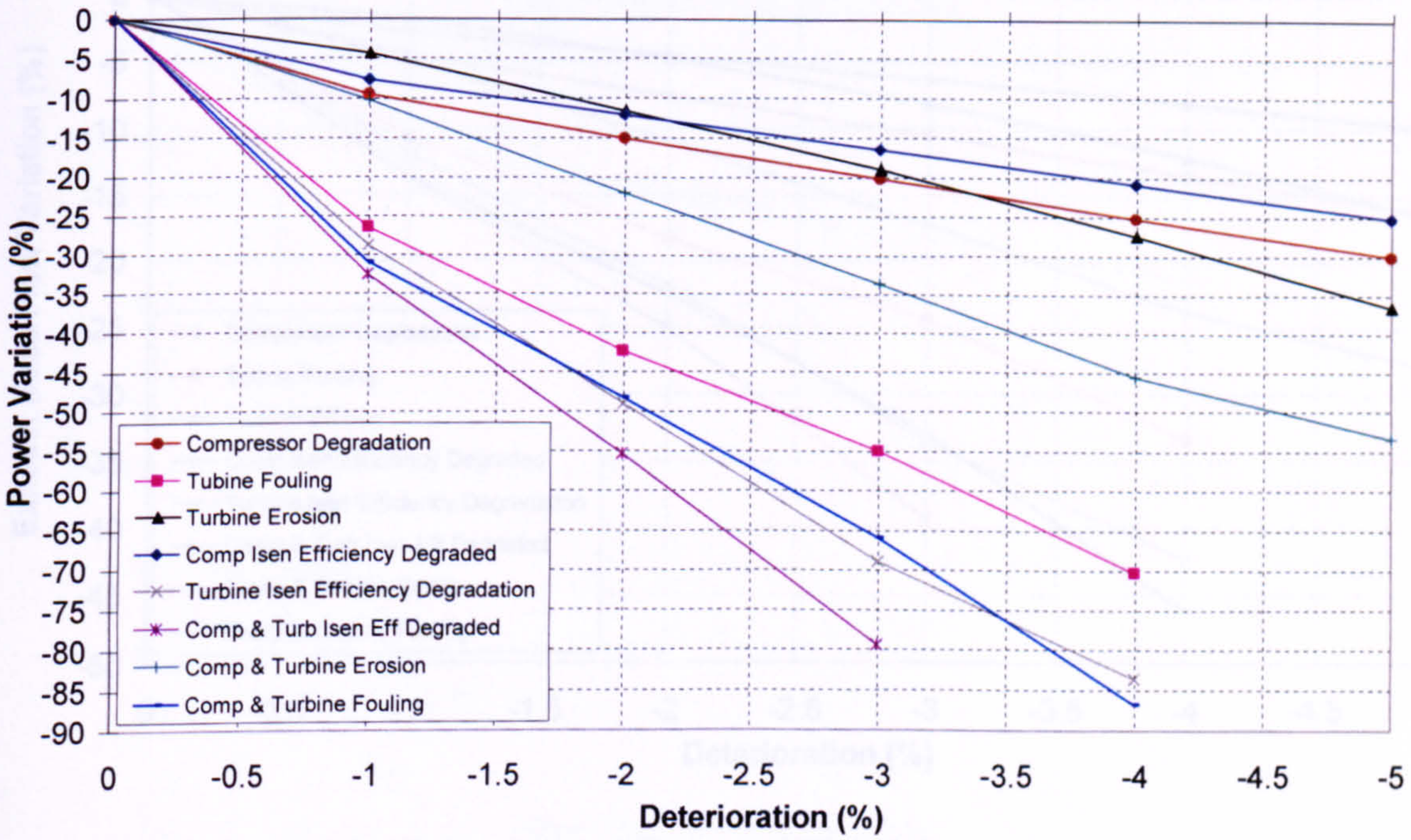

Figure 11.14 - Degradation effect on GTM#4 power

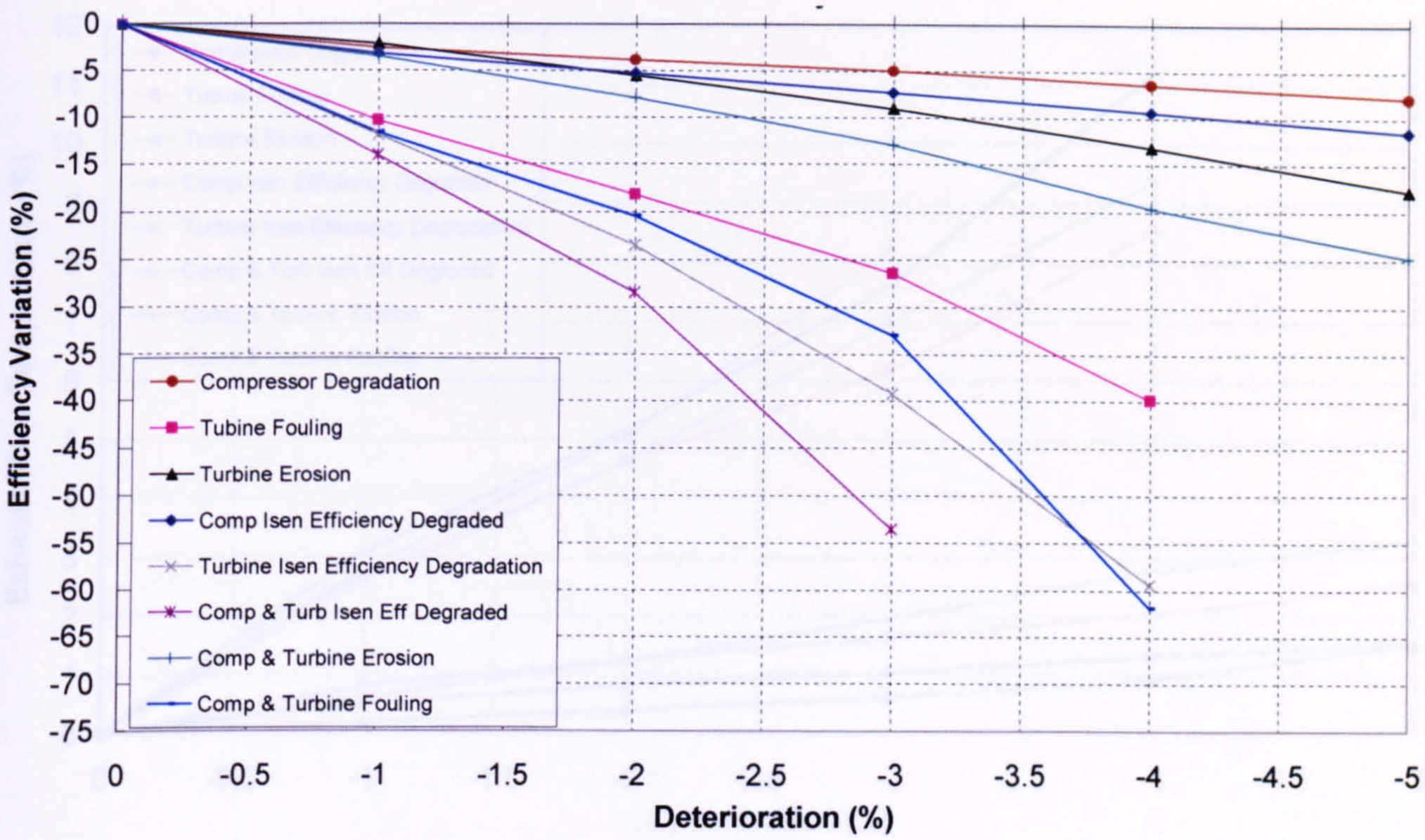

Figure 11.15 - Degradation effect on GTM#4 efficiency

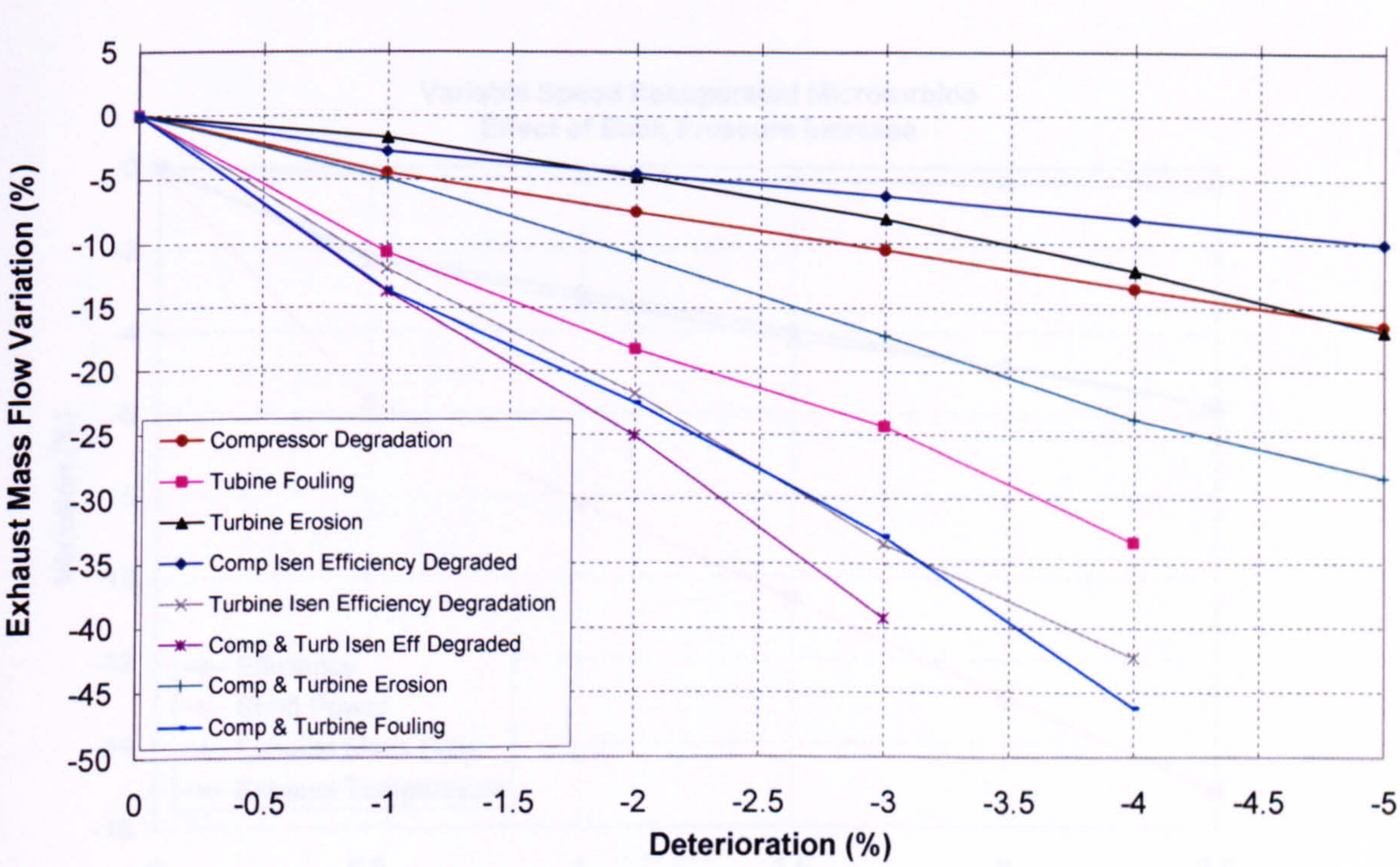

Figure 11.16 - Degradation effect on GTM#4 exhaust mass flow

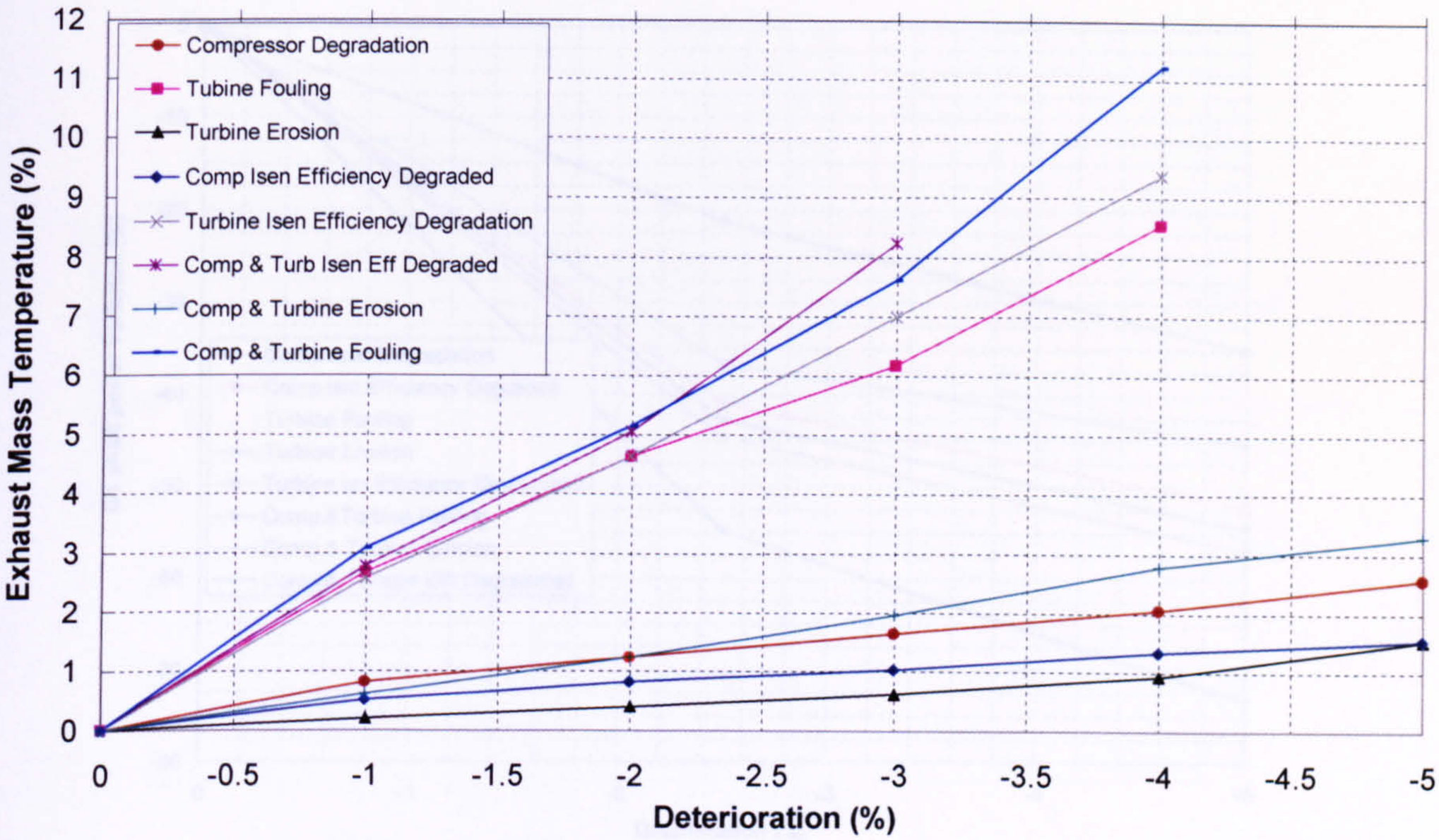

Figure 11.17 - Degradation effect on GTM#4 exhaust temperature

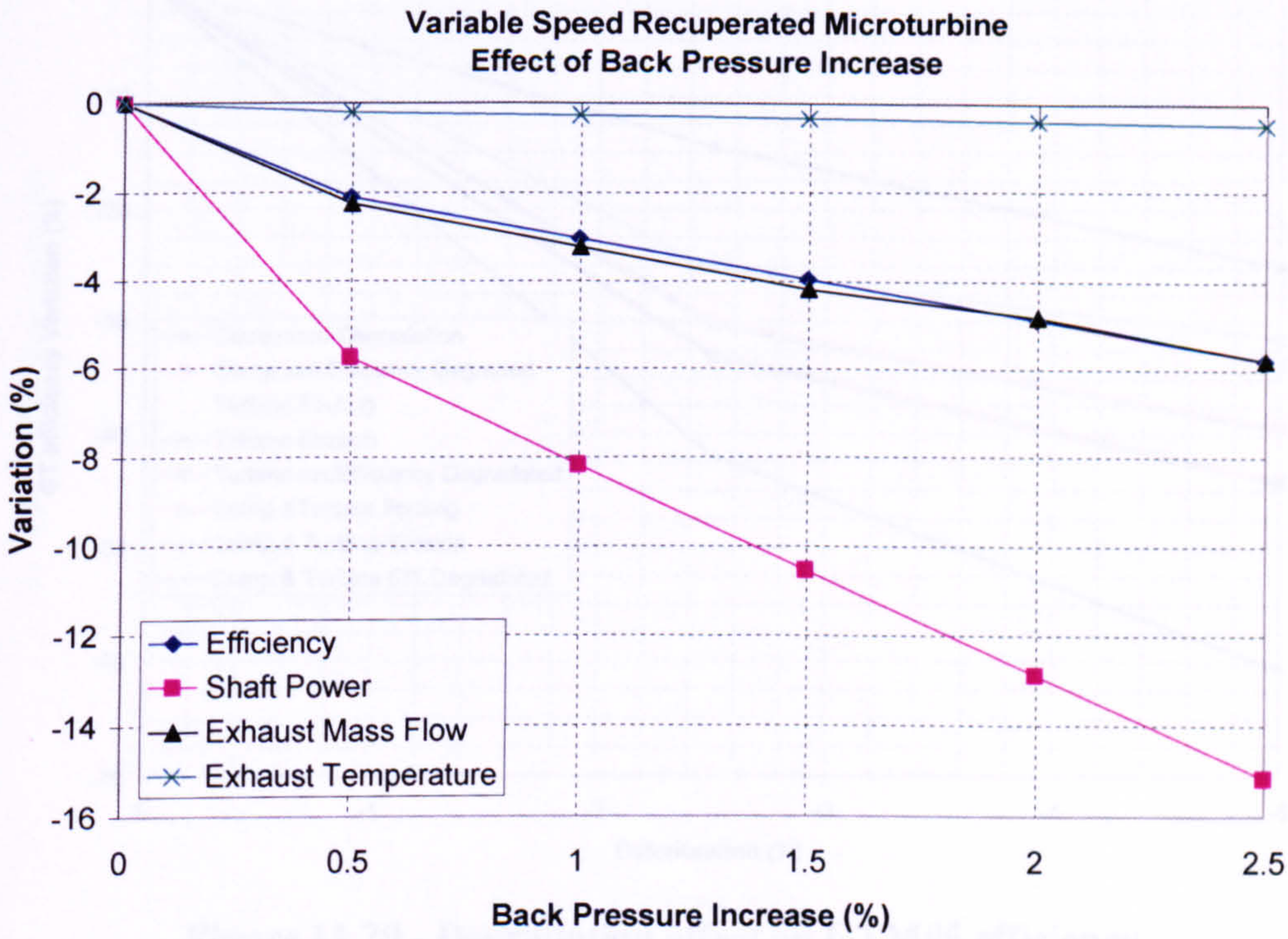

Figure 11.18 – Back Pressure effect on GTM#4 performance due recuperator degradation

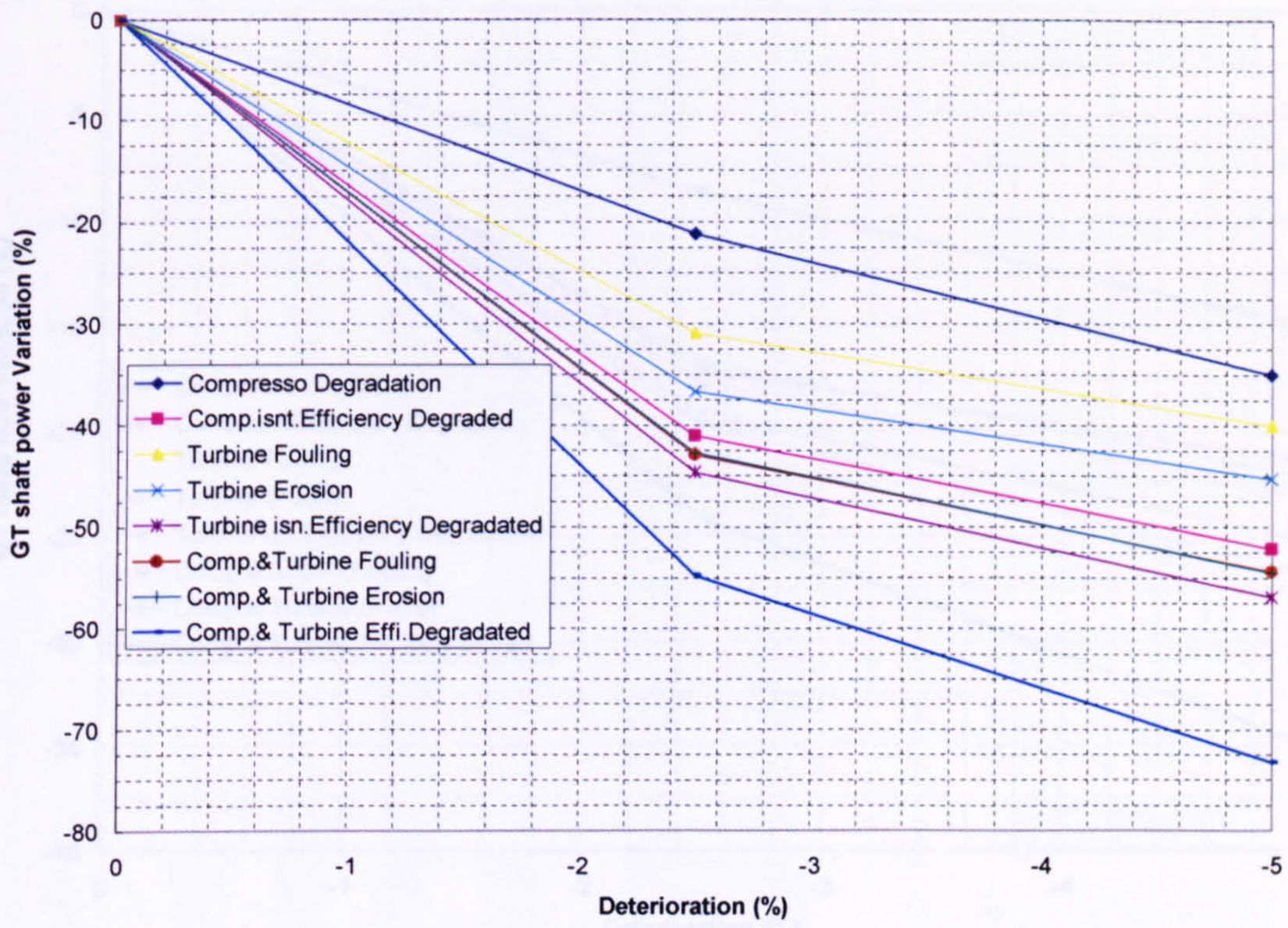

Figure 11.19 - Degradation effect on GTM#5 power

Figure 11.20 - Degradation effect on GTM#5 efficiency

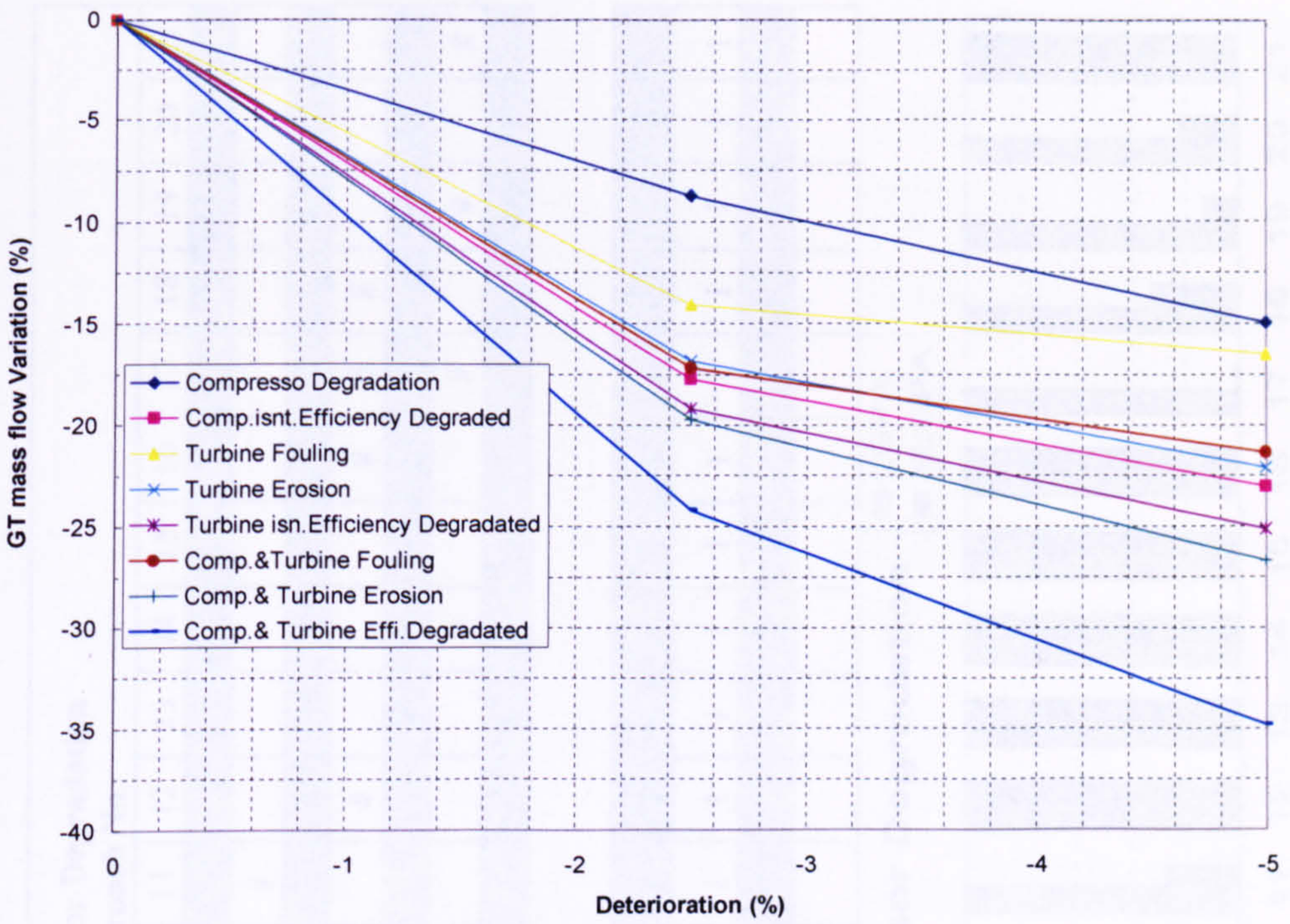

Figure 11.21 - Degradation effect on GTM#5 exhaust mass flow

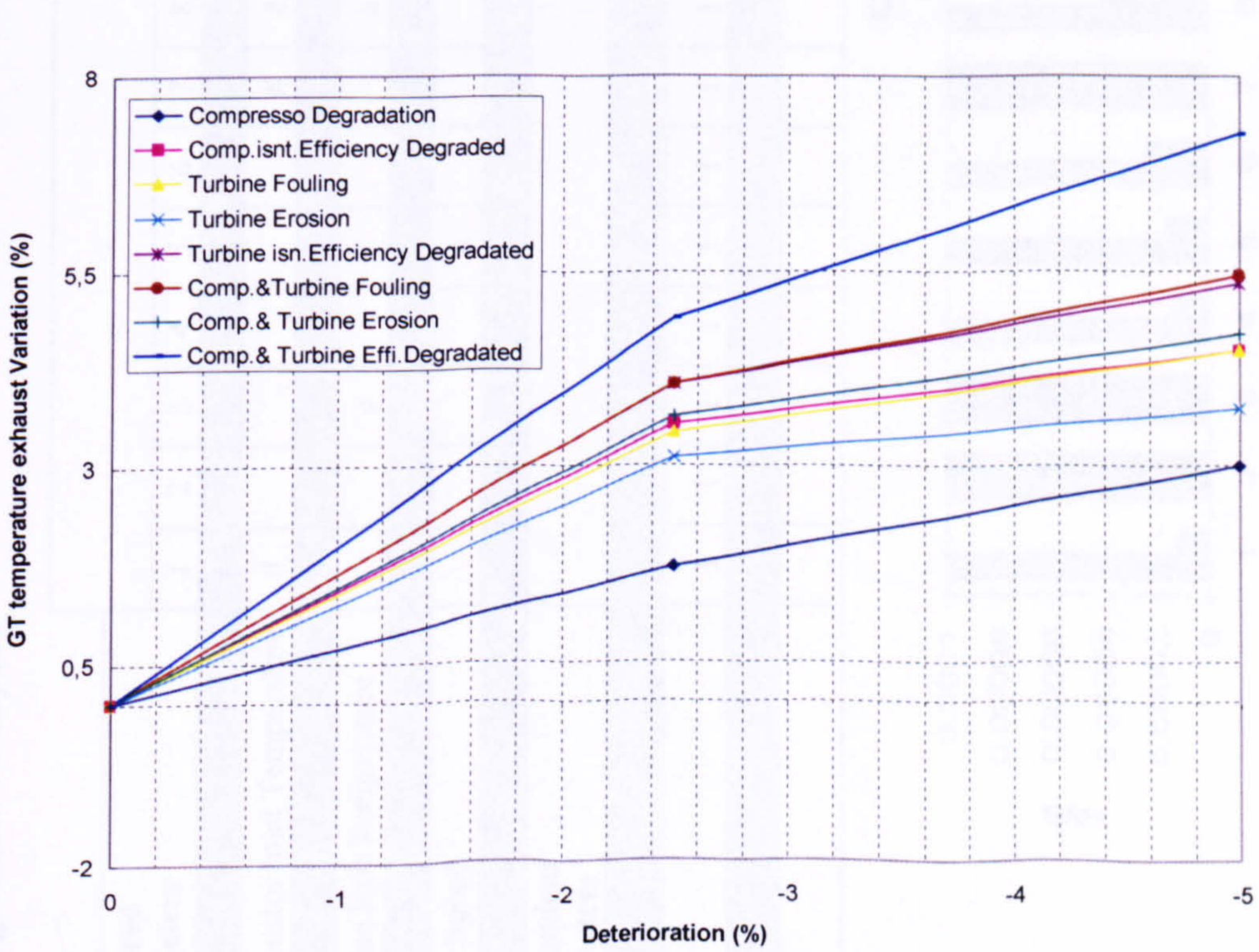

Figure 11.22 - Degradation effect on GTM#5 exhaust temperature

11.2 - Diagnostic Analysis

Measured Parameters	Compressor Degradation Approach No.																				
	1	2	3	4	5	6	7	8	9	10	11	12	13	14	15	16	17	18	19	20	21
Combustor Inlet Pressure	#	#	#	#	#	#															
Combustor Inlet Temperature	#						#	#	#	#	#										
Turbine Exit Pressure		#					#					#	#	#	#						
Turbine Exit Temperature			#					#				#				#	#	#			
Fuel Flow				#					#				#			#			#	#	
Shaft Speed					#					#				#			#		#		#
Shaft Power						#					#				#			#		#	#
Independent Parameters																					
Γ_C	I	I	I	I	I	I	I	I	I	I	I	I	I	I	I	I	I	I	I	I	I
η_C	I	I	I	I	I	I	I	I	I	I	I	I	I	I	I	I	I	I	I	I	I
Γ_T																					
η_C																					

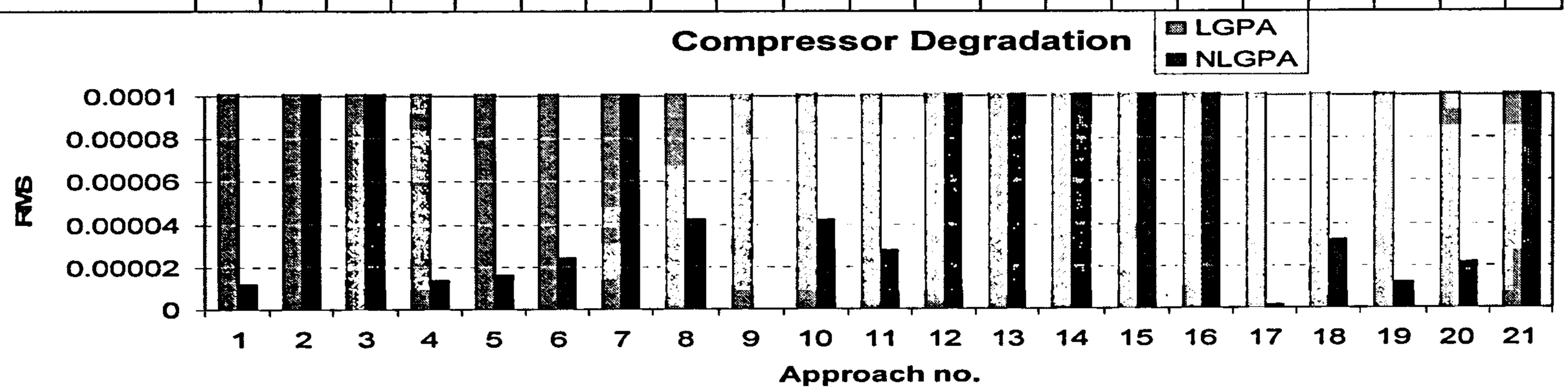

Figure 11.23 – Compressor Degradation Diagnostic – GTM#4

Measured Parameters	Turbine Fouling Approach No.																				
	1	2	3	4	5	6	7	8	9	10	11	12	13	14	15	16	17	18	19	20	21
Combustor Inlet Pressure	#	#	#	#	#	#															
Combustor Inlet Temperature	#						#	#	#	#	#										
Turbine Exit Pressure		#					#					#	#	#	#						
Turbine Exit Temperature			#					#				#				#	#	#			
Fuel Flow				#					#				#			#			#	#	
Shaft Speed					#					#				#			#		#		#
Shaft Power						#					#				#			#		#	#
Independent Parameters																					
Γ_C																					
η_C																					
Γ_T	I	I	I	I	I	I	I	I	I	I	I	I	I	I	I	I	I	I	I	I	I
η_C	I	I	I	I	I	I	I	I	I	I	I	I	I	I	I	I	I	I	I	I	I

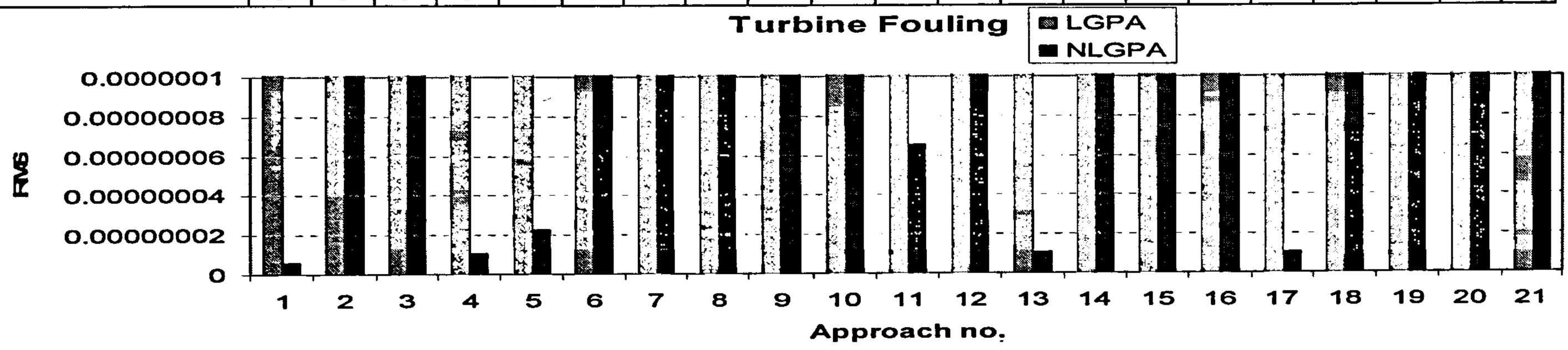

Figure 11.24 – Turbine Fouling Diagnostic – GTM#4

Measured Parameters	Turbine Erosion Approach No.																				
	1	2	3	4	5	6	7	8	9	10	11	12	13	14	15	16	17	18	19	20	21
Combustor Inlet Pressure	#	#	#	#	#	#															
Combustor Inlet Temperature	#						#	#	#	#	#										
Turbine Exit Pressure		#					#					#	#	#	#						
Turbine Exit Temperature			#					#				#				#	#	#			
Fuel Flow				#					#				#			#			#	#	
Shaft Speed					#					#				#			#		#		#
Shaft Power						#					#				#			#		#	#
Independent Parameters																					
Γ_C																					
η_C																					
Γ_T	I	I	I	I	I	I	I	I	I	I	I	I	I	I	I	I	I	I	I	I	I
η_C	I	I	I	I	I	I	I	I	I	I	I	I	I	I	I	I	I	I	I	I	I

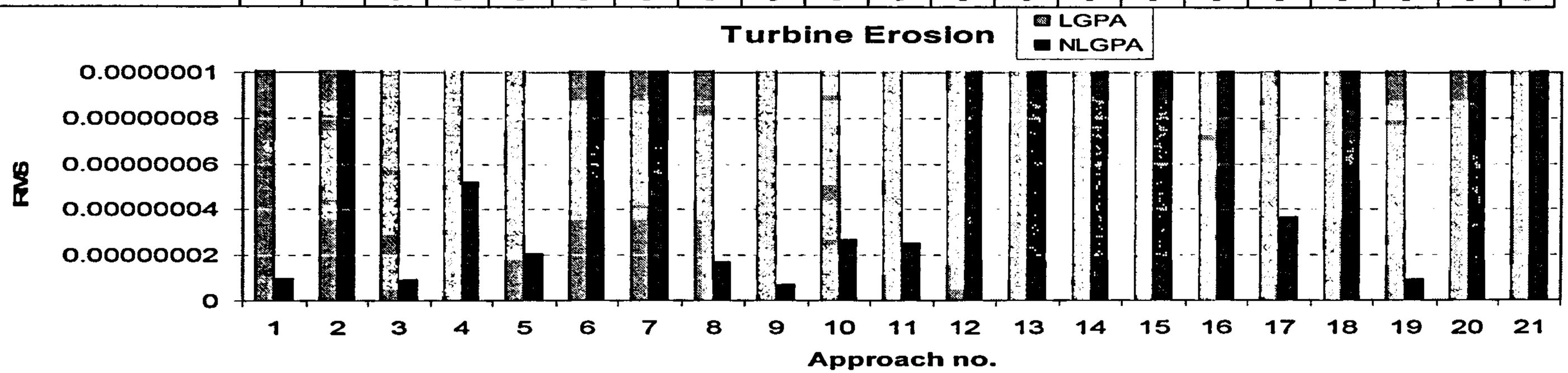

Figure 11.25 – Turbine Erosion Diagnostic – GTM#4

Measured Parameters	Compressor Degradation and Turbine Fouling Approach No.																															
	1	2	3	4	5	6	7	8	9	10	11	12	13	14	15	16	17	18	19	20	21	22	23	24	25	26	27	28	29	30	31	32
Combustor Inlet Pressure	#	#	#	#	#	#		#	#	#	#		#	#	#		#	#	#	#	#	#		#	#					#		#
Combustor Inlet Temperature	#	#	#	#	#		#	#	#	#			#			#	#	#	#	#	#			#			#		#	#	#	
Turbine Exit Pressure	#	#	#	#		#	#	#	#			#	#	#	#	#	#		#	#					#	#	#	#				#
Turbine Exit Temperature	#	#	#		#	#	#	#			#	#	#	#	#	#			#				#		#	#	#	#	#	#	#	#
Fuel Flow	#	#		#	#	#	#	#		#	#	#		#	#	#		#				#	#		#	#	#	#			#	
Shaft Speed	#	#	#	#	#	#	#		#	#	#	#			#	#	#	#			#	#	#	#				#	#	#		#
Shaft Power	#		#	#	#	#	#		#	#	#	#	#	#			#	#		#	#	#	#	#		#			#		#	
Independent Parameters		**6 Measured Parameters**						**5 Measured Parameters**											**4 Measured Parameters**													
Γ_C	I	I	I	I	I	I	I	I	I	I	I	I	I	I	I	I	I	I	I	I	I	I	I	I	I	I	I	I	I	I	I	I
η_C	I	I	I	I	I	I	I	I	I	I	I	I	I	I	I	I	I	I	I	I	I	I	I	I	I	I	I	I	I	I	I	I
Γ_t	I	I	I	I	I	I	I	I	I	I	I	I	I	I	I	I	I	I	I	I	I	I	I	I	I	I	I	I	I	I	I	I
η_C	I	I	I	I	I	I	I	I	I	I	I	I	I	I	I	I	I	I	I	I	I	I	I	I	I	I	I	I	I	I	I	I

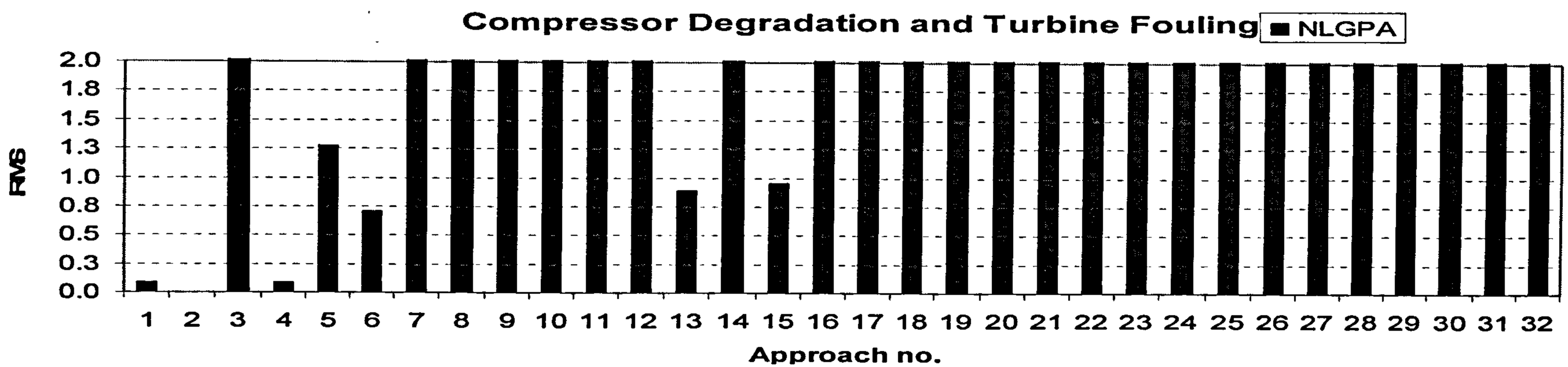

Figure 11.26 - Compressor Degradation and Turbine Fouling Diagnostic– GTM#4

Measured Parameters	Compressor Degradation and Turbine Erosion Approach No.																													
	1	2	3	4	5	6	7	8	9	10	11	12	13	14	15	16	17	18	19	20	21	22	23	24	25	26	27	28	29	30	31	32
Combustor Inlet Pressure	#	#	#	#	#	#		#	#	#	#		#	#	#		#	#	#	#	#	#		#	#					#		#
Combustor Inlet Temperature	#	#	#	#	#		#	#	#	#			#			#	#	#	#	#	#			#			#		#	#	#	
Turbine Exit Pressure	#	#	#	#		#	#	#	#			#	#	#	#	#	#		#	#					#	#	#	#			#
Turbine Exit Temperature	#	#	#		#	#	#	#			#	#	#	#	#	#			#				#		#	#	#	#	#	#	#
Fuel Flow	#	#		#	#	#	#	#		#	#	#		#	#	#		#				#	#		#	#	#	#		#	
Shaft Speed	#	#	#	#	#	#	#		#	#	#	#			#	#	#	#			#	#	#	#				#	#	#	#
Shaft Power	#		#	#	#	#	#		#	#	#	#	#	#			#	#		#	#	#	#	#		#			#		#	
Independent Parameters		**6 Measured Parameters**						**5 Measured Parameters**											**4 Measured Parameters**													
Γ_C	I	I	I	I	I	I	I	I	I	I	I	I	I	I	I	I	I	I	I	I	I	I	I	I	I	I	I	I	I	I	I	I
η_C	I	I	I	I	I	I	I	I	I	I	I	I	I	I	I	I	I	I	I	I	I	I	I	I	I	I	I	I	I	I	I	I
Γ_T	I	I	I	I	I	I	I	I	I	I	I	I	I	I	I	I	I	I	I	I	I	I	I	I	I	I	I	I	I	I	I	I
η_C	I	I	I	I	I	I	I	I	I	I	I	I	I	I	I	I	I	I	I	I	I	I	I	I	I	I	I	I	I	I	I	I

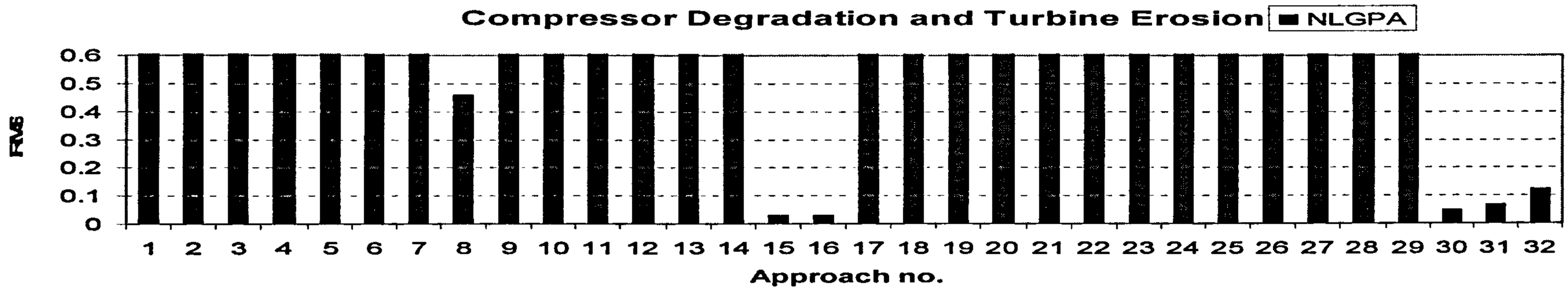

Figure 11.27 - Compressor Degradation and Turbine Erosion Diagnostics – GTM#4

Measured Parameters	Compressor Degradation Approach No.																				
	1	2	3	4	5	6	7	8	9	10	11	12	13	14	15	16	17	18	19	20	21
Combustor Inlet Pressure	#	#	#	#	#	#															
Combustor Inlet Temperature	#						#	#	#	#	#										
Turbine Exit Pressure		#					#					#	#	#	#						
Turbine Exit Temperature			#					#				#				#	#	#			
Fuel Flow				#					#				#			#			#	#	
Shaft Speed					#					#				#			#		#		#
Shaft Power						#					#				#			#		#	#
Independent Parameters																					
Γ_C	I	I	I	I	I	I	I	I	I	I	I	I	I	I	I	I	I	I	I	I	I
η_C	I	I	I	I	I	I	I	I	I	I	I	I	I	I	I	I	I	I	I	I	I
Γ_T																					
η_C																					

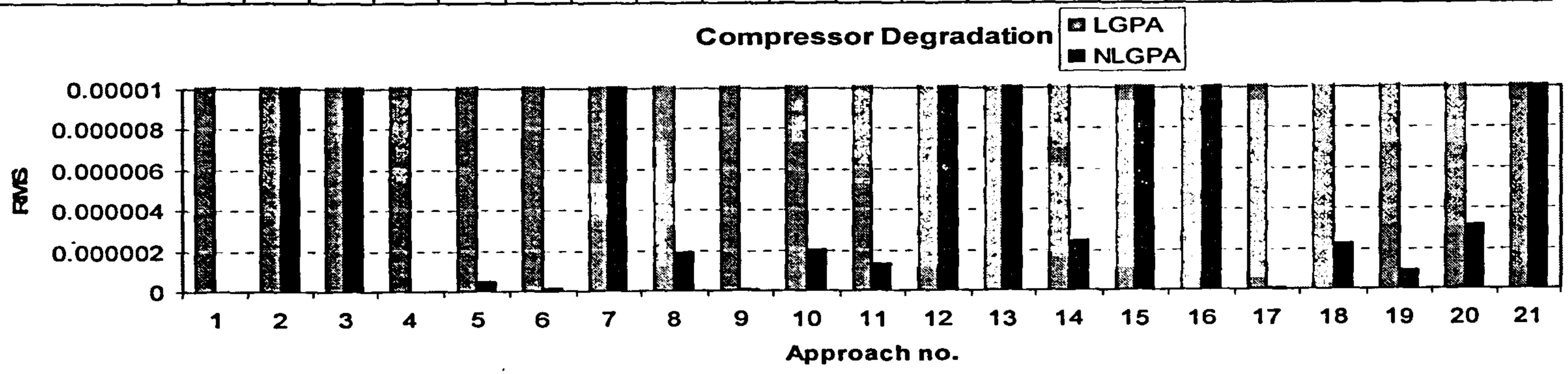

Figure 11.28 - Compressor Degradation Diagnostic – GTM#3

Measured Parameters	Turbine Fouling Approach No.																				
	1	2	3	4	5	6	7	8	9	10	11	12	13	14	15	16	17	18	19	20	21
Combustor Inlet Pressure	#	#	#	#	#	#															
Combustor Inlet Temperature	#						#	#	#	#	#										•
Turbine Exit Pressure		#					#					#	#	#	#						
Turbine Exit Temperature			#					#				#				#	#	#			
Fuel Flow				#					#				#			#			#	#	
Shaft Speed					#					#				#			#		#		#
Shaft Power						#					#				#			#		#	#
Independent Parameters																					
Γ_C																					
η_C																					
Γ_T	I	I	I	I	I	I	I	I	I	I	I	I	I	I	I	I	I	I	I	I	I
η_C	I	I	I	I	I	I	I	I	I	I	I	I	I	I	I	I	I	I	I	I	I

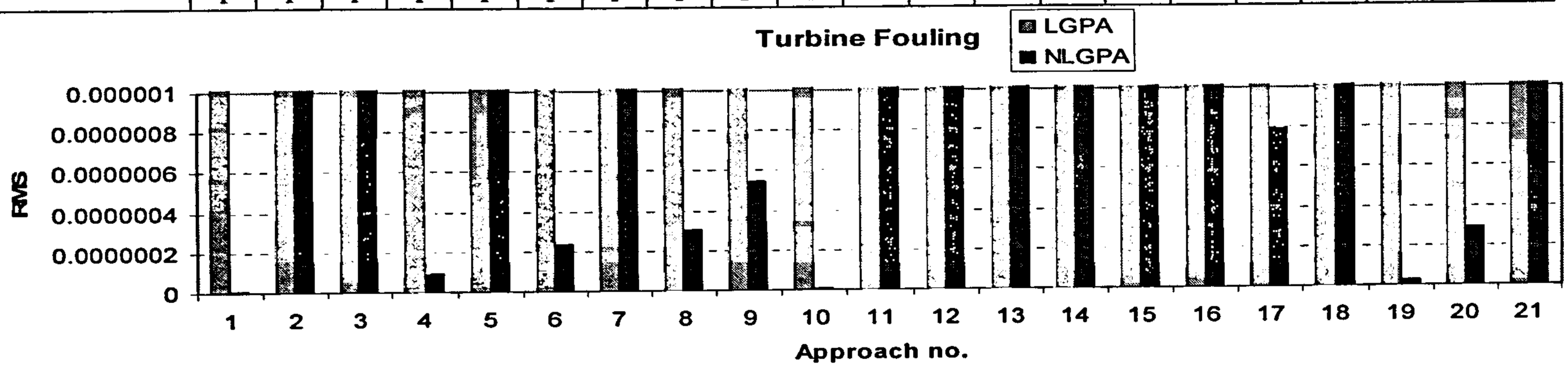

Figure 11.29 - Turbine Fouling Diagnostic - – GTM#3

Measured Parameters	Turbine Erosion Approach No.																				
	1	2	3	4	5	6	7	8	9	10	11	12	13	14	15	16	17	18	19	20	21
Combustor Inlet Pressure	#	#	#	#	#	#															
Combustor Inlet Temperature	#						#	#	#	#	#										
Turbine Exit Pressure		#					#					#	#	#	#						
Turbine Exit Temperature			#					#				#				#	#	#			
Fuel Flow				#					#				#			#			#	#	
Shaft Speed					#					#				#			#		#		#
Shaft Power						#					#				#			#		#	#
Independent Parameters																					
Γ_C																					
η_C																					
Γ_T	I	I	I	I	I	I	I	I	I	I	I	I	I	I	I	I	I	I	I	I	I
η_C	I	I	I	I	I	I	I	I	I	I	I	I	I	I	I	I	I	I	I	I	I

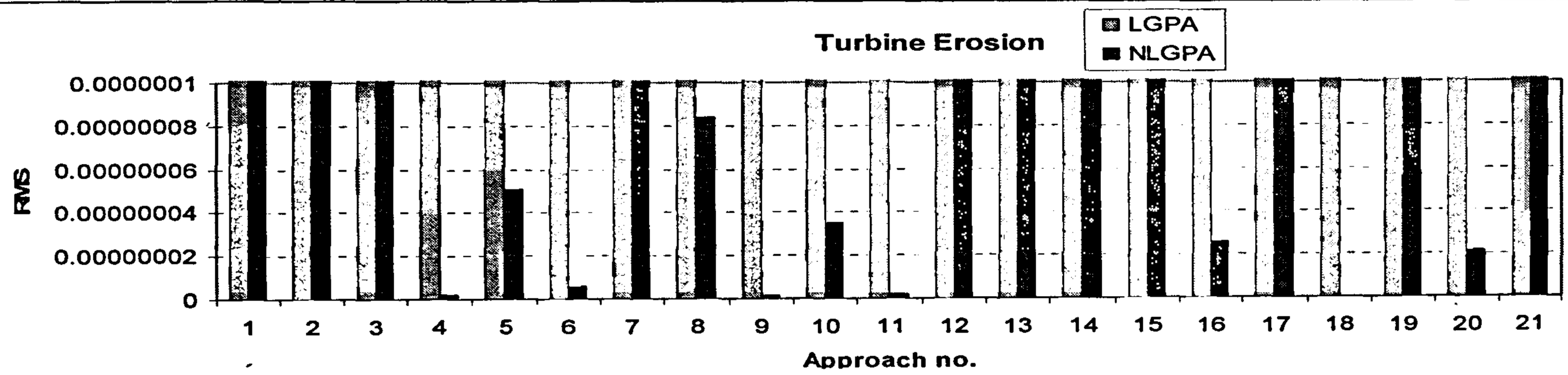

Figure 11.30 – Turbine Erosion Diagnostic – GTM#3

Measured Parameters	Compressor Degradation and Turbine Fouling Approach No.																														
	1	2	3	4	5	6	7	8	9	10	11	12	13	14	15	16	17	18	19	20	21	22	23	24	25	26	27	28	29	30	31	32
Combustor Inlet Pressure	#	#	#	#	#	#		#	#	#	#		#	#	#		#	#	#	#	#	#		#	#					#		#
Combustor Inlet Temperature	#	#	#	#	#		#	#	#	#			#			#	#	#	#	#	#			#			#		#	#	#	
Turbine Exit Pressure	#	#	#	#		#	#	#	#			#	#	#	#	#	#		#	#						#	#	#	#			#
Turbine Exit Temperature	#	#	#		#	#	#	#			#	#	#	#	#	#			#				#		#	#	#	#	#	#	#
Fuel Flow	#	#		#	#	#	#	#		#	#	#		#	#	#		#				#	#		#	#	#	#			#	
Shaft Speed	#	#	#	#	#	#	#		#	#	#	#			#	#	#	#			#	#	#	#				#	#	#		#
Shaft Power	#		#	#	#	#	#		#	#	#	#	#	#			#	#		#	#	#	#	#		#		#		#	#	
Independent Parameters		**6 Measured Parameters**						**5 Measured Parameters**											**4 Measured Parameters**													
Γ_C	I	I	I	I	I	I	I	I	I	I	I	I	I	I	I	I	I	I	I	I	I	I	I	I	I	I	I	I	I	I	I	I
η_C	I	I	I	I	I	I	I	I	I	I	I	I	I	I	I	I	I	I	I	I	I	I	I	I	I	I	I	I	I	I	I	I
Γ_T	I	I	I	I	I	I	I	I	I	I	I	I	I	I	I	I	I	I	I	I	I	I	I	I	I	I	I	I	I	I	I	I
η_C	I	I	I	I	I	I	I	I	I	I	I	I	I	I	I	I	I	I	I	I	I	I	I	I	I	I	I	I	I	I	I	I

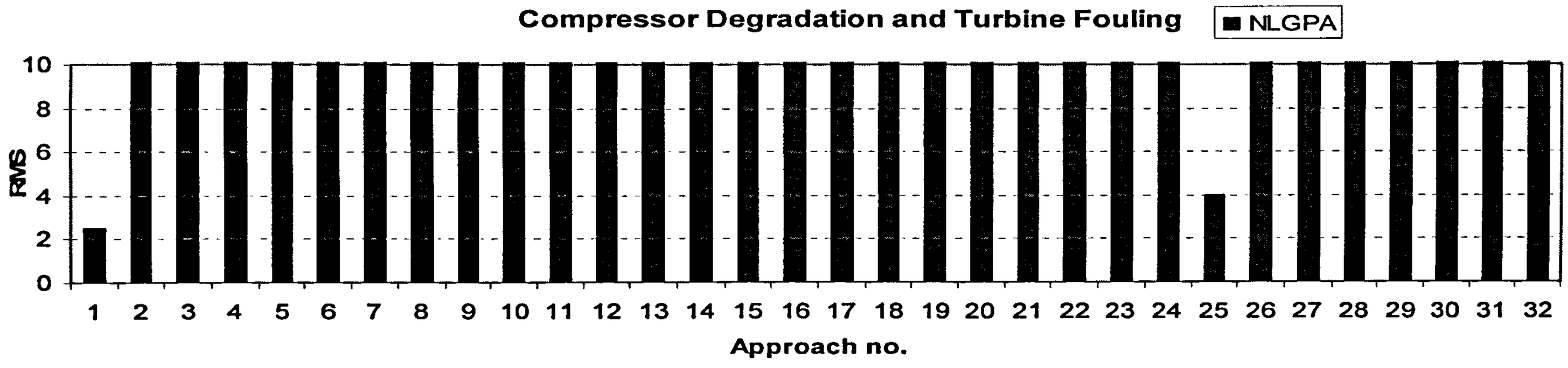

Figure 11.31 - Compressor Degradation and Turbine Fouling Diagnostic – GTM#3

Measured Parameters	Compressor Degradation and Turbine Erosion Approach No.																													
	1	2	3	4	5	6	7	8	9	10	11	12	13	14	15	16	17	18	19	20	21	22	23	24	25	26	27	28	29	30	31	32
Combustor Inlet Pressure	#	#	#	#	#	#		#	#	#	#		#	#	#		#	#	#	#	#	#		#	#					#		#
Combustor Inlet Temperature	#	#	#	#	#		#	#	#	#			#			#	#	#	#	#	#			#			#		#	#	#	
Turbine Exit Pressure	#	#	#	#		#	#	#	#			#	#	#	#	#	#		#	#					#	#	#	#				#
Turbine Exit Temperature	#	#	#		#	#	#	#			#	#	#	#	#	#			#				#		#	#	#	#	#	#	#	#
Fuel Flow	#	#		#	#	#	#	#		#	#	#		#	#	#		#				#	#		#	#	#	#			#	
Shaft Speed	#	#	#	#	#	#	#		#	#	#	#			#	#	#	#			#	#	#	#				#	#	#		#
Shaft Power	#		#	#	#	#	#		#	#	#	#	#	#			#	#		#	#	#	#	#		#			#		#	
Independent Parameters		**6 Measured Parameters**						**5 Measured Parameters**											**4 Measured Parameters**													
Γ_C	I	I	I	I	I	I	I	I	I	I	I	I	I	I	I	I	I	I	I	I	I	I	I	I	I	I	I	I	I	I	I	I
η_C	I	I	I	I	I	I	I	I	I	I	I	I	I	I	I	I	I	I	I	I	I	I	I	I	I	I	I	I	I	I	I	I
Γ_T	I	I	I	I	I	I	I	I	I	I	I	I	I	I	I	I	I	I	I	I	I	I	I	I	I	I	I	I	I	I	I	I
η_C	I	I	I	I	I	I	I	I	I	I	I	I	I	I	I	I	I	I	I	I	I	I	I	I	I	I	I	I	I	I	I	I

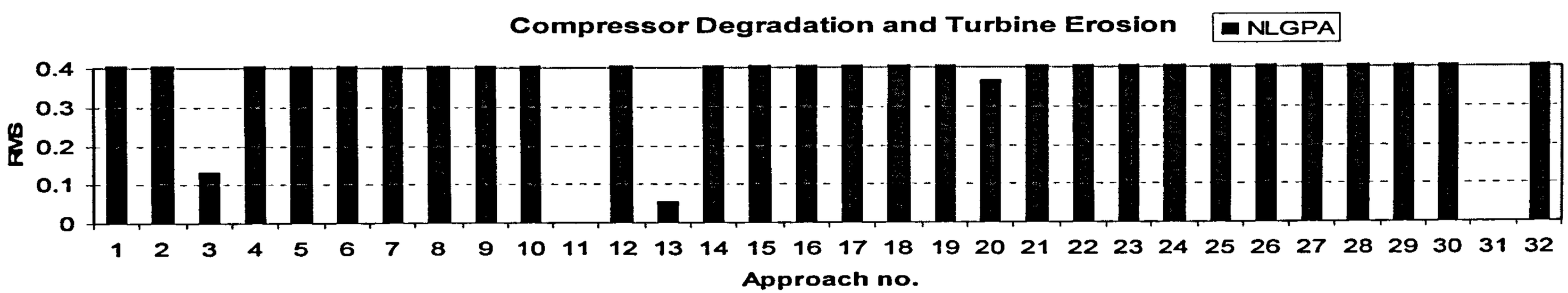

Figure 11.32 - Compressor Degradation and Turbine Erosion Diagnostic – GTM#3

Measured Parameters	Compressor Degradation Approach No.																				
	1	2	3	4	5	6	7	8	9	10	11	12	13	14	15	16	17	18	19	20	21
Compressor Delivery Pressure	#	#	#	#	#	#															
Compressor Delivery Temperature	#						#	#	#	#	#										
Turbine Exit Pressure		#					#					#	#	#	#						
Turbine Exit Temperature			#					#				#				#	#	#			
Fuel Flow				#					#				#			#			#	#	
Shaft Speed					#					#				#			#		#		#
Shaft Power						#					#				#			#		#	#
Independent Parameters																					
Γ_C	I	I	I	I	I	I	I	I	I	I	I	I	I	I	I	I	I	I	I	I	I
η_C	I	I	I	I	I	I	I	I	I	I	I	I	I	I	I	I	I	I	I	I	I
Γ_T																					
η_C																					

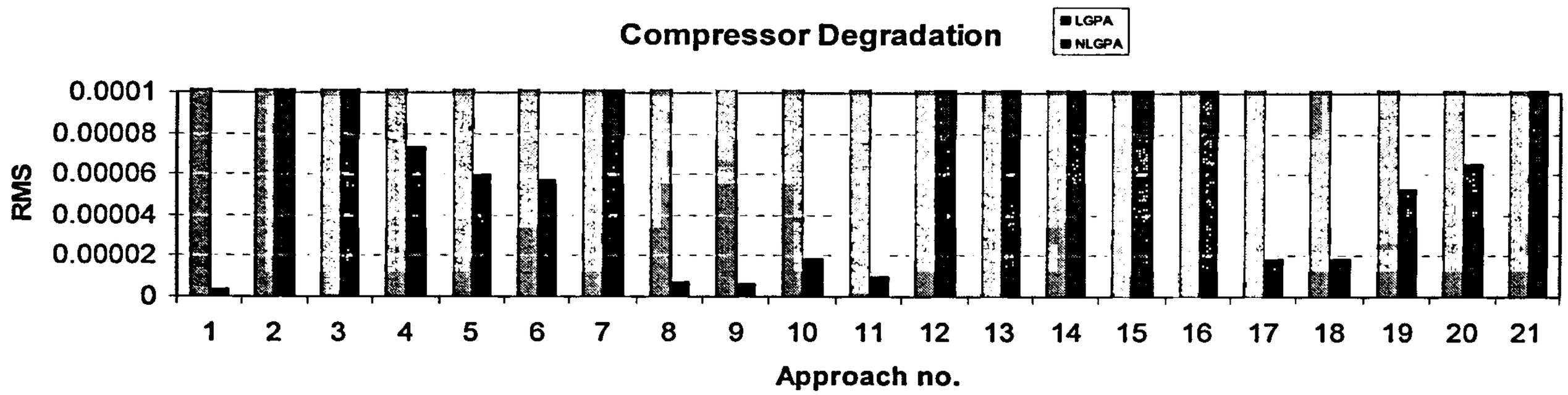

Figure 11.33 - Compressor Degradation Diagnostics – GTM#2

Measured Parameters	Turbine Fouling Approach No.																			
	1	2	3	4	5	6	7	8	9	10	11	12	13	14	15	16	17	18	19	20	21
Compressor Delivery Pressure	#	#	#	#	#	#															
Compressor Delivery Temperature	#						#	#	#	#	#										
Turbine Exit Pressure		#					#					#	#	#	#						
Turbine Exit Temperature			#					#				#				#	#	#			
Fuel Flow				#					#				#			#			#	#	
Shaft Speed					#					#				#			#		#		#
Shaft Power						#					#				#			#		#	#
Independent Parameters																					
Γ_C	I	I	I	I	I	I	I	I	I	I	I	I	I	I	I	I	I	I	I	I	I
η_C	I	I	I	I	I	I	I	I	I	I	I	I	I	I	I	I	I	I	I	I	I
Γ_T	I	I	I	I	I	I	I	I	I	I	I	I	I	I	I	I	I	I	I	I	I
η_C	I	I	I	I	I	I	I	I	I	I	I	I	I	I	I	I	I	I	I	I	I

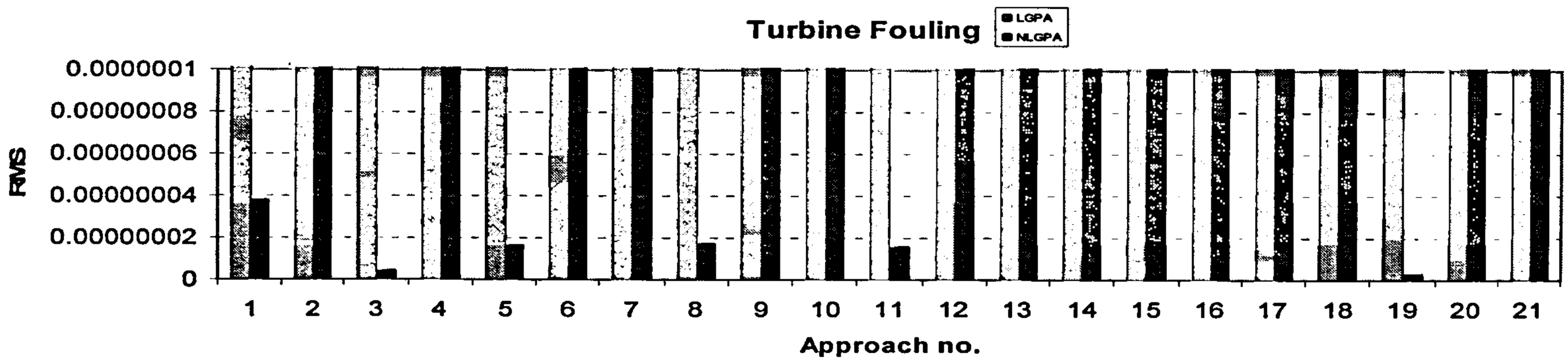

Figure 11.34 - Turbine Fouling Diagnostics – GTM#2

Measured Parameters	Turbine Erosion Approach No.																				
	1	2	3	4	5	6	7	8	9	10	11	12	13	14	15	16	17	18	19	20	21
Compressor Delivery Pressure	#	#	#	#	#	#															
Compressor Delivery Temperature	#						#	#	#	#	#										
Turbine Exit Pressure		#					#					#	#	#	#						
Turbine Exit Temperature			#					#				#				#	#	#			
Fuel Flow				#					#				#			#			#	#	
Shaft Speed					#					#				#			#		#		#
Shaft Power						#					#				#			#		#	#
Independent Parameters																					
Γ_C																					
η_C																					
Γ_T	I	I	I	I	I	I	I	I	I	I	I	I	I	I	I	I	I	I	I	I	I
η_C	I	I	I	I	I	I	I	I	I	I	I	I	I	I	I	I	I	I	I	I	I

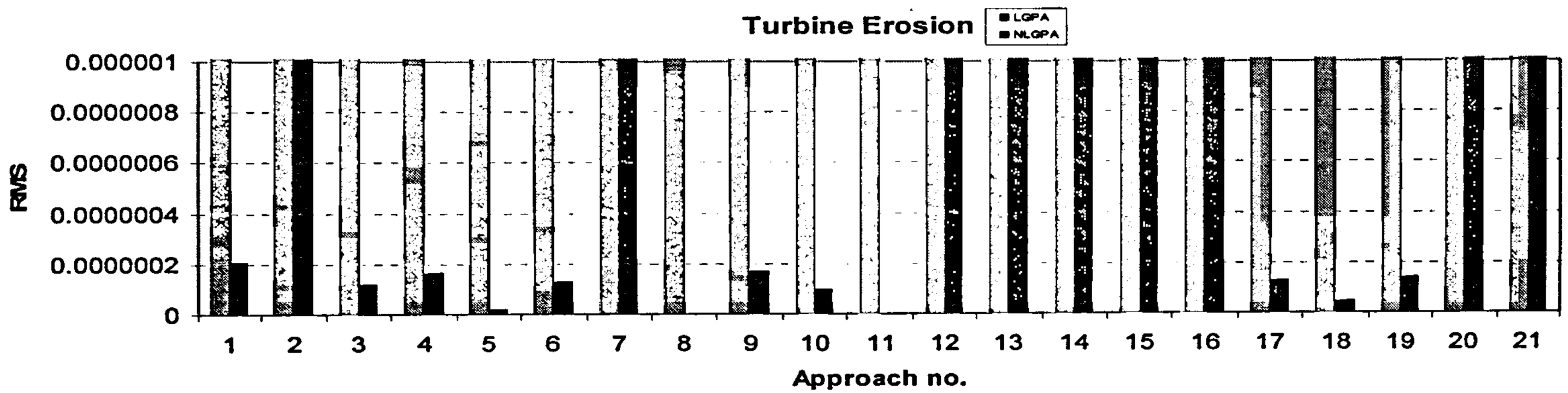

Figure 11.35 –Turbine Erosion Diagnostic – GTM#2

Measured Parameters	Compressor Degradation and Turbine Fouling Approach No.																														
	1	2	3	4	5	6	7	8	9	10	11	12	13	14	15	16	17	18	19	20	21	22	23	24	25	26	27	28	29	30	31	32
Comp. Exit Pressure	#	#	#	#	#	#		#	#	#	#		#	#	#		#	#	#	#	#	#		#	#					#		#
Comp. Exit Temp.	#	#	#	#	#		#	#	#	#			#			#	#	#	#	#	#			#			#		#	#	#	
Turb. Exit Pressure	#	#	#	#		#	#	#	#			#	#	#	#	#	#		#	#					#	#	#	#			#
Turb. Exit Temp.	#	#	#		#	#	#	#			#	#	#	#	#	#			#				#		#	#	#	#	#	#	#
Fuel Flow	#	#		#	#	#	#	#		#	#	#		#	#	#		#				#	#		#	#	#	#			#	
Shaft Speed	#	#	#	#	#	#	#		#	#	#	#			#	#	#	#			#	#	#	#				#	#	#		#
Shaft Power	#		#	#	#	#	#		#	#	#	#	#	#			#	#		#	#	#	#	#		#			#		#	
Independent Parameters		**6 Measured Parameters**						**5 Measured Parameters**											**4 Measured Parameters**													
Γ_C	I	I	I	I	I	I	I	I	I	I	I	I	I	I	I	I	I	I	I	I	I	I	I	I	I	I	I	I	I	I	I	I
η_C	I	I	I	I	I	I	I	I	I	I	I	I	I	I	I	I	I	I	I	I	I	I	I	I	I	I	I	I	I	I	I	I
Γ_T	I	I	I	I	I	I	I	I	I	I	I	I	I	I	I	I	I	I	I	I	I	I	I	I	I	I	I	I	I	I	I	I
η_C	I	I	I	I	I	I	I	I	I	I	I	I	I	I	I	I	I	I	I	I	I	I	I	I	I	I	I	I	I	I	I	I

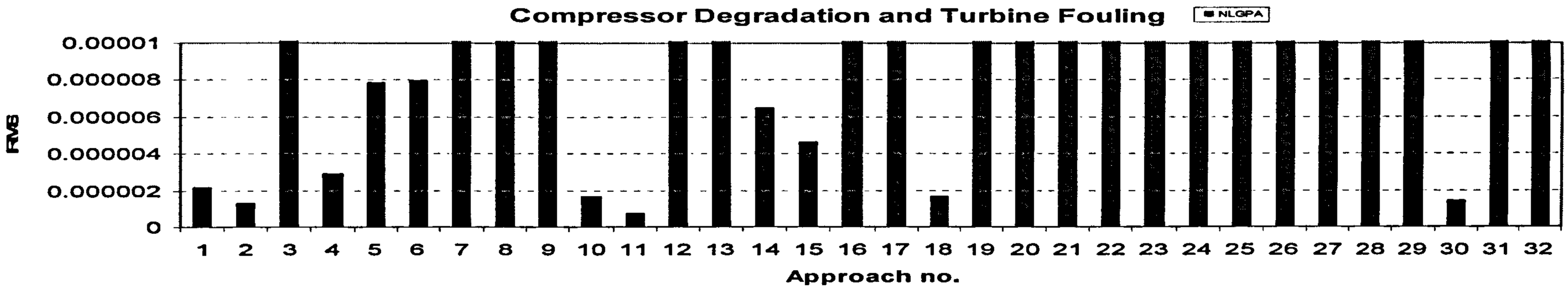

Figure 11.36 - Compressor Degradation and Turbine Fouling Diagnostic – GTM#2

Measured Parameters	Compressor Degradation and Turbine Erosion Approach No.																														
	1	2	3	4	5	6	7	8	9	10	11	12	13	14	15	16	17	18	19	20	21	22	23	24	25	26	27	28	29	30	31	32
Comp. Exit Pressure	#	#	#	#	#	#		#	#	#	#		#	#	#		#	#	#	#	#	#		#	#					#		#
Comp. Exit Temp.	#	#	#	#	#		#	#	#	#			#			#	#	#	#	#	#			#			#		#	#	#	
Turb. Exit Pressure	#	#	#	#		#	#	#	#			#	#	#	#	#	#		#	#					#	#	#	#			#
Turb. Exit Temp.	#	#	#		#	#	#	#			#	#	#	#	#	#			#				#		#	#	#	#	#	#	#
Fuel Flow	#	#		#	#	#	#	#		#	#	#		#	#	#		#				#	#		#	#	#	#			#	
Shaft Speed	#	#	#	#	#	#	#		#	#	#	#			#	#	#	#			#	#	#	#				#	#	#		#
Shaft Power	#		#	#	#	#	#		#	#	#	#	#	#			#	#		#	#	#	#	#		#			#		#	
Independent Parameters		**6 Measured Parameters**						**5 Measured Parameters**											**4 Measured Parameters**													
Γ_C	I	I	I	I	I	I	I	I	I	I	I	I	I	I	I	I	I	I	I	I	I	I	I	I	I	I	I	I	I	I	I	I
η_C	I	I	I	I	I	I	I	I	I	I	I	I	I	I	I	I	I	I	I	I	I	I	I	I	I	I	I	I	I	I	I	I
Γ_T	I	I	I	I	I	I	I	I	I	I	I	I	I	I	I	I	I	I	I	I	I	I	I	I	I	I	I	I	I	I	I	I
η_C	I	I	I	I	I	I	I	I	I	I	I	I	I	I	I	I	I	I	I	I	I	I	I	I	I	I	I	I	I	I	I	I

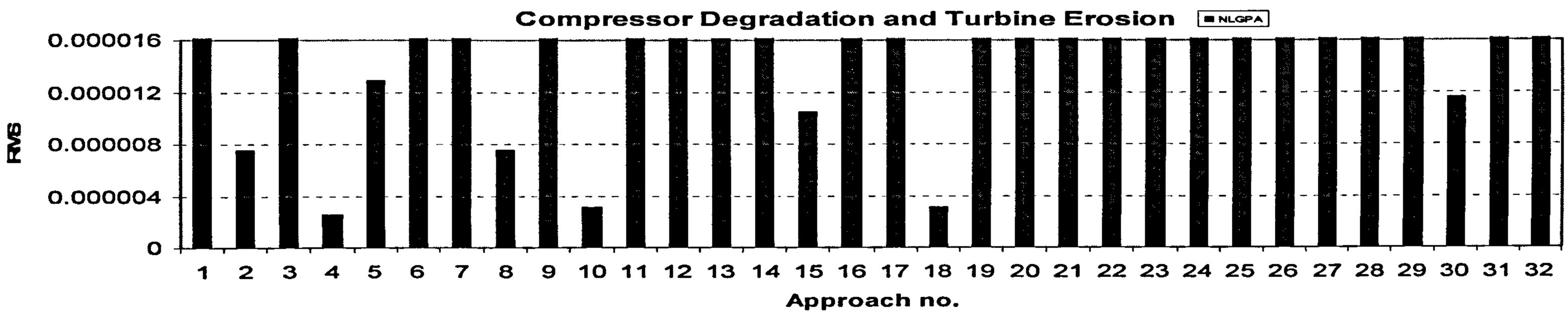

Figure 11.37 - Compressor Degradation and Turbine Erosion Diagnostic – GTM#2

Measured Parameters	Compressor Degradation Approach No.																				
	1	2	3	4	5	6	7	8	9	10	11	12	13	14	15	16	17	18	19	20	21
Compressor Delivery Pressure	#	#	#	#	#	#															
Compressor Delivery Temperature	#						#	#	#	#	#										
Turbine Exit Pressure		#					#					#	#	#	#						
Turbine Exit Temperature			#					#				#				#	#	#			.
Fuel Flow				#					#				#			#			#	#	
Shaft Speed					#					#				#			#		#		#
Shaft Power						#					#				#			#		#	#
Independent Parameters																					
Γ_C	I	I	I	I	I	I	I	I	I	I	I	I	I	I	I	I	I	I	I	I	I
η_C	I	I	I	I	I	I	I	I	I	I	I	I	I	I	I	I	I	I	I	I	I
Γ_T																					
η_C																					

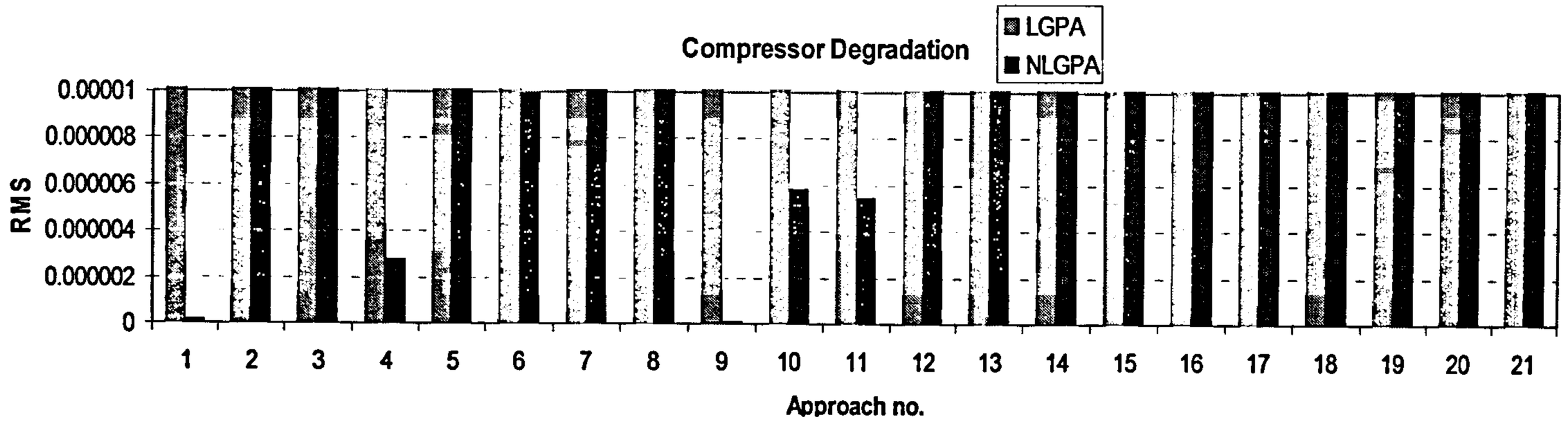

Figure 11.38 - Compressor Degradation Diagnostic – GTM#1

Measured Parameters	Turbine Fouling Approach No.																				
	1	2	3	4	5	6	7	8	9	10	11	12	13	14	15	16	17	18	19	20	21
Compressor Delivery Pressure	#	#	#	#	#	#															
Compressor Delivery Temperature	#						#	#	#	#	#										
Turbine Exit Pressure		#					#					#	#	#	#						
Turbine Exit Temperature			#					#				#				#	#	#			
Fuel Flow				#					#				#			#			#	#	
Shaft Speed					#					#				#			#		#		#
Shaft Power						#					#				#			#		#	#
Independent Parameters																					
Γ_C	I	I	I	I	I	I	I	I	I	I	I	I	I	I	I	I	I	I	I	I	I
η_C	I	I	I	I	I	I	I	I	I	I	I	I	I	I	I	I	I	I	I	I	I

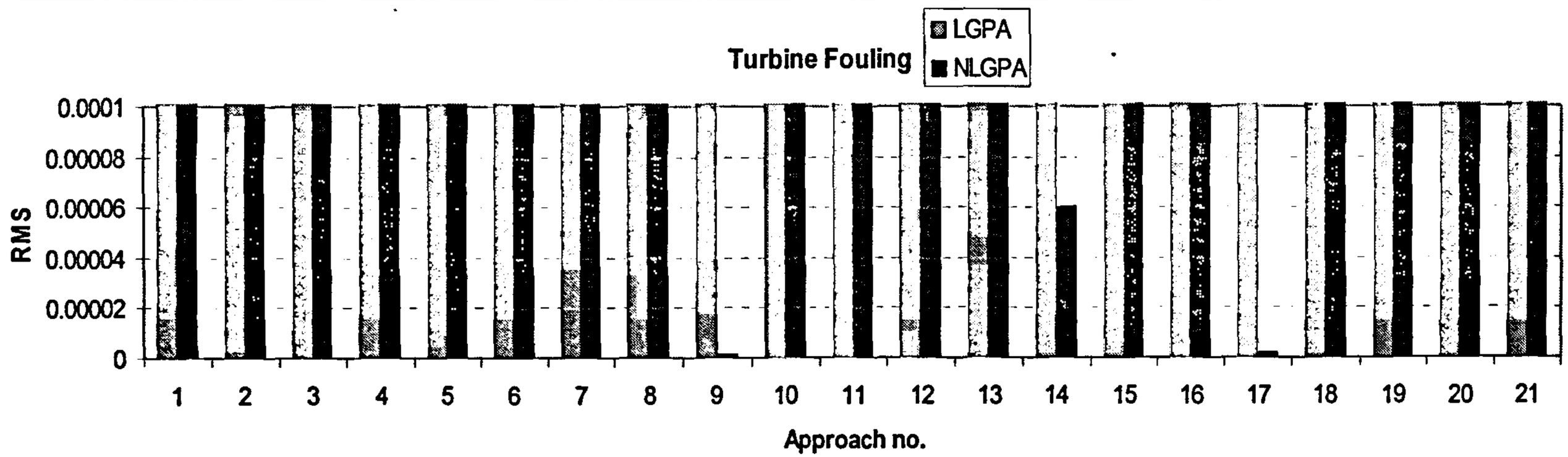

Figure 11.39 - Turbine Fouling Diagnostic – GTM#1

Measured Parameters	Turbine Erosion Approach No.																				
	1	2	3	4	5	6	7	8	9	10	11	12	13	14	15	16	17	18	19	20	21
Compressor Delivery Pressure	#	#	#	#	#	#															
Compressor Delivery Temperature	#						#	#	#	#	#										
Turbine Exit Pressure		#					#					#	#	#	#	#					
Turbine Exit Temperature			#					#				#				#	#	#			
Fuel Flow				#					#				#			#			#	#	
Shaft Speed					#					#				#			#		#		#
Shaft Power						#					#				#			#		#	#
Independent Parameters																					
Γ_C	I	I	I	I	I	I	I	I	I	I	I	I	I	I	I	I	I	I	I	I	I
η_C	I	I	I	I	I	I	I	I	I	I	I	I	I	I	I	I	I	I	I	I	I
Γ_T	I	I	I	I	I	I	I	I	I	I	I	I	I	I	I	I	I	I	I	I	I
η_C	I	I	I	I	I	I	I	I	I	I	I	I	I	I	I	I	I	I	I	I	I

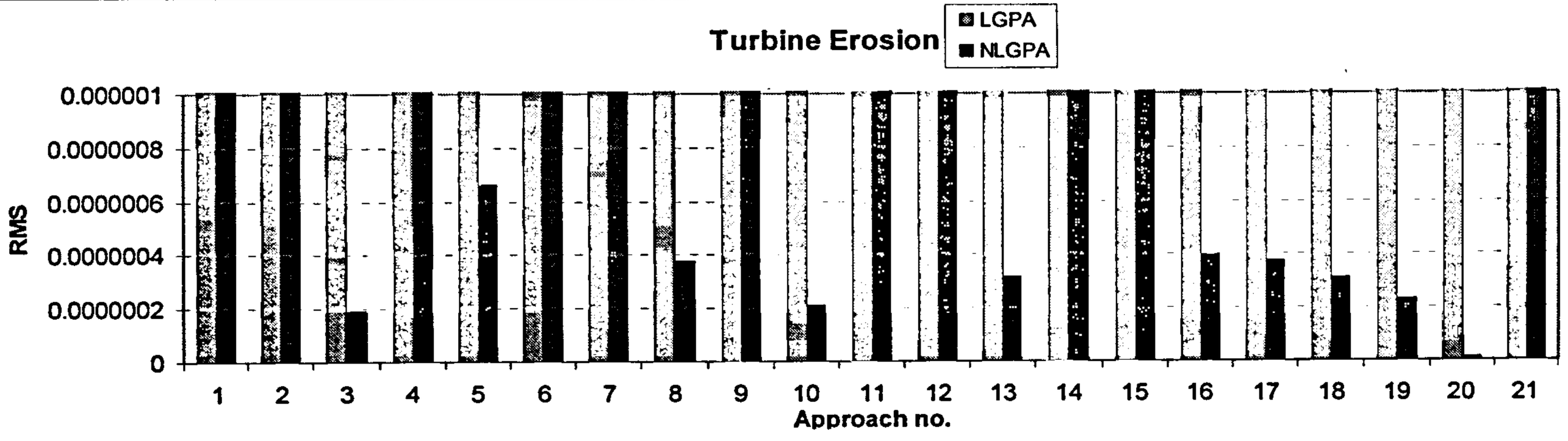

Figure 11.40 - Turbine Erosion Diagnostic – GTM#1

Measured Parameters	Compressor Degradation and Turbine Fouling Approach No.																															
	1	2	3	4	5	6	7	8	9	10	11	12	13	14	15	16	17	18	19	20	21	22	23	24	25	26	27	28	29	30	31	32
Comp. Exit Pressure	#	#	#	#	#	#		#	#	#	#		#	#	#		#	#	#	#	#	#		#	#					#		#
Comp. Exit Temp.	#	#	#	#	#		#	#	#	#			#			#	#	#	#	#	#			#			#		#	#	#	
Turb. Exit Pressure	#	#	#	#		#	#	#	#			#	#	#	#	#	#		#	#					#	#	#	#				#
Turb. Exit Temp.	#	#	#		#	#	#	#			#	#	#	#	#	#			#				#		#	#	#	#	#	#	#	#
Fuel Flow	#	#		#	#	#	#	#		#	#	#		#	#	#		#				#	#		#	#	#	#			#	
Shaft Speed	#	#	#	#	#	#	#		#	#	#	#			#	#	#	#			#	#	#	#				#	#	#		#
Shaft Power	#		#	#	#	#	#		#	#	#	#	#	#			#	#		#	#	#	#	#		#			#		#	
Independent Parameters		**6 Measured Parameters**						**5 Measured Parameters**											**4 Measured Parameters**													
Γ_C	I	I	I	I	I	I	I	I	I	I	I	I	I	I	I	I	I	I	I	I	I	I	I	I	I	I	I	I	I	I	I	I
η_C	I	I	I	I	I	I	I	I	I	I	I	I	I	I	I	I	I	I	I	I	I	I	I	I	I	I	I	I	I	I	I	I
Γ_T	I	I	I	I	I	I	I	I	I	I	I	I	I	I	I	I	I	I	I	I	I	I	I	I	I	I	I	I	I	I	I	I
η_C	I	I	I	I	I	I	I	I	I	I	I	I	I	I	I	I	I	I	I	I	I	I	I	I	I	I	I	I	I	I	I	I

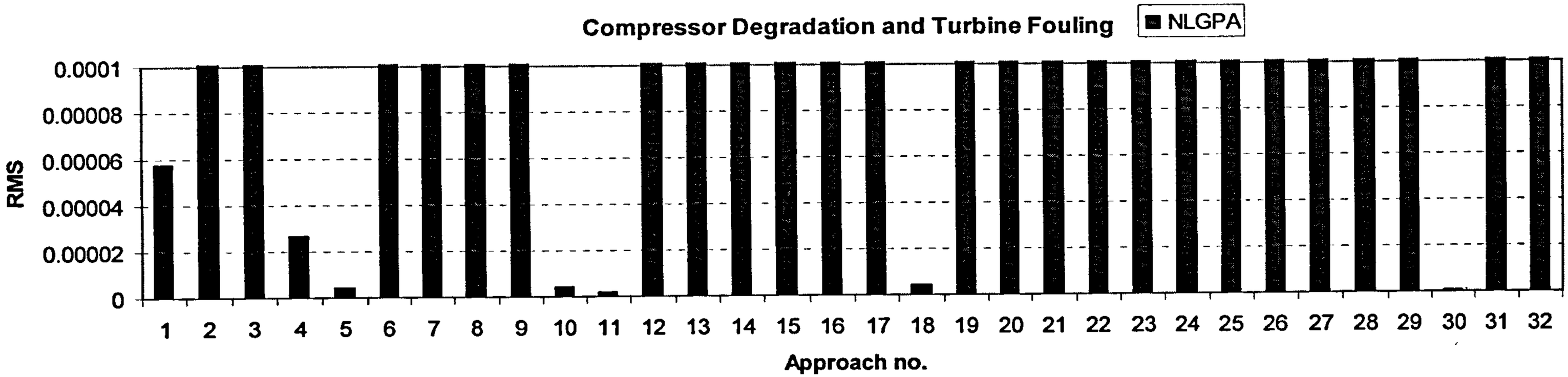

Figure 11.41 - Compressor Degradation and Turbine Fouling Diagnostic – GTM#1

Measured Parameters	Compressor Degradation and Turbine Erosion Approach No.																													
	1	2	3	4	5	6	7	8	9	10	11	12	13	14	15	16	17	18	19	20	21	22	23	24	25	26	27	28	29	30	31	32
Comp. Exit Pressure	#	#	#	#	#	#		#	#	#	#		#	#	#		#	#	#	#	#	#		#	#					#		#
Comp. Exit Temp.	#	#	#	#	#		#	#	#	#			#			#	#	#	#	#	#			#			#		#	#	#	
Turb. Exit Pressure	#	#	#	#		#	#	#	#			#	#	#	#	#	#		#	#					#	#	#	#				#
Turb. Exit Temp.	#	#	#		#	#	#	#			#	#	#	#	#	#			#				#		#	#	#	#	#	#	#	#
Fuel Flow	#	#		#	#	#	#	#		#	#	#		#	#	#		#				#	#		#	#	#	#			#	
Shaft Speed	#	#	#	#	#	#	#		#	#	#	#			#	#	#	#			#	#	#	#				#	#	#		#
Shaft Power	#		#	#	#	#	#		#	#	#	#	#	#			#	#		#	#	#	#	#		#		#		#		
Independent Parameters		**6 Measured Parameters**						**5 Measured Parameters**											**4 Measured Parameters**													
Γ_C	I	I	I	I	I	I	I	I	I	I	I	I	I	I	I	I	I	I	I	I	I	I	I	I	I	I	I	I	I	I	I	I
η_C	I	I	I	I	I	I	I	I	I	I	I	I	I	I	I	I	I	I	I	I	I	I	I	I	I	I	I	I	I	I	I	I
Γ_T	I	I	I	I	I	I	I	I	I	I	I	I	I	I	I	I	I	I	I	I	I	I	I	I	I	I	I	I	I	I	I	I
η_C	I	I	I	I	I	I	I	I	I	I	I	I	I	I	I	I	I	I	I	I	I	I	I	I	I	I	I	I	I	I	I	I

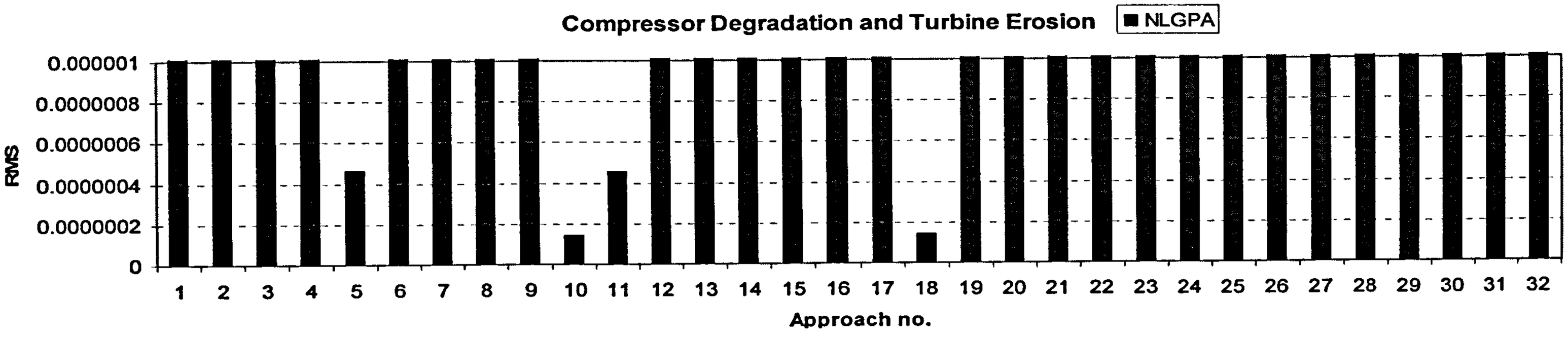

Figure 11.42 - Compressor Degradation and Turbine Erosion Diagnostic – GTM#1

Chapter 12 – Appendix C Applications of Multi-units Generation Schedule Optimisation

12 - Appendix C Applications of Multi-units Generation Schedule Optimisation

12.1 - Generation Schedule Optimisation for an 8-unit mini-pool with system constraints

Table 12.1 – Power setting and demand of an 8-units mini-pool

	$P_{i,t}$	[kW]																						
t [h]	1	2	3	4	5	6	7	8	9	10	11	12	13	14	15	16	17	18	19	20	21	22	23	24	Total
Units#1	4,699	4,934	5,188	5,253	5,253	5,253	5,253	5,108	4,848	4,629	4,522	4,462	4,372	4,332	4,307	4,336	4,394	4,439	4,504	4,529	4,554	4,608	4,636	4,698	113,111
Units#2	11,573	11,573	11,573	11,573	11,573	11,573	11,573	11,573	11,488	11,101	10,812	10,496	10,148	10,028	9,905	9,977	10,127	10,254	10,481	10,815	11,039	11,271	11,421	11,531	263,478
Units#3	3,132	3,271	3,461	3,496	3,496	3,496	3,496	3,414	3,230	3,081	3,006	2,957	2,896	2,872	2,872	2,872	2,920	2,948	2,994	2,994	3,029	3,062	3,062	3,000	75,055
Units#4	3,988	3,988	4,016	4,016	4,075	4,075	4,075	4,002	4,002	3,926	3,926	3,856	3,856	3,856	3,856	3,856	3,856	3,856	3,878	3,878	3,911	3,911	3,945	3,945	94,546
Units#5	4,823	4,823	4,864	4,864	4,937	4,937	4,937	4,851	4,825	4,757	4,729	4,666	4,666	4,666	4,638	4,638	4,660	4,660	4,686	4,686	4,728	4,728	4,772	4,772	114,315
Units#6	10,716	10,716	10,799	10,799	10,949	10,949	10,949	10,771	10,718	10,575	10,519	10,388	10,388	10,388	10,331	10,331	10,375	10,375	10,429	10,472	10,472	10,562	10,562	10,644	254,179
Units#7	1,755	1,755	1,768	1,786	1,786	1,822	1,800	1,776	1,749	1,732	1,696	1,662	1,641	1,641	1,619	1,619	1,647	1,647	1,647	1,696	1,723	1,723	1,736	1,758	41,184
Units#8	193	194	194	196	198	197	197	196	192	185	182	176	172	171	168	169	172	174	176	181	182	187	189	191	4,432
Subtotal	40,879	41,254	41,865	41,984	42,267	42,303	42,280	41,690	41,051	39,986	39,391	38,662	38,140	37,953	37,697	37,798	38,150	38,353	38,795	39,250	39,638	40,053	40,323	40,539	960,300
	$MFC_{i,t}$	[kg/s]																							
t [h]	1	2	3	4	5	6	7	8	9	10	11	12	13	14	15	16	17	18	19	20	21	22	23	24	Total
Units#1	0.2876	0.2984	0.3093	0.3113	0 3113	0.3113	0 3113	0.3062	0.2941	0.2847	0.2801	0.2780	0.2743	0.2722	0.2710	0.2719	0.2743	0.2763	0.2790	0.2804	0.2815	0.2836	0.2850	0.2875	6 921
Units#2	0 6899	0.6899	0 6899	0 6899	0 6899	0.6899	0.6899	0.6899	0 6862	0 6675	0 6563	0.6396	0.6235	0.6192	0.6135	0.6155	0 6218	0.6279	0 6396	0.6552	0.6635	0 6741	0 6816	0 6869	15 891
Units#3	0.2227	0.2312	0.2400	0.2416	0.2416	0.2416	0.2416	0.2375	0.2279	0.2203	0.2166	0 2149	0.2120	0.2103	0 2093	0.2100	0.2120	0.2136	0.2158	0.2170	0.2177	0.2194	0 2207	0.2164	5.352
Units#4	0.2814	0.2621	0.2630	0.2639	0.2656	0.2667	0.2652	0.2631	0.2617	0.2595	0.2581	0.2560	0.2554	0.2551	0 2546	0.2549	0.2552	0.2557	0.2563	0.2572	0 2578	0.2587	0 2595	0.2602	6.227
Units#5	0.2930	0.2937	0.2948	0.2959	0.2977	0.2990	0.2973	0.2949	0.2935	0.2908	0 2894	0.2869	0.2862	0 2858	0.2855	0.2858	0.2861	0.2866	0.2872	0.2882	0 2889	0.2899	0.2908	0.2917	6 979
Units#6	0 6494	0.6511	0 6534	0.6558	0 6598	0 6627	0.6590	0 6537	0 6505	0 6445	0 6414	0 6358	0 6343	0 6335	0 6327	0 6335	0 6341	0 6353	0.6365	0 6386	0 6406	0 6424	0 6448	0.6463	15.470
Units#7	0 1241	0 1244	0 1248	0.1256	0 1261	0.1271	0.1266	0 1255	0.1242	0.1233	0 1218	0.1201	0 1190	0.1184	0.1179	0.1179	0.1188	0 1187	0 1192	0 1216	0.1224	0 1230	0.1232	0.1242	2 938
Units#8	0 0133	0 0133	0 0133	0 0133	0 0133	0 0133	0 0133	0 0133	0 0133	0 0132	0 0132	0 0132	0 0132	0 0131	0 0131	0 0131	0 0132	0 0132	0 0132	0 0132	0 0132	0 0133	0 0133	0 0133	0 318
Subtotal	3	3	3	3	3	3	3	3	3	3	2	2	2	2	2	2	2	2	2	2	2	3	3	3	60 095
	$ED_{i,t}$	[kW]																							
t [h]	1	2	3	4	5	6	7	8	9	10	11	12	13	14	15	16	17	18	19	20	21	22	23	24	Total
Units#1	4576	4542	4498	4509	4453	4442	4520	4642	4753	4487	4564	4642	4820	4964	5053	5109	5020	4942	4698	4531	4331	4209	4064	4164	110,536
Units#2	9366	7929	7778	7475	7475	6416	7173	7778	9366	9669	10198	10274	10576	10425	10350	9896	10047	10123	10176	10479	10662	11087	10652	9442	224,814
Units#3	1607	1485	1415	1293	1275	1258	1188	1433	1660	1852	1834	2027	2097	2009	1992	1887	1922	1974	2131	2289	2446	2324	2044	1957	43,399
Units#4	1915	1765	1792	1851	1855	1960	1836	2113	2190	2040	1980	1871	2053	2692	2712	2767	2821	2276	1180	1792	1577	1432	1488	1735	47,693
Units#5	3185	3152	3123	3189	3178	3427	3477	3409	3383	3196	3600	3497	3592	2950	3065	3220	3182	3092	2716	3481	3087	2969	3028	3144	77,342
Units#6	6762	6489	6653	6612	6694	6639	5983	6543	6680	7199	6844	5956	7991	7978	7800	7295	8060	7896	6092	5532	4959	5109	5300	5724	158,790
Units#7	790	710	683	719	674	799	925	1033	1042	1087	1141	1141	1105	1069	1078	1096	1177	1195	1341	1231	1069	1033	916	871	23,925
Units#8	70	63	60	58	57	51	53	60	67	75	83	85	88	91	86	84	82	84	89	102	107	98	83	81	1,852
Subtotal	28,270	26,135	26,001	25,706	25,662	24,993	25,154	27,011	29,142	29,604	30,245	29,493	32,322	32,178	32,136	31,353	32,311	31,582	28,423	29,437	28,238	28,260	27,576	27,118	688,350

Table 12.2 – Running cost of an 8-units mini-pool over schedule time

t [h]	1	2	3	4	5	6	7	8	9	10	11	12	13	14	15	16	17	18	19	20	21	22	23	24	Total
Unit#1	0.01	85 11	83 91	0 01	0 01	88.99	84.58	82.97	79 49	76.71	75.35	74 69	73 59	73.01	72 67	72.96	73 67	74.27	75 07	75 44	75.76	76 40	76.80	77.55	1,629.00
Unit#2	0 01	196 57	187.18	0 01	0 01	196 57	187.18	187.18	186 07	180.74	177.33	172 68	168 03	166 68	165 04	165.72	167.60	169 34	172 63	177.11	179 67	182.75	184 87	186 38	3,757.35
Unit#3	0 01	0.01	0 01	0.01	0 01	0 01	66 46	62.37	0.01	0 01	0.01	0 01	58.05	0 01	0 01	57.56	55.21	55 66	56.26	56 54	0 01	0 01	0 01	0 01	468.30
Unit#4	0.01	0.01	0.01	0 01	0 01	0 01	74.23	69 90	0 01	0 01	0.01	0 01	71.37	67.68	67.58	67.65	67.71	67 81	68 01	68.20	0 01	0 01	0 01	0 01	690.27
Unit#5	0.01	0 01	0 01	0.01	0.01	0 01	84.90	79 67	79.27	78 46	78 05	77 30	77.16	77.08	76.90	76 98	77.11	77.22	77.44	77 66	77 95	78 17	78 51	0 01	1,329 92
Unit#6	0 01	185.28	176 67	0.01	0.01	188.58	178.41	176 65	175.78	174 00	173.13	171 49	171 16	171 00	170 63	170.79	171.08	171.33	171.78	172 38	172 79	173 51	174 01	174 62	3,665 09
Unit#7	0.01	0.01	0 01	0.01	0 01	0 01	34 73	32.86	0.01	0 01	0 01	0 01	32.55	0.01	0 01	32.24	30 98	30 96	31.06	31.76	0 01	0 01	0 01	0.01	257.30
Unit#8	0 01	0 01	0 01	0 01	0 01	0 01	3 69	3 52	0 01	0 01	0 01	0 01	3 57	0 01	0 01	3 56	3 40	3 41	3 42	3 45	0 01	0 01	0 01	0 01	28 18
Subtotal	0 08	467 00	447 81	0 08	0 08	474 19	714 18	695 13	520 66	509 94	503 91	496.20	655 47	555 47	552 86	647 46	646 75	649 99	655 69	662 53	506 21	510 88	514 23	438 60	11,825 39

Table 12.3 – Optimisation results of an 8-units mini-pool over schedule time with minimum up and down time constraint

t [h]	1	2	3	4	5	6	7	8	9	10	11	12	13	14	15	16	17	18	19	20	21	22	23	24	Total
ESP_t [£/MWh]	19.96	16.27	15.88	15.74	15 66	16.27	20.29	21.73	17.19	17.16	17.04	16.85	22.78	17.37	19 62	24.70	30.23	61.29	34 18	25.78	16.87	16 53	15.84	15.01	-
EBP_t [£/MWh]	22.50	17.53	15.88	15.74	15.96	20.11	33.91	32 96	27.07	26 68	26.14	24.71	24.25	21.79	47.81	48 16	79.13	104.05	74 93	51 45	23 43	22 92	19.26	17.20	-
DP_t [kW]	28270	0	0	25708	25662	0	0	0	0	0	0	0	0	0	0	0	0	0	0	0	0	0	0	245	79,883
SP_t [kW]	0	1087	1559	0	0	2783	17125	14679	2737	1458	337	519	5818	1091	902	6445	5839	6771	10371	9813	2555	2909	3815	0	98,613
$RC_{t,t}$ [£]	0.08	467.00	447.81	0.08	0.08	474 19	714.18	695.13	520 66	509.94	503 91	496.20	655 47	555.47	552.86	647.46	646.75	649 99	655.69	662.53	506.21	510 88	514.23	438.60	11,825
$CDP_{t,t}$ [£] -	636 08	0.00	0.00	404.73	409.50	0.00	0.00	0.00	0 00	0.00	0 00	0.00	0.00	0 00	0.00	0 00	0 00	0.00	0.00	0.00	0.00	0.00	0.00	4.20	1,455
$TEC_{t,t}$ [£]	507.84	470.02	467.21	461.56	460.56	449.24	451.96	485 73	523.92	532.81	544.31	532 17	582.10	578.54	577.81	563.80	580 73	568.48	514 49	532.71	511.92	511.36	497.58	489 32	12,396
$TESM_{t,t}$ [£]	0.00	17.70	24.76	0 00	0.00	45.28	347.48	318.99	47.06	25.02	5 74	8.74	132.50	18.96	17.69	159 18	176.53	414.99	354.44	252.94	43.10	48 09	60 43	0 00	2,520
$R_{t,t}$ [£]	507.84	487.71	491 97	461.56	460 56	494 52	799.43	804 72	570.98	557.83	550 05	540.91	714 60	597 49	595.50	722.98	757.25	983 47	868 94	785.65	555 02	559.44	558.00	489 32	14,916
$PC_{t,t}$ [£]	636.16	467 00	447.81	404 81	409.58	474 19	714 18	695.13	520 66	509 94	503.91	496.20	655 47	555 47	552.86	647 46	646 75	649.99	655.69	662.53	506.21	510 88	514.23	442.80	13,280
$Prf_{t,t}$ [£]	-128 32	20 71	44 16	56 75	50 98	20 33	85.25	109 60	50 32	47 88	46 14	44 71	59 14	42 02	42 64	75 53	110 50	333 48	213 25	123 12	48 81	48 56	43 78	46 52	1,636

Table 12.4 - Optimal 8-units mini-pool schedule obtained by multi-units commitment algorithm with minimum up and down time constraint

t [h]	1	2	3	4	5	6	7	8	9	10	11	12	13	14	15	16	17	18	19	20	21	22	23	24
Unit#1	0	1	1	0	0	1	1	1	1	1	1	1	1	1	1	1	1	1	1	1	1	1	1	1
Unit#2	0	1	1	0	0	1	1	1	1	1	1	1	1	1	1	1	1	1	1	1	1	1	1	1
Unit#3	0	0	0	0	0	0	1	1	0	0	0	0	1	0	0	1	1	1	1	1	0	0	0	0
Unit#4	0	0	0	0	0	0	1	1	0	0	0	0	1	1	1	1	1	1	1	1	0	0	0	0
Unit#5	0	0	0	0	0	0	1	1	1	1	1	1	1	1	1	1	1	1	1	1	1	1	1	0
Unit#6	0	1	1	0	0	1	1	1	1	1	1	1	1	1	1	1	1	1	1	1	1	1	1	1
Unit#7	0	0	0	0	0	0	1	1	0	0	0	0	1	0	0	1	1	1	1	1	0	0	0	0
Unit#8	0	0	0	0	0	0	1	1	0	0	0	0	1	0	0	1	1	1	1	1	0	0	0	0

Table 12.5 – Cumulative time of operation of an 8-units mini-pool schedule obtained by multi-units commitment algorithm with minimum up and down time constraint

t [h]	1	2	3	4	5	6	7	8	9	10	11	12	13	14	15	16	17	18	19	20	21	22	23	24
Unit#1	-2	1	2	-1	-2	1	2	3	4	5	6	7	8	9	10	11	12	13	14	15	16	17	18	19
Unit#2	-2	1	2	-1	-2	1	2	3	4	5	6	7	8	9	10	11	12	13	14	15	16	17	18	19
Unit#3	-2	-3	-4	-5	-6	-7	1	2	-1	-2	-3	-4	1	-1	-2	1	2	3	4	5	-1	-2	-3	-4
Unit#4	-2	-3	-4	-5	-6	-7	1	2	-1	-2	-3	-4	1	2	3	4	5	6	7	8	-1	-2	-3	-4
Unit#5	-2	-3	-4	-5	-6	-7	1	2	3	4	5	6	7	8	9	10	11	12	13	14	15	16	17	-1
Unit#6	-2	1	2	-1	-2	1	2	3	4	5	6	7	8	9	10	11	12	13	14	15	16	17	18	19
Unit#7	-2	-3	-4	-5	-6	-7	1	2	-1	-2	-3	-4	1	-1	-2	1	2	3	4	5	-1	-2	-3	-4
Unit#8	-2	-3	-4	-5	-6	-7	1	2	-1	-2	-3	-4	1	-1	-2	1	2	3	4	5	-1	-2	-3	-4

12.2 - Generation Schedule Optimisation for a 40-unit mini-pool

Table 12.6 – Power setting and demand of a 40 units mini-pool

	P_{Lt} [kW]																							
t [h]	1	2	3	4	5	6	7	8	9	10	11	12	13	14	15	16	17	18	19	20	21	22	23	24	Total
Units#1, 9, 17, 25, 33	4,699	4,934	5,188	5,253	5,253	5,253	5,253	5,108	4,848	4,629	4,522	4,462	4,372	4,332	4,307	4,336	4,394	4,439	4,504	4,529	4,554	4,608	4,636	4,698	565,557
Units#2, 10, 18, 26, 34	11,573	11,573	11,573	11,573	11,573	11,573	11,573	11,573	11,488	11,101	10,812	10,496	10,148	10,028	9,905	9,977	10,127	10,254	10,481	10,815	11,039	11,271	11,421	11,531	1,317,388
Units#3, 11, 19, 27, 35	3,132	3,271	3,461	3,496	3,496	3,496	3,496	3,414	3,230	3,081	3,006	2,957	2,896	2,872	2,872	2,872	2,920	2,948	2,994	2,994	3,029	3,062	3,062	3,000	375,276
Units#4, 12, 20, 28, 36	3,988	3,988	4,016	4,016	4,075	4,075	4,075	4,002	4,002	3,926	3,926	3,856	3,856	3,856	3,856	3,856	3,856	3,856	3,878	3,878	3,911	3,911	3,945	3,945	472,730
Units#5, 13, 21, 29, 37	4,823	4,823	4,864	4,864	4,937	4,937	4,937	4,851	4,825	4,757	4,729	4,668	4,668	4,666	4,638	4,638	4,660	4,660	4,686	4,686	4,728	4,728	4,772	4,772	571,577
Units#6, 14, 22, 30, 38	10,716	10,716	10,799	10,799	10,949	10,949	10,949	10,771	10,718	10,575	10,519	10,388	10,388	10,388	10,331	10,331	10,375	10,375	10,429	10,472	10,472	10,562	10,562	10,644	1,270,893
Units#7, 15, 23, 31, 39	1,755	1,755	1,768	1,786	1,786	1,822	1,800	1,776	1,749	1,732	1,696	1,662	1,641	1,641	1,619	1,619	1,647	1,647	1,647	1,696	1,723	1,723	1,736	1,758	205,918
Units#8, 16, 24, 32, 40	193	194	194	196	198	197	197	196	192	185	182	176	172	171	168	169	172	174	176	181	182	187	189	191	22,162
Subtotal	204,395	206,268	209,327	209,919	211,336	211,514	211,399	208,451	205,257	199,930	196,954	193,312	190,701	189,764	188,483	188,989	190,751	191,766	193,973	196,252	198,189	200,263	201,614	202,696	4,801,501
	MFC_{Lt} [kg/s]																								
t [h]	1	2	3	4	5	6	7	8	9	10	11	12	13	14	15	16	17	18	19	20	21	22	23	24	Total
Units#1, 9, 17, 25, 33	0.2876	0.2984	0.3093	0.3113	0 3113	0.3113	0 3113	0 3062	0.2941	0.2847	0.2801	0.2780	0.2743	0.2722	0.2710	0.2719	0.2743	0.2763	0.2790	0.2804	0.2815	0.2836	0.2850	0.2875	34 603
Units#2, 10, 18, 26, 34	0 6899	0 6899	0.6899	0 6899	0.6899	0 6899	0 6899	0.6899	0 6862	0 6675	0.6563	0.6396	0 6235	0.6192	0 6135	0 6155	0 6218	0 6279	0 6396	0 6552	0.6635	0 6741	0.6816	0 6869	79 457
Units#3, 11, 19, 27, 35	0.2227	0.2312	0.2400	0.2416	0.2416	0 2416	0 2416	0.2375	0.2279	0.2203	0.2166	0.2149	0.2120	0.2103	0.2093	0 2100	0.2120	0 2136	0.2158	0.2170	0 2177	0 2194	0.2207	0.2164	26.759
Units#4, 12, 20, 28, 36	0.2614	0 2621	0.2630	0.2639	0.2656	0.2667	0.2652	0.2631	0 2617	0.2595	0.2581	0.2560	0.2554	0.2551	0.2546	0.2549	0.2552	0.2557	0.2563	0.2572	0 2578	0.2587	0.2595	0.2602	31.135
Units#5, 13, 21, 29, 37	0.2930	0.2937	0.2948	0.2959	0.2977	0 2990	0.2973	0.2949	0.2935	0.2908	0 2894	0.2869	0.2862	0.2858	0.2855	0.2858	0.2861	0.2866	0.2872	0.2882	0.2889	0.2899	0.2908	0.2917	34 897
Units#6, 14, 22, 30, 38	0 6494	0.6511	0 6534	0 6558	0 6598	0 6627	0 6590	0.6537	0.6505	0 6445	0 6414	0 6358	0 6343	0 6335	0 6327	0.6335	0 6341	0 6353	0 6365	0 6386	0 6406	0 6424	0 6448	0.6463	77.348
Units#7, 15, 23, 31, 39	0.1241	0 1244	0.1248	0.1256	0 1261	0.1271	0 1266	0 1255	0 1242	0 1233	0.1218	0.1201	0 1190	0 1184	0.1179	0.1179	0.1188	0.1187	0 1192	0.1216	0 1224	0.1230	0.1232	0 1242	14.689
Units#8, 16, 24, 32, 40	0 0133	0.0133	0 0133	0 0133	0 0133	0 0133	0 0133	0 0133	0 0133	0 0132	0 0132	0 0132	0 0132	0 0131	0 0131	0 0131	0 0132	0 0132	0 0132	0 0132	0 0132	0 0133	0 0133	0 0133	1 589
Subtotal	12 707	12 820	12 942	12 987	13 027	13 058	13 022	12 921	12 757	12 519	12.384	12.223	12 089	12 038	11 989	12.014	12 077	12 136	12 234	12 357	12 428	12 523	12 594	12 632	300 477
	ED_{Lt} [kW]																								
t [h]	1	2	3	4	5	6	7	8	9	10	11	12	13	14	15	16	17	18	19	20	21	22	23	24	Total
Units#1, 9, 17, 25, 33	4576	4542	4498	4509	4453	4442	4520	4642	4753	4487	4564	4642	4820	4964	5053	5109	5020	4942	4698	4531	4331	4209	4064	4164	552,678
Units#2, 10, 18, 26, 34	9366	7929	7778	7475	7475	6416	7173	7778	9366	9669	10198	10274	10576	10425	10350	9896	10047	10123	10176	10479	10662	11087	10652	9442	1,124,069
Units#3, 11, 19, 27, 35	1607	1485	1415	1293	1275	1258	1188	1433	1660	1852	1834	2027	2097	2009	1992	1887	1922	1974	2131	2289	2446	2324	2044	1957	216,995
Units#4, 12, 20, 28, 36	1915	1765	1792	1851	1855	1960	1836	2113	2190	2040	1980	1871	2053	2692	2712	2767	2821	2276	1180	1792	1577	1432	1488	1735	238,465
Units#5, 13, 21, 29, 37	3185	3152	3123	3189	3178	3427	3477	3409	3383	3196	3600	3497	3592	2950	3065	3220	3182	3092	2716	3481	3087	2969	3028	3144	386,710
Units#6, 14, 22, 30, 38	6762	6489	6653	6612	6694	6639	5983	6543	6680	7199	6844	5956	7991	7978	7800	7295	8060	7896	6092	5532	4959	5109	5300	5724	793,950
Units#7, 15, 23, 31, 39	790	710	683	719	674	799	925	1033	1042	1087	1141	1141	1105	1069	1078	1096	1177	1195	1341	1231	1069	1033	916	871	119,625
Units#8, 16, 24, 32, 40	70	63	60	58	57	51	53	60	67	75	83	85	88	91	86	84	82	84	89	102	107	98	83	81	9,260
Subtotal	141,352	130,676	130,006	128,529	128,310	124,964	125,772	135,056	145,710	148,021	151,223	147,465	161,611	160,891	160,678	156,766	161,554	157,908	142,116	147,185	141,191	141,302	137,879	135,589	3,441,752

Table 12.7 – Running cost of a 40 units mini-pool over schedule time

t [h]	1	2	3	4	5	6	7	8	9	10	11	12	13	14	15	16	17	18	19	20	21	22	23	24	Total
Unit#1	82.11	80 64	0.01	0 01	0.01	88.96	84.54	82.96	79 49	76.80	75.36	74.72	73 55	72.99	72.69	73.00	73.64	74.22	75 09	75.39	75.69	0 01	0.01	0 01	1,391.90
Unit#2	196 65	187.26	187.26	187.26	187.26	187.26	187.26	187.26	186 10	180.70	177.34	172 82	168.19	166.70	165.21	165.68	167 69	169 42	172.77	177.14	179 63	182.79	185 02	186.47	4,311.14
Unit#3	61.25	0 01	0.01	0.01	0 01	0.01	66 57	62.50	0.01	0 01	0.01	0 01	58 08	0.01	57.36	54 64	55.24	55.76	56.35	56 56	0 01	0 01	0.01	0 01	584 45
Unit#4	73.04	0 01	0.01	0 01	0 01	0.01	74.20	69 90	0.01	0 01	0.01	0.01	71.30	67 68	67.68	67.68	67.68	67 89	67.97	68.18	0.01	0 01	0.01	0 01	763.33
Unit#5	83 61	79.40	79 76	79 97	80.66	80 87	80.45	79 71	79.20	78.53	78 01	77 36	77.15	77.15	76.84	77.05	77.12	77.34	77 43	77 64	78.00	78.21	78.58	78 80	1,888 84
Unit#6	184.90	175 94	176 66	177.29	178.68	179 31	178 47	176.77	175.94	174 16	173.12	171 59	171.17	170 96	170.75	170.75	171.12	171.33	171.74	172 53	172 95	173 48	174.12	174.62	4,188.35
Unit#7	34.02	0 01	0.01	0.01	0 01	0.01	34 82	32.77	0.01	0.01	0.01	0.01	32 56	0.01	32.27	30.73	31.04	31 04	31.04	31.85	0.01	0 01	0 01	0.01	322.28
Unit#8	3 62	0 01	0 01	0 01	0 01	0.01	3 63	3 46	0 01	0 01	0.01	0 01	3 54	0 01	0 01	3 53	3 37	3 38	3 39	3 40	0 01	0 01	3 60	0 01	35 06
Unit#9	82.11	0 01	0 01	0 01	0.01	88 96	84.54	82.96	79.49	76.80	75.36	74.72	73 55	72.99	72 69	73 00	73 64	74.22	75 09	75 39	75 69	76.51	0 01	0.01	1,387.77
Unit#10	196 65	187.26	187.26	187.26	187.26	187.26	187.26	187.26	186.10	180.70	177 34	172.82	168.19	166 70	165.21	165.68	167 69	169.42	172.77	177 14	179 63	182.79	185.02	186 47	4,311.14
Unit#11	61.25	0 01	0 01	0 01	0 01	0.01	66 57	62.50	0.01	0 01	0.01	0.01	58 08	0.01	57.36	54 64	55.24	55 76	56.35	56 56	0 01	0 01	0 01	0 01	584 45
Unit#12	73.04	0.01	0 01	0 01	0 01	0 01	74.20	69.90	69.69	68.78	68.57	67.89	67 68	67.68	67.68	67.68	67 68	67.89	67.97	68.18	0 01	0 01	0.01	0.01	1,034 60
Unit#13	83 61	0.01	0 01	0.01	0.01	0 01	84.87	79.71	79.20	78 53	78 01	77.36	77.15	77.15	76.84	77.05	77.12	77.34	77 43	77 64	78 00	78.21	78.58	0.01	1,413.86
Unit#14	184 90	175.94	0 01	0 01	0 01	0.01	187.86	176 77	175 94	174.16	173 12	171.59	171 17	170.96	170.75	170 75	171.12	171.33	171.74	172 53	172 95	173 48	174.12	174 62	3,485.84
Unit#15	34.02	0.01	0 01	0 01	0.01	0.01	34.82	32.77	0 01	0.01	0 01	0 01	32 56	0.01	32.27	30.73	31 04	31 04	31.04	31.85	0 01	0.01	0 01	0 01	322.28
Unit#16	3 62	0 01	0 01	3 63	0 01	0 01	3 63	3 46	0 01	0 01	0 01	0 01	3 54	0 01	0 01	3 53	3 37	3 38	3 39	3 40	0 01	0 01	3 60	0 01	38 68
Unit#17	82.11	80.64	83.88	84 54	84 54	84 54	84.54	82 96	79 49	76 80	75.36	74 72	73 55	72 99	72 69	73.00	73.64	74.22	75 09	75.39	75 69	76 51	76 83	77.48	1,871.20
Unit#18	196.65	187.26	0 01	0 01	0.01	196 65	187.26	187.26	186.10	180 70	177 34	172 82	168.19	166 70	165.21	165 68	167 69	169 42	172 77	177.14	179 63	182 79	185 02	186 47	3,758.78
Unit#19	61 25	0 01	0 01	0 01	0 01	0 01	66.57	62 50	0.01	0.01	0 01	0 01	58.08	0 01	57.36	54 64	55.24	55 76	56 35	56 56	0 01	0.01	0.01	0 01	584 45
Unit#20	73.04	0.01	0.01	0.01	0.01	0.01	74 20	69 90	0 01	0.01	0.01	0 01	71.30	67 68	67 68	67 68	67 68	67 89	67 97	68 18	0 01	0 01	0.01	0.01	763.33
Unit#21	83 61	79.40	79 76	79 97	80 66	80.87	80.45	79 71	79.20	78.53	78.01	77.36	77 15	77.15	76 84	77.05	77.12	77 34	77 43	77.64	78 00	78.21	78.58	78 80	1,888 84
Unit#22	184.90	0 01	0 01	0 01	0.01	188 70	178 47	176 77	175.94	174.16	173.12	171 59	171.17	170 96	170 75	170 75	171.12	171.33	171.74	172 53	172 95	173 48	174.12	174 62	3,489 21
Unit#23	34 02	0.01	0 01	0.01	0 01	0 01	34 82	32.77	0 01	0 01	0.01	0 01	32 56	0.01	32.27	30.73	31.04	31.04	31 04	31 85	0 01	0 01	0 01	0 01	322.28
Unit#24	3 62	0 01	0 01	0 01	0 01	0.01	3 63	3 46	0 01	0 01	0 01	0 01	3 54	0 01	0 01	3 53	3 37	3 38	3 39	3 40	0 01	0.01	3 60	3 44	38 49
Unit#25	82.11	80 64	83 88	84 54	84 54	84.54	84.54	82 96	79 49	76 80	75 36	74 72	73.55	72.99	72.69	73.00	73 64	74.22	75 09	75.39	75 69	76.51	76 83	77.48	1,871.20
Unit#26	196.65	187.26	0.01	0 01	0 01	196.65	187.26	187.26	186 10	180 70	177.34	172.82	168.19	166.70	165.21	165 68	167 69	169 42	172.77	177.14	179 63	182 79	185 02	186 47	3,758 78
Unit#27	61.25	0.01	0 01	0 01	0 01	0.01	66 57	62 50	0 01	0 01	0 01	0 01	58 08	0 01	57.36	54 64	55.24	55.76	56 35	56 56	0.01	0 01	0 01	0.01	584.45
Unit#28	73 04	0 01	0 01	0 01	0.01	0 01	74.20	69 90	0.01	0.01	0 01	0 01	71.30	67.68	67.68	67 68	67 68	67.89	67 97	68.18	0 01	0 01	0 01	0.01	763.33
Unit#29	83.61	79 40	79 76	79 97	80 66	80.87	80.45	79.71	79.20	78 53	78 01	77.36	77.15	77.15	76.84	77.05	77.12	77.34	77 43	77 64	78 00	78.21	78 58	78.80	1,888 84
Unit#30	184 90	175 94	0 01	0 01	0.01	188.70	178.47	176 77	175.94	174 16	173 12	171.59	171 17	170 96	170.75	170.75	171.12	171 33	171.74	172 53	172 95	173.48	0.01	0.01	3,316 42
Unit#31	34.02	0.01	0 01	0 01	0 01	0 01	34 82	32.77	0 01	0 01	0.01	0 01	32 56	0 01	32.27	30.73	31.04	31.04	31 04	31.85	0 01	0 01	0.01	0 01	322.28
Unit#32	3 62	0 01	0 01	0 01	0 01	0.01	3 63	3 46	0 01	0 01	0 01	0 01	0 01	0 01	0 01	3 53	3 37	3 38	3 39	3 40	0 01	0 01	3 60	0 01	31 53
Unit#33	82.11	0.01	0 01	0 01	0.01	88 96	84 54	82 96	79 49	76.80	75.36	74 72	73 55	72 99	72 69	73.00	73 64	74.22	75.09	75 39	75 69	76 51	76.83	77 48	1,542 06
Unit#34	196 65	187.26	187.26	187.26	187.26	187.26	187.26	187.26	186 10	180.70	177 34	172 82	168 19	166 70	165.21	165 68	167.69	169 42	172.77	177 14	179 63	182 79	185 02	186 47	4,311.14
Unit#35	61.25	0 01	0 01	0 01	0 01	0.01	66.57	62.50	0 01	0 01	0 01	0 01	58 08	0 01	57 36	54 64	55.24	55.76	56 35	56.56	0 01	0 01	0 01	0 01	584 45
Unit#36	73.04	0 01	0 01	0 01	0 01	0 01	74.20	69 90	0 01	0 01	0 01	0.01	0 01	71 30	67.68	67 68	67.68	67 68	67.89	67.97	68.18	0 01	0 01	0 01	763 33
Unit#37	83.61	79 40	0 01	0 01	0 01	0.01	84 87	79 71	79.20	78.53	78.01	77.36	77 15	77.15	76.84	77.05	77.12	77.34	77.43	77 64	78 00	78.21	78 58	78 80	1,572 04
Unit#38	184.90	175 94	0 01	0 01	0 01	0 01	187.86	176 77	175 94	174 16	173.12	171.59	171.17	170 96	170.75	170 75	171 12	171.33	171.74	172 53	172 95	173 48	174 12	174 62	3,485 84
Unit#39	34.02	0 01	0.01	0 01	0 01	0 01	34 82	32.77	0 01	0 01	0.01	0 01	32 56	0.01	32.27	30.73	31.04	31 04	31 04	31.85	0 01	0 01	0 01	0 01	322.28
Unit#40	3 62	0 01	0 01	0 01	0 01	0 01	3 63	3 46	0 01	0 01	0 01	0 01	3 54	0 01	0 01	3 53	3 37	3 38	3 39	3 40	0 01	0 01	0 01	3 61	35 07
Subtotal	3,596 00	2,199 82	1,145 79	1,151 99	1,151 83	2,190 60	3,577 32	3,476 65	2,673 53	2,619 92	2,587 91	2,550 53	3,270 55	2,777 55	3,214 05	3,215 30	3,234 50	3,251 90	3,278 90	3,313 45	2,531 55	2,478 65	2,259 56	2,185 74	63,933 59

Table 12.8 – Optimisation results of a 40 units mini-pool over schedule time

t [h]	1	2	3	4	5	6	7	8	9	10	11	12	13	14	15	16	17	18	19	20	21	22	23	24	Total
ESP_t [€/MWh]	19 96	16.27	15 88	15 74	15 66	16.27	20.29	21.73	17.19	17.16	17.04	16 85	22.78	17.37	19 62	24.70	30.23	61.29	34.18	25 78	16 87	16 53	15 84	15.01	-
EBP_t [€/MWh]	22.50	17.53	15 88	15 74	15 96	20.11	33.91	32 96	27 07	26 68	26 14	24.71	24.25	21.79	47.81	48 16	79.13	104.05	74 93	51 45	23 43	22 92	19.26	17.20	-
DP_t [kW]	0	0	59518	57715	57324	0	0	0	0	0	0	0	0	0	0	0	0	0	0	0	0	0	4	1794	176,356
SP_t [kW]	63043	4147	0	0	0	6826	85627	73395	17688	11215	5609	6451	28917	5457	26964	32223	29198	33858	51858	49068	12773	9936	0	0	554,250
RC_{Ui} [€]	3596 03	2199 80	1145 79	1151 98	1151.80	2190 57	3577.27	3476 61	2673 57	2619 95	2587 86	2550 55	3270 59	2777.55	3214.01	3215 30	3234 52	3251.89	3278 84	3313 42	2531 56	2478 73	2259 56	2185 72	63,933
CDP_{Ui} [€]	0 00	0.00	945 15	908.44	914 89	0 00	0.00	0.00	0 00	0.00	0.00	0 00	0 00	0 00	0.00	0 00	0.00	0.00	0 00	0 00	0.00	0.00	0 08	30 86	2,799
TEC_{Ui} [€]	2540.09	2350 78	2336 69	2308 43	2303.39	2246 58	2260.39	2429 31	2620 47	2664 81	2722 40	2661.87	2911.25	2893 63	2890 05	2820 04	2904 50	2843.21	2573 43	2664 61	2560 78	2558.00	2489.01	2447 49	62,001
$TESM_{Ui}$ [€]	1258 34	67.47	0 00	0.00	0.00	111.07	1737.37	1594.87	304 06	192 44	95 58	108 69	658.73	94 78	529 02	795.90	882 64	2075.13	1772 49	1264 96	215 47	164.25	0 00	0 00	13,923
R_{Ui} [€]	3796 43	2418.24	2336 69	2308 43	2303 39	2357 65	3997.77	4024.18	2924.53	2857.26	2817.98	2770.57	3569 98	2988 41	3419 08	3615.93	3787.14	4918.34	4345.92	3929 57	2776.25	2722.24	2489 01	2447.49	75,924
PC_{Ui} [€]	3596.03	2199 80	2090 94	2060 42	2066.70	2190.57	3577.27	3476 61	2673 57	2619 95	2587 86	2550 55	3270 59	2777.55	3214.01	3215.30	3234.52	3251 89	3278 84	3313.42	2531.56	2478 73	2259 63	2216 58	66,733
Prf_{Ui} [€]	202 39	218 44	245 75	248 01	236 69	167 08	420 50	547 58	250 96	237 30	230 12	220 02	299 39	210 86	205 06	400 64	552 61	1666 45	1067 08	616 14	244 69	243 52	229 37	230 91	9,192

Table 12.9 - Optimal 40 units mini-pool schedule obtained by multi-units commitment algorithm

t [h]	1	2	3	4	5	6	7	8	9	10	11	12	13	14	15	16	17	18	19	20	21	22	23	24
Unit#1	1	1	0	0	0	1	1	1	1	1	1	1	1	1	1	1	1	1	1	1	1	0	0	0
Unit#2	1	1	1	1	1	1	1	1	1	1	1	1	1	1	1	1	1	1	1	1	1	1	1	1
Unit#3	1	0	0	0	0	0	1	1	0	0	0	0	1	0	1	1	1	1	1	1	0	0	0	0
Unit#4	1	0	0	0	0	0	1	1	0	0	0	0	1	1	1	1	1	1	1	1	0	0	0	0
Unit#5	1	1	1	1	1	1	1	1	1	1	1	1	1	1	1	1	1	1	1	1	1	1	1	1
Unit#6	1	1	1	1	1	1	1	1	1	1	1	1	1	1	1	1	1	1	1	1	1	1	1	1
Unit#7	1	0	0	0	0	0	1	1	0	0	0	0	1	0	1	1	1	1	1	1	0	0	0	0
Unit#8	1	0	0	0	0	0	1	1	0	0	0	0	1	0	0	1	1	1	1	1	0	0	1	0
Unit#9	1	0	0	0	0	1	1	1	1	1	1	1	1	1	1	1	1	1	1	1	1	1	0	0
Unit#10	1	1	1	1	1	1	1	1	1	1	1	1	1	1	1	1	1	1	1	1	1	1	1	1
Unit#11	1	0	0	0	0	0	1	1	0	0	0	0	1	0	1	1	1	1	1	1	0	0	0	0
Unit#12	1	0	0	0	0	0	1	1	1	1	1	1	1	1	1	1	1	1	1	1	0	0	0	0
Unit#13	1	0	0	0	0	0	1	1	1	1	1	1	1	1	1	1	1	1	1	1	1	1	1	0
Unit#14	1	1	0	0	0	0	1	1	1	1	1	1	1	1	1	1	1	1	1	1	1	1	1	1
Unit#15	1	0	0	0	0	0	1	1	0	0	0	0	1	0	1	1	1	1	1	1	0	0	0	0
Unit#16	1	0	0	1	0	0	1	1	0	0	0	0	1	0	0	1	1	1	1	1	0	0	1	0
Unit#17	1	1	1	1	1	1	1	1	1	1	1	1	1	1	1	1	1	1	1	1	1	1	1	1
Unit#18	1	1	0	0	0	1	1	1	1	1	1	1	1	1	1	1	1	1	1	1	1	1	1	1
Unit#19	1	0	0	0	0	0	1	1	0	0	0	0	1	0	1	1	1	1	1	1	0	0	0	0
Unit#20	1	0	0	0	0	0	1	1	0	0	0	0	1	1	1	1	1	1	1	1	0	0	0	0
Unit#21	1	1	1	1	1	1	1	1	1	1	1	1	1	1	1	1	1	1	1	1	1	1	1	1
Unit#22	1	0	0	0	0	1	1	1	1	1	1	1	1	1	1	1	1	1	1	1	1	1	1	1
Unit#23	1	0	0	0	0	0	1	1	0	0	0	0	1	0	1	1	1	1	1	1	0	0	0	0
Unit#24	1	0	0	0	0	0	1	1	0	0	0	0	1	0	0	1	1	1	1	1	0	0	1	1
Unit#25	1	1	1	1	1	1	1	1	1	1	1	1	1	1	1	1	1	1	1	1	1	1	1	1
Unit#26	1	1	0	0	0	1	1	1	1	1	1	1	1	1	1	1	1	1	1	1	1	1	1	1
Unit#27	1	0	0	0	0	0	1	1	0	0	0	0	1	0	1	1	1	1	1	1	0	0	0	0
Unit#28	1	0	0	0	0	0	1	1	0	0	0	0	1	1	1	1	1	1	1	1	0	0	0	0
Unit#29	1	1	1	1	1	1	1	1	1	1	1	1	1	1	1	1	1	1	1	1	1	1	1	1
Unit#30	1	1	0	0	0	1	1	1	1	1	1	1	1	1	1	1	1	1	1	1	1	1	0	0
Unit#31	1	0	0	0	0	0	1	1	0	0	0	0	1	0	1	1	1	1	1	1	0	0	0	0
Unit#32	1	0	0	0	0	0	1	1	0	0	0	0	0	0	0	1	1	1	1	1	0	0	1	0
Unit#33	1	0	0	0	0	1	1	1	1	1	1	1	1	1	1	1	1	1	1	1	1	1	1	1
Unit#34	1	1	1	1	1	1	1	1	1	1	1	1	1	1	1	1	1	1	1	1	1	1	1	1
Unit#35	1	0	0	0	0	0	1	1	0	0	0	0	1	0	1	1	1	1	1	1	0	0	0	0
Unit#36	1	0	0	0	0	0	1	1	0	0	0	0	1	1	1	1	1	1	1	1	0	0	0	0
Unit#37	1	1	0	0	0	0	1	1	1	1	1	1	1	1	1	1	1	1	1	1	1	1	1	1
Unit#38	1	1	0	0	0	0	1	1	1	1	1	1	1	1	1	1	1	1	1	1	1	1	1	1
Unit#39	1	0	0	0	0	0	1	1	0	0	0	0	1	0	1	1	1	1	1	1	0	0	0	0
Unit#40	1	0	0	0	0	0	1	1	0	0	0	0	1	0	0	1	1	1	1	1	0	0	0	1

Table 12.10 - Sequence of units dispatched of a 40 units mini-pool achieved with APL

	GCi [£/kWh]	PL Position
Unit#01	0.01291	16th
Unit#02	0.01256	1st
Unit#03	0.01500	36th
Unit#04	0.01378	21st
Unit#05	0.01279	11th
Unit#06	0.01275	6th
Unit#07	0.01488	31st
Unit#08	0.01418	26th
Unit#09	0.01291	17th
Unit#10	0.01256	2nd
Unit#11	0.01500	37th
Unit#12	0.01378	22nd
Unit#13	0.01279	12th
Unit#14	0.01275	7th
Unit#15	0.01488	32nd
Unit#16	0.01418	27th
Unit#17	0.01291	18th
Unit#18	0.01256	3rd
Unit#19	0.01500	38th
Unit#20	0.01378	23rd
Unit#21	0.01279	13th
Unit#22	0.01275	8th
Unit#23	0.01488	33rd
Unit#24	0.01418	28th
Unit#25	0.01291	19th
Unit#26	0.01256	4th
Unit#27	0.01500	39th
Unit#28	0.01378	24th
Unit#29	0.01279	14th
Unit#30	0.01275	9th
Unit#31	0.01488	34th
Unit#32	0.01418	29th
Unit#33	0.01291	20th
Unit#34	0.01256	5th
Unit#35	0.01500	40th
Unit#36	0.01378	25th
Unit#37	0.01279	15th
Unit#38	0.01275	10th
Unit#39	0.01488	35th
Unit#40	0.01418	30th

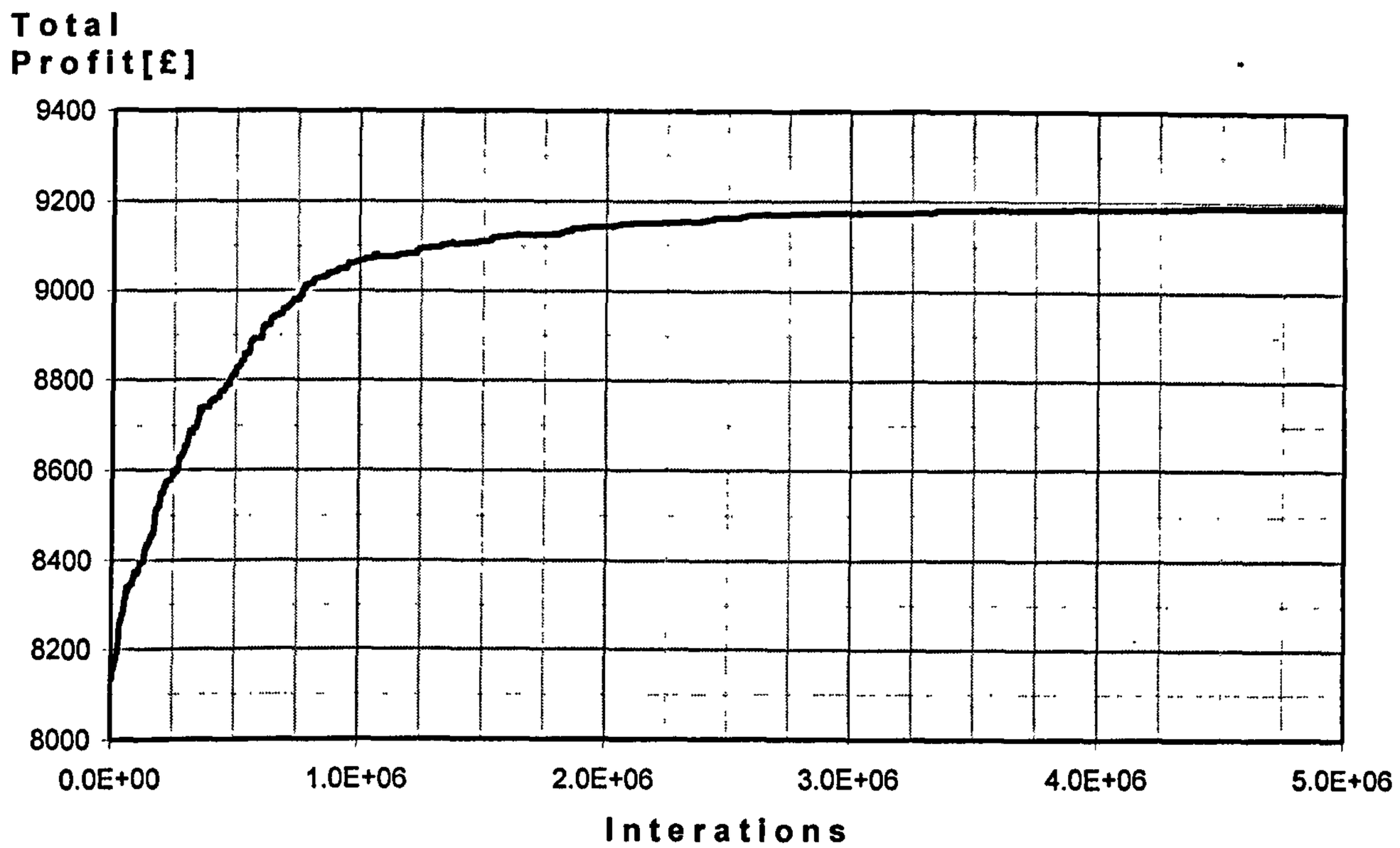

Figure 12.1 – Convergence obtained by Hybrid GA-APL (40 units mini-pool)

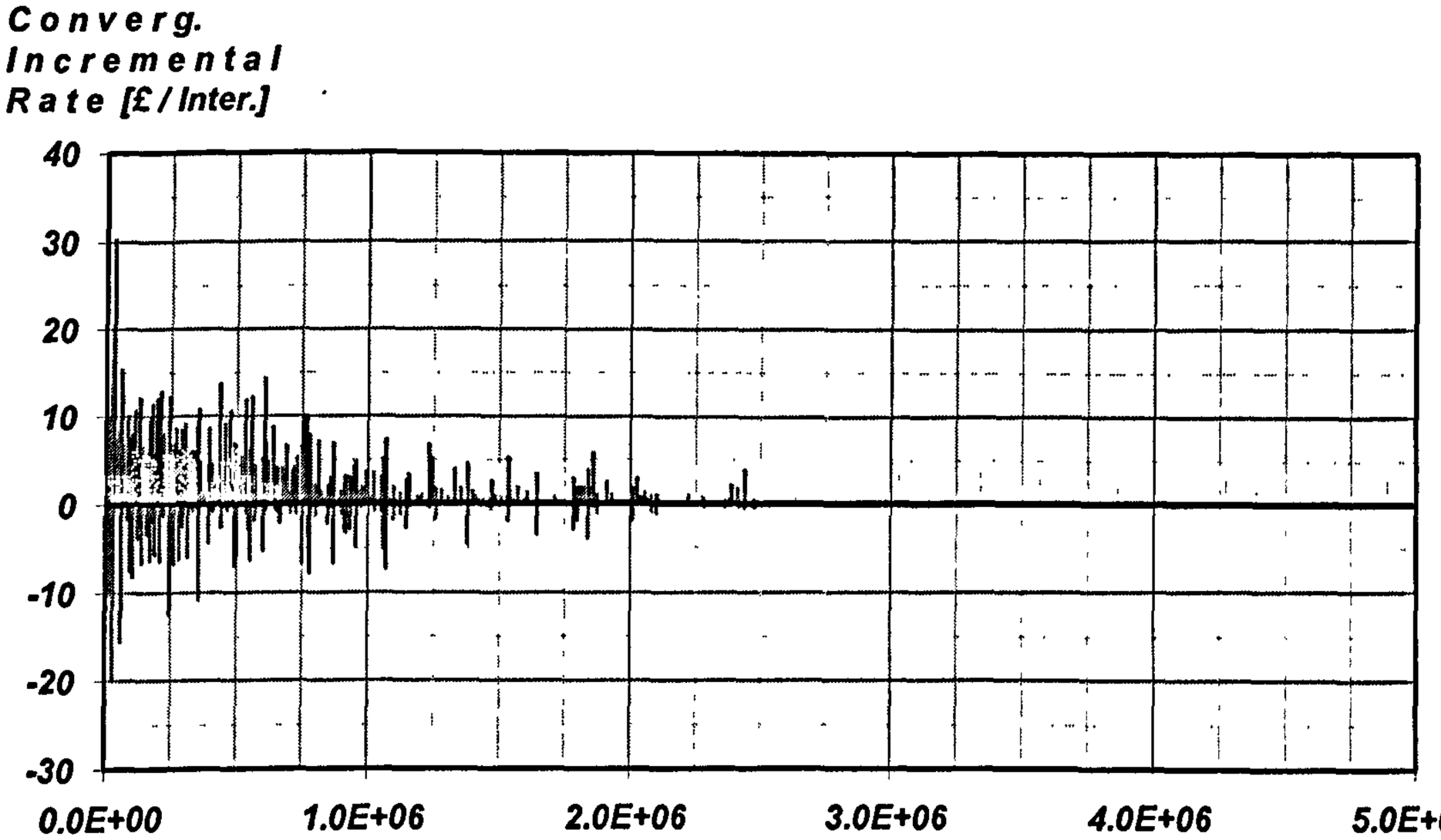

Figure 12.2 – Convergence incremental rate obtained by Hybrid GA-APL (40 units mini-pool)